frontiers | Research Topics

Model organisms in plant developmental biology — their effectiveness and limitations

Edited by
Neelima Roy Sinha and Verónica S. Di Stilio

Published in
Frontiers in Plant Science

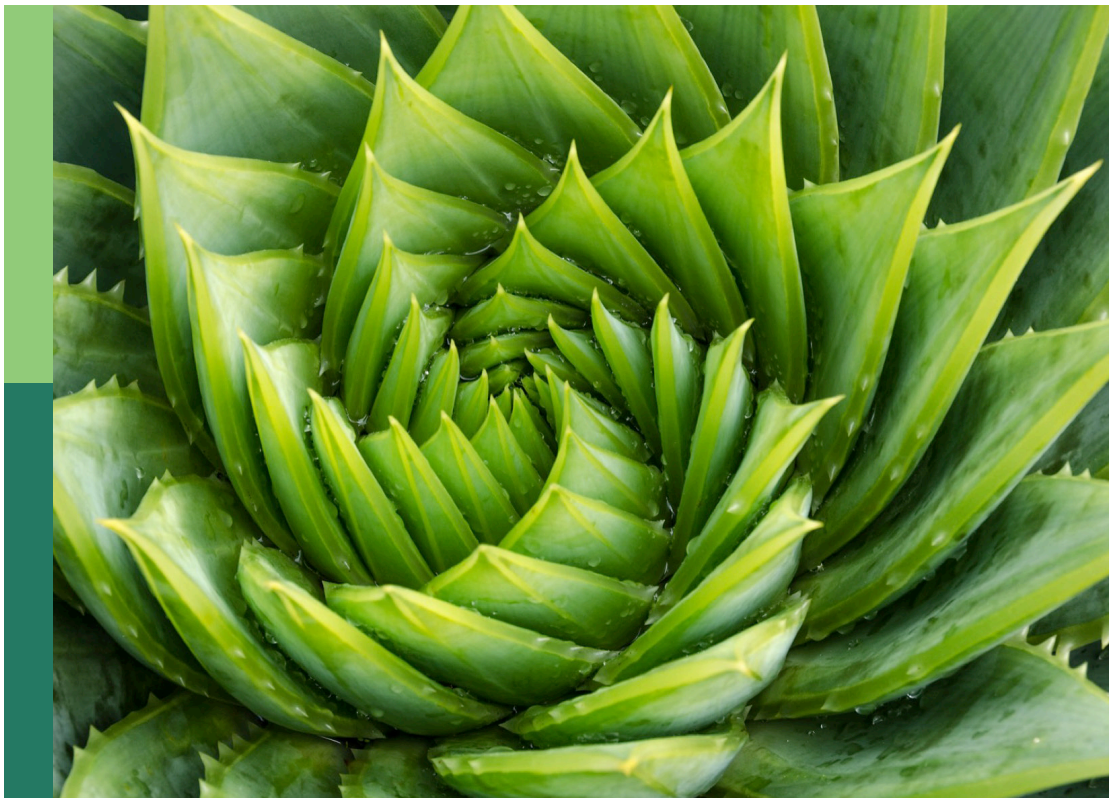

ISSN 1664-8714
ISBN 978-2-8325-5478-4
DOI 10.3389/978-2-8325-5478-4

About Frontiers

Frontiers is more than just an open access publisher of scholarly articles: it is a pioneering approach to the world of academia, radically improving the way scholarly research is managed. The grand vision of Frontiers is a world where all people have an equal opportunity to seek, share and generate knowledge. Frontiers provides immediate and permanent online open access to all its publications, but this alone is not enough to realize our grand goals.

Frontiers journal series

The Frontiers journal series is a multi-tier and interdisciplinary set of open-access, online journals, promising a paradigm shift from the current review, selection and dissemination processes in academic publishing. All Frontiers journals are driven by researchers for researchers; therefore, they constitute a service to the scholarly community. At the same time, the *Frontiers journal series* operates on a revolutionary invention, the tiered publishing system, initially addressing specific communities of scholars, and gradually climbing up to broader public understanding, thus serving the interests of the lay society, too.

Dedication to quality

Each Frontiers article is a landmark of the highest quality, thanks to genuinely collaborative interactions between authors and review editors, who include some of the world's best academicians. Research must be certified by peers before entering a stream of knowledge that may eventually reach the public - and shape society; therefore, Frontiers only applies the most rigorous and unbiased reviews. Frontiers revolutionizes research publishing by freely delivering the most outstanding research, evaluated with no bias from both the academic and social point of view. By applying the most advanced information technologies, Frontiers is catapulting scholarly publishing into a new generation.

What are Frontiers Research Topics?

Frontiers Research Topics are very popular trademarks of the *Frontiers journals series*: they are collections of at least ten articles, all centered on a particular subject. With their unique mix of varied contributions from Original Research to Review Articles, Frontiers Research Topics unify the most influential researchers, the latest key findings and historical advances in a hot research area.

Find out more on how to host your own Frontiers Research Topic or contribute to one as an author by contacting the Frontiers editorial office: frontiersin.org/about/contact

Model organisms in plant developmental biology — their effectiveness and limitations

Topic editors

Neelima Roy Sinha — University of California, Davis, United States

Verónica S. Di Stilio — University of Washington, United States

Citation

Sinha, N. R., Di Stilio, V. S., eds. (2024). *Model organisms in plant developmental biology — their effectiveness and limitations*. Lausanne: Frontiers Media SA.

doi: 10.3389/978-2-8325-5478-4

Table of contents

05 Editorial: Model organisms in plant developmental biology—their effectiveness and limitations
Verónica S. Di Stilio and Neelima R. Sinha

08 Evolutionary analyses and expression patterns of TCP genes in Ranunculales
Catherine Damerval, Carmine Claudot, Martine Le Guilloux, Natalia Conde e Silva, Véronique Brunaud, Ludivine Soubigou-Taconnat, José Caius, Etienne Delannoy, Sophie Nadot, Florian Jabbour and Yves Deveaux

25 *SEP*-like genes of *Gossypium hirsutum* promote flowering *via* targeting different loci in a concentration-dependent manner
Liting Chen, Yuanyuan Yan, Huifeng Ke, Zihao Zhang, Chengsheng Meng, Limei Ma, Zhengwen Sun, Bin Chen, Zhengwen Liu, Guoning Wang, Jun Yang, Jinhua Wu, Zhikun Li, Liqiang Wu, Guiyin Zhang, Yan Zhang, Xingfen Wang and Zhiying Ma

42 Insight into the formation of trumpet and needle-type leaf in *Ginkgo biloba* L. mutant
Fang Tang, Pengbo Sun, Qian Zhang, Fengwei Zhong, Ying Wang and Mengzhu Lu

53 *Cuscuta* species: Model organisms for haustorium development in stem holoparasitic plants
Min-Yao Jhu and Neelima R. Sinha

63 Nectary development in *Cleome violacea*
Shane Carey, Brandi Zenchyzen, A. J. Deneka and Jocelyn C. Hall

88 California poppy (*Eschscholzia californica*), the Papaveraceae golden girl model organism for evodevo and specialized metabolism
Annette Becker, Yasuyuki Yamada and Fumihiko Sato

100 What can hornworts teach us?
Eftychios Frangedakis, Alan O. Marron, Manuel Waller, Anna Neubauer, Sze Wai Tse, Yuling Yue, Stephanie Ruaud, Lucas Waser, Keiko Sakakibara and Péter Szövényi

117 Regulation of secondary growth by poplar *BLADE-ON-PETIOLE* genes in Arabidopsis
Sibei Li, Bhaswati Devi, Gamalat Allam, Armaan Bhullar, Jhadeswar Murmu, Eryang Li and Shelley R. Hepworth

129 The monoicous secondarily aquatic liverwort *Ricciocarpos natans* as a model within the radiation of derived Marchantiopsida
Shilpi Singh and John L. Bowman

145 A eudicot *MIXTA* family ancestor likely functioned in both conical cells and trichomes
Simra Zahid, Anjelique F. Schulfer and Verónica S. Di Stilio

160 Plant elicitor Peptides regulate root hair development in *Arabidopsis*
Yanping Jing, Fugeng Zhao, Ke Lai, Fei Sun, Chenjie Sun, Xingyue Zou, Min Xu, Aigen Fu, Rouhallah Sharifi, Jian Chen, Xiaojiang Zheng and Sheng Luan

172 Deciphering the maize gene ZmGF14–3: implications for plant height based on co-expression networks
Hengsheng Wang, Bo Wei, Lulu Qi, Yansong Chen, Kelong Chen, Dong Liu, Xu Su, Yan Zhang and Lingling Li

185 *Delphinium* as a model for development and evolution of complex zygomorphic flowers
Bharti Sharma, Mankirat Kaur Pandher, Ana Quetzali Alcaraz Echeveste, Rene Kenny Romo and Marianellie Bravo

frontiers | Frontiers in Plant Science

TYPE Editorial
PUBLISHED 13 September 2024
DOI 10.3389/fpls.2024.1478483

OPEN ACCESS

EDITED AND REVIEWED BY
Chi-Lien Cheng,
The University of Iowa, United States

*CORRESPONDENCE
Verónica S. Di Stilio
distilio@uw.edu

RECEIVED 09 August 2024
ACCEPTED 14 August 2024
PUBLISHED 13 September 2024

CITATION
Di Stilio VS and Sinha NR (2024) Editorial: Model organisms in plant developmental biology—their effectiveness and limitations. *Front. Plant Sci.* 15:1478483. doi: 10.3389/fpls.2024.1478483

Editorial: Model organisms in plant developmental biology—their effectiveness and limitations

Verónica S. Di Stilio[1]* and Neelima R. Sinha[2]

[1]Department of Biology, University of Washington, Seattle, WA, United States, [2]Department of Plant Biology, University of California, Davis, CA, United States

KEYWORDS

model organisms, model clade, plant development, Evo-Devo, #collectionseries

Editorial on the Research Topic

Model organisms in plant developmental biology—their effectiveness and limitations

Model organisms represent an invaluable resource for fundamental and applied research allowing the identification of the mechanistic basis of evolutionary innovations. This Research Topic showcases studies performed on established and emerging model organisms in Plant Developmental Biology that have broad significance to the field. Increased phylogenetic breadth and availability of genomes and transgenic techniques have fostered innovative ideas and syntheses spanning the range from fossil analyses to single-cell sequencing. However, broad taxonomic applicability of the knowledge gained from studies on model organisms and relevance to the field of Evolutionary Developmental Biology (Evo-Devo) often remains unresolved.

To address such questions, this Research Topic focuses on new insights, latest discoveries, current challenges, and future perspectives on the use of model organisms and the extent to which the knowledge gained from them can be extrapolated. Authors were encouraged to identify the greatest unifying concepts in their sub-disciplines, as well as to put forward potential solutions to address the challenges emerging from the use of model plants.

Core eudicots

There is still much to be learned in the classic core eudicot model *Arabidopsis thaliana*, such as description of a novel signaling pathway used by plant elicitor peptides to regulate root hair development (Jing et al.). *Cleome violacea* (Cleomaceae), in the sister lineage to Brassicaceae, utilizes comparisons to *Arabidopsis* to illuminate conserved genetic pathways in the evolution of nectary development suggesting a unique origin of nectaries in these sister lineages, while adding a reference point to only four other core eudicots with functional data on this aspect of flower development (Carey et al.).

Economically significant models: In the dicot model crop cotton (*Gossypium hirsutum*, Malvaceae), novel insights were gained on the role of the floral E class genes, the MADS box

transcription factors *SEPALLATA*. Via targeted gene silencing combined with heterologous overexpression in *Arabidopsis*, the authors find that the cotton orthologs GhSEP interact with regulators of the transition to flowering, such as GhAP1 and GhLFY, leading them to propose a model of tetramer interaction in leaves, meristems, and floral organs (Chen et al.). In the model tree poplar (Salicaceae), Li et al. demonstrate that two BLADE ON PETIOLE orthologs function in secondary growth affecting wood production via heterologous overexpression in *Arabidopsis*.

The widespread stem parasitic plants in the *Cuscuta* genus (Convolvulaceae) offer a unique model to investigate this divergent plant growth strategy that results in enormous loss in agricultural fields. The authors present the advantages of using *Cuscuta* species as model organisms to illuminate the haustorium formation process using unique features such as self, hyper-, and cross-organ parasitism (Jhu and Sinha).

In the monocot model crop maize, the ubiquitous developmental regulators GF14 emerged as candidates for plant height from gene regulatory network analyses. Heterologous testing via overexpression in *Arabidopsis* resulted in decreased plant height providing further evidence that these genes are involved in regulating plant growth that directly impacts crop yield (Wang et al.).

Early-diverging eudicots (Ranunculales)

The order Ranunculales occupies an interesting phylogenetic position as an early-diverging eudicot and sister group to the core eudicots. Four representatives of this order, encompassing two families, are included in this Research Topic.

The iconic state flower California poppy (*Eschscholzia californica*, Papaveraceae) is an emerging model with a genome in the making and the ability to conduct transient gene silencing. California poppy promises to help integrate traditional enquiries into the regulation of morphogenesis with emerging interest in secondary metabolites due to its abundance of benzylisoquinoline alkaloids in floral organs (Becker et al.).

Thalictrum thalictroides (Ranunculaceae) is amenable to high-efficiency targeted gene silencing. Combined with gene duplication from multiple rounds of polyploidy in the genus and expression analyses, the authors demonstrate the multiple roles of the MYB transcription factor family *MIXTA-like* and bridge the gap to reconstruct its ancestral function. In addition to its previously demonstrated role in papillate cells on the floral perianth, the authors demonstrate its involvement in leaf trichome development in *T. thalictroides*. Heterologous overexpression in tobacco demonstrates a conserved trichome function, supporting the dual role in the eudicot ancestor, presumably later parsed into distinct paralogs (Zahid et al.).

Damerval et al. characterize the land plant-specific TCP family of transcription factors in *Nigella damascena* (Ranunculaceae). On the one hand, the authors identify six clades of Class I TCP genes in *Nigella* tracing back to the origin of angiosperms, and three clades of Class II TCP with mostly redundant expression. On the other hand, the CYC/TB1 lineage are expressed distinctly suggesting more specific roles.

Sharma et al. review the unique ways in which the *Delphinieae* tribe, another Ranunculaceae model clade, contributes to understanding of the evolution, ecology, and development of complex flower symmetry involving a "hyperorgan" of synorganized spurred petaloid organs.

Gymnosperms

In non-flowering seed plants (gymnosperms), where very few model systems have been developed, Tang et al. characterize a *Ginkgo biloba* variety with a range of abnormal leaf shapes from needle- to trumpet- type. The authors find anatomical and genetic evidence for changes in leaf polarity via shifts in the adaxial (dorsal) and abaxial (ventral) domains in combination with boundary defects resulting in tissue fusion.

Bryophytes

Two articles highlight representatives of the non-vascular bryophytes, a liverwort and a hornwort. Singh and Bowman introduce us to the enigmatic *Ricciocarpos natans*, a liverwort that has secondarily evolved to be aquatic and monoicous from ancestral dioicy with sex chromosomes. *R. natans* thus provides an excellent platform to investigate the genomic consequences of sexual system and life habit transitions while also broadening the land plant perspective. Frangedakis et al. provide a valuable comparison of the hornwort *Anthoceros agrestis* to other model land plants while illustrating the unique features whose evolution it is well positioned to address, such as polyplastidy and symbiotic associations with fungi and cyanobacteria.

In closing, model organisms continue to be developed across land plants enriching the landscape for Evo-Devo studies. Here, we compiled contributions encompassing two non-vascular plants, a gymnosperm and ten angiosperms, comprising one monocot, four early-diverging eudicots, and five core eudicots. This sampling of model systems illustrates the possibilities for extending the frontiers of plant evolution and development, as well as pointing out current limitations.

Author contributions

VD: Writing – original draft. NS: Writing – review & editing.

Funding

The author(s) declare financial support was received for the research, authorship, and/or publication of this article. VD acknowledges funding from National Science Foundation (NSF, USA), Division of Integrated and Organismal Systems (IOS), Developmental Mechanisms, Grant number 1920408, and Division of Environmental Biology, Evolutionary Processes, Grant number 1911539. NS acknowledges funding from NSF IOS-211980 and FFAR grant number 23-000823.

Conflict of interest

The authors declare that the research was conducted in the absence of any commercial or financial relationships that could be construed as a potential conflict of interest.

The author(s) declared that they were an editorial board member of Frontiers, at the time of submission. This had no impact on the peer review process and the final decision.

Publisher's note

frontiers | Frontiers in Plant Science

TYPE Original Research
PUBLISHED 01 December 2022
DOI 10.3389/fpls.2022.1055196

OPEN ACCESS

EDITED BY
Verónica S. Di Stilio,
University of Washington,
United States

REVIEWED BY
Aniket Sengupta,
St. John's University, United States
Cecilia Zumajo-Cardona,
University of Milan, Italy

*CORRESPONDENCE
Catherine Damerval
catherine.damerval@universite-paris-saclay.fr

†PRESENT ADDRESS
Ludivine Soubigou-Taconnat,
Groupe d'Étude et de Contrôle des Variétés et des Semences (GEVES), Station Nationale d'Essais de Semences (SNES), Beaucouzé, France

SPECIALTY SECTION
This article was submitted to Plant Development and EvoDevo, a section of the journal Frontiers in Plant Science

RECEIVED 27 September 2022
ACCEPTED 04 November 2022
PUBLISHED 01 December 2022

CITATION
Damerval C, Claudot C, Le Guilloux M, Conde e Silva N, Brunaud V, Soubigou-Taconnat L, Caius J, Delannoy E, Nadot S, Jabbour F and Deveaux Y (2022) Evolutionary analyses and expression patterns of TCP genes in Ranunculales. *Front. Plant Sci.* 13:1055196. doi: 10.3389/fpls.2022.1055196

Evolutionary analyses and expression patterns of TCP genes in Ranunculales

Catherine Damerval[1]*, Carmine Claudot[1], Martine Le Guilloux[1], Natalia Conde e Silva[1], Véronique Brunaud[2], Ludivine Soubigou-Taconnat[2†], José Caius[2], Etienne Delannoy[2], Sophie Nadot[3], Florian Jabbour[4] and Yves Deveaux[1]

[1]Université Paris-Saclay, INRAE, CNRS, AgroParisTech, Génétique Quantitative et Evolution-Le Moulon, IDEEV, Gif-sur-Yvette, France, [2]Université Paris-Saclay, CNRS, INRAE, Univ Evry, Institute of Plant Sciences Paris-Saclay (IPS2), Orsay, France, [3]Université Paris-Saclay, CNRS, AgroParisTech, Ecologie Systématique Evolution, Orsay, France, [4]Institut de Systématique, Evolution, Biodiversité (ISYEB), Muséum National d'Histoire Naturelle, CNRS, Sorbonne Université, EPHE, Université des Antilles, Paris, France

TCP transcription factors play a role in a large number of developmental processes and are at the crossroads of numerous hormonal biosynthetic and signaling pathways. The complete repertoire of TCP genes has already been characterized in several plant species, but not in any species of early diverging eudicots. We focused on the order Ranunculales because of its phylogenetic position as sister group to all other eudicots and its important morphological diversity. Results show that all the TCP genes expressed in the floral transcriptome of *Nigella damascena* (Ranunculaceae) are the orthologs of the TCP genes previously identified from the fully sequenced genome of *Aquilegia coerulea*. Phylogenetic analyses combined with the identification of conserved amino acid motifs suggest that six paralogous genes of class I TCP transcription factors were present in the common ancestor of angiosperms. We highlight independent duplications in core eudicots and Ranunculales within the class I and class II subfamilies, resulting in different numbers of paralogs within the main subclasses of TCP genes. This has most probably major consequences on the functional diversification of these genes in different plant clades. The expression patterns of TCP genes in *Nigella damascena* were consistent with the general suggestion that CIN and class I TCP genes may have redundant roles or take part in same pathways, while CYC/TB1 genes have more specific actions. Our findings open the way for future studies at the tissue level, and for investigating redundancy and subfunctionalisation in TCP genes and their role in the evolution of morphological novelties.

KEYWORDS

Ranunculales, *Nigella damascena*, TCP gene family, gene phylogeny, amino acid motifs, gene duplication

Introduction

The TCP family of transcription factors is specific to Viridiplantae. Whether this gene family originated in the most recent common ancestor of Embryophyta (land plants) or in aquatic Streptophyta prior to the divergence of Zygnematophyta remains controversial (Navaud et al., 2007; Liu et al., 2019; Wang et al., 2022). Over the course of evolution, the number of TCP genes has increased markedly in seed plants and especially in angiosperms compared with other embryophytes (Navaud et al., 2007; Li, 2015; Liu et al., 2019; Wang et al., 2022). The TCP gene family was initially defined from structural homologies in the three founding gene members, *TEOSINTE-BRANCHED1* (*TB1*) in maize, *CYCLOIDEA* (*CYC*) in snapdragon and *PROLIFERATING CELL NUCLEAR ANTIGEN FACTOR1* (*PCF1*) and *PCF2* in rice (Luo et al., 1996; Doebley et al., 1997; Kosugi & Ohashi, 1997; Cubas et al., 1999). Their characteristic domain (the TCP domain) is a non-canonical basic helix-loop-helix (bHLH) domain (Cubas et al., 1999). Two classes of TCP transcription factors have been defined based on structural characteristics in the basic and second helix regions of the TCP domain. Class I proteins, first described in PCFs, are characterized by a 55-62 amino acid long TCP domain, with a four amino acid shorter basic region and a longer second helix than class II proteins. Class II proteins, such as CYC and TB1, are characterized by a 58-59 amino acid long TCP domain (Cubas et al., 1999; Aggarwal et al., 2010). While phylogenetic reconstructions are presently unable to resolve which of the two classes evolved first, they reveal that class I genes are less divergent from each other than class II genes. Indeed, two subfamilies of class II genes have been defined. The CIN subfamily, named after the snapdragon TCP gene *CINCINNATA* (*CIN*) (Nath et al., 2003), is present in all land plants. By contrast, the CYC/TB1 subfamily is found only in angiosperms, suggesting that this subfamily may have evolved from the CIN subfamily within class II (González-Grandío and Cubas, 2016; Liu et al., 2019).

It appears that TCP transcription factors bind to DNA as homo or heterodimers, mainly with members of the same class (Kosugi and Ohashi, 2002; Costa et al., 2005; Aggarwal et al., 2010; Danisman et al., 2013). TCP proteins recognize 6-10 bp motifs containing a GGNCC or GGNNCC core sequence (reviewed in González-Grandío and Cubas, 2016). More precisely, class I proteins bind to the consensus sequence GTGGGNCC and class II proteins to GTGGNCCC (Kosugi and Ohashi, 2002; Uberti-Manassero et al., 2013). Binding specificity appears to be determined mainly by specific amino acids in the basic region of the TCP domain, i.e. Gly at position 11 in class I and Asp at position 15 in class II (Kosugi and Ohashi, 1997; Aggarwal et al., 2010; Viola et al., 2012; González-Grandío and Cubas, 2016). A leucine-rich motif present in the second helix of the TCP domain could promote protein-protein interactions (Li, 2015). The arginine-rich R domain found in several class II proteins is predicted to form a coiled coil that could also promote protein-protein interactions (Cubas et al., 1999).

TCP transcription factors have been found to play a role in a large spectrum of developmental processes, such as floral symmetry, flowering time, leaf development and senescence, shoot branching, circadian clock and plant defense responses (Luo et al., 1996; Nath et al., 2003; Palatnik et al., 2003; Takeda et al., 2003; Crawford et al., 2004; Ori et al., 2007; Kim et al., 2008; Yuan et al., 2009; Giraud et al., 2010; Koyama et al., 2011; Hao et al., 2012; Aguilar-Martínez and Sinha, 2013; Juntheikki-Palovaara et al., 2014; Huang and Irish, 2015; Lucero et al., 2015; Koyama et al., 2017; Challa et al., 2018; Vadde et al., 2018; Challa et al., 2019; Li et al., 2019; Camoirano et al., 2020; Gastaldi et al., 2020; Zhang et al., 2020). In addition to their role in the transcriptional control of cell cycle genes (Kosugi and Ohashi, 1997; Gaudin et al., 2000; Nath et al., 2003), TCP proteins act in several regulatory networks including other transcription factors, miRNA-controlled pathways, and hormone biosynthesis and signaling pathways (Danisman et al., 2012; Das Gupta et al., 2014; Schommer et al., 2014; Nicolas and Cubas, 2016a; Nicolas and Cubas, 2016b; van Es et al., 2018; Zhou et al., 2018; Challa et al., 2019; Gastaldi et al., 2020). An increasing number of studies have revealed that the initial dichotomy of growth activator *vs* repressor role of class I *vs* class II genes is in fact much more complex, with both classes displaying antagonistic as well as synergistic actions in various growth processes (Nicolas and Cubas, 2016b; van Es et al., 2019).

Functional studies require knowledge of the complete repertoire of proteins in a multigene family such as the TCP family to track possible redundancy and investigate the specificity of action of its members. It is also important to understand the evolutionary relationship of gene family members and the large scale history of the gene family in question. Several complete genomes have been screened for the full repertoire of TCP genes, especially in core eudicots and monocots (e.g. Parapunova et al., 2014; Francis et al., 2016; Zheng et al., 2018; Huo et al., 2019; Jiu et al., 2019; Leng et al., 2019; Li et al., 2021; Zhao et al., 2021), but data is scarce in early diverging eudicots (Citerne et al., 2013; Liu et al., 2019). In this paper, we set out to characterize the gene repertoire and evolutionary history of the TCP family in the order Ranunculales, the sister group to all other eudicots. We took advantage of the available floral transcriptome of the Ranunculaceae species *Nigella damascena* L. to characterize expressed TCP genes, and we combined phylogenetic reconstruction with the presence and arrangement of conserved amino acid motifs as additional phylogenetic markers to (i) assess the orthology relationship of *N. damascena* genes with genes from the fully sequenced genome of another Ranunculaceae species *Aquilegia coerulea*, and (ii) reconstruct the evolutionary history of both class I and class II transcription factor genes in selected angiosperm species with fully sequenced genomes, as well as specifically within Ranunculales. Our results suggest that the fourteen transcripts characterized in *N. damascena* are the orthologs of the fourteen

TCP genes found in the fully sequenced genome of *A. coerulea*, and that the evolutionary history of TCP genes differs between Ranunculales and core eudicots, with evidence of independent large scale (i.e. concerning high rank taxa) gene duplications. Finally, we characterized TCP gene expression profiles in aerial tissues of *N. damascena* and discuss the results in the light of repertoire complexity and developmental processes where TCP genes are known to play a role in model eudicot species.

Material and methods

TCP homologs in *Nigella damascena*

We mined the annotated floral reference transcriptome of *N. damascena* for TCP proteins, identified from homology with the TCP proteins in the inferred proteomes of *Arabidopsis thaliana* and/or *Aquilegia coerulea* as described in Deveaux et al. (2021). Seventeen contigs encoding peptides with homology with 12 *Arabidopsis* TCP proteins and/or 14 *Aquilegia* TCP proteins were found.

Primers were designed to specifically amplify these sequences from genomic DNA in order to validate the transcriptome assembly and detect the presence of introns (Supplementary Table 1). When necessary, semi-nested PCRs were done to amplify the 3' end of the gene using an 18-base oligodT anchored with an A, G or C and two nested primers in the known 5' part of the candidate gene (Supplementary Table 1). Amplification products were sequenced (Eurofin Genomics). The initial contig sequence was aligned with the amplified sequence and corrected if necessary. The comparison of the two sequences allowed us to detect the presence of introns (Table 1).

A genome walking strategy was used to obtain the full ORFs of TCP genes known from contigs with incomplete 5' end coding sequences (*NdTCP22* and *NdCYL1*) using a protocol adapted from Balzergue et al. (2001). To summarize, 300 ng of genomic DNA were simultaneously digested by the PvII, EcoRI or DraI restriction enzyme and ligated to the asymmetric adapters in the T4 DNA ligase buffer (New England Biolabs). Specific nested primers were designed in the known 5' region of the gene fragments and combined with nested adapter-specific primers. Amplification products were sequenced (Eurofin Genomics) and aligned to produce the consensus sequence. Gene-specific primers are listed in Supplementary Table 1. Genomic sequences were deposited in Genbank (accession numbers OP493852-865).

Full repertoire of TCP proteins

Full repertoires of TCP genes were obtained from the annotated complete genomes of *Arabidopsis thaliana*, *Vitis*

TABLE 1 Characteristics of TCP sequences in *Nigella damascena*, and their homologs in *Aquilegia coerulea*.

Contig name	*Nigella* gene name	Contig length (bp)	cds length (bp)	5'/3' UTR minimum length (bp)	Intron (bp)	*Aquilegia* homolog	*Aquilegia* gene name
class I							
RN005256	*NdTCP7*	1607	777	95/735	–	Aqcoe3G008000	*AqTCP7*
RN006358	*NdTCP9-1*	1291	1098	157/17	–	Aqcoe7G051800	*AqTCP9-1*
RN065983	*NdTCP9-2*	1316	948	154/214	–	Aqcoe5G422600	*AqTCP9-2*
RN071097	NdTCP11	922	660	174/69	–	Aqcoe1G137200	*AqTCP11*
RN048267	*NdTCP15-1*	1665	1131	331/203	–	Aqcoe3G335300	*AqTCP15-1*
RN067927	*NdTCP15-2*	1447	1149	116/182	–	Aqcoe3G081500	*AqTCP15-2*
RN010851/2	*NdTCP20-1*	1497/1411	888	74/535	86 (3' UTR)	Aqcoe5G347900	*AqTCP20-1*
RN015628/29	*NdTCP20-2*	1644/1748	921	239/484	104 (3' UTR)	Aqcoe3G164300	*AqTCP20-2*
RN054028	*NdTCP22*	1611	1533 [a]	nd/276	96 (3' UTR)	Aqcoe6G015800	*AqTCP22*
class II							
RN066863/RN057437	*NdCYL1*	333 477	1122 (1050) [a,b]	nd/110	–	Aqcoe3G048600	*AqCYL1*
RN004309	*NdCYL2*	1314	1077	160/77	–	Aqcoe3G395500	*AqCYL2*
RN009083	*NdTCP2*	2766	1386	902/478	? (3'UTR)	Aqcoe4g007100	*AqTCP2*
RN002982	*NdTCP4*	2713	1191	1082/440	87 (3' UTR)	Aqcoe1g240000	*AqTCP4*
RN003972	*NdTCP5*	1819	1176	356/287	378 (5'UTR)	Aqcoe3g370100	*AqTCP5*

[a] 5' end sequence obtained by chromosome walking; [b] two possible ATG codons; nd, not determined.

vinifera, *Nelumbo nucifera*, *Aquilegia coerulea*, *Oryza sativa* and *Amborella trichopoda*. For *Vitis* and *Nelumbo*, we combined data retrieved from PlantTFDB (v5.0, http://planttfdb.gao-lab.org/) and BLASTp analyses using *Arabidopsis* proteins as queries in the non-redundant database of Genbank (https://www.ncbi.nlm.nih.gov/genbank/). For *Oryza sativa* TCP transcription factor sequences were obtained from PlantTFDB and confirmed by the PFAM 03634 identifier at http://rice.plantbiology.msu.edu. For *Aquilegia coerulea*, we compared data from Plant TFDB and annotations in Phytozome (https://phytozome.jgi.doe.gov/). For *Amborella trichopoda*, 15 sequences were retrieved from Plant TFDB and Phytozome (Supplementary Table 2).

Floral transcriptomes from four species of Ranunculaceae

Aconitum napellus and *Clematis stans* were grown at the Botanical garden of the French National Museum of Natural History, Paris, France. *Ficaria verna* and *Helleborus orientalis* were grown at the Jardin botanique de Launay, Orsay, France. Floral buds of various sizes covering the entire sequence of floral development for each species were harvested and immediately frozen in liquid nitrogen. Total RNA was extracted using the RNeasy Plant Mini Kit (Qiagen) with the additional DNAse I step according to the manufacturer's instructions. Total RNA from each sample (one per species) was checked for integrity on an RNA_Nano chip using an Agilent 2100 bioanalyzer (Agilent Technologies, Waldbroon, Germany). Libraries were constructed with the TruSeq stranded mRNA library Prep kit (Illumina®, California, U.S.A.). They were paired-end (PE) sequenced with a read length of 100 bp using an Illumina HiSeq2000 at the Genoscope Laboratory (Evry, France). Lane distribution and barcoding gave approximately 25 to 35 million PE reads per sample. For each sample, raw data (fastq) were trimmed with Trimmomatic (Bolger et al., 2014) with a Phred Quality Score (Qscore) >20 and read lengths >30 bases. Ribosome sequences were removed with the sortMeRNA tool (Kopylova et al., 2012).

For each species, transcriptome assembly was made using Trinity (version 2.8.4, Grabherr et al., 2011) with default parameters and a kmer size of 32. Contigs that were smaller than 200 bases were removed. iAssembler (version 1.3, Zheng et al., 2011) was then used for scaffolding contigs and reducing redundancy, with –c option for strand specific assembly and 97% identity for sequence clustering, generating 53,205 (*A. napellus*), 35,842 (*H. orientalis*), 36,900 (*F. verna*) and 36,536 (*C. stans*) contigs (N50 respectively 1,147 bp, 1,529 bp, 1,434 bp and 1,330 bp). Proteomes were then generated using Transdecoder (version 5.3, Haas et al., 2013) with best orfs parameter, generating 31,831 (*A. napellus*), 25,647 (*H. orientalis*), 23,056 (*F. verna*) and 22,382 (*C. stans*) proteins. Data are available at https://doi.org/10.57745/2G1VCP.

TCP sequences in Ranunculales

TCP sequences from Ranunculales were obtained from three sources. First, the 24 *Arabidopsis* TCP proteins were used as query for mining Genbank by tBLASTn, restricting the search to the seven Ranunculales families. Second, the 14 *Aquilegia coerulea* sequences were used as query for mining the Onekp database (https://db.cngb.org/onekp/) using tBLASTn, and sequences from Ranunculales species were selected. Third, we mined the floral transcriptomes of *Helleborus orientalis*, *Ficaria verna*, *Aconitum napellus* and *Clematis stans* (see above). The proteomes inferred from each of these transcriptomes were analyzed alongside the proteomes of *A. coerulea* and *N. damascena* using Orthofinder (Emms and Kelly, 2015; Emms and Kelly, 2019) with default options. Orthogroups that included at least one TCP protein from *A. coerulea* and/or *N. damascena* were kept, and transcripts of the homologous TCP proteins in *H. orientalis*, *F. verna*, *A. napellus* and *C. stans* were included in subsequent analyses.

The TCP sequence datasets obtained using the different strategies were then pruned to keep only unique amino acid sequences. In Papaveraceae, although we found sequences from several *Papaver* species in the databases, we retained only those of *P. somniferum*. The final dataset comprised in total 178 class II sequences and 145 class I sequences (Supplementary Table 3A, B). It is worth underlining that in most cases, these are expressed sequences and that the origin of multiple transcripts in a species is unknown (allelism, paralogy or alternative splicing).

Phylogenetic analyses

Protein sequences were aligned using the online version of MAFFT (version 7) using the L-INS-i method (https://mafft.cbrc.jp/alignment/server/). Alignments were inspected and manually adjusted using BioEdit v.7.0.5 (Hall, 1999). The phylogeny of the full repertoire of TCP genes from seven angiosperm species (listed above) was reconstructed using protein sequences because of codon bias in the *Oryza sativa* nucleotide sequences. Phylogenetic analyses of TCP genes in Ranunculales were conducted on codon-based nucleotide alignments obtained from protein alignments using TranslatorX (http://translatorx.co.uk/, Abascal et al., 2010). Regions where primary homology could not be confidently established were manually removed from the alignments. Alignments were deposited on dryad (doi:10.5061/dryad.zcrjdfngw).

Phylogenetic analyses were done using PhymL (http://www.atgc-montpellier.fr/phyml/) with the automatic model selection by SMS option (Lefort et al., 2017); branch support was determined by the aLRT SH-like method (Guindon et al., 2010).

Search for protein motifs

MEME in the MEME suite v5.3.3 (https://meme-suite.org) was used to identify conserved amino acid motifs in TCP class I and class II sequences. Default options were used except for the motif maximum width, which was fixed at 60 and 55 for class II and class I, respectively, and the number of motifs, which was fixed at 10 for both classes. Motifs are named as follows: Mx=motif x; I/II (superscript)=TCP class; R/nothing (subscript)=Ranunculales/full repertoire analysis. The presence and arrangement of conserved amino acid motifs along the whole length of the proteins were used to add support to the different groups identified in the phylogeny.

TCP expression patterns in *N. damascena*

Seeds derived from six generations of selfing of a heterozygous plant from a commercial seed lot (Royal Fleur) were sown in a growth chamber under controlled conditions (18h day at 25°C, 6h night at 16°C). Plants were arranged in three replicates of 5 individuals. When the terminal bud was 12-13.5 mm in diameter, plants were harvested as follows: bracts, sepals, petals, stamens and carpels were dissected from the terminal flower, and the second lower bud (7-8 mm diameter), stem internodes and mature cauline leaves were collected separately (Supplementary Figure 5). All tissues were frozen in liquid nitrogen and stored at -80°C until RNA extraction.

For each organ sample and replicate, total RNA was extracted using the RNeasy Plant Mini Kit (Qiagen) with the additional DNAse I step according to the manufacturer's instructions. An additional DNAse step was done before single stranded cDNAs were produced using SuperScriptII reverse transcriptase (Invitrogen) and a polyT primer. DNA contamination was excluded by performing no-RT negative controls using *ACTIN* specific primers (Supplementary Table 1). Each gene was amplified with specific primers, a specific annealing temperature and a specific number of cycles (Supplementary Table 4). *ACTIN* was used as a loading reference for comparison among samples.

Results

Characterization of TCP transcription factors in the floral transcriptome of *Nigella damascena*

Sixteen contigs encoding peptides with homology with 12 *Arabidopsis thaliana* and 14 *Aquilegia coerulea* TCP proteins were found in the annotated *N. damascena* floral transcriptome (Deveaux et al., 2021). An additional contig encoding a peptide that was only homologous to an *A. coerulea* TCP protein was also identified.

Genomic sequences corresponding to the *N. damascena* contigs were amplified to check the transcriptome assembly and determine the presence of introns. *N. damascena* sequences were then aligned and compared with their homologs in the *A. coerulea* genome (Table 1). Seven validated contigs (renamed *NdTCP7, NdTCP9-1, NdTCP9-2, NdTCP11, NdTCP15-1, NdTCP15-2* and *NdCYL2*) had complete coding sequences, 5' and 3' UTR of variable lengths and an absence of introns, like in their homologs in *A. coerulea*. The *NdTCP22* sequence was interrupted by an intron in the 3' UTR, like its closest homolog in *A. coerulea* (Aqcoe6G015800, renamed as *AqTCP22*). Contig pairs (*NdTCP20-1/NdTCP20-2*) were homologous to Aqcoe5G347900 and Aqcoe3G164300, respectively, both of which were annotated as TCP20-like in Phytozome (*AqTCP20-1/AqTCP20-2*). Gene annotation revealed the presence of an intron in the 3'UTR of these genes in *A. coerulea*. In *N. damascena*, the members of each pair differed by an indel in the 3' UTR, corresponding to alternative splicing of the intron. *NdTCP2* and *NdTCP4* had long 5' UTRs (902 bp and 1,082 bp, respectively) and complete coding sequences. However, the 3' UTR of *NdTCP2* could not be completely verified, and this may be due to the presence of a large intron, which is found in its closest homolog in *A. coerulea* (Aqcoe4g007100, *AqTCP2*). *NdTCP5* had both 5' and 3'UTRs, with an intron detected in the 5'UTR, like in *A. coerulea* Aqcoe3g370100 (*AqTCP5*). The sequence for *NdCYL1* was re-assembled from two contigs that aligned with the 5' and 3' parts of Aqcoe3g048600 (*AqCYL1*), corresponding to one Ranunculaceae CYC-like homolog (RanaCYL1, Jabbour et al., 2014). The sequence was extended upstream by genome walking to obtain the complete coding sequence. No intron was found, unlike *AqCYL1* that has three introns interrupting the coding sequence. In total, we validated and fully sequenced 14 transcribed genes encoding 14 TCP proteins in *N. damascena* (Table 1).

Relationships of *N. damascena* TCP proteins in the context of the evolutionary history of TCP proteins in angiosperms

To assess the orthology of *N. damascena* sequences with TCP genes from other angiosperms, we reconstructed the phylogeny of TCP proteins of selected angiosperm species with full genomes. The full inferred proteome of *Arabidopsis* comprises 24 TCP transcription factors, of which 13 belong to class I and 11 to class II (Cubas et al., 1999; Martín-Trillo & Cubas, 2010). In rice (*Oryza sativa* ssp *japonica*), we found 23 transcription factors corresponding to 21 different proteins in PlantTFDB, of which 11 belong to class II and 10 to class I. We found 11 *Amborella*, 7 *Nelumbo*, 9 *Vitis*, and 5 *Aquilegia* TCP proteins belonging to class II, and 9 *Aquilegia*, 9 *Vitis*, 9 *Nelumbo* and 6 *Amborella* proteins belonging to class I.

Phylogenetic analysis of class I TCP proteins, based on 69 amino acid positions, revealed high support (a-LRT≥0.80) for several clades (Figure 1). One clade (a-LRT 0.99) comprised a paraphyletic group that we called TCP22-like, from the name of one of its members in *Arabidopsis*, and a monophyletic group (a-LRT 1.0), TCP7-like. Another clade (a-LRT 0.95) comprised two well supported sub-clades, TCP11-like (a-LRT 0.85) and TCP9-like (a-LRT 0.97) and a paraphyletic group (including Nnu003157), TCP20-like. Two *Arabidopsis* genes in this group, AtTCP6 and AtTCP16, were highly divergent from all other sequences and possibly grouped together because of long branch attraction. A last set of sequences, which share motif $M^{I}3$ upstream of the TCP domain and for the most part motifs $M^{I}5$ and $M^{I}6$, was defined as TCP15-like (Supplementary Table 5A). While TCP11-like sequences were not characterized by any specific motif other than $M^{I}1$ (the TCP domain) and $M^{I}2$, the other clades had additional specific motifs (e.g. $M^{I}10$ in TCP9-like, $M^{I}7$ in TCP20-like) or specific combinations and order of motifs (Supplementary Table 5A). The $M^{I}2$ motif, which has been identified as a characteristic motif of class I proteins (Aggarwal et al., 2010), flanks the TCP domain and is lacking only in the *Arabidopsis* proteins AtTCP6, AtTCP11 and AtTCP16 (Supplementary Table 5A). Each of the six groups we have defined comprised one protein sequence from *Amborella* and at least one protein sequence from each of the other species, with the exception of *Nelumbo* (which does not have a TCP22-like ortholog), supporting the hypothesis that the same number of class I paralogs existed in the common ancestor of angiosperms.

The phylogenic analysis of class II proteins (61 amino acid positions) recovered the two previously characterized CYC/TB1 and CIN sub-classes (Figure 2). At least one protein sequence from each species except *Amborella* was found in the CYC/TB1 sub-class. Within this clade, some branches were well-supported, for example the two paralogous lineages previously described in Ranunculaceae (AqCYL1/NdCYL1 and AqCYL2/NdCYL2, respectively, Citerne et al., 2013; Jabbour et al., 2014), two pairs of *Arabidopsis* and *Vitis* proteins belonging to the previously described CYC2 (AtTCP1 and Vv36449) and CYC3 (AtTCP12 and Vv08234) clades (Howarth and Donoghue, 2006), and a small clade formed by AtTCP18 and three rice proteins. All proteins in this clade except Os08g33530 and Os09g24480 had an R domain ($M^{II}2$ motif, Supplementary Table 5B). Within the CIN sub-class, the CIN1 clade was weakly supported (a-LRT 0.74) while the CIN2 clade was well supported (a-LRT 0.97). The two sub-classes each have a specific motif upstream of the TCP domain ($M^{II}1$), i.e. $M^{II}4$ for CIN1 and $M^{II}6$ for CIN2 (Supplementary Table 5B). The CIN1 clade was poorly resolved, and comprised one rice sequence, three *Arabidopsis* (AtTCP3, AtTCP4 and AtTCP10) and three *Vitis* sequences, one sequence from each early diverging eudicot species and seven *Amborella* sequences, which were more closely related to each other than to sequences of the other species. There are two well supported clades, which we called CIN2a (a-LRT 0.87) and CIN2b (a-LRT 0.94), within the CIN2 clade, each containing a single *Amborella* sequence. CIN2b sequences differed from CIN2a sequences by the presence of several amino acid motifs (e.g. $M^{II}2$ (the R domain), $M^{II}9$ and to a lesser extent $M^{II}7$). The $M^{II}9$ motif is found in the closely related *Oryza* Os03g57190 and Os07g05720 ($M^{II}2$ is found in the latter), suggesting these sequences are closer to CIN2b; by contrast, the triplet including Os12g02090 has a low number of characteristic motifs so that its status remains uncertain (Supplementary Table 5B). As for early diverging eudicots, each CIN2 clade contained two paralogs from *Nelumbo* and one sequence from the two Ranunculaceae species.

In every clade described above, the phylogeny generally supported the orthology between one *N. damascena* sequence and one *A. coerulea* sequence, suggesting we obtained the full repertoire of TCP proteins from our *N. damascena* floral transcriptome.

Evolutionary history of TCP transcription factors in Ranunculales

Phylogenetic analysis of class I TCP genes

145 sequences belonging to 21 genera from five families out of the seven that are recognized in Ranunculales were retrieved from databases as well as from our own transcriptomic data. The phylogenetic analysis was based on an alignment of 207 nucleotide sites that included the TCP domain (Figure 3). The six groups of class I TCP proteins described above were recovered in the analysis of sequences from Ranunculales, each group containing sequences from species belonging to at least two different families. These groups were supported by specific combinations and order of protein motifs (Figure 3, Supplementary Figure 2). Most of these motifs were also detected in the complete repertoire analysis (see Supplementary Table 5A for correspondence of motifs). As expected, the $M^{I}_{R}1$ (TCP domain) and $M^{I}_{R}2$ (characteristic of class I TCP proteins) motifs were found in all sequences. The $M^{I}_{R}3$ motif was found upstream of the TCP domain in the RanTCP15 and RanTCP20 clades (a-LRT 0.99 and 0.81, respectively), whereas it was found downstream of the TCP domain in the RanTCP9 clade (a-LRT 0.89). The $M^{I}_{R}10$ motif was present in most RanTCP9 sequences, while the $M^{I}_{R}6$ motif was characteristic of the RanTCP20 clade. The RanTCP7 clade (a-LRT 0.99) was not characterized by any specific motif, but rather by the combination of five motifs in a specific order ($M^{I}_{R}7$, $M^{I}_{R}8$, $M^{I}_{R}4$, $M^{I}_{R}9$ and $M^{I}_{R}5$). A poorly supported group (RanTCP11, a-LRT 0.61) with long branches aggregated sequences without specific motifs except the characteristic $M^{I}_{R}1$ and $M^{I}_{R}2$ motifs. The sixth clade (RanTCP22) was well supported (a-LRT 0.93) and included sequences characterized by a low number of conserved amino acid motifs in addition to $M^{I}_{R}1$ and $M^{I}_{R}2$. Additional phylogenetic analyses of

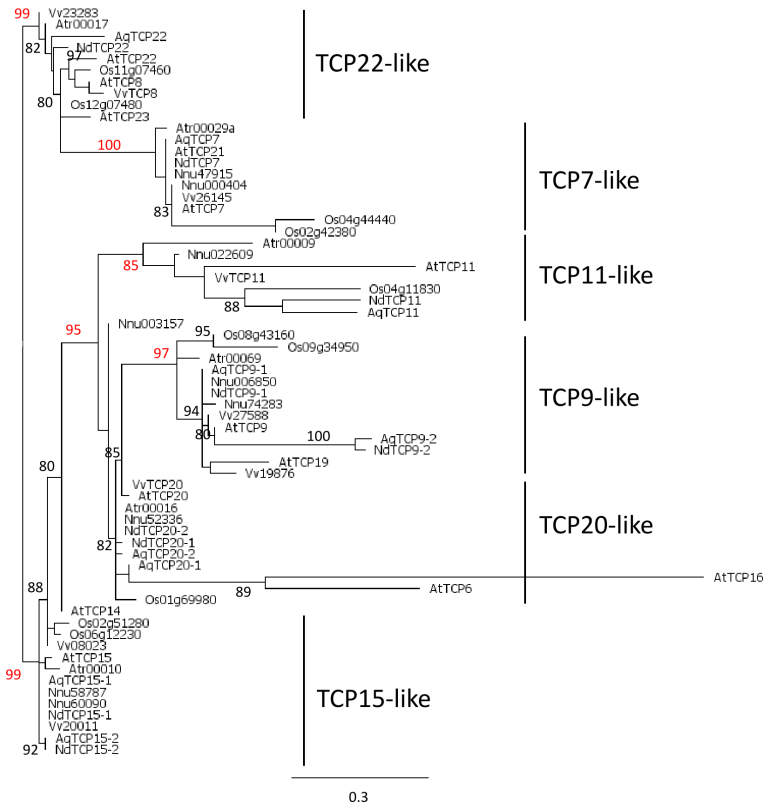

FIGURE 1
Phylogeny of class I TCP proteins in the complete inferred proteomes of *Amborella trichopoda* (Atr), *Arabidopsis thaliana* (At), *Vitis vinifera* (Vv), *Nelumbo nucifera* (Nnu), *Aquilegia coerulea* (Aq), *Oryza sativa* (Os), and the nine proteins deduced from the floral trancriptome of *Nigella damascena* (Nd). Maximum likelihood reconstruction was done with PhyML based on the alignment of 69 amino acid positions that included the TCP domain. Branch support values above 80% are indicated (a-LRT x100) with those discussed in the text in red.

each of the six groups rooted with the closest homologous sequences from *Nelumbo* (or *Vitis* for RanTCP22), showed that sequence relationships were generally congruent with species relationships (Supplementary Figures 1A-F). There was a duplication in the RanTCP20 clade in Ranunculaceae but the timing of this duplication in the evolutionary history of Ranunculales could not be ascertained due to insufficient sampling of the other families. A duplication was observed in the RanTCP15 clade, which could have taken place after the divergence of Papaveraceae. In the RanTCP9 clade, a duplication after the divergence of Eupteleaceae can be hypothesized (Supplementary Figures 1A-F).

Phylogenetic analysis of class II TCP genes

We compiled 178 sequences of class II TCP genes from 52 genera representing all seven families within Ranunculales. Similarly to class I, sequences from Ranunculaceae and Papaveraceae were over-represented. Phylogenetic reconstruction was based on a 199 nucleotide site alignment that included the TCP domain and its flanking regions, available in 173 out of the 178 sequences (Figure 4). The two subfamilies CYC/TB1 and CIN were well supported. Within the CIN clade, the three subfamilies described above were recovered, called here RanaCIL1, RanaCIL2a and RanaCIL2b. A characteristic difference between RanaCIL1 and RanaCIL2 was the presence of an alternative motif immediately upstream of the TCP domain ($M_R^{II}1$), i.e. $M_R^{II}7$ for RanaCIL1 and $M_R^{II}10$ for RanaCIL2 (Figure 4; Supplementary Figure 4, see also Supplementary Table 5B for correspondence of motifs with the full repertoire analysis). RanaCYL sequences were characterized by having an R domain ($M_R^{II}2$) and an ECE motif ($M_R^{II}3$). Two sequences in the RanaCIL2a clade had an R domain in addition to the TCP domain and the $M_R^{II}10$ motif. RanaCIL1 sequences had the largest number of conserved protein motifs (Figure 4). Detailed phylogenetic analyses of the RanaCIL clade showed that sequence relationships were congruent with species relationships, with some species specific gene duplications (Supplementary Figures 3A-C). Within the RanaCYL clade, a gene duplication may have taken place after the divergence of Eupteleaceae, which has two paralogs that are probably the result of a lineage specific duplication (Supplementary Figures 3A-D).

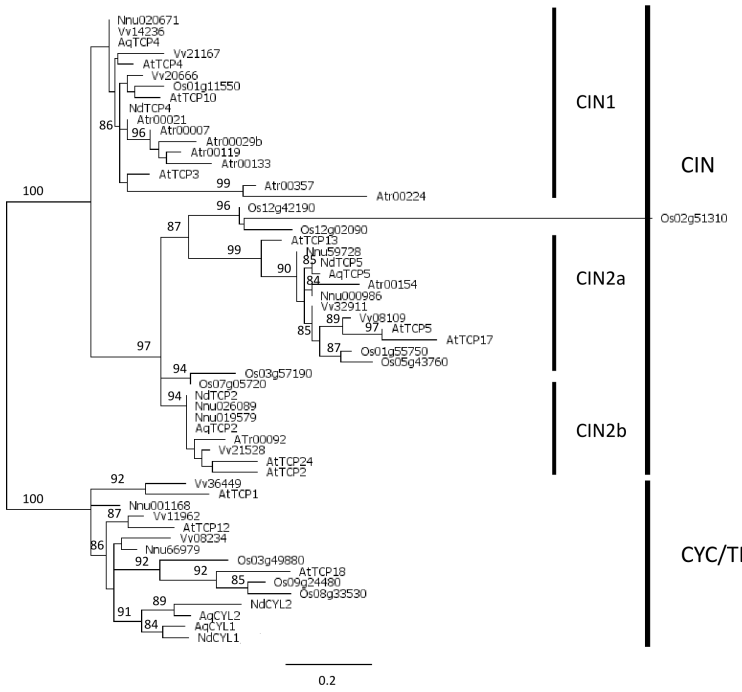

FIGURE 2
Phylogeny of class II TCP proteins in the complete inferred proteomes of *Amborella trichopoda* (Atr), *Arabidopsis thaliana* (At), *Vitis vinifera* (Vv), *Nelumbo nucifera* (Nnu), *Aquilegia coerulea* (Aq), *Oryza sativa* (Os), and the five proteins deduced from the floral trancriptome of *Nigella damascena* (Nd). Maximum likelihood reconstruction was done with PhyML and based on the alignment of 61 amino acid positions that included the TCP domain. Branch support values above 80% are indicated (a-LRT x100).

Expression patterns of TCP genes in aerial tissues of *Nigella damascena*

Semi-quantitative RT-PCR was used to obtain an overview of the expression profile of the 14 *N. damascena* TCP genes in aerial tissues of plants close to blooming (Supplementary Figure 5).

Results were generally consistent among the three biological replicates (Supplementary Figure 6). All TCP genes were expressed in most to all organs, with the exception of the two *NdCYLs* (Figure 5). Indeed, in the floral organs, *NdCYL2* was more strongly expressed in petals and stamens whereas *NdCYL1* was relatively more expressed in the gynoecium. The three *NdCIL* genes (*NdTCP2*, *NdTCP4* and *NdTCP5*) had a more even expression pattern among organs, with low expression in bracts and leaves for *NdTCP2*. *NdTCP2* and *NdTCP5* were comparatively less expressed in stamens than in other dissected floral organs. Similarly, the expression patterns of class I genes were generally similar across all organs. The expression of *NdTCP7* and *NdTCP11* in bracts and leaves was weak compared with the other organs. Among dissected floral organs, *NdTCP9-2* appeared less expressed in the reproductive organs than in the perianth organs, and expression of *NdTCP15-2* was highest in the gynoecium (Figure 5; Supplementary Figure 6).

Discussion

The Ranunculales appears to be the first order to have diverged within the eudicots. It stands out by its remarkable morphological diversity in both vegetative and reproductive traits. Its phylogenetic position as sister to all other eudicots makes it an important group for investigating the origin of morphological diversity in a comparative framework, in particular compared with other major angiosperm groups such as the successful monocots and core eudicots (Becker, 2016; Damerval and Becker, 2017; Zhao et al., 2018; Pabón-Mora et al., 2020; Martínez-Gómez et al., 2021). TCP transcription factor genes have been shown to be major actors of plant development since the initial characterization of the family (Cubas et al., 1999). While this gene family has been characterized in many core eudicot and monocot species, no systematic investigation has been conducted in early diverging eudicots and Ranunculales in particular. A comprehensive survey of TCP genes in Ranunculales will help clarify the evolutionary history of this gene family and understand the functional evolution of TCP genes in angiosperms as a whole. The recent availability of genomic resources, i.e. the full genome of *Aquilegia coerulea* (Filiault et al., 2018) and our floral transcriptome of *Nigella damascena* (Deveaux et al., 2021), allowed us to characterize

10.3389/fpls.2022.1055196

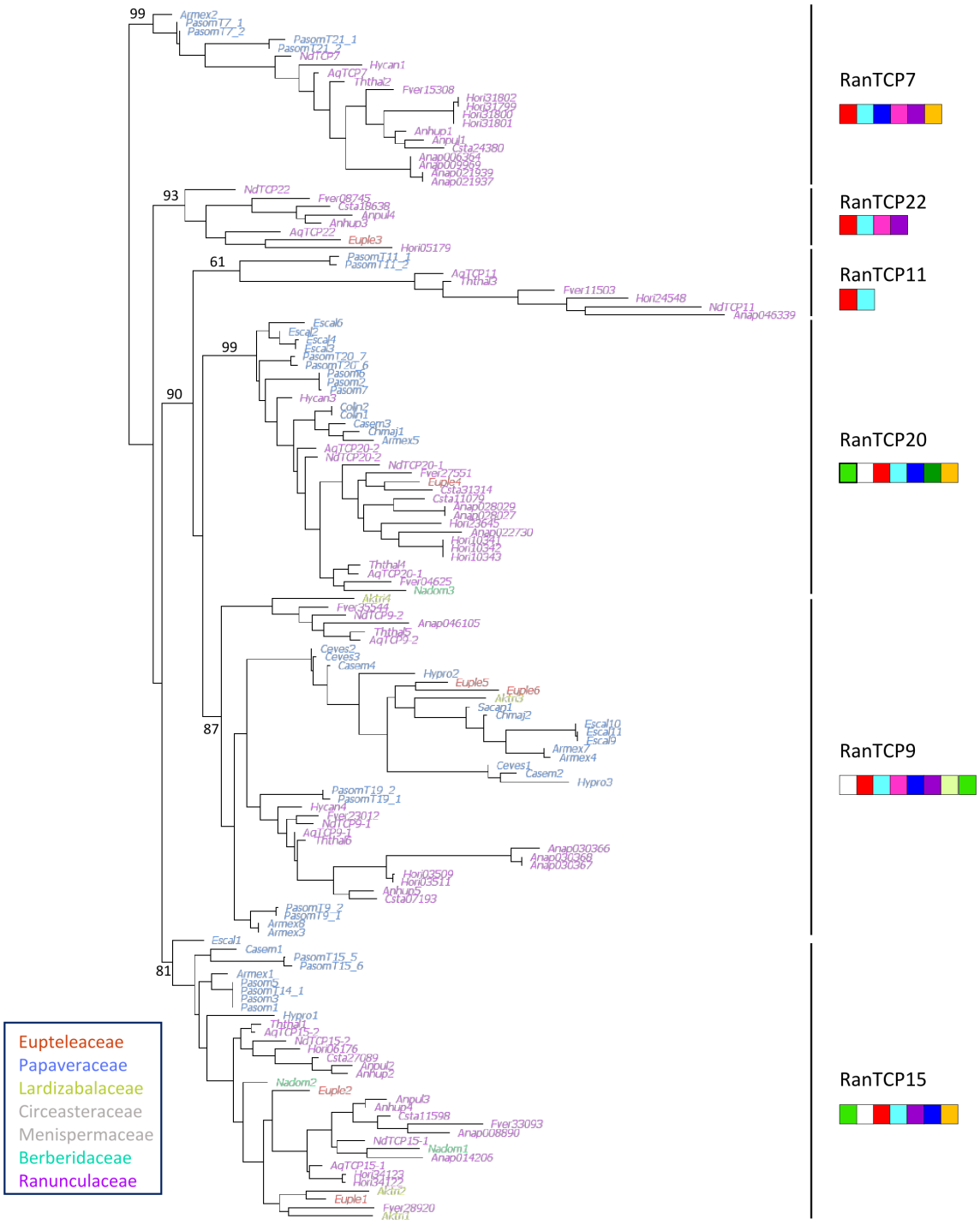

FIGURE 3
Phylogeny of 145 class I TCP coding nucleotide sequences from Ranunculales. Ranunculales families were color-coded as indicated (no sequences were available for Circeasteraceae and Menispermaceae, in grey). Support values (a-LRT x100) are given for the main branches, corresponding to the six groups identified in Figure 1. The specific combinations of amino acid motifs that characterize the six groups are drawn under each group name. A motif is represented if it is found in at least half of the sequences in that group. Red: $M^{I}_{R}1$; light blue: $M^{I}_{R}2$; mid green: $M^{I}_{R}3$; violet: $M^{I}_{R}4$; yellow: $M^{I}_{R}5$; dark green: $M^{I}_{R}6$; dark blue: $M^{I}_{R}7$; pink: $M^{I}_{R}8$; white: $M^{I}_{R}9$; yellow green: $M^{I}_{R}10$ (motifs defined in Supplementary Figure 2).

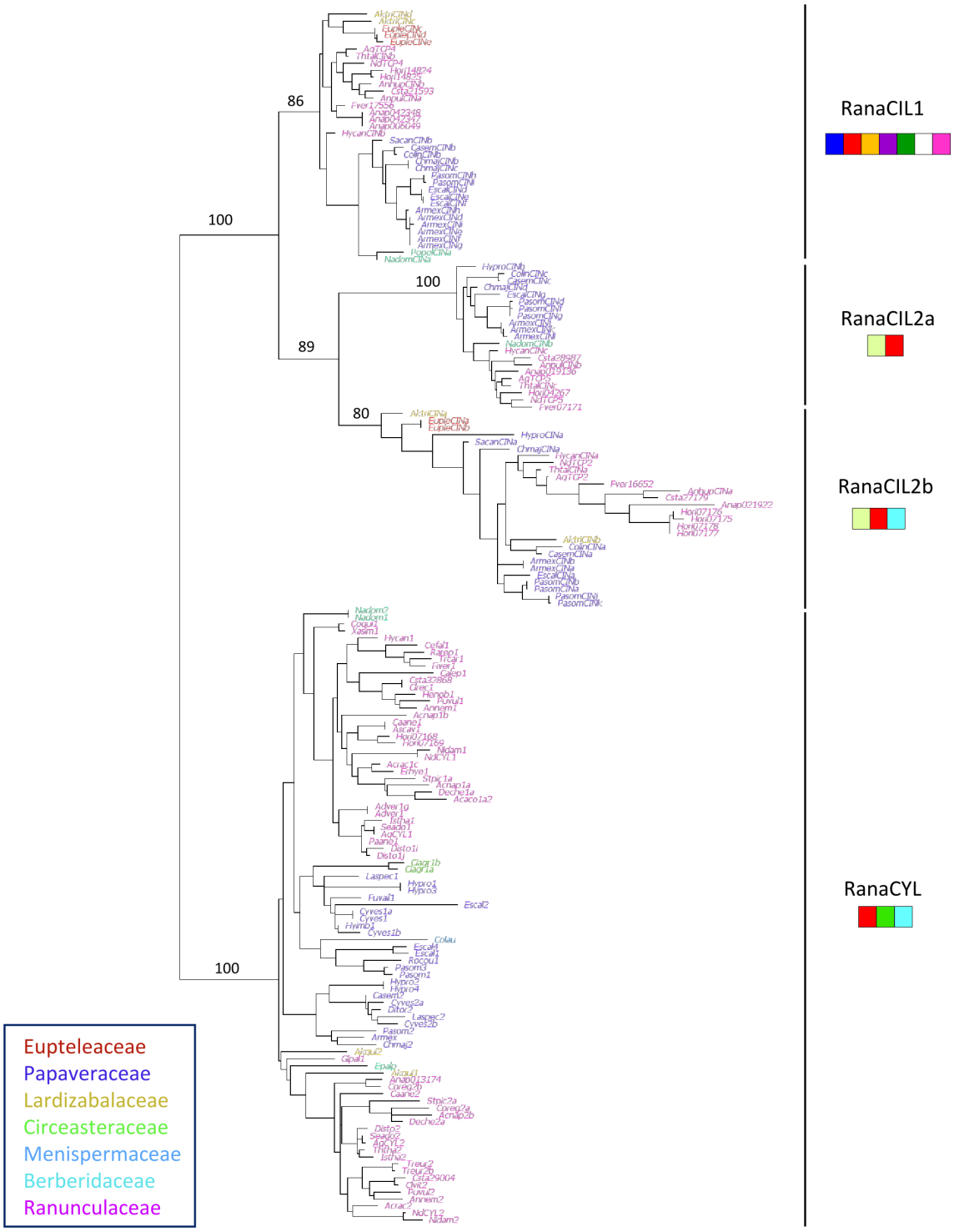

FIGURE 4
Phylogeny of 173 class II TCP coding sequences from Ranunculales. Ranunculales families were color-coded as indicated. Support values (a-LRT x100) are given for the main branches, corresponding to clades identified in Figure 2. The specific combinations of amino acid motifs that characterize the four clades are drawn under each clade name. A motif is represented if it is found in more than half of the sequences in that clade. Red: $M_R^{II}1$; light blue: $M_R^{II}2$; mid green: $M_R^{II}3$; violet: $M_R^{II}4$; yellow: $M_R^{II}5$; dark green: $M_R^{II}6$; dark blue: $M_R^{II}7$; pink: $M_R^{II}8$; white: $M_R^{II}9$; yellow green: $M_R^{II}10$ (motifs defined in Supplementary Figure 4).

10.3389/fpls.2022.1055196

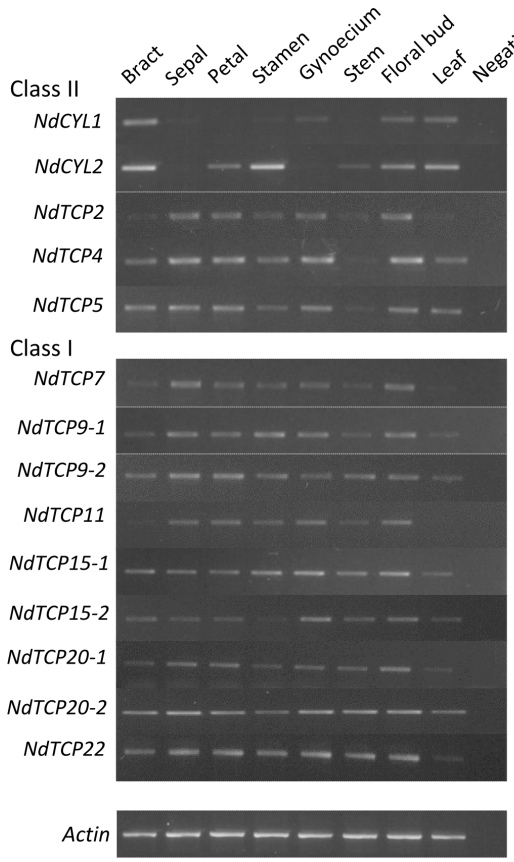

FIGURE 5
Expression patterns of all *Nigella damascena* TCP genes in eight aerial organs.

which could be the complete repertoire of both class I and class II TCP genes in *N. damascena*. Using phylogenetic reconstructions combined with analyses of conserved protein motifs, we propose a new evolutionary hypothesis for class I TCP transcription factors in angiosperms. Within the eudicot clade, we establish that the gene duplication history of the TCP family occurred independently in Ranunculales and core eudicots.

Accessing the full repertoire of TCP genes in a given species is an important step to assess the involvement of members of this family in developmental processes, as the analysis of individual genes may be blurred by redundancy (Danisman et al., 2013). Protein relatedness, as inferred from phylogenetic analyses, and similar spatio-temporal regulation are essential components of redundancy. We determine the expression patterns of all TCP genes in an early diverging eudicot species, *Nigella damascena*. We find that at the organ level, CIN and class I TCP genes have similar expression patterns, which could suggest redundant roles or involvement in the same pathways, as was found in some core eudicot species. By contrast, CYC/TB1 genes seem to have more differentiated expression domains.

Evolutionary history of class I TCP genes and independent duplications in Ranunculales and core eudicots

The complete repertoire of class I proteins amounted to 6 in *Amborella*, 13 in *Arabidopsis*, 10 in *Oryza* and 9 in *Vitis*, *Nelumbo*, *Aquilegia* and *Nigella*. Phylogenetic analysis showed that class I proteins are more conserved than class II proteins, as previously observed (Martín-Trillo and Cubas, 2010; Mondragón-Palomino and Trontin, 2011; Liu et al., 2019). Six groups of class I genes were identified in angiosperms on the phylogenetic tree, each of which contained a single sequence from *A. trichopoda*. The circumscription of these groups was confirmed by the specific association of conserved protein motifs. These results suggest that there were six paralogous copies of class I TCP genes in the common ancestor of angiosperms. Only one copy of TCP11-like was found in all species sampled. In the TCP22-like and TCP7-like groups, gene duplications were identified in *Oryza*, *Vitis* and *Arabidopsis*, but only one gene was found in Ranunculaceae. Duplications were also observed in all species in the TCP9-like, TCP20-like and TCP15-like groups, which were difficult to place reliably in the evolutionary history of class I genes because of low resolution (Figure 1). These six TCP groups were confirmed in the analysis of Ranunculales class I sequences, and provided a framework for more comprehensive analyses. The phylogenetic analyses of Ranunculales sequences in these groups rooted with sequences of a non-Ranunculales species support the occurrence of Ranunculales specific duplications, prior to the divergence of Ranunculaceae for TCP20-like, and possibly after the divergence of Eupteleaceae for TCP15-like and perhaps also for TCP9-like (Supplementary Figures 1D-F). These analyses suggest that although early diverging eudicots and core eudicots have the same number of class I paralogs [with the exception of *Arabidopsis*, which, unlike *Vitis*, has undergone additional whole genome duplications (Vision et al., 2000)], their duplication history is different. Independent whole genome duplications in core eudicots and at some points during the evolutionary history of the Ranunculales could account for these results (Cui et al., 2006; Jiao et al., 2012; Shi and Chen, 2020). The duplicate evolutionary history and therefore their potential functional specialization, were mostly taxon-specific.

Evolutionary history of class II TCP genes and low copy number in the CIN clade in Ranunculales

The classical subdivision of class II proteins into the CYC/TB1 and CIN clades was recovered (Martín-Trillo and Cubas, 2010; Mondragón-Palomino and Trontin, 2011; Liu et al., 2019). While CYC/TB1 sequences are specific to angiosperms (Navaud

et al., 2007; Horn et al., 2014; Liu et al., 2019), closely related sequences have recently been found in Gymnosperms (Wang et al., 2022). We confirmed the absence of CYC/TB1 in *Amborella trichopoda* (Liu et al., 2019; Wang et al., 2022), but our analysis could not determine whether CYC/TB1 had been lost in this species or if the CYC/TB1 lineage originated after the divergence of *Amborella* from the rest of angiosperms. Two to three paralogs were found in the complete repertoire of the other species sampled. The close phylogenetic relationship between the rice sequences and AtTCP18 suggests that only one CYC/TB1 gene was present in the common ancestor of the monocots and eudicots, with further taxon-specific duplications. Several studies have revealed the complex history of this clade in monocots (Mondragón-Palomino and Trontin, 2011; Bartlett and Specht, 2011; Preston and Hileman, 2012). The core eudicot specific CYC1, CYC2 and CYC3 clades that have been described previously (Howarth and Donoghue, 2006) may have been generated by the genome triplication which occurred in the common ancestor of this large clade. Independent duplications were reported in Ranunculales and in *Nelumbo* (Citerne et al., 2013). The present analysis supports the occurrence of a single duplication event in Ranunculales, most probably after the divergence of the Eupteleaceae (Supplementary Figure 3D).

Our analyses are consistent with the results obtained with more extensive taxonomic sampling, which suggested that two successive duplications had taken place in the CIN clade after the divergence of Lycophytes and Euphyllophytes (Liu et al., 2019; Lan and Qin, 2020). However, a study with an increased sampling of non-flowering plants has recently questioned the common ancestry of the CIN1 and CIN2 clades (Wang et al., 2022). We found seven CIN1 paralogs in *Amborella*, suggesting several species specific duplications; by contrast, there is only one *Amborella* sequence in each of the two CIN2 clades. A reduced complexity in terms of paralog number was observed in early diverging eudicots (3 sequences in *Aquilegia* and *Nigella*, 5 in *Nelumbo*) compared with the representatives of the core eudicots (6 in *Vitis*, and 8 in *Arabidopsis*) and monocots (8 in *Oryza*). Indeed, no duplications were observed in any of the three CIN sub-clades in Ranunculales (except possible species specific duplications, Supplementary Figures 3A-C), while two paralogs were found in the other early diverging eudicot *N. nucifera* in both CIN2 sub-clades. The different number of paralogs among taxa could suggest these are under different functional constraints, but this remains to be explored.

The so-called jaw-TCP genes identified in *Arabidopsis* (AtTCP2/24, AtTCP3/4/10) (Danisman et al., 2013) and other angiosperm species belonged to the CIN1 and CIN2b clades. These genes are specifically targeted by miR319 (Palatnik et al., 2003). No miR targeting site was found in the TCP genes of *Marchantia polymorpha*, *Physcomitrium patens* or *Selaginella mollendorfii*, suggesting that this mode of regulation of TCP genes has evolved after the divergence of Lycophytes (Lan and Qin, 2020), prior to the first duplication of the CIN clade, then lost in the CIN2a clade. In Ranunculales, two alternative variants of the miR targeting site existed, one in CIN1 and the other one in CIN2b, suggesting differential affinity for the miR possibly impacting gene regulation. In addition, the conceptual translation in these regions resulted in different amino acid motifs (QRGPLQSS which is part of $M_R^{II}9$ in CIN1, and NRGTLQSN in CIN2b), which may impact protein function. The R domain, first described in CYC/TB1 sequences, was present in CIN2b and rarely in CIN2a sequences. Because the R domain is also observed in class II *Physcomitrium* and *Selaginella* sequences (Floyd and Bowman, 2007; Liu et al., 2019), the most parsimonious hypothesis is that this domain is ancestral in class II sequences and was lost in the CIN1 lineage, and independently in many CIN2a sequences.

TCP gene expression patterns in *N. damascena* are differentiated for RanaCYL and more ubiquitous for RanaCIN and class I genes

The purpose of the analysis was to reveal trends in the expression patterns of TCP genes in aerial organs of *N. damascena*, to guide future trait, organ or tissue specific investigations. We found that all *N. damascena* TCP genes, with the notable exception of the *NdCYL* genes (in the CYC/TB1 clade), were expressed in all organs examined here (Figure 5), including at the very early stages of floral development, as revealed in our previous quantitative transcriptomic analysis (Deveaux et al., 2021). Such ubiquitous patterns suggest potential roles in various morphogenetic processes.

CYC/TB1 genes are known to be involved in the control of flower development, plant architecture and shoot branching (Luo et al., 1996; Doebley et al., 1997; Takeda et al., 2003; Kebrom et al., 2006; Kebrom et al., 2012). In *Arabidopsis*, *AtBRANCHED1* (*AtBRC1* a.k.a. *AtTCP18*) and to a lesser extent *AtBRC2* (*AtTCP12*) play a role in shoot branching, in concert with hormonal signals (Aguilar-Martínez et al., 2007; Seale et al., 2017). A similar role has been shown for *AtBRC1* homologs in pea and tomato (Martín-Trillo et al., 2011; Braun et al., 2012). Similarly, in the Papaveraceae species *Eschscholzia californica*, the *CYL1* paralog plays a role in the repression of axillary bud development with a possible redundant contribution of *CYL2*, suggesting that the role of CYC/TB1 genes in branching is conserved among angiosperms (Zhao et al., 2018). After being first characterized in *Antirrhinum majus* for their role in the establishment of zygomorphy (Luo et al., 1996), CYC/TB1 genes have been for the most part studied as candidates for the repeated origin of bilateral symmetry among angiosperms. Asymmetric expression during flower development has been found to be correlated with bilateral symmetry in many diverse angiosperm clades, and independent recruitement for the establishment of floral zygomorphy had been demonstrated in several groups (reviewed in

Hileman, 2014). In Lamiales, preliminary evidence suggested that the zygomorphic developmental program depending on CYC has been coopted "en bloc" early during the diversification of the order, from an ancestral role in carpel development (Sengupta and Hileman 2022). In early diverging eudicots and early diverging angiosperms, expression of CYC/TB1 genes is generally found in most floral organs, whether the flower is monosymmetric or polysymmetric (Damerval et al., 2013; Horn et al., 2014; Zhao et al., 2018; Pabón-Mora et al., 2020). Asymmetric floral expression was observed late in development, suggesting that although CYC/TB1 genes could play a role in the zygomorphic phenotype at anthesis, they are almost certainly not the initial triggers (Damerval et al., 2013; Horn et al., 2014; Jabbour et al., 2014; Citerne et al., 2017; Zhao et al., 2018; Pabón-Mora et al., 2020). In the radially symmetric *E. californica*, both *CYL* genes play a role in petal size in addition to having a role in controlling vegetative architecture (Zhao et al., 2018). The *CYL2* gene plays a specific role in controlling stamen number (Zhao et al., 2018). By contrast, in another Papaveraceae species, *Cysticapnos vesicaria*, no vegetative role was found, but *CYL* gene silencing did affect flower development, including sepal and petal identity and floral symmetry (Zhao et al., 2018). In Ranuculaceae, *CYL* paralogs were expressed in floral buds, being either uniformly or not expressed in the perianth organs of actinomorphic species (Jabbour et al., 2014). Our expression data refined these results in *N. damascena*. *NdCYL1* and *NdCYL2* have contrasted expression patterns in the floral organs at the developmental stage studied here, *NdCYL1* being more expressed in gynoecium and *NdCYL2* in petals and stamens, suggesting subfunctionalization (Figure 5). Additional duplications in both RanaCYL lineages occurred in the tribe Delphinieae, which contains all the zygomorphic species in the family. Species specific subfunctionalization was also observed among paralogs in Delphinieae species, some of them being asymmetrically expressed in the perianth (Jabbour et al., 2014). In all, available expression and functional data in Ranunculales reveal much species specific subfunctionalization between CYC/TB1 paralogs, advocating for further comparative analyses to better understand the role of these genes in vegetative and floral architecture and how it has evolved during the diversification of the order.

Most functional data on CIN genes have been obtained in the model species *Arabidopsis thaliana* and *Antirrhinum majus*. These genes appear to be at the crossroads of several hormonal biosynthesis and signaling pathways and as such they are involved in many developmental and biological processes (reviewed in Nicolas and Cubas, 2016a; Nicolas and Cubas, 2016b; Sarvepalli and Nath, 2018; Lan and Qin, 2020; Rath et al., 2022). In particular, CIN genes are involved in the control of leaf and petal development and cellular differentiation (Nath et al., 2003; Crawford et al., 2004; Koyama et al., 2011; Das Gupta et al., 2014; Huang and Irish, 2015; Huang and Irish, 2016; Nicolas and Cubas, 2016b; van Es et al., 2018; Chen et al., 2018). Less knowledge has been gained on the function of class I proteins, possibly be due to the difficulty in obtaining altered phenotypes from single gene mutants, suggesting a functional redundancy of these proteins. Additionally, in *Arabidopsis*, class I and CIN genes share several targets and act in the same pathways and processes, either redundantly or antagonistically (Kieffer et al., 2011; Uberti-Manassero et al., 2012; Danisman et al., 2012; Aguilar-Martínez and Sinha, 2013). Expression patterns of CIN and class I genes, and in some cases their functional role in organ development, have been recorded in a few non model species (Ori et al., 2007; Ikeuchi et al., 2013; Lin et al., 2016; Madrigal et al., 2017; Zhao et al., 2020, for review Lan and Qin, 2020). In Ranunculales, the CIN1 clade gene *AqTCP4* has been shown to be required for the proper development of the spurred petals of *Aquilegia coerulea* (Yant et al., 2015). In *Nigella damascena*, the three *NdCIL*s and the nine class I genes were found to be expressed in both the sepals and the elaborate petals as well as in the young floral bud. Both CIN2 paralogs (*NdTCP2* and *NdTCP5*) appeared weakly expressed in stamens compared with other floral organs. The expression pattern of *NdTCP15-2* was different from that of its close paralog *NdTCP15-1*, with a lower expression in the stamens and perianth organs compared with the gynoecium in the former, suggesting sub-functionalization. Overall, we observed quite limited differentiation in the expression patterns of CIN and class I TCP genes in our data. It is worth noting that we did not analyze roots and fruits, which may reveal specific patterns. In the aerial organs at least, functional redundancy could be common among these genes, as has been noticed in *Arabidopsis*. These seemingly redundant patterns advocate for more detailed analyses examining the fine tuning of TCP gene expression during developmental processes of interest in *Nigella damascena*, such as flower or leaf development, and additional functional studies to determine the role of specific genes. This should be enlightening from an evo-devo point of view, as many similar traits have evolved independently in Ranunculales and core eudicots species.

Data availability statement

The datasets presented in this study can be found in online repositories. The names of the repository/repositories and accession number(s) can be found below: The transcriptomic data are deposited in the CATdb repository http://tools.ips2.u-psud.fr/CATdb, under the accession ngs2015_16_ranunculaceae and are accessible in the dataverse INRAE at https://doi.org/10.57745/2G1VCP. The sequences and alignments are deposited in the Dryad repository and are accessible at https://doi.org/10.5061/dryad.zcrjdfngw. Nigella TCP sequences are deposited in Genbank with accession numbers OP493852-65.

Author contributions

CD, YD, NCS, FJ, and SN designed the study, CD, CC, MLG, YD performed the molecular work, LS-T and JC produced the

RNA-seq data, VB and ED performed the bioinformatic work, CD and CC performed the phylogenetic analyses, and all authors contributed to writing the manuscript. All authors contributed to the article and approved the submitted version.

Funding

The project received financial support from the Institut Diversité, Ecologie et Evolution du Vivant (IDEEV AAP2013 and AAP2015).

Acknowledgments

The GQE-Le Moulon and Institute of Plant Sciences Paris-Saclay benefit from the support of the LabExSaclay Plant Sciences-SPS (ANR-10-LABX-0040-SPS). The authors acknowledge Alioune Badara Ndiaye for help with the molecular work, Adrien Falce for helping with the OrthoFinder method, and Hélène Citerne for constructive comments on the manuscript.

Conflict of interest

The authors declare that the research was conducted in the absence of any commercial or financial relationships that could be construed as a potential conflict of interest.

Publisher's note

Supplementary material

The Supplementary Material for this article can be found online at: https://www.frontiersin.org/articles/10.3389/fpls.2022.1055196/full#supplementary-material

SUPPLEMENTARY TABLE 1
List of primers used.

SUPPLEMENTARY TABLE 2
TCP gene identifier and abbreviated name for the six angiosperm species included in the phylogenetic reconstruction of the TCP gene family.

SUPPLEMENTARY TABLE 3
(A, B) Class I and class II TCP gene identifier and abbreviated name for all Ranunculales sequences included in this study.

SUPPLEMENTARY TABLE 4
PCR conditions for the amplification of TCP genes in *N. damascena*.

SUPPLEMENTARY TABLE 5
(A, B) Conserved protein motifs detected in the six angiosperm species plus *N. damascena* (**A**: class I TCP proteins; **B**: class II TCP proteins). The motif order detected on the sequences in the seven species are first indicated. The logos of the motifs are shown in the image, and the correspondence between the motifs detected in the seven species and in the Ranunculales analyses are indicated. Partial overlap of the motif sequences detected in the two analyses is observed in some cases.

SUPPLEMENTARY FIGURE 1
(A-F) Phylogeny of coding nucleotide sequences of class I TCP genes in Ranunculales for each of the six major groups identified in the angiosperm TCP class I phylogeny separately. Phylogenetic trees were rooted with *Nelumbo* (or *Vitis* for RanTCP22) sequences belonging to the corresponding groups in the complete repertoire analysis. Trees were reconstructed using PhyML and branch supports are a-LRT. Regions where primary homology was uncertain were discarded. Reconstructions were based on 909 nucleotide positions out of 1,434 (RanTCP7), 843 out of 1,788 (RanTCP22), 606 out of 876 (RanTCP11), 876 out of 1,401 (RanTCP20), 1,569 out of 1,866 (RanTCP9) and 1,368 out of 1,965 (RanTCP15). Families were color-coded as follows: Eupteleaceae: brown; Lardizabalaceae: khaki green; Berberidaceae: green; Ranunculaceae: pink; Papaveraceae: blue.

SUPPLEMENTARY FIGURE 2
Sequence logos of the 10 amino acid motifs detected in 145 class I TCP proteins from Ranunculales using MEME.

SUPPLEMENTARY FIGURE 3
(A-D) Phylogeny of coding nucleotide sequences of class II TCP genes in Ranunculales for each subclade. Phylogenetic trees were rooted with the *Nelumbo* sequences used in the complete repertoire analysis. Trees were reconstructed using PhyML and branch supports are a-LRT. Regions where primary homology was uncertain were discarded. Reconstructions were based on 1,716 nucleotide positions out of 3,096 (RanaCIL1), 1,665 out of 1,677 (RanaCIL2a), and 423 out of 2,256 (RanaCYL). Families were color-coded as follows: Eupteleaceae: brown; Circeasteraceae: yellow; Lardizabalaceae: khaki green; Menispermaceae: dark blue; Berberidaceae: green; Ranunculaceae: pink; Papaveraceae: blue.

SUPPLEMENTARY FIGURE 4
Sequence logos of the 10 amino acid motifs detected in 178 class II TCP proteins from Ranunculales using MEME.

SUPPLEMENTARY FIGURE 5
(A) Picture of a *Nigella damascena* plant, showing the different organs collected for expression analysis. **(B)** Blooming flower with floral organs indicated.

SUPPLEMENTARY FIGURE 6
Comparison of the expression patterns of TCP gene in *Nigella damascena* in the three biological replicates. Figure 5 corresponds to R3.

References

Abascal, F., Zardoya, R., and Telford, M. J. (2010). TranslatorX: multiple alignment of nucleotide sequences guided by amino acid translations. *Nucleic Acids Res.* 38, W7–13. doi: 10.1093/nar/gkq291

Aggarwal, P., Gupta, M. D., Joseph, A. P., Chatterjee, N., Srinivasan, N., and Nath, U. (2010). Identification of specific DNA binding residues in the TCP family of transcription factors in *Arabidopsis*. *Plant Cell* 22, 1174–1189. doi: 10.1105/tpc.109.066647

Aguilar-Martínez, J. A., Poza-Carrión, C., and Cubas, P. (2007). *Arabidopsis* BRANCHED1 acts as an integrator of branching signals within axillary buds. *Plant Cell* 19, 458–472. doi: 10.1105/tpc.106.048934

Aguilar-Martínez, J. A., and Sinha, N. (2013). Analysis of the role of *Arabidopsis* class I TCP genes AtTCP7, AtTCP8, AtTCP22, and AtTCP23 in leaf development. *Front. Plant Sci.* 4. doi: 10.3389/fpls.2013.00406

Balzergue, S., Dubreucq, B., Chauvin, S., Le-Clainche, I., Le Boulaire, F., de Rose, R., et al. (2001). Improved PCR-walking for large-scale isolation of plant T-DNA borders. *Biotechniques* 30, 496–498, 502, 504. doi: 10.2144/01303bm06

Bartlett, M. E., and Specht, C. D. (2011). Changes in expression pattern of the *TEOSINTE BRANCHED1*-like genes in the zingiberales provide a mechanism for evolutionary shifts in symmetry across the order. *Am. J. Bot.* 98, 227–243. doi: 10.3732/ajb.1000246

Becker, A. (2016). Tinkering with transcription factor networks for developmental robustness of ranunculales flowers. *Ann. Bot.* 117, 845–858. doi: 10.1093/aob/mcw037

Bolger, A. M., Lohse, M., and Usadel, B. (2014). Trimmomatic: a flexible trimmer for illumina sequence data. *Bioinformatics* 30, 2114–2120. doi: 10.1093/bioinformatics/btu170

Braun, N., de Saint Germain, A., Pillot, J.-P., Boutet-Mercey, S., Dalmais, M., Antoniadi, I., et al. (2012). The pea TCP transcription factor PsBRC1 acts downstream of strigolactones to control shoot branching. *Plant Physiol.* 158, 225–238. doi: 10.1104/pp.111.182725

Camoirano, A., Arce, A. L., Ariel, F. A., Alem, A. L., Gonzalez, D. H., and Viola, I. L. (2020). Class I TCP transcription factors regulate trichome branching and cuticle development in *Arabidopsis*. *J. Exp. Bot.* 71, 5438–5453. doi: 10.1093/jxb/eraa257

Challa, K. R., Aggarwal, P., and Nath, U. (2018). Activation of YUCCA5 by the transcription factor TCP4 integrates developmental and environmental signals to promote hypocotyl elongation in *Arabidopsis*. *Plant Cell* 28, 2117–2130. doi: 10.1105/tpc.16.00360

Challa, K. R., Rath, M., and Nath, U. (2019). The CIN-TCP transcription factors promote commitment to differentiation in *Arabidopsis* leaf pavement cells *via* both auxin-dependent and independent pathways. *PloS Genet.* 1, e1007988. doi: 10.1371/journal.pgen.1007988

Chen, D., Yan, W., Fu, L. Y., and Kaufmann, K. (2018). Architecture of gene regulatory networks controlling flower development in *Arabidopsis thaliana*. *Nat. Commun.* 9, 4534. doi: 10.1038/s41467-018-06772-3

Citerne, H. L., Le Guilloux, M., Sannier, J., Nadot, S., and Damerval, C. (2013). Combining phylogenetic and syntenic analyses for understanding the evolution of TCP ECE genes in eudicots. *PloS One* 8, e74803. doi: 10.1371/journal.pone.0074803

Citerne, H. L., Reyes, E., Le Guilloux, M., Delannoy, E., Simonnet, F., Sauquet, H., et al. (2017). Characterization of *CYCLOIDEA*-like genes in proteaceae, a basal eudicot family with multiple shifts in floral symmetry. *Ann. Bot.* 119, 367–378. doi: 10.1093/aob/mcw219

Costa, M. M. R., Fox, S., Hanna, A. I., Baxter, C., and Coen, E. (2005). Evolution of regulatory interactions controlling floral asymmetry. *Development* 132, 5093–5101. doi: 10.1242/dev.02085

Crawford, B. C. W., Nath, U., Carpenter, R., and Coen, E. S. (2004). *CINCINNATA* controls both cell differentiation and growth in petal lobes and leaves of *Antirrhinum*. *Plant Physiol.* 135, 244–253. doi: 10.1104/pp.103.036368

Cubas, P., Lauter, N., Doebley, J., and Coen, E. (1999). The TCP domain: a motif found in proteins regulating plant growth and development. *Plant J.* 18, 215–222. doi: 10.1046/j.1365-13X.1999.00444.x

Cui, L., Wall, P. K., Leebens-Mack, J. H., Lindsay, B. G., Soltis, D. E., Doyle, J. J., et al. (2006). Widespread genome duplications throughout the history of flowering plants. *Genome Res.* 16, 738–749. doi: 10.1101/gr.4825606

Damerval, C., and Becker, A. (2017). Genetics of flower development in ranunculales – a new, basal eudicot model order for studying flower evolution. *New Phytol.* 216, 361–366. doi: 10.1111/nph.14401

Damerval, C., Citerne, H., Le Guilloux, M., Domenichini, S., Dutheil, J., De Craene, L. R., et al. (2013). Asymmetric morphogenetic cues along the transverse plane: shift from disymmetry to zygomorphy in the flower of fumarioideae. *Am. J. Bot.* 100, 391–402. doi: 10.3732/ajb.1200376

Danisman, S., van der Wal, F., Dhondt, S., Waites, R., de Folter, S., Bimbo, A., et al. (2012). *Arabidopsis* class I and class II TCP transcription factors regulate jasmonic acid metabolism and leaf development antagonistically. *Plant Physiol.* 159, 1511–1523. doi: 10.1104/pp.112.200303

Danisman, S., Van Dijk, A. D. J., Bimbo, A., van der Wal, F., Hennig, L., de Folter, S., et al. (2013). Analysis of functional redundancies within the *Arabidopsis* TCP transcription factor family. *J. Exp. Bot.* 64, 5673–5685. doi: 10.1093/jxb/ert337

Das Gupta, M., Aggarwal, P., and Nath, U. (2014). *CINCINNATA* in *Antirrhinum majus* directly modulates genes involved in cytokinin and auxin signaling. *New Phytol.* 204, 901–912. doi: 10.1111/nph.12963

Deveaux, Y., Conde e Silva, N., Manicacci, D., Le Guilloux, M., Brunaud, V., Belcram, H., et al. (2021). Transcriptome analysis reveals putative target genes of the *APETALA3-3* identity gene at early developmental stages in *Nigella damascena* l. *Front. Plant Sci.* 12, 660863. doi: 10.3389/fpls2021660803

Doebley, J., Stec, A., and Hubbard, L. (1997). The evolution of apical dominance in maize. *Nature* 386, 485–488. doi: 10.1038/386485a0

Emms, D. M., and Kelly, S. (2015). OrthoFinder: solving fundamental biases in whole genome comparisons dramatically improves orthogroup inference accuracy. *Genome Biol.* 16, 157. doi: 10.1186/s13059-015-0721-2

Emms, D. M., and Kelly, S. (2019). OrthoFinder: phylogenetic orthology inference for comparative genomics. *Genome Biol.* 20, 238. doi: 10.1186/s13059-019-1832-y

Filiault, D. L., Ballerini, E. S., Mandáková, T., Aköz, G., Derieg, N. J., Schmutz, J., et al. (2018). The *Aquilegia* genome provides insight into adaptive radiation and reveals an extraordinarily polymorphic chromosome with a unique history. *Elife* 7, e36426. doi: 10.7554/eLife.36426

Floyd, S. K., and Bowman, J. L. (2007). The ancestral developmental toolkit of land plants. *Int. J. Plant Sci.* 168, 1–35. doi: 10.1086/509079

Francis, A., Dhaka, N., Bakshi, M., Jung, K. H., Sharma, M. K., and Sharma, R. (2016). Comparative phylogenomic analysis provides insights into TCP gene functions in *Sorghum*. *Sci. Rep.* 6, 38488. doi: 10.1038/srep38488

Gastaldi, V., Lucero, L. E., Ferrero, L. V., Ariel, F. D. , and Gonzalez, D. H. (2020). Class-I TCP transcription factors activate the *SAUR63* gene subfamily in gibberellin-dependent stamen filament elongation. *Plant. Physiol.* 182, 2096–2110. doi: 10.1104/pp.19.01501

Gaudin, V., Lunness, P. A., Fobert, P. R., Towers, M., Riou-Khamlichi, C., Murray, J. A., et al. (2000). The expression of d-cyclin genes defines distinct developmental zones in snapdragon apical meristems and is locally regulated by the *Cycloidea* gene. *Plant Pysiol.* 122, 1137–1148. doi: 10.1104/pp.122.4.1137

Giraud, E., Ng, S., Carrie, C., Duncan, O., Low, J., Lee, C. P., et al. (2010). TCP Transcription factors link the regulation of genes encoding mitochondrial proteins with the circadian clock in *Arabidopsis thaliana*. *Plant Cell* 22, 3921–3934. doi: 10.1105/tpc.110.074518

González-Grandío, E., and Cubas, P. (2016). "TCP Transcription factors: evolution, structure, and biochemical functions," in *Plant transcription factors – evolutionary, structural, and functional aspects*. Ed. D. H. Gonzalez (San Diego, USA: Elsevier/Academic Press), pp139–pp151.

Grabherr, M. G., Haas, B. J., Yassour, M., Levin, J. Z., Thompson, D. A., Amit, I., et al. (2011). Full-length transcriptome assembly from RNA-seq data without a reference genome. *Nat. Biotechnol.* 29, 644–652. doi: 10.1038/nbt.1883

Guindon, S., Dufayard, J. F., Lefort, V., Anisimova, M., Hordijk, W., and Gascuel, O. (2010). New algorithms and methods to estimate maximum-likelihood phylogenies: assessing the performance of PhyML 3.0. *Syst. Biol.* 59, 307–321. doi: 10.1093/sysbio/syq010

Haas, B. J., Papanicolaou, A., Yassour, M., Grabherr, M., Blood, P. D., Bowden, J., et al. (2013). *De novo* transcript sequence reconstruction from RNA-seq using the trinity platform for reference generation and analysis. *Nat. Protoc.* 8, 1494–1512. doi: 10.1038/nprot.2013.084

Hall, T. A. (1999). BioEdit: a user-friendly biological sequence alignment editor and analysis program for windows 95/98/NT. *Nucl. Acids Symp. Ser.* 41, 95–98.

Hao, J., Tu, L., Hu, H., Tan, J., Deng, F., Tang, W., et al. (2012). GbTCP, a cotton TCP transcription factor, confers fibre elongation and root hair development by a complex regulating system. *J. Exp. Bot.* 63, 6267–62 81. doi: 10.1093/jxb/err313

Hileman, L. C. (2014). Trends in flower symmetry evolution revealed through phylogenetic and developmental genetic advances. *Philos. Trans. R. Soc Lond. B. Biol. Sci.* 369, 1–10. doi: 10.1098/rstb.2013.0348

Horn, S., Pabón-Mora, N., Theuß, V. S., Busch, A., and Zachgo, S. (2014). Analysis of the CYC/TB1 class of TCP transcription factors in basal angiosperms and magnoliids. *Plant J.* 81, 559–571. doi: 10.1111/tpj.12750

Howarth, D. G., and Donoghue, M. J. (2006). Phylogenetic analysis of the "ECE" (CYC/TB1) clade reveals duplications predating the core eudicots. *Proc. Natl. Acad. Sci. U.S.A.* 103, 9101–9106. doi: 10.1073/pnas.0602827103

Huang, T., and Irish, V. F. (2015). Temporal control of plant organ growth by TCP transcription factors. *Curr. Biol.* 25, 1765–1770. doi: 10.1016/j.cub.2015.05.024

Huang, T., and Irish, V. F. (2016). Gene networks controlling petal organogenesis. *J. Exp. Bot.* 67, 61–68. doi: 10.1093/jxb/erv444

Huo, Y., Xiong, W., Su, K., Li, Y., Yang, Y., Fu, C., et al. (2019). Genome-wide analysis of the *TCP* gene family in switchgrass (*Panicum virgatum* l.). *Int. J. Genomics* 2019, 8514928. doi: 10.1155/2019/8514928

Ikeuchi, M., Tatematsu, K., Yamaguchi, T., Okada, K., and Tsukaya, H. (2013). Precocious progression of tissue maturation instructs basipetal initiation of leaflets in *Chelidonium majus* subsp. *asiaticum* (Papaveraceae). *Am. J. Bot.* 100, 1116–1126. doi: 10.3732/ajb.1200560

Jabbour, F., Cossard, G., Le Guilloux, M., Sannier, J., Nadot, S., and Damerval, C. (2014). Specific duplication and dorsoventrally asymmetric expression patterns of *Cycloidea*-like genes in zygomorphic species of ranunculaceae. *PloS One* 9, e95727. doi: 10.1371/journal.pone.0095727

Jiao, Y., Leebens-Mack, J., Ayyampalayam, S., Bowers, J. E., McKain, M. R., McNeal, J., et al. (2012). A genome triplication associated with early diversification of the core eudicots. *Genome Biol.* 13, R3. doi: 10.1186/gb-2012-13-1-r3

Jiu, S., Xu, Y., Wang, J., Wang, L., Wang, S., Ma, C., et al. (2019). Genome-wide identification, characterization, and transcript analysis of the TCP transcription factors in *Vitis vinifera*. *Front. Genet.* 10. doi: 10.3389/fgene.2019.01276

Juntheikki-Palovaara, I., Tähtiharju, S., Lan, T., Broholm, S. K., Rijpkema, A. S., Ruonala, R., et al. (2014). Functional diversification of duplicated CYC2 clade genes in regulation of inflorescence development in *Gerbera hybrida* (Asteraceae). *Plant J.* 79, 783–796. doi: 10.1111/tpj.12583

Kebrom, T. H., Burson, B. L., and Finlayson, S. A. (2006). Phytochrome b represses *Teosinte Branched1* expression and induces sorghum axillary bud outgrowth in response to light signals. *Plant Physiol.* 140, 1109–1117. doi: 10.1104/pp.105.074856

Kebrom, T. H., Chandler, P. M., Swain, S. M., King, R. W., Richards, R. A., and Spielmeyer, W. (2012). Inhibition of tiller bud outgrowth in the tin mutant of wheat is associated with precocious internode development. *Plant Physiol.* 160, 308–318. doi: 10.1104/pp.112.197954

Kieffer, M., Master, V., Waites, R., and Davies, B. (2011). TCP14 and TCP15 affect internode length and leaf shape in *Arabidopsis*. *Plant J.* 68, 147–158. doi: 10.1111/j.1365-313X.2011.04674.x

Kim, M., Cui, M.-L., Cubas, P., Gillies, A., Lee, K., Chapman, M. A., et al. (2008). Regulatory genes control a key morphological and ecological trait transferred between species. *Science* 322, 1116–1119. doi: 10.1126/science.1164371

Kopylova, E., Noé, L., and Touzet, H. (2012). SortMeRNA: fast and accurate filtering of ribosomal RNAs in metatranscritomic data. *Bioinformatics* 28, 3211–3217. doi: 10.1093/bioinformatics/bts611

Kosugi, S., and Ohashi, Y. (1997). PCF1 and PCF2 specifically bind to cis elements in the rice proliferating cell nuclear antigen gene. *Plant Cell* 9, 1607–1619. doi: 10.1105/tpc.9.9.1607

Kosugi, S., and Ohashi, Y. (2002). DNA Binding and dimerization specificity and potential targets for the TCP protein family. *Plant J.* 30, 337–348. doi: 10.1046/j.1365-313X.2002.01294.x

Koyama, T., Ohme-Takagi, M., and Sato, F. (2011). Generation of serrated and wavy petals by inhibition of the activity of TCP transcription factors in *Arabidopsis thaliana*. *Plant Signal. Behav.* 6, 697–699. doi: 10.4161/psb.6.5.14979

Koyama, T., Sato, F., and Ohme-Takagi, M. (2017). Roles of miR319 and TCP transcription factors in leaf development. *Plant Physiol.* 175, 874–885. doi: 10.1104/pp.17.00732

Lan, J., and Qin, G. (2020). The regulation of CIN-like TCP transcription factors. *Int. J. Mol. Sci.* 21, 4498. doi: 10.3390/ijms21124498

Lefort, V., Longueville, J. E., and Gascuel, O. (2017). SMS: Smart model selection in PhyML. *Mol. Biol. Evol.* 34, 2422–2424. doi: 10.1093/molbev/msx149

Leng, X., Wei, H., Xu, X., Ghuge, S. A., Jia, D., Liu, G., et al. (2019). Genome-wide identification and transcript analysis of TCP transcription factors in grapevine. *BMC Genomics* 20, 786. doi: 10.1186/s12864-019-6159-2

Li, S. (2015). The *Arabidopsis thaliana* TCP transcription factors: A broadening horizon beyond development. *Plant Signal. Behav.* 10, e1044192. doi: 10.1080/15592324.2015

Li, Y., An, S., Cheng, Q., Zong, Y., Chen, W., Guo, W., et al. (2021). Analysis of evolution, expression and genetic transformation of TCP transcription factors in blueberry reveal that *VcTCP18* negatively regulates the release of flower bud dormancy. *Front. Plant Sci.* 12. doi: 10.3389/fpls.2021

Lin, Y. F., Chen, Y. Y., Hsiao, Y. Y., Shen, C. Y., Hsu, J. L., Yeh, C. M., et al. (2016). Genome-wide identification and characterization of TCP genes involved in ovule development of *Phalaenopsis equestris*. *J. Exp. Bot.* 67, 5051–5066. doi: 10.1093/jxb/erw273

Liu, M. M., Wang, M. M., Yang, J., Wen, J., Guo, P. C., Wu, Y. W., et al. (2019). Evolutionary and comparative expression analyses of TCP transcription factor gene family in land plants. *Int. J. Mol. Sci.* 20, 3591. doi: 10.3390/ijms20143591

Li, D., Zhang, H., Mou, M., Chen, Y., Xiang, S., Chen, L., et al. (2019). *Arabidopsis* class II TCP transcription factors integrate with the FT-FD module to control flowering. *Plant Physiol.* 181, 97–111. doi: 10.1104/pp.19.00252

Lucero, L. E., Uberti-Manassero, N. G., Arce, A. L., Colombatti, F., Alemano, S. G., and Gonzalez, D. H. (2015). TCP15 modulates cytokinin and auxin responses during gynoecium development in *Arabidopsis*. *Plant J.* 84, 267–282. doi: 10.1111/tpj.12992

Luo, D., Carpenter, R., Vincent, C., Copsey, L., and Coen, E. (1996). Origin of floral asymmetry in *Antirrhinum*. *Nature* 383, 794–799. doi: 10.1038/383794a0

Madrigal, Y., Alzate, J. F., and Pabón-Mora, N. (2017). Evolution and expression patterns of TCP genes in asparagales. *Front. Plant Sci.* 8. doi: 10.3389/fpls.2017.00009

Martínez-Gómez, J., Galimba, K. D., Coté, E. Y., Sullivan, A. M., and Di Stilio, V. S. (2021). Spontaneous homeotic mutants and genetic control of floral organ identity in a ranunculid. *Evol. Dev.* 23, 197–214. doi: 10.1111/ede.12357

Martín-Trillo, M., and Cubas, P. (2010). TCP Genes: a family snapshot ten years later. *Trends Plant Sci.* 15, 31–39. doi: 10.1016/j.tplants.2009.11.003

Martín-Trillo, M., Grandio, E. G., Serra, F., Marcel, F., Rodriguez-Buey, M. L., Schmitz, G., et al. (2011). Role of tomato BRANCHED1-like genes in the control of shoot branching. *Plant J.* 67, 701–714. doi: 10.1111/j.1365-313X.2011.04629.x

Mondragón-Palomino, M., and Trontin, C. (2011). High time for a roll call: gene duplication and phylogenetic relationships of TCP-like genes in monocots. *Ann. Bot.* 107, 1533–1544. doi: 10.1093/aob/mcr059

Nath, U., Crawford, B. C. W., Carpenter, R., and Coen, E. (2003). Genetic control of surface curvature. *Science* 299, 1404–1407. doi: 10.1126/science.1079354

Navaud, O., Dabos, P., Carnus, E., Tremousaygue, D., and Hervé, C. (2007). TCP Transcription factors predate the emergence of land plants. *J. Mol. Evol.* 65, 23–33. doi: 10.1007/s00239-006-0174-z

Nicolas, M., and Cubas, P. (2016a). TCP Factors: new kids on the signaling block. *Curr. Opin. Plant Biol.* 33, 33–41. doi: 10.1016/j.pbi.2016.05.006

Nicolas, M., and Cubas, P. (2016b). "The role of TCP transcription factors in shaping flower structure, leaf morphology, and plant architecture," in *Plant transcription factors – evolutionary, structural, and functional aspects*. Ed. D. H. Gonzalez (San Diego, USA: Elsevier/Academic Press), pp249–pp267.

Ori, N., Cohen, A. R., Etzioni, A., Brand, A., Yanai, O., Shleizer, S., et al. (2007). Regulation of *LANCEOLATE* by miR319 is required for compound-leaf development in tomato. *Nat. Genet.* 39, 787–791. doi: 10.1038/ng2036

Pabón-Mora, N., Madrigal, Y., Alzate, J. F., Ambrose, B. A., Ferrándiz, C., Wanke, S., et al. (2020). Evolution of class II TCP genes in perianth bearing piperales and their contribution to the bilateral calyx in *Aristolochia*. *New Phytol.* 228, 752–769. doi: 10.1111/nph.16719

Palatnik, J. F., Allen, E., Wu, X., Schommer, C., Schwab, R., Carrington, J. C., et al. (2003). Control of leaf morphogenesis by microRNAs. *Nature* 425, 257–263. doi: 10.1038/nature01958

Parapunova, V., Busscher, M., Busscher-Lange, J., Lammers, M., Karlova, R., Bovy, A. G., et al. (2014). Identification, cloning and characterization of the tomato TCP transcription factor family. *BMC Plant Biol.* 14, 157. doi: 10.1186/1471-2229-14-157

Preston, J. C., and Hileman, L. C. (2012). Parallel evolution of TCP and b-class genes in commelinaceae flower bilateral symmetry. *Evodevo* 3, 6. doi: 10.1186/2041-9139-3-6

Rath, M., Challa, K. R., Sarvepalli, K., and Nath, U. (2022). CINCINNATA-like TCP transcription factors in cell growth – an expanding portfolio. *Front. Plant Sci.* 13. doi: 10.3389/fpls.2022.825341

Sarvepalli, K., and Nath, U. (2018). CIN-TCP transcription factors: transiting cell proliferation in plants. *IUBMB* 70, 718–731. doi: 10.1002/iub.1874

Schommer, C., Debernardi, J. M., Bresso, E. G., Rodriguez, R. E., and Palatnik, J. F. (2014). Repression of cell proliferation by miR319-regulated TCP4. *Mol. Plant* 7, 1533–1544. doi: 10.1093/mp/ssu084

Seale, M., Bennett, T., and Leyser, O. (2017). *BRC1* expression regulates bud activation potential but is not necessary or sufficient for bud growth inhibition in *Arabidopsis*. *Development* 144, 1661–1673. doi: 10.1242/dev.145649

Sengupta, A., and Hileman, L. C. (2022). A CYC-RAD-DIV-DRIF interaction likely pre-dates the origin of floral monosymmetry in lamiales. *Evodevo* 13, 3. doi: 10.1186/s13227-021-00187-w

Shi, T., and Chen, J. (2020). A reappraisal of the phylogenetic placement of the aquilegia whole-genome duplication. *Genome Biol.* 21, 295. doi: 10.1186/s13059-020-02212-y

Takeda, T., Suwa, Y., Suzuki, M., Kitano, H., Ueguchi-Tanaka, M., Ashikari, M., et al. (2003). The *OsTB1* gene negatively regulates lateral branching in rice. *Plant J.* 33, 513–520. doi: 10.1046/j.1365-313X.2003.01648.x

Uberti-Manassero, N. G., Lucero, L. E., Viola, I. L., Vegetti, A. C., and Gonzalez, D. H. (2012). The class I protein AtTCP15 modulates plant development through a pathway that overlaps with the one affected by CIN-like TCP proteins. *J. Exp. Bot.* 63, 809–823. doi: 10.1093/jxb/err305

Uberti-Manassero, N. G., Viola, I. L., Welchen, E., and Gonzalez, D. H. (2013). TCP Transcription factors: architectures of plant form. *Biomol. Concepts.* 4, 111–127. doi: 10.1515/bmc-2012-0051

Vadde, B. V. L., Challa, K. R., and Nath, U. (2018). The TCP4 transcription factor regulates trichome cell differentiation by directly activating *GLABROUS INFLORESCENCE STEMS* in *Arabidopsis thaliana*. *Plant J.* 93, 259–269. doi: 10.1111/tpj.13772

van Es, S. W., Silveira, S. R., Rocha, D. I., Bimbo, A., Martinelli, A. P., Dornelas, M. C., et al. (2018). Novel functions of the *Arabidopsis* transcription factor TCP5 in petal development and ethylene biosynthesis. *Plant J.* 94, 867–879. doi: 10.1111/tpj.13904

van Es, S. W., van der Auweraert, E. B., Silveira, S. R., Angenent, G. C., van Dijk, A. D. J., and Immink, R. G. H. (2019). Comprehensive phenotyping reveals interactions and functions of *Arabidopsis thaliana* TCP genes in yield determination. *Plant J.* 99, 316–328. doi: 10.1111/tpj.14326

Viola, I. L., Reinheimer, R., Ripoll, R., Uberti-Manassero, N. G., and Gonzalez, D. H. (2012). Determinants of the DNA binding specificity of class I and class II TCP transcription factors. *J. Biol. Chem.* 287, 347–3356. doi: 10.1074/jbc.M111.256271

Vision, T. J., Brown, D. G., and Tanksley, S. D. (2000). The origins of genomic duplications in *Arabidopsis*. *Science* 290, 2114–2117. doi: 10.1126/science.290.5499.2114

Wang, J.-L., Wang, H.-W., Cao, Y.-N., Kan, S.-L., and Liu, Y.-Y. (2022). Comprehensive evolutionary analysis of the TCP gene family: Further insights for its origin, expansion, and diversification. *Front. Plant Sci.* 13. doi: 10.3389/fpls.2022.994567

Yant, L., Collani, S., Puzey, J., Levy, C., and Kramer, E. M. (2015). Molecular basis for three-dimensional elaboration of the *Aquilegia* petal spur. *Proc. R. Soc B.* 282, 20142778. doi: 10.1098/rspb.2014.2778

Yuan, Z., Gao, S., Xue, D. W., Luo, D., Li, L. T., Ding, S. Y., et al. (2009). *RETARDED PALEA1* controls palea development and floral zygomorphy in rice. *Plant Physiol.* 149, 235–244. doi: 10.1104/pp.108.128231

Zhang, F., Rossignol, P., Huang, T., Wang, Y., May, A., Dupont, C., et al. (2020). Reprogramming of stem cell activity to convert thorns into branches. *Curr. Biol.* 30, 2951–2961.e5. doi: 10.1016/j.cub.2020.05.068

Zhao, Y., Broholm, S. K., Wang, F., Rijpkema, A. S., Lan, T., Albert, V. A., et al. (2020). TCP And MADS-box transcription factor networks regulate heteromorphic flower type identity in *Gerbera hybrida*. *Plant Physiol.* 184, 1455–1468. doi: 10.1104/pp.20.00702

Zhao, Y., Pfannebecker, K., Dommes, A. B., Hidalgo, O., Becker, A., and Elomaa, P. (2018). Evolutionary diversification of CYC/TB1-like TCP homologs and their recruitment for the control of branching and floral morphology in papaveraceae (basal eudicots). *New Phytol.* 220, 317–331. doi: 10.1111/nph.15289

Zhao, Y., Su, X., Wang, X., Wang, M., Chi, X., Aamir Manzoor, M., et al. (2021). Comparative genomic analysis of TCP genes in six rosaceae species and expression pattern analysis in *Pyrus bretschneideri*. *Front. Genet.* 12. doi: 10.3389/fgene.2021.669959

Zheng, K., Ni, Z., Qu, Y., Cai, Y., Yang, Z., Sun, G., et al. (2018). Genome-wide identification and expression analyses of TCP transcription factor genes in *Gossypium barbadense*. *Sci. Rep.* 8, 14526. doi: 10.1038/s41598-018-32626-5

Zheng, Y., Zhao, L., Gao, J., and Fei, Z. (2011). iAssembler: a package for *de novo* assembly of Roche-454/Sanger transcriptome sequences. *BMC Bioinf.* 12, 453. doi: 10.1186/1471-2105-12-453

Zhou, Y., Zhang, D., An, J., Yin, H., Fang, S., Chu, J., et al. (2018). TCP Transcription factors regulate shade avoidance *via* directly mediating the expression of both *PHYTOCHROME INTERACTING FACTOR*s and auxin biosynthetic genes. *Plant Physiol.* 176, 1850–1861. doi: 10.1104/pp.17.01566

frontiers | Frontiers in Plant Science

TYPE Original Research
PUBLISHED 01 December 2022
DOI 10.3389/fpls.2022.990221

OPEN ACCESS

EDITED BY
Dongfang Wang,
Spelman College, United States

REVIEWED BY
Yang Zhu,
Zhejiang University, China
Hantao Wang,
Institute of Cotton Research (CAAS), China
Farrukh Azeem,
Government College University, Faisalabad, Pakistan
Hai Du,
Southwest University, China
Lu Long,
Henan University, China

*CORRESPONDENCE
Zhiying Ma
mzhy@hebau.edu.cn

†These authors have contributed equally to this work

SPECIALTY SECTION
This article was submitted to Plant Development and EvoDevo, a section of the journal Frontiers in Plant Science

RECEIVED 09 July 2022
ACCEPTED 02 November 2022
PUBLISHED 01 December 2022

CITATION
Chen L, Yan Y, Ke H, Zhang Z, Meng C, Ma L, Sun Z, Chen B, Liu Z, Wang G, Yang J, Wu J, Li Z, Wu L, Zhang G, Zhang Y, Wang X and Ma Z (2022) *SEP*-like genes of *Gossypium hirsutum* promote flowering *via* targeting different loci in a concentration-dependent manner. *Front. Plant Sci.* 13:990221. doi: 10.3389/fpls.2022.990221

SEP-like genes of *Gossypium hirsutum* promote flowering *via* targeting different loci in a concentration-dependent manner

Liting Chen†, Yuanyuan Yan†, Huifeng Ke, Zihao Zhang, Chengsheng Meng, Limei Ma, Zhengwen Sun, Bin Chen, Zhengwen Liu, Guoning Wang, Jun Yang, Jinhua Wu, Zhikun Li, Liqiang Wu, Guiyin Zhang, Yan Zhang, Xingfen Wang and Zhiying Ma*

State Key Laboratory of North China Crop Improvement and Regulation/North China Key Laboratory for Crop Germplasm Resources of Education Ministry/Key Laboratory for Crop Germplasm Resources of Hebei, Hebei Agricultural University, Baoding, China

SEP genes are famous for their function in the morphological novelty of bisexual flowers. Although the diverse functions of *SEP* genes were reported, only the regulatory mechanisms underlying floral organ development have been addressed. In this study, we identified *SEP*-like genes in *Gossypium* and found that *SEP3* genes were duplicated in diploid cotton varieties. *GhSEP4.1* and *GhSEP4.2* were abundantly transcribed in the shoot apical meristem (SAM), but only *GhSEP4.2* was expressed in the leaf vasculature. The expression pattern of *GhSEP*s in floral organs was conserved with that of homologs in *Arabidopsis*, except for *GhSEP2* that was preponderantly expressed in ovules and fibers. The overexpression and silencing of each single *GhSEP* gene suggested their distinct role in promoting flowering *via* direct binding to *GhAP1* and *GhLFY* genomic regions. The curly leaf and floral defects in overexpression lines with a higher expression of *GhSEP* genes revealed the concentration-dependent target gene regulation of GhSEP proteins. Moreover, GhSEP proteins were able to dimerize and interact with flowering time regulators. Together, our results suggest the dominant role of *GhSEP4.2* in leaves to promote flowering *via* *GhAP1-A04*, and differently accumulated GhSEP proteins in the SAM alternately participate in forming the dynamic tetramer complexes to target at the different loci of *GhAP1* and *GhLFY* to maintain reproductive growth. The regulatory roles of cotton *SEP* genes reveal their conserved and diversified functions.

KEYWORDS

SEP-like gene, *Gossypium*, flowering time control, cotton, concentration-dependent regulation

Introduction

Flowering is critical for angiosperms to evolve into the largest land plant lineage. The origin of this plant morphological novelty has been connected to the expansion of MADS-box genes during evolution. MADS-box proteins and their cofactors contribute to a large protein–protein interaction (PPI) network that is essential to virtually every aspect of plant reproductive development (Theissen, 2001; Smaczniak et al., 2012; Theissen et al., 2016).

The synteny studies of MADS-box genes across the plant kingdom have identified angiosperm-specific MADS-box gene clades including *FLOWERING LOCUS C* (*FLC*)-, *SQUAMOSA* (*SQUA*)-, and *SEPALLATA* (*SEP*)-like genes that share a common origin of gymnosperm *AGAMOUS-LIKE6* (*AGL6*)-like genes (Ruelens et al., 2013; Zhao et al., 2017). *SEP*-like genes encode the floral E-function proteins serving as hubs within the MADS PPI network to drive the formation of distinct tetrameric complexes that are proposed to facilitate the origin of angiosperm flowers (Theissen and Saedler, 2001; Zahn et al., 2005; Theissen and Melzer, 2007; Ruelens et al., 2017).

SEP genes participate in every step of reproductive growth ranging from the initiation of inflorescence meristems to the determination of floral organs. In *Arabidopsis*, four *SEP* genes function redundantly according to the severe developmental defects of *sep* multiple mutants rather than single mutants (Pelaz et al., 2000; Ditta et al., 2004). All floral organs are converted to sepals in the *sep1 sep2 sep3* triple mutant or show leaf-like structures in the *sep1 sep2 sep3 sep4* quadruple mutant, whereas they are not significantly perturbated in the *sep1 sep2 sep4* mutant (Pelaz et al., 2000; Ditta et al., 2004). The phenotypic variations of *SEP* mutants prove the role of *SEP4* in sepal determination and the dominant role of *SEP3* in determining the inner three whorls of a flower. These four proteins are capable to assemble other MADS-box proteins to form homotetrameric or heterotetrameric complexes that recognize two distanced CArG-boxes, the consensus MADS-domain binding motif (Immink et al., 2009; Melzer et al., 2009; Jetha et al., 2014). *FLORAL BINDING PROTEIN2* (*FBP2*) and *FBP5* (*SEP*-like genes in *petunia*) are required for B, C, and D genes to specify petal, stamen, carpel, and ovule development (Vandenbussche et al., 2003b). The *SEP* homologous in rice, tomato, soybean, birch, poplar, orchid, and lotus has been reported to participate in floral organogenesis and the identity of floral and inflorescence meristem (Pnueli et al., 1994; Lemmetyinen et al., 2004; Cseke et al., 2005; Cui et al., 2010; Gao et al., 2010; Huang et al., 2014; Pan et al., 2014; Morel et al., 2019; Lin et al., 2020).

Although the plant homeotic E class genes are highly conserved in flower development, plenty of evidence suggests a functional diversity of *SEP*-like genes. In *Arabidopsis*, *SEP3* is expressed in the floral organs of the inner three whorls, while the expression of *SEP1*, *SEP2*, and *SEP4* is activated earlier than *SEP3* in the floral meristem before the emergence of the organ primordia, and *SEP4* is detectable in all above-ground vegetative organs (Ma et al., 1991; Flanagan and Ma, 1994; Ditta et al., 2004). The temporal and spatial expression differences suggest the roles of *SEP* genes in regulating plant growth, which is in line with the early flowering and terminal flower phenotypes of *35S:SEP3* (Pelaz et al., 2001; Castillejo et al., 2005). Some *SEP3*-like genes promote flowering when constitutively expressed in *Arabidopsis* or tobacco including *FBP2*, *TaMADS1*, *LILY MADS BOX GENE3* (*LMADS3*), *OsMADS7/8*, *BpMADS1*, and *NsMADS3* (Kang et al., 1997; Jang et al., 1999; Elo et al., 2001; Ferrario, 2003; Tzeng et al., 2003; Zhao et al., 2006), whereas the silencing or knockdown of *SEP3*-like genes rarely causes changes in flowering time except the late flowering phenotype caused by the simultaneous silencing of *OsMADS7* and *8* (Cui et al., 2010). However, the function of *SEP1/2/4*-like genes in flowering time control is rarely reported. The *SEP1/2* homolog in poplar (*PTM3*) promotes tobacco flowering when overexpressed (Cseke et al., 2005). The overexpression of *PlacSEP* genes from *Platanus acerifolia* in *Arabidopsis* consistently promote floral transition except for *PlacSEP1.2* (Zhang et al., 2017). IiSEP4 in *Isatis indigotica* promotes the flowering of *Arabidopsis via* its interaction with the SHORT VEGETATIVE PHASE (SVP) to upregulate *FLOWERING LOCUS T* (*FT*) expression (Pu et al., 2020). The molecular mechanism of *SEP* genes in flowering time control is still unclear.

MADS box proteins form different complexes that perform diverse functions. The floral quartet model (FQM) poses the floral organ specification that is built on the tetrameric complexes glued by SEP proteins with different ABCD transcription factors to finely determine each whorl of a flower (Theissen et al., 2016). Dynamic tetramers with different binding affinity respond for the differential target gene regulation (Jetha et al., 2014). The broader involvement of SEP3 than SEP4 is supported by that SEP3 is capable to bind to a wider range of distance between two CArG-box motifs (Jetha et al., 2014). Furthermore, a large-scale analysis of protein interactions in *Arabidopsis* suggests that flowering time regulators, such as SVP, SUPPESSOR OF OVEREXPRESSION of CO 1 (SOC1), AGAMOUS-LIKE24 (AGL24) and APETALA1 (AP1), interact with SEP3 or SEP2 to form ternary complexes (De Folter et al., 2005; Immink et al., 2009). Protein interactions between SEPs and flowering time regulators are also identified in other species (Leseberg et al., 2008; Pu et al., 2020). The *SVP*-like genes are also regulated by SEP3 homologs in *Arabidopsis* and rice (Kaufmann et al., 2009; Khanday et al., 2016). Chromatin immunoprecipitation sequencing (ChIPSeq) data reveal the same binding loci of SEP3 as AP1 to the *SOC1* promoter (Liu et al., 2007; Kaufmann et al., 2009), suggesting a regulation of SEP3 and AP1 on *SOC1* transcription. Moreover, floral patterning is regulated by flowering time genes *SOC1*, *SVP*, and *AGL24*, targeted by SEP3 (Liu et al., 2009). These fragments

indicate a complex regulation of flowering time genes and *SEP* genes, which is essential for sequential developmental regulation from vegetative to reproductive growth.

Cotton fiber is the backbone of textile. Fiber development is the last step of cotton reproductive growth in which sequential development determines the success of fiber production. Early-maturing cotton is characterized by a short growth period, dwarf and compact plant architecture. They are becoming increasingly important for farmers to improve economic benefits through mechanical harvesting and double cropping. Early maturity is an important target trait of cotton breeding, and studies on flowering are the key to breed early-maturity varieties. The flowering time integrators of *FT*, *SOC1*, and *LEAFY (LFY)* play conserved functions to promote flowering in *Gossypium hirsutum* (Li et al., 2013; Liu et al., 2021; Ma and Yan, 2022). Genes involved in the photoperiod and gibberellin synthesis were reported to regulate cotton flowering time (Hao et al., 2021; Li et al., 2021a; Li et al., 2022). The MYB transcription factor (*GhAPL*) and epigenomic regulation (DNA methylation and histone deacetylation) are also involved in cotton flowering time control (Song et al., 2017; Zhang et al., 2021). However, the regulatory mechanism is largely unknown. In this study, we cloned cotton *SEP*-like genes from *G. hirsutum* (*GhSEP*s). The expression, overexpression, gene silencing, and interaction determination analysis found that GhSEPs (GhSEP proteins) promoted floral transition *via* interacting with their cofactors to form different protein tetramers that dynamically targeted the downstream genes directly *via* different loci, including *GhAP1* and *GhLFY*. This provides a molecular mechanism of how *SEP*-like genes regulate flowering time in cotton.

Materials and methods

Plant materials and growth condition

The cotton varieties CCRI50, Jiumian2, TM-1, and Yumian8 used in this study were preserved in Hebei Agricultural University and grown in a greenhouse (16 h light/8 h dark, 28°C day/25°C night) for experiments. The TM-1 variety was grown for tissue-specific analysis. The roots of the seedlings at the cotyledon stage and the stem, leaf, and SAM of seedlings at two true leaf stages (TLSs) were sampled, respectively. The calycle, sepal, petal, stamen, pistil, and ovule were collected 0 day postanthesis (DPA). Fibers were separated from ovules at 5 DPA. Two early-maturity cotton varieties CCRI50 [whole growth period (WGP) in Yellow River Basin Region (YRBR) is 110 days] and Jiumian2 (WGP in YRBR is 114 days) and two late-maturity cotton varieties TM-1 (WGP in YRBR is 135 days) and Yumian8 (WGP in YRBR is 136 days) were used for temporal expression analysis. A total of 10 shoot apexes were collected, respectively, at two, three, four, and five TLSs. The *Arabidopsis* and tobacco plants were grown in a plant growth chamber under 16 h light/8 h dark, 22°C. The whole seedlings of *Arabidopsis* homozygous plants were collected for expression analysis. All samples were immediately frozen in liquid nitrogen for further analysis.

Identification and sequence analysis of *SEP* genes

The four *Arabidopsis* SEP1/2/3/4 protein sequences were downloaded from the TAIR (https://www.arabidopsis.org/) and then blast against the published genomes of *G. hirsutum* on CottonFGD (https://cottonfgd.org/). The protein sequences and functional annotations were filtered for the protein family database (Pfam) identifiers of the MADS and K domains (PF00319 and PF01486), respectively. The candidate *GhSEP*s were confirmed with HMMER 3.0 and the Batch CD-Search service. The homologous genes of *SEP* in *Gossypium* (*G. raimondii*, *G. arboretum*, and *G. barbadense*) were determined in the same way.

The phylogenetic trees were constructed by MEGA 7.0 using the neighbor-joining (NJ) method with 1,000 bootstrap replications and default parameters and then displayed with the online iTOL tool (https://itol.embl.de/) (Kumar et al., 2016; Letunic and Bork, 2019). Segmental and tandem duplications were detected by MCScanX with default parameters. Homologous genes between the At and Dt subgenomes were determined using the bidirectional best hit method in BLAST. The duplication events were fetched and then displayed with TBtools (Chen et al., 2020).

Expression analysis

Plant total RNA was extracted using RNA Easy Fast Plant Kit (TIANGEN Beijing, China). DNase treatment was performed with RNase-free DNase (TIANGEN, Beijing, China) before purification. The cDNA was synthesized using cDNA Synthesis SuperMix (TRANS, Beijing, China). Gene transcription was detected by quantitative real-time PCR (qPCR) using AugeGreen^{TM} Master Mix for HRM (US EVERBRIGHT, Suzhou, China) on the ABI 7500 PCR Detection System (USA). Gene-specific primers for qPCR were verified for its specificity according to the single peak in the melting curve and are listed in Table S1. The relative expression level was calculated using the $2^{-\triangle Ct}$ formula. The expression was normalized to *AtTUB2* (AT5G62690) in *Arabidopsis* and *GhHis3* (GhM_D03G0424.1) in cotton and shown as relative values to the maximal gene expression level set at 100%. Three biological repeats were applied on each sample, and three technical repeats were performed on each reaction. The standard deviation (SD) of three biological repeats was calculated. R.E.L. stands for the relative expression level.

Construction of *Arabidopsis* transgenic lines

The coding regions of *GhSEP*s were cloned (primers listed in Table S1) and purified by the E.Z.N.A.® Gel Extraction Kit (Omega Bio-tek, Norcross, Georgia, USA). The resulting fragments were ligated into vector *pGreen0229* with a 35S promoter. The constructs were introduced into *Agrobacterium tumefaciens* strain GV3101 and transformed to *Arabidopsis* wild-type (WT) plants (Columbia) using the floral dip method. For each *GhSEP* gene, at least 25 T1 individual lines were obtained and confirmed by genotyping for the exogenous fragment. Then, five homozygous T3 lines were randomly selected and saved for a detailed observation of phenotypes. Expression analysis was performed on the seedlings of homozygous plants.

GUS analysis

The 2kb promoter sequence of each *GhSEP* was cloned and, finally, the genome regions of *GhSEP1A*, *GhSEP2D*, *GhSEP3.1A*, *GhSEP4.1D*, and *GhSEP4.2D* were obtained and inserted into the *pGreen-GUS* vector to generate *pro:GhSEP-GUS* constructs. Then, the construct was transformed into *Arabidopsis* using the methods described above. The homozygous lines were used for the histochemical assays of GUS activity. Different tissues were collected for GUS staining, including 13-day-old seedlings and cauline leaves, inflorescence, and floral organs from 6-week-old plants. Samples were immersed in the staining solution (Coolaber, Beijing, China) and incubated at 37°C overnight. Then, the samples were decolored in 70% (v/v) ethanol twice until the negative-control material (WT) turned white. Stained and cleared specimens were visualized and photographed using a stereoscope (AxioCam ICc 5; Carl Zeiss, Jena, Germany).

Subcellular location

To elucidate the subcellular localization of GhSEP proteins, the coding region without a stop codon was fused with GFP to generate a *35S:GhSEP-GFP* construct. *A. tumefaciens* strain GV3101 carrying plasmid *35S:GhSEP-GFP* was infiltrated into the abaxial surface of leaves of 4-week-old *N. benthamiana* plants. The infiltrated leaves were detected for GFP fluorescent by a confocal microscope (FV10i; Olympus, Tokyo, Japan) after 48 h infiltration. The cell nuclei were indicated by staining with 40,6-diamidino2-phenylindole (DAPI).

Virus-induced gene silencing

Due to the similarity of the *GhSEP*s' coding region, we chose the 3'UTR region (265/268/263/242/259-bp DNA fragment of *GhSEP1/GhSEP2/GhSEP3.1/GhSEP4.1/GhSEP4.2*) for PCR amplification. The fragments were inserted into the tobacco rattle virus (TRV) binary vector *pYL156* (*pTRV2*). In addition, the *pTRV1* and *pTRV2:GhSEP* vectors were coinfiltrated into the cotyledons of cotton CCRI50 to generate more than 40 individual silencing lines for each *GhSEP* gene. The same number of negative control plants were meanwhile generated by the infiltration of *pTRV1* and *pTRV2* empty vectors. To estimate the silencing effect, *pTRV : CLA1* was applied as a positive control. The expression of each *GhSEP* gene was detected in the SAM from randomly selected five silencing plants and five control plants when the photobleaching phenotype was obvious in the positive control (Figure S1). The gene expression was calculated as $2^{-\triangle Ct}$ normalizing to *GhHis3*. The SAM of another five silencing and negative-control plants were collected at four TLSs for the freezing section. The remaining plants were grown for the observation of phenotypes that were statistically analyzed with at least 20 plants. The experiments were repeated three times, and the SD of the silencing effect was calculated with three biological repeats using Student's t-test.

Freezing and paraffin section

The SAM of VIGS plants were embedded in Optical Cutting Temperature (OCT) compound (Leica Wetzlar, Germany) and fast-frozen in liquid nitrogen. Then, the samples were cross-sectioned by the freezing microtome (7500; Leica, Wetzlar, Germany) and the serial sections were expanded on a plus on a slide (CITOGLAS, Beijing, China) followed by observation under a microscope (DM2500; Leica Wetzlar, Germany).

The SAM of the early- and late-maturity cotton mentioned above was sampled and dehydrated in ethanal serial solutions (from 20% (v/v) to 100%). The tissues were visualized by adding eosin in 70% ethanal. Then, the tissues were incubated in a serial solution of ethanal/histonclear and histonclear/paraffin chips. The samples were finally embedded in the paraffin for section using a microtome (Leica, HistoCore AUTOCUT, Germany). The paraffin ribbon was expanded on plus on slides, and the paraffin was removed by a serial solution of ethanal/histonclear. The morphological characteristics of the SAM at each period were recorded and photographed under a microscope (DM2500; Leica, Germany).

Protein interaction assays

The coding regions of candidate genes were cloned into *pGADT7* (AD) and *pGBKT7* (BD) vectors (Clontech, San Francisco, California, USA). The two-hybrid assay was performed according to the Matchmaker® Gold Yeast Two-Hybrid System (Clontech San Francisco, California, USA).

The open reading frames (ORFs) of full-length genes were inserted into separate *pSAT1A-nEYFP-N1* and *pSAT1-cEYFP-C1-B* vectors and then transformed into *Agrobacterium*

(GV3103). These *Agrobacteria* were coinfiltrated into *Nicotiana benthamiana* leaves. The florescence signals were detected under confocal microscopy (FV10i; Olympus, Tokyo, Japan).

ChIP assays

The coding region of *GhSEP2* and *GhSEP4.2* were cloned into a *35S:-6HA* vector (pGreen). The mesophyll protoplasts transient expression system (Li et al., 2021b) was applied for the ChIP assay. The fifth leaves and shoot apexes from TM-1 at five TLSs were collected and sliced into fine filaments followed by gentle digestion for 9 h (1.5% cellulose, 0.4% macerozyme, 0.5 mol·L^{-1} mannitol, 20 mmol·L^{-1} KCl, 20 mmol·L^{-1} MES, 10 mmol·L^{-1} $CaCl_2$, and 1.0 g·L^{-1} BSA) to extract protoplasts. The plasmids *35S:GhSEP2-6HA* and *35S:GhSEP4.2-6HA* were transiently expressed in the protoplast by 40% PEG under isotonic pressure maintained by 0.5 mol·L^{-1} mannitol. Then, the protoplasts were cultured with a WI buffer (4 mmol·L^{-1} MES, 0.5 mol·L^{-1} mannitol, 20 mmol·L^{-1} KCl) in the dark for 16 h. More than 10^{-15} million cells were collected and fixed in 1% formaldehyde on ice for 20 min. The nuclei were isolated and sonicated to produce DNA fragments approximately 500 base pairs. Nucleoprotein was then immunoprecipitated by an anti-HA antibody conjugated with agarose (Sigma, St. Louis, Missouri, USA). The DNA fragments were purified by the E.Z.N.A.® Gel Extraction Kit (Omega Bio-tek, USA). Western blot was applied to detect the fusion protein using an HA antibody (Invitrogen, USA). The relative enrichment of each fragment was determined by qRT-PCR. Primers used for the ChIP assay are listed in Table S1. The enrichment fold of each fragment was calculated first by normalizing the amount of a target DNA fragment against *GhHis3* as an internal control and then by normalizing the value for transgenic protoplasts against non-transformed protoplasts. The SD of three biological repeats was calculated.

Results

Identification of *GhSEP*s

The MADS box family is highly conserved in the MADS-box domain. To distinguish *SEP*-like genes from other MADS family members in *Gossypium*, the four *Arabidopsis* SEP protein sequences were blasted against the published genomes. The results were filtered referring to the sequence similarity and the identified members of the cotton MADS-box family (Ren et al., 2017; Nardeli et al., 2018). Then, the selected sequences were confirmed by the phylogenetic tree constructed with SEP homologs (Table S2) and named according to the members in the same subgroup (Figure 1A and Table S3). Finally, 12 *SEP*-like genes were identified and distributed equally in the At and Dt subgenomes, which were named according to the sequence similarity (Figure S2A and Table S4). Consistent with the protein sequence similarity of each homologous gene pair in the Gh genome, their gene structures were conserved (Figures S2B, C). The GhSEPs contained MADS-box and K-box domains, and their C-terminals possessed a characterized SEP I motif and SEP II motif (Figures S2A, D) (Zahn et al., 2005; Pan et al., 2014). We also found conserved motifs between the cotton and *Arabidopsis* SEP1/2 and SEP3 proteins, respectively, designated as the SEP1 motif and SEP3 motif, respectively (Figure S2A).

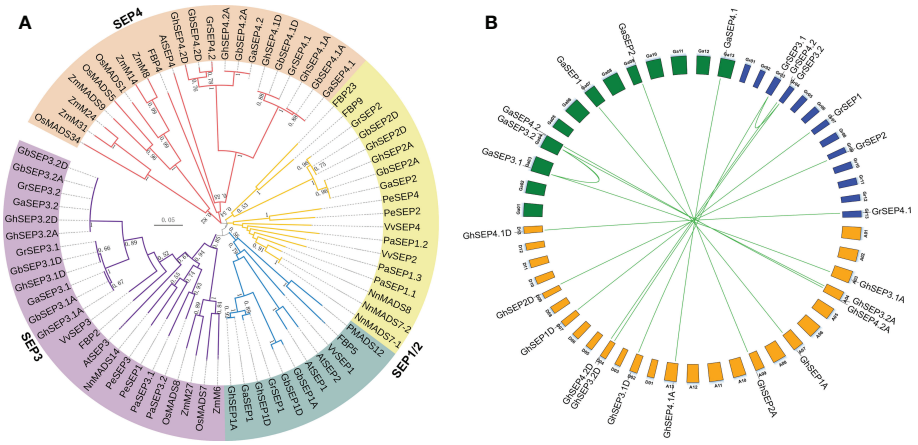

FIGURE 1
Evolution analysis of cotton SEP-like genes. **(A)** Phylogenetic relationships of SEP-like proteins from *Gossypium barbadense, G. hirsutum, G. raimondii, G. arboreum, Arabidopsis thaliana, Petunia hybrid, Oryza sativa, Phalaenopsis equestris, Vitis vinifera, Zea mays, Nelumbo nucifera*, and *Platanus acerifolia*. **(B)** Duplication events among SEP genes in diploid and tetraploid cotton varieties. Curves indicate segmental duplications. Lines link homologous genes between diploid and tetraploid genomes.

The phylogenetic tree was clustered into four groups (Figure 1A). The SEP3 group was closer to the SEP1 group, and the two groups were then rooted with the SEP2 group. The SEP4 group was located in a single evolutionary branch. Only the SEP3 group contained genes from all the chosen species, and other *SEP*-like genes in different species were clustered irregularly to other groups, suggesting that *SEP3*-like genes were mostly conserved in the angiosperm. Interestingly, *SEP4*-like genes in *Gossypium* were closely clustered with the rest of monocot *SEP*-like genes except for *SEP3*, indicating a different evolution of *SEP4*-like genes. These results supported that *SEP*-like genes originated from a single MADS gene and then extended during the whole genome duplication events followed by the evolution of diverse functions (Smaczniak et al., 2012; Chen et al., 2017; Zhao et al., 2017). To further elucidate the evolution of *SEP*s in the *Gossypium* species, their synteny was analyzed. The results showed the segmental duplications of *SEP3* genes in the diploid Gr and Ga genomes (Figure 1B), and the diploid *SEP3* sequences were highly similar to the *SEP3* genes in the tetraploid Gh genome (Figure S2A). Therefore, we speculate that *SEP* genes in the tetraploid Gh genome originated from their diploid progenitors.

Spatial and temporal expression of *GhSEP*s

The expression pattern of *GhSEP*s was studied first using the transcriptomic data obtained from CottonFGD (Hu et al., 2019). The transcripts of *GhSEP* homologies from At and Dt subgenomes displayed a consistent expression pattern in the heat map (Figure S3A). *GhSEP1/2/3.1* were highly transcribed during fiber development, whereas *GhSEP4*s were undetectable in the ovule or fiber. *GhSEP1* transcribed relatively higher during seed germination, and *GhSEP4.1* could be induced by cold, drought, and salt stress. However, the transcriptomic data lacked information about the *GhSEP3.2* gene, so we further compared the transcription of *GhSEP* genes in our unpublished transcriptomic data of the leaf and SAM during cotton floral transition (Figure S3B). The similar expression of *GhSEP* homologies from At and Dt subgenomes was also observed. Additionally, *GhSEP* genes displayed higher expression after floral transition (at five TLSs), especially in the SAM. The transcripts of *GhSEP3.2A* and *D* were not expressed in the leaf and SAM. The expression of *GhSEP*s were further examined in vegetative and reproductive tissues. Due to the extraordinarily high sequence similarity of homologies in At and Dt subgenomes, their transcripts were detected together and shown as *GhSEP1*, *GhSEP2*, *GhSEP3.1*, *GhSEP4.1*, and *GhSEP4.2*. The expression pattern of *GhSEP*s was different in flowers from the outside to the inner whorl (Figure S3C), which is similar as their homologies in *Arabidopsis*. *GhSEP4.1* and *GhSEP4.2* were expressed in the calycle. Except for *GhSEP3.1*, the other *GhSEP*s were expressed in the sepal. All the *GhSEP*s participated in the development of the petal and stamen. Only *GhSEP3.1* showed considerable transcripts in the pistil. Noticeably, *GhSEP2* expression raised up in the fiber, suggesting a novel function of cotton *SEP* genes in fiber development. In the SAM, *GhSEP*s consistently displayed higher expression, especially *GhSEP4.1* and *GhSEP4.2* (Figure 2A). In addition, *GhSEP2* and *GhSEP3.1* transcription in the SAM was relatively lower. Only *GhSEP4.2* showed a much higher expression in the vegetative tissues of leaves. Since *SEP*-like genes have been shown to control flowering time, we monitored the expression of *GhSEP*s in developing seedlings. Before expression analysis, the cytological morphology of the SAM was observed in early- and late-maturity cottons to illustrate the occurrence of floral transition. The eminence of the SAM was obvious in the early-maturity cotton CCRI50 and Jiumian2 when the fourth true leaf flattened, while the eminence was just visible in the SAMs of TM-1 and Yumian8 at five TLSs, suggesting a proximate 5-day delay of the floral transition in late-maturity cotton varieties (Figure 2B). Consistent with the occurrence of floral transition, the expression of *GhSEP*s was upregulated at the four TLSs in the early-maturity cotton varieties, while their expression only increased slightly in late-maturity cotton varieties. The *GhSEP* expression level was gradually increased along with the floral transition (Figure 2C), suggesting that they promote flowering time. In line with this, a higher expression level of *GhSEP*s was detected in the early-maturity cotton varieties than the late ones during floral transition (Figure S3D). The transcription of *GhSEP*s in tissue and developing seedlings suggested redundant roles in floral organ development and flowering time control.

Furthermore, we cloned the 2 kb upstream promoters of *GhSEP1A, GhSEP2D, GhSEP3.1A, GhSEP4.1D*, and *GhSEP4.2D* whose coding regions were obtained for functional study. GUS reporter lines were constructed driven by these promoters to mimic a detailed expression of *GhSEP* genes in *Arabidopsis* (Figure 2D). GUS signals were only observed in the SAM in *pro:GhSEP1/2/3.1-GUS Arabidopsis* lines. *GhSEP4.2* was expressed in the vascular bundle. GUS signals in *pro:GhSEP4.1-GUS* were observed in the whole leaf. After bolting, GUS signals were all detected in cauline leaves, flowers, and siliques. Interestingly, *GhSEP4.1* and *GhSEP4.2* displayed a consistent expression pattern in the cauline leaf and sepal as in the true leaf. The GUS signal of *pro:GhSEP3.1-GUS* was strong in the reproductive organ. *GhSEP2* showed unique transcription in ovules consisting of the qPCR results. It worth noticing that the *GhSEP4.1* transcriptional level in *Arabidopsis* leaves shown by GUS staining is not consistent with the low expression level in TM-1 cotton leaves detected by qPCR (Figures 2A, D). The dynamic transcription of *GhSEP* genes in a plant life cycle indicated at least partially independent functions.

Then, the coding region of each *GhSEP* gene was cloned and overexpressed with GFP in the tobacco epidermal cells. Consistent

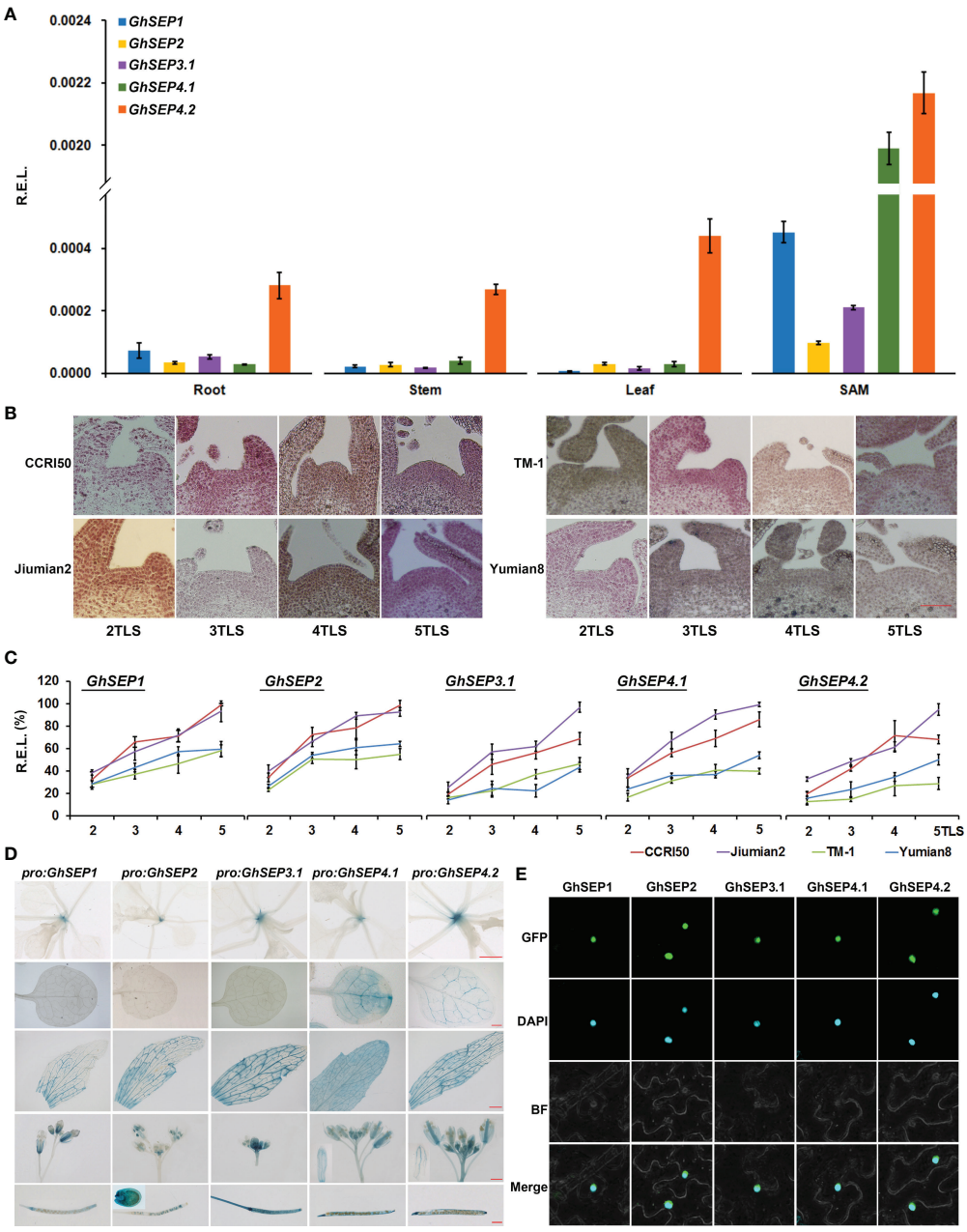

FIGURE 2
Expression patterns and subcellular localization of GhSEPs. **(A)** Expression of *GhSEP* genes in different tissues of TM-1. **(B)** Morphological changes of the shoot apical meristem (SAM) during the seedling development of early-(CCRI50 and Jiumian2) and late-maturity (TM-1 and Yumian8) varieties. Scale bar stands for 100 μm. **(C)** Temporal expression of *GhSEP*s in developing seedlings of the four varieties. **(D)** GUS activity in *pro:GhSEP-GUS* transgenic *Arabidopsis* plants in 15-day-old seedlings, cauline leaves, flowers, and seeds. Scale bars stand for 1 mm. **(E)** Subcellular localization of GhSEP-GFP proteins. *GhHis3* was used as internal controls for qPCR. Error bars denote standard deviation (SD).

with their roles as a transcription factor, the fluorescent signals of the GhSEPs-GFP were detectable in the nuclei (Figure 2E).

In summary, the overlapping and distinguished expression patterns of *GhSEP*s suggested functional redundancy and diversity. *GhSEP4*s might function dominantly during floral transition, and each *GhSEP* gene was likely to participate differently in the formation of each whorl of flowers. The prevalent expression of *GhSEP2* in ovule indicated a novel function.

*GhSEP*s promote flowering time

To elucidate the function of *GhSEP*s, their coding sequences were amplified and the resulting fragments shared the same sequences with *GhSEP1A, GhSEP2D, GhSEP3.1A, GhSEP4.1D*, and *GhSEP4.2D* after blasting against the *G. hirsutum* genome. Considering the high sequence similarity of *GhSEP* homologies in At and Dt subgenomes, the above sequences of *GhSEP* genes were overexpressed in *Arabidopsis* for functional study. There were more than 25 individual T1 lines of each *GhSEP* gene that flowered uniformly earlier than WT plants (Figures 3A, B). Some individuals even flowered with two rosette leaves (Figure S4A). Five lines of each transgene were randomly selected for transcriptional and phenotypic analysis. The results showed that the flowering time of transgenic plants reduced up to half of the WT plants (Figure 3B) and the flowering phenotype was closely associated with the expression levels in *35S:GhSEP*s (Figure 3C), suggesting that *GhSEP*s promoted flowering time in a dosage-dependent manner.

Next, due to the similarity of the *GhSEP*s' coding sequences, specific fragments from the 3' UTR of each *GhSEP* gene were amplified and constructed into the *pTRV* vector for the virus-induced gene silencing (VIGS) assay applied on an early-maturity cotton CCRI50 to silence the native *GhSEP* genes. The silencing effects were examined in the SAM (Figure 4A). VIGS caused a decreased expression of the relative gene in the silencing plants of *TRV : GhSEP3.1*, *TRV : GhSEP4.1*, and *TRV : GhSEP4.2.* However, the silencing of *GhSEP1* and *GhSEP2* was synchronal due to high sequence similarity. The silencing efficiency of each gene was above 70%. Compared with the control group, the silencing of *GhSEP*s delayed cotton squaring and flowering time (Figures 4B and S5A). The cross-section of the shoot apex at four TLSs demonstrated floral and inflorescence meristems of the control plants indicating the stage of reproductive growth, whereas the SAMs of *TRV : GhSEP*s were still flattened and only leaf primordia were observed, suggesting that the floral transition has not yet occurred (Figure 4C). A statistical analysis of the traits reflecting cotton maturity suggested that the silencing of *GhSEP*s resulted in a significant delay of maturity and the effects of *GhSEP3.1/4.1/4.2* were comparable (Figure 4D). The late-maturity phenotypes of *TRV : GhSEP1* and *TRV : GhSEP2*

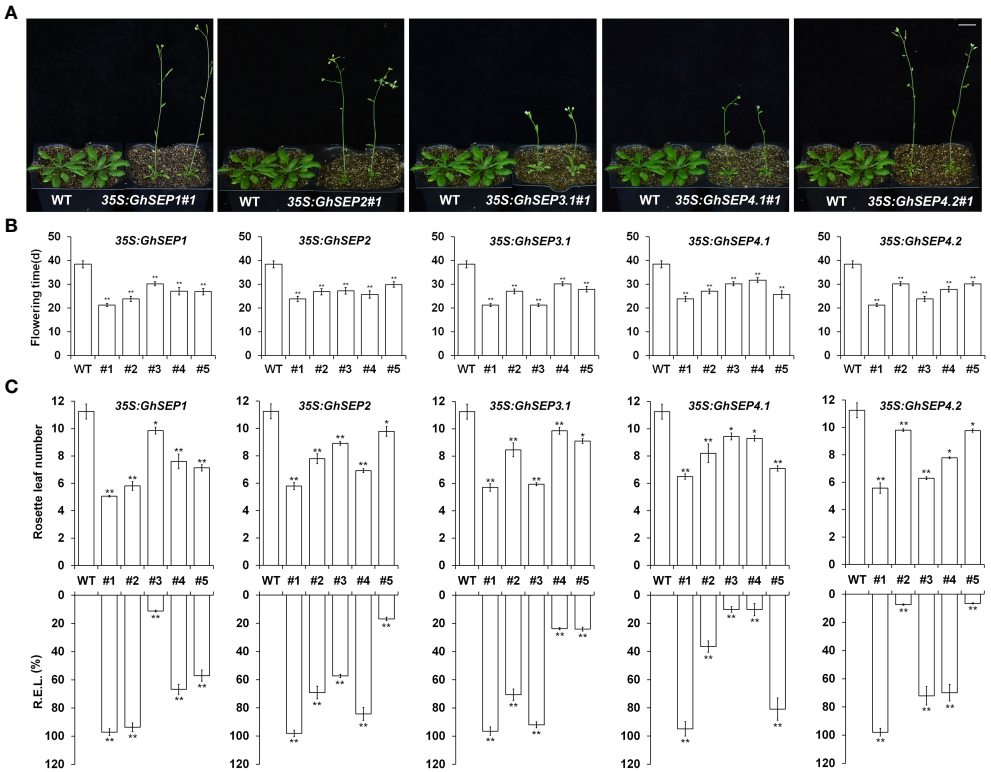

FIGURE 3
Phenotypes of *35S:GhSEP*s transgenic *Arabidopsis* plants. **(A, B)** *35S:GhSEP*s flowered earlier than wild-type (WT) plants under the long-day (LD) conditions. The same WT plants served as the controls of the transgenic plants for taking photos in A. Scale bar stands for 1 cm. **(C)** Upregulation of *GhSEP*s in independent *35S:GhSEP* transgenic plants is related to the degree of early flowering under LD conditions. Asterisks indicate significant differences (Student's *t*-test, $*p \leq 0.05$, $**p \leq 0.01$). Error bars denote SD.

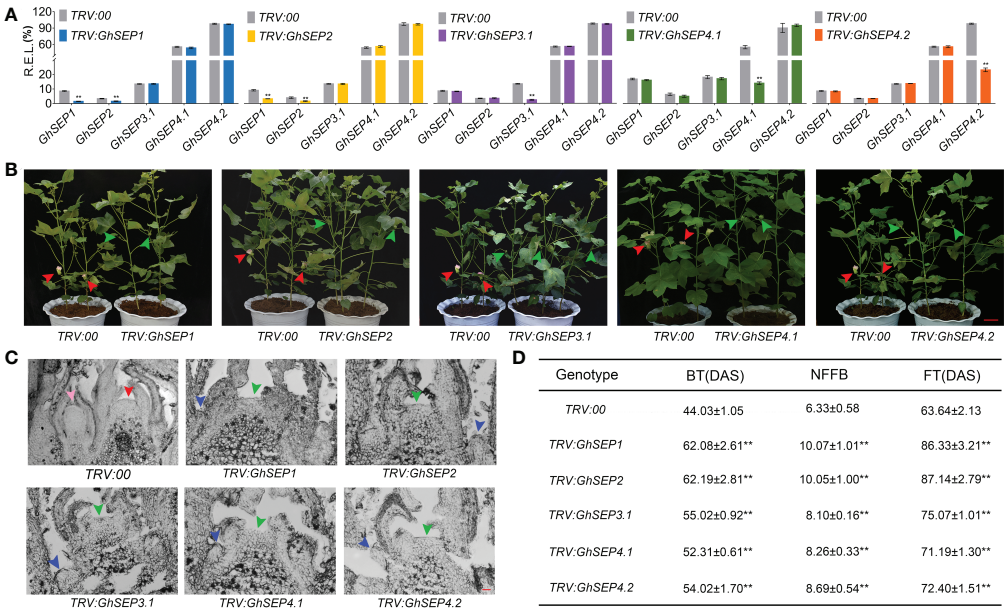

Genotype	BT(DAS)	NFFB	FT(DAS)
TRV:00	44.03±1.05	6.33±0.58	63.64±2.13
TRV:GhSEP1	62.08±2.61**	10.07±1.01**	86.33±3.21**
TRV:GhSEP2	62.19±2.81**	10.05±1.00**	87.14±2.79**
TRV:GhSEP3.1	55.02±0.92**	8.10±0.16**	75.07±1.01**
TRV:GhSEP4.1	52.31±0.61**	8.26±0.33**	71.19±1.30**
TRV:GhSEP4.2	54.02±1.70**	8.69±0.54**	72.40±1.51**

FIGURE 4
Phenotypes of virus-induced gene-silencing plants of *TRV : GhSEP*s. **(A)** Relative expression of each *GhSEP* gene in cotton silencing lines. Asterisks indicate significant differences according to Student's *t*-test at $p \leq 0.01$. Error bars denote SD. **(B)** Silencing of *GhSEP*s delayed the flowering of cotton. The green and red arrows represented the buds and flowers, respectively. The same control plants were used in the checking of the silencing plants of *GhSEP1*, *GhSEP3.1*, and *GhSEP4.2* for taking photos. Scale bar stands for 10 cm. **(C)** Section of the shoot apexes at four TLSs of control and silencing plants. The inflorescence meristem and floral meristem are labeled by red and pink arrows. Blue and green arrows point the young leaf and SAM. Scale bar stands for 1 mm. **(D)** Statistics of traits related to the early maturity of cotton silencing and control plants. Data were shown as the average ± SD. Asterisks indicate significant differences according to Student's *t*-test at $p \leq 0.01$. BT, budding time; NFFB, node of the first fruit branch; FT, flowering timing; DAS, days after sowing.

were more severe, which might be resulted from the synchronal silencing of *GhSEP1* and *GhSEP2*. These results described the participation of cotton *SEP*-like genes in floral transition in a dosage-dependent manner.

Overexpression of *GhSEP*s affects inflorescence development and leaf morphology

SEP genes are well known as the E function in floral development. Therefore, the organ morphological phenotypes were observed in the overexpression of *Arabidopsis* and the silencing of cotton plants. Some homozygous plants of *35S:GhSEP*s produced curly leaves (Figure S4B). The expression of GhSEPs in those lines were much higher compared with the lines that possessed normal rosette leaves and flowered later (Figure 3). However, the homozygous *35S:GhSEP*s consistently showed no significant perturbation of a flower (Figure S4C). Similarly, the silencing of any *GhSEP*s in the cotton plants had no effects on floral development (Figure S5B). However, some heterozygotes of the *Arabidopsis 35S:GhSEP*s T1 plants produced abnormal flowers with absent sepals from a leaf-like structure that was similar to bracts (Figure S4A). Moreover, terminal flowers were observed in some individuals. These plants flowered extremely early and failed to produce any seeds. These severe phenotypes could be caused by the higher expression level of any *GhSEP*s. These results suggested that *GhSEP*s acted in a dosage-dependent manner.

GhSEPs directly regulate *GhAP1* and *GhLFY*

To elucidate the regulatory mechanism of *GhSEP*s, the expression of flowering-time genes was first detected in *35S:GhSEP*s *Arabidopsis* plants. The transcription of *LFY* and *AP1* was dramatically upregulated in each of the *GhSEP* overexpression lines. In addition, the expression of the other flowering time regulators *FT*, *SOC1*, *CONSTANS* (*CO*), and *AGL24* was increased significantly (Figure S6). Although *GhSEP*s shed similar effects on *LFY* and *AP1* transcription, they upregulated the other detected genes differently in the overexpression lines. *GhSEP1* and *GhSEP4.1* were likely to perform similarly in flowering time control that *SOC1* expression change was weaker than *FT*, *CO*, and *AGL24*. *GhSEP2* had an even effect on the examined flowering time

genes. Only *FT* transcriptional increase was violent in the *35S:GhSEP3.1* lines. Additionally, *GhSEP4.2* regulated *FT* and *SOC1* at the similar level that was stronger than the regulation of *CO* and *AGL24*. The discrepancy of the effects of *GhSEP*s on flowering time regulators indicated the distinct roles of each *GhSEP* in flowering time control. Then, the expression trends of *LFY*, *AP1*, *FT*, and *SOC1* were monitored in *Arabidopsis* developing seedlings. *AP1* and *LFY* expression increased rapidly 5 days after germination of the *35S:GhSEP*s plants, while they remained at a relatively low level in the WT plants, suggesting that the floral transition occurred earlier in the *35S:GhSEP*s plants. However, the expression trends of *FT* and *SOC1* were similar in the *GhSEP* overexpression and WT plants, except for the *FT* expression trend in the *35S:GhSEP4.1* (Figure 5A). These results suggested that the upregulation of *SOC1* and *FT* in the *35S:GhSEP* plants might be indirect.

Furthermore, the expression of flowering time genes was analyzed in the *TRV : GhSEP* silencing plants (Figure 5B). Consistent with the expression change in *Arabidopsis*, the silencing of *GhSEP*s all caused significant expression decreases of *GhAP1* and *GhLFY*, among which the same expression variation was found in *TRV : GhSEP1* and *TRV : SEP2* that was greater than that in *TRV : GhSEP3.1* and *TRV : GhSEP4*s, which was probably due to the cosilencing effects on *GhSEP1/2*. However, *GhFT* and *GhSOC1* expression was undisturbed by the effective silence of *GhSEP*s (Figure S5C), which supported our speculation on the transcriptional increases of *SOC1* and *FT* in the *35S:GhSEP*s of *Arabidopsis*.

Therefore, *LFY* and *AP1* might be the downstream target genes of GhSEPs in the regulation of flowering time. To prove this, ChIP analysis was performed to examine the direct binding of GhSEPs to the *GhLFY* and *GhAP1* genomic DNA. In the upland cotton genome, there were four copies of *GhAP1* and two copies of *GhLFY* whose transcriptional regulation regions were different from each other. Thus, the CArG-box elements were predicted on their whole genome regions. The results showed that *GhAP1-A04* and *-D04* contained denser CArG-boxes, especially in the first introns (Figure 5C). Considering the higher expression of *GhSEP4.2* in cotton leaves (Figure 2A) and the specific expression of *GhSEP2* in the seed and fiber (Figure 2D and S3C), the DNA fragments bound with GhSEP2-HA and GhSEP4.2-HA were extracted from cotton protoplasts overexpressing the fusion proteins (Figure S7), respectively. The results suggested that GhSEP2 was strongly bound to the genomic region of *GhAP1-A04* around the start codon and the other two regions distributed in balance of the up- and downstream of the start codon (Figure 5D). The binding distribution of GhSEP2 to the *GhAP1-D04* was similar to that of *GhAP1-A04*, but the fold enrichment was quite lower than *GhAP1-A04*. Fold enrichments were also detected at a low level around the start codon of *GhAP1-A13* and the middle region of the first intron of *GhAP1-D13*. GhSEP2 was also strongly bound to *GhLFY-A07* at the end of second intron and weakly bound to the genomic region near the stat codon of *GhLFY-D07*. Different from GhSEP2, GhSEP4.2 did not bind to *GhAP1-D13* and displayed no binding superiority to the other *GhAP1* and *GhLFY*s. Two binding regions were detected located at the first and last introns of *GhAP1-A04* and 1.8 kb up- and downstream of the start codon of *GhLFY-A07*. GhSEP4.2 was bound to the transcription start region of *GhAP1-D04* and *GhAP1-A13* and the 1 kb upstream of the start codon in the *GhLFY-D07* genome. Additionally, it seemed that GhSEP2 binding affinity was stronger than GhSEP4.2, which is supported by *in vitro* EMSA results (Jetha et al., 2014), and GhSEPs were likely to loop DNA that was explained by the separated CArG-boxes in two binding sites (Melzer et al., 2009).

GhSEPs form a complex with flowering time regulators

DNA looping is formed with the binding of MADS tetramers (Theissen and Saedler, 2001). Hence, the protein interaction of GhSEPs were analyzed. First, we failed to study the dimerization between GhSEPs in two directions in yeast cells due to the strong self-activation of GhSEP2. Subsequently, the homodimers and heterodimers of GhSEPs were visualized by the bimolecular fluorescence complementation (BiFC) assay (Figure 6A). All the GhSEP proteins were capable to form heterodimers between each other, and homodimerizations were observed, except for GhSEP2. Then, the interaction between GhSEPs and flowering time regulators were tested, including GhAP1 (GhM_A13G0958), GhSOC1.4 (GhM_A11G0098), and GhSVP.5 (GhM_A12G1181). Strong interactions between GhSEPs and GhAP1, GhSOC1.4, and GhSVP.5 were detected both in the yeast two-hybrid assay and BiFC analysis (Figures 6B, C). These results suggested that GhSEPs were able to form tetramers with flowering time regulators and themselves.

Discussion

The function of *SEP*-like genes in flowering time control is preserved during evolution

Plant MADS-box transcription factors play essential roles in almost every developmental process. Many MADS-box genes have conserved functions across the angiosperms, but some have evolved novel functions in specific species. The morphological diversity of flower organs is closely related to functional divergence within the MADS-box genes. An evolutionary analysis of the MADS genes in plants points out a close link of *SEP*-like genes' origination with angiosperm evolution, especially in the formation of bisexual flowers (Zahn et al.,

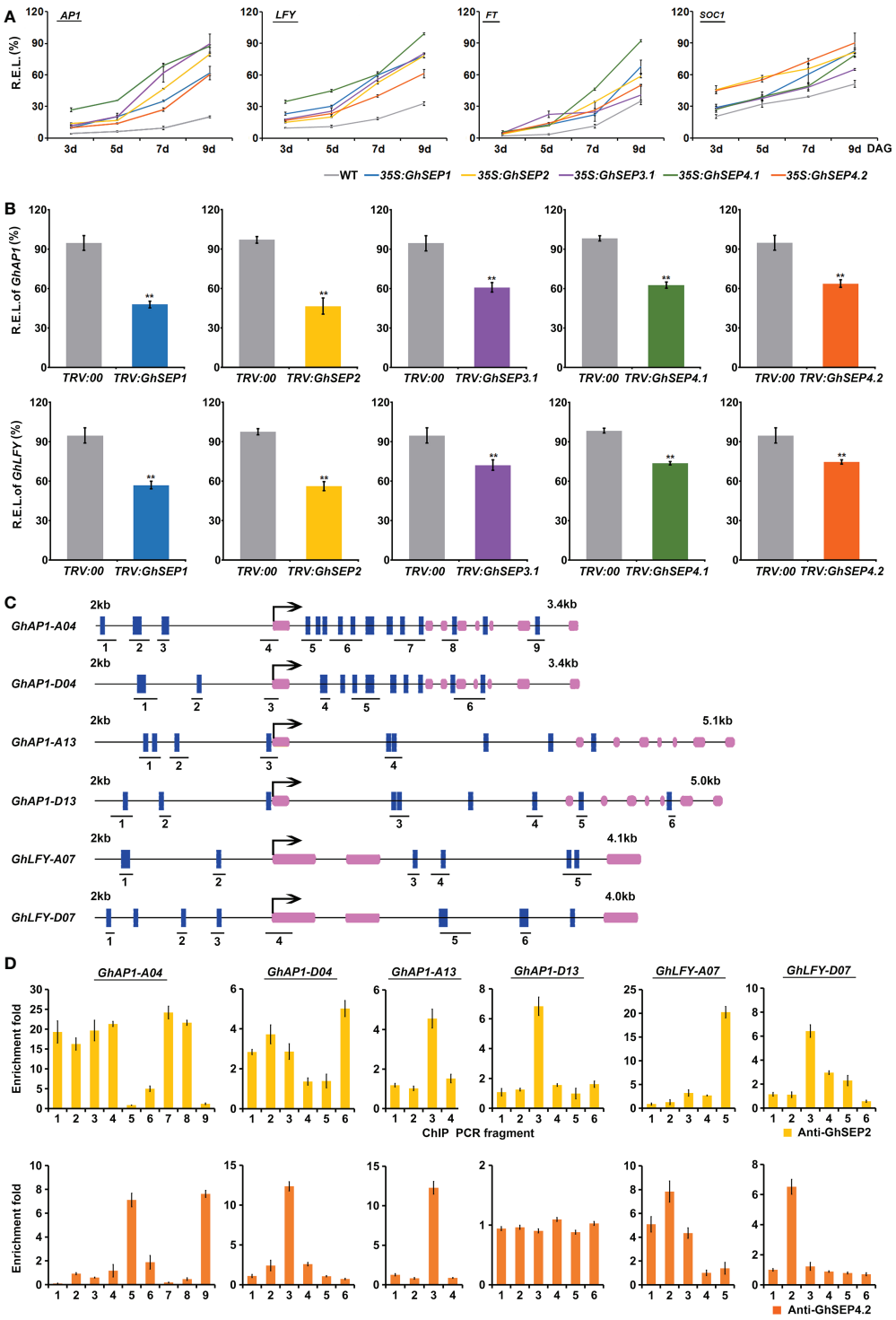

FIGURE 5
GhSEPs directly regulate *GhAP1* and *GhLFY*. **(A)** Temporal expression of *AtAP1*, *AtLFY*, *AtFT*, and *AtSOC1* in *Arabidopsis* developing seedlings of WT and *35S:GhSEP* plants. **(B)** Expression of *GhAP1* and *GhLFY* in cotton-silencing lines and control plants. Asterisks indicate significant differences according to Student's *t*-test at $p \leq 0.01$. **(C)** Prediction of the CArG box in the genome regions of *GhAP1* and *GhLFY*. Exons are represented by purple boxes, and the other genomic regions are represented by black lines. Blue boxes indicate the sites containing either a single mismatch or a perfect match to the consensus binding sequence (CArG-box) of MADS-domain proteins. The number under the schematic diagram means the DNA fragments designed for the ChIP analysis of the GhSEP binding site as shown in **(D)**. kb, kilobase. **(D)** ChIP analysis of GhSEP binding to the *GhAP1* and *GhLFY* genomic regions. Error bars denote SD.

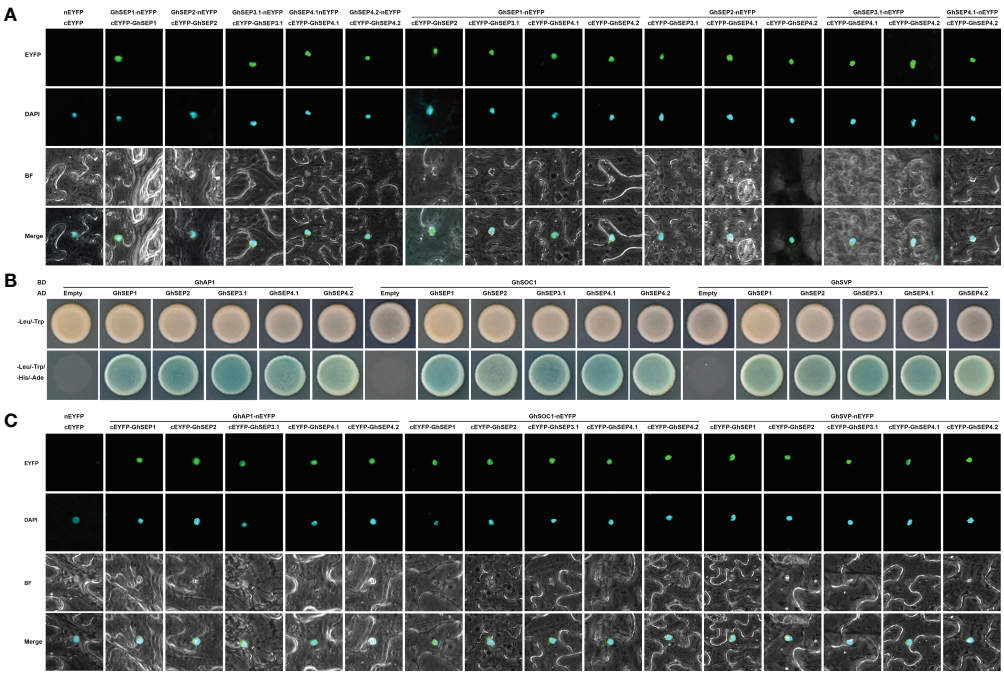

FIGURE 6
Protein interaction between GhSEP proteins and flowering time regulators. **(A)** Interaction between GhSEP proteins detected by the bimolecular fluorescence complementation (BiFC) assay. **(B)** Interaction of GhSEP proteins and flowering time regulators detected by the yeast two-hybrid assay. **(C)** Interaction of GhSEP proteins and flowering time regulators detected by the BiFC assay.

2005; Theissen and Melzer, 2007; Ruelens et al., 2017). The overexpression of cotton *SEP*-like genes affected inflorescence and floral development (Figure S4A), which is conserved in the angiosperm. Aside from floral development, the flowering time variation was observed in the overexpressing and silencing plants of a single *GhSEP* (Figures 3, 4), revealing the roles of *GhSEP*s in promoting flowering. However, the mutation or silencing of single *SEP*-like genes in *Arabidopsis*, petunia, orchid, rice, and tomato does not affect flowering time although an overexpression of them causes the early flowering of *Arabidopsis* (Ditta et al., 2004; Matsubara et al., 2008; Pan et al., 2014; Wu et al., 2018; Zhang et al., 2018). These phenotypes suggested that the function of *GhSEP*s in floral development is largely redundant, but their function in flowering time control is less redundant.

SEP-like genes share a most recent common ancestor with *AGL6* and *AP1* genes 296 MYA (Shen et al., 2019) and duplicated in the whole genome duplication event in flowering plants (Zhao et al., 2017). It could be observed in the phylogenetic tree of MADS-box genes that the lineages of *SEP*-, *SQUA*-, *FLC*-, and *AGL6*-like genes are nested within a strongly supported superfamily by evolutionary conserved tandem duplications between *SEP1* and *SQUA*, as well as *SEP3* and *FLC* (Ruelens et al., 2013; Zhao et al., 2017). Syntenic relationships are also supported by the conserved tandems of *SEP-SOC1* and *SEP-SVP* in the angiosperm (Zhao et al., 2017). The evolutionary evidence all points to a close relation of *SEP*-like genes with MADS flowering time regulators. The members of the *SOC1*-, *SVP*-, *FLC*-, and *SQUA*-like genes are generally the regulators of floral transition that determines the flowering time and reproductive success (Bowman et al., 1993; He, 2012). Additionally, the functional characterization of gymnosperm *AGL6*- and *SOC1*-like genes *CjMADS14* and *CjMADS15* show their conserved function in flowering time control (Katahata et al., 2014). Consistently, the clusters of *SVP*, *AG*, *AP1*, and *SOC1* genes diverge sequentially in this order to form the *SEP* genes in the lineage of cotton MADS genes (Nardeli et al., 2018), suggesting that cotton MADS transcription factors evolute conservedly. Therefore, we speculate that the function in the flowering time control of *GhSEP* genes was preserved from the ancestor during evolution.

It has always been considered that *SEP*-like genes in angiosperms are clustered into two groups: the SEP1/2/4 and SEP3 (Shen et al., 2019). However, cotton *SEP4* genes diverged independently with *AtSEP4* and monocot *SEP*-like genes other than *SEP3* orthologs (Figure 1A). In the *SEP4* clade, *OsMADS34*, *OsMADS1*, and *OsMADS5* contribute to the origin of distinct grass inflorescences and spikelets (Gao et al., 2010; Meng et al., 2017), whereas the other cotton *SEP* genes were clustered with *SEP1/2/3* orthologs that function as flowering time promoters

and floral organ determinators (Chung et al., 1994; Ferrario, 2003; Zhang et al., 2017; Lin et al., 2020). The sequence diversity and different conserved motifs in the C terminal of GhSEPs also supported the functional divergency (Figure S2) (Vandenbussche et al., 2003a). Consistently, the expression of each *GhSEP* gene differed spatially and temporally (Figure 2), suggesting that they have diverse functions. Hence, we propose that the neofunctionalization and redundancy that occurred following gene duplication jointly contribute to the functions of *GhSEP*s (Zahn et al., 2006).

GhSEP functions are dosage dependent

Dosage dependency is common in the regulation of quantitative traits. This principle coincided with the early flowering phenotype of *Arabidopsis* overexpression lines varied along with the expression level of *GhSEP*s (Figure 3C). The sterile *35S:GhSEP*s plants flowered with only two or fewer leaves (Figure S4A), which was reasonably caused by the excessive transcription levels of *GhSEP*s. Under these circumstances, floral defects were visible. In *Arabidopsis*, the inactivation of one *SEP1* allele in a *sep2 sep3* double-mutant background converts the normal flowers to severe abnormalities in ovule development (Favaro et al., 2003). A further reduction of *SEP1* activity in the *sep1 sep2 sep3* triple mutant results in flowers consisting of sepals only (Pelaz et al., 2000). The flower formation is fully disturbed in *sep1 sep2 sep3 sep4* quadruple mutants that only leaf-like organs exist (Ditta et al., 2004). The defects of rice spikelet progress in *osmads1-z osmads5-3 osmads34-1* triple mutants compared with double mutants *osmads1-z osmads5-3* and *osmads1-z osmads34-1* (Wu et al., 2018). The phenotypic evidence all reveals that the function of SEP proteins in floral development depends on their concentration.

The *in vitro* binding assay of SEPs and CArG fragments proved that protein concentration affects the binding affinity of SEPs and their cooperative complexes (Jetha et al., 2014; Rumpler et al., 2018), which lay a molecular foundation of the concentration-dependent regulation of SEP proteins to their target genes. Furthermore, the regulation of zygotic genes by maternal-effect genes during the *Drosophila* development sets a paradigmatic example for concentration-dependent target gene regulation (Lander, 2007). Whether SEP protein concentration is responsible for different target gene regulation lacks evidence. The *Arabidopsis GhSEP* overexpression lines could be summarized into three types according to the phenotypes (Figure 3). Type I only flowered earlier, and *GhSEP* expression levels were the lowest in the plants compared to the other transgenic lines. In Type II plants, the transcripts of *GhSEP*s were more abundant than Type I plants and curled leaves were additionally observed. Type III plants further demonstrated floral organ defects due to the excessive expression. The phenotypic variation is controlled by different genes downstream of GhSEPs. Therefore, a relatively minor accumulation of GhSEP proteins suffice to promote flowering, but the function in floral development requires more abundant GhSEPs.

GhSEPs form dynamic complexes to target different loci

Although the FQM describes the mechanism of SEP in floral development, the regulatory mechanism in flowering time control remains unclear. The overexpression of *SEP3* causes similar phenotypes as *35S:AP1* to promote the flowering of *Arabidopsis*, which could be masked by an elevated expression of *LFY*. As a floral meristem identity gene, *LFY* is a downstream of SEP3 (Castillejo et al., 2005), and the activation of *LFY* will, in turn, accelerate floral transition (Moon et al., 2005). *OsMADS7* (also named *OsMADS45*) is a *SEP3* homolog. The overexpression of *OsMADS7* can overcome photoperiod to upregulate *Hd3a* and *RFT1* simultaneously resulting in early flowering (Wang et al., 2013). The expression changes of *FT, SOC1, CO, LFY*, and *AP1* in *35S:GhSEP*s were consistent with the overexpression lines of other *SEP* orthologs (Figure S6) (Tzeng et al., 2003; Pu et al., 2020). However, the expression trend of *FT* and *SOC1* in the *35S:GhSEP* plants remained the same as in the WT, whereas the transcriptional elevation of *LFY* and *AP1* advanced suggesting earlier floral transition (Figure 5A). Meanwhile, the late flowering phenotype induced by the decrease of *GhSEP* expression was only related to the expression changes of *GhAP1* and *GhLFY* (Figures 5B and S5C). Thus, *AP1* and *LFY* were the downstream genes of GhSEPs in flowering time control. A genome-wide identification of AtSEP3 and OsMADS1 (SEP4 homolog) targets both demonstrate the direct binding of them to the gibberellic acid (GA) biosynthesis genes to regulate the GA level that is involved in regulating flowering time (Kaufmann et al., 2009; Khanday et al., 2016). Thus, the expression changes of other flowering time genes in *35S:GhSEP* plants might be due to the regulation of GA biosynthesis.

Previous studies revealed the transcription of *GhAP1* in the leaf and SAM (Cheng et al., 2021), whereas *GhLFY* expression was mainly detected in the SAM (Li et al., 2013). Only *GhSEP4.2* displayed commensurate expression in leaf with *GhAP1* (Figure 7A). Thus, we hypothesize that *GhAP1* is one of the targets of GhSEP4.2 in the leaf, where GhSEP4.2 interacts with GhSOC1, GhSVP, and itself to form tetramers (Figure 7B). In the SAM, GhSEPs were highly expressed at different time forming dynamic tetramers (Figure 7B). *GhSEP4.1* and *GhSEP4.2* were mainly expressed in the inflorescence meristem and maintained reproductive growth. They were also expressed earlier in the floral meristem to determine the formation of the calycle, sepal, and petals. *GhSEP1* was then expressed to participate in the growth of the sepal, petal, and stamen.

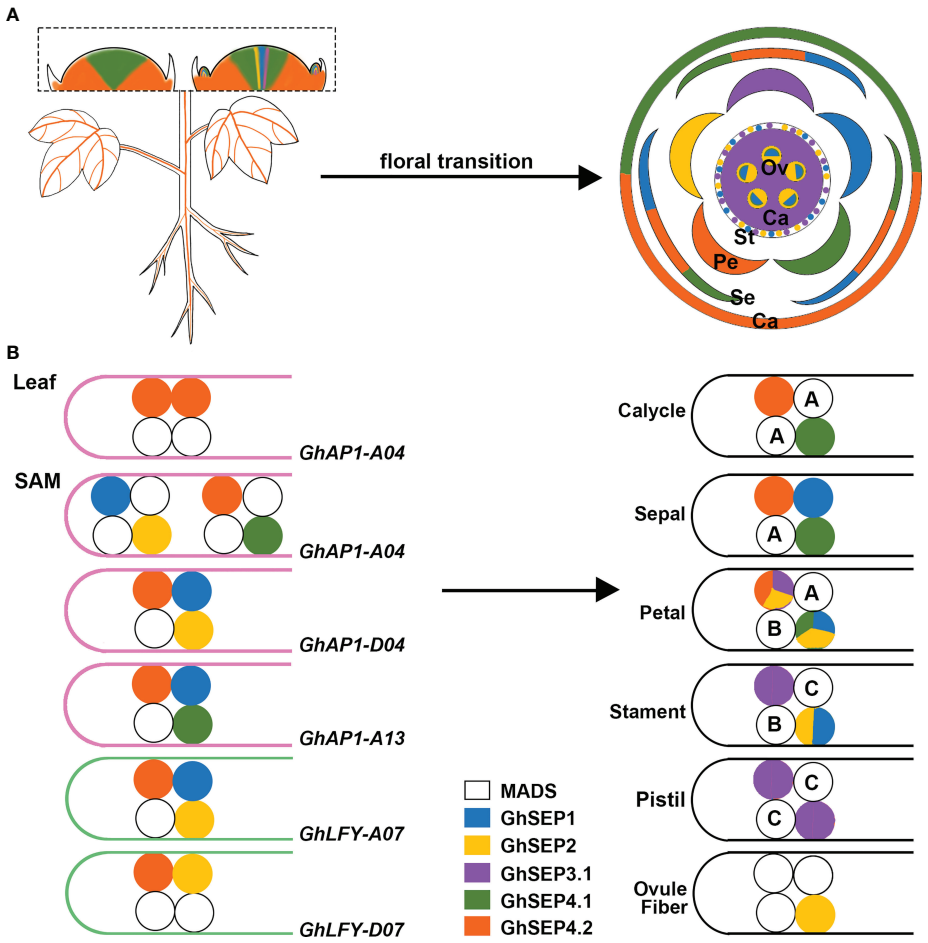

FIGURE 7
The proposed model of the *GhSEP* regulatory mechanism. **(A)** Spatial and temporal expression dynamic of *GhSEP* genes during reproductive growth. Ca, calycle; Se, sepal; Pe, petal; St, stamen; Pi, pistil; Ov, ovule. **(B)** Speculation of protein complexes involving different GhSEP proteins and their target loci. A, B, and C indicate the ABC genes. In the model, *GhSEP* genes are transcribed sequentially in the leaf and SAM resulting in dynamic protein tetramers containing other MADS proteins to directly regulate different target genes to promote floral transition and regulate the reproductive growth in the SAM.

GhSEP2 and *GhSEP3.1* were expressed latest to regulate petal and stamen formation. In addition, the pistil determination only involved *GhSEP3.1*. *GhSEP2* expression was upregulated in the ovule when the fiber initiates. The fine-tuning of the transcription of *GhSEP* genes was essential for their function in reproductive growth, and the resulting protein tetramers, in turn, regulated different target genes in the SAM.

MADS proteins form tetramers to loop DNA, and this process requires only a limited amount of interaction energy between the DNA-bound dimer (Melzer et al., 2009; Jetha et al., 2014). According to this principle, GhSEP4.2 binds to *GhAP1-A04* easier than other *GhAP1* regions as two separated binding sites were identified with an equal enrichment (Figures 5D and Figure 7). GhSEP4.1/4.2 accumulated dramatically due to their numerous transcripts, which is the same as *Arabidopsis SEP4* that transcribes earliest in the SAM (Ditta et al., 2004). The transcriptional superiority usually contributes to a dominant role. However, GhSEP4.2 bindings in *GhAP1* genome region were comparatively weaker than GhSEP2 binding to *GhAP1-A04* (Figure 5D). Moreover, GhSEP2 was unable to self-dimerize (Figure 6A). GhSEP2 binding to *GhAP1-A04* must be coordinated. GhSEP1, whose expression was higher in the SAM, was considered rather than GhSEP4.2 because the binding sites of GhSEP2 did not overlap with that of GhSEP4.2. Inferring from these, GhSEP1 and GhSEP2 regulate *GhAP1* dominantly on *A04* loci (Figure 7B). Furthermore, the binding sites of GhSEP4.2 coincide with that of GhSEP2 on *GhAP1-D04* and *-A13*. They form a heterodimer to regulate these two loci. Separated binding sites suggested a loop of *GhAP1-D04*. However the weak binding of GhSEP2 on *GhAP1-A13* should be strengthened *via* other GhSEPs. GhSEP4.1, GhSEP4.2, or GhSEP1, rather than GhSEP2, might cooperate with the regulation on *GhAP-A13* due

to their stronger interaction ability. Meanwhile, the binding on *GhAP1-D13* was only detected by GhSEP2 with a relatively low enrichment indicating a weak regulation of GhSEPs on this locus. Next, the binding superiority for *GhLFY* was also in the At subgenome. Heterodimerization is responsible for the strong binding. The similar enrichment and nearby binding sites of GhSEP2 and GhSEP4.2 suggested a cobinding on *GhLFY-D07* (Figure 5D). This regulatory model also needs the participation of flowering time regulators, such as GhSOC1 and GhSVP (Figures 6B,C). Members in a tetramer constrained each other to achieve a fine-tuning of the reproductive success of cotton to produce fibers.

Overall, the proposed model described a sequential developmental regulation from vegetative to reproductive growth linked by the temporal and spatial expression of *GhSEP* genes whose function is largely dependent on the cofactors to form different complexes dynamically to target different downstream genes. It provides new insights into the sequential regulation of cotton flowering and reproductive growth that contribute to fiber production.

Data availability statement

The original contributions presented in the study are included in the article/Supplementary Material. Further inquiries can be directed to the corresponding author.

Author contributions

ZM and YY supervised the project. YY conceived and designed the experiment. LC performed most of the experiments. YY and LC analyzed the data and wrote the paper. CM assisted in bioinformatic analysis. ZZ worked with the ChIP experiment. HK, LM, ZS, BC, ZWL, GW, JY, JW, ZKL, LW, GZ, YZ, and XW helped with the preparation of plant materials and expression analysis. All authors contributed to the article and approved the submitted version.

Funding

This work was supported by Natural Science Foundation of Hebei Province (grant no. C2020204079), National Natural Science Foundation of China (grant no. 31801410), Supporting Project of Hebei Agricultural University (grant no. ZD201601, PT2018004), and Top Talent Project of Hebei Province to ZM (031601801).

Conflict of interest

The authors declare that the research was conducted in the absence of any commercial or financial relationships that could be construed as a potential conflict of interest.

Publisher's note

All claims expressed in this article are solely those of the authors and do not necessarily represent those of their affiliated organizations, or those of the publisher, the editors and the reviewers. Any product that may be evaluated in this article, or claim that may be made by its manufacturer, is not guaranteed or endorsed by the publisher.

Supplementary material

The Supplementary Material for this article can be found online at: https://www.frontiersin.org/articles/10.3389/fpls.2022.990221/full#supplementary-material

SUPPLEMENTARY FIGURE 1
Photobleaching phenotype of the positive control.

SUPPLEMENTARY FIGURE 2
Sequence analysis of *GhSEP* genes.

SUPPLEMENTARY FIGURE 3
Expression of *GhSEP* genes.

SUPPLEMENTARY FIGURE 4
Phenotypes of *35S:GhSEP* transgenic *Arabidopsis* lines.

SUPPLEMENTARY FIGURE 5
Phenotypes and expression of flowering time regulators in *GhSEP* silencing plants.

SUPPLEMENTARY FIGURE 6
Expression of flowering time regulators in *35S:GhSEPs*.

SUPPLEMENTARY FIGURE 7
Detection of fusion proteins by Western blot.

SUPPLEMENTARY TABLE 1
Primer list.

SUPPLEMENTARY TABLE 2
List of the proteins used in the phylogenetic tree.

SUPPLEMENTARY TABLE 3
List of *SEP*-like genes in *G. hirsutum*.

SUPPLEMENTARY TABLE 4
Sequence similarity of *SEP*-like genes in *G. hirsutum*.

References

Bowman, J. L., Alvarez, J., Weigel, D., Meyerowitz, E. M., and Smyth, D. R. (1993). Control of flower development in arabidopsis thaliana by APETALA1 and interacting genes. *Development* 119, 721–743. doi: 10.1242/dev.119.3.721

Castillejo, C., Romera-Branchat, M., and Pelaz, S. (2005). A new role of the arabidopsis SEPALLATA3 gene revealed by its constitutive expression. *Plant J.* 43, 586–596. doi: 10.1111/j.1365-313X.2005.02476.x

Chen, C., Chen, H., Zhang, Y., Thomas, H. R., Frank, M. H., He, Y., et al. (2020). TBtools: An integrative toolkit developed for interactive analyses of big biological data. *Mol. Plant* 13, 1194–1202. doi: 10.1016/j.molp.2020.06.009

Cheng, X., Wang, H., Wei, H., Gu, L., Hao, P., Sun, H., et al. (2021). The MADS transcription factor GhAP1.7 coordinates the flowering regulatory pathway in upland cotton (). *Gene* 769, 145235. doi: 10.1016/j.gene.2020.145235

Chen, F., Zhang, X., Liu, X., and Zhang, L. (2017). Evolutionary analysis of MIKC(c)-type MADS-box genes in gymnosperms and angiosperms. *Front. Plant Sci.* 8, 895. doi: 10.3389/fpls.2017.00895

Chung, Y. Y., Kim, S. R., Finkel, D., Yanofsky, M. F., and An, G. (1994). Early flowering and reduced apical dominance result from ectopic expression of a rice MADS box gene. *Plant Mol. Biol.* 26, 657. doi: 10.1007/BF00013751

Cseke, L. J., Cseke, S. B., Ravinder, N., Taylor, L. C., Shankar, A., Sen, B., et al. (2005). SEP-class genes in populus tremuloides and their likely role in reproductive survival of poplar trees. *Gene* 358, 1–16. doi: 10.1016/j.gene.2005.05.035

Cui, R., Han, J., Zhao, S., Su, K., Wu, F., Du, X., et al. (2010). Functional conservation and diversification of class e floral homeotic genes in rice (Oryza sativa). *Plant J.* 61, 767–781. doi: 10.1111/j.1365-313X.2009.04101.x

De Folter, S., Immink, R. G., Kieffer, M., Parenicova, L., Henz, S. R., Weigel, D., et al. (2005). Comprehensive interaction map of the arabidopsis MADS box transcription factors. *Plant Cell* 17, 1424–1433. doi: 10.1105/tpc.105.031831

Ditta, G., Pinyopich, A., Robles, P., Pelaz, S., and Yanofsky, M. F. (2004). The SEP4 gene of arabidopsis thaliana functions in floral organ and meristem identity. *Curr. Biol.* 14, 1935–1940. doi: 10.1016/j.cub.2004.10.028

Elo, A., Lemmetyinen, J., Turunen, M. L., Tikka, L., and Sopanen, T. (2001). Three MADS-box genes similar to APETALA1 and FRUITFULL from silver birch (Betula pendula). *Physiol. Plant* 112, 95–103. doi: 10.1034/j.1399-3054.2001.1120113.x

Favaro, R., Pinyopich, A., Battaglia, R., Kooiker, M., Borghi, L., Ditta, G., et al. (2003). MADS-box protein complexes control carpel and ovule development in arabidopsis. *Plant Cell* 15, 2603–2611. doi: 10.1105/tpc.015123

Ferrario, S. (2003). The MADS-box gene FBP2 is required for SEPALLATA function in petunia. *Plant Cell* 15, 914–925. doi: 10.1105/tpc.010280

Flanagan, C. A., and Ma, H. (1994). Spatially and temporally regulated expression of the MADS-box gene AGL2 in wild-type and mutant arabidopsis flowers. *Plant Mol. Biol.* 26, 581–595. doi: 10.1007/BF00013745

Gao, X., Liang, W., Yin, C., Ji, S., Wang, H., Su, X., et al. (2010). The SEPALLATA-like gene OsMADS34 is required for rice inflorescence and spikelet development. *Plant Physiol.* 153, 728–740. doi: 10.1104/pp.110.156711

Hao, P., Wu, A., Chen, P., Wang, H., Ma, L., Wei, H., et al. (2021). GhLUX1 and GhELF3 are two components of the circadian clock that regulate flowering time of gossypium hirsutum. *Front. Plant Sci.* 12. doi: 10.3389/fpls.2021.691489

He, Y. (2012). Chromatin regulation of flowering. *Trends Plant Sci.* 17, 556–562. doi: 10.1016/j.tplants.2012.05.001

Huang, F., Xu, G., Chi, Y., Liu, H., Xue, Q., Zhao, T., et al. (2014). A soybean MADS-box protein modulates floral organ numbers, petal identity and sterility. *BMC Plant Biol.* 14, 89. doi: 10.1186/1471-2229-14-89

Hu, Y., Chen, J., Fang, L., Zhang, Z., Ma, W., Niu, Y., et al. (2019). Gossypium barbadense and gossypium hirsutum genomes provide insights into the origin and evolution of allotetraploid cotton. *Nat. Genet.* 51, 739–748. doi: 10.1038/s41588-019-0371-5

Immink, R. G. H., Tonaco, I. A. N., De Folter, S., Shchennikova, A., Van Dijk, A. D. J., Busscher-Lange, J., et al. (2009). SEPALLATA3: the 'glue' for MADS box transcription factor complex formation. *Genome Biol.* 10, R24. doi: 10.1186/gb-2009-10-2-r24

Jang, S., Hong, M. Y., Chung, Y. Y., and An, G. (1999). Ectopic expression of tobacco MADS genes modulates flowering time and plant architecture. *Molecules Cells* 9, 576–586.

Jetha, K., Theißen, G., and Melzer, R. (2014). Arabidopsis SEPALLATA proteins differ in cooperative DNA-binding during the formation of floral quartet-like complexes. *Nucleic Acids Res.* 42, 10927–10942. doi: 10.1093/nar/gku755

Kang, H. G., Jang, S., Chung, J. E., Cho, Y. G., and An, G. (1997). Characterization of two rice MADS box genes that control flowering time. *Molecules Cells* 7, 559–566.

Katahata, S.-I., Futamura, N., Igasaki, T., and Shinohara, K. (2014). Functional analysis of SOC1-like and AGL6-like MADS-box genes of the gymnosperm cryptomeria japonica. *Tree Genet. Genomes* 10, 317–327. doi: 10.1007/s11295-013-0686-9

Kaufmann, K., Muiño, J., Jauregui, R., Ca, A., Smaczniak, C., Krajewski, P., et al. (2009). Target genes of the MADS transcription factor SEPALLATA3: integration of developmental and hormonal pathways in the arabidopsis flower. *PloS Biol.* 7, e1000090. doi: 10.1371/journal.pbio.1000090

Khanday, I., Das, S., Chongloi, G. L., Bansal, M., Grossniklaus, U., and Vijayraghavan, U. (2016). Genome-wide targets regulated by the OsMADS1 transcription factor reveals its DNA recognition properties. *Plant Physiol.* 172, 372–388. doi: 10.1104/pp.16.00789

Kumar, S., Stecher, G., and Tamura, K. (2016). MEGA7: Molecular evolutionary genetics analysis version 7.0 for bigger datasets. *Mol. Biol. Evol.* 33, 1870–1874. doi: 10.1093/molbev/msw054

Lander, A. D. (2007). Morpheus Unbound: reimagining the morphogen gradient. *Cell* 128, 245–256. doi: 10.1016/j.cell.2007.01.004

Lemmetyinen, J., Hassinen, M., Elo, A., Porali, I., Keinonen, K., Makela, H., et al. (2004). Functional characterization of SEPALLATA3 and AGAMOUS orthologues in silver birch. *Physiol. Plant* 121, 149–162. doi: 10.1111/j.0031-9317.2004.00303.x

Leseberg, C. H., Eissler, C. L., Wang, X., Johns, M. A., Duvall, M. R., and Mao, L. (2008). Interaction study of MADS-domain proteins in tomato. *J. Exp. Bot.* 59, 2253–2265. doi: 10.1093/jxb/ern094

Letunic, I., and Bork, P. (2019). Interactive tree of life (iTOL) v4: recent updates and new developments. *Nucleic Acids Res.* 47, W256–W259. doi: 10.1093/nar/gkz239

Li, J., Fan, S. L., Song, M. Z., Pang, C. Y., Wei, H. L., Li, W., et al. (2013). Cloning and characterization of a FLO/LFY ortholog in gossypium hirsutum l. *Plant Cell Rep.* 32, 1675–1686. doi: 10.1007/s00299-013-1479-1

Lin, Z., Cao, D., Damaris, R. N., and Yang, P. (2020). Genome-wide identification of MADS-box gene family in sacred lotus (Nelumbo nucifera) identifies a SEPALLATA homolog gene involved in floral development. *BMC Plant Biol.* 20, 497. doi: 10.1186/s12870-020-02712-w

Liu, H., Huang, X., Ma, B., Zhang, T., Sang, N., Zhuo, L., et al. (2021). Components and functional diversification of florigen activation complexes in cotton. *Plant Cell Physiol.* 62, 1542–1555. doi: 10.1093/pcp/pcab107

Liu, C., Xi, W., Shen, L., Tan, C., and Yu, H. (2009). Regulation of floral patterning by flowering time genes. *Dev. Cell* 16, 711–722. doi: 10.1016/j.devcel.2009.03.011

Liu, C., Zhou, J., Bracha-Drori, K., Yalovsky, S., Ito, T., and Yu, H. (2007). Specification of arabidopsis floral meristem identity by repression of flowering time genes. *Development* 134, 1901–1910. doi: 10.1242/dev.003103

Li, X., Wu, Y., Chi, H., Wei, H., Wang, H., and Yu, S. (2022). Genomewide identification and characterization of the genes involved in the flowering of cotton. *Int. J. Mol. Sci.* 23, 7940. doi: 10.3390/ijms23147940

Li, Q., Yu, H., Zhang, Z., Sun, Z., Y., Z., D., Z., et al. (2021b). Optimization of cotton mesophyll protoplast transient expression system. *Scientia Agricultura Sin.* 54, 4514–4524. doi: 10.3864/j.issn.0578-1752.2021.21.003

Li, L., Zhang, C., Huang, J., Liu, Q., Wei, H., Wang, H., et al. (2021a). Genomic analyses reveal the genetic basis of early maturity and identification of loci and candidate genes in upland cotton (Gossypium hirsutum L.). *Plant Biotechnol. J.* 19, 109–123. doi: 10.1111/pbi.13446

Matsubara, K., Shimamura, K., Kodama, H., Kokubun, H., Watanabe, H., Basualdo, I. L., et al. (2008). Green corolla segments in a wild petunia species caused by a mutation in FBP2, a SEPALLATA-like MADS box gene. *Planta* 228, 401–409. doi: 10.1007/s00425-008- 0744-y

Ma, L., and Yan, Y. (2022). GhSOC1s evolve to respond differently to the environmental cues and promote flowering in partially independent ways. *Front. Plant Sci.* 13, 882946. doi: 10.3389/fpls.2022.882946

Ma, H., Yanofsky, M. F., and Meyerowitz, E. M. (1991). AGL1-AGL6, an arabidopsis gene family with similarity to floral homeotic and transcription factor genes. *Genes Dev.* 5, 484–495. doi: 10.1101/gad.5.3.484

Melzer, R., Verelst, W., and Theissen, G. (2009). The class e floral homeotic protein SEPALLATA3 is sufficient to loop DNA in 'floral quartet'-like complexes *in vitro*. *Nucleic Acids Res.* 37, 144–157. doi: 10.1093/nar/gkn900

Meng, Q., Li, X., Zhu, W., Yang, L., Liang, W., Dreni, L., et al. (2017). Regulatory network and genetic interactions established by OsMADS34 in rice inflorescence and spikelet morphogenesis. *J. Integr. Plant Biol.* 59, 693–707. doi: 10.1111/jipb.12594

Moon, J., Lee, H., Kim, M., and Lee, I. (2005). Analysis of flowering pathway integrators in arabidopsis. *Plant Cell Physiol.* 46, 292–299. doi: 10.1093/pcp/pci024

Morel, P., Chambrier, P., Boltz, V., Chamot, S., Rozier, F., Rodrigues Bento, S., et al. (2019). Divergent functional diversification patterns in the SEP/AGL6/AP1 MADS-box transcription factor superclade. *Plant Cell* 31, 3033–3056. doi: 10.1105/tpc.19.00162

Nardeli, S. M., Artico, S., Aoyagi, G. M., De Moura, S. M., Da Franca Silva, T., Grossi-De-Sa, M. F., et al. (2018). Genome-wide analysis of the MADS-box gene family in polyploid cotton (Gossypium hirsutum) and in its diploid parental species (Gossypium arboreum and gossypium raimondii). *Plant Physiol. Biochem.* 127, 169–184. doi: 10.1016/j.plaphy.2018.03.019

Pan, Z. J., Chen, Y. Y., Du, J. S., Chen, Y. Y., Chung, M. C., Tsai, W. C., et al. (2014). Flower development of phalaenopsis orchid involves functionally divergent SEPALLATA-like genes. *New Phytol.* 202, 1024–1042. doi: 10.1111/nph.12723

Pelaz, S., Ditta, G. S., Baumann, E., Wisman, E., and Yanofsky, M. F. (2000). B and c floral organ identity functions require SEPALLATA MADS-box genes. *Nature* 405, 200–203. doi: 10.1038/35012103

Pelaz, S., Gustafson-Brown, C., Kohalmi, S. E., Crosby, W. L., and Yanofsky, M. F. (2001). APETALA1 and SEPALLATA3 interact to promote flower development. *Plant J.* 26, 385–394. doi: 10.1046/j.1365-313X.2001.2641042.x

Pnueli, L., Hareven, D., Broday, L., Hurwitz, C., and Lifschitz, E. (1994). The TM5 MADS box gene mediates organ differentiation in the three inner whorls of tomato flowers. *Plant Cell* 6, 175–186. doi: 10.2307/3869637

Pu, Z.-Q., Ma, Y.-Y., Lu, M.-X., Ma, Y.-Q., and Xu, Z.-Q. (2020). Cloning of a SEPALLATA4-like gene (IiSEP4) in isatis indigotica fortune and characterization of its function in arabidopsis thaliana. *Plant Physiol. Biochem.* 154, 229–237. doi: 10.1016/j.plaphy.2020.05.031

Ren, Z., Yu, D., Yang, Z., Li, C., Qanmber, G., Li, Y., et al. (2017). Genome-wide identification of the MIKC-type MADS-box gene family in unravels their roles in flowering. *Front. Plant Sci.* 8, 384. doi: 10.3389/fpls.2017.00384

Ruelens, P., De Maagd, R. A., Proost, S., Theissen, G., Geuten, K., and Kaufmann, K. (2013). FLOWERING LOCUS c in monocots and the tandem origin of angiosperm-specific MADS-box genes. *Nat. Commun.* 4, 2280. doi: 10.1038/ncomms3280

Ruelens, P., Zhang, Z., Van Mourik, H., Maere, S., Kaufmann, K., and Geuten, K. (2017). The origin of floral organ identity quartets. *Plant Cell* 29, 229–242. doi: 10.1105/tpc.16.00366

Rumpler, F., Theissen, G., and Melzer, R. (2018). A conserved leucine zipper-like motif accounts for strong tetramerization capabilities of SEPALLATA-like MADS-domain transcription factors. *J. Exp. Bot.* 69, 1943–1954. doi: 10.1093/jxb/ery063

Shen, G., Yang, C. H., Shen, C. Y., and Huang, K. S. (2019). Origination and selection of ABCDE and AGL6 subfamily MADS-box genes in gymnosperms and angiosperms. *Biol. Res.* 52, 25. doi: 10.1186/s40659-019-0233-8

Smaczniak, C., Immink, R. G., Angenent, G. C., and Kaufmann, K. (2012). Developmental and evolutionary diversity of plant MADS-domain factors: insights from recent studies. *Development* 139, 3081–3098. doi: 10.1242/dev.074674

Song, Q., Zhang, T., Stelly, D. M., and Chen, Z. J. (2017). Epigenomic and functional analyses reveal roles of epialleles in the loss of photoperiod sensitivity during domestication of allotetraploid cottons. *Genome Biol.* 18, 99. doi: 10.1186/s13059-017-1229-8

Theissen, G. (2001). Development of floral organ identity: stories from the MADS house. *Curr. Opin. Plant Biol.* 4, 75–85. doi: 10.1016/S1369-5266(00)00139-4

Theissen, G., and Melzer, R. (2007). Molecular mechanisms underlying origin and diversification of the angiosperm flower. *Ann. Bot.* 100, 603–619. doi: 10.1093/aob/mcm143

Theissen, G., Melzer, R., and Rumpler, F. (2016). MADS-domain transcription factors and the floral quartet model of flower development: linking plant development and evolution. *Development* 143, 3259–3271. doi: 10.1242/dev.134080

Theissen, G., and Saedler, H. (2001). Plant biology. floral quartets. *Nature* 409, 469–471. doi: 10.1038/35054172

Tzeng, T.-Y., Hsiao, C.-C., Chi, P.-J., and Yang, C.-H. (2003). Two lily SEPALLATA-like genes cause different effects on floral formation and floral transition in arabidopsis. *Plant Physiol.* 133, 1091–1101. doi: 10.1104/pp.103.026997

Vandenbussche, M., Theissen, G., Van De Peer, Y., and Gerats, T. (2003a). Structural diversification and neo-functionalization during floral MADS-box gene evolution by c-terminal frameshift mutations. *Nucleic Acids Res.* 31, 4401–4409. doi: 10.1093/nar/gkg642

Vandenbussche, M., Zethof, J., Souer, E., Koes, R., Tornielli, G. B., Pezzotti, M., et al. (2003b). Toward the analysis of the petunia MADS box gene family by reverse and forward transposon insertion mutagenesis approaches: B, c, and d floral organ identity functions require SEPALLATA-like MADS box genes in petunia. *Plant Cell* 15, 2680–2693. doi: 10.1105/tpc.017376

Wang, J.-D., Lo, S.-F., Li, Y.-S., Chen, P.-J., Lin, S.-Y., Ho, T.-Y., et al. (2013). Ectopic expression of OsMADS45 activates the upstream genes Hd3a and RFT1 at an early development stage causing early flowering in rice. *Botanical Stud.* 54, 1–13. doi: 10.1186/1999-3110-54-12

Wu, D., Liang, W., Zhu, W., Chen, M., Ferrandiz, C., Burton, R. A., et al. (2018). Loss of LOFSEP transcription factor function converts spikelet to leaf-like structures in rice. *Plant Physiol.* 176, 1646–1664. doi: 10.1104/pp.17.00704

Zahn, L. M., Kong, H., Leebens-Mack, J. H., Kim, S., Soltis, P. S., Landherr, L. L., et al. (2005). The evolution of the SEPALLATA subfamily of MADS-box genes: a preangiosperm origin with multiple duplications throughout angiosperm history. *Genetics* 169, 2209–2223. doi: 10.1534/genetics.104.037770

Zahn, L. M., Leebens-Mack, J. H., Arrington, J. M., Hu, Y., Landherr, L. L., Depamphilis, C. W., et al. (2006). Conservation and divergence in the AGAMOUS subfamily of MADS-box genes: evidence of independent sub- and neofunctionalization events. *Evol. Dev.* 8, 30–45. doi: 10.1111/j.1525-142X.2006.05073.x

Zhang, J., Hu, Z., Wang, Y., Yu, X., Liao, C., Zhu, M., et al. (2018). Suppression of a tomato SEPALLATA MADS-box gene, SlCMB1, generates altered inflorescence architecture and enlarged sepals. *Plant Sci.* 272, 75–87. doi: 10.1016/j.plantsci.2018.03.031

Zhang, J., Jia, X., Guo, X., Wei, H., Zhang, M., Wu, A., et al. (2021). QTL and candidate gene identification of the node of the first fruiting branch (NFFB) by QTL-seq in upland cotton (). *BMC Genomics* 22, 882. doi: 10.1186/s12864-021-08164-2

Zhang, S., Lu, S., Yi, S., Han, H., Liu, L., Zhang, J., et al. (2017). Functional conservation and divergence of five SEPALLATA -like genes from a basal eudicot tree, platanus acerifolia. *Planta* 245, 1–19. doi: 10.1007/s00425-016-2617-0

Zhao, X. Y., Cheng, Z. J., and Zhang, X. S. (2006). Overexpression of TaMADS1, a SEPALLATA-like gene in wheat, causes early flowering and the abnormal development of floral organs in arabidopsis. *Planta* 223, 698–707. doi: 10.1007/s00425-005-0123-x

Zhao, T., Holmer, R., De Bruijn, S., Angenent, G. C., Van Den Burg, H. A., and Schranz, M. E. (2017). Phylogenomic synteny network analysis of MADS-box transcription factor genes reveals lineage-specific transpositions, ancient tandem duplications, and deep positional conservation. *Plant Cell* 29, 1278–1292. doi: 10.1105/tpc.17.00312

frontiers | Frontiers in Plant Science

TYPE Original Research
PUBLISHED 09 December 2022
DOI 10.3389/fpls.2022.1081280

OPEN ACCESS

EDITED BY
Verónica S. Di Stilio,
University of Washington,
United States

REVIEWED BY
Li Wang,
Yangzhou University, China
Daniel H. Chitwood,
Michigan State University,
United States

*CORRESPONDENCE
Mengzhu Lu
lumz@zafu.edu.cn
Ying Wang
tslkywy@163.com

SPECIALTY SECTION
This article was submitted to Plant Development and EvoDevo, a section of the journal Frontiers in Plant Science

RECEIVED 27 October 2022
ACCEPTED 21 November 2022
PUBLISHED 09 December 2022

CITATION
Tang F, Sun P, Zhang Q, Zhong F, Wang Y and Lu M (2022) Insight into the formation of trumpet and needle-type leaf in *Ginkgo biloba* L. mutant. *Front. Plant Sci.* 13:1081280. doi: 10.3389/fpls.2022.1081280

Insight into the formation of trumpet and needle-type leaf in *Ginkgo biloba* L. mutant

Fang Tang[1,2], Pengbo Sun[1], Qian Zhang[3], Fengwei Zhong[3], Ying Wang[3]* and Mengzhu Lu[1,2,4]*

[1]State Key Laboratory of Tree Genetics and Breeding, Key Laboratory of Tree Breeding and Cultivation of The National Forestry and Grassland Administration, Research Institute of Forestry, Chinese Academy of Forestry, Beijing, China, [2]Co-Innovation Center for Sustainable Forestry in Southern China, Nanjing Forestry University, Nanjing, China, [3]Taishan Academy of Forestry Sciences, Tai'an, China, [4]State Key Laboratory of Subtropical Silviculture, School of Forestry and Biotechnology, Zhejiang A&F University, Hangzhou, China

The leaf type of a plant determines its photosynthetic efficiency and adaptation to the environment. The normal leaves of modern *Ginkgo biloba*, which is known as a "living fossil" in gymnosperm, evolved from needle-like to fan-shaped with obvious dichotomous venation. However, a newly discovered *Ginkgo* variety "SongZhen" have different leaf types on a tree, including needle-, trumpet-, strip-, and deeply split fan-shaped leaves. In order to explore the mechanism in forming these leaf types, the microscopy of different leaf types and transcriptome analysis of apical buds of branches with normal or abnormal leaves were performed. We found that the normal leaf was in an intact and unfolded fan shape, and the abnormal leaf was basically split into two parts from the petiole, and each exhibited different extent of variation. The needle-type leaves were the extreme, having no obvious palisade and spongy tissues, and the phloem cells were scattered and surrounded by xylem cells, while the trumpet-type leaves with normal vascular bundles curled inward to form a loop from the abaxial to adaxial side. The other type of leaves had the characteristics among needle-type, trumpet-type, or normal leaves. The transcriptome analysis and quantitative PCR showed that the genes related to abaxial domain were highly expressed, while the adaxial domain promoting genes were decreasingly expressed in abnormal-type leaf (ANL) buds and abnormal leaves, which might lead to the obvious abaxialized leaves of "SongZhen." In addition, the low expression of genes related to leaf boundary development in ANL buds indicated that single- or double-needle (trumpet) leaves might also be due to the leaf tissue fusion. This study provides an insight into the mechanism of the development of the abnormal leaves in "SongZhen" and lays a foundation for investigating the molecular mechanism of the leaf development in gymnosperms.

KEYWORDS

***Ginkgo biloba* L., leaf shape regulation, anatomical structure, transcriptome analysis, adaxial-abaxial polarity, leaf boundary**

Introduction

The leaf is the main organ for plants to receive light energy and absorb carbon dioxide to produce carbohydrates. It is the most sensitive and plastic organ to environmental changes, and its morphological structure evolves and changes under different ecological conditions to adapt to the environment (Chitwood and Sinha, 2016). The earliest vascular plants had no leaves at all, only sparse stomata distributed on the stems. The flat megaphyll leaves with vein first appeared in the Devonian period 360 million years ago (Kenrick and Crane, 1997). The generation of flat leaves is an important time point in the evolution of leaves because flat and stretched leaves greatly improve the area to receive light, thus increasing the efficiency of carbon fixation, which plays an important role in the dominant position of giant leaf plants in many ecosystems (David, 2005). The development of leaf is mainly divided into three processes: leaf primordium initiation, leaf polarity establishment, and leaf expansion (Dkhar and Pareek, 2014). When leaf development initiates at the peripheral zone (PZ), which surrounds the central zone of the shoot apical meristem (SAM), a boundary region partitions the new leaf primordium from the SAM on the adaxial side. Subsequently, the leaf primordia undergo asymmetric division and differentiation along the adaxial–abaxial, medio–lateral, and proximal–distal axes to form leaf organs (Du et al., 2018). The abnormal development of adaxial–abaxial axis will cause leaf curl, leading to the reduced area of light acceptance and even plant death. Adaxial–abaxial polarity is maintained and further strengthened *via* adaxial- and abaxial-promoting genes, encoding transcription factors, and small RNAs that act in conserved and partially redundant pathways (Bar and Ori, 2014; Du et al., 2018).

The study on adaxial–abaxial axis of leaves began from the mutants of *PHANTASTICA* (*PHAN*) in *Antirrhinum*. The adaxial side of leaves of the mutants showed an abaxial character, and the severe mutants even had needle-like leaves, which revealed that *Phan* gene promotes the differentiation of adaxial tissues of leaves (Waites and Hudson, 1995). Although *PHAN* and its orthologues are uniformly expressed in young leaf primordia of respective species, their roles in adaxial specification are not strictly conserved. The knockdown of *PHAN* orthologues can lead to abaxialization in tomato (*LePHAN*) (Kim et al., 2003) but not in maize (*RS2*) (Timmermans et al., 1999) or *Arabidopsis* (*AS1*) (Byrne et al., 2000). In addition, *KANADI* (*KAN*) gene, encoding a transcription factor containing MYB-like GARP DNA binding domain, promotes abaxial domain (Kerstetter et al., 2001). *YABBY* (*YAB*) genes function relatively later in leaf development and are considered to act downstream of the *KAN*. In *Arabidopsis*, *YAB* genes are expressed in the abaxial domain and redundantly promote abaxial identity (Siegfried et al., 1999; Eshed et al., 2004). Antagonistically, the adaxial expression of homeodomain/leucine-zipper (HD-ZIP) genes, namely, *PHABULOSA* (*PHB*), *PHAVOLUTA* (*PHV*), and *REVOLUTA* (*REV*), are sufficient to define adaxial cell fate (Emery et al., 2003), but they are regulated by miR165 and miR166 (Tang et al., 2003). Gain-of-function *HD-ZIPIII* mutants and resistance to the inhibition by miR165/166 lead to the formation of adaxialized leaves, whereas loss-of-function *phb phv rev* triple-mutant plants form abaxialized leaves and exhibit loss-of-SAM phenotypes (Wenkel et al., 2007; Kim et al., 2008). The auxin signaling pathway is also involved in the regulation of adaxial–abaxial axis of leaves. Three redundant repressive AUXIN RESPONSE FACTORs (ARFs), namely, *ETTIN* (*ETT* or *ARF3*), *ARF4*, and *ARF2*, are expressed in the abaxial domain and promote abaxial cell fate (Pekker et al., 2005; Guan et al., 2017). The mutual antagonism exists between regulatory factors of the adaxial and abaxial domains of leaves. The adaxially localized ASYMMETRIC LEAF1 (AS1) and AS2 complex negatively regulates the expression of *ETT* and *ARF4* (Iwasaki et al., 2013) and also directly inhibits MIR166A and *YAB5* expression in the adaxial domain (Husbands et al., 2015). In the abaxial domain, KAN1 binds to the promoter regions of MIR166A and MIR166F and downregulates the expression of MIR166F but not MIR166A (Merelo et al., 2013), implying that complicated and fine-tuned regulations exist. In addition, ARF and KAN may form complexes and play a synergism role in promoting abaxial tissue differentiation (Kelley et al., 2012).

The formation of boundaries plays an important role in the development of plant lateral organs, and some transcriptional regulators are involved in the establishment and maintenance of boundaries (Žádníková and Simon, 2014). The CUP-SHAPED COTYLEDON (CUC) NAC-domain transcription factors *CUC1*, *CUC2*, and *CUC3* are specifically expressed in boundary positions, and mutations of *CUC* genes lead to varying degrees of shoot organ fusion phenotypes due to the failure of boundary formation (Aida et al., 1999; Vroemen et al., 2003). The class II TEOSINTE BRANCHED1/CYCLOIDEA/PROLIFERATING CELL FACTOR (TCP) transcription factors can regulate plant organ morphology by participating in cell proliferation and differentiation. They repress marginal meristem activity and control the morphogenesis of shoot lateral organs by negatively regulating the expression of boundary-specific genes. Gain of function of *TCP3* suppresses the expression of *CUC* genes and results in the fusion of cotyledons and defects in the formation of shoots (Koyama et al., 2007). The WUSCHEL-RELATED HOMEOBOX (WOX) transcription factors can regulate blade expansion specifically along the medio-lateral axis. PRESSED FLOWERS (PRS) and WOX1 redundantly promote lateral lamina outgrowth, and the *wox1 prs* double mutant produces narrow leaves with disturbed polarity but unaltered leaf length (Vandenbussche et al., 2009; Nakata et al., 2012). In addition, NGATHA (NGA) and TCP transcription factors redundantly inhibit *WOX* expression to terminate the marginal meristem in *Arabidopsis* (Alvarez et al., 2009).

Ginkgo biloba L. belongs to Ginkgoaceae and *Ginkgo* genus, one of the oldest living gymnosperms left over from the

Quaternary glacier movement, thus also known as "living fossil." Leaves in Ginkgoales tend to be laminated and petiolate due to planation, webbing, and fusion of telomes and mesomes (Zhou, 1991; Zhou, 2003). *Ginkgo* originated from the middle Carboniferous period of Paleozoic, which was dichophyllum with two main veins, and then evolved into *Trichopitys* having hairy leaves with four main veins in the Late Permian Period. The hairy leaves gradually became webbing, evolved into thin lobed type *Baiera*, and then into the four lobes type *Ginkgoites* sp. There were two branches of evolution that followed: one was *Ginkgoites pluripartita* in the cretaceous period of Mesozoic Era, which was totally extinct in Quaternary Period; the other developed into modern *G. biloba* having the fan-shaped leaves without cracks (Zhou and Zheng, 2003; Zhou, 2006). The ancient plants with megaphyll leaves had obvious dichotomous venation, but today, *G. biloba* still retains this ancient venation feature (Beerling et al., 2001). The leaf shape of the tertiary *Ginkgo* fossils unearthed in North Dakota is consistent with that of today's *G. biloba* (Zhou et al., 2012). "SongZhen" (pine needle) is a recently discovered *G. biloba* variety with many different leaf types in a tree. Besides the normal fan-shaped leaves, needle-, trumpet-type, and deeply split leaves sprout on one or different branches of "SongZhen" (Wang et al., 2009).

In order to explore the mechanism in the formation these leaf types of "SongZhen," microscopy observation of different leaf shapes and transcriptome analysis of apical buds of branches with normal and abnormal leaves were performed in this study. It was found that the obvious abaxialization could be the reason to form the "SongZhen" leaves. The expression of abaxial domain-promoting genes were higher, and the adaxial domain-promoting genes were lower in the abnormal-type leaf (ANL) buds, which might lead to the obvious abaxialized leaves of "SongZhen." In addition, the expression of genes related to leaf boundary development was generally low in ANL buds, indicating that the abnormal-type leaves of "SongZhen" may be also due to the leaf tissue fusion. These results lay a foundation for studying on the molecular evolution and regulation of the development of leaves in gymnosperms.

Materials and methods

Plant materials

The plant material used in this study is a 4-year-old *G. biloba* "SongZhen," which grew in a clonal plantation located in Tai'an, Shandong province, China. "SongZhen" is a new *Ginkgo* variety that was discovered and cultivated by Tai'an City Academy of Forestry Science (Wang et al., 2009). In the middle of April, when Ginkgo leaf buds were formed, about 120 apical buds of normal leaf (NL) and abnormal-type leaf (ANL) branches were collected separately with RNase-free blades and immediately frozen and stored in liquid nitrogen. The samples were divided into three parts as three biological repeats for transcriptome analysis. When the leaves of "SongZhen" were expanded, the different types of young leaves from ANL and NL branches were collected for quantitative PCR.

Sample collection and paraffin section of leaf

After the leaves were fully expanded, the representative leaves of different leaf types of "SongZhen" were collected. Among them, the fusion and division region of abnormal-type leaves and the widest sector of the unfolded leaves were prepared for cross-sections using paraffin cutting (He et al., 2014). The section thickness was <10 μm and stained with Safranin O-Fast Green for light microscope observation. The stained sections were observed and photographed under a Olympus BX51 microscope, and cellSens standard software was used to splice a complete image for long or large samples.

Total RNA extraction

The apical buds from NL and ANL branches were mixed in equal amount separately to extract the total RNAs using Total RNA Purification Kit (LC sciences, #TRK-1001) following the manufacturer's instructions. Briefly, 100 mg of tissues was grinded into powder in liquid nitrogen; then, 600 μl of extraction buffer with 6% Plant RNA Isolation Aid (Ambion, #Am9690) was added. The mixture was shaken vigorously, then incubated on ice for 15 min and centrifuged at 12,000 rpm for 10 min at room temperate, by which the yield of total RNA could be improved.

High-throughput sequencing and quality control

The cDNA libraries from the above total RNA samples and high-throughput sequencing were completed by BioMarker (BMK, Beijing). Sequencing libraries were generated using NEBNext UltraTM RNA Library Prep Kit for Illumina (NEB, USA) following the manufacturer's recommendations, and index codes were added to attribute sequences to each sample. Briefly, mRNA was purified from total RNA using poly-T oligo-attached magnetic beads and then was randomly broken into short fragments by fragmentation buffer. AMPure XP bead was selected for fragment selection, and the final sequencing library was obtained by PCR amplification. After the library passed the quality inspection, it was sequenced with Illumina NovaSeq 6000, and the length of the sequenced reading was 2×150 bp (PE150). The RNA-Seq raw data had been submitted to the

NCBI Sequence Read Archive under BioProject accession number PRJNA896381. The clean data were obtained by removing reads containing adapter, reads containing poly-N, and low-quality reads from raw data using fastp software. At the same time, Q20, Q30, GC content, and sequence duplication level of the clean data were calculated. All the downstream analyses were based on clean data with high quality.

Genome comparison and expression analysis

These clean reads were aligned with *G. biloba* genome (Guan et al., 2016) by HISAT2 software, and the allowed number of mismatch nucleotide was set to "0" or "1." StringTie was used for transcripts assembly and new transcripts prediction, and the alternative splicing type and corresponding expression amount of each sample were obtained through ASprofile software. Quantification of gene expression levels were estimated by fragments per kilobase of transcript per million fragments mapped (FPKM). Differential expression analysis of NL and ANL buds was performed using the DEseq. The FDR < 0.05 and fold change ≥2 was set as the threshold for significant differential expression. Gene Ontology (GO) enrichment analysis of the differentially expressed genes (DEGs) was implemented by the GOseq R packages based Wallenius non-central hyper-geometric distribution (Young et al., 2010), and KOBAS (Mao et al., 2005) software was used to test the statistical enrichment of DEGs in Kyoto Encyclopedia of Genes and Genomes (KEGG) pathways.

Quantitative real-time PCR

The reaction mixture contained 10 µl KAPA SYBR FAST qPCR Master Mix (KAPA Biosystems, # K4601), 2 µl 20-fold diluted cDNA, 0.4 µM of each forward and reverse primer (Supplementary Table S1), and ddH2O in a final volume of 20 µl. Amplifications were performed with the following program: 95°C for 3 s and 40 cycles of 95°C for 10 s, 60°C for 30 s, and 72°C for 3 s. No-template reactions were used as negative controls, and *PP2A-2* was the reference gene. The quantitative real-time PCR was performed on the LightCycler® 480 System (Roche Molecular Systems, Germany). Each sample was assessed in four technical replicates, and the data were analyzed using $-2^{-\triangle\triangle Ct}$ method.

Results

Leaf phenotypes of *Ginkgo biloba* "SongZhen"

"SongZhen" is *G. biloba* with variant leaf types including needle-shaped, trumpet-shaped, strip-shaped, deeply split semi fan-shaped, and normal fan-shaped leaves, and these leaf types appear at the same time on clonal individuals of "SongZhen" (Supplementary Figure S1A). The fan-shaped leaves similar to ordinary *Ginkgo* leaves are defined as "normal leaf, NL" and the leaves with other types as "abnormal leaf, ANL." The normal leaves and abnormal leaves were mostly clustered on different short branches (Supplementary Figures S1B, C). Therefore, the apical buds of the short branches with normal leaves or abnormal leaves were separately collected for the transcriptome analysis.

Morphology and tissue structure of "SongZhen" leaves

According to the variation degree, the leaves of "SongZhen" were mainly divided into nine types (Figure 1): single-needle, single-trumpet, double-trumpet, double-needle, needle and trumpet, unfolded and trumpet, unfolded and needle, deep-split, and normal leaf. The normal leaf was a typical modern ginkgo leaf in a fully developed fan shape. Except for the single-needle and single-trumpet leaves, the other variant leaves were basically separated into two parts from the petiole, one part was folded into a needle or trumpet shape, and the other part was expanded into fan shape, or both two parts formed needles or trumpets shape. The deep-split leaf was a partial fusion of two unfolded leaves at the bottom of the blade (Figure 1).

The cross-sections of different types of leaves in "SongZhen" were prepared. The single-needle leaves had secretory cavity (SC) and vein (Figure 2A), or vein only (Figure 2B). In double-needle leaves, there were one SC and two veins at the fusion part of the bottom of the leaf, and the SC was located at the ridge, while two veins were on both sides of the SC (Figure 2C). In double-trumpet leaves, two rings were formed at the junction of

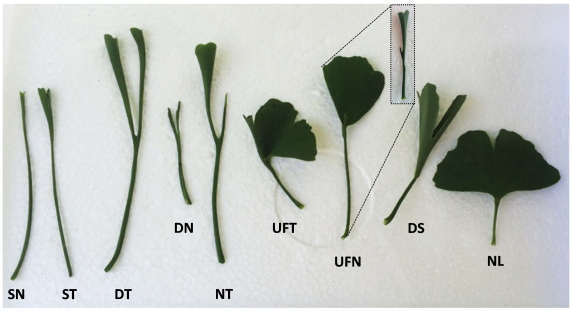

FIGURE 1
The different types of leaves of *Ginkgo biloba* "SongZhen." SN, single-needle; ST, single-trumpet; DT, double-trumpet; DN, double-needle; NT, needle and trumpet; UFT, unfolded and trumpet; UFN, unfolded and needle; DS, deep-split; NL, normal leaf. The small figure in the dotted box is a side view of UFN leaf.

10.3389/fpls.2022.1081280

the leaf and petiole where the two trumpets fused (Figure 2D). Then, the two rings could develop and split into two larger rings (Figure 2E). Needle type was the extreme for the undeveloped leaf, and other leaves were between it and the normal leaf type. For example, the needle and trumpet leaves consisted one needle- and one trumpet-type leaf (Figure 2F), while the unfolded and trumpet leaves had one side with half unfolded normal leaf and another side with trumpet-type leaf (Figures 2G, H). In contrast, the normal leaves were the same as wild-type *G. biloba* (Wang et al., 2011), which were long and flat, and composed of epidermis, mesophyll, vein, and secretory cavity (Figure 2I).

The enlarged images from the cross-section of "SongZhen" leaves in Figure 2 show that the normal leaves of "SongZhen" had a similar tissue structure with that of wild-type *G. biloba* (Wang et al., 2011). The upper and lower epidermis had only one layer of cells. The palisade tissue was composed of one to two layers of cells and arranged closely, while the sponge tissue was irregular and arranged loosely. In the mesophyll, veins were evenly distributed and alternated with the secretory cavity. The leaf vein was a complete vascular bundle with xylem on the adaxial side and phloem on the abaxial side (Figures 3A, B). On the other hand, single- and double-needle leaves were not typical leaves without obvious palisade and spongy tissues. The veins were not normal vascular bundle, where the phloem cells were scattered and surrounded by xylem cells (Figures 3C, D). The shape of single- and double-trumpet leaves were not flat and curled inward to form a loop from the abaxial side to adaxial side, i.e., the upper epidermis was inside, and the lower epidermis was outside (Figures 3E, F). The veins were normal vascular bundles, with xylem on the adaxial side and phloem on the abaxial side (Figures 3E–H). From the above description, the

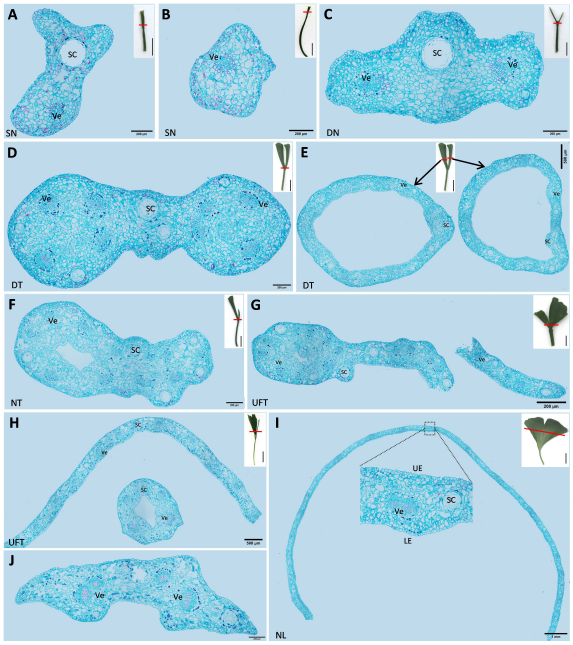

FIGURE 2
The cross-sections of different types of leaves of *Ginkgo biloba* "SongZhen." **(A, B)** Single-needle (SN) leaf; bar, 200 μm. **(C)** Double-needle (DN) leaf; bar, 200 μm. **(D)** The base part of double-trumpet (DT) leaf; bar, 200 μm. **(E)** The upper part of double-trumpet (DT) leaf; bar, 500 μm. **(F)** Needle and trumpet (NT) leaf; bar, 200 μm. **(G)** Unfolded and trumpet (UFT) leaf (unfold and trumpet part fused together; bar, 500 μm). **(H)** Unfolded and trumpet (UFT) leaf (unfold and trumpet part separated; bar, 500 μm). **(I)** Normal leaf (NL); bar, 1 mm. **(J)** The petiole of normal leaf; bar, 200 μm. Sc, secretory cavity; Ve, vein; UE, upper epidermis; LE, lower epidermis. The small pictures at the upper right corner of panels **(A–I)** are the complete leaves, where the red line shows the slicing position, and the black line is the scale; bar, 1 cm.

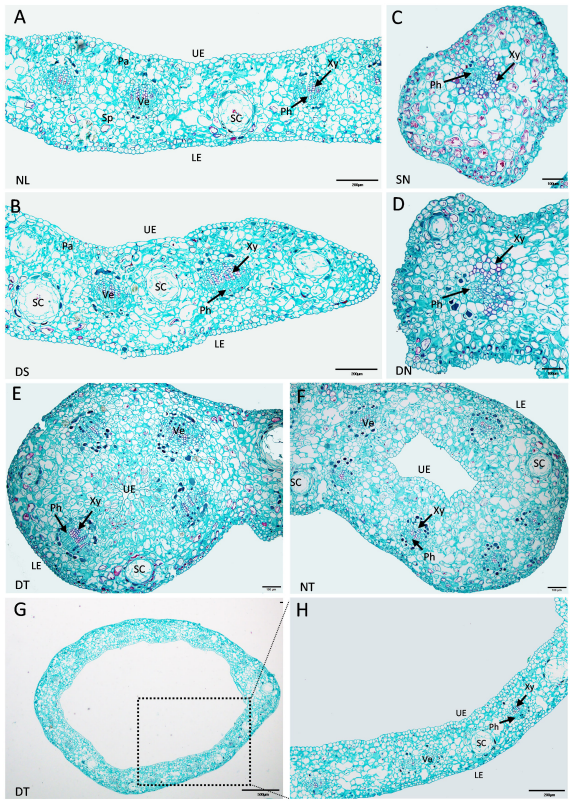

FIGURE 3
Enlarged cross-sections of leaves of *Ginkgo biloba* "SongZhen." **(A)** Normal leaf (NL); bar, 200 μm. **(B)** The leaf margin of the deep-split (DS) leaf; bar, 200 μm. **(C)** Single-needle (SN) leaf; bar, 100 μm. **(D)** One side of double-needle (DN) leaf; bar, 100 μm. **(E)** One side of double-trumpet (DT) leaf; bar, 100 μm. **(F)** The trumpet side of needle and trumpet (NT) leaf; bar, 100 μm. **(G)** The trumpet leaf; bar, 500 μm. **(H)** The enlarged view of the black dotted box in panel **(G)**; bar, 200 μm. Sc, secretory cavity; Ve, vein; UE, upper epidermis (adaxial side); LE, lower epidermis (abaxial side); Xy, xylem; Ph, phloem; Pa, palisade tissue; Sp, spongy tissue.

abnormal leaves could be all due to their incomplete unfolding, whose structure is more likely due to abaxialization.

Transcriptome change in ANL buds

To investigate the genetic basis for the ANL development, we performed transcriptome analysis. Six transcript libraries from the NL buds (NL1, NL2, and NL3) and ANL buds (ANL1, ANL2, and ANL3) were constructed and analyzed by high throughout RNA-seq. With the process of quality control for raw data, 65,905,424, 87,418,414, 98,233,334, 136,008,800, 72,083,256, and 65,922,944 clean reads were obtained from these libraries with Q30 above 85.20%. The clean data were mapped to the *G. biloba* genome (Guan et al., 2016), and the alignment ratio of samples ranges from 93.41% to 94.26% (Supplementary Table S2). Based on the comparison, 1,796 novel genes were discovered, of which 1,038 genes were annotated.

The transcript abundance of each gene from NL and ANL data were normalized into FPKM. Compared with NL, a total of 3,762 significant difference expression genes (DEGs) were identified in ANL libraries with the threshold of fold change ≥2 and FDR ≤ 0.05 (Supplementary Table S3), including 1,391 upregulated and 2,371 downregulated genes (Supplementary Figure S2). Among these identified DEGs, 1,917 DEGs were annotated with 21 biological processes, 16 cellular component, and 13 molecular functions in GO categories, and significantly enriched ($p \leq 0.01$) into 76 GO terms (Supplementary Table S4). Among downregulated genes, the term of "cellular glucan metabolic process," "oxidation–reduction process," "response to desiccation," "response to stress," and "lignin catabolic process" were the dominant groups in the biology process (Supplementary Figure S3A), while the upregulated genes mainly focused on "nucleosome assembly," "cell proliferation," and "flavonol biosynthetic process" (Supplementary Figure S3B). Furthermore, 3,762 significantly DEGs were compared with KEGG database to analyze their biology pathway. The 276 downregulated genes were enriched to 84 KEGG pathway (Supplementary Table S5), of which the most significant ones were "phenylpropanoid biosynthesis," "cutin, suberine, and wax biosynthesis," "flavonoid biosynthesis," and "plant hormone signal transduction" (Supplementary Figure S4A). While 76 enriched pathways were identified from 161 upregulated genes (Supplementary Table S5), and "betalain biosynthesis," "arginine biosynthesis," and "nitrogen metabolism" were the top 3 (Supplementary Figure S4B). The significant change in GO terms and KEGG pathway indicates the significant reprogramming of gene expression in ANL development.

The genes related to leaf formation

The anatomical structure of the trumpet-type leaves was similar to abaxialized leaves in the dicotyledons, and needle-type leaves might have resulted from severe abaxialization of leaf development. The adaxial–abaxial prepattern of leaf might be established prior to leaf initiation, and the adaxial–abaxial polarity genes had prepattern expressed at the PZ prior to leaf primordium formation (Yu et al., 2017). Therefore, we screened the adaxial–abaxial polarity genes in *Arabidopsis* that are mainly involved in the formation and maintenance of adaxial–abaxial polarity of leaves to find out their homologous genes in *G. biloba*. The differentially expressed genes (Supplementary Table S6) were assigned with their expression values in the regulatory network on the leaf adaxial–abaxial development (Figure 4).

Three *ARFs* (*ETTIN* (*ARF3*), *ARF4*, and *ARF2*), *KAN*, and *YAB* genes are expressed in the abaxial domain and redundantly promote abaxial identity. There were five *ARF*, two *KAN*, and two *YAB Ginkgo* homologous genes that were higher expressed in ANL buds, indicating that the increasing expression values of these abaxial dominant genes would promote leaf abaxial development. The *HD-ZIPIII* and *ASYMMETRIC LEAF1* genes are predominantly expressed on the adaxial domain and can promote adaxial cell fate. Two *Ginkgo HB* homologous genes exhibited lower expression values in ANL than in NL buds, while the expression of *AS1* and *AS2* homologous genes slightly decreased in ANL buds. The adaxially localized *AS1–AS2* complex negatively regulates the expression of *ETT*, *ARF4*, *KAN*, and *YAB* (Iwasaki et al., 2013) but positively regulates *HD-ZIPIII* expression (Fu et al., 2007). Therefore, the decreased expression of these adaxial dominant genes might weaken their promotion on leaf adaxial domain while reducing their inhibition on abaxial dominant genes, leading to the enhanced development of abaxial domain in ANL.

The normal leaves of "SongZhen" were fully expanded fan-shaped blades, while most of the abnormal leaves were smaller

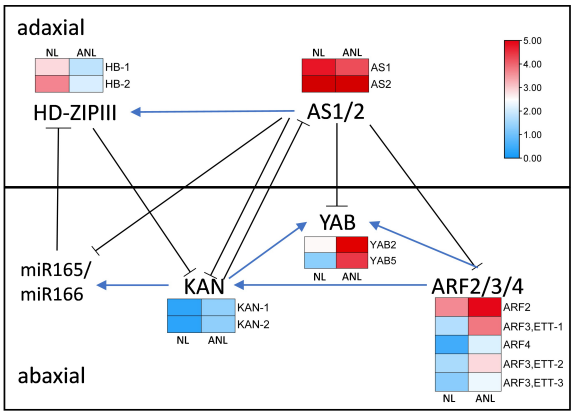

FIGURE 4
The gene regulatory network on leaf adaxial–abaxial development with their expression change in NL and ANL buds. AS, asymmetric leaf; HD-ZIPIII, homeodomain-leucine zipper III; ARF, AUXIN RESPONSE FACTOR; YAB, YABBY; KAN, KANADI; miR165/166, microRNA165/166.

and narrower than normal ones. The abnormal leaves were divided into two parts from the leaf stalk, in which the expanded side was half fan shaped, and the unfolded side was fused into trumpet or into more serious needle shaped. The *CUC* and *TCP* transcription factors are crucial for boundary formation and margin separation. The homologous *CUC1*, *CUC2*, and *CUC3* genes exhibited lower expression, while the two *TCP* genes showed higher expression in ANL buds (Figure 5). This indicated that the formation of needle-type, trumpet-type, and deep-split leaves in ANL might be due to the downregulation of *CUC* genes and upregulation of *TCP* genes, which limited the tissue development and separation. The *WOX* genes are expressed at the adaxial–abaxial boundary layer, where they can promote leaf blade outgrowth. In ANL buds, the expression values of *WOX1* genes were lower compared with that in NL buds. This might also explain why the abnormal leaves are smaller and narrower compared to the normal leaves.

The expression of DEGs in abnormal leaves

In order to determine whether the expression levels of above genes in different morphological leaves of "SongZhen" were related to the variation degree of abnormal leaves, quantitative PCR was performed in the collected samples of six different leaf types, including normal leaf, unfolded and trumpet leaf, unfolded and needle leaf, double-trumpet leaf, double-needle leaf, single-trumpet leaf, and single-needle leaf according to the degree of leaf variation. The gene expression in abnormal and normal leaves was consistent with that in buds (Figure 6). The abaxial dominant genes, such as *YAB2*, *YAB5*, *ARF2*, and *ARF3*, were highly expressed in abnormal leaves, and the expression levels increased with the degree of leaf variation, especially *YAB2* whose expression values were increased gradually from NL to SN. In contrary, the expression levels of *AS2* in different types of abnormal leaves were similar, but they all were lower than that in normal leaves, and *HB-1* was lowly expressed from UNT to DT accordingly (Figure 6A). In abnormal leaves, the expression levels of *CUC* genes were much lower than that of normal leaves, and their expression values reduced gradually from UNT to SN except *CUC2-2*, while the *TCP* genes were highly expressed in needle and trumpet leaves (Figure 6B). This indicates that these genes related to adaxial–abaxial formation and boundary development might affect the formation of abnormal leaves in "SongZhen."

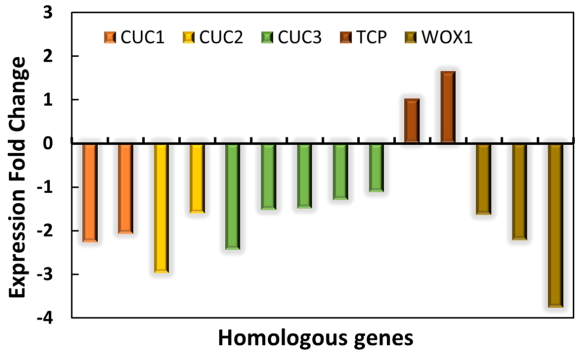

FIGURE 5
The expression changes in *CUC*, *TCP*, and *WOX* genes in ANL buds compared with NL buds.

Discussion

The development of the leaf is mainly through the formation and maintenance of polarity of the medial–lateral, proximal–distal, and adaxial–abaxial axis to achieve the three-dimensional structure, which is determined by a complex network of genes. *Ginkgo biloba* has a typical dichotomous bifurcate leaf structure, while different leaf types of the *G. biloba* variety "SongZhen" provide materials to access the mechanism of the formation of variant leaf types of *G. biloba*, which may shed light on the unique leaf development of *G. biloba* in an evolutionary view.

The variant materials of "SongZhen" could reflect the leaf evolution in *Ginkgo*. The double-needle- and double-trumpet-shaped leaves are similar to that of the Middle Jurassic *Ginkgo* leaf fossils unearthed in Uzbekistan (Nosova, 2013) from coniferous *Ginkgo* dated back about 200 million years ago. According to the telome theory, the leaves of *G. biloba* had undergone a series of evolution from dichophyllum with two main veins, to *Trichopitys* having the hairy leaves with four main

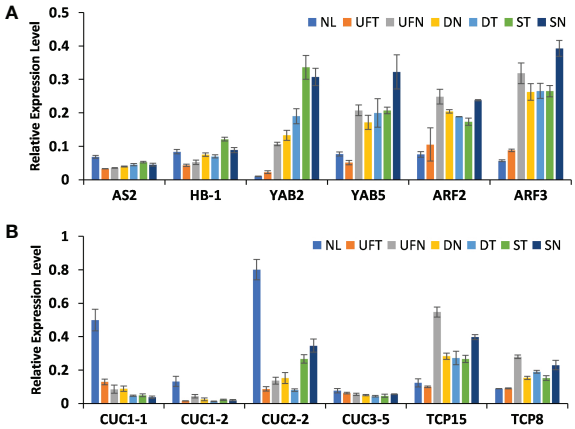

FIGURE 6
The relative expression profiles of genes in abnormal and normal leaves. The relative expression levels of genes related to **(A)** leaf adaxial–abaxial formation and **(B)** leaf boundary formation. NL, normal leaf; UFT, unfolded and trumpet leaf; UFN, unfolded and needle leaf; DN, double-needle leaf; DT, double-trumpet leaf; ST, single-trumpet leaf; SN, single-needle leaf.

veins, then the hairy leaves became thin and lobed type *Baiera*, and finally evolved into the four-lobe type *Ginkgoites* sp., which was the most recent ancestor to the modern *G. biloba* leaves (Zhou and Zheng, 2003; Zhou, 2006). There are paired vascular bundles transiting from the stem to the petiole, and each vascular bundle in the petiole gradually produces bifurcated branches to form four parallel vascular bundles; then, the four vascular bundles in the petiole produce three- and four-level bifurcated branches in *Ginkgo* leaves (Zhou, 2006). The double-needle (trumpets) leaf, needle and trumpet leaf, unfolded and needle (trumpet) leaf, or deep-split leaf in "SongZhen" have the vascular bundles joined together in the petiole but divided into two parts in the blade, which can be seen from the cross-section of the base of the double-trumpet leaves (Figure 2D) and of trumpet leaf with the separated vascular bundles (Figure 2E). The variant leaf types of "SongZhen" have the characteristics of *dichophyllum*, *Trichopitys*, and *Baiera*, having bifurcated, deeply split, or unfolded leaves. Therefore, it is speculated that the appearance of "SongZhen" may be a kind of atavism caused by bud mutation. The needle-like and the fused vascular bundles in abnormal leaves are regarded as "atavism" (Bauer et al., 2013; Nosova, 2013). The failure of adaxial–abaxial polarity formation and boundary separation are probably the reason to give rise to needle (trumpet) leaves with abaxialization and boundary fusion.

The most obvious variation of "SongZhen" were needle- and trumpet-type leaves. It can be seen from the transverse anatomy that the trumpet-type leaves form one or two closed rings on both sides of the central axis of the leaves, but they have a complete leaf structure with the upper epidermis in the inner ring and the lower epidermis in the outer ring. This is similar to the abaxialized leaves in dicotyledons, with promoted development of the abaxial domain to surrounding the adaxial domain. The needle-type leaves are the most severe case, which are similar to *phan* mutant in *Antirrhinum* and *as1/as2* double mutant in *Arabidasis* that lack laminae and adaxial cell types (Xu et al., 2003). It can be inferred that the development of the abaxial region of abnormal-type leaves may be greater than the adaxial region or even no adaxial region.

At present, the research on leaf polarity development is mainly focused in *Arabidopsis*, but the expression and function of the adaxial- and abaxial-domain-promoting genes may be diversified among various species. There are four *KANADI* paralogs in *Arabidopsis* with *KAN1* and *KAN2* specifying in abaxial leaf identity. Loss-of-function *kan1* and *kan2* mutants develop narrow cotyledons and leaves with ectopic outgrowths on their abaxial side and display adaxialized lateral organs, while *KAN1* and *KAN2* overexpression causes abaxialization and SAM termination (Eshed et al., 2001; Kerstetter et al., 2001). Phylogenetic analysis and *in situ* hybridization showed that the KAN function in leaf polarity is likely conserved across ferns, gymnosperms, and angiosperms except lycophyte (Zumajo-Cardona et al., 2019). In addition, severe polarity defects were observed in *Arabidopsis ett-1 arf4-1* and *ett-1 arf4-2* double-mutant plants resulting in abaxialized leaves similar to *kan1 kan2* mutants (Pekker et al., 2005). In fact, ARF and KAN proteins may form complexes and play a synergism role in promoting abaxial region differentiation (Kelley et al., 2012). The YABBY transcription factor family is expressed on the abaxial side of lateral organs and redundantly promote abaxial identity in *Arabidopsis*. Loss of function of two redundant *YAB* genes, namely, *FILAMENTOUS FLOWER* (*FIL*) and *YABBY3* (*YAB3*), results in narrow leaves and a partial loss of abaxial cell identity, whereas ectopic expression of *FIL* or *YAB3* in leaves and petals causes partial abaxialization (Siegfried et al., 1999; Eshed et al., 2001). However, the *YAB* gene expression is adaxialized in maize (Juarez et al., 2004) and is not polarized in rice (Yamaguchi et al., 2004), wheat (Zhao et al., 2006), soybean (Yang et al., 2019), and bamboo (Liu et al., 2020). Ectopic expressions of wheat *TaYAB1* and soybean *GmFILa* in *Arabidopsis* both cause the partial abaxialization of the adaxial epidermises of leaves (Zhao et al., 2006; Yang et al., 2019). These results indicate that the expression patterns and function of *YAB* genes have diverged between monocots and dicots. In ANL buds, *KAN* (*KAN1* and *KAN2*), *ARF* (*ETT*, *ARF2*, and *ARF4*), and *YAB* genes were upregulated. The higher expression of these abaxial domain-promoting genes in ANL buds and abnormal leaves might promote the overdevelopment of the abaxial domain of abnormal leaves, and the adaxial mesophyll cells are replaced by abaxial cells that leads to abaxialization leaves of "SongZhen."

HD-ZIPIII expression is sufficient to define adaxial cell fate, and they have conserved functional roles in *Arabidopsis*, rice, maize, and most likely across angiosperms (Dkhar and Pareek, 2014). Dominant gain-of-function *phb*, *phv*, and *rev* mutants show loss of abaxial identity and adaxialization of leaves, while loss-of-function *phb phv rev* triple-mutant plants form severe abaxialized leaves and exhibit loss-of-SAM phenotypes in *Arabidopsis* (McConnell et al., 2001; Emery et al., 2003). Two *HB* genes had lower expression values in ANL buds, and *HB-1* was also lowly expressed in abnormal leaves, suggesting that the abnormal leaf development was abaxialized. Adaxial cell fate is also promoted by *AS2*. The overexpression of *AS2* in *Arabidopsis* resulted in plants with narrower curly leaves displaying dramatic alteration in the identity of both adaxial and abaxial epidermal cells, and the abaxial side showed mostly adaxial features (Xu et al., 2003). The expression values of *AS2* had lower expression in abnormal leaves than normal ones, which further caused the abaxialization of "SongZhen" leaves. Therefore, *HD-ZIPIII* and *AS1–AS2* that had lower expression in ANL buds and abnormal leaves will weaken their inhibition on genes specified in the leaf abaxial side and eventually lead to the leaf abaxialization. To sum up, the expression of adaxial–abaxial polarity genes in "SongZhen" was similar to that in *Arabidopsis*, indicating that these genes may play a decisive role in leaf development, thus showing some conservatism between gymnosperms and angiosperms. However, the regulatory mechanism in leaf development among different species remains to be further studied.

Boundary separation is probably hurdled in single- or double-needle (trumpet) leaves in "SongZhen." The low expression of *CUC*s and high expression of *TCPs* in ANL may explain this type of development. *cuc1 cuc2* double mutation causes a complete lack of embryonic shoot meristem formation and a fusion of the cotyledons

(Aida et al., 1999; Hibara et al., 2006). *CUC3* also participates in embryonic shoot meristem formation and cotyledon boundary formation redundantly with *CUC1* and *CUC2* (Vroemen et al., 2003). Furthermore, inactivation of TCP function in *Arabidopsis* (Efroni et al., 2008), or its orthologs CINCINNATA (CIN) in *Antirrhinum* (Nath et al., 2003) and LANCEOLATE (LA) in tomato (Ori et al., 2007), causes overproliferation at the leaf margin, which leads to expanded, crinkly leaves or leaflets with serrated margin. In addition, overexpression of TCP3 suppresses the expression of *CUC* genes and results in the fusion of cotyledons and defects in formation of shoots (Koyama et al., 2007; Koyama et al., 2017). In ANL buds, the low expression of *CUC*s while the high expression of *TCP*s would affect the boundary formation in "SongZhen" with needle or fused trumpet-type leaves. Quantitative PCR results also showed that the expression of *CUC* genes in abnormal leaves was much lower than that in normal ones, while the expression of *TCP* genes was higher in abnormal leaves, indicating that *CUC* and *TCP* play an important role in the formation of abnormal leaves of "SongZhen."

Overall, the leaf phenotype of "SongZhen" variety is heritable. The plants obtained through grafting can have these abnormal leaf types continuously for more than years. However, the appearance and amount of these abnormal leaves are random, and the leaf type on a long branch may change in different years, although the abnormal and normal leaves are always clustered on different short branches, respectively. This indicates that the environment fluctuation may influence gene expression, leading to the phenotypic change. Transcriptome data in this study also show that "oxidation reduction process," "response to desiccation," and "response to stress" are the main biological processes among downregulated genes, indicating that "SongZhen" mutants are more vulnerable to the physiological and environmental changes, resulting in the randomness and variability of genetic variation. The results of microscopy and transcriptome analysis showed that the abnormal leaves of *G. biloba* "SongZhen" are mainly caused by the imbalance of abaxial and adaxial development of leaf and the impairment of leaf boundary. The genes related to abaxial domain are highly expressed, while the expression levels of adaxial-domain promoting genes are decreased in ANL buds. In addition, the low expression of genes related to leaf boundary development in ANL buds indicates that single- or double-needle (trumpet) leaves may be due to the leaf tissue fusion. This study provides an insight into the mechanism of the development of the abnormal leaves in "SongZhen" and the hint in evolution of *G. biloba* leaves.

Data availability statement

The original contributions presented in the study are publicly available. This data can be found here: NCBI, PRJNA896381.

Author contributions

ML and YW designed the study. FT and PS collected the tissues used for this study and analyzed the data. FT completed the section and microscopic observation of different types of leaves in "SongZhen." FT drafted the manuscript, and ML revised it. QZ and FZ gave valuable suggestions to the manuscript. All authors contributed to the article and approved the submitted version.

Funding

This work was supported by the Special Support Funds for the National Ten-thousand Talents Program of China to ML.

Acknowledgments

We thank Yanyan Huang, Taishan Academy of Forestry Sciences, for her valuable technical support in collecting samples and Xuejiao He, Chinese Academy of Forestry, for her assistance in microscopy and image preparation.

Conflict of interest

The authors declare that the research was conducted in the absence of any commercial or financial relationships that could be construed as a potential conflict of interest.

Publisher's note

Supplementary material

The Supplementary Material for this article can be found online at: https://www.frontiersin.org/articles/10.3389/fpls.2022.1081280/full#supplementary-material

References

Aida, M., Ishida, T., and Tasaka, M. (1999). Shoot apical meristem and cotyledon formation during *Arabidopsis* embryogenesis: interaction among the *Cup-shaped cotyledon* and *Shoot meristemless* genes. *Development* 126 (8), 1563–1570. doi: 10.1242/dev.126.8.1563

Alvarez, J. P., Goldshmidt, A., Efroni, I., Bowman, J. L., and Eshed, Y. (2009). The NGATHA distal organ development genes are essential for style specification in arabidopsis. *Plant Cell.* 21 (5), 1373–1393. doi: 10.1105/tpc.109.065482

Bar, M., and Ori, N. (2014). Leaf development and morphogenesis. *Development* 141 (22), 4219–4230. doi: 10.1242/dev.106195

Bauer, K., Grauvogel-Stamm, L., Kustatscher, E., and Krings, M. (2013). Fossil ginkgophyte seedlings from the Triassic of France resemble modern ginkgo biloba. *BMC Evol. Biol.* 13 (1), 177. doi: 10.1186/1471-2148-13-177

Beerling, D. J., Osborne, C. P., and Chaloner, W. G. (2001). Evolution of leaf-form in land plants linked to atmospheric CO_2 decline in the late Palaeozoic era. *Nature* 410 (6826), 352–354. doi: 10.1038/35066546

Byrne, M. E., Barley, R., Curtis, M., Arroyo, J. M., Dunham, M., Hudson, A., et al. (2000). *Asymmetric leaves1* mediates leaf patterning and stem cell function in *Arabidopsis*. *Nature* 408 (6815), 967–971. doi: 10.1038/35050091

Chitwood, D. H., and Sinha, N. R. (2016). Evolutionary and environmental forces sculpting leaf development. *Curr. Biol.* 26 (7), R297–R306. doi: 10.1016/j.cub.2016.02.033

David, J. B. (2005). Leaf evolution: Gases, genes and geochemistry. *Ann. Bot.* 96 (3), 345–352. doi: 10.1093/aob/mci186

Dkhar, J., and Pareek, A. (2014). What determines a leaf's shape? *EvoDevo* 5 (1), 47. doi: 10.1186/2041-9139-5-47

Du, F., Guan, C., and Jiao, Y. (2018). Molecular mechanisms of leaf morphogenesis. *Mol. Plant* 11 (9), 1117–1134. doi: 10.1016/j.molp.2018.06.006

Efroni, I., Blum, E., Goldshmidt, A., and Eshed, Y. (2008). A protracted and dynamic maturation schedule underlies *Arabidopsis* leaf development. *Plant Cell.* 20 (9), 2293–2306. doi: 10.1105/tpc.107.057521

Emery, J. F., Floyd, S. K., Alvarez, J., Eshed, Y., Hawker, N. P., Izhaki, A., et al. (2003). Radial patterning of *Arabidopsis* shoots by class III HD-ZIP and KANADI genes. *Curr. Biol.* 13 (20), 1768–1774. doi: 10.1016/j.cub.2003.09.035

Eshed, Y., Baum, S. F., Perea, J. V., and Bowman, J. L. (2001). Establishment of polarity in lateral organs of plants. *Curr. Biol.* 11 (16), 1251–1260. doi: 10.1016/S0960-9822(01)00392-X

Eshed, Y., Izhaki, A., Baum, S. F., Floyd, S. K., and Bowman, J. L. (2004). Asymmetric leaf development and blade expansion in *Arabidopsis* are mediated by KANADI and YABBY activities. *Development* 131 (12), 2997–3006. doi: 10.1242/dev.01186

Fu, Y., Xu, L., Xu, B., Yang, L., Ling, Q., Wang, H., et al. (2007). Genetic interactions between leaf polarity-controlling genes and *ASYMMETRIC LEAVES1* and *2* in *Arabidopsis* leaf patterning. *Plant Cell Physiol.* 48 (5), 724–735. doi: 10.1093/pcp/pcm040

Guan, C., Wu, B., Yu, T., Wang, Q., Krogan, N. T., Liu, X., et al. (2017). Spatial auxin signaling controls leaf flattening in *Arabidopsis*. *Curr. Biol.* 27 (19), 2940–2950. doi: 10.1016/j.cub.2017.08.042

Guan, R., Zhao, Y., Zhang, H., Fan, G., Liu, X., Zhou, W., et al. (2016). Draft genome of the living fossil *Ginkgo biloba*. *GigaScience* 5 (1), 49. doi: 10.1186/s13742-016-0154-1

He, B., Li, Z., Hao, X., and He, Y. (2014). A new technique of fast paraffin sectioning in plant tissues. *Chin. Bull. Bot.* 48 (2), 203–208. doi: 10.3724/SP.J.1259.2014.00203

Hibara, K.-i., Karim, M.R., Takada, S., Taoka, K.-i., Furutani, M., Aida, M., et al. (2006). *Arabidopsis CUP-SHAPED COTYLEDON3* regulates postembryonic shoot meristem and organ boundary formation. *Plant Cell.* 18 (11), 2946–2957. doi: 10.1105/tpc.106.045716

Husbands, A. Y., Benkovics, A. H., Nogueira, F. T. S., Lodha, M., and Timmermans, M. C. P. (2015). The ASYMMETRIC LEAVES complex employs multiple modes of regulation to affect adaxial-abaxial patterning and leaf complexity. *Plant Cell.* 27 (12), 3321–3335. doi: 10.1105/tpc.15.00454

Iwasaki, M., Takahashi, H., Iwakawa, H., Nakagawa, A., Ishikawa, T., Tanaka, H., et al. (2013). Dual regulation of *ETTIN* (*ARF3*) gene expression by AS1-AS2, which maintains the DNA methylation level, is involved in stabilization of leaf adaxial-abaxial partitioning in *Arabidopsis*. *Development* 140 (9), 1958–1969. doi: 10.1242/dev.085365

Juarez, M. T., Twigg, R. W., and Timmermans, M. C. P. (2004). Specification of adaxial cell fate during maize leaf development. *Development* 131 (18), 4533–4544. doi: 10.1242/dev.01328

Kelley, D. R., Arreola, A., Gallagher, T. L., and Gasser, C. S. (2012). ETTIN (ARF3) physically interacts with KANADI proteins to form a functional complex essential for integument development and polarity determination in *Arabidopsis*. *Development* 139 (6), 1105–1109. doi: 10.1242/dev.067918

Kenrick, P., and Crane, P. R. (1997). The origin and early evolution of plants on land. *Nature* 389 (6646), 33–39. doi: 10.1038/37918

Kerstetter, R. A., Bollman, K., Taylor, R. A., Bomblies, K., and Poethig, R. S. (2001). *KANADI* regulates organ polarity in *Arabidopsis*. *Nature* 411 (6838), 706–709. doi: 10.1038/35079629

Kim, Y.-S., Kim, S.-G., Lee, M., Lee, I., Park, H.-Y., Seo, P. J., et al. (2008). HD-ZIP III activity is modulated by competitive inhibitors *via* a feedback loop in *Arabidopsis* shoot apical meristem development. *Plant Cell.* 20 (4), 920–933. doi: 10.1105/tpc.107.057448

Kim, M., Mccormick, S., Timmermans, M., and Sinha, N. (2003). The expression domain of *PHANTASTICA* determines leaflet placement in compound leaves. *Nature* 424 (6947), 438–443. doi: 10.1038/nature01820

Koyama, T., Furutani, M., Tasaka, M., and Ohme-Takagi, M. (2007). TCP Transcription factors control the morphology of shoot lateral organs *via* negative regulation of the expression of boundary-specific genes in *Arabidopsis*. *Plant Cell.* 19 (2), 473–484. doi: 10.1105/tpc.106.044792

Koyama, T., Sato, F., and Ohme-Takagi, M. (2017). Roles of miR319 and TCP transcription factors in leaf development. *Plant Physiol.* 175 (2), 874–885. doi: 10.1104/pp.17.00732

Liu, S., Li, X., Yang, H., Qian, Q., and Lin, X. (2020). Ectopic expression of *BoYAB1*, a member of *YABBY* gene family in *Bambusa oldhamii*, causes leaf curling and late flowering in *Arabidopsis thaliana*. *J. Hortic. Sci. Biotechnol.* 95 (2), 169–174. doi: 10.1080/14620316.2019.1661289

Mao, X., Cai, T., Olyarchuk, J. G., and Wei, L. (2005). Automated genome annotation and pathway identification using the KEGG orthology (KO) as a controlled vocabulary. *Bioinformatics* 21 (19), 3787–3793. doi: 10.1093/bioinformatics/bti430

McConnell, J. R., Emery, J., Eshed, Y., Bao, N., Bowman, J., and Barton, M. K. (2001). Role of *PHABULOSA* and *PHAVOLUTA* in determining radial patterning in shoots. *Nature* 411 (6838), 709–713. doi: 10.1038/35079635

Merelo, P., Xie, Y., Brand, L., Ott, F., Weigel, D., Bowman, J. L., et al. (2013). Genome-wide identification of KANADI1 target genes. *PloS One* 8 (10), e77341. doi: 10.1371/journal.pone.0077341

Nakata, M., Matsumoto, N., Tsugeki, R., Rikirsch, E., Laux, T., and Okada, K. (2012). Roles of the middle domain–specific *WUSCHEL-RELATED HOMEOBOX* genes in early development of leaves in *Arabidopsis*. *Plant Cell.* 24 (2), 519–535. doi: 10.1105/tpc.111.092858

Nath, U., Crawford, B. C. W., Carpenter, R., and Coen, E. (2003). Genetic control of surface curvature. *Science* 299 (5611), 1404–1407. doi: 10.1126/science.1079354

Nosova, N. (2013). Revision of the genus grenana samylina from the middle Jurassic of angren, Uzbekistan. *Rev. Palaeobo. Palynol.* 197, 226–252. doi: 10.1016/j.revpalbo.2013.06.005

Ori, N., Cohen, A. R., Etzioni, A., Brand, A., Yanai, O., Shleizer, S., et al. (2007). Regulation of *LANCEOLATE* by miR319 is required for compound-leaf development in tomato. *Nat. Genet.* 39 (6), 787–791. doi: 10.1038/ng2036

Pekker, I., Alvarez, J. P., and Eshed, Y. (2005). Auxin response factors mediate *Arabidopsis* organ asymmetry *via* modulation of KANADI activity. *Plant Cell.* 17 (11), 2899–2910. doi: 10.1105/tpc.105.034876

Siegfried, K. R., Eshed, Y., Baum, S. F., Otsuga, D., Drews, G. N., and Bowman, J. L. (1999). Members of the *YABBY* gene family specify abaxial cell fate in *Arabidopsis*. *Development* 126 (18), 4117–4128. doi: 10.1242/dev.126.18.4117

Tang, G., Reinhart, B. J., Bartel, D. P., and Zamore, P. D. (2003). A biochemical framework for RNA silencing in plants. *Genes Dev.* 17 (1), 49–63. doi: 10.1101/gad.1048103

Timmermans, M. C. P., Hudson, A., Becraft, P. W., and Nelson, T. (1999). ROUGH SHEATH2: A myb protein that represses *knox* homeobox genes in maize lateral organ primordia. *Science* 284 (5411), 151–153. doi: 10.1126/science.284.5411.151

Vandenbussche, M., Horstman, A., Zethof, J., Koes, R., Rijpkema, A. S., and Gerats, T. (2009). Differential recruitment of *WOX* transcription factors for lateral development and organ fusion in petunia and *Arabidopsis*. *Plant Cell.* 21 (8), 2269–2283. doi: 10.1105/tpc.109.065862

Vroemen, C. W., Mordhorst, A. P., Albrecht, C., Kwaaitaal, M. A. C. J., and de Vries, S. C. (2003). The *CUP-SHAPED COTYLEDON3* gene is required for

boundary and shoot meristem formation in arabidopsis. *Plant Cell.* 15 (7), 1563–1577. doi: 10.1105/tpc.012203

Waites, R., and Hudson, A. (1995). *phantastica*: a gene required for dorsoventrality of leaves in *Antirrhinum majus*. *Development* 121, 2143–2154. doi: 10.1016/s0092-8674(00)81439-7

Wang, Y., Fang, R., Lin, M., Lu, Y., Wang, L., and Jin, B. (2011). Anatomical structure dynamics of *Ginkgo biloba* l. leaves during annual growth and development. *Acta Botanica Boreali-Occidentalia Sinica.* 31 (5), 0861–0867.

Wang, Y., Song, C., Guo, S., Zhang, T., and Huang, Y. (2009). A new variety *Ginkgo biloba* 'SongZhen'. *Sci. Silvae Sinicae.* 12 (9), 174–174. doi: 10.11707/j.1001-7488.20090930

Wenkel, S., Emery, J., Hou, B.-H., Evans, M. M. S., and Barton, M. K. (2007). A feedback regulatory module formed by LITTLE ZIPPER and HD-ZIPIII genes. *Plant Cell.* 19 (11), 3379–3390. doi: 10.1105/tpc.107.055772

Xu, L., Xu, Y., Dong, A., Sun, Y., Pi, L., Xu, Y., et al. (2003). Novel *as1* and *as2* defects in leaf adaxial-abaxial polarity reveal the requirement for *ASYMMETRIC LEAVES1* and *2* and *ERECTA* functions in specifying leaf adaxial identity. *Development* 130 (17), 4097–4107. doi: 10.1242/dev.00622

Yamaguchi, T., Nagasawa, N., Kawasaki, S., Matsuoka, M., Nagato, Y., and Hirano, H.-Y. (2004). The *YABBY* gene *DROOPING LEAF* regulates carpel specification and midrib development in *Oryza sativa*. *Plant Cell.* 16 (2), 500–509. doi: 10.1105/tpc.018044

Yang, H., Shi, G., Li, X., Hu, D., Cui, Y., Hou, J., et al. (2019). Overexpression of a soybean *YABBY* gene, *GmFILa*, causes leaf curling in *Arabidopsis thaliana*. *BMC Plant Biol.* 19 (1), 234. doi: 10.1186/s12870-019-1810-2

Young, M. D., Wakefield, M. J., Smyth, G. K., and Oshlack, A. (2010). Gene ontology analysis for RNA-seq: accounting for selection bias. *Genome Biol.* 11 (2), R14. doi: 10.1186/gb-2010-11-2-r14

Yu, T., Guan, C., Wang, J., Sajjad, M., Ma, L., and Jiao, Y. (2017). Dynamic patterns of gene expression during leaf initiation. *J. Genet. Genomics* 44 (12), 599–601. doi: 10.1016/j.jgg.2017.11.001

Žádníková, P., and Simon, R. (2014). How boundaries control plant development. *Curr. Opin. Plant Biol.* 17, 116–125. doi: 10.1016/j.pbi.2013.11.013

Zhao, W., Su, H. Y., Song, J., Zhao, X. Y., and Zhang, X. S. (2006). Ectopic expression of *TaYAB1*, a member of *YABBY* gene family in wheat, causes the partial abaxialization of the adaxial epidermises of leaves and arrests the development of shoot apical meristem in *Arabidopsis*. *Plant Sci.* 170 (2), 364–371. doi: 10.1016/j.plantsci.2005.09.008

Zhou, Z. (1991). Phylogeny and evolutionary trends of mesozoic ginkgoaleans - a preliminary assessment. *Rev. Palaeobo. Palynol.* 68 (3), 203–216. doi: 10.1016/0034-6667(91)90024-W

Zhou, Z. (2003). Mesozoic ginkgoaleans: Phylogeny, classification and evolutionary trends. *Acta Botanica Yunnanica.* 25 (4), 377–396. doi: 10.3969/j.issn.2095-0845.2003.04.001

Zhou, X. (2006). Development and evolution of leaves of *Ginkgo biloba*. *J. Shenyang Univ.* 18 (4), 83–86.

Zhou, Z., Quan, C., and Liu, Y.-S. (2012). Tertiary *Ginkgo* ovulate organs with associated leaves from north Dakota, U.S.A., and their evolutionary significance. *Int. J. Plant Sci.* 173 (1), 67–80. doi: 10.1086/662651

Zhou, Z., and Zheng, S. (2003). The missing link in *Ginkgo* evolution. *Nature* 423 (6942), 821–822. doi: 10.1038/423821a

Zumajo-Cardona, C., Vasco, A., and Ambrose, B. A. (2019). The evolution of the *KANADI* gene family and leaf development in lycophytes and ferns. *Plants* 8 (9), 313. doi: 10.3390/plants8090313

frontiers | Frontiers in Plant Science

TYPE Mini Review
PUBLISHED 12 December 2022
DOI 10.3389/fpls.2022.1086384

OPEN ACCESS

EDITED BY
Simon Scofield,
Cardiff University, United Kingdom

REVIEWED BY
Malay Das,
Presidency University, India

*CORRESPONDENCE
Min-Yao Jhu
myj23@cam.ac.uk
Neelima R. Sinha
nrsinha@ucdavis.edu

SPECIALTY SECTION
This article was submitted to Plant Development and EvoDevo, a section of the journal Frontiers in Plant Science

RECEIVED 01 November 2022
ACCEPTED 28 November 2022
PUBLISHED 12 December 2022

CITATION
Jhu M-Y and Sinha NR (2022) *Cuscuta* species: Model organisms for haustorium development in stem holoparasitic plants.
Front. Plant Sci. 13:1086384.
doi: 10.3389/fpls.2022.1086384

Cuscuta species: Model organisms for haustorium development in stem holoparasitic plants

Min-Yao Jhu[1]* and Neelima R. Sinha[2]*

[1]Crop Science Centre, Department of Plant Sciences, University of Cambridge, Cambridge, United Kingdom, [2]Department of Plant Biology, University of California, Davis, CA, United States

Parasitic plants are notorious for causing serious agricultural losses in many countries. Specialized intrusive organs, haustoria, confer on parasitic plants the ability to acquire water and nutrients from their host plants. Investigating the mechanism involved in haustorium development not only reveals the fascinating mystery of how autotrophic plants evolved parasitism but also provides the foundation for developing more effective methods to control the agricultural damage caused by parasitic plants. *Cuscuta* species, also known as dodders, are one of the most well-known and widely spread stem holoparasitic plants. Although progress has been made recently in understanding the evolution and development of haustoria in root parasitic plants, more and more studies indicate that the behaviors between root and stem haustorium formation are distinct, and the mechanisms involved in the formation of these organs remain largely unknown. Unlike most endoparasites and root holoparasitic plants, which have high host-specificity and self- or kin-recognition to avoid forming haustoria on themselves or closely related species, auto-parasitism and hyper-parasitism are commonly observed among *Cuscuta* species. In this review, we summarize the current understanding of haustorium development in dodders and the unique characteristics of their parasitizing behaviors. We also outline the advantages of using *Cuscuta* species as model organisms for haustorium development in stem holoparasitic plants, the current unknown mysteries and limitations in the *Cuscuta* system, and potential future research directions to overcome these challenges.

KEYWORDS

***Cuscuta*, parasitic plants, haustorium, model organisms, parasitism, holoparasite, organ development, organogenesis**

1 Introduction

Plants have often been defined as autotrophic eukaryotic photosynthetic organisms. Plants have chlorophyll, which enables them to convert inorganic carbons into carbohydrates utilizing light energy. However, parasitic plants are exceptions to this definition. They evolved to form a specialized organ, the haustorium, which allows parasitic plants to obtain water and nutrients from their host plants (Yoshida et al., 2016; Kokla and Melnyk, 2018). Depending on the haustorium attachment position on their host, parasitic plants are generally categorized as stem or root parasites. Based on their host dependency, parasitic plants are classified as hemiparasites or holoparasites. Holoparasitic plants have mostly lost their photosynthetic ability and need to rely entirely on their hosts to provide water and nutrients. Therefore, haustorium formation has been considered an essential element for plant parasitism (Yoshida et al., 2016; Kokla and Melnyk, 2018). Investigating the mechanism involved in haustorium development reveals how autotrophic plants evolved to acquire heterotrophic lifestyles. Our evolutionary developmental knowledge of haustorium formation also provides the foundation for developing more effective methods to control the agricultural damage caused by parasitic plants.

Cuscuta species (dodders) are the most well-known and widely spread stem holoparasitic plants. The *Cuscuta* genus comprises about 200 species and is the only genus that evolved parasitism in the Convolvulaceae (Yuncker, 1932). *Cuscuta* plants have degenerated roots and leaves and have stems that can coil around their host in a counterclockwise manner. Depending on the species and the growth conditions, *Cuscuta* stems are orange-yellow, yellow, or greenish-yellow because they only have a meagre amount of chlorophyll. Several previous studies on genomes of *Cuscuta* species indicate that *Cuscuta* species have lost some genes needed for efficient photosynthetic activity (McNeal et al., 2007; Braukmann et al., 2013; Sun et al., 2018; Vogel et al., 2018), which can be considered evidence for transitioning from hemiparasites to holoparasites. Therefore, obtaining water and nutrients from their host is the top priority for their survival. Unlike root parasitic plants that mostly depend on haustorium-inducing factors (HIFs) (Yoshida et al., 2016), the *Cuscuta* haustorium induction is also regulated by environmental signals such as light signals (Furuhashi et al., 2011). These unique lifestyles and morphological characteristics make *Cuscuta* species a good system to study how autotrophic plants evolved parasitism by attaching onto above-ground organs of their host plants.

Aside from the opportunities they present for investigating evo-devo mysteries, *Cuscuta* plants are the focus of intensive research since they cause massive agricultural losses. Several *Cuscuta* species are listed in multiple countries' noxious weed lists (Holm et al., 1997) because they parasitize a wide range of important vegetable and fruit crops, and ornamental plants (Lanini and Kogan, 2005). Comparing with *Striga* species that mostly target monocot hosts, the host plants for *Cuscuta* species are primarily eudicots, but a few monocot crops can also reportedly be attacked by *Cuscuta* species (Lanini and Kogan, 2005). *Cuscuta* species are parasites on 25 crops in at least 55 countries (Holm et al., 1997; Lanini and Kogan, 2005). If left uncontrolled, *Cuscuta* growth will decrease host nutrient status and lead to reduced stand, canopy, biomass and fruit weight (Musselman, 1987; Lanini and Kogan, 2005). Yield reductions of 50–72% in tomatoes and 70–90% in carrots have been reported (Lanini and Kogan, 2005; Mishra et al., 2006). In temperate climates, yield losses up to 80–100% have been reported in cranberry in the US due to *Cuscuta* (Devlin and Deubert, 1980). In California alone, over 12,000 ha. are affected by *Cuscuta* (Lanini and Kogan, 2005). Even when crop rotation is practised, *Cuscuta* is hard to eradicate due to long-term seed viability. Therefore, a better understanding of the mechanisms involved in *Cuscuta* haustorium development is required to build more effective control strategies to stop the agricultural damages brought on by *Cuscuta*. During the past decade, progress has been made in understanding the interaction between *Cuscuta* species and their hosts, especially on the mechanism involved in resistance responses against *Cuscuta* species (Kaiser et al., 2015; Jhu and Sinha, 2022), and the signal exchange and horizontal gene transfer between *Cuscuta* plants and their hosts (Kim and Westwood, 2015; Wu, 2018; Yang et al., 2019; Lin et al., 2022). These aspects have been reviewed recently (Kaiser et al., 2015; Kim and Westwood, 2015; Wu, 2018; Jhu and Sinha, 2022). On the other hand, although review articles cover some specific aspects of *Cuscuta* haustorium development and parasitism behaviours (Yoshida et al., 2016; Shimizu and Aoki, 2019), several recent discoveries in the field have not been systematically reviewed yet.

This review summarises our current knowledge of the mechanism involved in the four stages of *Cuscuta* haustorium development, including the initiation, adhesion, penetration, and vascular connection. We discuss the unique characteristics of the parasitizing behaviours in *Cuscuta* species compared with other well-studied root parasitic plants. These unique features are compelling reasons to use *Cuscuta* species as model organisms for studying haustorium development in stem holoparasitic plants. We outline the advantages, unknown mysteries, and current limitations of the *Cuscuta* system. We also propose potential models and directions that might overcome these challenges.

2 Before haustorium formation: Finding their hosts

Cuscuta seeds are about 1 mm in size and cannot store sufficient nutrients to support seedling growth for longer than

one week (Figures 1A–D). Therefore, finding a suitable host and forming successful haustorial attachments within a few days post-germination are important for seedling survival. Previous research indicates that *Cuscuta* seedlings can detect the volatiles released by their hosts and use these chemical cues to locate their preferred hosts (Runyon et al., 2006). In addition to airborne chemical signals, previous studies also indicate that the high far-red light relative to red light plays a vital role in controlling *Cuscuta* parasitism and growth directions (Furuhashi et al., 1995; Orr et al., 1996; Tada et al., 1996). This signal might help *Cuscuta* find green and healthy plants as their hosts (Orr et al., 1996). Blue light has been reported to be essential for the twining behavior of *Cuscuta* stems (Furuhashi et al., 1995; Furuhashi et al., 2021), which is tightly associated with the following haustorium induction phase.

3 Cuscuta haustorium organogenesis

Haustorium organogenesis in *Cuscuta* species has been well-reviewed (Yoshida et al., 2016; Kokla and Melnyk, 2018; Shimizu and Aoki, 2019). However, the developmental stages are reported differently among references and diverse names are used to refer to the same stage, leading to some confusion. Here, we aim to summarise the *Cuscuta* haustorium organogenesis process and standardize the vocabulary used. Based on cell types and morphological characteristics, we classified haustorium organogenesis in *Cuscuta* species into four development stages: the initiation phase, adhesion phase, penetration phase, and vascular connection phase (Figures 1E–H).

3.1 Initiation phase (prehaustorium)

Once *Cuscuta* plants find their hosts and successfully coil around them, the next step is the start of haustorium initiation and formation of the prehaustorium, which is the immature haustorial structure seen prior to penetration of the host tissues (Yoshida et al., 2016). A group of cortical cells begin to accumulate starch-containing amyloplasts and enlarged nuclei. These cells are identified as the initial cells, which will then dedifferentiate and develop into haustorial meristem cells. The disc-like meristem that emerges in the inner cortex of the *Cuscuta* stem is the prehaustorium primordia, consisting of two types of cells: file and digitate cells (Figure 1E) (Lee, 2007). This primordium is also known as the "endophyte primordium" because it develops into an "endophyte." An endophyte refers to the inner haustorial structure that grows into the host tissues during the penetration phase (Kuijt, 1977; Lee, 2007).

Based on previous studies, the two primary triggers for *Cuscuta* haustorium initiation are the far-red light signal and mechanical stimulation (Tada et al., 1996; Furuhashi et al., 2011) (Figure 2). Upon receiving these light signals and physical contacts, the prehaustorium structure starts to develop. *Cuscuta* species probably employ phytochromes to sense the change in red light and far-red light ratio and adopt phototropism signaling transduction to control the initiation of haustoria. In Arabidopsis, phytochromes are transformed from their inactive form (Pr) to their active form (Pfr) in high red-light environments. Pfr then translocates from the cytoplasm into the nucleus, where Pfr interacts with phytochrome interaction factors (PIFs). As a result of their interaction, PIFs are phosphorylated and then degraded. PIFs are transcription factors that regulate the downstream gene expression involved in skotomorphogenesis and photomorphogenesis in Arabidopsis. *Cuscuta* species likely co-opt similar signaling pathways and use phytochromes to control the genes involved in hormone transport or biosynthesis (Figure 2) (Furuhashi et al., 1997; Furuhashi et al., 2011; Furuhashi et al., 2021; Pan et al., 2022). A previous study indicates that strong far-red light or low red to far-red ratios (low red light and high far-red light mixture condition) promoted *Cuscuta* stem coiling and haustorium formation (Furuhashi et al., 1997; Haidar and Orr, 1999). The results of *in vivo* quantification of the percentage of phytochrome status also showed that a maximum number of prehaustoria were produced when a low percentage of phytochrome is in Pfr form (Haidar and Orr, 1999). This evidence supports the model that phytochromes are in the inactive (Pr) state under intense far-red light circumstances, which prevents phytochromes from entering the nucleus. PIFs are thus unrestricted from regulation and activate the genes, including those involved in auxin and cytokinin biosynthesis or transport, needed for haustorium initiation (Furuhashi et al., 2021; Pan et al., 2022) (Figure 2).

Another component needed for forming the *Cuscuta* haustorium is physical contact with its host (Tada et al., 1996; Furuhashi et al., 2011). Several herbaceous and woody plant species have been described that can perceive mechanical cues from their environment and respond physiologically to change their growth or morphology by a process known as thigmomorphogenesis (Börnke and Rocksch, 2018). During the past decade, progress has been made in investigating the underlying molecular mechanisms of mechanoperception and thigmomorphogenesis in several plant species (Monshausen and Gilroy, 2009; Hamilton et al., 2015; Börnke and Rocksch, 2018; Mano and Hasebe, 2021), but how these thigmomorphogenesis signaling pathways are involved in *Cuscuta* haustorium organogenesis remains largely unknown. Here, we propose a hypothetical model based on our current understanding of non-parasitic plant models (Figure 2). Ion channels and receptor-like kinases are examples of mechanosensory proteins (Monshausen and Gilroy, 2009; Hamilton et al., 2015; Börnke and Rocksch, 2018) that may be activated by a physical contact signal with hosts. Plasma membrane-localized mechanosensitive calcium

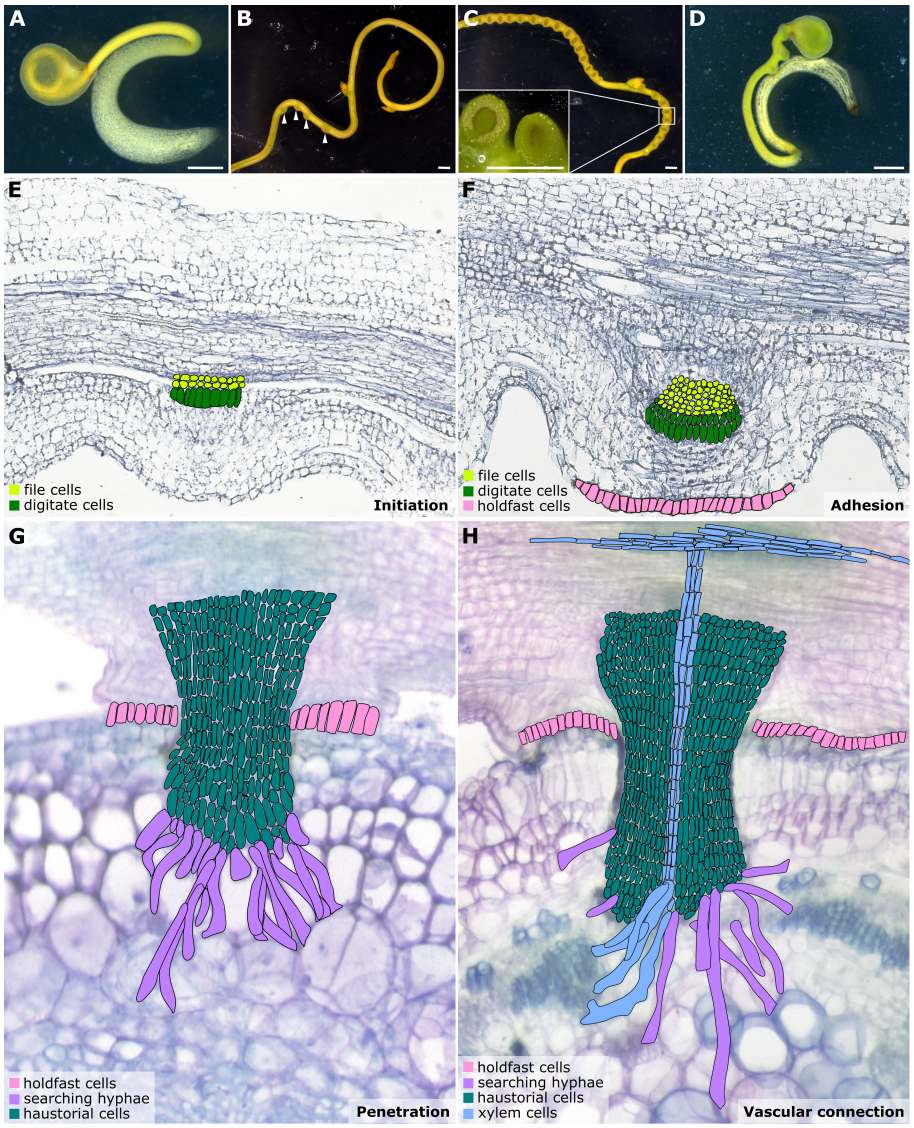

FIGURE 1
Illustrations of *Cuscuta* developmental stages and haustorium organogenesis. **(A–D)** *Cuscuta campestris* seedlings and strands with prehaustoria and haustoria at different developmental stages. **(A)** A *Cuscuta campestris* seedling. **(B)** A *Cuscuta campestris* strand with prehaustoria. White arrowheads indicate prehaustoria. **(C)** Haustoria with adhesive disks on a *Cuscuta campestris* strand. Adhesive disks are enlarged in the subfigure. **(D)** A *Cuscuta campestris* seedling autoparasitizes itself. **(A–D)** Scale bar = 1 mm. **(E–H)** Four major haustorium developmental phases in *Cuscuta* species. **(E)** Initiation phase: The prehaustorium structure appears because the disc-like meristem emerges in the inner cortex region of the *Cuscuta* stem. The prehaustorium primordia consist of file cells and digitate cells. **(F)** Adhesion phase: The epidermal cells of *Cuscuta* stems divide and differentiate into holdfast cells, which comprise the adhesive disk to secure the adhesion of haustorial attachments. **(G)** Penetration phase: The cortex-originated inner haustorial cells penetrate through the epidermis and cortex of their host tissues. At the tip of the haustorium, the inner haustorial cells elongate and differentiate into searching hyphae, which start invading through the apoplastic region of host cortex tissues and searching for host vasculature. **(H)** Vascular connection phase: Establishing a successful vascular connection is the final stage of haustorium organogenesis. If the searching hyphae reach host xylem cells or phloem cells, they obtain xylem or phloem identity and differentiate into xylem- or phloem-conductive elements, respectively. Part of this figure **(B, C)** is modified from images in a previously published paper Jhu et al., 2021 with new information added.

channels, like Mid1-complementing activity (MCA), trigger Ca^{2+} influx, cytosolic Ca^{2+}-dependent signaling, and activate the expression of downstream genes possibly through Ca^{2+} sensors, such as calmodulin or calcium-dependent protein kinases (Nakagawa et al., 2007; Kurusu et al., 2013; Börnke and Rocksch, 2018; Mano and Hasebe, 2021). Another potential candidate is the mechanosensitive channel of small conductance (MscS) -like (MSL) family proteins, which are reported to be stretch-activated anion channels for Cl^- and cause alteration in the membrane potential (Haswell et al., 2008; Maksaev and

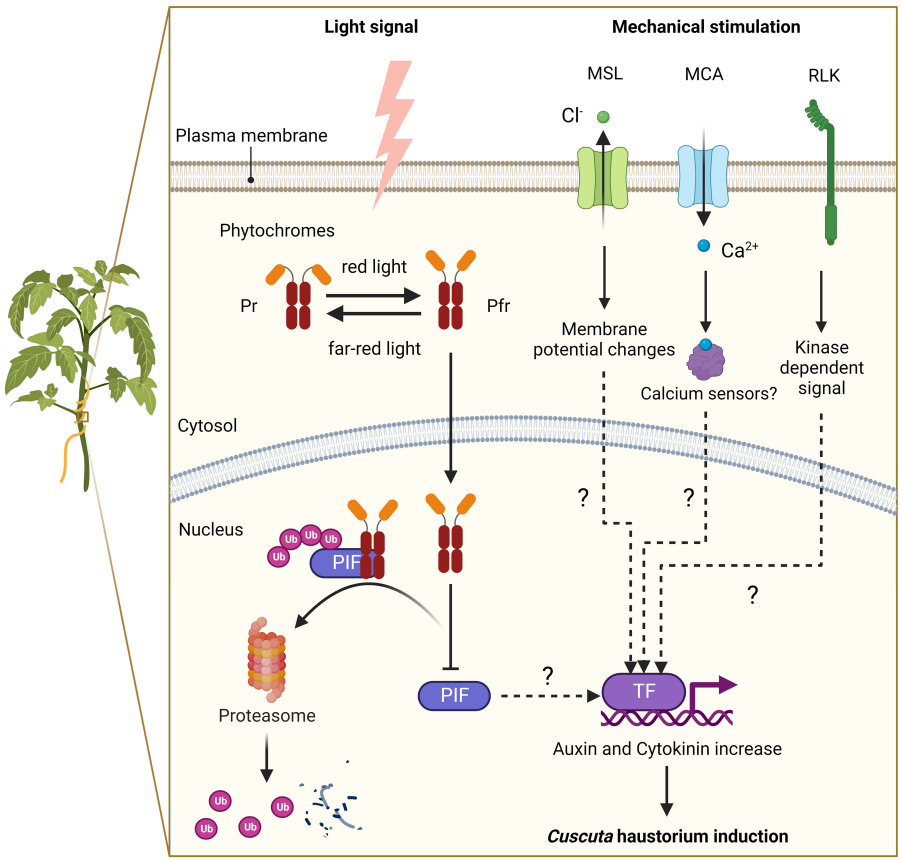

FIGURE 2
A putative model of signalling pathways for haustorium induction in *Cuscuta* species. Far-red light signal and mechanical stimulation are known to be the two major factors in inducing *Cuscuta* haustorium development. *Cuscuta* species likely have adopted far-red light signaling transduction and use phytochromes to regulate haustorium initiation. In high red-light conditions, phytochromes are converted from inactive form (Pr) to active form (Pfr), which will translocate from the cytosol into the nucleus and interact with phytochrome interacting factors (PIFs). PIFs are transcription factors, which are likely to regulate the downstream genes involved in hormone biosynthesis or transport. Interacting with Pfr phytochromes leads to PIFs phosphorylation and subsequent degradation. In high far-red light conditions, phytochromes are in the Pr inactive form and cannot enter the nucleus. Therefore, PIFs are released from repression and activate genes involved in haustorium initiation. Mechanosensing is another required element for *Cuscuta* haustorium development. A physical contact signal with hosts might activate mechanosensory proteins such as ion channels and receptor-like kinases. Mechanosensory ion channels elicit cytosolic Ca^{2+}-dependent signaling and regulate downstream gene expression via unknown mechanisms. Receptor-like kinases trigger protein kinase cascades and then influence downstream gene transcription, which can lead to hormone status changes and haustorium induction.

Haswell, 2012; Mano and Hasebe, 2021). Receptor-like kinases (RLKs) might also play a role in triggering protein kinase cascades and altering Ca^{2+} signaling (Humphrey et al., 2007; Shih et al., 2014; Börnke and Rocksch, 2018), which in turn may affect downstream gene transcription, change hormone status and induce haustorium formation (Figure 2).

3.2 Adhesion phase (attached haustorium)

In the adhesion phase, prehaustoria continue to grow toward the host and form adhesive disks (also known as holdfasts or upper haustorium). The *Cuscuta* haustorial epidermal cells in contact with the host proliferate anticlinally, elongate, and differentiate into secretory holdfast cells. These holdfast cells can secrete adhesive glue containing de-esterified pectins to secure the haustorium on their host's surface and seal the gap between themselves and their host (Figure 1F) (Vaughn, 2002).

3.3 Penetration phase (invading haustorium)

Once a haustorium securely attaches to its host, the haustorium development enters the penetration phase (also

known as intrusive phase), and the file and digitate cells in endophyte primordium continue to divide and form inner haustorial cells. These cortex-originated inner haustorial cells then penetrate through the epidermis and cortex of their host tissues. At the tip of the penetrating haustorium, the inner haustorial cells elongate and differentiate into searching hyphae (Vaughn, 2003). Searching hyphae continue invading through the apoplastic region of host cortex tissues and searching for host vasculature *via* tip growth (Figure 1G).

3.4 Vascular connection phase (mature haustorium)

The final stage of developing a functional haustorium is establishing a successful vascular connection between host and parasite. The searching hyphae continue tip growth to seek host vascular tissues. Once the searching hyphae reach the host vascular cells, they form interspecies plasmodesmata connections at the tip of the searching hyphae. These searching hyphae then convert their cell identity depending on the type of cells they contact. For instance, the searching hyphae that make contact with host xylem cells will obtain xylem identity and become xylic hyphae (Vaughn, 2006). The xylic hyphae differentiate into xylem conductive elements and form xylem bridges connecting the xylem system between the host and the parasite (Figure 1H). On the other hand, the searching hyphae that make contact with host phloem sieve elements will obtain phloem identity and become phloic hyphae (also known as absorbing hyphae) (Vaughn, 2006). The phloic hyphae differentiate into phloem-conductive elements with finger-like protrusions connecting the phloem system between the host and the parasite. The mechanisms involved in the transition of cell identity are currently unknown. However, based on the discovery of mRNA, small RNA, and small peptides exchanged between host and parasite *via* haustorial connection (Kim et al., 2014; Kim and Westwood, 2015; Shahid et al., 2018), we propose a potential hypothesis that these exchanged signals likely function as signals to facilitate cell identity conversion, which will be of interest for future investigation.

4 *Cuscuta* as a model for haustorium development in stem holoparasitic plants

Compared with our recent advances in understanding root parasitic plant haustorium development, our knowledge of haustorium development and parasitism behaviours on stem parasitic plants is relatively limited. According to an increasing number of research reports, the required signals for inducing haustorium formation are different, the parasitism behaviours between root and stem haustorium formation are distinct, and the mechanisms behind these phenomena are still not completely understood. Therefore, good model organisms representing stem holoparasitic plants will help investigate how parasitic plants evolved to have different strategies to effectively attach to various above-ground organs of their host. The *Cuscuta* genus is one of the most well-studied stem parasitic plants and here we summarized why they are the popular choices for scientists in this field.

4.1 Advantage 1: Distinct mechanisms involved in haustorium induction

A stem parasitic plant-specific model system is required because the mechanisms involved in haustorium induction differ between root and stem parasitic plants. For example, many studies indicate that detecting quinones or phenolics from the hosts, known as haustorium-inducing factors (HIFs), is a critical factor in inducing haustorium development for root parasitic plants, like those seen in the Orobanchaceae (Chang and Lynn, 1986; Goyet et al., 2019). On the other hand, stem parasites use tactile stimuli and light signals for haustorium induction (Tada et al., 1996; Furuhashi et al., 2011). These different factors required for triggering haustorium formation show the distinct strategies needed to adapt to underground and aboveground parasitism. For underground parasitism, physical contact and light signals would not be effective searching mechanisms for host root systems surrounded by soil. Consequently, the ability to detect host-specific HIFs would be the primary criteria for root parasitic plant haustorium induction. Therefore, using *Cuscuta* species for studying stem parasitic plant haustorium organogenesis could help us understand the unique mechanisms deployed in aboveground parasitism.

4.2 Advantage 2: Special parasitizing behaviors: Autoparasitism, hyperparasitism, cross-organ parasitism

Besides serving as a sound system for studying the distinctive mechanisms involved in haustorium initiation, *Cuscuta* species also perform some unique parasitizing behaviours that are currently underinvestigated, including hyperparasitism (Wilson and Calvin, 2017), autoparasitism (Krasylenko et al., 2021), and cross-organ parasitism (Jhu and Sinha, 2022). These unique parasitizing behaviours among multiple parasitic plants have been previously reviewed (Krasylenko et al., 2021; Jhu and Sinha, 2022). Therefore, here, we focus on providing clear definitions with concise discussion and then propose hypotheses to understand why *Cuscuta* species evolved these unique parasitizing behaviours.

Hyperparasitism indicates the phenomenon of a parasitic plant parasitizing another parasitic plant. For stem parasites that attach to the aerial part of their host, this phenomenon is also known as epiparasitism because they grow "on top of" another parasite (Wilson and Calvin, 2017). Several previous studies have reported *Cuscuta* hyperparasitism on other parasitic plants. Hyperparasitism can happen between species or within the same species (Hawksworth, 1996). When a parasitic plant parasitizes the same parasitic plant species, this is known as autoparasitism. One specific type of autoparasitism is when the parasitic plants form functional haustoria on themselves, which is also known as self-parasitism (Fineran, 1965). In *Cuscuta* species, both autoparasitism and self-parasitism are commonly observed (Krasylenko et al., 2021). This is a distinctive parasitism strategy compared with several facultative or obligate root parasitic plants, which have self- and kin-recognition mechanisms to avoid forming haustoria on themselves or their similar relatives.

Deploying hyperparasitism and autoparasitism strategies might be the evolutionary consequence of adapting to aboveground parasitism. One hypothesis proposed by McLuckie is that self-parasitic haustoria in *Cassytha* or *Cuscuta* species might facilitate water conduction and long-distance transport (McLuckie, 1924). In addition, based on the observation that *Cuscuta* species also often form attachments to non-biological materials (Bernal-Galeano et al., 2022), we propose that the formation of these non-conductive haustoria or self-parasitic haustoria might both serve as physical support for *Cuscuta* to spread over a wider area and reach longer distances, which increases the possibility of finding new hosts and is therefore, beneficial for parasite survival.

Cross-organ parasitism refers to the phenomenon of a parasitic plant forming nonconventional haustorial attachments with other host organs (Jhu and Sinha, 2022). For example, *C. campestris* is known as a parasitic stem plant but has been reported to be able to form haustoria on tomato seedling roots (Jhu and Sinha, 2022). The reason why *Cuscuta* species evolved to have the ability to parasitize different organs of their host is still a mystery. However, the mechanisms of haustorium induction and host-specificity might contribute to these characteristics. Previous studies indicate that parasitic plants that can form self-parasitic haustoria, like *Cuscuta*, *Cassytha* and some hemiparasitic Orobanchaceae, can form haustoria without depending on detecting host-specific HIFs and are also more likely to show hyperparasitism (Krasylenko et al., 2021). These parasites usually also have a wider host range. To parasitize different host species, which might have different anatomical structures, having a higher degree of haustorium plasticity and HIF-independent haustorium induction might be criteria to adapt to different host structures and form successful haustorial connections with them. Therefore, this higher degree of haustorium plasticity might also confer on *Cuscuta* the ability to form haustoria on different organs of their hosts.

4.3 Advantage 3: Whole genome and abundant transcriptome data are available

Another advantage of using *Cuscuta* species as a model organism is the availability of whole genome information and different types of transcriptome data. The genomes of *C. campestris* and *C. australis* were both published in 2018 (Sun et al., 2018; Vogel et al., 2018). The *Cuscuta* transcriptome profiles in different developmental stages and tissue types are readily available (Ranjan et al., 2014; Jhu et al., 2021; Jhu et al., 2022; Bawin et al., 2022). *Cuscuta* mobile mRNAs and miRNAs that can transfer into the host plants are also reported (Kim et al., 2014; Shahid et al., 2018). These resources will facilitate research on *Cuscuta* development and the interaction between hosts and *Cuscuta* plants.

4.4 Advantage 4: Easy propagation and *in vitro* haustorium system

Another key criterion that makes an organism a good model organism is the ability to propagate or reproduce easily in vast numbers. *Cuscuta* species can quickly propagate through vines and produce many fruits and seeds, which can remain viable for more than ten years (Lanini and Kogan, 2005; Goldwasser et al., 2012; Masanga et al., 2022). These characteristics make them excellent model organisms. In addition, as mentioned in previous sections, many studies have shown that far-red light signals and physical contacts can trigger *Cuscuta* haustorium formation (Furuhashi et al., 1995; Tada et al., 1996; Furuhashi et al., 1997; Haidar and Orr, 1999). Therefore, several *in vitro* methods of growing *Cuscuta* or inducing haustorium formation without hosts have also been developed simultaneously (Kaga et al., 2020; Jhu et al., 2021; Bernal-Galeano et al., 2022). These methods allow us to investigate the function of genes in haustorium organogenesis more effectively and remove the influence or variations created by host conditions.

4.5 Major limitations: Lack of efficient transformation systems to obtain stable *Cuscuta* transgenic lines

To study the function of genes, generating mutants or transgenic plants with specific gene knockouts or gene overexpression is one critical approach. Unfortunately, the current major limitation of using *Cuscuta* species as a model is lack of efficient transformation methods to obtain stable transgenic lines. Several methods for producing successful transformation events have been published in

different *Cuscuta* species, including *Cuscuta trifolii, Cuscuta reflexa*, and *Cuscuta europaea* (Borsics et al., 2002; Švubová and Blehová, 2013; Lachner et al., 2020). However, regenerating the transformed cells into calli and whole plants is still an unsolved issue. Developing a transformation system to generate stable transgenic *Cuscuta* plants will be a significant breakthrough technology.

At the same time, scientists have been developing different tools and methods for functional gene studies to bypass and overcome the current transformation obstacles. Based on previous studies, *Cuscuta* haustoria not only transport water and nutrients but also can transport small RNAs, messenger RNAs and small peptides (Kim et al., 2014; Kim and Westwood, 2015; Shahid et al., 2018; Wu, 2018; Johnson and Axtell, 2019). Therefore, host-induced gene silencing (HIGS) is a commonly used method to knock-down specific gene expressions in *Cuscuta* by attaching them to transgenic hosts that carry RNA interference (RNAi) constructs targeting *Cuscuta* genes (Albert et al., 2006; Alakonya et al., 2012; Jhu et al., 2021; Jhu et al., 2022). This method has been used widely in the *Cuscuta* research field to conduct functional analysis on genes of interest.

5 Conclusions

This review summarises the four major developmental stages of haustorium organogenesis in *Cuscuta* species. We organize the current understanding of haustorium induction by light signals and physical contacts and propose a potential pathway for haustorium formation. The detailed mechanisms of phytochrome signalling, hormone regulation, and thigmomorphogenesis in *Cuscuta* haustorium development are still elusive and will be of interest for future research. We also discuss the four significant advantages of using *Cuscuta* species as model organisms for haustorium development research, including the unique haustorium induction mechanisms, parasitizing behaviours, abundant genetic resources, and easy propagation. The current major limitation is absence of efficient transformation systems to obtain stable *Cuscuta* transgenic lines. However, host induces gene silencing has been widely used to overcome this limitation. With several reports on successful transformation events published recently from different research groups, we are optimistic that stable *Cuscuta* transformation systems might be established in the near future.

Author contributions

M-YJ wrote the initial draft and prepared the figures. M-YJ and NRS both revised and approved the final manuscript. All authors contributed to the article and approved the submitted version.

Funding

M-YJ was supported by Taiwan Government GSSA Scholarship, Loomis Robert S. and Lois Ann Graduate Fellowship, Katherine Esau Summer Graduate Fellowship, Elsie Taylor Stocking Memorial Fellowship, Yen Chuang Taiwan Fellowship, and the UCD Graduate Research Award. NRS was funded by USDA-NIFA (2013-02345) and funding from the California Tomato Research Institute, Inc.

Acknowledgments

We thank Eli Marable's feedback on the early draft of this manuscript, and Anindya Kundu and Victor Hugo Moura De Souza for their valuable discussion.

Conflict of interest

The authors declare that the research was conducted in the absence of any commercial or financial relationships that could be construed as a potential conflict of interest.

Publisher's note

References

Alakonya, A., Kumar, R., Koenig, D., Kimura, S., Townsley, B., Runo, S., et al. (2012). Interspecific RNA interference of SHOOT MERISTEMLESS-like disrupts cuscuta pentagona plant parasitism. *Plant Cell* 24, 3153–3166. doi: 10.1105/tpc.112.099994

Albert, M., Belastegui-Macadam, X., and Kaldenhoff, R. (2006). An attack of the plant parasite cuscuta reflexa induces the expression of attAGP, an attachment protein of the host tomato. *Plant J.* 48, 548–556. doi: 10.1111/j.1365-313X.2006.02897.x

Bawin, T., Bruckmüller, J., Olsen, S., and Krause, K. (2022). A host-free transcriptome for haustoriogenesis in cuscuta campestris: Signature gene expression identifies markers of successive development stages. *Physiol. Plant* 174(2). doi: 10.1111/ppl.13628

Bernal-Galeano, V., Beard, K., and Westwood, J. H. (2022). An artificial host system enables the obligate parasite cuscuta campestris to grow and reproduce *in vitro*. *Plant Physiol.* 189, 687–702. doi: 10.1093/plphys/kiac106

Börnke, F., and Rocksch, T. (2018). Thigmomorphogenesis – control of plant growth by mechanical stimulation. *Sci. Hortic.* 234, 344–353. doi: 10.1016/j.scienta.2018.02.059

Borsics, T., Mihálka, V., Oreifig, A. S., Bárány, I., Lados, M., Nagy, I., et al. (2002). Methods for genetic transformation of the parasitic weed dodder (Cuscuta trifolii bab. et gibs) and for PCR-based detection of early transformation events. *Plant Sci.* 162, 193–199. doi: 10.1016/S0168-9452(01)00536-2

Braukmann, T., Kuzmina, M., and Stefanović, S. (2013). Plastid genome evolution across the genus cuscuta (Convolvulaceae): two clades within subgenus grammica exhibit extensive gene loss. *J. Exp. Bot.* 64, 977–989. doi: 10.1093/jxb/ers391

Chang, M., and Lynn, D. G. (1986). The haustorium and the chemistry of host recognition in parasitic angiosperms. *J. Chem. Ecol.* 12, 561–579. doi: 10.1007/BF01020572

Devlin, R. M., and Deubert, K. H. (1980). Control of swamp dodder on cranberry bogs with butralin. *Proc. Northeastern Weed Sci. Society 1980.* 34, 399–405.

Fineran, B. A. (1965). Studies on the root parasitism of exocarpus bidwillii hook. f. VI. haustorial attachment and the phenomenon of self-parasitism. *Phytomorphology* 15, 387–399.

Furuhashi, T., Furuhashi, K., and Weckwerth, W. (2011). The parasitic mechanism of the holostemparasitic plant cuscuta. *J. Plant Interact.* 6, 207–219. doi: 10.1080/17429145.2010.541945

Furuhashi, K., Iwase, K., and Furuhashi, T. (2021). Role of light and plant hormones in stem parasitic plant (Cuscuta and cassytha) twining and haustoria induction. *Photochem. Photobiol.* 97, 1054–1062. doi: 10.1111/php.13441

Furuhashi, K., Kanno, M., and Morita, T. (1995). Photocontrol of parasitism in a parasitic flowering plant, cuscuta japonica chois, cultured in vitro. *Plant Cell Physiol.* 36, 533–536. doi: 10.1093/oxfordjournals.pcp.a078790

Furuhashi, K., Tada, Y., Okamoto, K., Sugai, M., Kubota, M., and Watanabe, M. (1997). Phytochrome participation in induction of haustoria in cuscuta japonica, a holoparasitic flowering plant. *Plant Cell Physiol.* 38, 935–940. doi: 10.1093/oxfordjournals.pcp.a029254

Goldwasser, Y., Sazo, M. R. M., and Lanini, W. T. (2012). Control of field dodder (Cuscuta campestris) parasitizing tomato with ALS-inhibiting herbicides. *Weed Technol.* 26, 740–746. doi: 10.1614/WT-D-11-00173.1

Goyet, V., Wada, S., Cui, S., Wakatake, T., Shirasu, K., Montiel, G., et al. (2019). Haustorium inducing factors for parasitic orobanchaceae. *Front. Plant Sci.* 10. doi: 10.3389/fpls.2019.01056

Haidar, M. A., and Orr, G. L. (1999). The response of cuscuta planiflora seedlings to red and far-red, blue light and end-of-day irradiations. *Ann. Appl. Biol.* 134, 117–120. doi: 10.1111/j.1744-7348.1999.tb05242.x

Hamilton, E. S., Schlegel, A. M., and Haswell, E. S. (2015). United in diversity: Mechanosensitive ion channels in plants. *Annu. Rev. Plant Biol.* 66, 113–137. doi: 10.1146/annurev-arplant-043014-114700

Haswell, E. S., Peyronnet, R., Barbier-Brygoo, H., Meyerowitz, E. M., and Frachisse, J. M. (2008). Two MscS homologs provide mechanosensitive channel activities in the arabidopsis root. *Curr. Biol.* 18, 730–734. doi: 10.1016/j.cub.2008.04.039

Hawksworth, F. G. (1996). *Dwarf mistletoes: biology, pathology, and systematics* (Forest Service: US Department of Agriculture).

Holm, L. R., Doll, J., Holm, E., Pancho, J., and Herberger, J. P. (1997). World weeds: natural histories and distribution. John Wiley & Sons.

Humphrey, T., Bonetta, D. T., and Goring, D. R. (2007). Sentinels at the wall: Cell wall receptors and sensors. *New Phytol.* 176, 7–21. doi: 10.1111/j.1469-8137.2007.02192.x

Jhu, M. Y., Farhi, M., Wang, L., Zumstein, K., and Sinha, N. R. (2022). Investigating host and parasitic plant interaction by tissue-specific gene analyses on tomato and cuscuta campestris interface at three haustorial developmental stages. *Front. Plant Sci.* 12. doi: 10.3389/fpls.2021.764843

Jhu, M. Y., Ichihashi, Y., Farhi, M., Wong, C., and Sinha, N. R. (2021). LATERAL ORGAN BOUNDARIES DOMAIN 25 functions as a key regulator of haustorium development in dodders. *Plant Physiol.* 186, 2093–2110. doi: 10.1093/plphys/kiab231

Jhu, M.-Y., and Sinha, N. R. (2022). Annual review of plant biology parasitic plants: An overview of mechanisms by which plants perceive and respond to parasites. doi: 10.1146/annurev-arplant-102820

Johnson, N. R., and Axtell, M. J. (2019). Small RNA warfare: exploring origins and function of trans-species microRNAs from the parasitic plant cuscuta. *Curr. Opin. Plant Biol.* 50, 76–81. doi: 10.1016/j.pbi.2019.03.014

Kaga, Y., Yokoyama, R., Sano, R., Ohtani, M., Demura, T., Kuroha, T., et al. (2020). Interspecific signaling between the parasitic plant and the host plants regulate xylem vessel cell differentiation in haustoria of cuscuta campestris. *Front. Plant Sci.* 11. doi: 10.3389/fpls.2020.00193

Kaiser, B., Vogg, G., Fürst, U. B., and Albert, M. (2015). Parasitic plants of the genus cuscuta and their interaction with susceptible and resistant host plants. *Front. Plant Sci.* 6. doi: 10.3389/fpls.2015.00045

Kim, G., LeBlanc, M. L., Wafula, E. K., dePamphilis, C. W., and Westwood, J. H. (2014). Genomic-scale exchange of mRNA between a parasitic plant and its hosts. *Sci. (1979)* 345, 808–811. doi: 10.1126/science.1253122

Kim, G., and Westwood, J. H. (2015). Macromolecule exchange in cuscuta-host plant interactions. *Curr. Opin. Plant Biol.* 26, 20–25. doi: 10.1016/j.pbi.2015.05.012

Kokla, A., and Melnyk, C. W. (2018). Developing a thief: Haustoria formation in parasitic plants. *Dev. Biol.* 442, 53–59. doi: 10.1016/j.ydbio.2018.06.013

Krasylenko, Y., Těšitel, J., Ceccantini, G., Oliveira-da-Silva, M., Dvořák, V., Steele, D., et al. (2021). Parasites on parasites: hyper-, epi-, and autoparasitism among flowering plants. *Am. J. Bot.* 108, 8–21. doi: 10.1002/ajb2.1590

Kuijt, J. (1977). Haustoria of phanerogamic parasites. *Annu. Rev. Phytopathol.* 15, 91–118. doi: 10.1146/annurev.py.15.090177.000515

Kurusu, T., Kuchitsu, K., Nakano, M., Nakayama, Y., and Iida, H. (2013). Plant mechanosensing and Ca2+ transport. *Trends Plant Sci.* 18, 227–233. doi: 10.1016/j.tplants.2012.12.002

Lachner, L. A. M., Galstyan, L., and Krause, K. (2020). A highly efficient protocol for transforming cuscuta reflexa based on artificially induced infection sites. *Plant Direct* 4 (8), e00254. doi: 10.1002/pld3.254

Lanini, W. T., and Kogan, M. (2005). Biology and management of cuscuta in crops. *Int. J. Agric. Natural Resour.* 32, 127–141. doi: 10.7764/rcia.v32i3.317

Lee, K. B. (2007). Structure and development of the upper haustorium in the parasitic flowering plant cuscuta japonica (Convolvulaceae). *Am. J. Bot.* 94, 737–745. doi: 10.3732/ajb.94.5.737

Lin, Q., Banerjee, A., and Stefanović, S. (2022). Mitochondrial phylogenomics of cuscuta (Convolvulaceae) reveals a potentially functional horizontal gene transfer from the host. *Genome Biol. Evol.* 14, evac091. doi: 10.1093/gbe/evac091

Maksaev, G., and Haswell, E. S. (2012). MscS-Like10 is a stretch-activated ion channel from arabidopsis thaliana with a preference for anions. *Proc. Natl. Acad. Sci. U.S.A.* 109, 19015–19020. doi: 10.1073/pnas.1213931109

Mano, H., and Hasebe, M. (2021). Rapid movements in plants. *J. Plant Res.* 134, 3–17. doi: 10.1007/s10265-020-01243-7

Masanga, J., Oduor, R., Alakonya, A., Ngugi, M., Ojola, P., Bellis, E. S., et al. (2022). Comparative phylogeographic analysis of cuscuta campestris and cuscuta reflexa in Kenya: Implications for management of highly invasive vines. *Plants People Planet* 4, 182–193. doi: 10.1002/ppp3.10236

McLuckie, J. (1924). Studies in parasitism. i. a contribution to the physiology of the genus cassytha, part 1. in. *Proc. Linn. Soc. New South Wales*, 55–78.

McNeal, J. R., Arumugunathan, K., Kuehl, J., Boore, J. L., and dePamphilis, C. W. (2007). Systematics and plastid genome evolution of the cryptically photosynthetic parasitic plant genus Cuscuta(Convolvulaceae). *BMC Biol.* 5, 55. doi: 10.1186/1741-7007-5-55

Mishra, J. S., Moorthy, B. T. S., and Bhan, M. (2006). Relative tolerance of linseed (Linum usitatissimum) varieties to dodder (Cuscuta campestris) infestation. *Indian Journal of Agricultural Sciences* 76, 380–382.

Monshausen, G. B., and Gilroy, S. (2009). Feeling green: mechanosensing in plants. *Trends Cell Biol.* 19, 228–235. doi: 10.1016/j.tcb.2009.02.005

Musselman, L. J. (1987). Parasitic flowering plants. *Econ Bot.* 41, 215. doi: 10.1007/BF02858968

Nakagawa, Y., Katagiri, T., Shinozaki, K., Qi, Z., Tatsumi, H., Furuichi, T., et al. (2007). Arabidopsis plasma membrane protein crucial for Ca2+ influx and touch sensing in roots. *Proc. Natl. Acad. Sci.* 104, 3639–3644. doi: 10.1073/pnas.0607703104

Orr, G. L., Haidar, M. A., and Orr, D. A. (1996). Smallseed dodder (Cuscuta planiflora) phototropism toward far- red when in white light. *Weed Sci.* 44, 233–240. doi: 10.1017/s0043174500093838

Pan, H., Li, Y., Chen, L., and Li, J. (2022). Molecular processes of dodder haustorium formation on host plant under low Red/Far red (R/FR) irradiation. *Int. J. Mol. Sci.* 23 (14), 7528. doi: 10.3390/ijms23147528

Ranjan, A., Ichihashi, Y., Farhi, M., Zumstein, K., Townsley, B., David-Schwartz, R., et al. (2014). *De novo* assembly and characterization of the transcriptome of the parasitic weed dodder identifies genes associated with plant parasitism. *Plant Physiol.* 166, 1186–1199. doi: 10.1104/pp.113.234864

Runyon, J. B., Mescher, M. C., and de Moraes, C. M. (2006). Volatile chemical cues guide host location and host selection by parasitic plants. *Sci. (1979)* 313, 1964–1967. doi: 10.1126/science.1131371

Shahid, S., Kim, G., Johnson, N. R., Wafula, E., Wang, F., Coruh, C., et al. (2018). MicroRNAs from the parasitic plant cuscuta campestris target host messenger RNAs. *Nature* 553, 82–85. doi: 10.1038/nature25027

Shih, H. W., Miller, N. D., Dai, C., Spalding, E. P., and Monshausen, G. B. (2014). The receptor-like kinase FERONIA is required for mechanical signal transduction in arabidopsis seedlings. *Curr. Biol.* 24, 1887–1892. doi: 10.1016/j.cub.2014.06.064

Shimizu, K., and Aoki, K. (2019). Development of parasitic organs of a stem holoparasitic plant in genus cuscuta. *Front. Plant Sci.* 10. doi: 10.3389/fpls.2019.01435

Sun, G., Xu, Y., Liu, H., Sun, T., Zhang, J., Hettenhausen, C., et al. (2018). Large-Scale gene losses underlie the genome evolution of parasitic plant cuscuta australis. *Nat. Commun.* 9 (9), 1–8. doi: 10.1038/s41467-018-04721-8

Švubová, R., and Blehová, A. (2013). Stable transformation and actin visualization in callus cultures of dodder (Cuscuta europaea). *Biol. (Poland)* 68, 633–640. doi: 10.2478/s11756-013-0188-0

Tada, Y., Sugai, M., and Furuhashi, K. (1996). Haustoria of cuscuta japonica, a holoparasitic flowering plant, are induced by the cooperative effects of far-red light and tactile stimuli. *Plant Cell Physiol.* 37, 1049–1053. doi: 10.1093/oxfordjournals.pcp.a029052

Vaughn, K. C. (2002). Attachment of the parasitic weed dodder to the host. *Protoplasma* 219, 227–237. doi: 10.1007/s007090200024

Vaughn, K. C. (2003). Dodder hyphae invade the host: A structural and immunocytochemical characterization. *Protoplasma* 220, 189–200. doi: 10.1007/s00709-002-0038-3

Vaughn, K. C. (2006). Conversion of the searching hyphae of dodder into xylic and phloic hyphae: A cytochemical and immunocytochemical investigation. *Int. J. Plant Sci.* 167, 1099–1114. doi: 10.1086/507872

Vogel, A., Schwacke, R., Denton, A. K., Usadel, B., Hollmann, J., Fischer, K., et al. (2018). Footprints of parasitism in the genome of the parasitic flowering plant cuscuta campestris. *Nat. Commun.* 9 (1), 1–11. doi: 10.1038/s41467-018-04344-z

Wilson, C. A., and Calvin, C. L. (2017). Metadata provide insights on patterns of epiparasitism in mistletoes (Santalales), an overlooked topic in forest biology. *Botany* 95, 259–269. doi: 10.1139/cjb-2016-0264

Wu, J. (2018). miRNAs as a secret weapon in the battlefield of haustoria, the interface between parasites and host plants. *Mol. Plant* 11, 354–356. doi: 10.1016/j.molp.2018.02.004

Yang, Z., Wafula, E. K., Kim, G., Shahid, S., McNeal, J. R., Ralph, P. E., et al. (2019). Convergent horizontal gene transfer and cross-talk of mobile nucleic acids in parasitic plants. *Nat. Plants* 5, 991–1001. doi: 10.1038/s41477-019-0458-0

Yoshida, S., Cui, S., Ichihashi, Y., and Shirasu, K. (2016). The haustorium, a specialized invasive organ in parasitic plants. *Annu. Rev. Plant Biol.* 67, 643–667. doi: 10.1146/annurev-arplant-043015-111702

Yuncker, T. G. (1932). The genus cuscuta. *Memoirs Torrey Botanical Club* 18, 109–331. Available at: https://www.biodiversitylibrary.org/part/250866.

frontiers | Frontiers in Plant Science

TYPE Original Research
PUBLISHED 09 February 2023
DOI 10.3389/fpls.2022.1085900

OPEN ACCESS

EDITED BY
Verónica S. Di Stilio,
University of Washington,
United States

REVIEWED BY
Yaowu Yuan,
University of Connecticut,
United States
Ana Maria Rocha De Almeida,
California State University, East Bay,
United States

*CORRESPONDENCE
Shane Carey
scarey@ualberta.ca

SPECIALTY SECTION
This article was submitted to Plant Development and EvoDevo, a section of the journal Frontiers in Plant Science

RECEIVED 31 October 2022
ACCEPTED 22 December 2022
PUBLISHED 09 February 2023

CITATION
Carey S, Zenchyzen B, Deneka AJ and Hall JC (2023) Nectary development in *Cleome violacea*. *Front. Plant Sci.* 13:1085900. doi: 10.3389/fpls.2022.1085900

Nectary development in *Cleome violacea*

Shane Carey*, Brandi Zenchyzen, A. J. Deneka and Jocelyn C. Hall

Department of Biological Sciences, University of Alberta, Edmonton, AB, Canada

Nectaries are a promising frontier for plant evo-devo research, and are particularly fascinating given their diversity in form, position, and secretion methods across angiosperms. Emerging model systems permit investigations of the molecular basis for nectary development and nectar secretion across a range of taxa, which addresses fundamental questions about underlying parallelisms and convergence. Herein, we explore nectary development and nectar secretion in the emerging model taxa, *Cleome violacea* (Cleomaceae), which exhibits a prominent adaxial nectary. First, we characterized nectary anatomy and quantified nectar secretion to establish a foundation for quantitative and functional gene experiments. Next, we leveraged RNA-seq to establish gene expression profiles of nectaries across three key stages of development: pre-anthesis, anthesis, and post-fertilization. We then performed functional studies on five genes that were putatively involved in nectary and nectar formation: *CvCRABSCLAW* (*CvCRC*), *CvAGAMOUS* (*CvAG*), *CvSHATTERPROOF (CvSHP)*, *CvSWEET9*, and a highly expressed but uncharacterized transcript. These experiments revealed a high degree of functional convergence to homologues from other core Eudicots, especially *Arabidopsis*. *CvCRC*, redundantly with *CvAG* and *CvSHP*, are required for nectary initiation. Concordantly, *CvSWEET9* is essential for nectar formation and secretion, which indicates that the process is eccrine based in *C. violacea*. While demonstration of conservation is informative to our understanding of nectary evolution, questions remain. For example, it is unknown which genes are downstream of the developmental initiators *CvCRC*, *CvAG*, and *CvSHP*, or what role the *TCP* gene family plays in nectary initiation in this family. Further to this, we have initiated a characterization of associations between nectaries, yeast, and bacteria, but more research is required beyond establishing their presence. *Cleome violacea* is an excellent model for continued research into nectary development because of its conspicuous nectaries, short generation time, and close taxonomic distance to *Arabidopsis*.

KEYWORDS

Cleomaceae, nectaries, nectar, transcriptomics, VIGS, parallel evolution, RNA-seq

1 Introduction

Flowers exhibit tremendous diversity of form, much of which is driven by plant-pollinator interactions. Responses to similar pollinator environments have resulted in repeated evolution of floral forms across angiosperms (reviewed in: (Endress, 2011; Sauquet et al., 2017; Wessinger and Hileman, 2020)). Such traits include, but are not limited to, monosymmetry (zygomorphy), organ fusion, spurs, and heterostyly (Specht and Howarth, 2015; Kramer, 2019; Phillips et al., 2020; Wessinger and Hileman, 2020). This repeated evolution raises fundamental questions about the developmental and genetic bases of their evolutionary shifts (Sobel and Streisfeld, 2013; Specht and Howarth, 2015; Kramer, 2019; Wessinger and Hileman, 2020). Among these questions is whether the same genetic pathways have been recruited in independent origins of these traits (Specht and Howarth, 2015; Wessinger and Hileman, 2020). Remarkable and repeated recruitment of the same genetic pathway is clear with certain traits, notably monosymmetry [reviewed in: (Preston et al., 2009; Preston et al., 2011; Hileman, 2014a; Hileman, 2014b; Wessinger and Hileman, 2020)], but whether the genetic basis of other features is conserved remains unclear.

Nectaries, and the nectar they secrete, are integral to plant-animal interactions and, as such, warrant detailed investigation across taxa (Liao et al., 2021). They have evolved multiple times across angiosperms and are remarkably variable in position, structure, and morphology (Bernardello, 2007; Nepi, 2007; Nepi et al., 2018; Liao et al., 2021; Slavkovic et al., 2021). Despite this variation, nectaries are united by the simple function of producing nectar, a complex sugar-rich solution that contains a wide range of metabolites and microbes (Nepi, 2007; Heil, 2011; Nepi et al., 2018; Slavkovic et al., 2021; Liao et al., 2021). As a critical reward to insects, and potential attractor, nectaries and their nectar drive many macroevolutionary patterns *via* relationships with pollinators and other animals (Parachnowitsch et al., 2019; Liao et al., 2021). Nectaries are associated with all plant organs except for roots, and floral nectaries can be associated with any floral organ (Nepi, 2007; Liao et al., 2021). Nectary morphology can be structured (i.e., distinct morphology with identifiable cell types) or unstructured (i.e., no specialized morphology) (Nepi, 2007; Slavkovic et al., 2021). Nectar secretion ranges from modified stomata (nectarostomata), to specialized trichomes, and even cell rupture (reviewed in: (Nepi, 2007; Slavkovic et al., 2021)). This diversity in morphology and secretion mechanisms differs across families and within genera (Bernardello, 2007). Also, variable nectar composition impacts pollinator interactions (Nepi et al., 2018; Parachnowitsch et al., 2019). This extensive diversity calls into question whether nectary development is underpinned by similar or different developmental programs in taxa with variable nectaries.

A genetic breakthrough in nectary research was the establishment of *CRABS CLAW* (*CRC*), a YABBY family transcription factor, as essential for nectary initiation (Alvarez and Smyth, 1998; Bowman and Smyth, 1999; Lee et al., 2005a). In *Arabidopsis*, *CRC* knockouts do not develop nectaries (Bowman and Smyth, 1999). *CRC* has since been shown as essential for nectary formation across the core eudicots (Lee et al., 2005b; Fourquin et al., 2014), and is expressed in extrafloral nectaries (Lee et al., 2005b). *CRC* protein dimerizes with other YABBY transcription factors and also has an important role in *Arabidopsis* carpel development (Alvarez and Smyth, 1998; Alvarez and Smyth, 1999; Alvarez and Smyth, 2002; Lee et al., 2005a) that is widely conserved (Orashakova et al., 2009; Fourquin et al., 2014; Pfannebecker et al., 2017). The expression of *CRC* across core eudicot nectaries, regardless of morphology or position, suggests that *CRC* regulation of nectary development is consistent across the clade (Lee et al., 2005b). To the best of our knowledge, functional studies of nectaries have only been conducted in four core Eudicot taxa: *Petunia* (Solonales) (Lee et al., 2005b; Morel et al., 2018), *Gossypium* (Malvales) (Pei et al., 2021), *Pisum* (Fabales) (Fourquin et al., 2014), and *Arabidopsis* (Brassicales) (Bowman and Smyth, 1999). *CRC* is shown as essential for nectary development in the aforementioned taxa, except for *Gossypium* where the gene *GoNe* is required for both floral and extra floral nectaries (Pei et al., 2021). Thus, investigations of additional taxa are needed to uncover the extent of this potential conserved role of *CRC*.

The role of *CRC* as essential for nectary development does not extend beyond the core eudicots. For example, all petals of *Aquilegia* have elongated spurs, which bear nectaries in their distal tips. In this taxa, three *STYLISH* (*STY*) homologs, a member of the *SHORT INTERNODES* (*SHI*) gene family, are redundantly necessary for the formation of nectaries in the spurs as well as style development (Min et al., 2019). Thus, both *CRC* and *STY* are involved in nectary and gynoecial development (Pfannebecker et al., 2017), which raises questions about developmental pathways shared between nectaries and carpels.

Upstream regulators of *CRC* are also shared between *Petunia* and *Arabidopsis* (Morel et al., 2018). *CRC* is insufficient for ectopic nectary formation (Baum et al., 2001), which reveals a necessity for upstream regulators. In *Arabidopsis*, these regulators include ABC(E) class genes *APETALA2/3* (*AP2/3*), *PISTILLATA* (*PI*), *AGAMOUS* (*AG*), and *SEPALLATA1/2/3* (*SEP1/2/3*), as well as MADS-box gene *SHATTERPROOF 1/2* (*SHP1/2*) (Reviewed in: (Slavkovic et al., 2021)). In sum, *SHP1/2* and *AG* act redundantly to promote *CRC*, such that knockouts of each one alone does not prevent nectary formation, although combined they do (Lee et al., 2005a). The floral meristem identity genes *LEAFY* (*LFY*) and *UNUSUAL FLORAL ORGANS* (*UFO*) are also upstream of *CRC* and function to restrict *CRC* expression to nectaries and carpels (Bowman and Smyth, 1999; Slavkovic et al., 2021). Loss of *SEP1/2/3* also prevents nectaries from developing (Lee et al., 2005a). Individual knockouts of any aforementioned gene do not prevent nectary formation, although they can impact shape

and size (e.g., *lfy, ufo, pi, ag*) (Baum et al., 2001). Double and triple knockouts however cause a loss of nectaries (e.g., *lfy & ufo, sep1/2/3*) (reviewed in: (Slavkovic et al., 2021)). Nectary inhibition may be indirect because meristem identity genes act upstream of ABC class genes, i.e., nectary formation may be halted because their associated organs fail to form. In *Petunia*, nectary formation is also dependent on C class genes, i.e., *euAG* and *PLEN* are essential for nectary formation (Morel et al., 2018). This redundancy of MADS-box genes implies that the entire regulatory pathway was established prior to the Rosid/Asterid split (Morel et al., 2018; Slavkovic et al., 2021).

Beyond nectary formation, genes have been identified that are important for nectary size and growth. In *Petunia*, two *euAP2* genes, *BLIND ENHANCER* (*BEN*) and *REPRESSOR OF B FUNCTION* (*ROB*), impact floral nectary size such that *rob1 rob2 rob3* triple mutants have flowers with larger nectaries than wildtype (Morel et al., 2018). This phenotype is enhanced when *BEN* is also knocked out, such that much of the carpel is converted to nectary tissue (Morel et al., 2018). Whereas in *Arabidopsis, BLADE ON PETIOLE 1/2* (*BOP1/2*) are essential for nectary growth independent of *CRC* (Mckim et al., 2008). Knockouts of *BOP1/2* result in nectaries that are small and not fully differentiated into parenchyma and secretory tissue (Mckim et al., 2008).

Phytohormones also play an important role in nectary development, composition, and secretion. *AUXIN RESPONSE FACTOR 6/8* (*ARF6/8*) promote and coordinate nectary formation in *Arabidopsis* (Reeves et al., 2012) and *Aquilegia* (Zhang et al., 2020). Thus, while these taxa differ in which key regulator promotes nectary formation, they have a shared response to hormone signalling, which reflects the central role of plant hormones in floral evolution (Wessinger and Hileman, 2020). Auxin plays an additional role in nectar secretion *via PIN FORMED 6* (*PIN6*) expression, which is positively correlated with nectar production (Bender et al., 2013). Also correlated with an increase in nectar production is jasmonic acid (JA), which peaks in concentration just prior to nectar secretion in *Brassica napus* (Radhika et al., 2010). Further, both auxin and JA are regulated by gibberellic acid (GA) (Reeves et al., 2012), which speaks to the complex interplay between auxin, JA and GA.

Investigations of additional taxa are critical for assessing not only the extent of the conserved role of *CRC*, but also how it is regulated, and the potential pathway deviations across taxa with different nectary shapes and positions. Towards addressing these outstanding questions, Cleomaceae is an excellent model for investigating floral development. Cleomaceae is a small, cosmopolitan family of circa 270 species placed in 25 genera (Bayat et al., 2018). This family houses floral variation in traits likely associated with pollinator interactions, including petal color, petal size, and gynophores/androgynophores (Iltis et al., 2011; Higuera-Diaz et al., 2015; Bayat et al., 2018). Importantly, members of the family exhibit a wide range of nectary size, shape, and position. Across the family, nectaries may be absent, adaxially positioned, or annular (Tucker and Vanderpool, 2010). Cleomaceae is sister to Brassicaceae and the phylogenetic framework within the family is established (Patchell et al., 2014; Barrett et al., 2017; Bayat et al., 2018). While some floral developmental patterns are described (Erbar and Leins, 1997b; Erbar and Leins, 1997a; Patchell et al., 2011), most information regarding nectaries is based on floristic work (e.g., (Tucker and Vanderpool, 2010)). There is also limited empirical information on pollinators, which has revealed generalist and specialist systems across the family (Cane, 2008; Fleming et al., 2009; Higuera-Diaz et al., 2015; Raju and Rani, 2016). Of note, functional approaches have been established for *Cleome violacea* (Carey et al., 2021). This species is amenable to investigations of nectaries as their flowers have prominent, 3-lobed nectaries adaxially positioned between petals and stamen (Figure 1).

The overarching goal of this study was to determine the genetic basis of floral nectaries of *Cleome violacea*. Towards this end, we first characterized nectary anatomy and nectar volume. Second, we conducted a detailed transcriptomic analysis of nectaries from pre-anthetic, anthetic, and post-anthetic (post-fertilization) flowers to document gene expression patterns during nectary development and assess possible convergences in underlying genetic pathways. Finally, we conducted functional studies on key genes to test their direct role and putative interactions in nectary development and nectar production.

2 Materials and methods

2.1 Plant growth conditions

Inbred lines of *C. violacea* were grown from lab seed stock. A voucher was deposited in the vascular plant herbarium at the University of Alberta (ALTA; Hall & Bolton s.n., 20 February 2008; #813 from Hortus Botanicus, Amsterdam). Seeds were sown individually in 7.5 cm diameter pots containing sterilized (20 min, liquid, 121.1°C) Sun Gro Sunshine Mix (Agawam, Massachusetts, USA). All plants were grown in a growth chamber at the University of Alberta, Department of Biological Sciences with 16 h of full spectrum LED light at 22°C and 8 h of darkness at 18°C.

2.2 Histology and scanning electron microscopy (SEM)

Inflorescence tips, small buds (<1 mm wide), medium buds (1-1.5 mm wide), large buds (2.5-3 mm wide), flowers, and post-anthesis flowers were collected and fixed in FAA solution (50% EtOH, 5% glacial acetic acid, 10% formalin, 35% MilliQ water) and vacuum infiltrated as outlined previously (Hall et al., 2006; Patchell et al., 2011). Plant samples were then dehydrated in an ethanol

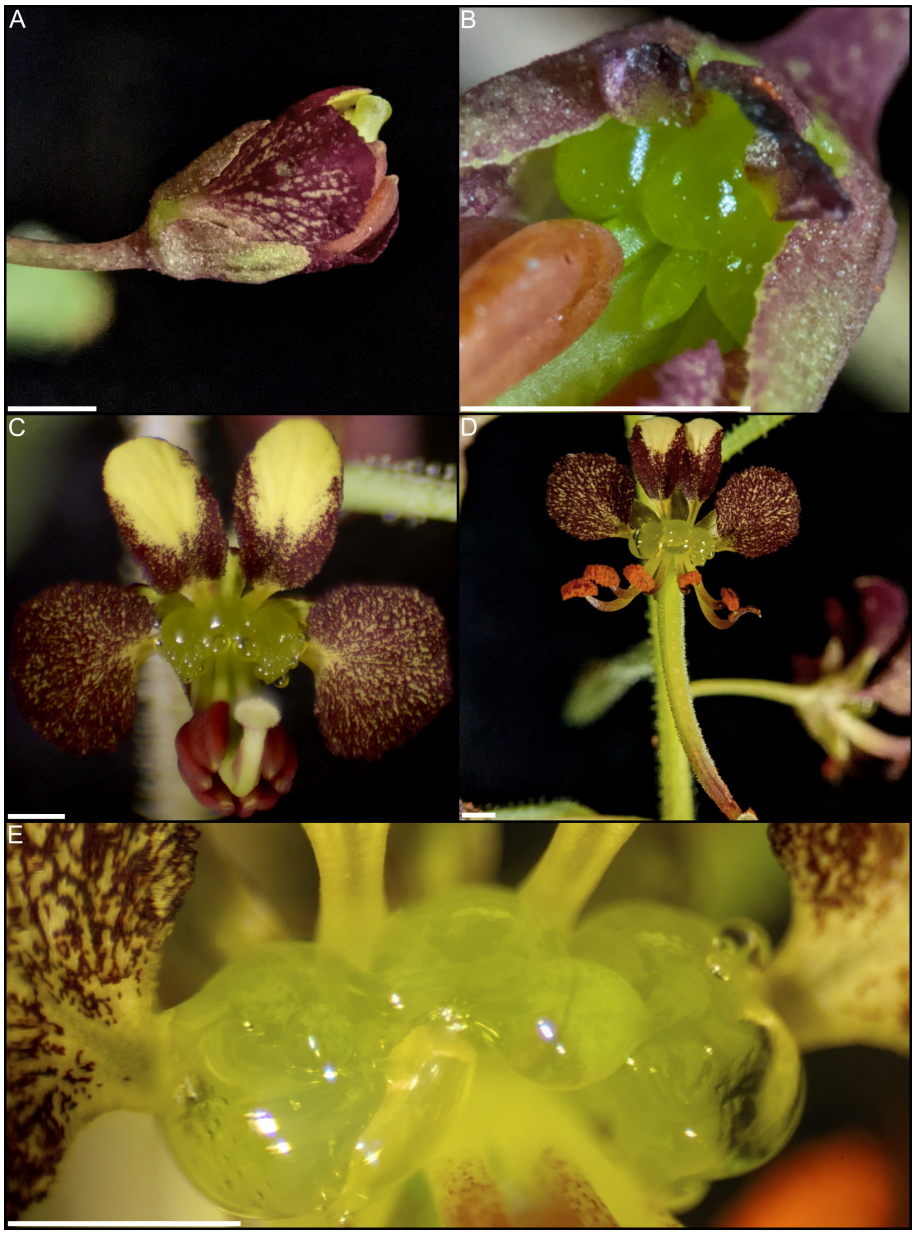

FIGURE 1
Cleome violacea flowers at various stages of development. **(A)** Large undissected floral bud. **(B)** Large dissected floral bud showing nectary. **(C)** Newly anthetic flower. **(D)** Post-anthetic flower with developing fruit. **(E)** Magnified view of anthetic nectary. Scale bars = 1 mm.

series (50% to 100%). All ethanol solutions were kept at 4°C and samples were incubated for 2 hours. The 100% ethanol solutions were left overnight. Samples were infiltrated with CitriSolv (Decon Labs, USA) by changing to a 1:1 ethanol:CitriSolv solution, then changing to 100% CitriSolv. Each CitriSolv solution was incubated for two hours at room temperature with shaking. Samples were infiltrated with Tissue-Prep paraplast (Leica Biosystems, Canada) with 2-3 changes daily for five days then embedded in paraplast. Samples were sectioned to 8 µm using a Microm HM 325 (GMI, Inc., Ramsey, MN, USA) microtome prior to mounting. Slides were cleared with CitriSolv and dehydrated in isopropanol before staining with 0.025% Alcian blue and 0.01% Safranin O in 0.1M acetate buffer for two hours. Slides were examined using a Nikon (Tokyo, Japan) Eclipse 801 microscope with a Nikon DS-Ri1 photo system.

Samples used for scanning electron microscopy (SEM) were fixed and dehydrated as indicated above. After dehydration, samples were critical point dried with carbon dioxide using a CPD 030 critical point dryer (Bal-Tec AG, Liechtenstein, Germany). Specimens were then dissected and mounted on

scanning electron microscopy stubs with conductive carbon tabs and sputter coated with gold using a Hummer 6.2 sputter coater (Anatech USA, Sparks, Nevada, USA). Finally, specimens were imaged using a ZEISS EVO 10 scanning electron microscope (Carl Zeiss AG, Oberkochen, Germany). Contrast and brightness of micrographs were adjusted using GIMP version 2.10.18 (https://gimp.org).

2.3 Nectar volume

Nectar volume of *C. violacea* was measured by pooling nectar from all the open flowers on each plant (2-7 flowers) in a capillary tube (Morrant et al., 2009). This measurement was taken for 20 plants and repeated at the same time each day for four consecutive days. Only flowers with visible nectar were measured. Individual flowers typically senesce three days after anthesis and stop producing nectar. Average nectar volume was calculated for each day and then graphed. A student's t-test was run for binary comparisons between day 1-4.

2.4 RNA isolation and cDNA library preparation

Nectaries were collected from *C. violacea* flowers at three stages of development: pre-anthetic (buds 2.5-3 mm wide), anthetic (first day of anthesis) and post-anthetic (fertilized flowers with fruits at approximately 10 mm in length). RNA from these three developmental stages of four biological replicates were extracted to provide 1) an overview of gene expression at the end of nectary development and 2) insight into how gene expression changes before, at, and after anthesis. Nectary tissue was excised, flash frozen in liquid nitrogen, and stored at -80°C. Following: Carey et al., (2019), RNA was extracted from manually-ground frozen tissue using a Qiagen RNeasy micro kit (Hilden, Germany) and cDNA was generated using the Illumina TruSeq stranded mRNA LT sample prep kit RS-122-2101 (California, U.S.). In this case, mRNA for each sample was isolated using nucleomag beads (Macherey-Nagel, Düren, Germany). Samples were sent to The Center for Applied Genetics (TCAG) at the Toronto Sick Kids Hospital in Ontario, Canada where they were normalized, pooled and sequenced on a HiSeq 2500.

2.5 *De novo* transcript assembly, differential expression, and annotation

Raw reads were downloaded from the TCAG webserver and processed as in (Carey et al., 2019) using updated software (Table S1). The raw reads are available at the Sequence Read Archive (SRA) database (BioProject: PRJNA912718). After differential expression analysis with edgeR (Robinson et al., 2009), transcripts were classified as significantly differentially expressed if they had a log2 (fold-change) greater than four and a False Discovery Rate (FDR)-corrected p-value (α) less than 0.001. The 'analyze_diff_expr.pl' script, provided with Trinity (Haas et al., 2013), was used to generate a matrix of all significantly differentially expressed contig clustered transcripts, which was then used to generate a z-score heatmap in R (R Core Team, 2013).

We performed an additional z-score analysis with trinity transcripts filtered using TransDecoder.LongOrfs and TransDecoder.Predict to remove potential misassemblies. In total, 81,151 of 143,919 transcripts remained. A list of the 81,151 transcripts was used to extract significant transcripts from the original matrix file produced by 'analyze_diff_expr.pl', as well as from a list of all transcripts with expression greater than 100 TPM. Additionally, any transcripts with one or more biological groupings below 10 TPM, or with a coefficient of variation greater than or equal to 50, were removed.

All transcripts from the larger (original) trinity fasta file were annotated using BLASTx (Altschul et al., 1990) with default parameters and a local copy of the Araport11 protein database. Transcripts with the highest bit-score from the TAIR database were used as representative transcripts. Gene specific heatmaps were generated using ggplot2 and ggplot in R (R Core Team, 2013), respectively. Assembly completeness was determined using Benchmarking Universal Single Copy Orthologs (BUSCO) (Simao et al., 2015), and an ExN90 profile.

Transcripts unique to each stage were uploaded to the KEGG automatic annotation server (KAAS) using the bi-directional best hit against the following organism databases: *Arabidopsis thaliana* (Brassicaceae), *Brassica napa* (Brassicaceae), and *Tarenaya hassleriana* (Cleomaceae). Transcripts were considered unique if their expression was $\geq$ 10 TPM with a coefficient of variation < 50. A list of all KEGG entries was compiled, excluding most human diseases and other mammalian-exclusive categories. Of note, some categories were kept because they are convergent with pathways in plants and/or yeast.

2.6 Virus-induced gene silencing (VIGS)

Viral vector constructs were designed following (Carey et al., 2021). Tobacco rattle virus vectors pTRV1 (donor stock no. YL192) and pTRV2 (donor stock no. YL156) were obtained from The *Arabidopsis* Information Resource (TAIR; https://www.arabidopsis.org) using their stock center (*Arabidopsis* Biological Resource Center [ABRC], Ohio State University, Columbus, Ohio, USA; https://abrc.osu.edu). The pTRV2 vector is used for downregulating genes of interest (Ratcliff et al., 2001) and the pTRV1 vector assists with viral movement (Ziegler-Graff et al., 1991). Six new endogenous constructs were generated for this study using *C. violacea* mRNA: pTRV2-*CvANS*, pTRV2-

CvAG, pTRV2-*CvAG-CvSHP*, pTRV2-*CvCRC-CvANS*, pTRV2-*CvSWEET9-CvANS*, and pTRV2-DN802_c0_g1_i4-*CvANS*. The *CvANS* construct was used as a marker gene and positive control. Treatment with pTRV2-*CvSHP* was explored in a preliminary round of VIGS but produced no remarkable floral phenotype and, as such, was abandoned in future trials.

All constructs were generated as follows. All cDNA was synthesized following manufacturer instructions using SuperScript III Reverse Transcriptase (Invitrogen), poly(T) primers, and random hexamer primers. All primers were designed using the transcriptomic data from this study. All amplification was done using Invitrogen recombinant Taq DNA Polymerase (Waltham, Massachusetts, USA) using the manufacturer protocol, 50 µL reaction volumes, and 35 cycles. All amplicons were verified using agarose gel electrophoresis, and colonies were screened *via* PCR with primers, 156F and 156R that span the TRV2 multiple cloning site (Gould and Kramer, 2007). Manufacturer protocols were used for each step unless otherwise noted. First, a 533 bp insert of *CvANS* was amplified using forward and reverse primers with added BAMHI [G^GATCC] and XHOI [C^TCGAG] restriction sites, respectively. Amplicons were purified using a QIAquick PCR purification kit and digested alongside empty TRV2 vector with NEB BAMHI and XHOI restriction enzymes (Ipswich, Massachusetts, USA). Digests were purified using the Quantum Prep Freeze 'N Squeeze DNA Gel Extraction protocol with 200 µL pipette tips and 2 mL tubes in lieu of spin columns. Eluate was further purified using ethanol precipitation (https://projects.iq.harvard.edu/hlalab/resources-0). Digests were ligated together using NEB T4 DNA ligase and immediately transformed using One Shot™ TOP10 Chemically Competent *E. coli*. *Escherichia coli* was incubated for 24 h at 37°C in Miller LB broth (Sigma-Aldrich, Burlington, Massachusetts, USA) containing 50 µg/mL kanamycin. The pTRV2-*CvANS* construct was verified using colony PCR, and colonies containing the appropriately sized plasmids were extracted using a GeneJET Plasmid Miniprep Kit (Thermo Fisher, Waltham, Massachusetts, USA), verified using agarose gel electrophoresis, and transformed into chemically competent Agrobacterium GV3101; cells were prepared and transformed according to protocol (Luo et al., 2008). All media used to grow *Agrobacterium* contained 50 µg/mL kanamycin, 50 µg/mL gentamycin, and 25 µg/mL rifampicin. Plasmids from transformed Agrobacterium were verified *via* restriction digestion and agarose gel electrophoresis, and finally sanger sequencing. Agrobacterium containing the appropriate pTRV2-*CvANS* vector were grown for 48 h at 28°C and mixed 1:1 with sterile 50% glycerol prior to storage at -80°C.

All other vectors were made following the same protocol. Amplicons from *CvCRC*, *CvSWEET9*, and DN802_c0_g1_i4 were ligated to pTRV2-*CvANS* vectors using XBAI [T^CTAGA] and BAMHI restriction sites; *ANS* acting both as a positive control and marker gene for facilitated phenotyping. The pTRV2-*CvAG* construct was generated using BAMHI and XHOI restriction sites, as with pTRV2-*CvANS*. The *CvSHP* amplicon was then ligated to the pTRV2-*CvAG* vector using XBAI and BAMHI restriction sites. No *CvANS* marker was used for the *CvAG* or *CvAG-CvSHP* constructs because downregulation of *CvAG* is distinct. Viral constructs were verified for off-target silencing using siFi21 (Lück et al., 2019).

Agrobacterium tumefaciens was prepared for DNA transformation as previously described (Carey et al., 2021). All vectors were transformed into *A. tumefaciens* using calcium chloride heat-shock transformation. For each, 100 ng of purified construct was combined with 250 µL of competent *A. tumefaciens*. Transformants were plated on LB media containing the aforementioned antibiotics. Transformants were then screened as before using 156F and 156R primers, and glycerol stocks were made and stored at −80°C (1:1 ratio of 50% glycerol and overnight *A. tumefaciens* culture).

The vacuum infiltration protocol, which has been shown to be an effective infiltration method with *C. violacea*, was modified from Carey et al. (2021). For each vector, *A. tumefaciens* cultures were serially inoculated up to 1000 mL cultures containing antibiotics, 1mM MES buffer and 0.02 mM acetosynringone. A 1:1 ratio of pTRV1 cultures were also serially inoculated up to 1000 mL. The final cultures were grown until they reached an OD600 between 0.8-1, and then immediately centrifuged and resuspended in infiltration buffer (10 mM MES, 10 mM MgCL2 and 0.2 mM acetosyringone) to an OD600 of 4.0 ± 0.1 and left for four hours to acclimatize. *Agrobacterium* containing pTRV1 should be inoculated 1-2 hours prior to pTRV2 cultures because they have a slower growth rate. An OD600 of four was chosen because it has been reported to achieve greater yields, and when pTRV2 and pTRV1 are combined their OD600 values half to an optimal OD600 of 2.0 (Wang et al., 2006). The serial inoculation was halted at OD600 0.8 to capture log-phase growth. The pTRV2 and pTRV1 suspensions were combined prior to infiltration at a 1:1 ratio. Silwet L-77 surfactant was added to each mixture at 100 µL/L. Groups of seedlings were extracted from the soil, rinsed in reverse osmosis water, briefly air-dried, submerged in *Agrobacterium*, and placed in a vacuum chamber. The chamber was evacuated to -20 inHg and held for 2 minutes. Vacuum pressure was then quickly released, and plants were rinsed and planted in fresh soil. Finally, plants were grown at 22° C for 16 h and 18°C for 8 h because it was found that lower temperatures consistently resulted in better VIGS efficacy in *Petunia* (Broderick and Jones, 2014).

All treated plants began showing phenotypes five weeks post-inoculation, and phenotypes lasted until plant senescence. Phenotypes for construct pTRV2-*CvANS* were scored based on reduction in maroon pigmentation in petals, which is hereafter referred to as yellowing, i.e., a reduction in anthocyanins resulted in petals with increased yellow pigmentation. A flower was scored as having a moderate phenotype when at least two petals displayed obvious yellowing. Flowers were scored as

having a strong phenotype if all four petals displayed obvious yellowing. Flowers with less yellowing than moderate flowers, but which were distinct from untreated flowers, were scored as having a mild phenotype. There were no observed instances of only a single petal yellowing.

The yellowing phenotype assisted with scoring of *CvCRC*, *CvSWEET9*, and DN802_c0_g1_i4 constructs. Phenotypes for pTRV2-*CvCRC-CvANS* were scored based on complete or partial absence of nectary. Yellowed flowers with complete nectaries, and non-yellow flowers without nectaries were also recorded because it is possible for only a single gene to be silenced even with multiple gene constructs. Phenotypes for pTRV2-*CvSWEET9-CvANS* were scored based on visual inspection of nectary gland for presence of nectary droplets using a dissection microscope. Phenotypes for pTRV2- DN802_c0_g1_i4-*CvANS* were indistinguishable from pTRV2-*CvANS*.

Phenotypes for *pTRV2-CvAG* and *pTRV2-CvAG-CvSHP* were scored based on *AG* silenced phenotypes in *Arabidopsis* because of conservation of ABC gene function (Mizukami and Ma 1997). Silencing efficacy was based on the extent of repetition of perianth whorls and the absence of reproductive whorls. For both constructs, presence/absence of nectaries, absence of reproductive whorls, and repetition of perianth whorls were noted. Plant tissue from treated and control plants was excised, flash-frozen in liquid nitrogen, and stored at -80°C. Phenotypes were imaged using a Nikon SMZ 1500 dissecting microscope (Nikon, Tokyo, Japan) and a handheld digital Canon DS126181 camera (Canon, Tokyo, Japan). Images were standardized, scaled, color balanced, and assembled into figures using Inkscape version 0.92.5 (https://inkscape.org) and GIMP.

3 Results

3.1 Morphology and nectar production in *Cleome violacea*

Anthetic nectaries of *C. violacea* are adaxially positioned between petals and stamen. These nectaries are prominent due to their relatively large size (i.e., roughly half the size of an abaxial petal). Nectaries are tri-lobulate with two larger lateral lobes and a smaller central lobe at anthesis (Figures 1B–E). Following the terminology of Nepi (2007), these structured nectaries have prominent epidermis, and mostly consist of specialized parenchyma with vascular tissue interspersed throughout (Figure 2). Nectar is secreted *via* nectarostomata, which are present prior to anthesis (Figure 3). Floral nectaries are first visible late in development when developing stamens reach the same length as petals. At this stage, sepals and petals are growing, stamens have differentiated into filaments and anthers, and the gynoecium is formed with papillate stigma. Nectaries mature concordantly with stamens and reach maturity just prior to anthesis (Figure 1B). Nectary primordia are visible in small buds (Figure 2) when sepals are maturing.

In small buds (<1.0 mm wide), nectaries are oblong and marginally lobed. At this stage, cells appear parenchymal with no differentiation of epidermis or vascular tissue, although the cuticle is apparent (Figures 2A–C). Medium buds (1-1.5 mm wide) have more pronounced lobes with differentiated epidermis (Figures 2D–F). Large buds (2.5-3.0 mm wide) have larger lobes comprised of parenchymal cells which make up the bulk of the nectary (Figures 2G–I). Epidermal cells are 1-2 layers thick on medial and lateral nectary lobes (Figure 2Q). In large buds, vascular tissue is distributed throughout the specialized parenchyma and likely connects with other vasculature near the receptacle base (Figure 2P) and with nectarostomata on the nectary surface (Figure 3). These nectarostomata are present on large buds (Figure 3A) and anthetic flowers (Figure 3B). Nectaries produce a low volume of nectar that decreases in volume after anthesis (Figure 4). Anthetic nectaries produce an average of 0.17 ± 0.07 µL) of nectar (Figure 4). Nectar volume decreases after day 1 but remains stable over three consecutive days of sampling at ~ 0.11 ± 0.04 µL) (Figure 4).

3.2 Expression profiles show distinct gene expression patterns pre to post anthesis

The transcriptome is of suitable quality and completeness for downstream analyses. The transcriptomic read depth averaged 19.9 million reads across 12 biological replicates, totaling just over 239M paired end trimmed reads. Median Phred scores are between 34 and 39 for each base pair of all 143,919 Trinity transcripts (Table S2), which indicates a base call accuracy between 99.7% and 99.99% (data not shown). The E90N50 value of the assembled transcriptome is 2227, and peaks at 2259 for Ex93 and Ex94 (Figure S1). A peak around Ex90 generally indicates a high level of transcriptome completeness. Further, the Benchmarking Universal Single Copy Orthologues (BUSCO) analysis of Viridiplantae orthologues (Simao et al., 2015) revealed that the transcriptome was 99.6% complete with 2 fragmented BUSCOs (Table S3).

Heatmap patterns of gene expression of pre-anthetic, anthetic and post-anthetic nectaries are consistent across two distinct thresholds. We compared all 4521 significantly differentially expressed transcripts, as well as the 1214 transcripts above 100 TPM (with a coefficient of variation < 50 in one or more biological groupings) (Figure 5). Pre and post-anthetic nectaries have opposing expression profiles, such that transcripts upregulated in pre-anthetic nectaries are generally downregulated in post-anthetic nectaries. Anthetic nectaries have no large clusters of up or downregulated transcripts and appear to be partially transitional, although they have a few unique clusters of differential expression (Figure 5). Expression patterns of

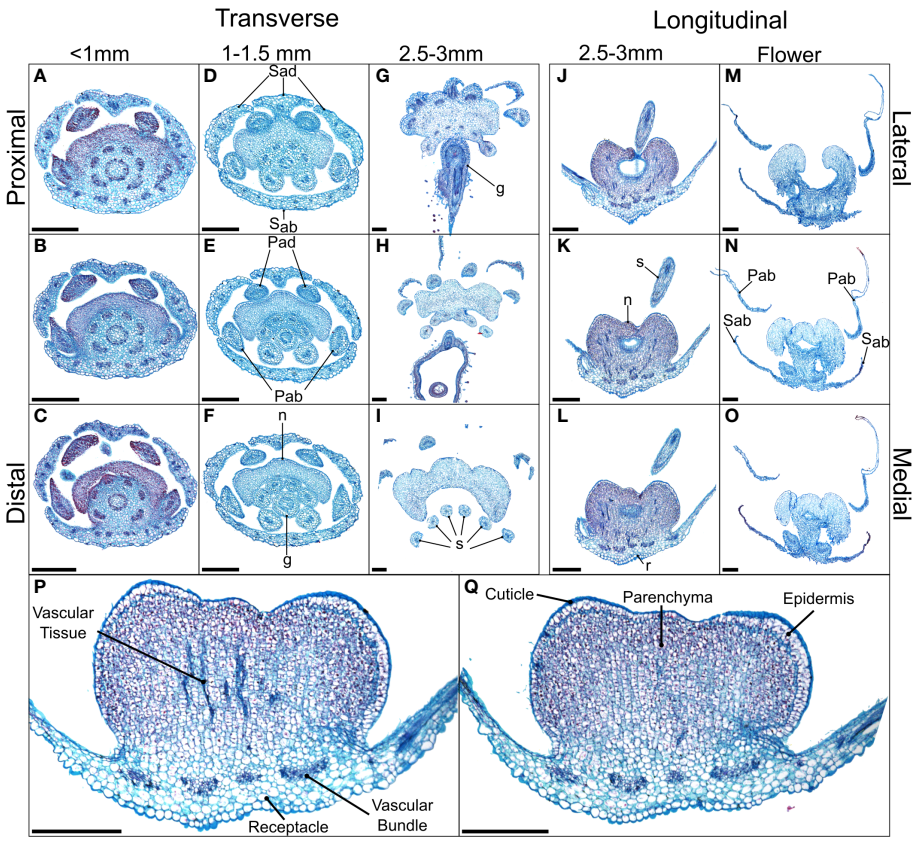

FIGURE 2
Alcian blue/safranin O-stained sections of *Cleome violacea* nectaries at pre-anthetic, anthetic and post-anthetic stages. From left to right: **(A–C)** small, **(D–F)** medium, and **(G–I)** large buds in transverse view with proximal-distal indicating relative distance to receptacle. **(J–L)** Large bud and **(M–O)** flowers in longitudinal view with lateral-medial indicating relative distance from center. **(P, Q)** Longitudinal view of 20 µm slices of the same large floral bud with and without vascular tissue, respectively. Scale bars = 250 µm. Sad = adaxial sepal; Sab = abaxial sepal; Pad = adaxial petal; Pab = abaxial petal; s = stamen; g = gynoecium, r = receptacle.

transcripts filtered using TransDecoder were similar to the unfiltered list for significantly differentially expressed transcripts, as well as those above 100 TPM (Figure S5). In sum, each of the three developmental stages is genetically distinct.

To provide additional insight into gene regulatory networks governing nectar secretion and nectary development, we also assembled the highest expressed transcripts across all stages from the TransDecoder-filtered dataset. This list included 20 of the highest expressed transcripts from pre-anthetic, anthetic and post-anthetic stages that were significantly differentially expressed in pairwise comparisons, and the top 20 highest overall expressed transcripts that were not differentially expressed. Due to overlap, there were 56 transcripts in total (40 among the differentially expressed and 16 non-differentially highly expressed transcripts). A few transcripts matched to the same genes leaving 51 unique accessions. Out of the 51, eight had no obvious role specific to nectary function (e.g., ubiquitous cellular process; Table S4). Five were related to photosynthesis, 14 to water transport and sugar production, 16 to stress response and six to cell growth. *YABBY5*, which can dimerize with *CRC* (Gross et al., 2018) was also among the highest expressed (Table S4). Putative gene function was estimated using gene description information from TAIR (www.arabidopsis.org), and a brief review of the literature.

3.3 Energy metabolism and hormonal regulation across nectary development

Genetic networks were assessed to determine which categories were active at each sampled stage of nectary development. KEGG analyses revealed several categories that had different relative counts (i.e., putative orthologs) in one or more stages: energy metabolism, biosynthesis of secondary metabolites, translation, replication and repair, environmental adaptation, and cell growth and death. We interpret greater counts as greater biological activity. A difference of three or less was disregarded to account for any potential noise in the data,

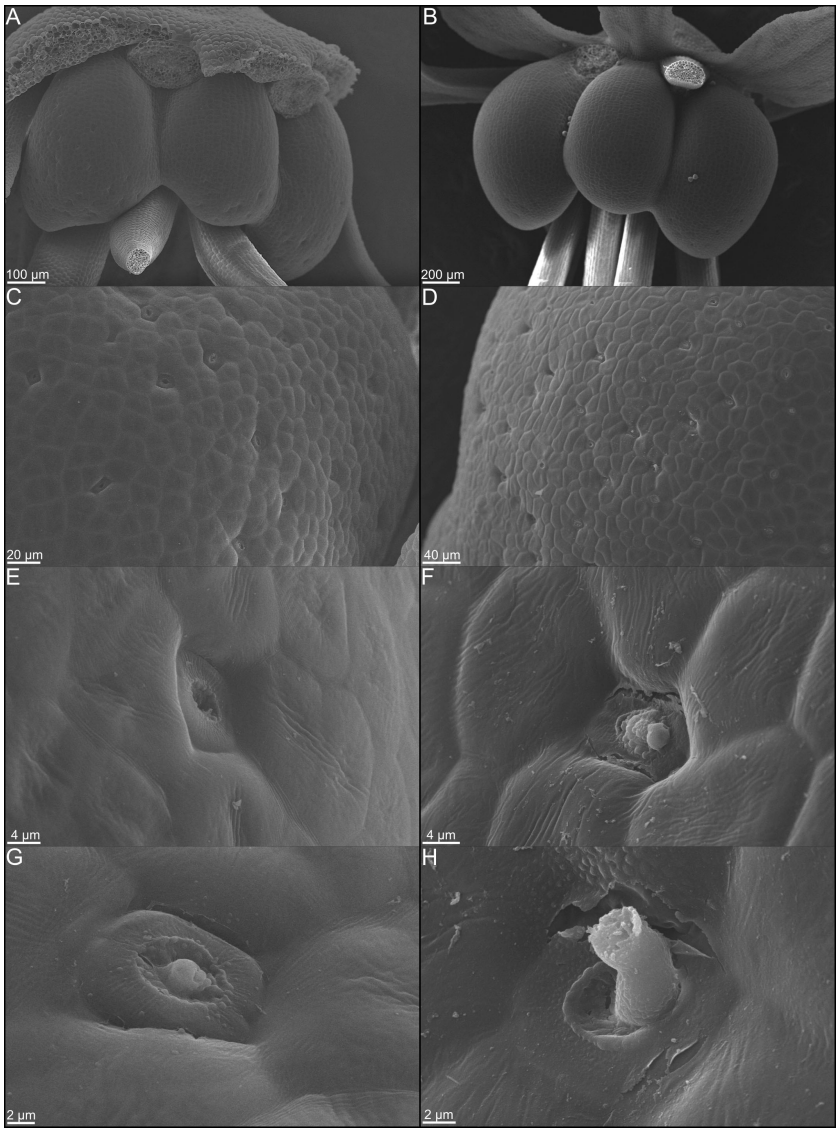

FIGURE 3
Scanning electron micrographs of whole nectaries from Cleome violacea at **(A)** pre-anthetic and **(B)** anthetic stages. **(C)** Distribution of nectarostomata on pre-anthetic nectary lobe and **(D)** anthetic nectary lobe. Examples of nectarostomata from **(E–G)** bud and **(F–H)** anthetic flowers.

e.g., invalid isoforms created during the assembly process. In pre-anthetic nectaries, oxidative phosphorylation (35 relative to 25 in the other two stages), and thermogenesis (40 relative to 32 in the other two stages) are the only subcategories with a greater number of putative orthologs (Table S5). Mitochondrial oxidative phosphorylation in plants is known to provide ATP for cellular functions (e.g., sucrose metabolism) and is tightly linked to photosynthesis (Braun, 2020). However, photosynthetic processes are similar between all stages (Table S5). Anthetic nectaries have no categories with greater hits than the other two stages (Table S5). Post-anthetic nectaries have increased biological activity in two categories, replication and repair, and cell growth and death; three of the five subcategories for cell growth and death are directly related to yeast (Table S5), i.e., nectary yeast are likely contributing to ortholog abundance in this category. Overall, most categories have a similar number of putative orthologues across all stages.

Although plant hormone signalling is important in nectary development and nectar secretion, there was no indication of differences between hormone signalling related orthologs between stages, based on the KEGG analysis (Table S5). However, expression analyses indicated significant differential expression in genes related to these pathways (Figure 6). Auxin, JA, and GA are known to regulate transcriptional expression

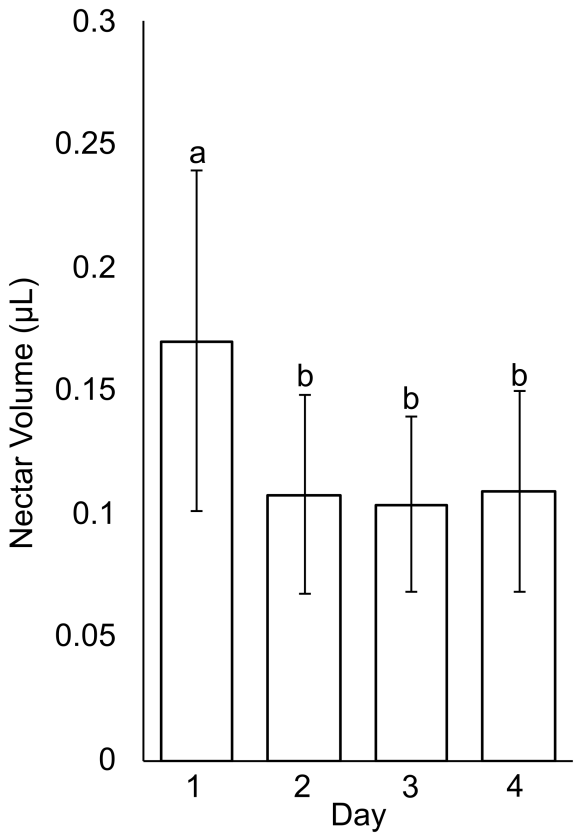

FIGURE 4
Nectar volume from *Cleome violacea* flowers taken on first day of anthesis (Day 1) and three days post-anthesis (Days 2, 3, and 4). Averaged value of flowers from 20 plants. Significance measured using paired, one-tailed, student's t-tests ($\alpha < 0.01$).

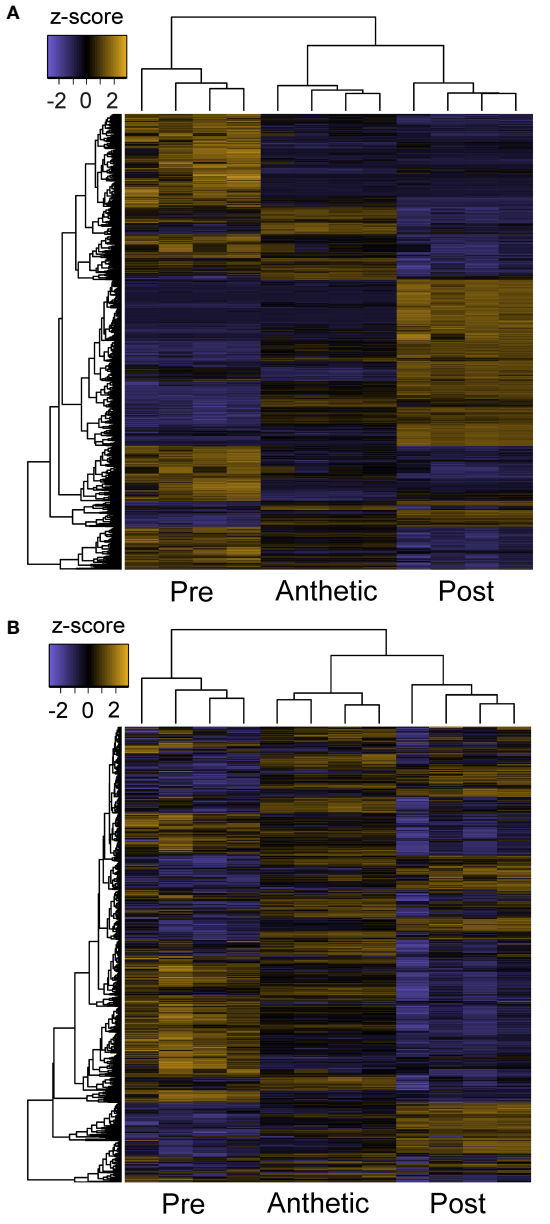

FIGURE 5
Z-score heatmaps of **(A)** all differentially expressed transcripts and **(B)** transcripts with TPM > 100 from *Cleome violacea* pre-anthetic, anthetic, and post-anthetic nectaries.

related to nectar secretion (Slavkovic et al., 2021), and ethylene interacts synergistically with auxin (Muday et al., 2012), although to our knowledge has no direct link to nectaries. Examples of highly expressed transcripts were *AUXIN RESPONSE FACTOR 6* (*ARF6*) and *JASMONATE ZIM-DOMAIN PROTEIN 1* (*JAZ1*) (Figures 6A, C). Three *GIBBERELLIN 2-OXIDASE* genes were expressed in pre-anthetic, anthetic and post-anthetic nectaries, respectively (Figure 6B). We also found significant upregulation of multiple ethylene related transcripts in pre-anthetic nectaries (e.g., *ETHYLENE RESPONSE FACTOR 1* (*ERF1*) and *ETHYLENE FORMING ENZYME* (*EFE1*). (Figure 6D). These data suggest that a combination of auxin, JA, and GA influence nectary development and nectar secretion in *C. violacea*.

3.4 Yeast and bacteria are present on Cleome *violacea* nectaries

Transcriptomic and SEM data provide evidence that yeast and bacteria colonize C. *violacea* nectaries. There are a total of 46 and 44 hits (e-value < 1e-50) to bacterial and yeast-related rRNA in the *C. violacea* transcriptome, respectively (Figure 7). Ribosomal rRNA can still be present in poly(A)-enriched libraries in appreciable percentages (Kim et al., 2019), which is valuable for finding non-plant related expression. Generally, expression of fungal and bacterial rRNA was inconsistent across biological replicates and stages; suggesting that colonization may be replicate specific. However, there are a few instances where expression is consistent across replicates and stages, which may indicate an established biological interaction (Figure 7). These data are further supported by the

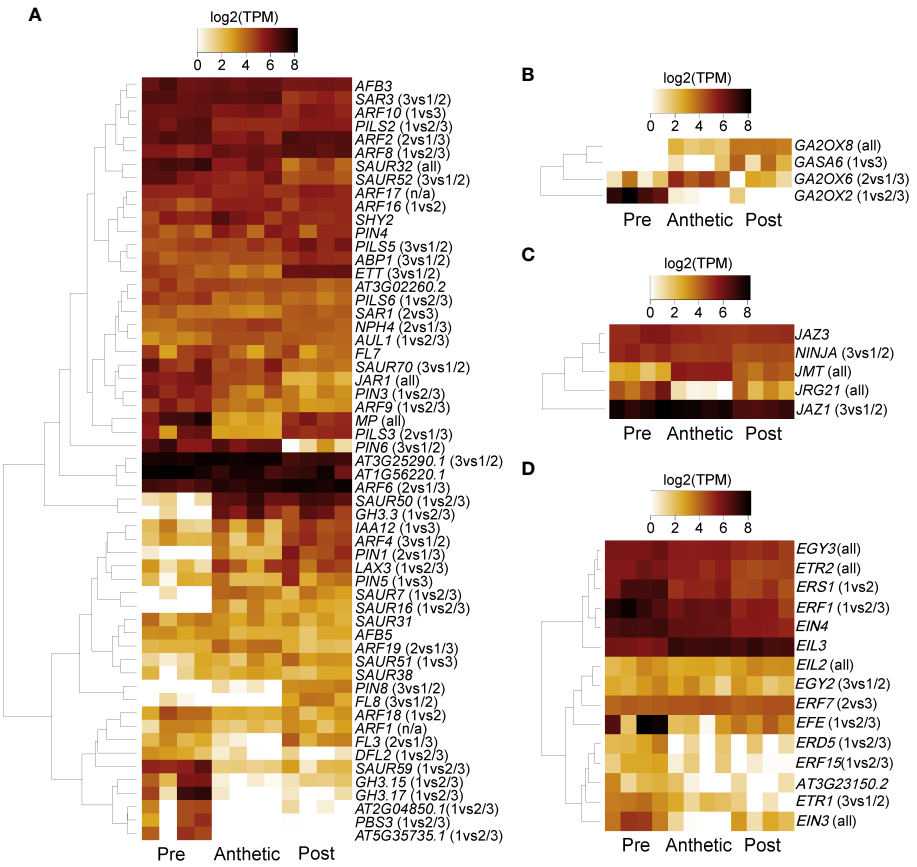

FIGURE 6
A heatmap of phytohormone-related transcripts expressed in pre-anthetic, anthetic, and post-anthetic nectaries of *Cleome violacea* displayed in log2(TPM). Representative transcripts of genes related to **(A)** auxin, **(B)** gibberellic acid **(C)** jasmonic acid, and **(D)** ethylene. Significance displayed in brackets. 1 = pre-anthetic; 2 = anthetic; 3 = post-anthetic.

obstructions surrounding and within the nectarostomata (e.g., what appears to be budding yeast cells) (Figures 3F–H) and are consistent with the abundance of yeast related KEGG terms (Table S5). For example, there are nearly twofold more KEGG terms related to the yeast cell cycle in post-anthetic nectaries (43) than pre-anthetic (22) or anthetic (20) nectaries (Table S5). Carotenoid related genes *FLAVONOL SYNTHASE* 1 (*FLS1*), *PHYTOENE SYNTHASE (PSY)*, and *CHALCONE SYNTHASE* (*CHS*) are also highly expressed at various developmental stages (Table 1 and Figure S2). All three genes have purported roles in combating biotic stress (Dao et al., 2011; Havaux, 2014; Naparlo et al., 2019).

3.5 Dynamic expression patterns of genes involved in nectar and nectary formation

After establishing global patterns and active biological networks, we examined expression patterns of 17 genes of interest with uncertain roles, nine genes known to be involved in nectar production, and ten genes with direct roles in nectary formation (e.g., expression in *Arabidopsis* nectaries) (Tables 1–3; Figure S2). These analyses reveal dynamic expression patterns from pre to post-anthetic nectaries. Seven genes linked to nectar production are significantly upregulated in either pre-anthetic and/or anthetic nectaries: *BAM1, PIN6, MYB21, SWEET9, JAZ, G20X* and *JMT* (Table 2). This pattern mirrors the onset of nectar production. Interestingly, expression profiles for nectary development genes (Table 3) are generally opposite to nectar production (Table 2). That is, of the genes examined with established roles in nectary development, most transcripts are downregulated in pre-anthetic nectaries, and three of ten genes explored are evenly expressed across all stages (Table 3). Downregulated genes include *PI*, *AG*, *ARF6*, *ARF8*, and *STY* (Table 3). Of the 17 genes with uncertain roles, six are evenly expressed across all three developmental stages: *SEP1/4, TOPLESS* (*TPL*), *SUPRESSOR OF OVEREXPRESSION OF CO 1* (*SOC1*), *GIGANTEA* (*GI*), and *FLOWERING LOCUS D LIKE* (*FLD-like*). Of the remaining, no clear pattern emerges (Table 1).

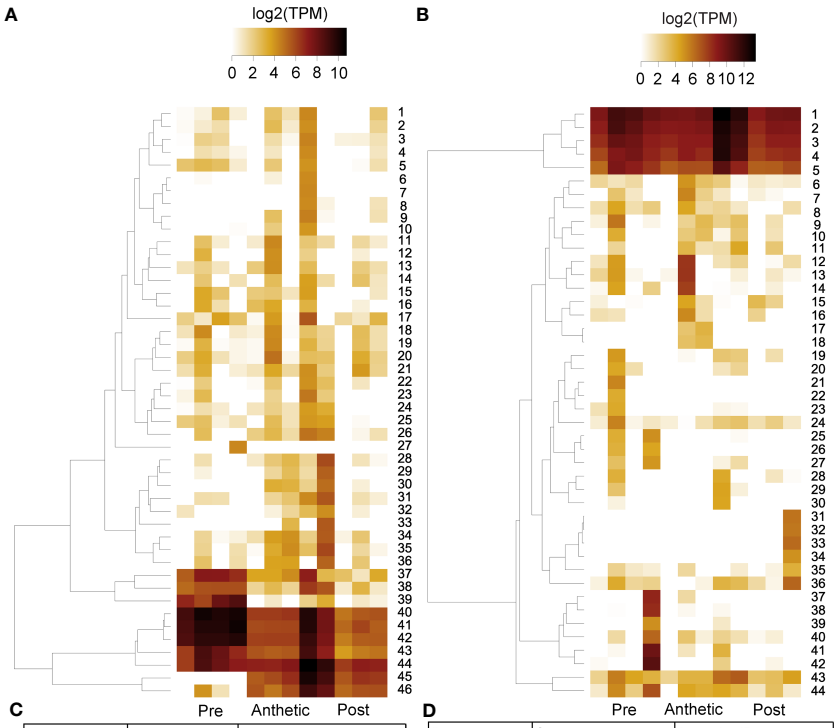

C

#	Genus	Accession ID
2;18	*Acinetobacter*	nr_102814.1/nr_148847.1
24;27		nr_115299.1/nr_026208.1
38;44	*Corynebacterium*	nr_026380.1/nr_029292.1
33	*Curvibacter*	nr_024702.1
8;13;20	*Cutibacterium*	nr_040847.1
28;35	*Cylindrospermum*	nr_102462.1
15	*Dokdonella*	nr_042397.1
22	*Domibacillus*	nr_108861.1
32	*Ehrlichia*	nr_121714.1
25;37	*Exiguobacterium*	nr_043478.1
5	*Insolitispirillum*	nr_044314.1
45	*Kribbella*	nr_025735.1
23	*Microbacterium*	nr_044934.1
43	*Micrococcus*	nr_172606.1
10	*Neochroococcus*	nr_172603.1
3;17	*Paracoccus*	nr_024658.1/nr_025857.1
21;34;40		nr_025714.1/nr_157668.1
16	*Prolinoborus*	nr_104948.1
26	*Propionibacterium*	nr_151943.1
4	*Propionivibrio*	nr_025455.1
1;6;11	*Pseudomonas*	nr_041715/116651/134795
14;29;42		nr_026395/024704/041715
9;36	*Schlegelella*	nr_043802.1
46	*Sphingomonas*	nr_108991.1
12	*Stella*	nr_025582.1
7;19;30	*Tepidimonas*	nr_042418.1
31;39;41		nr_109514.1

D

#	Genus	Accession ID
19	*Acremonium*	ng_062813.1
9;34	*Amycosphaerella*	ng_061084.1
41	*Ascochyta*	ng_061064.1
7;15;17;39;42	*Aspergillus*	ng_063229.1/ng_074950.1
8;14;23;30;40;43	*Brunneoclavispora*	ng_061284.1
13	*Candida*	ng_063392.1
1	*Chytridium*	ng_061075.1
37	*Cutaneotrichosporon*	ng_062024.1
5	*Erythrobasidium*	ng_063520.1
36	*Hyaloraphidium*	ng_017172.1
18	*Hyphozyma*	ng_070854.1
31	*Infundichalara*	ng_061112.1
27	*Leiothecium*	ng_061073.1
38	*Lentithecium*	ng_016507.1
10;28	*Loramyces*	ng_062693.1
21	*Malassezia*	ng_062732.1
3;12;20;44	*Mortierella*	ng_070277/070287/070251
6;25;35	*Olpidium*	ng_017176.1
29	*Penicillium*	ng_074879.1
26	*Phaeotremella*	ng_063469.1
22	*Ramicandelaber*	ng_070281.1
2;4	*Rhexocercosporidium*	ng_061015.1
16	*Rozella*	ng_017174.1
33	*Symbiotaphrina*	ng_070853.1
11	*Teratosphaeria*	ng_065572.1
24	*Westerdykella*	ng_016502.1
32	*Xenoacremonium*	ng_061110.1

FIGURE 7
Heatmap of **(A)** 16s bacterial rRNA and **(B)** 18s fungal rRNA related transcripts in pre-anthetic, anthetic, and post-anthetic nectaries of *Cleome violacea* displayed in log2(TPM). Genera and NCBI accessions of respective transcripts for bacteria and fungi outlined in **(C, D)**, respectively.

3.6 Functional studies demonstrate key roles of *CvAG, CvSHP, CvCRC*, and *CvSWEET9* in nectary development and nectar secretion

VIGS experiments tested the putative function of five genes. Four of the five genes targeted for downregulation were highly expressed and have established roles in nectary development and nectar production: *CvAG*, *CvSHP*, *CvCRC*, and *CvSWEET9* (Tables 2, 3 and Figure S2). We also downregulated an uncharacterized transcript (DN802_c0_g1_i4) because it was among the highest expressed in the transcriptome, has a similar profile to *CvSWEET9*, and has no significant match to either the TAIR11 database or the nr database, despite an ORF of 375 bp (Figure S3). It partially matches AT412520.1 (e-value = 8.19e-4) from the TAIR11 database and MW419336 (e-value = 6.33e-7) from the nr database. These hits were not considered further because of their large e-values.

TABLE 1 Genes of interest not directly implicated in nectary development with relative expression values from our transcriptomic dataset, putative roles, and relevant citations.

Gene	SDE	Putative Role	Citation
TPL	≈	Co-repressor of *AG* which is recruited by *AP2* in floral organ identity	Krogan et al., 2012
STM	↓S2 vs S1/S3	Controls carpel development and requires the function of *AG*	Scofield et al., 2007
SEP3	↓S2 vs S1/S3	Functions in combination with B and C class genes to activate *CRC*	Lee et al., 2005a
FTM4	↑S3 vs S2/S3	Encodes an intracellular LRR protein that interacts with *AG*	Torti et al., 2012
SEP4	≈	Functions in combination with B and C class genes to activate *CRC*	Lee et al., 2005a
SOC1	≈	Functions together with *FUL* to promote development of inflorescence	Preston et al., 2011
AP1	↑S3 vs S1/S2	Regulates fatty acid biosynthesis with *CRC* in *Arabidopsis*	Han et al., 2012
GI	≈	Regulates miR172, which in turn regulates *BEN* and *ROB* in *Petunia*	Jung et al., 2007
FLD-LIKE	≈	Required for systemic acquired resistance in *Arabidopsis*	Singh et al., 2013
FUL	↓S3 vs S1/S2	Expressed in *Arabidopsis* nectaries from stage 9 to stage 14	Baum et al., 2001
CO	↑S1 vs S2/S3	Promotes *SOC1* and *FT*	Jung et al., 2007
SEP1	≈	Functions in combination with B and C class genes to activate CRC	Lee et al., 2005a
YABBY5	↑S2 vs S1/S3	Can dimerize with *CRC via* the *YABBY* domain	Gross et al., 2018
TPS	↑S3 vs S1/S2	Levels of trehalose change in parallel with sucrose; regulates stomatal conductance and water use.	Lunn et al., 2014
FLS1	↑↑S3 vs ↑S2 vs S1	Accumulation of flavanols may increase survival of yeast by reducing oxidative stress	Naparlo et al., 2019
PSY	↑S2 vs S1/S3	Carotenoid oxidation products function as a plant stress signal	Havaux, 2014
CHS	↑S3 vs S1/S2	Linked to resistance of biotic stress	Dao et al., 2011

SDE, Significant Differential Expression with arrows representing either up or down regulation of expression between developmental stages (≈ indicates no SDE). S1, pre-anthetic nectary; S2, anthetic nectary; S3, post-anthetic nectary.

TABLE 2 Genes of interest with direct roles in nectar production with relative expression values from our transcriptomic dataset, putative roles, and relevant citations.

Gene	SDE	Putative Role	Citation
CWINV4	≈	Hydrolyzes sucrose into fructose and glucose; knockouts do not produce nectar	Ruhlmann et al., 2010
SBE2.2	≈	Involved in starch synthesis; upregulated early in development in ornamental tobacco	Ren et al., 2007
BAM1	↑S1 vs S2/S3	Starch breakdown; upregulated during secretory stage in Cucurbita pepo	Solhaug et al., 2019
PIN6	↓S3 vs S1/S2	Expression level is positively correlated with nectar production in *Arabidopsis*	Bender et al., 2013
MYB21	↑S2 vs S1/S3	Induces negative feedback loop on jasmonate biosynthesis	Reeves et al., 2012
SWEET9	↓S3 vs S1/S2	Required for nectar secretion in *Arabidopsis*	Lin et al., 2014
JAZ	↓S3 vs S1/S2	Represses jasmonic acid (JA) signalling in a negative feedback loop	Chico et al., 2008
GA2ox6	↑S2 vs S1/S3	Inactivates gibberellic acid (GA), which increases expression of genes involved in nectar production	Wiesen et al., 2016
JMT	↑S2 vs S1/S3	Forms Methyl Jasmonate from JA; JA conjugates are linked to increased nectar production.	Radhika et al., 2010

SDE, Significant Differential Expression with arrows representing either up or down regulation of expression between developmental stages (≈ indicates no SDE). S1, pre-anthetic nectary; S2, anthetic nectary; S3, post-anthetic nectary.

ANS was used both as a positive control vector (pTRV2-*CvANS*) and as a marker gene to facilitate scoring of phenotypes for *CvCRC* (pTRV2-*CvCRC-CvANS*), *CvSWEET9* (pTRV2-*CvSWEET9-CvANS*), and DN802_c0_g1_i4 (pTRV2-DN802-*CvANS*). Untreated *C. violacea* and plants treated with pTRV2-MCS constructs were also used as controls (Figures 8A–D). Treatment with pTRV2-*CvANS* produced flowers with primarily yellow pigmentation on adaxial and abaxial petals (Figures 8E, F).

TABLE 3 Genes of interest with direct roles in nectary formation with relative expression values from our transcriptomic dataset, putative roles and relevant citations.

Gene	SDE	Putative Role	Citation
AP3	↑S3 vs S1/S2	Downregulation disrupts nectary placement and nectar secretion in *Arabidopsis*	Baum et al., 2001
PI	↓S1 vs S3	Downregulation disrupts nectary placement and nectar secretion in *Arabidopsis*	Baum et al., 2001
AP2	≈	Downregulation disrupts nectar secretion in *Arabidopsis*	Baum et al., 2001
AG	↓S1 vs S2/S3	Redundantly activates *CRC* with *SHP1/2*	Morel et al., 2018
ARF8	↓S1 vs S2/S3	Affects nectary size and gene expression redundantly with *AUXIN RESPONSE FACTOR 6* (*ARF6*) in *Arabidopsis*	Reeves et al., 2012
ARF6	↓S1 vs S2/S3	Affects nectary size and gene expression redundantly with *ARF8* in *Arabidopsis*	Reeves et al., 2012
BOP2	≈	Promotes the formation of nectary glands independent of *CRC*	Mckim et al., 2008
SHP1/2	↑S2 vs S3	Redundantly regulates *CRC* with *AG*	Morel et al., 2018
STY	↓S1 vs S2/S3	Controls nectary development in *Aquilegia* independent of CRC	Min et al., 2019
CRC	≈	Essential but not sufficient for nectary formation in the core eudicots.	Lee et al., 2005b

SDE, Significant Differential Expression with arrows representing either up or down regulation of expression between developmental stages (≈ indicates no SDE). S1, pre-anthetic nectary; S2, anthetic nectary; S3, post-anthetic nectary.

Yellowing is purported to be from a disruption of the anthocyanin production pathway and was the visual marker used for other constructs because it is not expected to alter the form or function of nectaries. *CvANS* is only moderately expressed in post-anthetic nectaries (Figure S2).

With exception of pTRV2-DN802_c0_g1_i4 (Figure S4), all other treatment groups had marked phenotypes related to nectary and nectar formation. DN802_c0_g1_i4 was highly expressed in pre-anthetic and anthetic nectaries, and relatively downregulated in post-anthetic nectaries (Figure S2). Treatment with pTRV2-DN802_c0_g1_i4-*CvANS* resulted in flowers that were phenotypically indistinguishable from the *CvANS* control (Figure S4; Figures 8E, F), despite a high efficacy and mortality among treated flowers relative to control (Table S6). It is plausible that this transcript is related to water and/or nutrient transport because of its unusually high mortality during silencing (Table S6), absence of discernible silencing phenotype (Figure S4), and similar expression profile to *CvSWEET9* (Figure S2), but further research is required.

Functional studies suggest the role of *CvCRC* and *CvSWEET9* in nectary and nectar formation, respectively. *CvCRC* is expressed across all three developmental stages investigated, but with no significant difference between stages (Table 3). In contrast, *CvSWEET9* was downregulated in post-anthetic nectaries as compared to pre-anthetic and anthetic nectaries (Table 2). Treatment with pTRV2-*CvCRC-CvANS* resulted in either partial or total loss of nectaries in all flowers with yellowing phenotype (Figure 9; Table S6). Treatment with pTRV2-*CvSWEET9-CvANS* produced flowers with a visible reduction in nectar on their nectaries (Figure 10), and no detectable sugar using a refractometer (n = 10; data not shown).

Individual and combined constructs of *CvAG* and *CvSHP* demonstrate these genes are functionally redundant in regulation of nectary formation. Treatment with pTRV2-*CvAG* and pTRV2-*CvAG-CvSHP* produced flowers without reproductive whorls and repeating perianth (Figures 11, 12). Flowers treated with pTRV2-*CvAG* still produced nectaries, but their position and structure were altered relative to untreated flowers (Figure 11). This misplacement is likely due to a loss of reproductive whorls and repeated morphology. Flowers treated with pTRV2-*CvAG-CvSHP* generally produced no nectaries, although occasionally they were present and reduced in size (Figures 12A, F).

4 Discussion

4.1 *Cleome violacea* have structured nectaries that produce nectar secreted *via* nectarostomata

The nectary of *C. violacea* is striking in that it is a prominent feature of the flower, due to its large size and location (Figure 1). The nectary is adaxially positioned between stamens and adaxial petals, contributing to monosymmetry of the flower in addition to petal color patterning and reproductive organ curvature. Nectaries appear late in development, well after initiation of stamens and gynoecium. Once formed, mature nectaries are a large 3-lobulate structure (Figures 1–3). *Cleome violacea* nectaries are characteristic of many other structured nectaries (Nepi, 2007): (1) the nectary epidermis has thick cuticle, (2) the nectary parenchyma is made up of small, dense cells, and (3) the vasculature is interspersed throughout the nectary and likely connects with vascular bundles in the receptacle (Figure 2P). Presence of nectarostomata on nectaries of *C. violacea* has been described previously (Erbar and Leins, 1997b). In the annular nectary of *Cleomella sparsifolia* (= *Cleome sparsifolia*),

FIGURE 8
Cleome violacea flowers from untreated and treatment control groups. **(A)** Untreated newly anthetic flower and **(B)** maturing flower. pTRV2-MCS treated flower displaying **(C)** moderate and **(D)** mild viral phenotype. **(E, F)** pTRV2-*CvANS* treated flowers displaying moderate yellowing petal phenotypes. Scale bars = 1 mm.

nectarostomata appear on abaxial tips (Lee et al., 2005b), suggesting nectarostomata may be common in Cleomaceae. Nectarostomata are modified stomata that secrete carbohydrate rich solutions for pollinator reward; a similar genetic pathway regulates both nectarostomata and unmodified stomata (Pillitteri et al., 2008; Baylis et al., 2013).

Nectar is known to be secreted *via* a few different methods, and most commonly *via* nectarostomata in a granulocrine or eccrine based manner (Nepi, 2007). Outlined by Roy et al. (2017) eccrine based secretion begins with the breakdown of starch and subsequent synthesis of sucrose, which is then transported out of the cell and hydrolyzed before secretion out of nectarostomata in droplets of nectar. Key to the export of sucrose is *SWEET9*, which is essential for sugar transport in nectaries of *Arabidopsis*, *Brassica rapa*, and *Nicotiana* (Lin et al., 2014). Another relevant gene, *CWINV4* is important for nectar formation in *Arabidopsis*, specifically cleaving sucrose in the extracellular space which has the effect of moving water towards sugar, forming nectary

FIGURE 9
Flowers of *Cleome violacea* treated with pTRV2-*CvCRC*-*CvANS* constructs. **(A)** Flower with strong yellowing phenotype and no nectary. **(B)** Flower with moderate yellowing phenotype and no nectary. **(C)** Flower with moderate yellowing phenotype, no nectary, and enlarged gynoecium. **(D)** Flower with moderate yellowing phenotype and no nectary. **(E)** Flower with half normal and half yellowing petals with partially absent nectary. **(F)** Flower with strong yellowing phenotype and reduced lateral nectary lobes. Scale bars = 1 mm.

droplets (Ruhlmann et al., 2010). In *C. violacea*, multiple lines of evidence support eccrine-based nectar secretion. First, there are nectarostomata on the nectary surface (Figures 3C–H) which likely connect with the vasculature present throughout parenchymal tissue (Figure 2P). Second, both *CvSWEET9* and *CvCWINV4* are highly expressed in pre-anthetic and anthetic nectaries (Table 2 and Figure S2). Additionally, we identified 14 highly expressed transcripts that are related to sugar production or water transport, e.g., five of which are related to aquaporins found in *Aquilegia* (Singh et al., 2020) (Figure S5 and Table S4). Finally, nectar secretion is lessened when *CvSWEET9* is completely downregulated (Figure 10). In sum, nectary secretion in *C. violacea* is dependent on *CvSWEET9*, as demonstrated for *Arabidopsis*, *Brassica* and *Nicotiana*, which supports its key role in sucrose export across the core eudicots (Lin et al., 2014).

Nectar is secreted at anthesis, accumulates on C. *violacea* nectary lobes (Figure 1E) and has a low average secretion volume

FIGURE 10
Flowers of *Cleome violacea* treated with pTRV2-*CvSWEET9*-*CvANS* constructs. **(A)** Flower with moderate yellowing and nectary with reduced nectar accumulation. **(B)** Magnified view of nectary in A. **(C)** Flower with partial yellowing and partial normal phenotype. **(D)** Flower with near-normal pigmentation and reduced nectar production. **(E)** Magnified nectary from C displaying decreased nectar accumulation correlating with yellowing phenotype. Scale bars = 1 mm.

(0.17 ± 0.07 μL) (Figure 4). This volume is lower than averages of wild populations of other species of Cleomaceae: *Cleomella serrulata* (0.85 ± 0.96 μL) and *Polanisia dodecandra* (0.63 ± 0.32 μL) (Higuera-Diaz et al., 2015). However, it is similar to the average volume produced by one species of Brassicaceae: *Erysimum mediohispanicum* (0.136 ± 0.010 μL). The differences in nectar volume may be in part explained by flower size as *C. violacea* has much smaller flowers than *C. serrulata* and *P. dodecandra*. It may also reflect different pollinator environments; flowers of *C. serrulata* and *P. dodecandra* have a wide range of visitors and somewhat overlap in geography in some areas of North America (Higuera-Diaz et al., 2015). It is also unclear if there is a reduction of nectar in lab-grown inbred lines of *C. violacea* relative to wild populations. No empirical pollination study has been conducted on *C. violacea* to date, which is native to Spain (GBIF.org), so there is no information on which pollinators would be attracted to and rewarded by its nectar.

FIGURE 11
Flowers of *Cleome violacea* treated with pTRV2-*CvAG* constructs. **(A)** Flower with repeating perianth whorls. **(B)** Nectary from flower similar to A with petals removed. **(C)** Flower with normal adaxial petals, repeating perianth whorls and adaxial nectary. **(D)** Flower with repeating perianth whorls and distally positioned nectary. **(E)** Flower with petaloid stamens and adaxial nectary. **(F)** Flower with repeating perianth whorls and adaxial nectary. White arrowheads indicate nectary position. Scale bars = 1 mm.

4.2 Cv*CRC, CvSHP*, and *CvAG*, exhibit conserved roles with other core eudicots in nectary formation

CRC is essential for nectary formation in *Arabidopsis*, *Petunia*, *Pisum*, and *Medicago* in addition to having an important role in carpel formation (Baum et al., 2001; Lee et al., 2005b; Fourquin et al., 2014). As with these taxa and other core eudicots (Lee et al., 2005b; Slavkovic et al., 2021), *CvCRC* is expressed in developing nectaries without any significant difference in gene expression patterns from late-stage buds to post-anthetic flowers (Table 3 and Figure S2). Like with other species, loss of *CvCRC* resulted in an absence of nectaries (Figure 9), which demonstrates that *CvCRC* is essential for nectary formation in *C. violacea*. While strong *CsCRC* expression in nectaries of *C. sparsifolia* implied the conserved role of *CRC* (Lee et al., 2005b), this study provides the first functional evidence of the direct contribution of *CRC* to nectary

FIGURE 12
Flowers of *Cleome violacea* treated with pTRV2-*CvAG-CvSHP* constructs. **(A)** Flower with partial nectary. **(B–E)** Flowers with repeating perianth whorls and no nectary. **(F)** Flower with repeating perianth whorls and partial nectary. Black and white arrowheads represent reduced and absent nectary, respectively. Scale bars = 1 mm.

formation in Cleomaceae. Since the nectaries of *C. sparsifolia* are annular, forming a ring around the stamen base, as compared to the adaxial position of *C. violacea* nectaries (Figure 1), these data indicate that upstream regulators of *CRC* are likely important for nectary position and morphology within Cleomaceae flowers. In *Medicago* and *Pisum*, inconspicuous nectaries form at the base of the staminal tube. Like with Fabaceae, nectaries of *Arabidopsis* are found at the base of stamens, although in this instance forming six glands on the abaxial side. Nectaries in *Petunia* form a ring at the base of the gynoecium (Morel et al., 2018). Interestingly, unlike knockout or knockdowns of *CRC* in *Arabidopsis* (Alvarez and Smyth, 1999; Alvarez and Smyth, 2002), Fabaceae (Ferrandiz and Fourquin, 2014), and poppy (Orashakova et al., 2009), we did not observe many notable changes to gynoecium or fruit formation in *CvCRC* knockdowns (but see Figure 9C). Additional studies are necessary to explore the extent of *CRC's* role in gynoecium development and its conservation in *C. violacea*. The highly expressed *YABBY5* (Table 1, Figure S2) should also be explored due to its ability to dimerize with *CRC* (Gross et al., 2018), i.e., it may share a role with CRC in *C.*

violacea. *CRC* homologs have variable importance in carpel formation across core eudicots (Morel et al., 2018), which also warrants further examination in *C. violacea*. As shown in *Arabidopsis* (Pinyopich et al., 2003), we predict a high redundancy of gene function for gynoecial formation in *C. violacea* given its importance to plant fitness.

MADS-box genes *AG* and *SHP* act redundantly upstream of *CRC* in both *Arabidopsis* and *Petunia* to initiate nectary development (Morel et al., 2018). The regulatory roles of these genes appear to be conserved in nectary formation of *C. violacea.* Both *CvAG* and *CvSHP* are strongly expressed across all stages of development (Table 3 and Figure S2). Treatment with pTRV2-*CvSHP* or pTRV2-*CvAG* alone is insufficient to prevent nectaries from forming (Figure 11 & Table S6). Treatment with pTRV2-*CvSHP* alone has no effect on floral phenotype (Table S6) but treatment with pTRV2-*CvAG* disrupts the formation of whorls 3 and 4 (Figure 11). These phenotypes in *C. violacea* are like *Arabidopsis ag-1* mutants (Baum et al., 2001). Only doubly silenced flowers do not produce nectaries, although they are otherwise like flowers treated with pTRV2-*CvAG* (Figure 12). Our data is consistent with the model from Wollmann et al. (2010) which shows a balance between *AP2* and *AG* activities, i.e., in pTRV2-*CvAG* treated flowers, stamens occasionally appear petaloid (Figure 11F). Thus, there is the possibility that the overlapping of whorls may be the condition which contributes to nectary formation because all the ABC genes are expressed in nectaries to some degree (Table 3 and Figure S2). When flowers are treated with pTRV2-*CvAG*, and petals form haphazardly, nectary tissue surrounds each petal at the base of the flower and the lobe-like structure is lost. Perhaps this is because nectary tissue here has no boundary due to the absence of reproductive whorl (Figure 11B). These results are consistent with those observed in *Arabidopsis* and *Petunia* in that *CRC* expression is dependent on both *AG* and *SHP* lineages (Morel et al., 2018). It is striking that the upstream regulators are likely shared between these three taxa. However, like Morel et al. (2018) our data cannot distinguish whether this shared regulation is due to a single evolutionary origin of nectaries or due to the conservation of *CRC* in carpel development.

Intriguingly, when *CvTCP1* is downregulated in *C. violacea*, nectaries are altered with phenotypes ranging from reduced lobes to complete absence (Carey et al., in prep). Like *CRC*, the regulatory pathway upstream of *TCP1* is unclear, although the key contribution of *TCP* homologs towards many types of floral monosymmetry has been demonstrated across angiosperms (Preston and Hileman, 2009; Hileman, 2014b; Wessinger and Hileman, 2020). Given that expression domains of *AG* and *SHP* are much broader across the flowers, other genetic factors are required for restriction of nectaries to a single whorl (Morel et al., 2018). In *C. violacea*, *CvTCP1* may be involved, at least indirectly. As noted above, functional data for floral nectaries to date has been conducted on flowers whose nectaries are distributed evenly around floral organs (e.g., circular around *Petunia* gynoecium and at the base of all stamens in *Arabidopsis*), unlike the adaxial positioning of the nectary in *C. violacea.* Thus, adaxial floral identity may be required for nectary formation in *C. violacea*, although it is unclear if *TCP1* has a direct role in nectary initiation. Functional studies of Cleomaceae with annular nectaries, such as *Tarenaya hassleriana*, would inform on decoupling nectary position and identity in the family.

Less is known about nectary size than initiation. In *Petunia*, *BEN* and *ROB* are important for nectary size (Morel et al., 2018), whereas *BOP1/2* impacts nectary size in *Arabidopsis* (Mckim et al., 2008). It is perhaps unsurprising that no *BEN* or *ROB* homologs were expressed in nectaries of *C. violacea*, but *CvBOP2* is expressed throughout all stages examined (Table 3 and Figure S2). Unlike *BEN* and *ROB*, the interactions between *BOP1/2* and other floral homeotic genes, with regards to nectary formation and size, are not as well understood (Slavkovic et al., 2021). Further experiments are needed to determine whether *CvBOP2* contributes to nectary size in *C. violacea*. In our analysis of highly expressed transcripts (Figure S5 and Table S4), six transcripts are potentially linked to cell growth in nectaries, although they have only been characterized in leaves (e.g., *EXL2*) and roots (e.g., *PRX44*) (Schröder et al., 2009; Marzol et al., 2022). Future studies should explore genes similar to those identified in this study, as well as earlier stages of nectary development. Altogether, these expression patterns suggest that pathways determining nectary size are not conserved across the core eudicots.

Gene expression data suggests additional conservation as well as deviation in the genetic pathway of nectary development between *Arabidopsis* and *C. violacea*. Transcriptomic data shows many genes important for nectary formation are conserved across *Arabidopsis* and *Cleome*, including ABC genes *AG, AP2, AP3, PI*, and *MADS-box gene SHP* (Table 3 and Figure S4.2). Notably, *AqSTY* has been shown as essential for nectary formation in *Aquilegia* (Min et al., 2019) and *CvSTY* is expressed in nectaries of *C. violacea*. While expression is low, it is significantly differentially expressed and down regulated in pre-anthetic flowers (Table 3 and Figure S2). This co-expression presents a tantalizing hypothesis that *CvSTY* and *CvCRC* are not mutually exclusive pathways in *C. violacea* nectary development. *STY* likely interacts with *CRC* in developing carpels of *Arabidopsis* (Kuusk et al., 2002) such that interactions in other floral structures are feasible. In addition, *STY* is also linked to auxin biosynthesis (Baylis et al., 2013), which is important to nectary development.

4.3 The nectar of *Cleome violacea* is complex, as is its secretion method

Nectar is a multifaceted sugar solution that changes in composition over time and includes microorganisms as well as secondary metabolites made by both plant and microbes (Alvarez-Perez et al., 2012; Chappell and Fukami, 2018; Parachnowitsch et al., 2019; Liao et al., 2021; Jacquemyn et al., 2021). Our data are consistent with bacteria and fungi

colonization of *C. violacea* nectaries (Figure 7) and reflect complexities in these interactions. Unsurprisingly, many of the identified microorganisms from this study are commonplace in soil and/or have been previously isolated from nectar (e.g., *Sphingomonas*, *Pseudomonas*, and *Erythrobasidium*) (Figure 7) (Alvarez-Perez et al., 2012; Jacquemyn et al., 2013). However, the exact nature of the relationship (i.e., mutualism, commensalism, or parasitism) cannot be determined with gene expression data alone, especially since there was variation across replicates. Nonetheless, we found six transcripts that potentially play a role in combating biotic stress from our analysis of highly expressed transcripts (Figure S5 and Table S4), e.g., *LIPID TRANSFER PROTEIN 2* (*LTP2*) and *β-GLUCOSIDASE 19* (*BGLU19*) (Molina and García-Olmedo, 1997; Li et al., 2019) KEGG counts also showed enriched plant-pathogen interactions (26, 25, and 26 in pre-anthetic, anthetic, and post-anthetic nectaries, respectively.) (Table S5). Further, compounds typically produced by nectar-associated microbial communities (e.g., alcohols, isoprenoids, and ketones) (Rering et al., 2018) are difficult to distinguish with transcriptomics because many of these metabolites are also produced by the plant. Additionally, yeasts are known to chemically alter metabolites already present in nectar (Vannette and Fukami, 2016).

In all stages of developing nectaries of *C. violacea*, we found roughly even KEGG counts of carotenoid and flavonoid biosynthesis (~14 and ~8 across stages, respectively) (Table S5). Flavonoids have antioxidant activity, which reduces reactive oxygen species (ROS) in *Arabidopsis* (Vannette and Fukami, 2016), and they have also been linked to the reduction of *E.coli* fimbria, which may reduce biofilm formation (Lee et al., 2011). *FLS1* is significantly upregulated in anthetic and post-anthetic nectaries (Table 1 and Figure S2). Additionally, accumulation of flavanols have also been shown to increase survival of yeast by reducing oxidative stress (Naparlo et al., 2019). Thus, flavonoid accumulation may be a way to inhibit bacterial biofilms while simultaneously supporting symbiotic yeast. *CHS*, which is highly expressed in our transcriptome (Table 1, S4 and Figure S2), is also linked to resistance against biotic and abiotic stress such as UV, temperature, wounding, and bacteria (Dao et al., 2011). However, even though their role in the reduction of ROS can potentially impact biotic stress, carotenoids are more commonly linked to abiotic stress (Havaux, 2014), pollinator attraction (Cazzonelli, 2011), and photoprotection (Demmig-Adams, 1990), so further research is required.

Phytohormone expression in *C. violacea* is complex with evidence supporting convergence to other eudicots. In Brassicales, phytohormones play an important role in gland development and nectar secretion (Slavkovic et al., 2021). In both *Aquilegia* and *Arabidopsis*, auxin is linked to nectary initiation *via ARF6* and *ARF8* (Nagpal et al., 2005; Reeves et al., 2012) to nectar production *via PIN6* (Bender et al., 2013). *Cleome violacea* nectaries express multiple *ARFs* and *PINs* across development (Figure 6A), although not all expression is identical to that in *Arabidopsis* (Tables 2, 3). All PINs serve to promote the flow of auxin between cells (Křeček et al., 2009), so there is likely conservation of function between Cleomaceae and Brassicaceae. Auxin however does not function alone, and gland development is complicated by phytohormone interactions. For example, JA is positively and negatively regulated by auxin and GA, respectively. Both GA (Wiesen et al., 2016) and JA (Radhika et al., 2010) are linked to nectar secretion (Slavkovic et al., 2021), e.g., JA is positively correlated with nectar production. For other biological processes (e.g., seedling development) there is substantial crosstalk between auxin and ethylene (Muday et al., 2012). To our knowledge there have been no studies to date that characterize ethylene function in nectaries, although few do show ethylene-related genes present in nectary tissues (Tang et al., 1994) or ethylene production with *CRC* promoters (Switzenberg et al., 2015). Our transcriptome has multiple ethylene-related genes that are expressed across all developmental stages, e.g., *CvEIN4* (*ETHYLENE INSENSITIVE 4*) and *CvEIL3* (*ETHYLENE INSENSITIVE-LIKE 3*) (Figure 6C). Further, *CHITINASE LIKE 1* (*CLK1*), which modulates ethylene biosynthesis in root development, is among the highest expressed transcripts (Table S4). However, it is yet unclear what role these genes play, and whether they have a function unique to nectaries.

5 Conclusions

As no explicit ancestral reconstruction states of nectaries have been performed in Brassicales or core eudicots, it remains unknown whether nectaries in Cleomaceae and Brassicaceae represent a single or independent origin of nectaries. The data presented in this study demonstrate a high degree of conservation between Cleomaceae and Brassicaceae, which would be consistent with a single origin of nectaries in these sister lineages. *CvCRC* functions as it does in *Arabidopsis* and is regulated redundantly by MADS-box genes *AG* and *SHP*. *Cleome violacea* nectaries are eccrine-based and appear to regulate their own energy production. Given multiple origins of other traits (e.g., monosymmetry), we cannot exclude the possibility of independent recruitment in the roles of *CRC, AG, SHP* and *SWEET9* for nectary development and nectar secretion, respectively. Research on the evolution and development of nectaries and on nectar biology is ripe for interdisciplinary research (Liao et al., 2021). Here we show that *Cleome violacea* is a promising model for nectary development in the Cleomaceae that will pave the way forward for future nectary research on other key factors such as morphology and pollination.

Data availability statement

The raw reads used in this study are available at the sequence read archive (SRA) database under BioProject ID: PRJNA912718.

Author contributions

SC and JH conceived the study. SC collected and analysed the VIGS and transcriptomic data. AD collected nectar volume data. AD and SC prepared histological slides. BZ produced SEM micrographs. SC wrote the initial manuscript draft. SC, BZ, and JH edited the manuscript. All authors contributed to the article and approved the submitted version.

Funding

This work was supported by the Natural Sciences and Engineering Research Council of Canada (NSERC) (funding reference number 5014131).

Acknowledgments

The authors thank Nathan Gerein (Scanning Electron Microscopy Laboratory, Department of Earth and Atmospheric Sciences, University of Alberta) and Kacie Norton (Advanced Microscopy Facility, Department of Biological Sciences, University of Alberta) for assistance with scanning electron microscopy. We also thank Ida John for their help with generating SEM photos. We thank all Hall lab members for help with plant care and tissue collection.

Conflict of interest

The authors declare that the research was conducted in the absence of any commercial or financial relationships that could be construed as a potential conflict of interest.

Publisher's note

Supplementary material

The Supplementary Material for this article can be found online at: https://www.frontiersin.org/articles/10.3389/fpls.2022.1085900/full#supplementary-material

SUPPLEMENTARY FIGURE 1
ExN50 graph generated by the 'contig_ExN50_statistic.pl' and 'plot_ExN50_statistic.Rscript' scripts provided with Trinity.

SUPPLEMENTARY FIGURE 2
A heatmap of nectary-related genes displayed as log2(TPM).

SUPPLEMENTARY FIGURE 3
Sequence and ORF of uncharacterized Trinity transcript DN802_c0_g1_i4.. The ORF is highlighted and begins at bp 182.

SUPPLEMENTARY FIGURE 4
Flowers of *Cleome violacea* treated with pTRV2-DN802_c0_g1_i4-*CvANS* constructs. Phenotypes were indiscernible from pTRV2-*CvANS* control. **(A)** Flower with mild yellowing and underdeveloped stamens. **(B)** Flower with strong yellowing and no nectar production. **(C)** Flower with mild yellowing and underdeveloped stamens. **(D)** Flower with moderate yellowing. **(E)** Flower with moderate yellowing and underdeveloped stamen. **(F)** Flower with moderate yellowing. Scale bars = 1 mm.

SUPPLEMENTARY FIGURE 5
Z-score heatmaps of TransDecoder filtered transcripts; **(A)** All differentially expressed transcripts and **(B)** transcripts with TPM > 100 from Cleome violacea pre-anthetic, anthetic, and post-anthetic nectaries.

References

Altschul, S., Gish, W., Miller, W., Myers, E., and Lipman, D. (1990). Basic local alignment search tool. *J. Mol. Biol.* 215, 403–410. doi: 10.1016/S0022-2836(05)80360-2

Alvarez-Perez, S., Herrera, C. M., and De Vega, C. (2012). Zooming-in on floral nectar: a first exploration of nectar-associated bacteria in wild plant communities. *FEMS Microbiol. Ecol.* 80, 591–602. doi: 10.1111/j.1574-6941.2012.01329.x

Alvarez, J., and Smyth, D. R. (1998). Genetic pathways controlling carpel development in *Arabidopsis thaliana*. *J. Plant Res.* 111, 295–298. doi: 10.1007/BF02512187

Alvarez, J., and Smyth, D. R. (1999). *CRABS CLAW* and *SPATULA*, two arabidopsis genes that control carpel development in parallel with *AGAMOUS*. *Development* 126, 2377–2386. doi: 10.1242/dev.126.11.2377

Alvarez, J., and Smyth, D. R. (2002). *CRABS CLAW* and *SPATULA* genes regulate growth and pattern formation during gynoecium development in *Arabidopsis thaliana*. *Int. J. Plant Sci.* 163, 17–41. doi: 10.1086/324178

Andrews, S. (2010) *FastQC: a quality control tool for high throughput sequence data*. Available at: http://www.bioinformatics.babraham.ac.uk/projects/fastqc.

Barrett, R. L., Roalson, E. H., Ottewell, K., Byrne, M., Govindwar, S. P., Yadav, S. R., et al. (2017). Resolving generic boundaries in Indian-Australasian cleomaceae: Circumscription of *Areocleome*, *Arivela*, and *Corynandra* as distinct genera. *Systemat. Bot.* 42, 15. doi: 10.1600/036364417X696401

Baum, S. F., Eshed, Y., and Bowman, J. L. (2001). The arabidopsis nectary is an ABC-independent floral structure. *Development* 128, 4657–4667. doi: 10.1242/dev.128.22.4657

Bayat, S., Schranz, M. E., Roalson, E. H., and Hall, J. C. (2018). Lessons from cleomaceae, the sister of crucifers. *Trends Plant Sci.* 23, 808–821. doi: 10.1016/j.tplants.2018.06.010

Baylis, T., Cierlik, I., Sundberg, E., and Mattsson, J. (2013). *SHORT INTERNODES/STYLISH* genes, regulators of auxin biosynthesis, are involved in leaf vein development in *Arabidopsis thaliana*. *New Phytol.* 197, 737–750. doi: 10.1111/nph.12084

Bender, R. L., Fekete, M. L., Klinkenberg, P. M., Hampton, M., Bauer, B., Malecha, M., et al. (2013). *PIN6* is required for nectary auxin response and short stamen development. *Plant J.* 74, 893–904. doi: 10.1111/tpj.12184

Bernardello, G. (2007). *A systematic survey of floral nectaries* (Netherlands: Springer, Po Box 17, 3300 Aa Dordrecht).

Bowman, J. L., and Smyth, D. R. (1999). *CRABS CLAW*, a gene that regulates carpel and nectary development in arabidopsis, encodes a novel protein with zinc

finger and helix-loop-helix domains. *Development* 126, 2387–2396. doi: 10.1242/dev.126.11.2387

Braun, H. P. (2020). The oxidative phosphorylation system of the mitochondria in plants. *Mitochondrion* 53, 66–75. doi: 10.1016/j.mito.2020.04.007

Broderick, S. R., and Jones, M. L. (2014). An optimized protocol to increase virus-induced gene silencing efficiency and minimize viral symptoms in petunia. *Plant Mol. Biol. Rep.* 32, 219–233. doi: 10.1007/s11105-013-0647-3

Cane, J. H. (2008). Breeding biologies, seed production and species-rich bee guilds of *Cleome lutea* and *Cleome serrulata* (Cleomaceae). *Plant Species Biol.* 23, 152–158. doi: 10.1111/j.1442-1984.2008.00224.x

Carey, S., Higuera-Díaz, M., Mankowski, P., Rocca, A., and Hall, J. C. (2021). Virus-induced gene silencing as a tool for functional studies in *Cleome violacea*. *Appl. Plant Sci.* 9. doi: 10.1002/aps3.11435

Carey, S., Mendler, K., and Hall, J. C. (2019). How to build a fruit: Transcriptomics of a novel fruit type in the brassiceae. *PloS One* 14, 18. doi: 10.1371/journal.pone.0209535

Cazzonelli, C. I. (2011). Carotenoids in nature: insights from plants and beyond. *Funct. Plant Biol.* 38, 833–847. doi: 10.1071/FP11192

Chappell, C. R., and Fukami, T. (2018). Nectar yeasts: a natural microcosm for ecology. *Yeast* 35, 417–423. doi: 10.1002/yea.3311

Chico, J. M., Chini, A., Fonseca, S., and And Solano, R. (2008). JAZ repressors set the rhythm in jasmonate signaling. *Curr. Opin. Plant Biol.* 11, 486–494. doi: 10.1016/j.pbi.2008.06.003

Dao, T. T. H., Linthorst, H. J. M., and And Verpoorte, R. (2011). Chalcone synthase and its functions in plant resistance. *Phytochem. Rev.* 10, 397–412. doi: 10.1007/s11101-011-9211-7

Demmig-Adams, B. (1990). Carotenoids and photoprotection in plants: a role for the xanthophyll zeaxanthin. *Biochim. Biophys. Acta (BBA)-Bioenerget.* 1020, 1–24. doi: 10.1016/0005-2728(90)90088-L

Endress, P. K. (2011). Evolutionary diversification of the flowers in angiosperms. *Am. J. Bot.* 98, 370–396. doi: 10.3732/ajb.1000299

Erbar, C., and Leins, P. (1997a). Different patterns of floral development in whorled flowers, exemplified by apiaceae and brassicaceae. *Int. J. Plant Sci.* 158, 49–64. doi: 10.1086/297506

Erbar, C., and Leins, P. (1997b). Studies on the early floral development in cleomoideae (Capparaceae) with emphasis on the androecial development. *Plant Systematics Evol.* 206, 119–132. doi: 10.1007/BF00987944

Ferrandiz, C., and Fourquin, C. (2014). Role of the *FUL*-SHP network in the evolution of fruit morphology and function. *J. Exp. Bot.* 65, 4505–4513. doi: 10.1093/jxb/ert479

Fleming, T. H., Geiselman, C., and Kress, W. J. (2009). The evolution of bat pollination: a phylogenetic perspective. *Ann. Bot.* 104, 1017–1043. doi: 10.1093/aob/mcp197

Fourquin, C., Primo, A., Martinez-Fernandez, I., Huet-Trujillo, E., and Ferrandiz, C. (2014). The *CRC* orthologue from *Pisum sativum* shows conserved functions in carpel morphogenesis and vascular development. *Ann. Bot.* 114, 1535–1544. doi: 10.1093/aob/mcu129

Gould, B., and Kramer, E. M. (2007). Virus-induced gene silencing as a tool for functional analyses in the emerging model plant *Aquilegia* (columbine, ranunculaceae). *BMC Plant Methods* 3, 6. doi: 10.1186/1746-4811-3-6

Gross, T., Broholm, S., and And Becker, A. (2018). *CRABS CLAW* acts as a bifunctional transcription factor in flower development. *Front. Plant Sci.* 9. doi: 10.3389/fpls.2018.00835

Haas, B. J., Papanicolaou, A., Yassour, M., Grabherr, M., Blood, P. D., Bowden, J., et al. (2013). *De novo* transcript sequence reconstruction from RNA-seq using the trinity platform for reference generation and analysis. *Nat. Protoc.* 8, 1494. doi: 10.1038/nprot.2013.084

Hall, J. C., Tisdale, T. E., Donohue, K., and Kramer, E. M. (2006). Developmental basis of an anatomical novelty: heteroarthrocarpy in *Cakile lanceolata* and *Erucaria erucarioides* (Brassicaceae). *Int. J. Plant Sci.* 167, 771–789. doi: 10.1086/504928

Han, X., Yin, L., and And Xue, H. (2012). Co-Expression analysis identifies CRC and AP1 the regulator of arabidopsis fatty acid biosynthesis. *J. Integr. Plant Biol.* 54, 486–499. doi: 10.1111/j.1744-7909.2012.01132.x

Havaux, M. (2014). Carotenoid oxidation products as stress signals in plants. *Plant J.* 79, 597–606. doi: 10.1111/tpj.12386

Heil, M. (2011). Nectar: generation, regulation, and ecological functions. *Trends Plant Sci.* 16, 191–200. doi: 10.1016/j.tplants.2011.01.003

Higuera-Diaz, M., Manson, J. S., and Hall, J. C. (2015). Pollination biology of *Cleomella serrulata* and *Polanisia dodecandra* in a protected natural prairie in southern Alberta, Canada. *Botany* 93, 745–757. doi: 10.1139/cjb-2015-0084

Hileman, L. C. (2014a). Bilateral flower symmetry - how, when and why? *Curr. Opin. Plant Biol.* 17, 146–152. doi: 10.1016/j.pbi.2013.12.002

Hileman, L. C. (2014b). Trends in flower symmetry evolution revealed through phylogenetic and developmental genetic advances. *Philos. Trans. R Soc. Lond B Biol. Sci.* 369. doi: 10.1098/rstb.2013.0348

Iltis, H. H., Hall, J. C., Cochrane, T. S., and Sytsma, K. J. (2011). Studies in the cleomaceae I: On the separate recognition of capparaceae, cleomaceae, and brassicaceae. *Ann. Missouri Botan. Garden* 98, 28–36. doi: 10.3417/2007017

Jacquemyn, H., Lenaerts, M., Tyteca, D., and Lievens, B. (2013). Microbial diversity in the floral nectar of seven epipactis (Orchidaceae) species. *Microbiologyopen* 2, 644–658. doi: 10.1002/mbo3.103

Jacquemyn, H., Pozo, M. I., Alvarez-Perez, S., Lievens, B., and Fukami, T. (2021). Yeast-nectar interactions: metacommunities and effects on pollinators. *Curr. Opin. Insect Sci.* 44, 35–40. doi: 10.1016/j.cois.2020.09.014

Jung, J. H., Seo, Y. H., Pil, J. S., Reyes, J. L., Yun, J., Chua, N. H., et al. (2007). The *GIGANTEA*-regulated microRNA172 mediates photoperiodic flowering independent of *CONSTANS* in arabidopsis. *Plant Cell* 19, 2736–2748. doi: 10.1105/tpc.107.054528

Kim, I. V., Ross, E. J., Dietrich, S., Doring, K., Alvarado, A. S., and Kuhn, C. D. (2019). Efficient depletion of ribosomal RNA for RNA sequencing in planarians. *BMC Genomics* 20, 12. doi: 10.1186/s12864-019-6292-y

Kramer, E. M. (2019). Plus ca change, plus c'est la meme chose: The developmental evolution of flowers. *Curr. Top. Dev. Biol.* 131, 211–238. doi: 10.1016/bs.ctdb.2018.11.015

Křeček, P., Skůpa, P., Libus, J., Naramoto, S., Tejos, R., Friml, J., et al. (2009). Protein family review the PIN-FORMED (PIN) protein family of auxin transporters. *Genome Biology* 10, 1–11. doi: 10.1186/gb-2009-10-12-249

Krogan, N. T., Hogan, K., and And Long, J. A. (2012). *APETALA2* negatively regulates multiple floral organ identity genes in arabidopsis by recruiting the co-repressor TOPLESS and the histone deacetylase HDA19. *Development* 139, 4180–4190. doi: 10.1242/dev.085407

Krueger, F. (2012) *Trim galore!*. Available at: http://www.bioinformatics.babraham.ac.uk/projects/trim_galore/.

Kuusk, S., Sohlberg, J. J., Long, J. A., Fridborg, I., and Sundberg, E. (2002). *STY1* and *STY2* promote the formation of apical tissues during *Arabidopsis* gynoecium development. *Development* 129, 4707–4717. doi: 10.1242/dev.129.20.4707

Lee, J. Y., Baum, S. F., Alvarez, J., Patel, A., Chitwood, D. H., and Bowman, J. L. (2005a). Activation of *CRABS CLAW* in the nectaries and carpels of arabidopsis. *Plant Cell* 17, 25–36. doi: 10.1105/tpc.104.026666

Lee, J. Y., Baum, S. F., Oh, S. H., Jiang, C. Z., Chen, J. C., and Bowman, J. L. (2005b). Recruitment of *CRABS CLAW* to promote nectary development within the eudicot clade. *Development* 132, 5021–5032. doi: 10.1242/dev.02067

Lee, J. H., Regmi, S. C., Kim, J. A., Cho, M. H., Yun, H., Lee, C. S., et al (2011). Apple flavonoid phloretin inhibits Escherichia coli O157: H7 biofilm formation and ameliorates colon inflammation in rats. *Infection and immunity*, 79(12), 4819–4827.

Liao, I. T., Hileman, L. C., and Roy, R. (2021). On the horizon for nectar-related research. *Am. J. Bot.* 108, 2326–2330. doi: 10.1002/ajb2.1767

Li, B. B., Liu, Y. G., Tao, W. U., Wang, J. P., Xie, G. R., Chu, Z. H., et al. (2019). OsBGLU19 and OsBGLU23 regulate disease resistance to bacterial leaf streak in rice. *J. Integr. Agric.* 18, 1199–1210. doi: 10.1016/S2095-3119(18)62117-3

Lin, I. W., Sosso, D., Chen, L. Q., Gase, K., Kim, S. G., Kessler, D., et al. (2014). Nectar secretion requires sucrose phosphate synthases and the sugar transporter *SWEET9*. *Nature* 508, 546–549. doi: 10.1038/nature13082

Lück, S., Kreszies, T., Strickert, M., Schweizer, P., Kuhlmann, M., and Douchkov, D. (2019). siRNA-finder (si-Fi) software for RNAi-target design and off-target prediction. *Front. Plant Sci.* 10, 12. doi: 10.3389/fpls.2019.01023

Lunn, J. E., Delorge, I., Figueroa, C. M., Van Dijck, P., and And Stitt, M. (2014). Trehalose metabolism in plants. *Plant J.* 79, 544–567. doi: 10.1111/tpj.12509

Luo, K. M., Harding, S. A., and Tsai, C. J. (2008). A modified T-vector for simplified assembly of hairpin RNAi constructs. *Biotechnol. Lett.* 30, 1271–1274. doi: 10.1007/s10529-008-9673-x

Marzol, E., Borassi, C., Sardoy, M. C., Ranocha, P., Aptekmann, A. A., Bringas, M., et al. (2022). Class III peroxidases PRX01, PRX44, and PRX73 control root hair growth in arabidopsis thaliana. *Int. J. Mol. Sci.* 23, 5375. doi: 10.3390/ijms23105375

Mckim, S. M., Stenvik, G. E., Butenko, M. A., Kristiansen, W., Cho, S. K., Hepworth, S. R., et al. (2008). The *BLADE*-ON-*PETIOLE* genes are essential for abscission zone formation in arabidopsis. *Development* 135, 1537–1546. doi: 10.1242/dev.012807

Min, Y., Bunn, J. I., and Kramer, E. M. (2019). Homologs of the *STYLISH* gene family control nectary development in aquilegia. *New Phytol.* 221, 1090–1100. doi: 10.1111/nph.15406

Mizukami, Y., and Ma, H. (1997). Determination of Arabidopsis floral meristem identity by AGAMOUS. *The Plant Cell* 9(3), 393–408. doi: 10.1105/tpc.9.3.393

Molina, A., and García-Olmedo, F. (1997). Enhanced tolerance to bacterial pathogens caused by the transgenic expression of barley lipid transfer protein LTP2. *Plant J.* 12, 669–675. doi: 10.1046/j.1365-313X.1997.00605.x

Morel, P., Heijmans, K., Ament, K., Chopy, M., Trehin, C., Chambrier, P., et al. (2018). The floral c-lineage genes trigger nectary development in petunia and arabidopsis. *Plant Cell* 30, 2020–2037. doi: 10.1105/tpc.18.00425

Morrant, D. S., Schumann, R., and And Petit, S. (2009). Field methods for sampling and storing nectar from flowers with low nectar volumes. *Ann. Bot.* 103, 533–542. doi: 10.1093/aob/mcn241

Muday, G. K., Rahman, A., and Binder, B. M. (2012). Auxin and ethylene: collaborators or competitors? *Trends Plant Sci.* 17, 181–195. doi: 10.1016/j.tplants.2012.02.001

Nagpal, P., Ellis, C. M., Weber, H., Ploense, S. E., Barkawi, L. S., Guilfoyle, T. J., et al. (2005). Auxin response factors *ARF6* and *ARF8* promote jasmonic acid production and flower maturation. *Development* 132, 4107–4118. doi: 10.1242/dev.01955

Naparlo, K., Zyracka, E., Bartosz, G., and And Sadowska-Bartosz, I. (2019). Flavanols protect the yeast *Saccharomyces cerevisiae* against heating and freezing/thawing injury. *J. Appl. Microbiol.* 126, 872–880. doi: 10.1111/jam.14170

Nepi, M. (2007). *Nectary structure and ultrastructure* (Netherlands: Springer, Po Box 17, 3300 Aa Dordrecht).

Nepi, M., Grasso, D. A., and Mancuso, S. (2018). Nectar in plant–insect mutualistic relationships: From food reward to partner manipulation. *Front. Plant Sci.* 9. doi: 10.3389/fpls.2018.01063

Orashakova, S., Lange, M., Lange, S., Wege, S., and Becker, A. (2009). The CRABS CLAW ortholog from California poppy (*Eschscholzia californica*, papaveraceae), *EcCRC*, is involved in floral meristem termination, gynoecium differentiation and ovule initiation. *Plant J.* 58, 682–693. doi: 10.1111/j.1365-313X.2009.03807.x

Parachnowitsch, A. L., Manson, J. S., and Sletvold, N. (2019). Evolutionary ecology of nectar. *Ann. Bot.* 123, 247–261. doi: 10.1093/aob/mcy132

Patchell, M. J., Bolton, M. C., Mankowski, P., and Hall, J. C. (2011). Comparative floral development in cleomaceae reveals two distinct pathways leading to monosymmetry. *Int. J. Plant Sci.* 172, 352–365. doi: 10.1086/658158

Patchell, M. J., Roalson, E. H., and Hall, J. C. (2014). Resolved phylogeny of cleomaceae based on all three genomes. *Taxon* 63, 315–328. doi: 10.12705/632.17

Pei, Y. F., Zhang, J., Wu, P., Ye, L., Yang, D. F., Chen, J. D., et al. (2021). GoNe encoding a class VIIIb AP2/ERF is required for both extrafloral and floral nectary development in gossypium. *Plant J.* 106, 1116–1127. doi: 10.1111/tpj.15223

Pfannebecker, K. C., Lange, M., Rupp, O., and Becker, A. (2017). Seed plant-specific gene lineages involved in carpel development. *Mol. Biol. Evol.* 34, 925–942. doi: 10.1093/molbev/msw297

Phillips, H. R., Landis, J. B., and Specht, C. D. (2020). Revisiting floral fusion: the evolution and molecular basis of a developmental innovation. *J. Exp. Bot.* 71, 3390–3404. doi: 10.1093/jxb/eraa125

Pillitteri, L. J., Bogenschutz, N. L., and Torii, K. U. (2008). The bHLH protein, *MUTE*, controls differentiation of stomata and the hydathode pore in arabidopsis. *Plant Cell Physiol.* 49, 934–943. doi: 10.1093/pcp/pcn067

Pinyopich, A., Ditta, G. S., Savidge, B., Liljegren, S. J., Baumann, E., Wisman, E., et al. (2003). Assessing the redundancy of MADS-box genes during carpel and ovule development. *Nature* 424, 85–88. doi: 10.1038/nature01741

Preston, J. C., and Hileman, L. C. (2009). Developmental genetics of floral symmetry evolution. *Trends Plant Sci.* 14, 147–154. doi: 10.1016/j.tplants.2008.12.005

Preston, J. C., Hileman, L. C., and Cubas, P. (2011). Reduce, resuse and recycle: developmental evolution of trait diversification. *Am. J. Bot.* 98, 397–403. doi: 10.3732/ajb.1000279

Preston, J. C., Kost, M. A., and Hileman, L. C. (2009). Conservation and diversification of the symmetry developmental program among close relatives of snapdragon with divergent floral morphologies. *New Phytol.* 182, 751–762. doi: 10.1111/j.1469-8137.2009.02794.x

Radhika, V., Kost, C., Boland, W., and Heil, M. (2010). The role of jasmonates in floral nectar secretion. *PloS One* 5, 6. doi: 10.1371/journal.pone.0009265

Raju, A., and Rani, D. (2016). Reproductive ecology of *Cleome gynandra* and *Cleome viscosa* (Capparaceae). *Phytol. Balcanica* 22, 15–28.

Ratcliff, F., Martin-Hernandez, A. M., and Baulcombe, D. C. (2001). Tobacco rattle virus as a vector for analysis of gene function by silencing. *Plant J.* 25, 237–245. doi: 10.1046/j.0960-7412.2000.00942.x

R Core Team (2013). *R: A language and environment for statistical computing* (Vienna, Austria: R Foundation for Statistical Computing). Available at: http://www.r-project.org/.

Reeves, P. H., Ellis, C. M., Ploense, S. E., Wu, M. F., Yadav, V., Tholl, D., et al. (2012). A regulatory network for coordinated flower maturation. *PloS Genet.* 8, 17. doi: 10.1371/journal.pgen.1002506

Ren, G., Healy, R. A., Horner, H. T., James, M. G., and And Thornburg, R. W. (2007). Expression of starch metabolic genes in the developing nectaries of ornamental tobacco plants. *Plant Sci.* 173, 621–637. doi: 10.1016/j.plantsci.2007.08.012

Rering, C. C., Beck, J. J., Hall, G. W., Mccartney, M. M., and Vannette, R. L. (2018). Nectar-inhabiting microorganisms influence nectar volatile composition and attractiveness to a generalist pollinator. *New Phytol.* 220, 750–759. doi: 10.1111/nph.14809

Robinson, M., Mccarthy, D., and Smyth, G. (2009). edgeR: a bioconductor package for differential expression analysis of digital gene expression data. *Bioinformatics* 26, 139–140. doi: 10.1093/bioinformatics/btp616

Roy, R., Schmitt, A. J., Thomas, J. B., and Carter, C. J. (2017). Nectar biology: from molecules to ecosystems. *Plant Science* 262, 148–164.

Ruhlmann, J. M., Kram, B. W., and Carter, C. J. (2010). CELL WALL INVERTASE 4 is required for nectar production in arabidopsis. *J. Exp. Bot.* 61, 395–404. doi: 10.1093/jxb/erp309

Sauquet, H., Von Balthazar, M., Magallón, S., Doyle, J. A., Endress, P. K., Bailes, E. J., et al. (2017). The ancestral flower of angiosperms and its early diversification. *Nat. Commun.* 8, 16047. doi: 10.1038/ncomms16047

Schröder, F., Lisso, J., Lange, P., and Müssig, C. (2009). The extracellular EXO protein mediates cell expansion in arabidopsis leaves. *BMC Plant Biol.* 9, 1–12. doi: 10.1186/1471-2229-9-20

Scofield, S., Dewitte, W., and And Murray, J. A. H. (2007). The KNOX gene SHOOT MERISTEMLESS is required for the development of reproductive meristematic tissues in arabidopsis. *Plant J.* 50, 767–781. doi: 10.1111/j.1365-313X.2007.03095.x

Simao, F. A., Waterhouse, R. M., Ioannidis, P., Kriventseva, E. V., and Zdobnov, E. M. (2015). BUSCO: assessing genome assembly and annotation completeness with single-copy orthologs. *Bioinformatics* 31, 3210–3212. doi: 10.1093/bioinformatics/btv351

Singh, S., Bhatt, V., Kumar, V., Kumawat, S., Khatri, P., Singla, P., et al. (2020). Evolutionary understanding of aquaporin transport system in the basal eudicot model species *aquilegia coerulea*. *Plants* 9, 799. doi: 10.3390/plants9060799

Singh, V., Roy, S., Giri, M. K., Chaturvedi, R., Chowdhury, Z., Shah, J., et al. (2013). *Arabidopsis thaliana FLOWERING LOCUS* d is required for systemic acquired resistance. *Mol. Plant-Microbe Interact.* 26, 1079–1088. doi: 10.1094/MPMI-04-13-0096-R

Slavkovic, F., Dogimont, C., Morin, H., Boualem, A., and Bendahmane, A. (2021). The genetic control of nectary development. *Trends Plant Sci.* 26, 260–271. doi: 10.1016/j.tplants.2020.11.002

Sobel, J. M., and Streisfeld, M. A. (2013). Flower color as a model system for studies of plant evo-devo. *Front. Plant Sci.* 4, 321. doi: 10.3389/fpls.2013.00321

Solhaug, E. M., Roy, R., Chatt, E. C., Klinkenberg, P. M., Mohd-Fadzil, N., Hampton, M., et al. (2019). An integrated transcriptomics and metabolomics analysis of the *Cucurbita pepo* nectary implicates key modules of primary metabolism involved in nectar synthesis and secretion. *Plant Direct* 3, e00120. doi: 10.1002/pld3.120

Specht, C. D., and Howarth, D. G. (2015). Adaptation in flower form: a comparative evodevo approach. *New Phytol.* 206, 74–90. doi: 10.1111/nph.13198

Switzenberg, J. A., Beaudry, R. M., and And Grumet, R. (2015). Effect of CRC:: etr1-1 transgene expression on ethylene production, sex expression, fruit set and fruit ripening in transgenic melon (*Cucumis melo* l.). *Transgenic Res.* 24, 497–507. doi: 10.1007/s11248-014-9853-5

Tang, X., Gomes, R., Bhatia, A., and And Woodson, W. R. (1994). Pistil-specific and ethylene-regulated expression of l-Aminocyclopropane-l-Caaboxylate oxidase genes in petunia flowers. *Plant Cell* 6, 1227–1239. doi: 10.2307/3869821

Torti, S., Fornara, F., Vincent, C., Andrés, F., Nordström, K., Göbel, U., et al. (2012). Analysis of the arabidopsis shoot meristem transcriptome during floral transition identifies distinct regulatory patterns and a leucine-rich repeat protein that promotes flowering. *Plant Cell* 24, 444–462. doi: 10.1105/tpc.111.092791

Tucker, G. C., and Vanderpool, S. S. (2010). "Cleomaceae," in *Flora of north America north of Mexico: Magnoliophyta: Salicaceae to brassicaceae* (New York: Oxford University Press).

Vannette, R. L., and Fukami, T. (2016). Nectar microbes can reduce secondary metabolites in nectar and alter effects on nectar consumption by pollinators. *Ecology* 97, 1410–1419. doi: 10.1890/15-0858.1

Wang, C. C., Cai, X. Z., Wang, X. M., and Zheng, Z. (2006). Optimisation of tobacco rattle virus-induced gene silencing in arabidopsis. *Funct. Plant Biol.* 33, 347–355. doi: 10.1071/FP05096

Wessinger, C. A., and Hileman, L. C. (2020). Parallelism in flower evolution and development. *Annu. Rev. Ecol. Evol. Syst.* 51, 387–408. doi: 10.1146/annurev-ecolsys-011720-124511

Wiesen, L. B., Bender, R. L., Paradis, T., Larson, A., Perera, M. A. D. N., Nikolau, B. J., et al. (2016). A role for GIBBERELLIN 2-OXIDASE6 and gibberellins in regulating nectar production. *Mol. Plant* 9, 753–756. doi: 10.1016/j.molp.2015.12.019

Wollmann, H., Mica, E., Todesco, M., Long, J. A., and Weigel, D. (2010). On reconciling the interactions between APETALA2, miR172 and AGAMOUS with the ABC model of flower development. *Development* 137(21), 3633–3642.

Zhang, R., Min, Y., Holappa, L. D., Walcher-Chevillet, C. L., Duan, X. S., Donaldson, E., et al. (2020). A role for the auxin response factors ARF6 andARF8 homologs in petal spur elongation and nectary maturation in *Aquilegia*. *New Phytol.* 227, 1392–1405. doi: 10.1111/nph.16633

Ziegler-Graff, V., Guilford, P. J., and Baulcombe, D. C. (1991). Tobacco rattle virus RNA-1 29K gene product potentiates viral movement and also affects symptom induction in tobacco. *Virology* 182, 145–155. doi: 10.1016/0042-6822(91)90658-X

frontiers | Frontiers in Plant Science

TYPE Review
PUBLISHED 02 March 2023
DOI 10.3389/fpls.2023.1084358

OPEN ACCESS

EDITED BY
Verónica S. Di Stilio,
University of Washington, United States

REVIEWED BY
Zhichao Xu,
Northeast Forestry University, China
Rainer Melzer,
University College Dublin, Ireland

*CORRESPONDENCE
Annette Becker
annette.becker@bot1.bio.uni-giessen.de
Fumihiko Sato
fsato@lif.kyoto-u.ac.jp

SPECIALTY SECTION
This article was submitted to Plant Development and EvoDevo, a section of the journal Frontiers in Plant Science

RECEIVED 30 October 2022
ACCEPTED 16 February 2023
PUBLISHED 02 March 2023

CITATION
Becker A, Yamada Y and Sato F (2023) California poppy (*Eschscholzia californica*), the Papaveraceae golden girl model organism for evodevo and specialized metabolism.
Front. Plant Sci. 14:1084358.
doi: 10.3389/fpls.2023.1084358

California poppy (*Eschscholzia californica*), the Papaveraceae golden girl model organism for evodevo and specialized metabolism

Annette Becker[1]*, Yasuyuki Yamada[2] and Fumihiko Sato[3,4,5]*

[1]Plant Development Lab, Institute of Botany, Hustus-Liebig-University, Giessen, Germany, [2]Laboratory of Medicinal Cell Biology, Kobe Pharmaceutical University, Kobe, Japan, [3]Graduate School of Biostudies, Kyoto University, Kyoto, Japan, [4]Bioorganic Research Institute, Suntory Foundation for Life Science, Kyoto, Japan, [5]Graduate School of Science, Osaka Metropolitan University, Sakai, Japan

California poppy or golden poppy (*Eschscholzia californica*) is the iconic state flower of California, with native ranges from Northern California to Southwestern Mexico. It grows well as an ornamental plant in Mediterranean climates, but it might be invasive in many parts of the world. California poppy was also highly prized by Native Americans for its medicinal value, mainly due to its various specialized metabolites, especially benzylisoquinoline alkaloids (BIAs). As a member of the Ranunculales, the sister lineage of core eudicots it occupies an interesting phylogenetic position. California poppy has a short-lived life cycle but can be maintained as a perennial. It has a comparatively simple floral and vegetative morphology. Several genetic resources, including options for genetic manipulation and a draft genome sequence have been established already with many more to come. Efficient cell and tissue culture protocols are established to study secondary metabolite biosynthesis and its regulation. Here, we review the use of California poppy as a model organism for plant genetics, with particular emphasis on the evolution of development and BIA biosynthesis. In the future, California poppy may serve as a model organism to combine two formerly separated lines of research: the regulation of morphogenesis and the regulation of secondary metabolism. This can provide insights into how these two integral aspects of plant biology interact with each other.

KEYWORDS

flower development, benzylisoquinoline alkaloid, Ranunculales, evo devo, VIGS (virus-induced gene silencing)

1 Phylogeny, biogeography and growth conditions

Eschscholzia californica is a member of the Papaveraceae family of the order of Ranunculales, which is sister to the core eudicots (Figure 1A, Hoot et al., 2015; Lane et al., 2018). Sister to all Papaveraceae is the enigmatic *Pteridophyllum racemosum*, with fern-like leaves and bell-like white flowers in a loose inflorescence. *Eschscholzia californica*, with common name California poppy, Golden poppy, or Cup of Gold, belongs to the subfamily of Eschscholzioideae, which is the sister group to both, the Papaveroideae (including *Papaver somniferum*, opium poppy) and the Chelidonioideae (Figure 1B).

California poppy is growing as an annual or perennial and is native to western North America. Its native range covers the Columbia River in Northern Oregon to Baja California, a peninsula separating the Gulf of California from the Pacific Ocean. It is found from the Pacific Coast to the Great Basin, including the Sierra Nevada and the Mojave Desert (Cook, 1962). In the past 200 years, California poppy was introduced by man to Chile, South Africa, Australia including Tasmania, and New Zealand, where they became naturalized weeds (Cook, 1962; Leger and Rice, 2007). For the Chilean invasive population, the population history was documented in astonishing detail: California poppy was introduced to the Chilean coastal cities as an ornamental plant during the 1890s and spread from there along railway tracks. Within less than 100 years, the species spread 240 km south and 520 km north of their original points of introduction, including all of the Mediterranean climate region of Chile in its range. Furthermore, California poppy habitat covers an enormous altitudinal range between 0 and 2000 m.a.s.l. in Chile (Véliz et al., 2012) with traits differing between coastal and high altitude plants: coastal plants were shorter, required more time to flower, and produced fewer flowers and fewer seeds per fruit, regardless if the plants were collected from California or Chile. After being introduced to Chile, California poppy has improved its abilities to colonize disturbed environments and evolved robust patterns of local adaptations, all in only 150 years (Leger and Rice, 2007).

Owing to its invasive nature and Mediterranean climate natural range, California poppy is easy to grow and a commonly grown ornamental plant. The plants (Becker et al., 2005; Wege et al., 2007), require little space, 42 plants/m² can be grown comfortably, but up to 90 plants/m² are possible, and standard greenhouse conditions (6 cm pots, standard potting mix, 21°C – 25°C day, 15°C-18°C night, natural light supplemented with fluorescent tubes or mercury lamps, 16 h light/8 h darkness). California poppy does not require governmental permits to be raised and does not require CITES documentation as it is not an endangered plant species.

2 California poppy morphology

Cotyledons of California poppy are deeply lobed, and the shoot apical meristem (SAM) gives rise to highly dissected, silvery green leaves forming a rosette. Once the shoot elongates, the SAM converts into an inflorescence meristem, which continues to

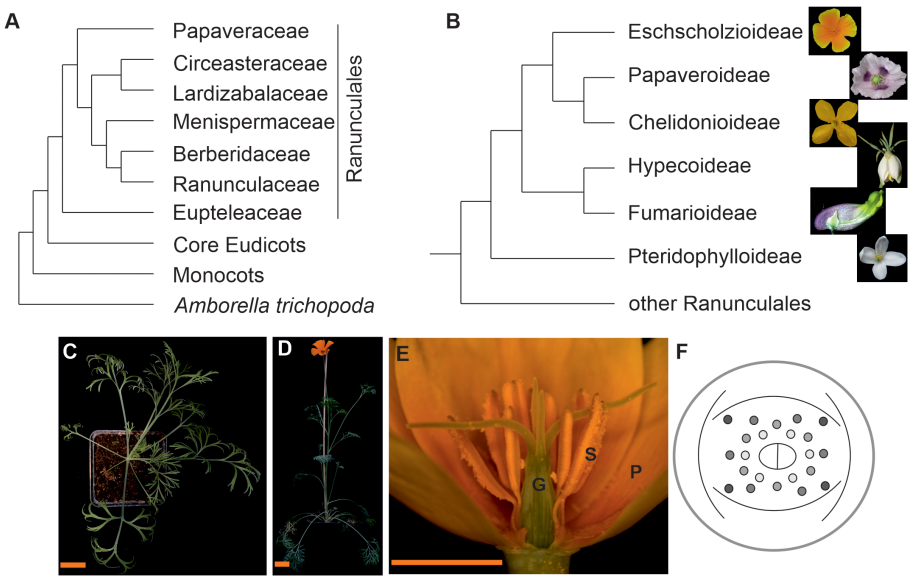

FIGURE 1
Simplified angiosperm phylogenies focusing on the phylogenetic position and morphology of California poppy. **(A)** Phylogeny of the Ranunculales [according to Lane et al. (2018) and Hoot et al. (2015)], **(B)** phylogeny of the Papaveraceae s.l. on subfamily level based on Hoot et al. (2015). Fotos next to the branches show subfamily representatives, from top to bottom California poppy, *Papaver somniferum, Chelidonium majus, Hypecoum leptocarpum, Capnoides sempervirens, Pteridophyllum racemosum.* **(C)** top view on California poppy in its vegetative phase, **(D)** side view of a flowering plant, **(E)** side view of a California poppy flower (G, gynoecium; P, petal; S, stamens) and **(F)** floral diagram showing the sepal cap, two whorls of petals, several whorls of stamens and a bicarpellate gynoecium (photos are from Dominik Lotz and Doudou Kong, Gießen, Germany, and Natalia Pabon-Mora, Medellin, Colombia). The size bar in C and D correspond to 3 cm, the size bar in E is 1 cm.

release leaves. When the uppermost two leaves are formed, the inflorescence meristem converts into a terminal flower meristem. In the leaf axils of the uppermost cauline leaves, new secondary meristems may form. California poppy leaf size and shape depends on the position and age of the leaves: length and degree of dissections increases with age during the vegetative phase, but decreases after transitioning to flowering (Becker et al., 2005).

California poppy has large flowers with four brightly colored petals. The flowers across natural populations are diverse, with petal color in the northern and coastal habitats of its native range being more yellow and the central and southern populations show a larger portion of orange petal color. Stamen numbers range between 16 and 39 with the southern population developing fewer stamens normally (Cook, 1962). California poppy flowers are composed of two sepals fused into a cap-like structure that dehisces when the petals fully elongate. Four petals are 1-3 cm in length and width and are arranged in two concentric whorls (Becker et al., 2005). The petals are not only intensely colored by carotenoids but also have a silky appearance. This effect is caused by a thick, prism-like ridge that runs along enormously elongated petal cells and focuses light to the pigments at the abaxial epidermis cell side (Wilts et al., 2018).

Further inside the flower, the stamens form, with four stamens in the first stamen whorl and all other consecutive whorls forming six stamens. The stamens are composed of a short filament and long, bilobed anthers. The basal part of the anthers is often dark brown with all other parts colored bright yellow. In the center of the flower, the gynoecium is composed of two fused carpels forming a long, superior ovary topped by a short style. Four stigmatic protrusions are covered with papillae that often bend down towards the floral base. A floral tube forms that surrounds the ovary, which is adorned with a torus rim to which the sepals and petals are attached. In the ovary, two rows of ovules are attached to the two placentae (Becker et al., 2005).

After fertilization, the gynoecium develops into a slender capsule of around 5 cm in length at maturity. The capsule dries out and the valves separate from bottom to top from each other releasing the seeds explosively, scattering them up to 1.5 m (Cook, 1962; Becker et al., 2005).

2.1 Molecular regulation of vegetative and reproductive development, examples from functional studies in California poppy

Several studies examining the role of California poppy orthologs of *Arabidopsis thaliana* developmental regulators in recent years contributed to our understanding of gene function conservation. The focus of these studies was on floral development, with an emphasis on carpel development. The advantage of California poppy in these studies is its comparatively simple floral and fruit morphology allowing direct comparisons with long established model species like *Arabidopsis*.

Highly conserved developmental regulators, such as MADS-box transcription factors from California poppy show partially similar functions to *Arabidopsis*, such as specification of floral organ identity. However, their regulation differs from that of *Arabidopsis* and a higher number of genes in the poppy allows for sub- and possibly neofunctionalization. For example, the *AGAMOUS* (*AG*) orthologs of California poppy are required for stamen and carpel organ identity, and the *APETALA3* (*AP3*) and *PISTILLATA (PI)* orthologs for petal and stamen organ identity (Yellina et al., 2010; Lange et al., 2013). The two *AG* orthologs and three *AP3* orthologs are differentially expressed in the flower. *EScaAG1* shows a stronger expression, especially in carpels and fruits. *EScaAG2* is expressed mainly in stamens and only very little in other floral tissues. This divergence in expression suggests that *EScaAG1* is more important for carpel identify and possibly also for the regulation of floral meristem termination, and *EScaAG2* is more important for stamen formation. Expression of the three *DEF/AP3*-like genes shows organ-level differences, such that *EScaDEF3* is most strongly expressed in petals, as is *EScaDEF2*, but the latter to a lesser extent, and *EScaDEF1* is hardly expressed in petals and stamens (Yellina et al., 2010; Lange et al., 2013). In terms of trimeric protein interactions, *EScaAG1* participates in complexes of floral homeotic proteins including BBC and BCE class proteins, but *EScaAG2* does not, suggesting that the floral homeotic C function may be carried out by *EScaAG1*. Further, EScaAG2 can form homodimers, while EScaAG1 cannot, suggesting novel, yet unknown functions for *EScaAG2*. It is also notable that EScaDEF1, the E-function protein Ec-SEP3 and EScaAG1 complexes form, as well as EScaDEF2/Ec-SEP3/EScaAG1, but not EScaDEF3/Ec-SEP3/EScaAG1 (Lange et al., 2013), suggesting subfunctionalization on the level of protein interactions for these floral homeotic proteins.

The regulation of California poppy floral homeotic B and C genes differs from that of *A. thaliana*: the *AG* orthologs are activated by the *AP3* and *PI* orthologs while the *AG* orthologs repress *AP3* and *PI* activity in the carpels, as shown using VIGS experiments and by analysis of the B mutant *sei-1* (Yellina et al., 2010; Lange et al., 2013).

California poppy also served to show that the function of *INAPERTURATE POLLEN (INP1)*, a gene required for aperture formation in pollen grains to allow pollen grain germination, is conserved throughout monocots and dicots, even though sequence divergence of orthologs is comparatively high (Mazuecos-Aguilera et al., 2021).

Like in *Arabidopsis*, the *SHOOT MERISTEMLESS* (*STM*) homologs of California poppy are required for floral meristem activity (Scofield et al., 2007) and are, in combination with California poppy *CRABS CLAW* (*CRC*) orthologs required for floral meristem maintenance and timely termination. As the carpels are the last organs to be formed in the flower, their presence and number critically depends on floral meristem activity, and when the poppy *STM* genes are silenced, the floral meristem terminates prematurely leading to failure of carpel formation, as observed in *A. thaliana* (Scofield et al., 2007; Stammler et al., 2013). Conversely, more carpels are produced when the California poppy *CRC* ortholog transcription is silenced. This suggests antagonistic functions in floral meristem maintenance for the poppy *STM* and *CRC* genes (Orashakova et al., 2009; Stammler et al., 2013). *A. thaliana crc* mutants show only rarely more carpels, but the gynoecia often fail to fuse at the apex and lack nectaries. Recent work has shown that *CRC* acts as a repressing transcription factor in floral meristem termination and

as a transcriptional activator in carpel fusion and nectary development (Bowman and Smyth, 1999; Groß et al., 2018). Also, in the *Phalaenopsis equestris* orchid, *CRC* homologs regulate reproductive development, specifically in the gynostemium, an organ consisting of stamens fused to the gynoecium, suggesting that the regulation of gynoecium development by *CRC* homologs is conserved between monocots and dicots (Chen et al., 2021).

FRUITFUL (*FUL*) and *NGATHA* (*NGA*) orthologs of poppy were shown to be involved in carpel and fruit development, indicative of deeply conserved gene functions between California poppy genes and their orthologs from *Arabidopsis*. *EcFUL1, EcFUL2* down regulated by VIGS results in shorter fruits that open prematurely and occurrence of leaf-like sepals, suggesting that sepal organ identity is compromised and the lignin deposition pattern in fruits is disturbed (Pabón-Mora et al., 2012). Lignin deposition is also disturbed in the *A. thaliana ful* mutant, resulting in a failure to form a dehiscence zone leading to fruits that rupture at random positions (Ferrandiz et al., 2000). Outside the eudicots, *FUL*-like genes are not involved in fruit dehiscence, for example, *WAP1* from wheat is required for vernalization and phase transition (Murai et al., 2003), suggesting that the involvement of *FUL*-like genes in regulation of lignification pattern for dehiscence zone formation is restricted to eudicots.

For *NGA*-like genes, California poppy VIGS-treated plants provide the only functional data outside the core eudicots, as information on mutants in grasses is lacking so far. Within eudicots, the *NGA* orthologs of *A. thaliana*, tobacco and California poppy all share that they are required for style and stigma tissue specification (Fourquin and Ferrándiz, 2014).

CYCLOIDEA/TEOSINTE BRANCHED1-like (*CYL/TB1*) genes of California poppy regulate plant stature, such that down regulation by VIGS enhances axillary branching, a function conserved throughout dicots and monocots. Further, the *CYL/TB1*-like genes in California poppy regulate stamen number and petal size. However, the link between stamen number regulation and *CYL/TB1*-like genes does not seem to be special to Papaveraceae, but floral organ size regulation of *CYL/TB1*-like genes is in line with a conserved function of these genes in the repeated establishment of zygomorphy within the pentapetalae. In the Papaveraceae, *CYL/TB1*-like genes do not establish zygomorphy but may regulate the extent of morphological differences between the floral organs by controlling growth (Zhao et al., 2018).

These studies show that knowledge about the conservation of developmental regulator's gene functions across dicots can be garnered by studying California poppy as genetically tractable representative of the sister lineage to the core eudicots, and the conservation of function between monocots and dicots can be inferred by incorporating California poppy mutants or VIGS-treated plants.

2.2 Floral pigments

California poppy flowers contain unique carotenoids, such as eschscholtzxanthin and retro-carotene-triol (Maoka et al., 2000), which show intense yellow to orange petal pigmentation of this ornamental flower. Whereas orange flowers are more popular, color variations from white to yellow and orange are known. Barrell et al. (2010) analyzed flower color inheritance in diverse variants and showed that all white and yellow variants showed the multiple effects and total of five complementation groups were identified as single recessive loci. Interestingly, all mutations influence both petal and pollen color, suggesting that the same gene controls petal and pollen color.

Zhou et al. (2018) further investigated the carotenoid biosynthetic pathway using a Tobacco Rattle Virus-based virus-induced-gene-silencing (VIGS) approach. VIGS of early (*PDS* and *ZDS*) and late (*βOH* and *ZEP*) biosynthetic enzymes in carotenoid pathway reduced the transcripts of the target genes in the petals without the effect on other carotenoid biosynthesis gene expressions. Silencing of *PDS*, *ZDS*, *βOH* and *ZEP* genes reduced total pigment concentration by 75-90% and altered petal color. HPLC and LC-MS measurements suggested that petal color changes were caused by substantially altered pigment profiles and quantity. More recently, Pollack et al. (2019) discovered a single deletion leading to altered splicing and C-terminal truncation of phytoene synthase (*PSY*), a key enzyme in carotenoid biosynthesis mutated in multiple white petal varieties.

Whereas the key enzyme genes for retro-carotene-triol biosynthesis are still not identified yet, some candidate genes are predicted based on the draft genome sequence and transcriptome analysis for future breeding (Sato et al. unpublished data).

3 Medicinal use

California poppy was highly prized by Native Americans for its medicinal value based on its specialized metabolite biosynthesis, with the most prominent class being the benzylisoquinoline alkaloids (BIAs). Phytochemical analysis revealed that aerial parts and roots accumulate alkaloids, with roots showing a higher concentration of up to 1.6% alkaloids of the dry weight. These alkaloids are mainly BIAs and include benzophenanthridine alkaloids (such as sanguinarine, chelirubine, macarpine, chelerythrine, chelilutine), protopines (protopine, allocryptopine), aporphine alkaloids (magnoflorine, corydine, isoboldine, *N*-methyllaurotetanine), simple benzylisoquinolines (reticuline), pavine alkaloids (californidine, caryachine, escholtzine), as well as the dihydro-intermediates (Figure 2). Roots contain mainly benzophenanthridine alkaloids and protopines, whereas aerial parts are especially rich in pavine and some aporphine alkaloids (Liscombe et al., 2009; Fedurco et al., 2015; Hori et al., 2018).

Pharmacological studies of these BIAs revealed their antifungal, analgesic, anxiolytic, sedative activities (Al-Snafi, 2017). For example, extracts prepared from aerial parts of California poppy as herbal supplement show analgesic, anxiolytic and sedative effects. Rolland et al. (1991) reported that the aqueous extract reduced the behavioral performance in mice with regard to novelty preference, locomotion and rearing in two compartments parameters measured (in a familiar environment test). Further, the California poppy extract treated mice underperformed in the staircase test (non-familiar environment tests). These findings support the traditional

10.3389/fpls.2023.1084358

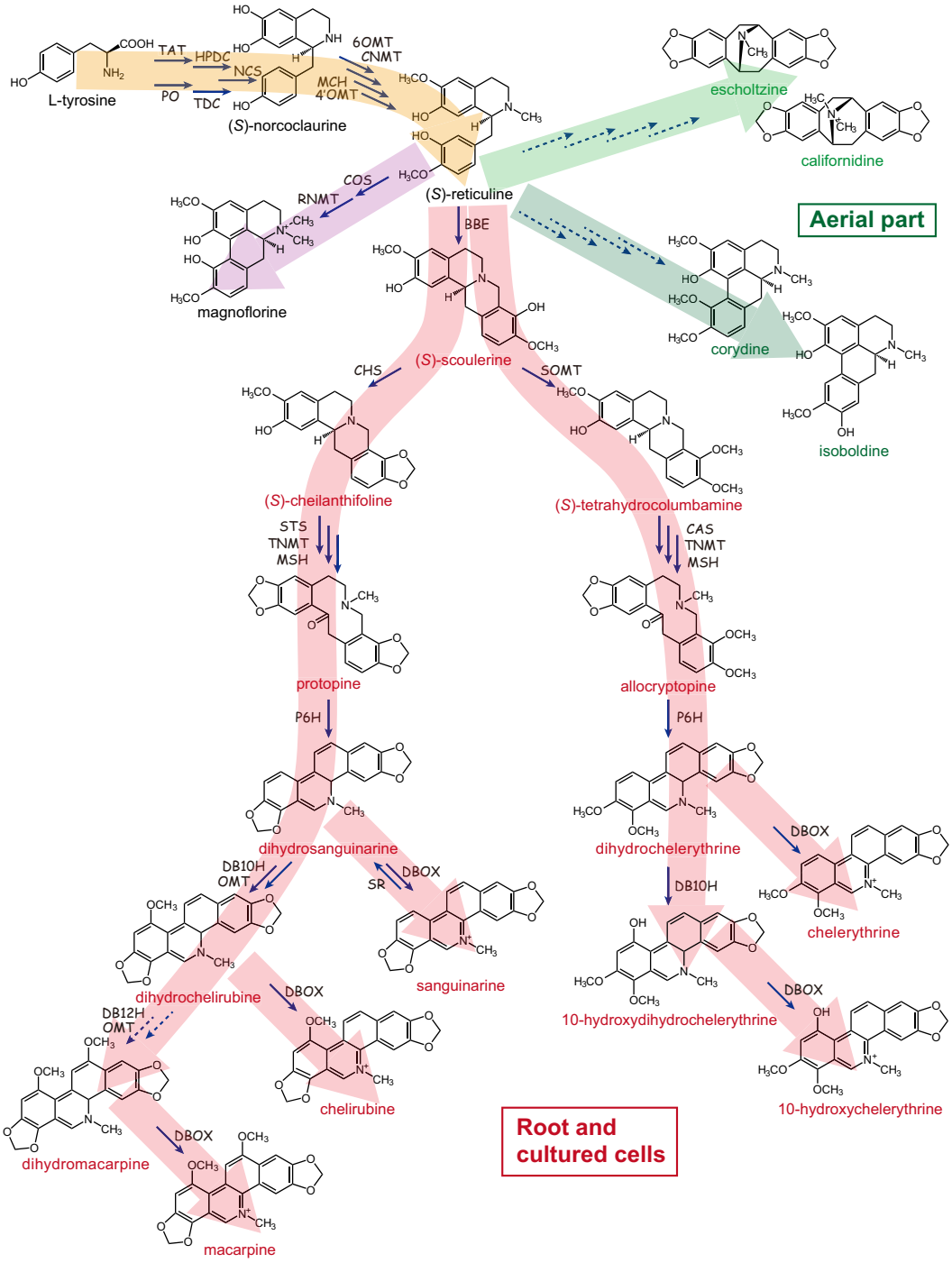

FIGURE 2
Benzylisoquinoline alkaloid biosynthetic pathway in California poppy. California poppy produces diverse array of benzylisoquinoline type alkaloids (BIAs), which include benzophenanthridine alkaloids (such as sanguinarine, chelirubine, macarpine, chelerythrine, chelilutine), protopines (protopine, allocryptopine), aporphine alkaloids (magnoflorine, corydine, isoboldine), simple benzylisoquinolines (reticuline), pavine alkaloids (californidine, escholtzine), as well as the dihydro-intermediates. The broken lines indicate that the biosynthetic enzyme-encoding genes have not been identified. TAT, tyrosine aminotransferase; HPDC, *p*-hydroxyphenylpyruvate decarboxylase; PO, phenol oxidase; TDC, tyrosine/DOPA decarboxylase; NCS, (*S*)-norcoclaurine synthase; 6OMT, (*S*)-norcoclaurine 6-*O*-methyltransferase; CNMT, (*S*)-coclaurine *N*-methyltransferase; MCH, (*S*)-*N*-methylcoclaurine 3'-hydroxylase; 4'OMT, (*S*)-3'-hydroxy-*N*-methylcoclaurine 4'-*O*-methyltransferase; COS, (*S*)-corytuberine synthase; RNMT, (*S*)-reticuline *N*-methyltransferase; BBE, berberine bridge enzyme; SOMT, (*S*)-scoulerine 9-*O*-methyltransferase; CHS, (*S*)-cheilanthifoline synthase; STS, (*S*)-stylopine synthase; CAS, (*S*)-canadine synthase; TNMT, (*S*)-tetrahydroprotoberberine *N*-methyltransferase; MSH, (*S*)-*N*-methylstylopine 14-hydroxylase; P6H, protopine 6-hydroxylase; DBOX, dihydrobenzophenanthridine alkaloid oxidase; SR, sanguinarine reductase; DB10H, dihydrobenzophenanthridine alkaloid 10-hydroxylase; DB12H, dihydrobenzophenanthridine alkaloid 12-hydroxylase. Large arrows in red denote compounds synthesized in root and cultured cells, yellow indicates starting products of BIA synthesis, and green indicates alkaloids found in aerial part.

use of California poppy herbal extract to induce sleep due to sedative properties. Fedurco et al. (2015) further assigned the depressant properties of aerial California poppy parts to chloride-current modulation at the alpha(3)beta(2)gamma(2) and alpha(5) beta(2)gamma(2) GABA(A) receptors by (*S*)-reticuline, a minor alkaloid in the herbal extract,

The biological activities of sanguinarine, the main alkaloid in California poppy root and cell cultures, have been investigated in depth and were recently reviewed by Laines-Hidalgo et al. (2022). In brief, sanguinarine shows herbivore deterrent activity as well as antimicrobial effects (Schmeller et al., 1997). These effects may be related to its cytotoxic activity, such as intercalation in nucleic acids, and inhibition of DNA and RNA synthesis. Moreover, sanguinarine can bind to negatively charged membrane surfaces and proteins as heteroaromatic iminium cation (Han et al., 2016) and it inhibits choline acetyltransferase activity in arthropods and vertebrates.

Sanguinarine, chelerythrine, and other BIAs also show antibacterial and antifungal activities (Zhao et al., 2019), whereas their direct effects on these pathogens was not analyzed *in planta*. Interestingly, antiplaque mouth washes and toothpaste containing sanguinarine were once commercially available, but were later removed from supermarket shelves due to their dramatic side effect: leukoplakia, a pre-malignant condition, of the maxillary vestibule had occurred in some consumers (Laines-Hidalgo et al., 2022).

It is further important to notice that some plant-derived alkaloids, such as protopine and (+)-*N*-methyllaurotetanine reduced the human cardiac ether-a-go-go-related gene (hERG) expression and poses a potential risk for human hERG toxicity (Schramm et al., 2014).

3.1 Alkaloids

The BIA pathway in California poppy provides a convenient system to study the regulation of biosynthesis and the physiological roles of BIAs (Figure 2). And while *Coptis japonica* (https://www.sciencedirect.com/topics/biochemistry-genetics-and-molecular-biology/coptis), *Thalictrum thalictroides* (https://www.sciencedirect.com/topics/pharmacology-toxicology-and-pharmaceutical-science/thalictrum), and *Papaver somniferum* (https://www.sciencedirect.com/topics/biochemistry-genetics-and-molecular-biology/papaver-somniferum) are also used to study BIAs, California poppy provides practical advantages. The plants are easy and permit-free to cultivate, efficient methods for cell cultures and genetic transformations are available as discussed below (Hagel and Facchini, 2013; Sato, 2013; Lotz et al., 2022).

HPLC or LC-MS analyses easily reveal alkaloid composition of California poppy (Liscombe et al., 2009; Hori et al., 2018), whereas the more traditional TLC method is also still in use (Balažová et al., 2020). Kukula-Koch (2017) reported an optimized method for the LC-ESI-Q-TOF-MS analysis for the extracts of Papaveraceae and Berberidaceae families (genera: *Papaver, Argemone, Eschscholzia, Chelidonium, Glaucium*, and *Berberis*), providing even more sensitive and precise method for BIA characterization. Based on the identification of alkaloid chemical structures and tracer experiments, the major alkaloid biosynthesis pathways and biosynthetic enzymes of BIAs have been characterized at the molecular level (Hagel and Facchini, 2013; Sato, 2013; Sato, 2020)

BIA biosynthesis commences with the conversion of tyrosine to both dopamine and 4-hydroxyphenylacetaldehyde (4HPAA) by tyrosine/dopa decarboxylase (TDC), or 4-hydroxyphenylpyruvate decarboxylase (HPDC), phenol oxidase (PO), and tyrosine amino transferase (TAT) (Figure 2, brown pathway). Dopamine and 4HPAA are condensed by norcoclaurine synthase (NCS) and yield (*S*)-norcoclaurine (Samanani and Facchini, 2001). (*S*)-Norcoclaurine is sequentially converted to (*S*)-reticuline by norcoclaurine 6-*O*-methyltransferase (6OMT) (Inui et al., 2007), coclaurine *N*-methyltransferase (CNMT), *N*-methylcoclaurine hydroxylase (CYP80B1; MCH) (Pauli and Kutchan, 1998), and 3'-hydroxy *N*-methylcoclaurine 4'-*O*-methyltransferase (4'OMT) (Inui et al., 2007).

(*S*)-Reticuline is converted to (*S*)-scoulerine by berberine bridge enzyme (BBE), then benzophenanthridine alkaloids (e.g., sanguinarine and macarpine) (Figure 2, red pathway in root and cultured cells) (Dittrich and Kutchan, 1991; Fujii et al., 2007; Ikezawa et al., 2007, 2009; Liscombe et al., 2009; Hagel et al., 2012; Beaudoin and Facchini, 2013; Takemura et al., 2013; Purwanto et al., 2017). Two enzymes unique to California poppy and identified based on draft genome sequence mining are dihydrobenzophenathridine hydroxylase (DB10H) and OMT required for dihydrochelirubine biosynthesis (Hori et al., 2018). Importantly, California poppy cell cultures can self-detoxify exogenously added benzophenanthridines by sanguinarine reductase (SR; Vogel et al., 2010). As shown in Figure 2, the biosynthetic pathway of sanguinarine and related chelerythrine and chelirubine in underground parts and cultured cells of California poppy has been almost completely elucidated.

The characterization of BIA biosynthetic enzymes was the prerequisite to elucidate the mechanisms of their transcriptional regulation (Yamada and Sato, 2021). Firstly, *CjWRKY1* and *CjbHLH1* were identified as comprehensive transcriptional activators of biosynthetic enzyme genes in BIA biosynthesis of *C. japonica* cells (Kato et al., 2007; Yamada et al., 2011a). Later, their homologs were isolated from California poppy (*Ec*WRKY and *Ec*bHLH1-1/1-2) allowing for the characterization of the regulation of BIA biosynthesis in California poppy (Yamada et al., 2015; Yamada et al., 2021b). Interestingly, *Cj*bHLH1 and *Ec*bHLH1-1/1-2 are non-MYC2-type bHLH transcription factors and their homologs are only found in BIA-producing plant species (Yamada et al., 2011b). Whereas WRKYs were also identified in California poppy genome, the heterologous expression of *Cj*WRKY1 in California poppy showed limited activation of BIA biosynthetic enzyme genes and only partial increase in BIA production, suggesting that their function is not fully interchangeable (Yamada et al., 2017). Detailed genome-wide analysis of the California poppy WRKY transcription factor family combined with transcriptome analysis suggested that this gene family is involved in the regulation of BIA biosynthesis and is possibly also associated with the accumulation and translocation of BIAs in California poppy (Yamada et al., 2021b).

Further transcriptome analysis and genome mining revealed several transcription factor genes that are strongly upregulated in

response to methyl jasmonate (MeJA), such as *EcAP2/ERF2*, *EcAP2/ERF3* and *EcAP2/ERF4* (Yamada et al., 2020). MeJA also sequentially induced the expression of *bHLH* and *WRKY* genes as well as of BIA biosynthetic enzyme and transporter genes (Yamada and Sato, 2021). This information on additional BIA regulatory transcription factors and MeJA as inducing phytohormone, all obtained in California poppy, can be highly useful to dissect the regulation of BIA biosynthesis in diverse plant species.

Unfortunately, molecular information of the genes encoding the biosynthetic enzymes for pavine-type BIAs in the aerial parts of California poppy, such as californidine and escholtzine (Figure 2, green pathway) is still missing (Hori et al., 2018). Moreover, while pavine-type alkaloids are most prominent in leaves, their physiological role is unknown. And, the important question on why pavine-type alkaloids are found in leaves and benzophenanthridine alkaloids accumulate in roots and how this relates to the defense against different pathogens would be interesting to study in California poppy.

We also note that California poppy has limitations, due to the lack of some commercially important BIAs, such as noscapine and morphinan alkaloids (Hagel and Facchini, 2013; Sato, 2020). The biosynthesis of morphinan alkaloids in opium poppy requires cell-type-specific localization of the biosynthetic enzymes. *In situ* localization of their transcripts indicated that seven biosynthetic enzymes (6OMT, CNMT, CYP80B, 4'OMT and BBE involved in reticuline biosynthesis, and SAT and COR in the morphine pathway) were localized in sieve elements, whereas proteins were localized in the supporting companion cells, demonstrating a complex spatial organization of morphinan alkaloids (Lee et al., 2013; Ozber et al., 2022). California poppy could serve as preferred host system to reconstruct the morphinan pathway including genes encoding for the biosynthetic enzymes, translocators, and transcription factors genes involved in cell differentiation. This would be a prime example for synthetic biology to recreate a highly complex biosynthetic pathway of a commercially extremely valuable pharmaceutical.

Undoubtedly, the California poppy draft genome provides a useful platform to study the evolution of BIA biosynthesis and its regulation. Phylogenomic approaches using whole genome sequences of five benzylisoquinoline alkaloid (BIA)-producing species from the Ranunculales and Proteales orders including California poppy revealed the sequence and timing of evolutionary events leading to the diversification of BIA alkaloids (Li et al., 2020). 1-Benzylisoquinoline is a pivotal intermediate in the synthesis of many BIAs and phylogenomic analyses revealed parallel evolution in the orders of Ranunculales and Proteales, which diverged ~122 million years ago (MYA), with the Ranunculales producing (*S*)-reticuline and the Proteales the related (R/S)-norcoclaurine. Berberine is present in species across the Ranunculales but lacking in Proteales, and homologs of genes essential for the protoberberine class production were found throughout the Ranunculales. However, benzophenanthridine class is specific to the Papaveraceae family within Ranunculales (Figure 1), and its biosynthetic genes emerged after the Papaveraceae separated from the other Ranunculales, around 110 MYA. Their origin also predates the split of the three Papaveraceae species (opium poppy, California poppy, and *Macleaya cordata*) at approximately 77 MYA. The phthalideisoquinoline noscapine and morphinan classes of BIAs are exclusive to the opium poppy lineage (Li et al., 2020). In addition, predicted protein-encoding genes and comparative analysis using genome sequences of BIA-producing plants, opium poppy and *Aquilegia coerulea*, showed many additional candidate genes encoding for biosynthetic enzymes, transcription factors, and transporter genes involved in the BIA pathway (Yamada et al., 2021a).

4 Genetic resources

The species California poppy shows a stunning variation in floral and vegetative traits observed in natural populations and its adaptability suggests high genetic variation. Cytological observations and classical genetic experiments by Ernst and Cook (Ernst, 1958; Cook, 1962) revealed that California poppy has 6 chromosomes, and is self-incompatible to the largest extent, even in the naturalized populations, and genetic barriers to outcrossing were not identified so far. The powdery nature of the pollen allows also for wind pollination, but the flowers are mainly pollinated by insects. While the large flowers do not exudate nectar, they abundantly provide pollen. Beetles, bees and bumblebees contribute significantly to California poppy pollination, but also thrips and hover flies were observed to visit the flowers (Cook, 1962). The open breeding system of this species allows novel adaptive trait combinations and permits differentially adapted population existing close to each other (Cook, 1962) and may be a prerequisite of its invasiveness.

4.1 Sequence resources

Several genetic resources have been developed to facilitate California poppy research with the advantages of relatively small genome size (503.8 Mb): 14 microsatellite markers are available for population genetic analysis that have been utilized to characterize the highly invasive populations in Chile (Véliz et al., 2012). And EST database has been established to facilitate gene discovery (Carlson et al., 2006), and the sequence information garnered from the ESTs was used to generate microarrays for differential gene expression studies (Zahn et al., 2010). In addition to these transcriptomes, RNAseq data for different stages of carpel development obtained by laser microdissection are available from California poppy (Kivivirta et al., 2019).

Meanwhile, a draft genome sequence was published (Hori et al., 2018; Eschscholzia Genome DataBase, http://eschscholzia.kazusa.or.jp) and a reference-quality genome sequencing effort in combination with a transcriptome atlas is about to be completed by the Open Green Genome initiative with the data being deposited in the phytozome database (OGG, https://phytozome-next.jgi.doe.gov/ogg/) for easy access. Further, we are generating a large number of high quality transcriptome data for diverse tissues and these will be available for the research community *via* a web-based multi-omics platform. This will allow *in silico* analysis of the genome and digital gene expression

analysis along the entire transcriptome and be useful for gene network constructions.

4.2 Resources for genetic manipulation

In addition to sequence information, questions regarding the conservation of gene functions can be addressed by knocking down gene expression of target genes by Virus-Induced Gene Silencing (VIGS). This method allows gene function analysis in a simple and time efficient way by manipulating the plant's immune reaction towards RNA viruses such that the expression of endogenous genes is reduced (Wege et al., 2007; Rössner et al., 2022). This method was employed several times to elucidate the function of transcription factors involved in vegetative and reproductive development (Orashakova et al., 2009; Yellina et al., 2010; Lange et al., 2013; Stammler et al., 2013; Zhao et al., 2018). While the effect of VIGS is transient and cannot be transferred to subsequent generations, a second, reliable method for stable transformation and regeneration of mature plants is now available (Park and Facchini, 2000; Lotz et al., 2022). Here, *Agrobacterium tumefaciens*-mediated transformation of cotyledons and subsequent regeneration is works efficiently but is time-consuming in California poppy, requiring at least eight months from the transformation event to mature plants (Park and Facchini, 2000; Lotz et al., 2022).

Whereas prolonged modulation of gene expression with *A. tumefaciens* mediated stable transformation, or VIGS/virus-based expression is useful for the functional characterization of biosynthetic enzyme or developmental genes, transient assays using protoplasts are faster to characterize certain gene functions such as transcription factor genes regulating BIA biosynthesis. Protoplasts are prepared from plant cells after the digestion of cell walls with cellulase, pectinase and other cell wall digesting enzymes. Protoplasts take up DNA, RNA, or proteins easily when treated with polyethylene glycol (PEG), or electric stimulus. For example, the efficacy of double-stranded (ds) RNAs prepared against candidate transcription factor encoding genes or over-expression plasmids for transcription factor encoding genes were examined in protoplasts of *C. japonica*, a relevant model for BIA-producing plants using PEG-mediated transformation. Suppression effects of TFs on biosynthetic enzyme genes were successfully monitored by quantitative reverse transcription (RT)-polymerase chain reaction (PCR) in *C. japonica* (Dubouzet et al., 2005). Since mesophyll protoplasts are rather easily isolated from California poppy leaves (data not shown), similar system will be applicable, for example to characterize the pavine-biosynthesis in leaf tissue.

4.3 Cell culture systems

California poppy cell cultures have been intensively used to study BIA pathway, since cell cultures produce the major BIAs and provides sufficient materials for biochemical and molecular genetics characterization (Sato, 2013). Cell culture systems are also useful to modify biosynthetic pathways using genetically transformed cultures (Sato et al., 2001; Fujii et al., 2007; Inui et al., 2007), and to test the effect of chemicals such as elicitors from pathogens or MeJA as BIA pathway activator (Tanahashi and Zenk, 1990; Färber et al., 2003; Ikezawa et al., 2009).

In fact, introduction of the *C. japonica* scoulerine 9-*O*-methyltransferase (*Cj*SMT) gene into BIA biosynthesis in a California poppy cell culture system shifted the metabolic flow from the sanguinarine type to chelerythrine type (Sato et al., 2001, Figure 2). Whereas both introduced *Cj*SMT and endogenous cheilanthifoline synthase (*Ec*CYP719A2/A3) accept scoulerine as substrate, the highly reactive *Cj*SMT dominated the pathway when compared to the endogenous *Ec*CYP719A2/A3. Similarly, when the *C. japonica* (*S*)-tetrahydroberberine oxidase (*Cj*THBO) was introduced to California poppy cells, *Cj*THBO hijacked the intermediates in benzophenanthridine biosynthesis to convert them into protoberberine type products (Matsushima et al., 2012).

The physiological role of down-regulation using antisense RNA, co-suppression or gene-knockout with CRISPR/Cas 9 is also effectively monitored in cell culture systems. For example, the effects of RNA-interference (RNAi) of berberine bridge enzyme (BBE) gene in BIA pathway can be detected as the accumulation of the key intermediate reticuline with substantial production of 7-*O*-methylated derivative of reticuline, laudanine, which indicates the dynamics of metabolism (Fujii et al., 2007).

Sterilized California poppy seedlings grown on 1% agar medium containing Murashige–Skoog inorganic salts under continuous light (100 μE/m^2/s) at 25°C are preferable materials for cell culture or transformation with *Agrobacterium tumefaciens*. Calli generally form after 2 months (about three successive selection cultures) on culture medium containing appropriate plant growth factors such as auxin, cytokinin, and antibiotics for selecting the transgenics. Transformation efficiency, regeneration/callus formation efficiency, and secondary metabolite productivity can vary considerably and require seed variety comparisons as preliminary experiments. For the establishment of an embryogenic culture, juvenile tissues such as shoot meristem and immature seed are often preferred materials (Takemura et al., 2010). Whereas Cauliflower Mosaic Virus 35S is a commonly used promoter sequence to over-express desired genes constitutively in host plant cells, gene expression in specific tissues or developmental stages requires carefully selected promoters and even enhancers. Thus, for alkaloid engineering, more research on the regulation of metabolic pathway and specific gene expression profiles is needed. One example for a comprehensive characterization of biosynthetic enzymes was done with the genes encoding for the two *C. japonica* enzymes norcoclaurine 6-*O* methyltransferase (*Cj*6OMT) and 3'-hydroxy-*N*-methylcoclaurine 4'-*O*-methyltransferase (*Cj*4'OMT). They were over-expressed in California poppy cell cultures and showed different effects. Over-expression of *Cj*6OMT increased the alkaloid content to 7.5 times greater than that of the wild type, whereas the over-expression of *Cj*4'OMT had only a marginal effect (Inui et al., 2007).

Cell culture systems proved also useful to dissect BIA induction and its role in the molecular mechanism of phytopathogen defense. Whereas jasmonate treatment is commonly used to activate BIA biosynthesis (Färber et al., 2003; Ikezawa et al., 2009), Balažová et al. (2020) examined salicylic acid (SA), and simultaneous or sequential treatment of SA and L-tyrosine in cell cultures to enhance production of macarpine, a BIA specific to few Papaveraceae

species only. Angelova et al. (2010) used root-derived cell cultures to characterize the elicitation mechanism, initiated by a short contact to low concentrations of a yeast glycoprotein elicitor, which led to the transient acidification of the cytoplasm. In contrast to low concentration treatment, high elicitor concentration signal increased jasmonate concentration and triggered hypersensitive cell death, resulting in massive mRNA decay.

Taken together, transient and stable genetic transformation methods have been established for California poppy to interrogate gene functions in different contexts. For metabolic engineering and the analysis of metabolite biosynthesis regulation, stable genetic transformation of cell culture systems have been used extensively. For the analysis of developmental regulators, fully grown plants are required and VIGS was used efficiently to unravel their function and regulatory circuits, even though this method is transient. The novel method for stable transformation and regeneration of California poppy will provide even more possibilities, especially for targeted, heritable mutagenesis by CRISPR-Cas.

5 Outlook

California poppy's high level of genetic diversity comes with the cost of being an obligate outcrossing plant. This suggests that the level of heterozygosity is high and the isogenic and even near-isogenic lines production is very challenging. However, homozygous mutants can be created by sibling crossing. Moreover, CRISPR-Cas guided genome editing introduced by *Agrobacterium*-mediated transformation and regeneration provides an efficient means to elucidate gene function in homozygous knock-out mutants. Further, VIGS can be combined with CRISPR-Cas such that the guide RNAs may be delivered by VIGS to a plant carrying a CRISPR-Cas expressing transgene. These future developments of the California poppy toolkit will enhance the potential of this already established model organism to study, for example, BIA biosynthesis and its regulation in fully grown plants and link this with developmental genetics analyses. Availability of many high quality transcriptome datasets allows the calculation of gene networks based on genes' co-expression to identify whole modules of putatively interacting genes. This type of analysis is independent of candidate genes associated to biological processes in other species, such as *Arabidopsis*, and is thus bias-free.

Additionally to California poppy genome and transcriptome datasets being generated, these datasets are becoming available also for other Ranunculales, allowing comparative analyses. Several Ranunculales genomes have been published recently, some even at chromosome-level, including *M. cordata* (Liu et al., 2017), *Coptis chinensis* (Liu et al., 2021), *P. somniferum* (Guo et al., 2018), *Papaver rhoeas, Papaver setigerum* (Yang et al., 2021), and *A. coerulea* (Filiault et al., 2018), *Aquilegia oxysepala* (Xie et al., 2020), *Thalictrum thalictroides* (Arias et al., 2021), *Kingdonia uniflora* (Sun et al., 2020), *Akebia trifoliat*a (Huang et al., 2021), and *Corydalis tomentella* (Xu et al., 2022).

While genome sequencing requires the extraction of a single sample of high molecular weight DNA, transcriptome analysis requires the collection of several biological replicates for many tissues, stages, and/or treatments, rendering this method more time consuming and laborious. While for *Nigella damascena, A. coerule*a, and *T. thalictroides* more extensive transcriptomes datasets have already been published facilitating gene identification in Ranunculales and gene expression analysis to a limited extent (Meaders et al., 2020; Zhang et al., 2020; Arias et al., 2021). However, the datasets often comprise only few tissues and an insufficient number of replicates to allow for digital gene expression analysis. Furthermore, gene expression comparison of orthologous genes is challenging at the present state, if possible at all. Comparable datasets including representatives covering all Ranunculales subfamilies is desirable for cross-species comparison of gene expression data. Sufficient expression data for each representative species is further required for co-expressed gene network calculations and to compare these networks between species to learn about novel network nodes that may correspond to morphological or metabolic novelties in the Ranunculales.

Furthermore, California poppy allows the fusion of two formerly separated fields in plant biology: developmental genetics and regulation of metabolism: floral homeotic genes specify floral organ identity and any anomaly in the structure or expression of these genes apparently may result in morphological variations of the flower/capsule and consequently in the alkaloid yield. One such recessive mutation, *aco* (*androcarpel organ*), has been described in the opium poppy (Prajapati, 2002), in which androcarpels are formed in place of stamens in the mutant flowers. The androcarpel walls synthesized and accumulated alkaloids similar to the main carpel walls and thus provided a means for increasing the carpel wall husk mass and alkaloid yield. Singh et al. (2017) also reported the presence of major BIAs in the carpeloid stamens of the floral homeotic mutant *OM*, unlike in wild type stamens, indicating functional similarities between the carpeloid stamen and the capsule wall in their capacity to synthesize BIAs. Whereas California poppy does not synthesize morphinan alkaloids, it also accumulates BIAs in floral organs and thus allows the study of the interplay of regulatory genes in flower morphogenesis and specialized metabolism, i.e., carotenoid and BIA biosynthesis for crop improvement in future breeding programs of Papaveraceae species.

Author contributions

AB, YY, and FS wrote the draft and final version of the manuscript. All authors contributed to the article and approved the submitted version.

Funding

Research on *California poppy* in AB's group has been funded continuously by the German Research Foundation (DFG, grants BE2547/3-1; 6-1; 6-2; 7-2; 14-1; 24-1, 27-1). *California poppy* research in YY's group was funded by the Ministry of Education, Culture, Sports, Science and Technology of Japan (MEXT, Grant-in-Aid for Young Scientists 21K14830) and partially by JSPS, PRESTO (Grant Number JPMJPR21DA), Japan. Work in FS's lab

on *California poppy* was funded by MEXT (Grant-in-Aid for Scientific Research (S) 26221201).

Conflict of interest

The authors declare that the research was conducted in the absence of any commercial or financial relationships that could be construed as a potential conflict of interest.

Publisher's note

References

Al-Snafi, A. E. (2017). *Eschscholzia californica*: A phytochemical and pharmacological - review. doi: 10.5281/zenodo.344931

Angelova, S., Buchheim, M., Frowitter, D., Schierhorn, A., and Roos, W. (2010). Overproduction of alkaloid phytoalexins in California poppy cells is associated with the co-expression of biosynthetic and stress-protective enzymes. *Mol. Plant* 3, 927–939. doi: 10.1093/mp/ssq043

Arias, T., Riaño-Pachón, D. M., and Di Stilio, V. S. (2021). Genomic and transcriptomic resources for candidate gene discovery in the ranunculids. *Appl. Plant Sci.* 9, e11407. doi: 10.1002/aps3.11407

Balažová, A., Urdová, J., Forman, V., and Mučaji, P. (2020). Enhancement of macarpine production in *Eschscholzia californica* suspension cultures under salicylic acid elicitation and precursor supplementation. *Molecules* 25, 1261. doi: 10.3390/molecules25061261

Barrell, P. J., Wakelin, A. M., Gatehouse, M. L., Lister, C. E., and Conner, A. J. (2010). Inheritance and epistasis of loci influencing carotenoid content in petal and pollen color variants of california poppy (*Eschscholzia californica* cham.). *J. Hered* 101, 750–756. doi: 10.1093/jhered/esq079

Beaudoin, G. A. W., and Facchini, P. J. (2013). Isolation and characterization of a cDNA encoding (S)-cis-N-methylstylopine 14-hydroxylase from opium poppy, a key enzyme in sanguinarine biosynthesis. *Biochem. Biophys. Res. Commun.* 431, 597–603. doi: 10.1016/j.bbrc.2012.12.129

Becker, A., Gleissberg, S., and Smyth, D. R. (2005). Floral and vegetative morphogenesis in California poppy (*Eschscholzia californica* cham.). *Int. J. Plant Sci.* 166, 537–555. doi: 10.1086/429866

Bowman, J. L., and Smyth, D. R. (1999). CRABS CLAW, a gene that regulates carpel and nectary development in *Arabidopsis*, encodes a novel protein with zinc finger and helix-loop-helix domains. *Development* 126, 2387–2396. doi: 10.1242/dev.126.11.2387

Carlson, J. E., Leebens-Mack, J. H., Wall, P. K., Zahn, L. M., Mueller, L. A., Landherr, L. L., et al. (2006). EST database for early flower development in California poppy (*Eschscholzia californica* cham., Papaveraceae) tags over 6,000 genes from a basal eudicot. *Plant Mol. Biol.* 62, 351–369. doi: 10.1007/s11103-006-9025-y

Chen, Y.-Y., Hsiao, Y.-Y., Li, C.-I., Yeh, C.-M., Mitsuda, N., Yang, H.-X., et al. (2021). The ancestral duplicated DL/CRC orthologs, PeDL1 and PeDL2, function in orchid reproductive organ innovation. *J. Exp. Bot.* 72, 5442–5461. doi: 10.1093/jxb/erab195

Cook, S. A. (1962). Genetic system, variation, and adaptation in *Eschscholzia californica*. *Evolution* 16, 278. doi: 10.2307/2406277

Dittrich, H., and Kutchan, T. M. (1991). Molecular cloning, expression, and induction of berberine bridge enzyme, an enzyme essential to the formation of benzophenanthridine alkaloids in the response of plants to pathogenic attack. *Proc. Natl. Acad. Sci. U.S.A.* 88, 9969–9973. doi: 10.1073/pnas.88.22.9969

Dubouzet, J. G., Morishige, T., Fujii, N., An, C.-I., Fukusaki, E., Ifuku, K., et al. (2005). Transient RNA silencing of scoulerine 9-*O*-methyltransferase expression by double stranded RNA in *Coptis japonica* protoplasts. *Biosci. Biotechnol. Biochem.* 69, 63–70. doi: 10.1271/bbb.69.63

Ernst, W. R. (1958). Chromosome numbers of some western Papaveraceae. *Contr. Dudley Herb.* 5, 109–115.

Färber, K., Schumann, B., Miersch, O., and Roos, W. (2003). Selective desensitization of jasmonate- and pH-dependent signaling in the induction of benzophenanthridine biosynthesis in cells of *Eschscholzia californica*. *Phytochemistry* 62, 491–500. doi: 10.1016/S0031-9422(02)00562-9

Fedurco, M., Gregorová, J., Šebrlová, K., Kantorová, J., Peš, O., Baur, R., et al. (2015). Modulatory effects of *Eschscholzia californica* alkaloids on recombinant GABAA receptors. *Biochem. Res. Int.* 2015, 617620. doi: 10.1155/2015/617620

Ferrandiz, C., Liljegren, S. H., and Yanofsky, M. (2000). Negative regulation of the *SHATTERPROOF* genes by FRUITFULL during *Arabidopsis* fruit development. *Science* 289, 436–438. doi: 10.1126/science.289.5478.436

Filiault, D. L., Ballerini, E. S., Mandáková, T., Aköz, G., Derieg, N. J., Schmutz, J., et al. (2018). The *Aquilegia* genome provides insight into adaptive radiation and reveals an extraordinarily polymorphic chromosome with a unique history. *Elife* 7, e36426. doi: 10.7554/eLife.36426

Fourquin, C., and Ferrándiz, C. (2014). The essential role of NGATHA genes in style and stigma specification is widely conserved across eudicots. *New Phytol.* 202, 1001–1013. doi: 10.1111/nph.12703

Fujii, N., Inui, T., Iwasa, K., Morishige, T., and Sato, F. (2007). Knockdown of berberine bridge enzyme by RNAi accumulates (*S*)-reticuline and activates a silent pathway in cultured California poppy cells. *Transgenic Res.* 16, 363–375. doi: 10.1007/s11248-006-9040-4

Groß, T., Broholm, S., and Becker, A. (2018). CRABS CLAW acts as a bifunctional transcription factor in flower development. *Front. Plant Sci.* 9, 835. doi: 10.1093/pcp/pct020

Guo, L., Winzer, T., Yang, X., Li, Y., Ning, Z., He, Z., et al. (2018). The opium poppy genome and morphinan production. *Science* 362, 343–347. doi: 10.1126/science.aat4096

Hagel, J. M., Beaudoin, G. A. W., Fossati, E., Ekins, A., Martin, V. J. J., and Facchini, P. J. (2012). Characterization of a flavoprotein oxidase from opium poppy catalyzing the final steps in sanguinarine and papaverine biosynthesis. *J. Biol. Chem.* 287 (51), 42972–42983. doi: 10.1074/jbc.M112.420414

Hagel, J. M., and Facchini, P. J. (2013). Benzylisoquinoline Alkaloid Metabolism: A Century of Discovery and a Brave New World. *Plant Cell Physiol.* 54, 647–672. doi: 10.1093/pcp/pct020

Han, N., Yang, Z., Liu, Z., Liu, H., and Yin, J. (2016). Research progress on natural benzophenanthridine alkaloids and their pharmacological functions: A review. *Nat. Prod. Commun.* 11, 1181–1188. doi: 10.1177/1934578X1601100838

Hoot, S. B., Wefferling, K. M., and Wulff, J. A. (2015). Phylogeny and character evolution of Papaveraceae s. l. (Ranunculales). *Syst. Bot.* 40, 474–488. doi: 10.1600/036364415X688718

Hori, K., Yamada, Y., Purwanto, R., Minakuchi, Y., Toyoda, A., Hirakawa, H., et al. (2018). Mining of the uncharacterized cytochrome P450 genes involved in alkaloid biosynthesis in California poppy using a draft genome sequence. *Plant Cell Physiol.* 59, 222–233. doi: 10.1093/pcp/pcx210

Huang, H., Liang, J., Tan, Q., Ou, L., Li, X., Zhong, C., et al. (2021). Insights into triterpene synthesis and unsaturated fatty-acid accumulation provided by chromosomal-level genome analysis of *Akebia trifoliata* subsp. *australis*. *Hortic. Res.* 8, 33. doi: 10.1038/s41438-020-00458-y

Ikezawa, N., Iwasa, K., and Sato, F. (2007). Molecular cloning and characterization of methylenedioxy bridge-forming enzymes involved in stylopine biosynthesis in *Eschscholzia californica*. *FEBS J.* 274, 1019–1035. doi: 10.1111/j.1742-4658.2007.05652.x

Ikezawa, N., Iwasa, K., and Sato, F. (2009). CYP719A subfamily of cytochrome P450 oxygenases and isoquinoline alkaloid biosynthesis in *Eschscholzia californica*. *Plant Cell Rep.* 28, 123–133. doi: 10.1007/s00299-008-0624-8

Inui, T., Tamura, K.-I., Fujii, N., Morishige, T., and Sato, F. (2007). Overexpression of *Coptis japonica* norcoclaurine 6-*O*-methyltransferase overcomes the rate-limiting step in benzylisoquinoline alkaloid biosynthesis in cultured *Eschscholzia californica*. *Plant Cell Physiol.* 48, 252–262. doi: 10.1093/pcp/pcl062

Kato, N., Dubouzet, E., Kokabu, Y., Yoshida, S., Taniguchi, Y., Dubouzet, J. G., et al. (2007). Identification of a WRKY protein as a transcriptional regulator of benzylisoquinoline alkaloid biosynthesis in *Coptis japonica*. *Plant Cell Physiol.* 48, 8–18. doi: 10.1093/pcp/pcl041

Kivivirta, K., Herbert, D., Lange, M., Beuerlein, K., Altmüller, J., and Becker, A. (2019). A protocol for laser microdissection (LMD) followed by transcriptome analysis of plant reproductive tissue in phylogenetically distant angiosperms. *Plant Methods* 15, 151. doi: 10.1186/s13007-019-0536-3

Kukula-Koch, W. (2017). The elevation of LC-ESI-Q-TOF-MS response in the analysis of isoquinoline alkaloids from some Papaveraceae and Berberidaceae representatives. *J. Anal. Methods Chem.* 2017, 8384107. doi: 10.1155/2017/8384107

Laines-Hidalgo, J. I., Muñoz-Sánchez, J. A., Loza-Müller, L., and Vázquez-Flota, F. (2022). An update of the sanguinarine and benzophenanthridine alkaloids' biosynthesis and their applications. *Molecules* 27, 1378. doi: 10.3390/molecules27041378

Lane, A. K., Augustin, M. M., Ayyampalayam, S., Plant, A., Gleissberg, S., Di Stilio, V. S., et al. (2018). Phylogenomic analysis of Ranunculales resolves branching events across the order. *Bot. J. Linn. Soc.* 187, 157–166. doi: 10.1093/botlinnean/boy015

Lange, M., Orashakova, S., Lange, S., Melzer, R., Theißen, G., Smyth, D. R., et al. (2013). The seirena b class floral homeotic mutant of California poppy (*Eschscholzia californica*) reveals a function of the enigmatic PI motif in the formation of specific multimeric MADS domain protein complexes. *Plant Cell* 25, 438–453. doi: 10.1105/tpc.112.105809

Lee, E.-J., Hagel, J. M., and Facchini, P. J. (2013). Role of the phloem in the biochemistry and ecophysiology of benzylisoquinoline alkaloid metabolism. *Front. Plant Sci.* 4. doi: 10.3389/fpls.2013.00182

Leger, E. A., and Rice, K. J. (2007). Assessing the speed and predictability of local adaptation in invasive California poppies (*Eschscholzia californica*). *J. Evol. Biol.* 20, 1090–1103. doi: 10.1111/j.1420-9101.2006.01292.x

Li, Y., Winzer, T., He, Z., and Graham, I. A. (2020). Over 100 million years of enzyme evolution underpinning the production of morphine in the Papaveraceae family of flowering plants. *Plant Commun.* 1, 100029. doi: 10.1016/j.xplc.2020.100029

Liscombe, D. K., Ziegler, J., Schmidt, J., Ammer, C., and Facchini, P. J. (2009). Targeted metabolite and transcript profiling for elucidating enzyme function: isolation of novel *N*-methyltransferases from three benzylisoquinoline alkaloid-producing species. *Plant J.* 60, 729–743. doi: 10.1111/j.1365-313X.2009.03980.x

Liu, X., Liu, Y., Huang, P., Ma, Y., Qing, Z., Tang, Q., et al. (2017). The genome of medicinal plant *Macleaya cordata* provides new insights into benzylisoquinoline alkaloids metabolism. *Mol. Plant* 10, 975–989. doi: 10.1016/j.molp.2017.05.007

Liu, Y., Wang, B., Shu, S., Li, Z., Song, C., Liu, D., et al. (2021). Analysis of the *Coptis chinensis* genome reveals the diversification of protoberberine-type alkaloids. *Nat. Commun.* 12, 3276. doi: 10.1038/s41467-021-23611-0

Lotz, D., Imani, J., Ehlers, K., and Becker, A. (2022). Towards a genetic model organism: an efficient method for stable genetic transformation of *Eschscholzia californica* (Ranunculales). *Plant Cell Tiss Organ Cult.* 149, 823–832. doi: 10.1007/s11240-021-02223-y

Maoka, T., Fujiwara, Y., Hashimoto, K., Takeda, S., Takaragaki, S., and Ida, K. (2000). A new retro-carotenoid from the petals of the Californian yellow poppy *Eschscholzia californica*. *J. Nat. Prod.* 63, 1288–1289. doi: 10.1021/np0000670

Matsushima, Y., Minami, H., Hori, K., and Sato, F. (2012). Pathway engineering of benzylisoquinoline alkaloid biosynthesis in transgenic California poppy cells with ectopic expression of tetrahydroberberine oxidase from *Coptis japonica*. *Plant Biotechnol.* 29, 473–481. doi: 10.5511/plantbiotechnology.12.1101a

Mazuecos-Aguilera, I., Romero-García, A. T., Klodová, B., Honys, D., Fernández-Fernández, M. C., Ben-Menni Schuler, S., et al. (2021). The role of INAPERTURATE POLLEN1 as a pollen aperture factor is conserved in the basal eudicot *Eschscholzia californica* (Papaveraceae). *Front. Plant Sci.* 12. doi: 10.3389/fpls.2021.701286

Meaders, C., Min, Y., Freedberg, K. J., and Kramer, E. (2020). Developmental and molecular characterization of novel staminodes in *Auilegia*. *Ann. Bot.* 126, 231–243. doi: 10.1093/aob/mcaa029

Murai, K., Miyamae, M., Kato, H., Takumi, S., and Ogihara, Y. (2003). WAP1, a wheat APETALA1 homolog, plays a central role in the phase transition from vegetative to reproductive growth. *Plant Cell Phys.* 44, 1255–1265. doi: 10.1093/pcp/pcg171

Orashakova, S., Lange, M., Lange, S., Wege, S., and Becker, A. (2009). The CRABS CLAW ortholog from California poppy (*Eschscholzia californica*, Papaveraceae), EcCRC, is involved in floral meristem termination, gynoecium differentiation and ovule initiation. *Plant J.* 58, 682–693. doi: 10.1111/j.1365-313X.2009.03807.x

Ozber, N., Carr, S. C., Morris, J. S., Liang, S., Watkins, J. L, Caldo, K. M., et al (2022). Alkaloid binding to opium poppy major latex proteins triggers structural modification and functional aggregation. *Nat. Commun.* 13, 6768. doi: 10.1038/s41467-022-34313-6

Pabón-Mora, N., Ambrose, B. A., and Litt, A. (2012). Poppy APETALA1/FRUITFULL orthologs control flowering time, branching, perianth identity, and fruit development. *Plant Physiol.* 158, 1685–1704. doi: 10.1104/pp.111.192104

Park, S.-U., and Facchini, P. J. (2000). Agrobacterium-mediated genetic transformation of California poppy, *Eschscholzia californica* cham., *via* somatic embryogenesis. *Plant Cell Rep.* 19, 1006–1012. doi: 10.1007/s002990000213

Pauli, H. H., and Kutchan, T. M. (1998). Molecular cloning and functional heterologous expression of two alleles encoding (S)-*N*-methylcoclaurine 3'-hydroxylase (CYP80B1), a new methyl jasmonate-inducible cytochrome P-450-dependent mono-oxygenase of benzylisoquinoline alkaloid biosynthesis. *Plant J.* 13, 793–801. doi: 10.1046/j.1365-313x.1998.00085.x

Pollack, A. J., Gong, X., and Pollack, J. R. (2019). A common phytoene synthase mutation underlies white petal varieties of the California poppy. *Sci. Rep.* 9, 11615. doi: 10.1038/s41598-019-48122-3

Prajapati, S., Bajpai, S., and Gupta, M.M. (2001). The floral androcarpel organ (ACO) mutation permits high alkaloid yields in opium poppy, *Papaver somniferum*. *Curr. Sci.* 81, 1109–1112.

Prajapati, S. (2002). The floral androcarpel (ACO) permits high alkaloid yields in opium poppy papaver somiferum. *Curr. Sci.*, 1109–1112.

Purwanto, R., Hori, K., Yamada, Y., and Sato, F. (2017). Unraveling additional O-methylation steps in benzylisoquinoline alkaloid biosynthesis in California poppy (*Eschscholzia californica*). *Plant Cell Physiol.* 58, 1528–1540. doi: 10.1093/pcp/pcx093

Rolland, A., Fleurentin, J., Lanhers, M. C., Younos, C., Misslin, R., Mortier, F., et al. (1991). Behavioural effects of the American traditional plant *Eschscholzia californica*: sedative and anxiolytic properties. *Planta Med.* 57, 212–216. doi: 10.1055/s-2006-960076

Rössner, C., Lotz, D., and Becker, A. (2022). VIGS goes viral: How VIGS transforms our understanding of plant science. *Annu. Rev. Plant Biol.* 73, 703–728. doi: 10.1146/annurev-arplant-102820-020542

Samanani, N., and Facchini, P. J. (2001). Isolation and partial characterization of norcoclaurine synthase, the first committed step in benzylisoquinoline alkaloid biosynthesis, from opium poppy. *Planta* 213, 898–906. doi: 10.1007/s004250100581

Sato, F. (2013). Characterization of plant functions using cultured plant cells, and biotechnological applications. *Biosci. Biotechnol. Biochem.* 77, 1–9. doi: 10.1271/bbb.120759

Sato, F. (2020). "Plant alkaloid engineering," in *Comprehensive natural products III* (Oxford, UK: Elsevier), 700–755. doi: 10.1016/B978-0-12-409547-2.14696-7

Sato, F., Hashimoto, T., Hachiya, A., Tamura, K., Choi, K. B., Morishige, T., et al. (2001). Metabolic engineering of plant alkaloid biosynthesis. *Proc. Natl. Acad. Sci. U.S.A.* 98, 367–372. doi: 10.1073/pnas.98.1.367

Schmeller, T., Latz-Brüning, B., and Wink, M. (1997). Biochemical activities of berberine, palmatine and sanguinarine mediating chemical defense against microorganisms and herbivores. *Phytochemistry* 44, 257–266. doi: 10.1016/S0031-9422(96)00545-6

Schramm, A., Saxena, P., Chlebek, J., Cahlíková, L., Baburin, I., Hering, S., et al. (2014). Natural products as potential human ether-a-go-go-related gene channel inhibitors - screening of plant-derived alkaloids. *Planta Med.* 80, 740–746. doi: 10.1055/s-0034-1368590

Scofield, S., Dewitte, W., and Murray, J. A. H. (2007). The *KNOX* gene *SHOOT MERISTEMLESS* is required for the development of reproductive meristematic tissues in *Arabidopsis*. *Plant J.* 50, 767–781. doi: 10.1111/j.1365-313X.2007.03095.x

Singh, S. K., Gupta, S., Ahmad, N., Shukla, A. K., Shasany, A. K., Lal, R. K., et al. (2017). Variability and heritability studies in floral homeotic mutants of *Papaver somniferum* l. *Ind. Crops Prod.* 95, 276–285. doi: 10.1016/j.indcrop.2016.10.032

Stammler, A., Meyer, S. S., Plant, A. R., Townsley, B. T., Becker, A., and Gleissberg, S. (2013). Duplicated *STM*-like *KNOX I* genes act in floral meristem activity in *Eschscholzia californica* (Papaveraceae). *Dev. Genes Evol.* 223, 289–301. doi: 10.1007/s00427-013-0446-8

Sun, Y., Deng, T., Zhang, A., Moore, M. J., Landis, J. B., Lin, N., et al. (2020). Genome sequencing of the endangered *Kingdonia uniflora* (Circaeasteraceae, Ranunculales) reveals potential mechanisms of evolutionary specialization. *iScience* 23, 101124. doi: 10.1016/j.isci.2020.101124

Takemura, T., Chow, Y., Todokoro, T., Okamoto, T., and Sato, F. (2010). Over-expression of rate-limiting enzymes to improve alkaloid productivity. *Methods Mol. Biol.* 643, 95–109. doi: 10.1007/978-1-60761-723-5_7

Takemura, T., Ikezawa, N., Iwasa, K., and Sato, F. (2013). Molecular cloning and characterization of a cytochrome P450 in sanguinarine biosynthesis from *Eschscholzia californica* cells. *Phytochemistry* 91, 100–108. doi: 10.1016/j.phytochem.2012.02.013

Tanahashi, T., and Zenk, M. H. (1990). Elicitor induction and characterization of microsomal protopine-6-hydroxylase, the central enzyme in benzophenanthridine alkaloid biosynthesis. *Phytochemistry* 29, 1113–1122. doi: 10.1016/0031-9422(90)85414-B

Véliz, D., Gauci, R., and Bustamante, R. O. (2012). Characterization of novel microsatellite markers for *Eschscholzia californica* (Papaveraceae), an invasive species in central Chile. *Am. J. Bot.* 99, e366–e368. doi: 10.3732/ajb.1200076

Vogel, M., Lawson, M., Sippl, W., Conarad, U., and Roos, W. (2010). Structure and mechanism of sanguinarine reductase, an enzyme of alkaloid detoxification. *J. Biol. Chem.* 285, 18397–18406. doi: 10.1074/jbc.M109.088989

Wege, S., Scholz, A., Gleissberg, S., and Becker, A. (2007). Highly efficient virus-induced gene silencing (VIGS) in California poppy (*Eschscholzia californica*): an evaluation of VIGS as a strategy to obtain functional data from non-model plants. *Ann. Bot.* 100, 641–649. doi: 10.1093/aob/mcm118

Wilts, B. D., Rudall, P. J., Moyroud, E., Gregory, T., Ogawa, Y., Vignolini, S., et al. (2018). Ultrastructure and optics of the prism-like petal epidermal cells of *Eschscholzia californica* (California poppy). *New Phytol.* 219, 1124–1133. doi: 10.1111/nph.15229

Xie, J., Zhao, H., Li, K., Zhang, R., Jiang, Y., Wang, M., et al. (2020). A chromosome-scale reference genome of *Aquilegia oxysepala* var. *kansuensis*. *Hortic. Res.* 7, 113. doi: 10.1038/s41438-020-0328-y

Xu, Z., Li, Z., Ren, F., Gao, R., Wang, Z., Zhang, J., et al. (2022). The genome of *Corydalis* reveals the evolution of benzylisoquinoline alkaloid biosynthesis in Ranunculales. *Plant J.* 111, 217–230. doi: 10.1111/tpj.15788

Yamada, Y., Hirakawa, H., Hori, K., Minakuchi, Y., Toyoda, A., Shitan, N., et al. (2021a). Comparative analysis using the draft genome sequence of California poppy (*Eschscholzia californica*) for exploring the candidate genes involved in benzylisoquinoline alkaloid biosynthesis. *Biosci. Biotechnol. Biochem.* 85, 851–859. doi: 10.1093/bbb/zbaa091

Yamada, Y., Kokabu, Y., Chaki, K., Yoshimoto, T., Ohgaki, M., Yoshida, S., et al. (2011a). Isoquinoline alkaloid biosynthesis is regulated by a unique bHLH-type transcription factor in *Coptis japonica*. *Plant Cell Physiol.* 52, 1131–1141. doi: 10.1093/pcp/pcr062

Yamada, Y., Koyama, T., and Sato, F. (2011b). Basic helix-loop-helix transcription factors and regulation of alkaloid biosynthesis. *Plant Signal Behav.* 6, 1627–1630. doi: 10.4161/psb.6.11.17599

Yamada, Y., Motomura, Y., and Sato, F. (2015). CjbHLH1 homologs regulate sanguinarine biosynthesis in *Eschscholzia californica* cells. *Plant Cell Physiol.* 56, 1019–1030. doi: 10.1093/pcp/pcv027

Yamada, Y., Nishida, S., Shitan, N., and Sato, F. (2020). Genome-wide identification of AP2/ERF transcription factor-encoding genes in California poppy (*Eschscholzia californica*) and their expression profiles in response to methyl jasmonate. *Sci. Rep.* 10, 18066. doi: 10.1038/s41598-020-75069-7

Yamada, Y., Nishida, S., Shitan, N., and Sato, F. (2021b). Genome-wide profiling of *WRKY* genes involved in benzylisoquinoline alkaloid biosynthesis in California poppy (*Eschscholzia californica*). *Front. Plant Sci.* 12. doi: 10.3389/fpls.2021.699326

Yamada, Y., and Sato, F. (2021). Transcription factors in alkaloid engineering. *Biomolecules* 11, 1719. doi: 10.3390/biom11111719

Yamada, Y., Shimada, T., Motomura, Y., and Sato, F. (2017). Modulation of benzylisoquinoline alkaloid biosynthesis by heterologous expression of CjWRKY1 in *Eschscholzia californica* cells. *PloS One* 12, e0186953. doi: 10.1371/journal.pone.0186953

Yang, X., Gao, S., Guo, L., Wang, B., Jia, Y., Zhou, J., et al. (2021). Three chromosome-scale *Papaver* genomes reveal punctuated patchwork evolution of the morphinan and noscapine biosynthesis pathway. *Nat. Commun.* 12, 6030. doi: 10.1038/s41467-021-26330-8

Yellina, A. L., Orashakova, S., Lange, S., Erdmann, R., Leebens-Mack, J., and Becker, A. (2010). Floral homeotic c function genes repress specific b function genes in the carpel whorl of the basal eudicot California poppy (*Eschscholzia californica*). *Evodevo* 1, 13. doi: 10.1186/2041-9139-1-13

Zahn, L. M., Ma, X., Altman, N. S., Zhang, Q., Wall, P. K., Tian, D., et al. (2010). Comparative transcriptomics among floral organs of the basal eudicot *Eschscholzia californica* as reference for floral evolutionary developmental studies. *Genome Biol.* 11, R101. doi: 10.1186/gb-2010-11-10-r101

Zhang, R., Fu, X., Zhao, C., Cheng, J., Liao, H., Wang, P., et al. (2020). Identification of the key regulatory genes involved in elaborate petal development and specialized character formation in *Nigella damascena* (Ranunculaceae). *Plant Cell* 32, 3095–3112. doi: 10.1105/tpc.20.00330

Zhao, Y., Pfannebecker, K., Dommes, A. B., Hidalgo, O., Becker, A., and Elomaa, P. (2018). Evolutionary diversification of *CYC/TB1*-like TCP homologs and their recruitment for the control of branching and floral morphology in Papaveraceae (basal eudicots). *New Phytol.* 220, 317–331. doi: 10.1111/nph.15289

Zhao, Z. M., Shang, X. F., Lawoe, R. K., Liu, Y. Q., Zhou, R., Sun, Y. F., et al. (2019). Anti-phytopathogenic activity and the possible mechanisms of action of isoquinoline alkaloid sanguinarine. *Pest Biochem. Physiol.* 159, 51–58. doi: 10.1016/j.pestbp.2019.05.015

Zhou, J., Hunter, D. A., Lewis, D. H., McManus, M. T., and Zhang, H. (2018). Insights into carotenoid accumulation using VIGS to block different steps of carotenoid biosynthesis in petals of California poppy. *Plant Cell Rep.* 37, 1311–1323. doi: 10.1007/s00299-018-2314-5

frontiers | Frontiers in Plant Science

TYPE Review
PUBLISHED 08 March 2023
DOI 10.3389/fpls.2023.1108027

OPEN ACCESS

EDITED BY
Verónica S. Di Stilio,
University of Washington, United States

REVIEWED BY
Eduardo Flores-Sandoval,
Monash University, Australia
Jeffrey Graham Duckett,
Natural History Museum, United Kingdom

*CORRESPONDENCE
Eftychios Frangedakis
efragedakis@gmail.com
Péter Szövényi
Peter.szoevenyi@uzh.ch

SPECIALTY SECTION
This article was submitted to Plant Development and EvoDevo, a section of the journal Frontiers in Plant Science

RECEIVED 25 November 2022
ACCEPTED 13 February 2023
PUBLISHED 08 March 2023

CITATION
Frangedakis E, Marron AO, Waller M, Neubauer A, Tse SW, Yue Y, Ruaud S, Waser L, Sakakibara K and Szövényi P (2023) What can hornworts teach us? *Front. Plant Sci.* 14:1108027. doi: 10.3389/fpls.2023.1108027

What can hornworts teach us?

Eftychios Frangedakis[1]*, Alan O. Marron[1], Manuel Waller[2,3], Anna Neubauer[2,3], Sze Wai Tse[1], Yuling Yue[2,3], Stephanie Ruaud[2,3], Lucas Waser[2,3,4], Keiko Sakakibara[5] and Péter Szövényi[2,3]*

[1]Department of Plant Sciences, University of Cambridge, Cambridge, United Kingdom, [2]Department of Systematic and Evolutionary Botany, University of Zurich, Zurich, Switzerland, [3]Zurich-Basel Plant Science Center, Zurich, Switzerland, [4]Department of Plant and Microbial Biology, University of Zürich, Zurich, Switzerland, [5]Department of Life Science, Rikkyo University, Tokyo, Japan

The hornworts are a small group of land plants, consisting of only 11 families and approximately 220 species. Despite their small size as a group, their phylogenetic position and unique biology are of great importance. Hornworts, together with mosses and liverworts, form the monophyletic group of bryophytes that is sister to all other land plants (Tracheophytes). It is only recently that hornworts became amenable to experimental investigation with the establishment of *Anthoceros agrestis* as a model system. In this perspective, we summarize the recent advances in the development of *A. agrestis* as an experimental system and compare it with other plant model systems. We also discuss how *A. agrestis* can help to further research in comparative developmental studies across land plants and to solve key questions of plant biology associated with the colonization of the terrestrial environment. Finally, we explore the significance of *A. agrestis* in crop improvement and synthetic biology applications in general.

KEYWORDS

terrestrialization of plants, land plants, polyplastidy, pyrenoid, RNA editing, evo-devo, plant-cyanobacteria symbiosis, plant-mycorrhizal symbiosis

1 Introduction

As indicated by biochemical, morphological and molecular data, land plants evolved from aquatic green algae (Karol, 2001; Lewis and McCourt, 2004; Becker and Marin, 2009) around 500 million years ago. Land plants diverged into seven main groups: liverworts, mosses, hornworts, lycophytes, ferns, gymnosperms and angiosperms (Leebens-Mack et al., 2019). Our efforts to understand key events in the evolution of land plants are hindered by the fact that the majority of tractable land plant experimental systems belong to angiosperms (Szövényi et al., 2021). A few tractable non-seed plant models are available but only four are well-established: the fern *Ceratopteris richardii* (Plackett et al., 2015), the liverwort *Marchantia polymorpha* (Bowman et al., 2022), the moss *Physcomitrium patens* (Rensing et al., 2020) and very recently the hornwort *Anthoceros agrestis* (Szövényi et al., 2015; Frangedakis et al., 2021b). Liverworts, mosses and hornworts form the monophyletic group of bryophytes, a deeply divergent lineage of plants. The recent development of a

hornwort model, *A. agrestis*, makes comparative studies employing model systems from each of these deeply divergent clades feasible for the first time. This can eventually provide a more accurate insight into major events of land plant evolution (Dolan, 2009; Donoghue et al., 2021; Frangedakis et al., 2021a). Importantly, the development of a transformation technique for *A. agrestis*, and for three additional species (Waller et al., 2022), paves the way for detailed molecular and genetic studies to elucidate hornwort biology. Furthermore, it opens the way to experimentally study the enigmatic features of hornworts that are absent or rarely occur in other land plants, such as the single algal-like chloroplast per cell or the basal sporophyte meristem (Villarreal and Renzaglia, 2015; Frangedakis et al., 2021a). In this review we first provide an overview of the recently developed tools that enable experimental work on hornworts. We then highlight the key aspects of hornwort biology and their significance for general plant biology, applied plant science and synthetic biology. Finally, we discuss the challenges that need to be tackled in the future.

2 The significance of hornworts in understanding key questions of land plant evolution

Current phylogenetic evidence strongly supports the idea that land plants comprise two major monophyletic clades, the vascular plants (tracheophytes) and the bryophytes (Puttick et al., 2018; Leebens-Mack et al., 2019; Harris et al., 2020; Su et al., 2021; Harris et al., 2022). There is also accumulating evidence that within bryophytes, the hornworts are sister to the monophyletic clade of mosses and liverworts (Setaphytes) with a divergence time of approximately 400 MYA (Harrison and Morris, 2018; Puttick et al., 2018; Harris et al., 2022). This new phylogenetic backbone is in stark contrast to the traditional view that treated bryophytes as a paraphyletic grade of mosses, liverworts and hornworts (Buck et al., 2008). Importantly it has also revolutionized the way we think about character evolution in land plants. Traditional evolutionary hypotheses suggested that the common ancestor of land plants had a simple morphology, probably similar to extant bryophytes (Buck et al., 2008; Gerrienne et al., 2016). However, the discovery of bryophyte monophyly makes statements about the complexity and nature of the land plant common ancestor as well as character evolution in land plants challenging (Puttick et al., 2018; Harris et al., 2022). The monophyly of bryophytes and vascular plants implies that the land plant common ancestor could have had a haploid-dominant, a diploid-dominant, or an isomorphic (haploid and diploid phases with comparable complexity) life cycle. Therefore, the haploid-dominant life cycle and the organizational level of bryophytes may not be the ancestral state and could be the result of a reductive evolutionary process (Bowman et al., 2016; Chater et al., 2016; Harris et al., 2020; Harris et al., 2022). This is supported by recent findings indicating that the evolution of bryophytes might have been accompanied by massive gene losses after the split from the common ancestor of land plants (Clark et al., 2022; Harris et al., 2022). Furthermore, the new phylogenetic backbone of bryophytes combined with both genomic and evo-devo studies also imply that various complex traits could have been gained and lost among the three deeply divergent clades of bryophytes (Li et al., 2020; Rensing, 2020; Clark et al., 2022; Harris et al., 2022). Therefore, it is important to have at least one tractable model species for each major lineage of bryophytes. This will help to recognize and study the evolution of traits shared by most bryophyte groups and vascular plants, identify ancestral traits only retained by a specific group of bryophytes, as well as traits representing bryophyte-specific innovations. Such comparative analyses became increasingly possible with the establishment of the new hornwort model *A. agrestis.*

3 The hornwort model *Anthoceros agrestis*

For hornworts, *A. agrestis* (Figure 1A) has recently emerged as the model experimental system, with two geographic isolates (Oxford and Bonn) being available (Szövényi et al., 2015). Both *A. agrestis* isolates are derived from a single spore and can be routinely grown axenically. High quality genome assemblies are available (Li et al., 2020) and an efficient *Agrobacterium*-mediated transformation method, using regenerating thallus fragments, has been developed (Frangedakis et al., 2021b; Waller et al., 2022). Up to 100 and 40 stable transgenic lines can be obtained from 0.2 g of tissue for the Oxford and Bonn isolate, respectively. Protoplast isolation and transient transformation protocols are also available (Neubauer et al., 2022). Finally, a new growth medium for *A. agrestis* has been developed, that yields four times more tissue mass compared to the traditionally used KNOP medium (Gunadi et al., 2022). For cloning, the OpenPlant toolkit (Sauret-Güeto et al., 2020) originally developed for *M. polymorpha* has been adopted. The OpenPlant kit is a Golden Gate Cloning method, based on Type IIS restriction enzymes, that enables the fast generation of complex DNA circuits from standardized basic DNA parts (e.g., promoters, coding sequences and terminators).

In addition to the widely used CaMV 35S promoter, two native constitutive promoters have been developed for *A. agrestis*, the promoter regions of the *Elongation Factor 1 Alpha (Ef1a)* and the *Gamma Tonoplast Intrinsic Protein 1;1 (Tip1;1)* genes (Frangedakis et al., 2021b; Waller et al., 2022). Hygromycin is used as an antibiotic selection marker and chlorsulfuron as a herbicide selection marker. Four fluorescent proteins (eGFP, mVenus, mTurquoise2 and mScarlet) can be expressed successfully in *A. agrestis* without toxic effects. A set of targeting peptides for subcellular localization into the chloroplast, mitochondria, Golgi, Endoplasmic reticulum, peroxisomes, nucleus, cytoskeleton and the plasma membrane are also available (Waller et al., 2022). The palette of hornwort species that can be genetically modified was recently expanded by the addition of *Anthoceros punctatus*, which has been used as a model for plant symbiosis with cyanobacteria, *Leiosporoceros dussii*, which is the sister to all other hornworts and *Phaeoceros carolinianus* (Waller et al., 2022).

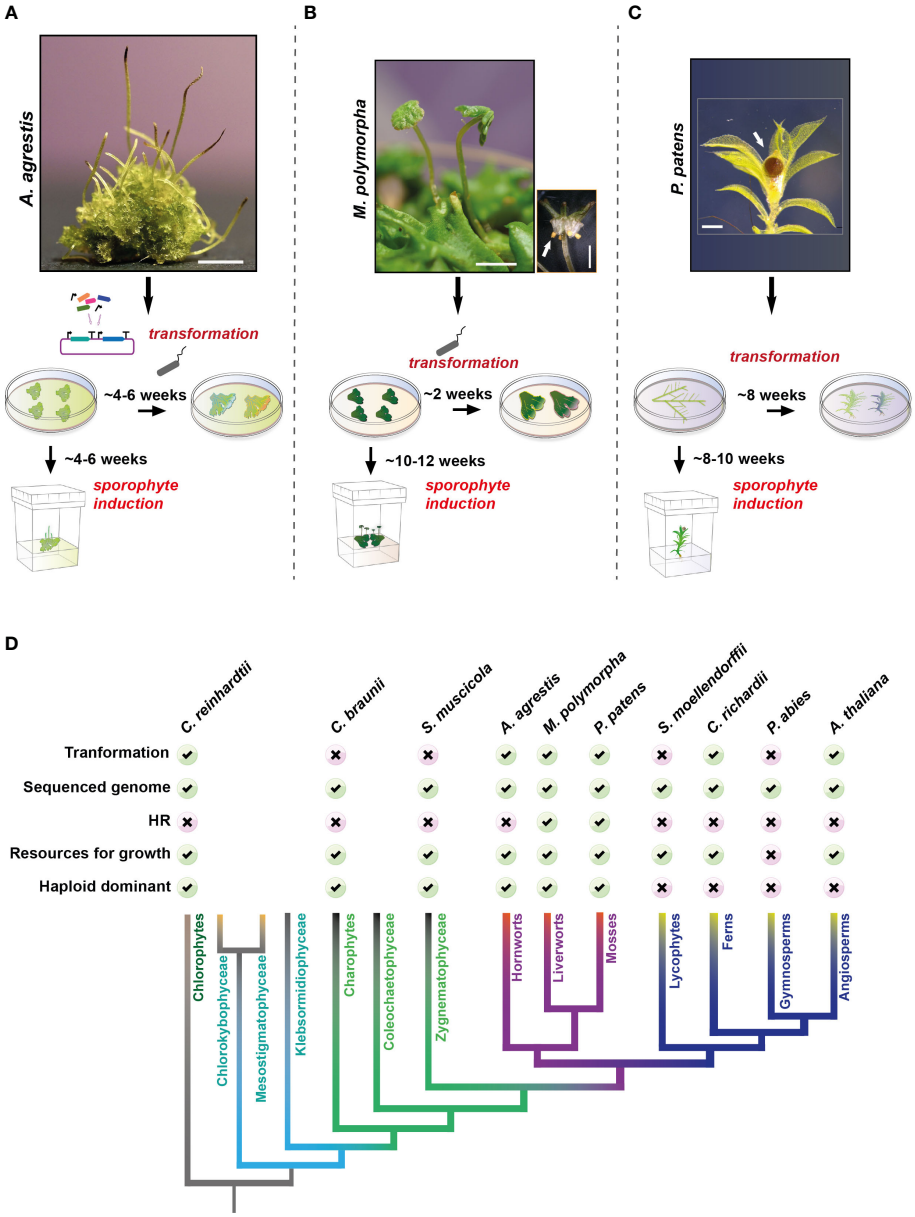

FIGURE 1
Anthoceros agrestis compared to other model plants. **(A–C)**: Top: Representative images of *Anthoceros agrestis* **(A)**, *Marchantia polymorpha* **(B)** and *Physcomitrium patens* **(C)** gametophytes and sporophytes. Bottom: Comparison of time required to obtain stable transgenic plants and sporophyte induction. Scale bars A: 2 mm, B: 2 mm, bottom right 1 mm and C: 0.5 mm. In **(B, C)** white arrow indicates sporophyte. **(D)** Phylogenetic relationships of the major lineages of land plants illustrating the monophyly of bryophytes and the monophyly of lycophytes, ferns, gymnosperms, and angiosperms (de Vries et al., 2016; Li et al., 2020). Comparison of model systems for key phylogenetic clades is shown on top.

4 *A. agrestis* compared to other model plants

A. agrestis like any other bryophyte, has a gametophyte/haploid dominant life cycle (Buck et al., 2008). Axenic tissue propagation is simple and achieved by careful fragmentation of thallus tissue (Szövényi et al., 2015), however, *A. agrestis* does not tolerate high light intensities (Frangedakis et al., 2021b). The thallus tissue can be stored at 4° C for up to two months. Sporophyte induction is more efficient in the case of the Bonn isolate compared to the Oxford isolate and it takes about 6 weeks for mature sporophytes to develop (Figure 1A). Mature sporophytes can be removed and stored at 4° C for up to six months. In *A. agrestis* genetic studies are made easier, compared to angiosperms, by its small gene families, lack of redundancy and a dominant haploid phase in its life cycle (Szövényi, 2016; Li et al., 2020). For transformation, thallus fragments are co-cultivated with *Agrobacterium* and successful transformants are visible within 4-6 weeks after antibiotic/herbicide selection. Finally, *A. agrestis* provides an accessible platform for live-tissue microscopy where cell division can be easily tracked. CRISPR/cas9 genome editing technology is currently under development.

Model systems have been available for many years for the other two bryophyte groups, liverworts and mosses. For liverworts, *M. polymorpha* is a well-established model species (Figure 1B). *Agrobacterium* based transformation techniques are available and stable transformants can be obtained in approximately two weeks (Ishizaki et al., 2008; Kubota et al., 2013). The genome of *M. polymorpha* is available (Bowman et al., 2017; Diop et al., 2020; Montgomery et al., 2020) including extensive transcriptomic resources that are currently being improved (Kawamura et al., 2022). Homologous recombination is also feasible in *M. polymorpha*, however, it is not as efficient as in the moss *P. patens* (Ishizaki et al., 2013). It takes up to 12 weeks for mature sporophytes to develop. CRISPR/cas9 technology for genome editing is also well established (Sugano et al., 2014; Sugano et al., 2018). Transformation protocols are also available for two other liverworts: *Marchantia palacea*, commonly used for mycorrhizal symbiosis studies (Rich et al., 2021), and *Riccia fluitans* (Althoff and Zachgo, 2020).

For mosses, *P. patens* has been established as a model in 1924 by Wettstein (Wettstein, 1924) representing one of the oldest land plant model systems with the most extensive genomic resources among bryophytes (Figure 1C). Effective methods for *in vitro* propagation, protoplast-based, and *Agrobacterium*-mediated genetic transformations are available (Kammerer and Cove, 1996; Schaefer and Zrÿd, 1997; Cho et al., 1999; Li et al., 2010). Transgenic lines can be obtained in approximately 12 weeks. *P. patens* is unique for its ability to undergo homologous recombination with an efficiency similar to that of yeast (Schaefer and Zrÿd, 1997). It takes up to 10 weeks for mature sporophytes to develop, which is longer compared to *A. agrestis*. CRISPR/cas9 technology for genome editing is also available (Mallett et al., 2019; Guyon-Debast et al., 2021).

Other non-seed land plant model systems include lycophytes and ferns (Figure 1D). For lycophytes *Selaginella moellendorffii* has been proposed as a model and its genome was sequenced in 2011 (Banks et al., 2011). However, the lack of a transformation technique for S. *moellendorffii* and the length of time needed to complete its life cycle are major hurdles in genetic studies. For ferns, *C. richardii* was developed as a model system in 1960 (Hickok et al., 1987). *C. richardii* has a short life cycle under laboratory conditions, biolistic and *Agrobacterium* based transformation techniques (Plackett et al., 2014; Bui et al., 2015) are available and its genome was sequenced recently (Marchant et al., 2022). No CRISPR/cas9 protocol is available for editing *C. richardii*`s genome.

For angiosperms *Arabidopsis thaliana* is the system of choice (Figure 1D). *Agrobacterium* based transformation techniques are available and a high-quality reference genome is publicly available (http://www.arabidopsisbook.org/ and *Arabidopsis* Genome Initiative, 2000). Its life cycle can be completed within 6-8 weeks and an extensive set of molecular tools and genome editing techniques have been available for a long time. Several gymnosperm genomes are available (Rigault et al., 2011; Nystedt et al., 2013; Liu et al., 2021), however, their size and the length of their life cycles are major obstacles for laboratory-based experimentation.

Multiple model systems are available for green algae (Figure 1D). The most frequently used system is the unicellular green alga *Chlamydomonas reinhardtii* for which a genome assembly (Merchant et al., 2007) and efficient genetic transformation methods are available (Mussgnug, 2015). *Chara braunii* (Nishiyama et al., 2018) and *Spirogloea muscicola* (Cheng et al., 2019) have been proposed as multicellular green algae models, however despite their genomes being sequenced, genetic manipulation is still challenging.

Altogether, the hornwort model system performs well in comparison to other plant model (Figure 1D) systems in terms of ease of growth in laboratory conditions, life-cycle length and transformation efficiency. Nevertheless, important molecular tools, routinely used in the other two land plant models, are still under development.

5 The unique biology of hornworts

Hornworts have a handful of unique traits absent from other bryophytes or even any other land plants. The unique traits of hornworts include but are not restricted to (Figures 2, 3A): (i) zygote and sporophyte development, (ii) a single chloroplast per cell, (iii) high-rates of RNA-editing and reverse editing, (iv) a pyrenoid based carbon concentrating mechanism, and (v) symbiotic relationships with arbuscular mycorrhiza fungi and cyanobacteria.

Hornworts comprise 11 families/genera which include: *Leiosporoceros, Anthoceros*, *Folioceros*, *Paraphymatoceros*, *Phaeoceros, Notothylas*, *Phymatoceros*, *Phaeomegaceros*, *Nothoceros*, *Megaceros* and *Dendroceros* (Figure 3B) (Villarreal and Renner, 2012). Interestingly, some of the unique hornwort characters vary even between different families. For example, the number of chloroplasts per cell or the presence of pyrenoids, stomata and arbuscular mycorrhizal symbiosis (Villarreal and Renner, 2012; Desiro et al., 2013; Frangedakis et al., 2021a; MacLeod et al., 2022) (Figure 3B). Thus, comparative studies within hornworts can help identify the genetic mechanisms that control these characters.

5.1 Zygote and sporophyte development

The orientation of the first zygote division in hornworts is longitudinal compared to the longitudinal axis of the archegonium unlike other land plants, with the exception of leptosporangiate ferns (Johnson et al., 2009) (Figures 2A, 3A). The functional significance of this unique hornwort feature is unclear. It is hypothesized that the longitudinal division is a consequence of anatomical and mechanistic constraints (Shaw and Renzaglia, 2004). Unlike in mosses and liverworts where archegonia are superficial, hornwort archegonia and the zygotes are sunken in the gametophyte thallus and surrounded by gametophyte tissues. This mechanical constraint may have led to changing direction of the first division plane in hornworts and have likely independently evolved in leptosporangiate ferns (Johnson et al., 2009). Nevertheless, this hypothesis needs further testing and the genetic networks determining the first division plane must be thoroughly investigated. A potential component of such networks is the *A. agrestis* single *FLORICAULA/LEAFY (FLO/LFY)* gene, homologs of

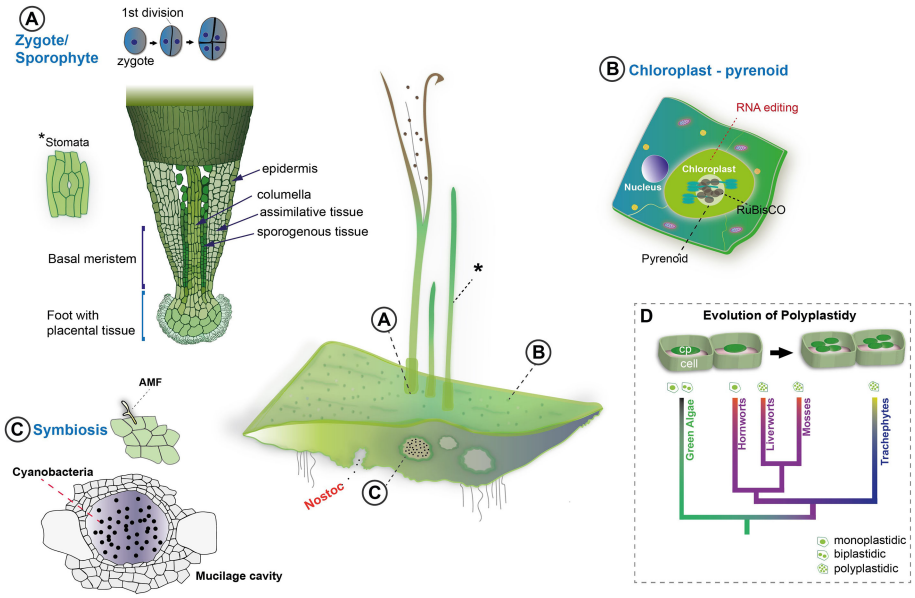

FIGURE 2
Unique biological traits of hornworts. Center: *Anthoceros agrestis* forms simple thallus tissues. Sporophytes grow on the gametophyte from thallus embedded zygotes, the first division of which is longitudinal. Stomata (indicated with "*") are present in the sporophyte **(A)**. Thallus cells have a single chloroplast that contains a pyrenoid and exhibits high levels of RNA editing **(B)**. The body of the thallus features mucilage cavities which play a role in cyanobacteria symbiosis **(C)**. Mucilage clefts are the entry point for *Nostoc* cyanobacteria. Arbuscular mycorrhizal fungi symbiosis can also be established in the thallus **(D)**. In general, *A. agrestis* thanks to its unique traits, can help to shed light on the evolution of key land plant innovations such as the evolution of polyplastidy (cp: chloroplast).

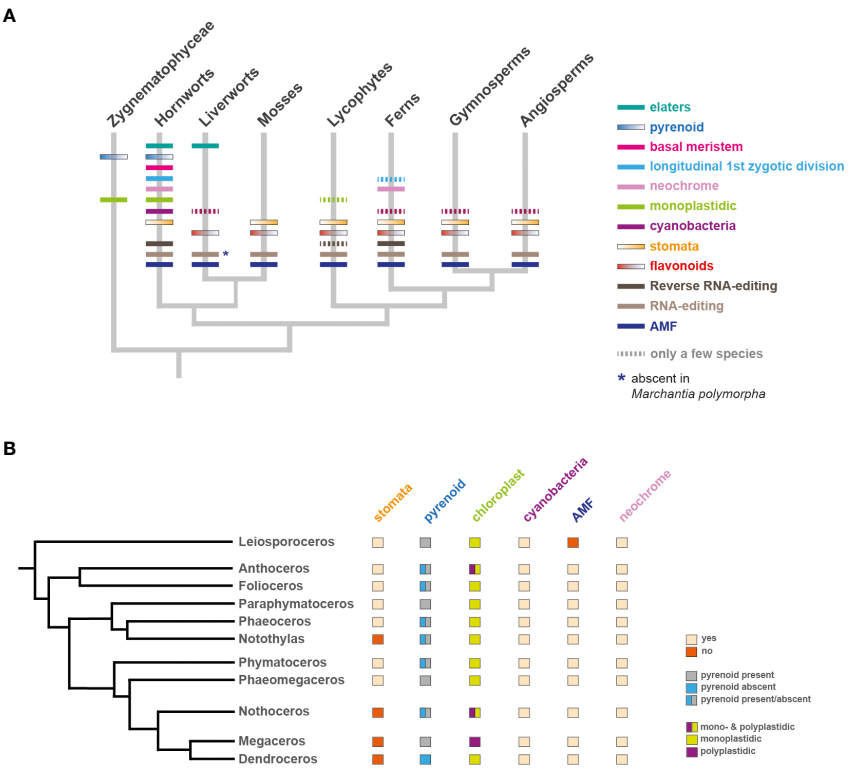

FIGURE 3
Occurrence of unique and evolutionary significant hornwort characters across land plants and within hornworts. **(A)** Land plant phylogeny (Li et al., 2020). The presence and/or absence of various traits is indicated with colored bars on corresponding tree branches. Zygnematophyceae are also biplastidic. **(B)** Phylogeny of hornworts based on (Villarreal and Renner, 2012). The presence and/or absence of various traits is indicated next to each genera name. Exception: stomata absent in *Folioceros incurvus*.

which have been shown to be necessary for the first zygotic division in *P. patens* (Maizel, 2005; Tanahashi et al., 2005).

Hornwort sporophytes are also unique amongst other bryophytes (Figures 4A–C) and land plants in general. A remarkable feature of the hornwort sporophyte is that most of it is formed by a multicellular basal meristem (Ligrone et al., 2012a) (Figures 2A, 3A, 4D). By contrast, the sporophyte of *P. patens* develops from an apical cell, a transient intercalary meristem, and various secondary meristems (Bower, 1935; Smith, 1955; Wardlaw, 1955; Kato and Akiyama, 2005; Lopez-Obando et al., 2022). Sporophyte tissues of the liverwort *M. polymorpha* do not contain a well-defined meristematic region (Ligrone et al., 2012a; Szövényi et al., 2019). The hornwort multicellular meristem is located at the base of the sporophyte, just above the foot connecting the sporophyte to the gametophyte, and continuously produces cells upwards that differentiate into the various cell types of the sporophyte (Bartlett, 1928; Ligrone et al., 2012a; Field et al., 2015). More specifically, the internal structure of the basal meristem resembles that of the root apical meristem of vascular plants (Ligrone et al., 2012a; Uchida and Torii, 2019; Dubrovsky and Vissenberg, 2021). Cells derived from the basal meristem are arranged in well-defined rows (Figure 2A, circles in 3D view) that give rise to the various tissue types of the sporophyte: the columella, the sporogenous tissue, the assimilative tissue and the epidermis. Each row consists of basally arranged meristematic cells that continuously differentiate into the major tissue types towards the apex of the sporophyte. Very little is known about the molecular mechanisms governing the development of this meristem and its evolutionary homology to the multicellular meristems of land plants is highly debated (Ligrone et al., 2012a; Ligrone et al., 2012b; Harrison and Morris, 2018; Fouracre and Harrison, 2022). Nevertheless, the continuous differentiation gradient present along

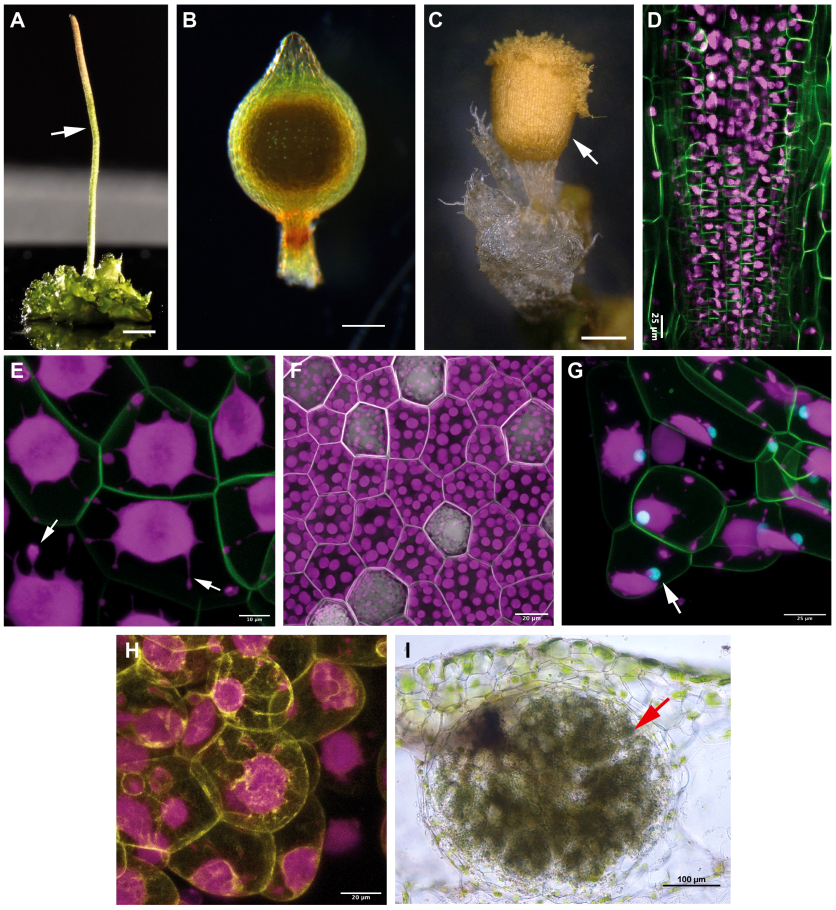

FIGURE 4
Sporophyte morphology, chloroplast and cellular features, and symbiotic interaction of the three bryophyte models. **(A)** *Anthoceros agrestis* Bonn gametophyte bearing a single sporophyte (indicated with white arrow). Scale bar 1.5 mm. **(B)** *Physcomitrium patens* sporophyte. Scale bar 200 µm. **(C)** *Marchantia polymorpha* sporophyte. Scale bar 500 µm. **(D)** Multiphoton microscopy images (whole mount) of the sporophyte base of *A. agrestis* Bonn expressing eGFP targeted to the plasma membrane. eGFP signal is visible in overlying cell rows of the basal meristem. Chloroplast autofluorescence in magenta. Scale bar: 25 µm. **(E)** Confocal microscopy image of *A. agrestis* Bonn gametophyte expressing eGFP targeted to the plasma membrane. Chloroplast autofluorescence in magenta. Stromules indicated with arrows. Scale bar: 25 µm. **(F)** Confocal microscopy image of *M. polymorpha* gemma with plasma membrane marked with mScarlet. Scale bar: 25 µm. **(G)** Confocal image of *A. agrestis* Oxford gametophyte tissue expressing eGFP targeted to the plasma membrane and mTurquoise2 targeted to the nucleus (indicated with arrow). Chloroplast autofluorescence in magenta. Scale bar: 50 µm. **(H)** Confocal microscopy image of *A. agrestis* Oxford with the actin labelled with mVenus. Scale bar: 20 µm. **(I)** Hand sections of *Anthoceros punctatus* thallus showing cavities colonized by cyanobacteria (indicated with arrow). Scale bar: 100 µm. Image provided by Masaki Shimamura.

the longitudinal axis of the sporophyte provides an excellent model to understand conserved features of cell fate determination across bryophytes and vascular plants, and potentially the origin of multicellular meristems in vascular plants.

The genetic network underlying the establishment and maintenance of the hornwort sporophyte meristem is poorly understood. *KNOTTED1-LIKE HOMEOBOX (KNOX1)* genes known to be critical for sporophyte development in *P. patens* (Sakakibara et al., 2008) and embryo formation in liverworts (Dierschke et al., 2021) are not present in the genome of *A. agrestis* (Li et al., 2020). While *KNOX1* genes are missing from the *A. agrestis* genome, a single *KNOX2* gene is present and preferentially expressed during sporophyte development. It can be speculated that the hornwort *KNOX2* gene may be able to compensate for the function of the absent *KNOX1* gene, however functional verification is needed to confirm such a hypothesis.

In angiosperms, a negative feedback pathway involving *CLAVATA* genes and the *WUSCHEL* transcription factor maintains the stem-cell population in the shoot apical meristem (SAM). In *A. thaliana* there are three *CLAVATA* genes, *CLV1*, *CLV2* and *CLV3*. *CLV3* encodes a small secreted protein and is expressed in the L1 and L2 layers of the SAM central zone while *CLV1* and *CLV2* genes encode receptor-like proteins and are expressed mainly in the L3 (Clark et al., 1997; Jeong et al., 1999). CLV3 interacts with CLV1 and CLV2 (Müller et al., 2008) to limit the *WUS* expression zone and consequently to limit the size of the stem cell/central zone (Reddy and Meyerowitz, 2005). Finally, *WUS* positively regulates *CLV3* activity, generating a feedback loop that stabilizes stem cell activity in the SAM. CLAVATA3/Embryo Surrounding Region-Related (CLE) peptides have been shown to promote the formation of gametophyte apical cells in *M. polymorpha* (Hirakawa et al., 2020; Hirakawa, 2022) and to antagonize stem cell formation in *P. patens* gametophyte (Cammarata et al., 2022). More recently, it has been shown that some CLE peptides (CLE40 in *Arabidopsis*) also have the capacity to promote meristematic activity in angiosperms (Schlegel et al., 2021), contrary to their canonical role antagonizing the meristem *via* WUSCHEL repression. Thus, experimental studies of CLE peptide/CLV receptors in hornworts will further clarify whether CLE peptides repressed or promoted meristematic activity in the land plant ancestor.

YABBY transcription factors have been shown to be involved in the regulation of lateral organ development, the proper maintenance of the SAM and initiation of axillary meristems in flowering plants (Bowman and Smyth, 1999; Siegfried et al., 1999; Kumaran et al., 2002; Goldshmidt et al., 2008; Tanaka et al., 2012). A *YABBY* gene has also been shown to be expressed in the simplex SAM, the microphyll primordia and the sporangium-primordia of the lycophyte *Huperzia selago* (Evkaikina et al., 2017). While no *YABBY* genes were found in *P. patens* or *M. polymorpha*, a single *YABBY* gene has been shown to be expressed in a sporophyte specific manner in the hornwort *A. agrestis* (Li et al., 2020). Investigating the functional role of the single hornwort *YABBY* gene will give insight into its potential role during basal meristem regulation and thus about the role of YABBY transcription factors during the evolution of land plant body plans in general.

The hornwort sporophyte also bears stomata (Figures 2A, 3A). Stomata also occur in mosses but are absent in liverworts. (Renzaglia et al., 2017; Harrison and Morris, 2018; Clark et al., 2022). Unlike stomata of vascular plants, stomata of hornworts do not respond to environmental cues, they remain open once the stomata pore is formed and eventually collapse, facilitating sporophyte dehiscence and subsequent spore dispersal. In mosses stomata also play a role in sporophyte dehiscence but do respond to environmental cues such as light and abscisic acid (Chater et al., 2011; Lind et al., 2015). While the function and morphological features of moss stomata differ from those of vascular plants, their development is regulated by a set of orthologous genes (Pressel et al., 2014; Chater et al., 2017; Clark et al., 2022). The development, morphology and function of hornwort stomata further differs from those of mosses but shows remarkable similarity to Silurian-Devonian early land plant fossils (Edwards et al., 1998; Renzaglia et al., 2017). Elucidating the function of stomata in hornworts and determining the genetic network driving their development will help to resolve the long-standing debate about the ancestral function of stomata.

Studies of hornwort sporophytes can also help to understand the evolution and developmental biology of some unique features of bryophytes. For instance, both liverwort and hornwort sporophytes contain so-called elaters/pseudoelaters (elaters in liverworts and pseudoelaters in hornworts) aiding spore dispersal, while such structures are absent (likely lost) in all mosses (Ligrone et al., 2012a). Similarly, while most moss sporophytes contain a special opening structure (the annulus) enabling controlled dehiscence and regulated release of spores, most liverwort and all hornwort sporophytes open along two or more preformed slits (Crandall-Stotler and Stotler, 2008; Renzaglia et al., 2009). Additionally, while moss, liverwort and hornwort sporophytes are all nurtured by the gametophyte, nutrient transfer cells occur only in the gametophyte of hornworts while they are present in both the gametophyte and sporophyte tissues of several mosses and liverworts (Alfayate et al., 2000; Buck and Goffinet, 2000; Carafa et al., 2003; Crandall-Stotler and Stotler, 2008; Villarreal and Renzaglia, 2015). Finally, unlike mosses and liverworts, hornworts lack both water- and nutrient-conducting cells (Ligrone et al., 2000), with the evolutionary, physiological, and developmental aspects of this still not understood.

5.2 Chloroplast

5.2.1 Monoplastidy-polyplastidy

Chloroplasts originated from an endosymbiotic event between a cyanobacterium and a eukaryotic cell over one billion years ago (Archibald, 2009). The ancient organism that resulted from the endosymbiotic event evolved into three main groups: 1) the Glaucophyta, 2) the Rhodophyta (red algae) and 3) the Viridiplantae (green algae and land plants), with various secondary endosymbiosis events giving rise to other algal groups such as stramenopiles and haptophytes (Keeling, 2004; de Vries and Gould, 2018). Gene transfers from the genome of the endosymbiotic cyanobacterium to the nuclear genome of the eukaryotic host saw the cyanobacterium progressively losing

independence, thus evolving into a plastid (Bock and Timmis, 2008; de Vries et al., 2016; de Vries and Gould, 2018). However, this process remains incomplete: eukaryotic cells cannot produce a plastid *de novo* and only a plastid can make a new plastid by dividing *via* binary fission. Therefore, a daughter cell must inherit a plastid from its mother cell, otherwise the daughter cell lineage would be in an aplastidic state (de Vries and Gould, 2018). One solution is to have only one chloroplast per cell (monoplastidy) and to tightly link plastid division to cell division. Plastid division gene expression is coupled to cell cycle gene expression, with the mother cell only dividing once the chloroplast has multiplied so there is one chloroplast ready and available for each daughter cell. Most algal lineages are monoplastidic, including all the unicellular, basal branching groups in the chlorophyte green algae (de Vries and Gould, 2018). Some groups have escaped this bottleneck to evolve into a condition with multiple chloroplasts per cell: polyplastidy. This innovation appears to have evolved several times in photosynthetic eukaryotes, including within the streptophyte lineage that gave rise to the land plants (de Vries et al., 2016). Polyplastidy is suggested to be linked to the transfer of the plastid division *minicell* genes *MinD* and *MinE* from the chloroplast to the nuclear genome (Lopez-Juez and Pyke, 2005; de Vries and Gould, 2018). The increase in the number of plastids per cell coincided with the transition to terrestrial ecosystems and aided the development of macroscopic growth forms with specialized photosynthetic tissues. Multiple chloroplasts per cell allows for better photosynthetic efficiency and adaptation to variable environmental light conditions (Park et al., 1996; Königer et al., 2008; Ogasawara et al., 2013) in ways that are more difficult to achieve with the monoplastidic condition (Vaughn et al., 1992). Polyplastidic cells have a greater degree of back-up in case of damage or deleterious mutations in the chloroplast (Dutta et al., 2017; de Vries and Gould, 2018). The emergence of more complex body plans in vascular plants and seed plants also saw the evolution of new plastid types beyond the chloroplast (de Vries et al., 2016).

How polyplastidy evolved is poorly understood, and hornworts represent the ideal system to tackle this question. Most hornwort species, including the fully sequenced *Anthoceros* species, are monoplastidic (Figures 2B, 3B, 4E), however some groups (*e.g.*, *Megaceros*) are polyplastidic. Phylogenetic mapping suggests that bryophytes were originally polyplastidic, and within hornworts (Figure 3B) there were multiple independent transitions to monoplastidy (MacLeod et al., 2022). This provides opportunities to study the mono/polyplastidic transition both amongst the hornworts and within the bryophytes, with liverworts (for example the polyplastidic *M. polymorpha*, Figure 4F) and mosses providing convenient outgroups for comparison. By contrast such transitions are rare in other land plant groups (e.g. the giant plastids of the bizonoplast lycophytes, (Liu et al., 2020)). Furthermore, there are also cases of mono/polyplastidic transitions within one hornwort species, for example during *Megaceros* meristem regeneration. During the formation of an undifferentiated callus-like stage, the usual polyplastidic condition reverts to monoplastidy *via* an association between the chloroplast and nucleus that produces asymmetric cell divisions. After the emergence of apical cells and meristematic growth the usual polyplastidic state is restored (Burr, 1969). A similar transition from a polyplastidic to a monoplastidic conditions occurs in liverworts, such as *M. polymorpha*. Sporocytes (the cells that give rise to spores) have a single chloroplast per cells but during meiosis, they make a transition from a monoplastidic to a polyplastidic state (Renzaglia et al., 1994; Shimamura, 2016). Exploring the mechanism governing such transitions can provide insight into the evolution of polyplastidy.

In land plants, plastid division is largely independent from the cell cycle. However, the two processes cannot be entirely decoupled to avoid mis-segregation between daughter cells and the loss of plastids in one lineage. Birky's model (Birky, 1983; Birky and Skavaril, 1984; Birky, 2001) suggests a way of controlling for this: if plastids occupy a sufficient percentage of cell volume (50%) or if there are a large enough number of plastids (>6) then the probability of inheritance is such that it is almost certain that each daughter cell will have at least one plastid, and from this can produce new additional plastids. Yet it is still unknown how land plant cells sense the number or size of the plastids they contain, or what the molecular mechanism linking plastid and cell division is. The process of plastid division by binary fission is carried out by the formation of contractile rings that are linked across the plastid inner and outer envelopes. The genes involved in the formation and function of these divisional rings are a combination of those inherited from the cyanobacterial ancestor (e.g. *MinD*, *MinE*) and innovations from the eukaryotic host (e.g. *Plastid Division (PDV)* genes) (Chen F. et al., 2018). Bryophytes also have a more streamlined repertoire of plastid-related genes versus model angiosperm species. This smaller gene repertoire, together with lineage-specific gene losses, provides a useful avenue to investigate their role in polyplastidy evolution. There have also been losses of plastid-related genes specifically within hornworts (MacLeod et al., 2022). Most notable in this regard are the distributions of *Accumulation and Replication of Chloroplasts 3* (*ARC3*) and the *Filamentous Temperature Sensitive Z (FtsZ)* gene family (*FtsZ 1, 2* and *3*) in hornworts. All green algae and land plants possess *FtsZ* genes. Within the bryophytes, mosses such as *P. patens* have multiple *FtsZ* genes (two *FtsZ1*, two *FtsZ2* and one *FtsZ3*), while liverworts (e.g. *M. polymorpha*) have one copy of each of *FtsZ1*, *FtsZ2* and *FtsZ3* (Grosche and Rensing, 2017). *ARC3* appeared early in chlorophyte evolution and is found throughout the land plants, with rare exceptions e.g. *P. patens* (though this may be compensated for by a *MinC*-like gene) (Miyagishima et al., 2011; Osteryoung and Pyke, 2014). Crucially, all hornworts analyzed thus far only possess a copy of *FtsZ1* and *FtsZ3*, that is, they lack *FtsZ2*, and have lost *ARC3* (MacLeod et al., 2022). *ftsZ2* and *arc3* mutants in *A. thaliana* and *P. patens* have impaired chloroplast division dynamics, displaying extreme phenotypes of large, misshapen chloroplasts (Martin et al., 2009; Schmitz et al., 2009; Zhang et al., 2013). The unique hornwort situation has been suggested to be a crucial factor in the evolution of monoplastidy, analogous to the *A. thaliana* and *P. patens ftsZ2* and *arc3* mutants. Another interesting observation is that the nucleus in an *A. agrestis* cell is always next to the plastid (Figure 4G). In addition, *A. agrestis* lines with the actin fluorescently labeled, reveal a close interaction of the actin-cytoskeleton with the chloroplast (Figure 4H). These observations point towards a

potential mechanism that allows the coordination of plastid with cell division potentially *via* links with the cytoskeleton. Thus, hornworts provide a natural laboratory with simple, accessible systems to study FtsZ protein functions, FtsZ-ARC3 interactions, and the nucleus-plastid coordination.

Hornworts also provide an attractive system to study the least investigated *FtsZ* gene, *FtsZ3*, which is found in streptophyte green algae, bryophytes and lycophytes, but has been lost in ferns and seed plants (gymnosperms and angiosperms) (Grosche and Rensing, 2017) FtsZ3 differs from FtsZ1 or 2 in that the protein is localized to both the chloroplast and the cytoplasm in *P. patens*. *PpftsZ3* mutants possess misshapen chloroplasts and impaired phyllid growth, again distinct from phenotypes in *ftsz1* or *ftsz2* mutants (Martin et al., 2009). The fact that most traditional model plant species lack *FtsZ3* has hindered investigation into its function, yet the fact that it is ancestral in land plants makes it important in understanding the evolution of plastids and chloroplast division. One observation is that *FtsZ3* is correlated with a peptidoglycan layer between the chloroplast inner and outer envelopes, as is the case in cyanobacterial cell walls (and presumably in the ancestral endosymbiont). The suggestion is that FtsZ3 is somehow involved in forming or coordinating the peptidoglycan layer during plastid division (Grosche and Rensing, 2017), but the details surrounding this remain unclear (Chen C. et al., 2018). Hornworts provide an excellent opportunity to tackle this issue, having large, easily observable chloroplasts, established transgenic protocols and a single *FtsZ3* gene.

How polyplastidy evolved and controlled is a question of fundamental interest in plant biology, and the answers hold enormous biotechnological promise. Eventually controlling polyplastidy could facilitate applications such as the engineering of C4 traits in C3 crop species (e.g. to increase the chloroplast compliment in bundle sheath cells (Schuler et al., 2016; Stata et al., 2016)), manipulating plastid type interchange (Jarvis and López-Juez, 2013; Daniell et al., 2016; Solymosi et al., 2018) or producing morphologically-tailored plastids optimized for synthetic biology and protein biosynthesis (Daniell et al., 2016; Frangedakis et al., 2021c). Hornworts therefore represent a key system to study the regulatory mechanisms of chloroplast division, size and segregation, a "rosetta stone" for understanding the evolution of polyplastidy in land plants.

5.2.2 Stromules

Hornworts allow other aspects of chloroplast morphology and function to be explored. One example of this are the numerous, prominent projections that extend from hornwort chloroplasts (see arrows, Figure 4E). These projections have been termed stromules (Frangedakis et al., 2021a), under the assumption that they are homologous and functionally equivalent to stromules in other plant groups (Gray et al., 2001; Natesan, 2005). Stromules are projections from plastids and can form independent of the cytoskeleton, in isolated chloroplasts (Brunkard et al., 2015). Despite a long history of observation (Gray et al., 2001), even in model angiosperm species such as *A. thaliana* and tomato, stromule biology remains mysterious (Waters et al., 2004; Schattat et al., 2012). There is experimental evidence for stromules having a role in chromoplasts during fruit ripening (Waters et al., 2004) and a role in reactive oxygen signaling during immune responses (Caplan et al., 2015), but other suggested functions in inter-plastid connectivity have been disproven (Schattat et al., 2012). In general, there is an inverse relationship between stromules and plastid density (Waters et al., 2004), including in chloroplast division mutants (Holzinger et al., 2008), and this is also the case for monoplastidic hornworts (Frangedakis et al., 2021a). This points towards stromules being involved in increasing chloroplast surface area, possibly for transfer of substances to/from the cytoplasm. This would be of greater importance for large hornwort chloroplasts, considering their high volume-surface area ratio. The *A. agrestis* genome has homologs of known stromule-related genes, such as the *Chloroplast Outer Envelope Protein 1* (Caplan et al., 2015), a prime target for further study.

5.3 RNA editing

RNA editing refers to the conversion of cytidine (C) to uridine (U) in plant mitochondria and chloroplasts (Maier et al., 1996; Gott and Emeson, 2000) and is found in most land plants including hornworts, but not in green algae (Figure 3A). C-to-U RNA editing is mediated by nuclear encoded proteins called Pentatricopeptide Repeat (PPR) proteins. Hornwort plastid genomes are unique, having one of the highest RNA editing rates amongst land plants executed by over 1400 PPR proteins (Gutmann et al., 2020). Furthermore, RNA editing rates appear to be variable within hornworts, providing a unique opportunity to investigate the relationship between PPR protein diversification and RNA editing rates (Kugita et al., 2003; Juan Carlos Villarreal et al., 2018; Gerke et al., 2020). Hornworts also exhibit a special type of RNA editing, called reverse editing (U-to-C), which is otherwise found only in some lycophytes and ferns (Knie et al., 2016; Knoop, 2022) (Figure 3A). Genetic studies in hornworts can provide valuable insight into the molecular basis and biological significance of this poorly understood phenomenon (Bernath-Levin et al., 2021).

Plant lineages capable of reverse editing, including hornworts, have evolved special types of PPR proteins (Gerke et al., 2020; Gutmann et al., 2020). Reverse RNA editing PPR proteins are of particular interest since they might have applications in chloroplast engineering similar to C-to-U RNA editing PPR proteins (Bernath-Levin et al., 2021; McDowell et al., 2022). For example, it has recently been reported that synthetic PPR proteins can be used to specifically direct C-to-U RNA editing in the chloroplast (Royan et al., 2021) Similarly, hornwort reverse RNA editing PPR proteins have also the potential to be engineered to direct reverse U-to-C editing, offering additional tools for the control of chloroplast transgenes.

5.4 Carbon concentrating mechanisms

To improve photosynthetic efficiency, various organisms have evolved mechanisms to increase intracellular carbon concentration. CO_2 fixation is usually limited by the low CO_2 attraction (Whitney et al., 2011) and catalytic rate (Bar-Even et al., 2011) of the

Ribulose-1,5-bisphosphate carboxylase/oxygenase (RuBisCO) enzyme, and can be compensated by a mechanism, called carbon concentrating mechanism (CCM), that increases the CO_2 concentration in the immediate vicinity of RuBisCO (Tcherkez et al., 2006). While this is achieved by employing complex multicellular structures in C4 and CAM plants, various algae and a single lineage of land pants, the hornworts, carry out biophysical carbon concentration at a single cell level in pyrenoids (Figure 3A) (Li et al., 2017). Pyrenoids are a chloroplast based biophysical CCM that incorporates transporters to actively move HCO_3^- into the chloroplast, which is then converted into CO_2 and concentrated around RuBisCO (Li et al., 2017; Meyer et al., 2017; Barrett et al., 2021).

To date, information on biophysical CCM and pyrenoid biology is mainly available for the unicellular alga *C. reinhardtii* and very little is known about hornwort pyrenoids (Barrett et al., 2021). Pyrenoids have repeatedly been gained and lost over the course of hornwort evolution (Figure 3B) enabling comparative analyses of pyrenoid-bearing and pyrenoid-absent species (Villarreal and Renner, 2012). This framework, combined with the currently established transformation techniques, provides an ideal opportunity to answer key questions related to pyrenoids in hornworts as well as to reveal conserved and divergent features with *C. reinhardtii* (Li et al., 2017; Frangedakis et al., 2021b; Waller et al., 2022). In particular:

(i) Measurements indicate that pyrenoid-bearing hornworts carry out active carbon concentration (Smith E. and Griffiths, 1996; Smith E. C. and Griffiths, 1996; Smith and Griffiths, 2000; Hanson et al., 2002; Meyer et al., 2008). Nevertheless, whether the CCM is inducible or rather constitutive is poorly known. Furthermore, the ultimate factors inducing CCM and their biological significance are unknown. Past and present atmospheric CO_2 concentrations and habitat do not seem to correlate with the presence/absence of pyrenoids and CCM in hornworts (Villarreal and Renner, 2012). (ii) Pyrenoids are highly dynamic liquid phase separated structures in *C. reinhardtii*. By contrast, hornwort pyrenoids appear to be more stable and whether they form liquid phase separated bodies is unclear (Ligrone and Fioretto, 1987). (iii) Pyrenoids in *C. reinhardtii* consist mainly of RuBisCO scaffolded by a special protein matrix (Mackinder et al., 2016). While RuBisCO is concentrated in the pyrenoid in pyrenoid-bearing hornwort species and dispersed in the stroma in pyrenoid-absent species, the mechanism of pyrenoid assembly and components of the pyrenoid matrix are unknown (Vaughn et al., 1990; Vaughn et al., 1992). Whether pyrenoid assembly in hornworts occurs in an analogous way to *C. reinhardtii* is unclear (Barrett et al., 2021). (iii) Finally, the overall molecular mechanisms, the various enzymes/channels, and their localization within the hornwort cell and chloroplast are unknown and remain to be investigated.

Currently, there are attempts towards engineering algal pyrenoids into crops. This mainly includes proof of concept application in *A. thaliana* and tobacco (Adler et al., 2022). For example, engineering a chimeric *A. thaliana* RuBisCO by replacement of the two surface α-helices of its small subunit (S-subunit) with those of *C. reinhardtii*, results in a functional RuBisCO (Atkinson et al., 2017). *C. reinhardtii* RuBisCO S-subunit contains surface α-helices that have been shown to be necessary for the recruitment of RuBisCO into the pyrenoid *via* the interaction with the essential pyrenoid component 1 (EPYC1) (Engel et al., 2015; Mackinder et al., 2016). Recent evidence shows that co-expression of the chimeric *A. thaliana* RuBisCO with *C. reinhardtii* EPYC1 can result in functional pyrenoid-like structures in *A. thaliana* chloroplast (Atkinson et al., 2020). Given the vast evolutionary time separating chlorophytes from angiosperm crop species it can be hypothesized that it might be an easier endeavor to engineer a hornwort type pyrenoid into crops. Because the amino acid sequence of the hornwort RuBisCO S-subunit α-helices is more similar to that of *A. thaliana* compared to the *C. reinhardtii* one, introducing a hornwort EPYC1 analog to crops may induce pyrenoid formation with the native RuBisCO. Furthermore, pyrenoids produced this way may be more stable and have better biochemical properties than those induced using chimeric RuBisCO molecules and scaffolding proteins of algal origin.

5.5 Symbiotic interactions

Hornworts form beneficial (mutualistic) associations with arbuscular mycorrhizal (AM) fungi and cyanobacteria (Adams and Duggan, 2008; Rimington et al., 2020) (Figures 2C, 3B). In exchange for photosynthetic carbon, the plant gains fixed nitrogen or phosphorus (Enderlin and Meeks, 1983; Desiro et al., 2013). These associations of plants with AM fungi and cyanobacteria played an important role in land plant evolution (Delaux and Schornack, 2021). Supplying the plants with essential nutrients might have enabled the adaptation to a terrestrial life in which organic matter was scarce (Rensing, 2018; Puginier et al., 2022).

5.5.1 Arbuscular mycorrhizal fungi

Most hornwort species form a symbiosis with fungal partners (Figure 3B) (Desiro et al., 2013; Hoysted et al., 2017; Rimington et al., 2020). These associations involve two Mucoromycota subphyla, Mucoromycotina (that colonize 69% of hornworts) and Glomeromycotina (that colonize 78% of hornworts) (Rimington et al., 2020). Both the Glomeromycotina and Mucoromycotina are known to have played a key role in the plant adaptation to the land (Puginier et al., 2022). Often these different types of AM fungi occur simultaneously in the same thallus (Desiro et al., 2013). Fungal hyphae penetrate all parts of the thallus and occur inter- and intracellularly. Sometimes, the hyphae even interact with the cyanobacteria colonies (see next section) present in the mucilage cavities. While most hornwort species form a symbiosis with fungal partners, some species have apparently lost these symbioses (Read et al., 2000; Desiro et al., 2013). For example, the sister to all other hornworts *L. dussii*, has never been recorded in association with a fungus. In contrast, the family of Phymatocerotaceae has only been reported to occur in "a fungal association" (Rimington et al., 2020). Despite the presence of AM fungi in hornworts being well-documented using both morphological and molecular data (Schüßler, 2000; Desiro et al., 2013; Rimington et al., 2020), very

little is known about the functional aspects of symbiosis and its underlying regulatory networks. The sequenced *Anthoceros* genomes contain the full complement (orthologs/homologs) of major common symbiosis pathway genes necessary to regulate the signaling between the host plant and the symbiont (Li et al., 2020). Nevertheless, the conservation of genetic networks governing the initiation, establishment and stabilization of symbiotic interaction has yet to be investigated. Evidence is mounting that the common ancestor of all land plants was capable of establishing symbiosis with AM fungi (Rich et al., 2021). Information about the gene network regulating AM fungal interactions in liverworts is emerging (Radhakrishnan et al., 2020; Rich et al., 2021; Kodama et al., 2022). However, due to the deep divergence between hornworts and liverworts some findings may represent liverwort-specific innovations and cannot be generalized. Therefore, establishing a hornwort system to study AM fungal interactions is of high significance. Revealing conserved regulatory mechanisms shared by hornworts and other land plants will help to reconstruct the ancestral symbiosis molecular tool kit. A hornwort study system will also enable studying the potential three-way interaction between plant host, cyanobacteria, and AM fungi. To do so, research in isolating AM fungi from various hornworts is in progress and initial experiments indicate that the symbiotic interaction can be reconstituted under axenic conditions (Ono et al., 1992).

5.5.2 Cyanobacteria

Hornworts also establish a symbiosis with cyanobacteria providing the host plant with fixed nitrogen in exchange for photosynthates (Figures 2C, 3B, 4I) (Meeks and Elhai, 2002; Adams and Duggan, 2008). Unlike plant interaction with AM fungi, the endophytic interaction between plants and cyanobacteria is rarer and seems to have evolved independently in just a few phylogenetically diverse groups of land plants: in bryophytes (all hornworts and two species of liverworts), ferns (*Azolla*), gymnosperms (*Cycads*), and angiosperms (*Gunnera* and *Oryza*) (Meeks, 1998; Meeks and Elhai, 2002; Santi et al., 2013; Álvarez et al., 2020).

The cyanobionts hosted by hornworts are usually from the genus *Nostoc* spp. (Adams and Duggan, 2008) but can be phylogenetically diverse (Nelson et al., 2021; Rahmatpour et al., 2021). Hornworts host the cyanobacteria in mucilage cavities that can be accessed through ventral mucilage clefts, which superficially resemble stomata (Renzaglia et al., 2000; Villarreal A and Renzaglia, 2006). An exception is *L. dussii* that hosts cyanobacteria in canals that branch and form an integrated network within the thallus (de Vries and de Vries; Meeks, 2003).

Initiation of the cyanobacteria-plant symbiosis requires mobilization and chemical attraction of cyanobacteria. In the majority of plant-cyanobacteria symbioses this is achieved by molecules collectively called hormogonia-inducing factors (HIF) that are produced by the plant host and transform the cyanobacterial cells to hormogonia. Hormogonia are motile cells that can detach from the parent organism and function as dispersal units (Adams and Duggan, 2008; Liu and Rousk, 2022; Rousk, 2022). The hornwort-cyanobacteria symbiosis is relatively easy to reconstruct under axenic conditions, with *A. punctatus* being used as the model system to study the morphological, functional, molecular, and chemical processes underlying the symbiosis (Enderlin and Meeks, 1983). In *A. punctatus* (Enderlin and Meeks, 1983), a HIF is released when the hornwort is deprived of fixed nitrogen, enabling the colonization of the cyanobiont (Campbell and Meeks, 1989). Once the mucilage-rich cavities are colonized, the hornwort releases a hormogonia-repressing factor triggering the production of vegetative cyanobacterial filaments enriched with specialized N-fixing cells, the heterocysts (Campbell et al., 1997). While the cyanobacterial genes regulating symbiosis initiation, establishment, and stabilization are relatively well-investigated, very little is known about the host (de Vries and de Vries). It is thought that attraction of the cyanobiont may rely on some mechanisms conserved across the diverse lineages of land plants in which endophytic plant-cyanobacteria symbiosis occur (de Vries and de Vries). A recent RNA sequencing study identified a suite of candidate genes that might mediate the hornwort-cyanobacteria symbiotic relationship (Li et al., 2020; Chatterjee et al., 2022). These include a SWEET transporter, receptor kinases, and transcription factors but many questions remain to be answered.

Experimental tractability of the hornwort-cyanobacteria model system and the ability to genetically transform *A. punctatus* (Frangedakis et al., 2021b; Waller et al., 2022) will enable detailed exploration of various aspects of the symbiotic interaction in detail. Firstly, one could use this system to clarify how nitrogen starvation preconditions the host plants to attract and establish the initial interaction with the cyanobiont. It was hypothesized that symbiont attraction could have evolved by the extension of a conserved nutrient starvation response mechanism (Isidra-Arellano et al., 2021). Furthermore, forward genetic experiments could be used to identify the genes necessary for the initiation, establishment, and stabilization of the symbiotic interaction. Finally, reverse genetic tools could be employed to functionally verify the effect of candidate genes. Collectively, the hornwort-cyanobacteria system provides a tractable tool to thoroughly explore the origin and evolution of plant-cyanobacteria interactions.

It is expected that this knowledge can be used in the future to engineer crops capable of initiating the mutualistic interaction with cyanobacteria (Liu and Rousk, 2022; Rousk, 2022). This type of interaction has received increasing interest in recent years due to its significant translational potential to boost crop yield without applying additional artificial fertilizer (Alvarenga and Rousk, 2022; Rousk, 2022). Compared to AM fungi, cyanobacteria, especially the members of the genus *Nostoc* dominantly present in hornworts, are less dependent on the host, do not necessarily require specialized plant structures like arbuscules, and therefore hold a promising translational potential (Adams and Duggan, 2008).

5.6 Photoreceptors and flavonoids

Hornworts have a unique photoreceptor called neochrome, which is a chimeric gene composed of a red/far-red-sensing module from a phytochrome and a blue-sensing phototropin (Li

et al., 2014; Li et al., 2015). Apart from hornworts, neochrome is only found in ferns (Figure 3A). Interestingly, it has been proposed that ferns acquired neochrome by horizontal gene transfer from hornworts (Li et al., 2014). It remains to be understood whether the function of neochrome in hornworts is similar to ferns, where it increases light sensitivity by perceiving both red and blue light signals and ultimately mediates phototropism and chloroplast relocation (Kawai et al., 2003; Suetsugu et al., 2005; Li et al., 2014; Li et al., 2015).

Hornworts do not produce flavonoids (Davies et al., 2020) (Figure 3A). Flavonoids are polyphenolic secondary metabolite compounds with approximately 8000 being reported so far in land plants (Andersen and Markham, 2005). Flavonoids play a wide variety of important roles, ranging from UV radiation and pathogen protection to providing color to flowers and fruits to attract pollinators and seed dispersers. It is hypothesized that the evolution of flavonoid biosynthesis pathways coincided with the transition of plants to terrestrial ecosystems and that flavonoid biosynthetic pathways were present in the common ancestor of all land plants. The presence of degenerated sequences of genes encoding enzymes that catalyze the initial steps of the flavonoid biosynthesis pathway in *A. agrestis* and *A. punctatus* genomes suggest that the absence of flavonoids in hornworts likely represents a secondary loss. However, functional analysis is needed to confirm whether or not those genes that are present in hornworts can compensate for homologous genes in other plant groups and still produce functional enzymes.

6 Current challenges and conclusions

While significant advancements have been made in the last ten years in the genetic manipulation of hornworts, many challenges remain to be tackled in the future. Testing and optimization of a CRISPR/Cas9-based genome editing method is underway but has not yet been reliably established. Genetic editing using transient expression of CRISPR/Cas9 components in protoplasts appears feasible, but progress is currently hindered by the low regeneration potential of protoplasts. Preliminary experiments suggest that genetic transformation *via* homologous recombination may be possible. Nevertheless, further experiments are needed to identify the optimal parameters required. Until now, no inducible promoter systems have been tested in the hornworts. Further progress should be made on the long-term storage of hornwort plants. While spores provide a potential agent for long-term storage, many hornwort species do not develop sporophytes under laboratory conditions. Therefore, conditions necessary for long term storage of gametophyte fragments must be established. It is also necessary to extend the available genomic and transcriptomic resources, and efforts in that direction are currently underway. Finally, functional annotation of the hornwort genes is still in its initial phase. Considerable efforts must be directed towards the functional characterization of genes. This could be partially achieved by applying forward genetic techniques involving mutagenesis. Classical genetic approaches using genetic mapping *via* crossing of genetically diverse individuals must be also established.

A. agrestis has already been adopted by several groups as an experimental system and appears in literature with increasing frequency. The development of additional tools, especially CRISPR/cas9 technology, will spark further interest in hornworts and will further facilitate research in comparative developmental studies across bryophytes and vascular plants to answer long-standing questions of plant evolution and plant biology in general.

Author contributions

EF, AOM, MW, AN, SWT, YY, SR, LW, KS and PS collaboratively wrote the manuscript. EF, PS and MW coordinated the writing and finalized the manuscript. All authors contributed to the article and approved the submitted version.

Funding

JSPS Bridge Fellowship (BR220302) to EF. This project was carried out as part of the Deutsche Forschungsgemeinschaft (DFG) priority program 2237: "MAdLand—Molecular Adaptation to Land: plant evolution to change" (http://madland.science), through which PS received financial support (PSLJ1111/1). Additional funding was received from the Swiss National Science Foundation (grant nos. 160004, 184826, and 212509 to PS); project funding through the University Research Priority Program "Evolution in Action" of the University of Zurich to PS and LW; a Georges and Antoine Claraz Foundation grant to AN, YY, SR, LW, MW, and PS; UZH Forschungskredit Candoc grant no. FK-19-089 and an SNSF Doc.Mobility Projekt grant no. P1ZHP3_200030 to MW, and FK-22-098 to SR. AOM was funded by the BBSRC/EPSRC OpenPlant Synthetic Biology Research Centre Grant BB/L014130/1. This work was also supported by a Foundation of German Business (SDW) Scholarship to AN. SWT is funded by the Doris Zimmern HKU-Cambridge Hughes Hall Scholarship. KS was supported by JSPS KAKENHI Grant Number JP22H05177.

Acknowledgments

The authors thank Dora Huszar (ISEB, University of Zurich, Switzerland) for her help with plant culturing, Celia Baroux and Christof Eichenberger (IPMB, University of Zurich, Switzerland) for their expertise in fluorescence microscopy and providing us with the necessary equipment.

Conflict of interest

The authors declare that the research was conducted in the absence of any commercial or financial relationships that could be construed as a potential conflict of interest.

Publisher's note

References

Álvarez, C., Navarro, J. A., Molina-Heredia, F. P., and Mariscal, V. (2020). Endophytic colonization of rice (*Oryza sativa* l.) by the symbiotic strain *Nostoc punctiforme* PCC 73102. *Mol. Plant Microbe Interact.* 33, 1040–1045. doi: 10.1094/MPMI-01-20-0015-SC

Adams, D. G., and Duggan, P. S. (2008). Cyanobacteria-bryophyte symbioses. *J. Exp. Bot.* 59, 1047–1058. doi: 10.1093/jxb/ern005

Adler, L., Díaz-Ramos, A., Mao, Y., Pukacz, K. R., Fei, C., and McCormick, A. J. (2022). New horizons for building pyrenoid-based CO2-concentrating mechanisms in plants to improve yields. *Plant Physiol.* 190, 1609–1627. doi: 10.1093/plphys/kiac373

Alfayate, C., Estébanez, B., and Ron, E. (2000). The sporophyte-gametophyte junction in five species of pleurocarpous mosses. *Bryologist* 103, 467–474. doi: 10.1639/0007-2745(2000)103[0467:TSGJIF]2.0.CO;2

Althoff, F., and Zachgo, S. (2020). Transformation of *Riccia fluitans*, an amphibious liverwort dynamically responding to environmental changes. *Int. J. Mol. Sci.* 21(15), 5410. doi: 10.3390/ijms21155410

Alvarenga, D. O., and Rousk, K. (2022). Unraveling host-microbe interactions and ecosystem functions in moss-bacteria symbioses. *J. Exp. Bot.* 73, 4473–4486. doi: 10.1093/jxb/erac091

Andersen, O. M., and Markham, K. R. (Eds.). (2005). *Flavonoids: Chemistry, Biochemistry and Applications* (*1st* ed.). Boca Raton, CRC Press. doi: 10.1201/9781420039443

Arabidopsis Genome Initiative (2000). Analysis of the genome sequence of the flowering plant *Arabidopsis thaliana*. *Nature* 408, 796–815. doi: 10.1038/35048692

Archibald, J. M. (2009). The puzzle of plastid evolution. *Curr. Biol.* 19, R81–R88. doi: 10.1016/j.cub.2008.11.067

Atkinson, N., Leitão, N., Orr, D. J., Meyer, M. T., Carmo-Silva, E., Griffiths, H., et al. (2017). Rubisco small subunits from the unicellular green alga *Chlamydomonas* complement rubisco-deficient mutants of *Arabidopsis*. *New Phytol.* 214, 655–667. doi: 10.1111/nph.14414

Atkinson, N., Mao, Y., Chan, K. X., and McCormick, A. J. (2020). Condensation of rubisco into a proto-pyrenoid in higher plant chloroplasts. *Nat. Commun.* 11, 6303. doi: 10.1038/s41467-020-20132-0

Banks, J. A., Nishiyama, T., Hasebe, M., Bowman, J. L., Gribskov, M., DePamphilis, C., et al. (2011). The *Selaginella* genome identifies genetic changes associated with the evolution of vascular plants. *Science* 332, 960–963. doi: 10.1126/science.1203810

Bar-Even, A., Noor, E., Savir, Y., Liebermeister, W., Davidi, D., Tawfik, D. S., et al. (2011). The moderately efficient enzyme: evolutionary and physicochemical trends shaping enzyme parameters. *Biochemistry* 50, 4402–4410. doi: 10.1021/bi2002289

Barrett, J., Girr, P., and Mackinder, L. C. M. (2021). Pyrenoids: CO2-fixing phase separated liquid organelles. *Biochim. Biophys. Acta Mol. Cell Res.* 1868, 118949. doi: 10.1016/j.bbamcr.2021.118949

Bartlett, E. M. (1928). A comparative study of the development of the sporophyte in the anthocerotaceae, with especial reference to the genus *Anthoceros*. *Ann. Bot.* 42, 409–430. doi: 10.1093/jxb/13.1.161

Becker, B., and Marin, B. (2009). Streptophyte algae and the origin of embryophytes. *Ann. Bot.* 103, 999–1004. doi: 10.1093/aob/mcp044

Bernath-Levin, K., Schmidberger, J., Honkanen, S., Gutmann, B., Sun, Y. K., Pullakhandam, A., et al. (2021). Cofactor-independent RNA editing by a synthetic s-type PPR protein. *Synth. Biol. (Oxford England)* 7, ysab034. doi: 10.1093/synbio/ysab034

Birky, C. W. (1983). The partitioning of cytoplasmic organelles at cell division. *Int. Rev. Cytol. Suppl.* 15, 49–89. doi: 10.1016/B978-0-12-364376-6.50009-0

Birky, C. W. (2001). The inheritance of genes in mitochondria and chloroplasts: Laws, mechanisms, and models. *Annu. Rev. Genet.* 35, 125–148. doi: 10.1146/annurev.genet.35.102401.090231

Birky, C. W., and Skavaril, R. V. (1984). Random partitioning of cytoplasmic organelles at cell division: the effect of organelle and cell volume. *J. Theor. Biol.* 106, 441–447. doi: 10.1016/0022-5193(84)90001-8

Bock, R., and Timmis, J. N. (2008). Reconstructing evolution: Gene transfer from plastids to the nucleus. *BioEssays* 30, 556–566. doi: 10.1002/bies.20761

Bower, F. O. (1935). *Primitive land plants: Also known as the archegoniatae* (Macmillan, London).

Bowman, J. L., and Smyth, D. R. (1999). CRABS CLAW, a gene that regulates carpel and nectary development in *Arabidopsis*, encodes a novel protein with zinc finger and helix-loop-helix domains. *Development* 126, 2387–2396. doi: 10.1242/dev.126.11.2387

Bowman, J. L., Arteaga-Vazquez, M., Berger, F., Briginshaw, L. N., Carella, P., Aguilar-Cruz, A., et al. (2022). The renaissance and enlightenment of *Marchantia* as a model system. *Plant Cell* 34, 3512–3542. doi: 10.1093/plcell/koac219

Bowman, J. L., Kohchi, T., Yamato, K. T., Jenkins, J., Shu, S., Ishizaki, K., et al. (2017). Insights into land plant evolution garnered from the *Marchantia polymorpha* genome. *Cell* 171, 287–304.e15. doi: 10.1016/j.cell.2017.09.030

Bowman, J. L., Sakakibara, K., Furumizu, C., and Dierschke, T. (2016). Evolution in the cycles of life. *Annu. Rev. Genet.* 50, 133–154. doi: 10.1146/annurev-genet-120215-035227

Brunkard, J. O., Runkel, A. M., and Zambryski, P. C. (2015). Chloroplasts extend stromules independently and in response to internal redox signals. *Proc. Natl. Acad. Sci.* 112, 10044–10049. doi: 10.1073/pnas.1511570112

Buck, W., and Goffinet, B. (2000). "Morphology and classification of mosses," in *Bryophyte biology*. Eds. A. J. Shaw and B. Goffinet (Cambridge: Cambridge University Press), 71–123.

Buck, W. R., Shaw, A. J., and Goffinet, B. (2008). "Morphology, anatomy, and classification of the bryophyta," in *Bryophyte biology*. Ed. A. J. Shaw (Cambridge: Cambridge University Press), 55–138. doi: 10.1017/CBO9780511754807.003

Bui, L. T., Cordle, A. R., Irish, E. E., and Cheng, C.-L. (2015). Transient and stable transformation of *Ceratopteris richardii* gametophytes. *BMC Res. Notes* 8, 214. doi: 10.1186/s13104-015-1193-x

Burr, F. A. (1969). Reduction in chloroplast number during gametophyte regeneration in *Megaceros flagellaris*. *Bryologist* 72, 200. doi: 10.2307/3241669

Cammarata, J., Morales Farfan, C., Scanlon, M. J., and Roeder, A. H. K. (2022). Cytokinin-CLAVATA cross-talk is an ancient mechanism regulating shoot meristem homeostasis in land plants. *Proc. Natl. Acad. Sci. U. S. A.* 119, e2116860119. doi: 10.1073/pnas.2116860119

Campbell, E. L., and Meeks, J. C. (1989). Characteristics of hormogonia formation by symbiotic *Nostoc* spp. in response to the presence of *Anthoceros punctatus* or its extracellular products. *Appl. Environ. Microbiol.* 55, 125–131. doi: 10.1128/aem.55.1.125-131.1989

Campbell, E. L., Cohen, M. F., and Meeks, J. C. (1997). A polyketide-synthase-like gene is involved in the synthesis of heterocyst glycolipids in *Nostoc punctiforme* strain ATCC 29133. *Arch. Microbiol.* 167, 251–258. doi: 10.1007/s002030050440

Caplan, J. L., Kumar, A. S., Park, E., Padmanabhan, M. S., Hoban, K., Modla, S., et al. (2015). Chloroplast stromules function during innate immunity. *Dev. Cell* 34, 45–57. doi: 10.1016/j.devcel.2015.05.011

Carafa, A., Duckett, J. G., and Ligrone, R. (2003). The placenta in *Monoclea forsteri* hook. and *Treubia lacunosa* (Col.) prosk: insights into placental evolution in liverworts. *Ann. Bot.* 92, 299–307. doi: 10.1093/aob/mcg140

Chater, C., Caine, R. S., Fleming, A. J., and Gray, J. E. (2017). Origins and evolution of stomatal development. *Plant Physiol.* 174, 183. doi: 10.1104/pp.17.00183

Chater, C. C., Caine, R. S., Tomek, M., Wallace, S., Kamisugi, Y., Cuming, A. C., et al. (2016). Origin and function of stomata in the moss *Physcomitrella patens*. *Nat. Plants* 2, 16179. doi: 10.1038/nplants.2016.179

Chater, C., Kamisugi, Y., Movahedi, M., Fleming, A., Cuming, A. C., Gray, J. E., et al. (2011). Regulatory mechanism controlling stomatal behavior conserved across 400 million years of land plant evolution. *Curr. Biol.* 21, 1025–1029. doi: 10.1016/j.cub.2011.04.032

Chatterjee, P., Schafran, P., Li, F.-W., and Meeks, J. C. (2022). Nostoc talks back: Temporal patterns of differential gene expression during establishment of anthoceros-nostoc symbiosis. *Mol. Plant-Microbe Interact.* 35, 917–932. doi: 10.1094/mpmi-05-22-0101-r

Chen, C., MacCready, J. S., Ducat, D. C., and Osteryoung, K. W. (2018). The molecular machinery of chloroplast division. *Plant Physiol.* 176, 138–151. doi: 10.1104/pp.17.01272

Chen, F., Dong, W., Zhang, J., Guo, X., Chen, J., Wang, Z., et al. (2018). The sequenced angiosperm genomes and genome databases. *Front. Plant Sci.* 9. doi: 10.3389/fpls.2018.00418

Cheng, S., Xian, W., Fu, Y., Marin, B., Keller, J., Wu, T., et al. (2019). Genomes of subaerial Zygnematophyceae provide insights into land plant evolution. *Cell* 179, 1057–1067.e14. doi: 10.1016/j.cell.2019.10.019

Cho, S.-h., Chung, Y., Cho, S.-k., Rim, Y., and Shin, J. (1999). Particle bombardment mediated transformation and GFP expression in the moss *Physcomitrella patens* 9, 14–19.

Clark, J. W., Harris, B. J., Hetherington, A. J., Hurtado-Castano, N., Brench, R. A., Casson, S., et al. (2022). The origin and evolution of stomata. *Curr. Biol.* 32, R539–R553. doi: 10.1016/j.cub.2022.04.040

Clark, S. E., Williams, R. W., and Meyerowitz, E. M. (1997). The CLAVATA1 gene encodes a putative receptor kinase that controls shoot and floral meristem size in *Arabidopsis*. *Cell* 89, 575–585. doi: 10.1016/s0092-8674(00)80239-1

Crandall-Stotler, B., and Stotler, R. E. (2008). "Morphology and classification of the Marchantiophyta," in *Bryophyte biology* (Cambridge: Cambridge University Press), 21–70. doi: 10.1017/CBO9781139171304.003

Daniell, H., Lin, C.-S., Yu, M., and Chang, W.-J. (2016). Chloroplast genomes: diversity, evolution, and applications in genetic engineering. *Genome Biol.* 17, 134. doi: 10.1186/s13059-016-1004-2

Davies, K. M., Jibran, R., Zhou, Y., Albert, N. W., Brummell, D. A., Jordan, B. R., et al. (2020). The evolution of flavonoid biosynthesis: A bryophyte perspective. *Front. Plant Sci.* 11. doi: 10.3389/fpls.2020.00007

Delaux, P.-M., and Schornack, S. (2021). Plant evolution driven by interactions with symbiotic and pathogenic microbes. *Science* 371(6531), eaba6605. doi: 10.1126/science.aba6605

Desiro, A., Duckett, J. G., Pressel, S., Villarreal, J. C., Bidartondo, M. I., Desirò, A., et al. (2013). Fungal symbioses in hornworts: a chequered history. *Proc. R. Soc B-Biological Sci.* 280, 20130207. doi: 10.1098/Rspb.2013.0207

de Vries, J., and Gould, S. B. (2018). The monoplastidic bottleneck in algae and plant evolution. *J. Cell Sci.* 131, jcs203414. doi: 10.1242/jcs.203414

de Vries, J., Stanton, A., Archibald, J. M., and Gould, S. B. (2016). Streptophyte terrestrialization in light of plastid evolution. *Trends Plant Sci.* 21, 467–476. doi: 10.1016/j.tplants.2016.01.021

de Vries, S., and de Vries, J. (2022). Evolutionary genomic insights into cyanobacterial symbioses in plants. *Quant. Plant Biol.* 3, e16. doi: 10.1017/qpb.2022.3

Dierschke, T., Flores-Sandoval, E., Rast-Somssich, M. I., Althoff, F., Zachgo, S., and Bowman, J. L. (2021). Gamete expression of TALE class HD genes activates the diploid sporophyte program in *Marchantia polymorpha*. *Elife* 10, 1–25. doi: 10.7554/eLife.57088

Diop, S. I., Subotic, O., Giraldo-Fonseca, A., Waller, M., Kirbis, A., Neubauer, A., et al. (2020). A pseudomolecule-scale genome assembly of the liverwort marchantia polymorpha. *Plant J.* 101, 1378–1396. doi: 10.1111/tpj.14602

Dolan, L. (2009). Body building on land - morphological evolution of land plants. *Curr. Opin. Plant Biol.* 12, 4–8. doi: 10.1016/j.pbi.2008.12.001

Donoghue, P. C. J., Harrison, C. J., Paps, J., and Schneider, H. (2021). The evolutionary emergence of land plants. *Curr. Biol.* 31, R1281–R1298. doi: 10.1016/j.cub.2021.07.038

Dubrovsky, J. G., and Vissenberg, K. (2021). The quiescent centre and root apical meristem: organization and function. *J. Exp. Bot.* 72, 6673–6678. doi: 10.1093/jxb/erab405

Dutta, S., Cruz, J. A., Imran, S. M., Chen, J., Kramer, D. M., and Osteryoung, K. W. (2017). Variations in chloroplast movement and chlorophyll fluorescence among chloroplast division mutants under light stress. *J. Exp. Bot.* 68, 3541–3555. doi: 10.1093/jxb/erx203

Edwards, D., Kerp, H., and Hass, H. (1998). Stomata in early land plants: An anatomical and ecophysiological approach. *J. Exp. Bot.* 49, 255–278. doi: 10.1093/jxb/49.special_issue.255

Enderlin, C. S., and Meeks, J. C. (1983). Pure culture and reconstitution of the anthoceros-nostoc symbiotic association. *Planta* 158, 157–165. doi: 10.1007/BF00397709

Engel, B. D., Schaffer, M., Cuellar, L. K., Villa, E., Plitzko, J. M., and Baumeister, W. (2015). Native architecture of the *Chlamydomonas* chloroplast revealed by *in situ* cryo-electron tomography. *Elife* 2015, 1–29. doi: 10.7554/eLife.04889

Evkaikina, A. I., Berke, L., Romanova, M. A., Proux-Wéra, E., Ivanova, A. N., Rydin, C., et al. (2017). The huperzia selago shoot tip transcriptome sheds new light on the evolution of leaves. *Genome Biol. Evol.* 9, 2444–2460. doi: 10.1093/gbe/evx169

Field, K. J., Duckett, J. G., Cameron, D. D., and Pressel, S. (2015). Stomatal density and aperture in non-vascular land plants are non-responsive to above-ambient atmospheric CO2 concentrations. *Ann. Bot.* 115, 915–922. doi: 10.1093/aob/mcv021

Fouracre, J. P., and Harrison, C. J. (2022). How was apical growth regulated in the ancestral land plant? insights from the development of non-seed plants. *Plant Physiol.* 190, 100–112. doi: 10.1093/plphys/kiac313

Frangedakis, E., Guzman-Chavez, F., Rebmann, M., Markel, K., Yu, Y., Perraki, A., et al. (2021c). Construction of DNA Tools for Hyperexpression in Marchantia Chloroplasts Eftychios. *ACS Synth. Biol.* 10(7), 1651–66. doi: 10.1021/acssynbio.0c00637

Frangedakis, E., Shimamura, M., Villarreal, J. C., Li, F.-W., Tomaselli, M., Waller, M., et al. (2021a). The hornworts: morphology, evolution and development. *New Phytol.* 229, 735–754. doi: 10.1111/nph.16874

Frangedakis, E., Waller, M., Nishiyama, T., Tsukaya, H., Xu, X., Yue, Y., et al. (2021b). An agrobacterium-mediated stable transformation technique for the hornwort model *Anthoceros agrestis*. *New Phytol.* 232, 1488–1505. doi: 10.1111/nph.17524

Gerke, P., Szövényi, P., Neubauer, A., Lenz, H., Gutmann, B., McDowell, R., et al. (2020). Towards a plant model for enigmatic U-to-C RNA editing: the organelle genomes, transcriptomes, editomes and candidate RNA editing factors in the hornwort *Anthoceros agrestis*. *New Phytol.* 225, 1974–1992. doi: 10.1111/nph.16297

Gerrienne, P., Servais, T., and Vecoli, M. (2016). Plant evolution and terrestrialization during Palaeozoic times–the phylogenetic context. *Rev. Palaeobot. Palynol.* 227, 4–18. doi: 10.1016/j.revpalbo.2016.01.004

Goldshmidt, A., Alvarez, J. P., Bowman, J. L., and Eshed, Y. (2008). Signals derived from YABBY gene activities in organ primordia regulate growth and partitioning of *Arabidopsis* shoot apical meristems. *Plant Cell* 20, 1217–1230. doi: 10.1105/tpc.107.057877

Gott, J. M., and Emeson, R. B. (2000). Functions and mechanisms of RNA editing. *Annu. Rev. Genet.* 34, 499–531. doi: 10.1146/annurev.genet.34.1.499

Gray, J. C., Sullivan, J. A., Hibberd, J. M., and Hansen, M. R. (2001). Stromules: Mobile protrusions and interconnections between plastids. *Plant Biol.* 3, 223–233. doi: 10.1055/s-2001-15204

Grosche, C., and Rensing, S. A. (2017). Three rings for the evolution of plastid shape: a tale of land plant FtsZ. *Protoplasma* 254, 1879–1885. doi: 10.1007/s00709-017-1096-x

Gunadi, A., Li, F.-W., and Van Eck, J. (2022). Accelerating gametophytic growth in the model hornwort *Anthoceros agrestis*. *Appl. Plant Sci.* 10, e11460. doi: 10.1002/aps3.11460

Gutmann, B., Royan, S., Schallenberg-Rüdinger, M., Lenz, H., Castleden, I. R., McDowell, R., et al. (2020). The expansion and diversification of pentatricopeptide repeat RNA-editing factors in plants. *Mol. Plant* 13, 215–230. doi: 10.1016/j.molp.2019.11.002

Guyon-Debast, A., Alboresi, A., Terret, Z., Charlot, F., Berthier, F., Vendrell-Mir, P., et al. (2021). A blueprint for gene function analysis through base editing in the model plant *Physcomitrium* (Physcomitrella) *patens*. *New Phytol.* 230, 1258–1272. doi: 10.1111/nph.17171

Hanson, D., Andrews, T. J., and Badger, M. R. (2002). Variability of the pyrenoid-based CO2 concentrating mechanism in hornworts (Anthocerotophyta). *Funct. Plant Biol.* 29, 407–416. doi: 10.1071/PP01210

Harris, B. J., Clark, J. W., Schrempf, D., Szöllősi, G. J., Donoghue, P. C. J., Hetherington, A. M., et al. (2022). Divergent evolutionary trajectories of bryophytes and tracheophytes from a complex common ancestor of land plants. *Nat. Ecol. Evol.* 6, 1634–1643. doi: 10.1038/s41559-022-01885-x

Harris, B. J., Harrison, C. J., Hetherington, A. M., and Williams, T. A. (2020). Phylogenomic evidence for the monophyly of bryophytes and the reductive evolution of stomata. *Curr. Biol.* 30, 2001–2012.e2. doi: 10.1016/j.cub.2020.03.048

Harrison, C. J., and Morris, J. L. (2018). The origin and early evolution of vascular plant shoots and leaves. *Philos. Trans. R. Soc Lond. B. Biol. Sci.* 373, 20160496. doi: 10.1098/rstb.2016.0496

Hickok, L. G., Warne, T. R., and Slocum, M. K. (1987). *Ceratopteris richardii*: Applications for experimental plant biology. *Am. J. Bot.* 74, 1304. doi: 10.2307/2444165

Hirakawa, Y. (2022). Evolution of meristem zonation by CLE gene duplication in land plants. *Nat. Plants* 8, 735–740. doi: 10.1038/s41477-022-01199-7

Hirakawa, Y., Fujimoto, T., Ishida, S., Uchida, N., Sawa, S., Kiyosue, T., et al. (2020). Induction of multichotomous branching by CLAVATA peptide in *Marchantia polymorpha*. *Curr. Biol.* 30, 3833–3840.e4. doi: 10.1016/j.cub.2020.07.016

Holzinger, A., Kwok, E. Y., and Hanson, M. R. (2008). Effects of arc3, arc5 and arc6 mutations on plastid morphology and stromule formation in green and nongreen tissues of *Arabidopsis thaliana*. *Photochem. Photobiol.* 84, 1324–1335. doi: 10.1111/j.1751-1097.2008.00437.x

Hoysted, G. A., Kowal, J., Jacob, A., Rimington, W. R., Duckett, J. G., Pressel, S., et al. (2017). A mycorrhizal revolution. *Curr. Opin. Plant Biol.* 44, 1–6. doi: 10.1016/j.pbi.2017.12.004

Ishizaki, K., Chiyoda, S., Yamato, K. T., and Kohchi, T. (2008). Agrobacterium-mediated transformation of the haploid liverwort *Marchantia polymorpha* l., an emerging model for plant biology. *Plant Cell Physiol.* 49, 1084–1091. doi: 10.1093/pcp/pcn085

Ishizaki, K., Johzuka-Hisatomi, Y., Ishida, S., Iida, S., and Kohchi, T. (2013). Homologous recombination-mediated gene targeting in the liverwort *Marchantia polymorpha* l. *Sci. Rep.* 3, 1–6. doi: 10.1038/srep01532

Isidra-Arellano, M. C., Delaux, P. M., and Valdés-López, O. (2021). The phosphate starvation response system: Its role in the regulation of plant–microbe interactions. *Plant Cell Physiol.* 62, 392–400. doi: 10.1093/pcp/pcab016

Jarvis, P., and López-Juez, E. (2013). Biogenesis and homeostasis of chloroplasts and other plastids. *Nat. Rev. Mol. Cell Biol.* 14, 787–802. doi: 10.1038/nrm3702

Jeong, S., Trotochaud, A. E., and Clark, S. E. (1999). The *Arabidopsis* CLAVATA2 gene encodes a receptor-like protein required for the stability of the CLAVATA1 receptor-like kinase. *Plant Cell* 11, 1925–1934. doi: 10.1105/tpc.11.10.1925

Johnson, G. P., Renzaglia, Æ.K.S., Lycophyte, F.Á., Suspensor, Á.P.Á., and Transfer, Á. (2009). Evaluating the diversity of pteridophyte embryology in the light of recent phylogenetic analyses leads to new inferences on character evolution. *Plant Syst. Evol.* 283, 149–164. doi: 10.1007/s00606-009-0222-4

Juan Carlos Villarreal, A., Turmel, M., Bourgouin-Couture, M., Laroche, J., Allen, N. S., Li, F. W., et al. (2018). Genome-wide organellar analyses from the hornwort *Leiosporoceros dussii* show low frequency of RNA editing. *PloS One* 13, 1–18. doi: 10.1371/journal.pone.0200491

Kammerer, W., and Cove, D. J. (1996). Genetic analysis of the effects of re-transformation of transgenic lines of the moss *Physcomitrella patens*. *Mol. Gen. Genet.* 250, 380–382. doi: 10.1007/BF02174397

Karol, K. G. (2001). The closest living relatives of land plants. *Science*. 294, 2351–2353. doi: 10.1126/science.1065156

Kato, M., and Akiyama, H. (2005). Interpolation hypothesis for origin of the vegetative sporophyte of land plants. *Taxon* 54, 443–450. doi: 10.2307/25065371

Kawai, H., Kanegae, T., Christensen, S., Kiyosue, T., Sato, Y., Imaizumi, T., et al. (2003). Responses of ferns to red light are mediated by an unconventional photoreceptor. *Nature* 421, 287–290. doi: 10.1038/nature01310

Kawamura, S., Romani, F., Yagura, M., Mochizuki, T., Sakamoto, M., Yamaoka, S., et al. (2022). MarpolBase expression: A web-based, comprehensive platform for visualization and analysis of transcriptomes in the liverwort *Marchantia polymorpha*. *Plant Cell Physiol.* 1. 11, 1745–1755. doi: 10.1093/pcp/pcac129

Keeling, P. J. (2004). Diversity and evolutionary history of plastids and their hosts the tree of eukaryotes. *Am. J. Bot.* 91, 1481–1493. doi: 10.3732/ajb.91.10.1481

Knie, N., Grewe, F., Fischer, S., and Knoop, V. (2016). Reverse U-to-C editing exceeds c-to-U RNA editing in some ferns - a monilophyte-wide comparison of chloroplast and mitochondrial RNA editing suggests independent evolution of the two processes in both organelles. *BMC Evol. Biol.* 16, 134. doi: 10.1186/s12862-016-0707-z

Knoop, V. (2022). C-to-U and U-to-C: RNA editing in plant organelles and beyond. *J. Exp. Bot*. doi: 10.1093/jxb/erac488

Kodama, K., Rich, M. K., Yoda, A., Shimazaki, S., Xie, X., Akiyama, K., et al. (2022). An ancestral function of strigolactones as symbiotic rhizosphere signals. *Nat. Commun.* 13, 3974. doi: 10.1038/s41467-022-31708-3

Königer, M., Delamaide, J. A., Marlow, E. D., and Harris, G. C. (2008). *Arabidopsis thaliana* leaves with altered chloroplast numbers and chloroplast movement exhibit impaired adjustments to both low and high light. *J. Exp. Bot.* 59, 2285–2297. doi: 10.1093/jxb/ern099

Kubota, A., Ishizaki, K., Hosaka, M., and Kohchi, T. (2013). Efficient agrobacterium-mediated transformation of the liverwort *Marchantia polymorpha* using regenerating thalli. *Biosci. Biotechnol. Biochem.* 77, 167–172. doi: 10.1271/bbb.120700

Kugita, M., Yamamoto, Y., Fujikawa, T., Matsumoto, T., and Yoshinaga, K. (2003). RNA Editing in hornwort chloroplasts makes more than half the genes functional. *Nucleic Acids Res.* 31, 2417–2423. doi: 10.1093/nar/gkg327

Kumaran, M. K., Bowman, J. L., and Sundaresan, V. (2002). YABBY polarity genes mediate the repression of KNOX homeobox genes in *Arabidopsis*. *Plant Cell* 14, 2761–2770. doi: 10.1105/tpc.004911

Leebens-Mack, J. H., Barker, M. S., Carpenter, E. J., Deyholos, M. K., Gitzendanner, M. A., Graham, S. W., et al. (2019). One thousand plant transcriptomes and the phylogenomics of green plants. *Nature* 574, 679–685. doi: 10.1038/s41586-019-1693-2

Lewis, L. A., and McCourt, R. M. (2004). Green algae and the origin of land plants. *Am. J. Bot.* 91, 1535–1556. doi: 10.3732/ajb.91.10.1535

Li, F.-W., Melkonian, M., Rothfels, C. J., Villarreal, J. C., Stevenson, D. W., Graham, S. W., et al. (2015). Phytochrome diversity in green plants and the origin of canonical plant phytochromes. *Nat. Commun.* 6, 7852. doi: 10.1038/ncomms8852

Li, F.-W., Nishiyama, T., Waller, M., Frangedakis, E., Keller, J., Li, Z., et al. (2020). *Anthoceros* genomes illuminate the origin of land plants and the unique biology of hornworts. *Nat. Plants* 6, 259–272. doi: 10.1038/s41477-020-0618-2

Li, F.-W., Villarreal, J. C., Kelly, S., Rothfels, C. J., Melkonian, M., Frangedakis, E., et al. (2014). Horizontal transfer of an adaptive chimeric photoreceptor from bryophytes to ferns. *Proc. Natl. Acad. Sci. U. S. A.* 111, 6672–6677. doi: 10.1073/pnas.1319929111

Li, F.-W., Villarreal, J. C., and Szövényi, P. (2017). Hornworts: An overlooked window into carbon-concentrating mechanisms. *Trends Plant Sci.* 22, 275–277. doi: 10.1016/j.tplants.2017.02.002

Li, L., Yang, J., Qiu, H. L., and Liu, Y. Y. (2010). Genetic transformation of *Physcomitrella patens* mediated by *Agrobacterium tumefaciens*. *African Journal of Biotechnology* 9, 3719–3725. doi: 10.5897/AJB2010.000-3237

Ligrone, R., Ducket, J. G., and Renzaglia, K. S. (2000). Conducting tissues and phyletic relationships of bryophytes. *Philos. Trans. R. Soc Lond. B. Biol. Sci.* 355, 795–813. doi: 10.1098/rstb.2000.0616

Ligrone, R., Duckett, J. G., and Renzaglia, K. S. (2012a). The origin of the sporophyte shoot in land plants: a bryological perspective. *Ann. Bot.* 110, 935–941. doi: 10.1093/aob/mcs176

Ligrone, R., Duckett, J. G., and Renzaglia, K. S. (2012b). Major transitions in the evolution of early land plants: a bryological perspective. *Ann. Bot.* 109, 851–871. doi: 10.1093/aob/mcs017

Ligrone, R., and Fioretto, A. (1987). Chloroplast development in light-and dark-grown sporophytes of *Phaeoceros laevis* (L.) prosk. (Anthocerotophyta). *New Phytol.* 105, 301–308. doi: 10.1111/j.1469-8137.1987.tb00868.x

Lind, C., Dreyer, I., López-Sanjurjo, E. J., Von Meyer, K., Ishizaki, K., Kohchi, T., et al. (2015). Stomatal guard cells co-opted an ancient ABA-dependent desiccation survival system to regulate stomatal closure. *Curr. Biol.* 25, 928–935. doi: 10.1016/j.cub.2015.01.067

Liu, J., Li, S., Wu, C., Valdespino, I. A., Ho, J., Wu, Y., et al. (2020). Gigantic chloroplasts, including bizonoplasts, are common in shade-adapted species of the ancient vascular plant family {Selaginellaceae}. *Am. J. Bot.* 107, 562–576. doi: 10.1002/ajb2.1455

Liu, H., Wang, X., Wang, G., Cui, P., Wu, S., Ai, C., et al. (2021). The nearly complete genome of *Ginkgo biloba* illuminates gymnosperm evolution. *Nat. Plants* 7, 748–756. doi: 10.1038/s41477-021-00933-x

Liu, X., and Rousk, K. (2022). The moss traits that rule cyanobacterial colonization. *Ann. Bot.* 129, 147–160. doi: 10.1093/aob/mcab127

Lopez-Juez, E., and Pyke, K. A. (2005). Plastids unleashed: their development and their integration in plant development. *The International Journal of Developmental Biology* 49, 557–577. doi: 10.1387/ijdb.051997el

Lopez-Obando, M., Landberg, K., Sundberg, E., and Thelander, M. (2022). Dependence on clade II bHLH transcription factors for nursing of haploid products by tapetal-like cells is conserved between moss sporangia and angiosperm anthers. *New Phytol.* 235, 718–731. doi: 10.1111/nph.17972

Mackinder, L. C. M., Meyer, M. T., Mettler-altmann, T., Chen, V., and Madeline, C. (2016). A repeat protein links Rubisco to form the eukaryotic carbon concentrating organelle. *Pnas*. 113, 5958–5963. doi: 10.1073/pnas.1522866113

MacLeod, A. I., Raval, P. K., Stockhorst, S., Knopp, M. R., Frangedakis, E., and Gould, S. B. (2022). Loss of plastid developmental genes coincides with a reversion to monoplastidy in hornworts. *Front. Plant Sci.* 13. doi: 10.3389/fpls.2022.863076

Maier, R. M., Zeltz, P., Kössel, H., Bonnard, G., Gualberto, J. M., and Grienenberger, J. M. (1996). RNA Editing in plant mitochondria and chloroplasts. *Plant Mol. Biol.* 32, 343–365. doi: 10.1007/BF00039390

Maizel, A. (2005). The floral regulator LEAFY evolves by substitutions in the DNA binding domain. *Science*. 308, 260–263. doi: 10.1126/science.1108229

Mallett, D. R., Chang, M., Cheng, X., and Bezanilla, M. (2019). Efficient and modular CRISPR-Cas9 vector system for *Physcomitrella patens*. *Plant Direct* 3, 1–15. doi: 10.1002/pld3.168

Marchant, D. B., Chen, G., Cai, S., Chen, F., Schafran, P., Jenkins, J., et al. (2022). Dynamic genome evolution in a model fern. *Nat. Plants* 8, 1038–1051. doi: 10.1038/s41477-022-01226-7

Martin, A., Lang, D., Hanke, S. T., Mueller, S. J. X., Sarnighausen, E., Vervliet-Scheebaum, M., et al. (2009). Targeted gene knockouts reveal overlapping functions of the five *Physcomitrella patens* FtsZ isoforms in chloroplast division, chloroplast shaping, cell patterning, plant development, and gravity sensing. *Mol. Plant* 2, 1359–1372. doi: 10.1093/mp/ssp076

McDowell, R., Small, I., and Bond, C. S. (2022). Synthetic PPR proteins as tools for sequence-specific targeting of RNA. *Methods* 208, 19–26. doi: 10.1016/j.ymeth.2022.10.003

Meeks, J. C. (1998). Symbiosis between nitrogen-fixing cyanobacteria and plants. *Bioscience* 48, 266–276. doi: 10.2307/1313353

Meeks, J. C. (2003). Symbiotic interactions between *Nostoc punctiforme*, a multicellular cyanobacterium, and the hornwort *Anthoceros punctatus*. *Symbiosis* 35, 55–71.

Meeks, J. C., and Elhai, J. (2002). Regulation of cellular differentiation in filamentous cyanobacteria in free-living and plant-associated symbiotic growth states. *Microbiol. Mol. Biol. Rev.* 66, 94–121. doi: 10.1128/MMBR.66.1.94-121.2002

Merchant, S. S., Prochnik, S. E., Vallon, O., Harris, E. H., Karpowicz, S. J., Witman, G. B., et al. (2007). The *Chlamydomonas* genome reveals the evolution of key animal and plant functions. *Science* 318, 245–250. doi: 10.1126/science.1143609

Meyer, M., Seibt, U., and Griffiths, H. (2008). To concentrate or ventilate? carbon acquisition, isotope discrimination and physiological ecology of early land plant life forms. *Philos. Trans. R. Soc Lond. B. Biol. Sci.* 363, 2767–2778. doi: 10.1098/rstb.2008.0039

Meyer, M. T., Whittaker, C., and Griffiths, H. (2017). The algal pyrenoid: key unanswered questions. *J. Exp. Bot.* 68, 3739–3749. doi: 10.1093/jxb/erx178

Miyagishima, S., Nakanishi, H., and Kabeya, Y. (2011). Structure, regulation, and evolution of the plastid division machinery. *Int. Rev. Cell Mol. Biol.* 291, 115–53. doi: 10.1016/B978-0-12-386035-4.00004-5

Montgomery, S. A., Tanizawa, Y., Galik, B., Wang, N., Ito, T., Mochizuki, T., et al. (2020). Chromatin organization in early land plants reveals an ancestral association between H3K27me3, transposons, and constitutive heterochromatin. *Curr. Biol.* 30, 573–588.e7. doi: 10.1016/j.cub.2019.12.015

Müller, R., Bleckmann, A., and Simon, R. (2008). The receptor kinase CORYNE of *Arabidopsis* transmits the stem cell-limiting signal CLAVATA3 independently of CLAVATA1. *Plant Cell* 20, 934–946. doi: 10.1105/tpc.107.057547

Mussgnug, J. H. (2015). Genetic tools and techniques for *Chlamydomonas reinhardtii*. *Appl. Microbiol. Biotechnol.* 99, 5407–5418. doi: 10.1007/s00253-015-6698-7

Natesan, S. K. A. (2005). Stromules: a characteristic cell-specific feature of plastid morphology. *J. Exp. Bot.* 56, 787–797. doi: 10.1093/jxb/eri088

Nelson, J. M., Hauser, D. A., and Li, F.-W. (2021). The diversity and community structure of symbiotic cyanobacteria in hornworts inferred from long-read amplicon sequencing. *Am. J. Bot.* 108, 1731–1744. doi: 10.1002/ajb2.1729

Neubauer, A., Ruaud, S., Waller, M., Frangedakis, E., Li, F., Nötzold, S. I., et al. (2022). Step-by-step protocol for the isolation and transient transformation of hornwort protoplasts. *Appl. Plant Sci.* 10, e11456. doi: 10.1002/aps3.11456

Nishiyama, T., Sakayama, H., de Vries, J., Buschmann, H., Saint-Marcoux, D., Ullrich, K. K., et al. (2018). The *Chara* genome: Secondary complexity and implications for plant terrestrialization. *Cell*. 174, 448–464.e24. doi: 10.1016/j.cell.2018.06.033

Nystedt, B., Street, N. R., Wetterbom, A., Zuccolo, A., Lin, Y. C., Scofield, D. G., et al. (2013). The Norway spruce genome sequence and conifer genome evolution. *Nature* 497, 579–584. doi: 10.1038/nature12211

Ogasawara, Y., Ishizaki, K., Kohchi, T., and Kodama, Y. (2013). Cold-induced organelle relocation in the liverwort *Marchantia polymorpha* l. *Plant Cell Environ.* 36, 1520–1528. doi: 10.1111/pce.12085

Ono, K., Izumi, Y., and Takamiya, M. (1992). Isolation, culture and thallus regeneration of protoplasts from the hornwort *Anthoceros punctatus* l. *Cultured Cells Plant Tissue Cult. Lett.* 9, 27–31.

Osteryoung, K. W., and Pyke, K. A. (2014). Division and dynamic morphology of plastids. *Annu. Rev. Plant Biol.* 65, 443–472. doi: 10.1146/annurev-arplant-050213-035748

Park, Y. I., Chow, W. S., and Anderson, J. M. (1996). Chloroplast movement in the shade plant *Tradescantia albiflora* helps protect photosystem II against light stress. *Plant Physiol.* 111, 867–875. doi: 10.1104/pp.111.3.867

Plackett, A. R. G., Di Stilio, V. S., and Langdale, J. A. (2015). Ferns: the missing link in shoot evolution and development. *Front. Plant Sci.* 6. doi: 10.3389/fpls.2015.00972

Plackett, A. R. G., Huang, L., Sanders, H. L., and Langdale, J. A. (2014). High-efficiency stable transformation of the model fern species *Ceratopteris richardii via* microparticle bombardment. *Plant Physiol.* 165, 3–14. doi: 10.1104/pp.113.231357

Pressel, S., Goral, T., and Duckett, J. G. (2014). Stomatal differentiation and abnormal stomata in hornworts. *J. Bryol.* 36, 87–103. doi: 10.1179/1743282014y.0000000103

Puginier, C., Keller, J., and Delaux, P.-M. (2022). Plant-microbe interactions that have impacted plant terrestrializations. *Plant Physiol.* 190, 72–84. doi: 10.1093/plphys/kiac258

Puttick, M. N., Morris, J. L., Williams, T. A., Cox, C. J., Edwards, D., Kenrick, P., et al. (2018). The interrelationships of land plants and the nature of the ancestral embryophyte. *Curr. Biol.* 28, 733–745.e2. doi: 10.1016/j.cub.2018.01.063

Radhakrishnan, G. V., Keller, J., Rich, M. K., Vernié, T., Mbadinga Mbadinga, D. L., Vigneron, N., et al. (2020). An ancestral signalling pathway is conserved in intracellular symbioses-forming plant lineages. *Nat. Plants* 6, 280–289. doi: 10.1038/s41477-020-0613-7

Rahmatpour, N., Hauser, D. A., Nelson, J. M., Chen, P. Y., Villarreal A, J. C., Ho, M.-Y., et al. (2021). A novel thylakoid-less isolate fills a billion-year gap in the evolution of cyanobacteria. *Curr. Biol.* 31, 2857–2867.e4. doi: 10.1016/j.cub.2021.04.042

Read, D. J., Ducket, J. G., Francis, R., Ligron, R., and Russell, A. (2000). Symbiotic fungal associations in "lower" land plants. *Philos. Trans. R. Soc Lond. B. Biol. Sci.* 355, 815–830; discussion 830-831. doi: 10.1098/rstb.2000.0617

Reddy, G. V., and Meyerowitz, E. M. (2005). Stem-cell homeostasis and growth dynamics can be uncoupled in the *Arabidopsis* shoot apex. *Science* 310, 663–667. doi: 10.1126/science.1116261

Rensing, S. A. (2018). Great moments in evolution: the conquest of land by plants. *Curr. Opin. Plant Biol.* 42, 49–54. doi: 10.1016/j.pbi.2018.02.006

Rensing, S. A. (2020). How plants conquered land. *Cell* 181, 964–966. doi: 10.1016/j.cell.2020.05.011

Rensing, S. A., Goffinet, B., Meyberg, R., Wu, S. Z., and Bezanilla, M. (2020). The moss *Physcomitrium* (*Physcomitrella*) *patens*: A model organism for non-seed plants. *Plant Cell* 32, 1361–1376. doi: 10.1105/tpc.19.00828

Renzaglia, K. S., Brown, R. C., Lemmon, B. E., Duckett, J. G., and Ligrone, R. (1994). Occurrence and phylogenetic significance of monoplastidic meiosis in liverworts. *Can. J. Bot.* 72, 65–72. doi: 10.1139/b94-009

Renzaglia, K. S., Duff, R. J. T., Nickrent, D. L., and Garbary, D. J. (2000). Vegetative and reproductive innovations of early land plants: implications for a unified phylogeny. *Philos. Trans. R. Soc Lond. B. Biol. Sci.* 355, 769–793. doi: 10.1098/rstb.2000.0615

Renzaglia, K. S., Villarreal, J. C., and Duff, J. R. (2009). "New insights into morphology, anatomy and systematics of hornworts," in *Bryophyte biology*. Eds. B. Goffinet and A. J. Shaw (Cambridge: Cambridge University Press), 139–172. doi: 10.1017/cbo9780511754807.004

Renzaglia, K. S., Villarreal, J. C., Piatkowski, B. T., Lucas, J. R., and Merced, A. (2017). Hornwort stomata: Architecture and fate shared with 400 million year old fossil plants without leaves. *Plant Physiol.* 174, 156. doi: 10.1104/pp.17.00156

Rich, M. K., Vigneron, N., Liboure, C., Keller, J., Xue, L., Hajheidari, M., et al. (2021). Lipid exchanges drove the evolution of mutualism during plant terrestrialization. *Science*. 372, 864–868. doi: 10.1126/science.abg0929

Rigault, P., Boyle, B., Lepage, P., Cooke, J. E. K., Bousquet, J., and MacKay, J. J. (2011). A white spruce gene catalog for conifer genome analyses. *Plant Physiol.* 157, 14–28. doi: 10.1104/pp.111.179663

Rimington, W. R., Duckett, J. G., Field, K. J., Bidartondo, M. I., and Pressel, S. (2020). The distribution and evolution of fungal symbioses in ancient lineages of land plants. *Mycorrhiza* 30, 23–49. doi: 10.1007/s00572-020-00938-y

Rousk, K. (2022). Biotic and abiotic controls of nitrogen fixation in cyanobacteria-moss associations. *New Phytol.* 235, 1330–1335. doi: 10.1111/nph.18264

Royan, S., Gutmann, B., Colas des Francs-Small, C., Honkanen, S., Schmidberger, J., Soet, A., et al. (2021). A synthetic RNA editing factor edits its target site in chloroplasts and bacteria. *Commun. Biol.* 4, 545. doi: 10.1038/s42003-021-02062-9

Sakakibara, K., Nishiyama, T., Deguchi, H., and Hasebe, M. (2008). Class 1 KNOX genes are not involved in shoot development in the moss *Physcomitrella patens* but do function in sporophyte development. *Evol. Dev.* 10, 555–566. doi: 10.1111/j.1525-142X.2008.00271.x

Santi, C., Bogusz, D., and Franche, C. (2013). Biological nitrogen fixation in non-legume plants. *Ann. Bot.* 111, 743–767. doi: 10.1093/aob/mct048

Sauret-Güeto, S., Frangedakis, E., Silvestri, L., Rebmann, M., Tomaselli, M., Markel, K., et al. (2020). Systematic tools for reprogramming plant gene expression in a simple model, *Marchantia polymorpha*. *ACS Synth. Biol.* 9, 864–882. doi: 10.1021/acssynbio.9b00511

Schaefer, D. G., and Zrÿd, J. P. (1997). Efficient gene targeting in the moss *Physcomitrella patens*. *Plant J.* 11, 1195–1206. doi: 10.1046/j.1365-313x.1997.11061195.x

Schattat, M. H., Griffiths, S., Mathur, N., Barton, K., Wozny, M. R., Dunn, N., et al. (2012). Differential coloring reveals that plastids do not form networks for exchanging macromolecules. *Plant Cell* 24, 1465–1477. doi: 10.1105/tpc.111.095398

Schlegel, J., Denay, G., Wink, R., Pinto, K. G., Stahl, Y., Schmid, J., et al. (2021). Control of *Arabidopsis* shoot stem cell homeostasis by two antagonistic CLE peptide signalling pathways. *Elife* 10, 1–30. doi: 10.7554/eLife.70934

Schmitz, A. J., Glynn, J. M., Olson, B. J. S. C., Stokes, K. D., and Osteryoung, K. W. (2009). *Arabidopsis* FtsZ2-1 and FtsZ2-2 are functionally redundant, but FtsZ-based plastid division is not essential for chloroplast partitioning or plant growth and development. *Mol. Plant* 2, 1211–1222. doi: 10.1093/mp/ssp077

Schüßler, A. (2000). Glomus claroideum forms an arbuscular mycorrhiza-like symbiosis with the hornwort *Anthoceros punctatus*. *Mycorrhiza* 10, 15–21. doi: 10.1007/s005720050282

Schuler, M. L., Mantegazza, O., and Weber, A. P. M. (2016). Engineering C4 photosynthesis into C3 chassis in the synthetic biology age. *Plant J.* 87, 51–65. doi: 10.1111/tpj.13155

Shaw, J., and Renzaglia, K. (2004). Phylogeny and diversification of bryophytes. *Am. J. Bot.* 91, 1557–1581. doi: 10.3732/ajb.91.10.1557

Shimamura, M. (2016). *Marchantia polymorpha*: Taxonomy, phylogeny and morphology of a model system. *Plant Cell Physiol.* 57, 230–256. doi: 10.1093/pcp/pcv192

Siegfried, K. R., Eshed, Y., Baum, S. F., Otsuga, D., Drews, G. N., and Bowman, J. L. (1999). Members of the YABBY gene family specify abaxial cell fate in *Arabidopsis*. *Development* 126, 4117–4128. doi: 10.1242/dev.126.18.4117

Smith, G. M. (1955). Cryptogamic Botany. Vol. II. Bryophytes and Pteridophytes. *AIBS Bull.* 5, 15–15. doi: 10.1093/aibsbulletin/5.2.15-a

Smith, E., and Griffiths, H. (1996). A pyrenoid-based carbon-concentrating mechanism is present in terrestrial bryophytes of the class Anthocerotae. *Planta* 200, 203–212. doi: 10.1007/BF00208310

Smith, E. C., and Griffiths, H. (1996). The occurrence of the chloroplast pyrenoid is correlated with the activity of a CO2-concentrating mechanism and carbon isotope discrimination in lichens and bryophytes. *Planta* 198, 6–16. doi: 10.1007/BF00197580

Smith, E. C., and Griffiths, H. (2000). The role of carbonic anhydrase in photosynthesis and the activity of the carbon-concentrating-mechanism in bryophytes of the class Anthocerotae. *New Phytol.* 145, 29–37. doi: 10.1046/j.1469-8137.2000.00559.x

Solymosi, K., Lethin, J., and Aronsson, H. (2018). "Diversity and plasticity of plastids in land plants,". Ed. E. Maréchal In *Plastids: Methods and Protocols, Methods in Molecular Biology*. (New York, NY: Springer US), 55–72. doi: 10.1007/978-1-4939-8654-5_4

Stata, M., Sage, T. L., Hoffmann, N., Covshoff, S., Ka-Shu Wong, G., and Sage, R. F. (2016). Mesophyll chloroplast investment in C3 , C4 and C2 species of the genus flaveria. *Plant Cell Physiol.* 57, 904–918. doi: 10.1093/pcp/pcw015

Su, D., Yang, L., Shi, X., Ma, X., Zhou, X., Hedges, S. B., et al. (2021). Large-Scale phylogenomic analyses reveal the monophyly of bryophytes and neoproterozoic origin of land plants. *Mol. Biol. Evol.* 38, 3332–3344. doi: 10.1093/molbev/msab106

Suetsugu, N., Mittmann, F., Wagner, G., Hughes, J., and Wada, M. (2005). A chimeric photoreceptor gene, NEOCHROME, has arisen twice during plant evolution. *Proc. Natl. Acad. Sci. U. S. A.* 102, 13705–13709. doi: 10.1073/pnas.0504734102

Sugano, S. S., Nishihama, R., Shirakawa, M., Takagi, J., Matsuda, Y., Ishida, S., et al. (2018). Efficient CRISPR/Cas9-based genome editing and its application to conditional genetic analysis in *Marchantia polymorpha*. *PloS One* 13, e0205117. doi: 10.1371/journal.pone.0205117

Sugano, S. S., Shirakawa, M., Takagi, J., Matsuda, Y., Shimada, T., Hara-Nishimura, I., et al. (2014). CRISPR/Cas9-mediated targeted mutagenesis in the liverwort *Marchantia polymorpha* l. *Plant Cell Physiol.* 55, 475–481. doi: 10.1093/pcp/pcu014

Szövényi, P. (2016). "The genome of the model species *Anthoceros agrestis*," in *Advances in botanical research*. Ed. S. A. Rensing (London: Elsevier), 189–211. doi: 10.1016/bs.abr.2015.12.001

Szövényi, P., Frangedakis, E., Ricca, M., Quandt, D., Wicke, S., and Langdale, J. A. (2015). Establishment of *Anthoceros agrestis* as a model species for studying the biology of hornworts. *BMC Plant Biol.* 15, 98. doi: 10.1186/s12870-015-0481-x

Szövényi, P., Gunadi, A., and Li, F.-W. (2021). Charting the genomic landscape of seed-free plants. *Nat. Plants* 7, 554–565. doi: 10.1038/s41477-021-00888-z

Szövényi, P., Waller, M., and Kirbis, A. (2019). Evolution of the plant body plan. *Curr. Topics Dev. Biol.* 131, 1–34. doi: 10.1016/bs.ctdb.2018.11.005

Tanahashi, T., Sumikawa, N., Kato, M., and Hasebe, M. (2005). Diversification of gene function: homologs of the floral regulator FLO/LFY control the first zygotic cell division in the moss *Physcomitrella patens*. *Development* 132, 1727–1736. doi: 10.1242/dev.01709

Tanaka, W., Toriba, T., Ohmori, Y., Yoshida, A., Kawai, A., Mayama-Tsuchida, T., et al. (2012). The YABBY gene TONGARI-BOUSHI1 is involved in lateral organ development and maintenance of meristem organization in the rice spikelet. *Plant Cell* 24, 80–95. doi: 10.1105/tpc.111.094797

Tcherkez, G. G. B., Farquhar, G. D., and Andrews, T. J. (2006). Despite slow catalysis and confused substrate specificity, all ribulose bisphosphate carboxylases may be nearly perfectly optimized. *Proc. Natl. Acad. Sci. U. S. A.* 103, 7246–7251. doi: 10.1073/pnas.0600605103

Uchida, N., and Torii, K. U. (2019). Stem cells within the shoot apical meristem: identity, arrangement and communication. *Cell. Mol. Life Sci.* 76, 1067–1080. doi: 10.1007/s00018-018-2980-z

Vaughn, K. C., Campbell, E. O., Hasegawa, J., Owen, H. A., and Renzaglia, K. S. (1990). The pyrenoid is the site of ribulose 1,5-bisphosphate carboxylase/oxygenase accumulation in the hornwort (Bryophyta: Anthocerotae) chloroplast. *Protoplasma* 156, 117–129. doi: 10.1007/BF01560650

Vaughn, K. C., Ligrone, R., Owen, H. A., Hasegawa, J., Campbell, E. O., Renzaglia, K. S., et al. (1992). The anthocerote chioroplast: a review. *New Phytol.* 120, 169–190. doi: 10.1111/j.1469-8137.1992.tb05653.x

Villarreal A, J. C., and Renzaglia, K. S. (2006). Structure and development of nostoc strands in *Leiosporoceros dussii* (Anthocerotophyta): a novel symbiosis in land plants. *Am. J. Bot.* 93, 693–705. doi: 10.3732/ajb.93.5.693

Villarreal, J. C., and Renner, S. S. (2012). Hornwort pyrenoids, carbon-concentrating structures, evolved and were lost at least five times during the last 100 million years. *Proc. Natl. Acad. Sci.* 109, 18873–18878. doi: 10.1073/pnas.1213498109

Villarreal, J. C., and Renzaglia, K. S. (2015). The hornworts: important advancements in early land plant evolution. *J. Bryol.* 37, 157–170. doi: 10.1179/1743282015Y.0000000016

Waller, M., Frangedakis, E., Marron, A., and Sauret-gueto, S. (2022). An optimised transformation protocol for *Anthoceros agrestis* and three more hornwort species. *bioRxiv*. doi: 10.1101/2022.08.10.503456

Wardlaw, C. W. (1955). *Embryogenesis in plants* (San Diego: Methuen, the University of California).

Waters, M. T., Fray, R. G., and Pyke, K. A. (2004). Stromule formation is dependent upon plastid size, plastid differentiation status and the density of plastids within the cell. *Plant J.* 39, 655–667. doi: 10.1111/j.1365-313X.2004.02164.x

Wettstein, F. (1924). Morphologie und Physiologie des Formwechsels der Moose auf genetischler Grundlage. I. Zeitschrift für Indukt. Abstammungs-und Vererbungslehre 33, 1–236.

Whitney, S. M., Houtz, R. L., and Alonso, H. (2011). Advancing our understanding and capacity to engineer nature's CO2-sequestering enzyme, rubisco. *Plant Physiol.* 155, 27–35. doi: 10.1104/pp.110.164814

Zhang, M., Schmitz, A. J., Kadirjan-Kalbach, D. K., Terbush, A. D., and Osteryoung, K. W. (2013). Chloroplast division protein ARC3 regulates chloroplast FtsZ-ring assembly and positioning in *Arabidopsis* through interaction with FtsZ2. *Plant Cell* 25, 1787–1802. doi: 10.1105/tpc.113.111047

frontiers | Frontiers in Plant Science

TYPE Original Research
PUBLISHED 14 November 2023
DOI 10.3389/fpls.2023.1244583

OPEN ACCESS

EDITED BY
Verónica S. Di Stilio,
University of Washington, United States

REVIEWED BY
Ana Campilho,
University of Porto, Portugal
Jesse L. Labbé,
Technology Holding, United States

*CORRESPONDENCE
Shelley R. Hepworth
shelley.hepworth@carleton.ca

†PRESENT ADDRESS
Gamalat Allam,
Department of Biology, Western University,
London, ON, Canada

‡These authors have contributed equally to this work

RECEIVED 22 June 2023
ACCEPTED 17 October 2023
PUBLISHED 14 November 2023

CITATION
Li S, Devi B, Allam G, Bhullar A, Murmu J, Li E and Hepworth SR (2023) Regulation of secondary growth by poplar *BLADE-ON-PETIOLE* genes in Arabidopsis. *Front. Plant Sci.* 14:1244583. doi: 10.3389/fpls.2023.1244583

Regulation of secondary growth by poplar *BLADE-ON-PETIOLE* genes in Arabidopsis

Sibei Li‡, Bhaswati Devi‡, Gamalat Allam†, Armaan Bhullar, Jhadeswar Murmu, Eryang Li and Shelley R. Hepworth*

Department of Biology, Carleton University, Ottawa, ON, Canada

BLADE-ON-PETIOLE (*BOP*) genes are essential regulators of vegetative and reproductive development in land plants. First characterized in *Arabidopsis thaliana* (Arabidopsis), members of this clade function as transcriptional co-activators by recruiting TGACG-motif binding (TGA) basic leucine zipper (bZIP) transcription factors. Highly expressed at organ boundaries, these genes are also expressed in vascular tissue and contribute to lignin biosynthesis during secondary growth. How these genes function in trees, which undergo extensive secondary growth to produce wood, remains unclear. Here, we investigate the functional conservation of *BOP* orthologs in *Populus trichocarpa* (poplar), a widely-used model for tree development. Within the poplar genome, we identified two *BOP*-like genes, *PtrBPL1* and *PtrBPL2*, with abundant transcripts in stems. To assess their functions, we used heterologous assays in Arabidopsis plants. The promoters of *PtrBPL1* and *PtrBPL2*, fused with a β-glucuronidase (GUS) reporter gene showed activity at organ boundaries and in secondary xylem and phloem. When introduced into Arabidopsis plants, *PtrBPL1* and *PtrBPL2* complemented leaf and flower patterning defects in *bop1 bop2* mutants. Notably, Arabidopsis plants overexpressing *PtrBPL1* and *PtrBPL2* showed defects in stem elongation and the lignification of secondary tissues in the hypocotyl and stem. Finally, PtrBPL1 and PtrBPL2 formed complexes with TGA bZIP proteins in yeast. Collectively, our findings suggest that PtrBPL1 and PtrBPL2 are orthologs of Arabidopsis BOP1 and BOP2, potentially contributing to secondary growth regulation in poplar trees. This work provides a foundation for functional studies in trees.

KEYWORDS

BLADE-ON-PETIOLE, TGA bZIP, *Populus trichocarpa*, secondary growth, lignin

Introduction

Populus trichocarpa is a deciduous tree species that is commonly known as black cottonwood or western balsam poplar. A long-lived, mostly diploid species that is native to western North America, it is widely distributed in temperate and cold temperate regions (Cooke and Rood, 2007). *P. trichocarpa* and companion species in the genus *Populus*

(poplar) are valuable model organisms for tree research (Taylor, 2002; Jansson and Douglas, 2007). The genus is closely related to the model plant *Arabidopsis thaliana* (Arabidopsis) and many poplar gene functions are conserved. An available variety of molecular tools, such as genetic transformation methods, CRISPR-based gene editing systems, and a growing number of sequenced genomes, make poplar species ideal for molecular studies (Jansson and Douglas, 2007; Bryant et al., 2020).

BLADE-ON-PETIOLE (BOP) co-transcriptional regulators, first described in Arabidopsis, belong to a family in land plants that have a BTB/POZ (Broad-complex, Tramtrack, and Bric-a-brac/POX virus and zinc finger) domain and ankyrin repeats for interaction with other proteins (Khan et al., 2014; Backer et al., 2019). Family members are classified into two phylogenetic subclades (Khan et al., 2014; Backer et al., 2019). The first subclade contains NPR1-type proteins involved in plant defense whereas BOP-type proteins primarily regulate plant development (Khan et al., 2014; Backer et al., 2019). Proteins from both subclades lack a DNA binding domain and interact TGACG-motif binding (TGA) basic leucine zipper (bZIP) transcription factors for the co-activation or co-repression of target genes. BTB-ankyrin proteins from both subclades can also function as E3 ubiquitin ligase adaptors involved in regulating protein abundance (Fu et al., 2012; Zhang et al., 2017; Chahtane et al., 2018; He et al., 2020). In monocots and dicots, BOPs contribute to a surprisingly large number of developmental processes, including lignin deposition as a defense (Zhang et al., 2019) and during secondary growth (Khan et al., 2012b; Woerlen et al., 2017; Shen et al., 2021; Liu et al., 2022).

In Arabidopsis, *BOP1* and *BOP2* genes are strongly expressed at organ boundaries, zones that connect organs to the plant body (Žádníková and Simon, 2014; Hepworth and Pautot, 2015). These areas regulate growth at the base of organs and produce axillary meristems for the development of lateral branches, flowers, and appendages such as stipules or nectaries. Boundaries are also sites where organs separate by abscission or dehiscence to release foliage, fruits, or seeds (Hepworth and Pautot, 2015). Phenotypic defects in *bop1 bop2* double mutants are concentrated at lateral organ boundaries resulting in elongated leafy petioles, five-petalled flowers with a subtending bract, and defects in abscission (Hepworth et al., 2005; Norberg et al., 2005; McKim et al., 2008). In monocots and dicots, BOP1 and BOP2 paralogs participate in many of the same developmental processes (Wu et al., 2012; Tavakol et al., 2015; Couzigou et al., 2016; Jost et al., 2016; Xu et al., 2016; Toriba et al., 2019; Magne et al., 2020; Liu et al., 2022).

In Arabidopsis, *BOP1* and *BOP2* genes are also expressed in vascular tissues (Hepworth et al., 2005; Khan et al., 2012a). The overexpression of either gene inhibits stem elongation and disrupts secondary growth in stems and the root-hypocotyl (Khan et al., 2012a; Woerlen et al., 2017). In the inflorescence stem, lignified phloem and interfascicular fibers are completed earlier and the central pith becomes lignified in severe lines (Khan et al., 2012a). Secondary growth in the root-hypocotyl is also disrupted, with loss of xylem fiber differentiation (Liebsch et al., 2014; Woerlen et al., 2017). Unlike trees, secondary growth in the majority of the Arabidopsis stem is limited to the secondary thickening of xylem and phloem cell walls and the lignification of interfascicular fibers spaced between the primary vascular bundles. These fibers complete the vascular ring and provide mechanical support (Rogers and Campbell, 2004; Ehlting et al., 2005).

In woody dicot plants, cambium activity initiates in the primary vascular bundles (fascicular cambium) and spreads out to the interfascicular regions where differentiated cells regain the ability to divide (interfascicular cambium). In Arabidopsis, continuous vascular cambium only forms in the root-hypocotyl and at the base of the primary inflorescence 1-2 mm above the rosette (Sehr et al., 2010; Sanchez et al., 2012). The end result is a tube-like sheath of meristematic activity. Daughter cells on the outer rim of the cambium produce secondary phloem (inner bark) whereas daughter cells on the inside make secondary xylem (wood). In forest trees, this activity results in the radial thickening of stems and supports the development of large body architectures (Groover et al., 2006; Sehr et al., 2010; Sanchez et al., 2012).

P. trichocarpa and its relatives have emerged as an excellent platform for the study of trees (Jansson and Douglas, 2007; Bryant et al., 2020). The industrial impact of poplar is significant as hybrid poplars are among the fastest growing temperate forest trees in the world, ready for harvesting at 10 to 20 years. Trees can be grown on forest lands or marginal crop lands. Plantations, totalling some 9.6 million hectares worldwide, contribute to the storage of atmospheric CO_2 as biomass, which is harvested for the production of wood chips, plywood, biofuels, and other materials. Lignin and wood engineering in forest trees can benefit from a detailed understanding of the molecular mechanisms controlling tree architecture and wood development (Sannigrahi et al., 2010; Chanoca et al., 2019).

Here, we investigate the function of two *BOP*-like genes in *P. trichocarpa*. Highly expressed in poplar xylem and phloem, we provide evidence that these genes when heterologously expressed in Arabidopsis can function at organ boundaries and regulate lignin deposition in tissues undergoing secondary growth. We also provide evidence of complex formation with TGA bZIP proteins indicating that gene functional networks might be conserved in poplar trees. The potential evolutionary implications of these findings are discussed.

Materials and methods

Plant material and growth conditions

The *P. trichocarpa* female clone "Nisqually-1" was used (Song et al., 2006). Cuttings from a tree grown on the University of British Columbia campus (a gift of Sean Mansfield) were rooted in soil and grown under natural lighting in a greenhouse. The *Arabidopsis thaliana* Columbia (Col-0) accession was used as the wild type. The double mutant *bop1 bop2* (Hepworth et al., 2005), activation-tagged overexpression line *bop1-6D* and transgenic line *35S:BOP2* (Norberg et al., 2005) were previously described. Surface-sterilized seeds were sown on minimal media agar plates (Haughn and Somerville, 1986). Ten-day-old seedlings were planted in sterilized soil (Promix BX, Premier Tech, Quebec) supplemented

with 20-20-20 fertilizer (Plant Product Co. Ltd, Brampton, Ontario). The plants were grown to maturity in chambers at 21°C under long days (8 h dark/16 h light, intensity 100 μmol m^{-2} s^{-1}).

PtrBPL1 and *PtrBPL2* complementation of Arabidopsis *bop1 bop2* mutant

PtrBPL1 and *PtrBPL2* genes were expressed under the control of a *BOP1* promoter in Arabidopsis *bop1 bop2* mutant plants. This promoter has been previously used for complementation studies (Khan et al., 2015). The cDNA sequences of *PtrBPL1* (Potri.016G040500) and *PtrBPL2* (Potri.006G043400) were amplified by polymerase chain reaction (PCR) using cDNA from mixed poplar tissue as the template and high-fidelity iProof polymerase (Biorad, Hercules, CA). The primers annealed to the 5' and 3' untranslated regions of each gene to ensure that amplification was specific. The resulting products were cloned into pCR™-BluntII-TOPO™ (Invitrogen, ThermoFisher Scientific, Waltham, MA) and verified by DNA sequencing (Eurofins Genomics, Louisville, KY). Verified clones were used as template to amplify the coding regions of *PtrBPL1* and *PtrBPL2* using PtrBPL-XbaI-F and PtrBPL-Sac1-R as the primers. The resulting products were cloned into the corresponding sites of binary vector pBAR (a gift from the Dangl lab, University of North Carolina) downstream of the *AtBOP1* promoter (McKim et al., 2008). The resulting constructs named *BOP1p:PtrBPL1* and *BOP1p:PtrBPL2* were introduced into *Agrobacterium tumefaciens* strain C58C1 pGV101 pMP90 (Koncz and Schell, 1986). Arabidopsis *bop1 bop2* plants were transformed by floral dipping (Clough and Bent, 1998). Glufosinate-resistant primary transformant (T1) plants were selected on soil using the herbicide Finale (Bayer Environmental Sciences, Sacramento, CA). Complementation of *bop1 bop2* leaf, flower, and abscission defects was scored in the T1 generation. The progeny of ten independent T1 lines showing strong complementation were genotyped to confirm that they were *bop1 bop2* double mutants. Three to five independent transgenic lines were selected for further analysis. Primers used for cloning are listed in Supplementary Table S1.

PtrBPL1 and *PtrBPL2* promoter GUS reporter constructs

To determine the expression pattern of *PtrBPL1* and *PtrBPL2* genes, the promoters were PCR-amplified from genomic DNA template extracted from young poplar leaves using a Genomic DNA Mini Kit (Plant) (FroggaBio Inc., Concord, Ontario). A 3938-bp *PtrBPL1* promoter (nucleotides -3867 to +112) was assembled using an overlap PCR approach because the full-length sequence was difficult to amplify. A 2.9-kb *PtrBPL1* promoter fragment (nucleotides -3867 to -2876) was PCR-amplified using ptBPL1-pro-F10 and ptBPL1-pro-R1 as the primers. A 1.1-kb *PtrBPL1* promoter fragment (-2807 to +112) was PCR amplified using BPL1-pro-F8 and BPL1-May14-R as the primers. These two *PtrBPL1* overlapping promoter fragments were gel purified, mixed, and used as template to amplify a full-length product using PtBPL1-pro-F10 and BPL1-May14-R as the primer pair. The resulting *PtrBPL1* promoter (including 112-bp of *PtrBPL1* coding sequence) was column-purified and cloned into a Zero Blunt™ TOPO™ vector (Invitrogen, ThermoFisher Scientific). DNA sequencing identified a 42-bp sequence deletion (nucleotides -3757 to -3715) compared to publicly available database sequence. To create the reporter gene, the *PtrBPL1* promoter was amplified from the above plasmid using BPL1-pro-BamH1-F and BPL1-pro-Nco1-R as the primer pair. The resulting product was column-purified, digested with *Bam*H1 and *Nco*1 restriction enzymes and ligated into the corresponding sites of the pGreen-based $pTGA9_{pro}$:GUS plasmid (Hellens et al., 2000; Murmu et al., 2010). This ligation placed the *PtrBPL1* promoter upstream of a GUS reporter gene as a translational fusion. Similarly, a 4092-bp *PtrBPL2* promoter sequence (nucleotide -4059 to +33) was PCR-amplified using BPL2-4kb-F and BPL2-Promo-R as the primers and cloned into the Zero Blunt™ TOPO™ vector (Invitrogen, ThermoFisher Scientific). The *PtrBPL2* promoter insert was then amplified using BPL2-pro-BamH1-F and BPL2-pro-Nco1-R as the primers, digested with *Bam*HI and *Nco*I restriction enzymes, and cloned into the corresponding sites of $pTGA9_{pro}$:GUS (Murmu et al., 2010). DNA fragments destined for cloning were amplified using iProof high-fidelity polymerase (Biorad, Hercules, CA). All clones were verified by DNA sequencing (Eurofins Genomics). The resulting GUS reporter constructs were co-transformed with pSOUP into *Agrobacterium tumefaciens* strain C58C1 pGV101 pMP90 (Koncz and Schell, 1986; Hellens et al., 2000). Wild-type plants were transformed by floral dipping (Clough and Bent, 1998). Glufosinate-resistant primary transformant (T1) plants were selected on soil using the herbicide Finale (Bayer Environmental Sciences). Multiple independent transgenic lines per construct were evaluated for reporter GUS activity. Three independent transgenic lines were selected for further analysis. Primers used for cloning are listed in Supplementary Table S1.

Constructs for overexpression of *PtrBPL1* and *PtrBPL2*

The coding sequences of *PtrBPL1* and *PtrBPL2* were PCR-amplified from cloned cDNA template using iProof as the polymerase (Biorad) and Pt6s04010CDS-F and Pt6s04010CDS-R primer set, and Pt6s04190CDS-F and Pt6s04190CDS-R primer set, respectively. The resulting products were placed into the Gateway entry vector pCR™8/GW/TOPO™ (Invitrogen, ThermoFisher Scientific) and moved into the pSM3 binary vector (Unda et al., 2017) downstream of a double 35S CaMV promoter (D35S) using Gateway™ LR Clonase™ (Invitrogen, ThermoFisher Scientific). Wild-type plants were transformed as described above. Hygromycin-resistant primary transformants were selected on agar plates. Phenotypes were scored in the T1 generation. Three to five independent transformants were selected for further analysis. Primers used for cloning are listed in Supplementary Table S1.

Reverse transcription-quantitative PCR

Total RNA was isolated from dissected poplar tissues (a gift of the Carl Douglas lab). 2 µg of RNA was used for cDNA synthesis using Superscript III reverse transcriptase (Invitrogen, ThermoFisher Scientific). PCR reactions in triplicate containing 2 µl of 10-fold diluted cDNA, gene-specific primers (Supplementary Table S1) and Power SYBR™ Green Master mix (Invitrogen, ThermoFisher Scientific) were carried out using a StepOnePlus thermocycler (Applied Biosystems, ThermoFisher Scientific). Relative transcript levels were calculated according to Pfaffl (2001). Values were normalized to the poplar elongation factor reference gene *C672* (Wang et al., 2014) and then to young leaf. Data are the average of four measurements for each of two biological replicates. Error bars show standard deviation.

Localization of lignin deposition

Tissues were analyzed for lignin deposition as previously described (Khan et al., 2012b; Woerlen et al., 2017). Arabidopsis stems were harvested from five-week-old plants. A razor blade was used to hand-cut sections from the base of the primary inflorescence about 1 cm above the rosette leaves (Khan et al., 2012b). Hypocotyls were harvested from seven-week-old plants. A razor blade was used to hand-cut sections about 1.5 mm below the rosette leaves. Samples were placed in 2% phloroglucinol dissolved in 95% ethanol for five minutes. Then, five drops of concentrated hydrochloric acid were added. Two minutes were allowed for color development. Immediately, samples were transferred onto a glass slide and a cover slip was added. Images were collected using a Discovery V20 stereomicroscope (Carl Zeiss Canada, North York, Ontario).

Localization of GUS activity

Tissues were analyzed for β-glucuronidase (GUS) activity as previously described (Woerlen et al., 2017) with minor changes. The staining solution contained 4 mM KFe(CN) and 2 mM of 5-bromo-4-chloro-3-indoxyl-β-D-glucuronide (X-Gluc). The samples were incubated at 37°C for 3 to 24 hours until a localized blue precipitate was visible. After clearing in 70% ethanol, the samples were imaged using a Discovery V20 stereomicroscope (Carl Zeiss). For sections, the stained tissue was embedded in Paraplast Plus® (Sigma-Aldrich, St. Louis, MO) and processed using *tert*-butanol instead of xylenes (Woerlen et al., 2017). Tissue sections (20 µm) were fixed onto glass slides and dewaxed with *tert*-butanol. The samples were imaged using an Axio Imager M2 compound microscope (Carl Zeiss).

Yeast two-hybrid assay

Protein-protein interactions were assayed using a Matchmaker™ GAL4-based yeast two-hybrid system (Clontech, Takara Bio USA Inc, San Jose, CA) and Gateway-compatible pGBKT7-DEST (bait) and pGADT7-DEST (prey) plasmids modified from pGBKT7 and pGADT7-Res vectors, respectively (Lu et al., 2009). PtrBPL1 and PtrBPL2 proteins fused to the DNA-binding domain of yeast GAL4 were used as bait. AtTGA1, AtTGA4, AtTGA3, AtTGA7 and AtTGA8/PAN proteins fused to the transcriptional activation domain of yeast GAL4 were used as prey. To prepare Gateway entry vectors, the full-length coding sequences of bait and prey genes were cloned into pCR™8/GW/TOPO™TA (Invitrogen, ThermoFisher Scientific). All entry vector inserts were sequenced to confirm authenticity. To make the final plasmids, recombination reactions were performed using Gateway™ LR Clonase™ II enzyme mix according to the manufacturer's instructions (Invitrogen, ThermoFisher Scientific). Bait and prey plasmid were co-transformed into yeast AH109 strain (Gietz and Schiestl, 2007). Transformed yeast colonies were identified by selection on synthetic complete (SC) media plates lacking Leu and Trp (SC/-Leu/-Trp). Dilution series were spotted onto SC/-Leu/-Trp medium or SC/-Leu-Trp-His medium plus 10 mM 3-amino-1,2,4-triazole (3-AT; Sigma-Aldrich) for assessment of His reporter gene activity. A 3-AT concentration (10 mM) sufficient to distinguish positive growth from background was determined empirically.

Bioinformatics

P. trichocarpa homologs of Arabidopsis BTB-ankyrin and TGA bZIP proteins were identified using the plant homologs tool at The Arabidopsis Information Resource (TAIR) (www.arabidopsis.org). The corresponding *P. trichocarpa* protein sequences were retrieved from Phytozome (Goodstein et al., 2012; phytozome-next.jgi.doe.gov). MEGA version 11 was used for the alignment of protein sequences by MUSCLE (Edgar, 2004) using the default parameters (www.megasoftware.net). Maximum Likelihood trees were constructed based on 100 bootstrap replicates using the Jones-Taylor-Thornton Model. The BOXSHADE alignment and sequence logos were prepared using Geneious Prime 2022.1 (www.geneioius.com). The percent similarity of protein pairs was calculated using the Expasy SIM tool (www.expasy.org/sim).

Promoter analysis

The 500-bp promoter sequences upstream of the translational start sites of *AtBOP1*, *AtBOP2*, *PtrBPL1*, and *PtrBPL2* genes were retrieved from their genome assemblies found at TAIR (https://www.arabidopsis.org/) or Phytozome (https://phytozome-next.jgi.doe.gov/). Scanning for Transcription Factor Binding Sites (TFBS) was carried out using PlantPAN 3.0 (http://plantpan.itps.ncku.edu.tw/index.html). Selected TFBS were aligned to statistically enriched 6-mers identified by the motif finder tool at TAIR. Binding site locations were visualized by using TBtools v1.123 (Chen et al., 2020).

10.3389/fpls.2023.1244583

Results

Identification of BTB-ankyrin and TGA bZIP gene families in poplar

In the *P. trichocarpa* (poplar) genome, six BTB-ankyrin proteins were identified. The phylogenetic relationship Arabidopsis and poplar BTB-ankyrin proteins was investigated (Figure 1A). This analysis revealed one NPR1 protein (Potri.006G148100), three NPR3/4 proteins (Potri.012G118300; Potri.012G118500; Potri.015G117200) and two poplar BOP-like proteins designated as PtrBPL1 (Potri.016G040500) and PtrBPL2 (Potri.006G043400), respectively. Multiple sequence alignment showed that PtrBPL1 and PtrBPL2 are 94.3% similar to each other at the amino acid level and 80.2% versus 75.6% similar to AtBOP1, respectively. The similarity is broadly distributed across the length of the proteins, not just within the BTB/POZ and ankyrin repeat domain (Figures 1B–D; Supplementary Figure S1). Less conserved regions are situated within the BTB/POZ domain and near the C-terminus. For example, PtrBPL1 contains a deletion in the C-terminus compared to AtBOP1/2 and PtrBPL2 proteins (Figure 1B; Supplementary Figure S1). In parallel, we investigated the phylogenetic relationship of poplar TGA bZIP proteins as potential functional partners. Representatives from all five TGA clades found in Arabidopsis are present (Figure 1E; Supplementary Figure S2). Given these overall similarities, we anticipated that PtrBPL1 and PtrBPL2 might have conserved activities similar to AtBOP1 and AtBOP2.

PtrBPL1 and *PtrBPL2* expression pattern

We next obtained expression data for *PtrPBL1* and *PtrBPL2* from the Bio-Analytic Resource for Plant Biology (BAR, www.utoronto.ca/bar). These data showed the wide expression of both genes in poplar tissues including seedlings, young leaves, catkins, roots, and xylem (Figures 2A, B). We then used RT-qPCR to monitor transcript abundance in selected tissues. These data showed that *PtrBPL1* and *PtrBPL2* transcripts are enriched in the petiole region of leaves compared to the blade. Significant expression was also observed in xylem and phloem tissues of young poplar stems (Figure 2C).

We next investigated the spatial and temporal expression of *PtrBPL1* and *PtrBPL2* genes, by monitoring the expression of *PtrBPL1p:GUS* and *PtrBPL2p:GUS* reporter genes in Arabidopsis plants (Figure 2D). In seedlings, both genes were expressed in boundaries at the base of the cotyledons. During flowering, both genes were expressed at nodes in the stem where a boundary forms at the base of the flower pedicel. GUS expression was evident in floral organ boundaries and abscission zones at the base of young siliques for *PtrBPL1* but not *PtrBPL2* (Supplementary Figure S3). The vasculature of cotyledons, leaves, and the hypocotyl also showed differential expression. *PtrBPL2* but not *PtrBPL1* was expressed

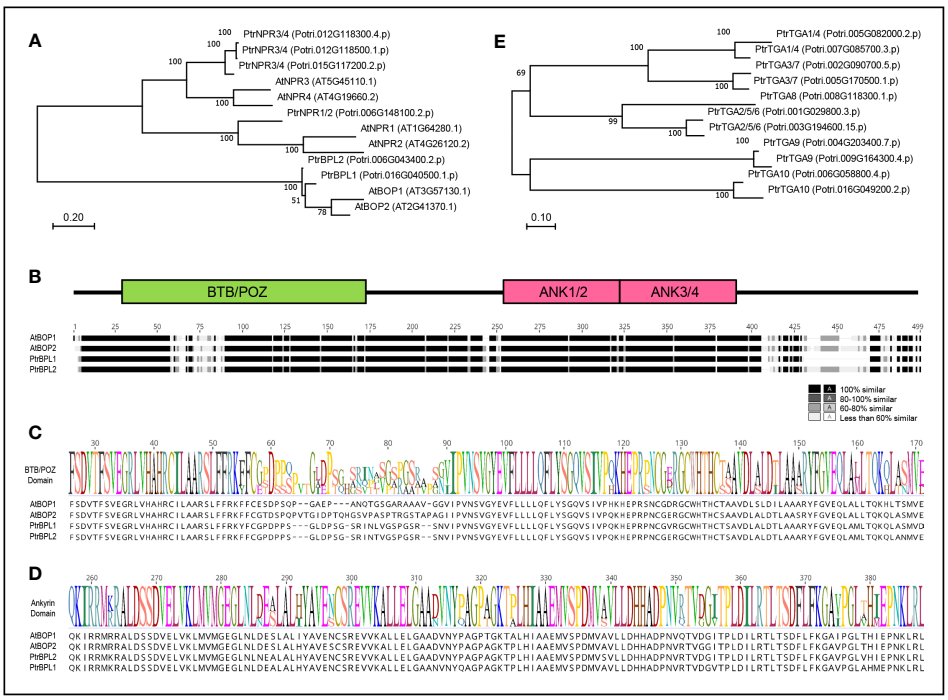

FIGURE 1
Proteins encoded by BTB-ankyrin and TGA bZIP genes from Arabidopsis and poplar. **(A)** Maximum Likelihood tree showing phylogenetic relationships between Arabidopsis (At) and poplar (Ptr) BTB-ankyrin proteins. **(B)** Multiple sequence alignment of AtBOP and PtrBPL proteins with corresponding domain map showing the relative position of conserved BTB/POZ and ankyrin (ANK) domains. Segments of highest similarity or identity are colored darkest and segments of lowest identity or similarity are colored lightest. **(C)** BTB/POZ domain sequence logo. **(D)** Ankyrin domain sequence logo. Protein sequences with listed identification numbers were retrieved from TAIR (www.arabidopsis.org) or Phytozome (phytozome-next.jgi.doe.gov). **(E)** Maximum Likelihood tree showing phylogenetic relationships between PtrTGA proteins.

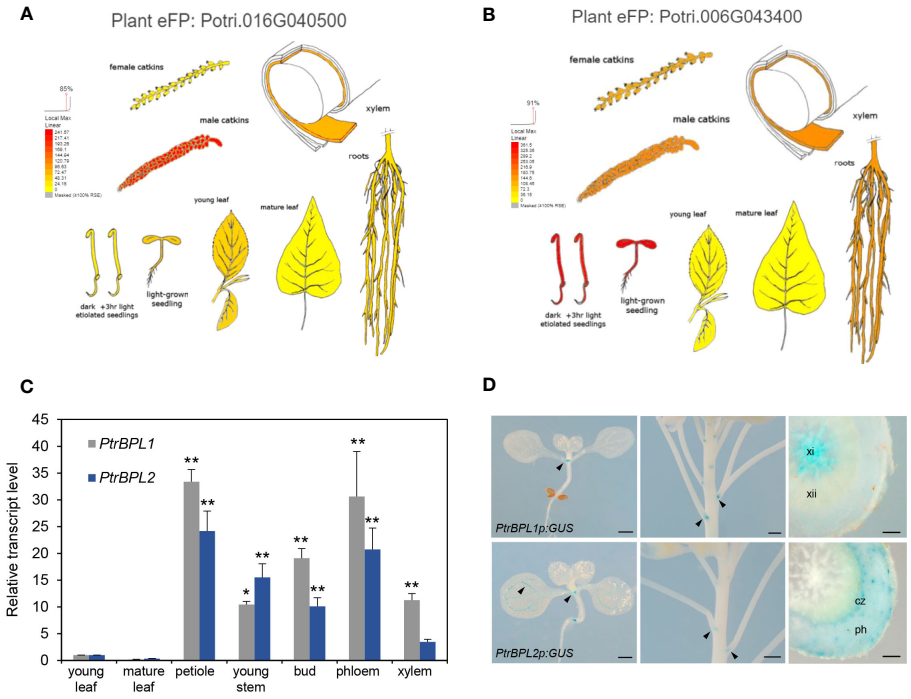

FIGURE 2
Expression of *PtrBPL1* and *PtrBPL2* in poplar and Arabidopsis. **(A, B)** Transcriptome data for *P. trichocarpa* compiled by the Bio-Analytic Resource for Plant Biology (www.bar.utoronto.ca). Red, high expression; orange, medium expression; yellow, lower expression. Plant eFP viewer output for **(A)** *PtrBPL1* and **(B)** *PtrBPL2*. **(C)** The relative abundance of *PtrBPL1* and *PtrBPL2* transcript was independently measured using RT-qPCR in dissected poplar tissues. Data are the average ± SD of four measurements performed on each of two biological replicates. Values were normalized to young leaf. Asterisks indicate significant differences between tissues compared with young leaf (ANOVA with Tukey's test, $^{**}P<0.01$, $^{*}P<0.05$). **(D)** Expression patterns of *PtrBPL1p:GUS* and *PtrBPL2p:GUS* in Arabidopsis seedlings, inflorescences, and sectioned hypocotyls. Arrows denote expression at organ boundaries. xi, secondary xylem I; xii, secondary xylem II; ph, secondary phloem; cz, cambium zone. Scale bars, 500 µm except 100 µm for hypocotyl sections.

in veins of leaves (Figure 2D; Supplementary Figure S3). At the seedling stage, both genes were expressed at the root tip and at the base of lateral roots (Supplementary Figure S3). In the hypocotyl, *PtrBPL1* was strongly expressed in early secondary xylem (xylem I) whereas *PtrBPL2* was expressed at the outer edge of the cambial zone and in secondary phloem (Figure 2D; Supplementary Figure S3). Neither *AtBOP1* nor *AtBOP2* are expressed in secondary xylem (Liebsch et al., 2014; Woerlen et al., 2017) indicating a possible difference in gene regulation between the two species. To investigate this difference, a statistical motif analysis was carried out using the promoter regions (500 base pairs upstream of the start codon) of all four genes. This analysis showed an enrichment of MYB-related and NAC transcription factor binding sites in the promoters of *PtrBPL1* and *PtrBPL2* compared to *AtBOP1* and *AtBOP2* (Supplementary Figure S4) implicating these factors in the differential regulation of poplar orthologs.

PtrPBL1 and *PtrBPL2* can complement *bop1 bop2* leaf and flower patterning defects

To investigate to what extent PtrBPL1 and PtrBPL2 can substitute for AtBOP1 and AtBOP2, we expressed *PtrBPL1* and *PtrBPL2* under the control of an *AtBOP1* promoter in *bop1 bop2* mutants and tested for complementation. In total, we obtained 203 primary (T1) transformants for *BOP1p:PtrBPL1* and 212 primary transformants for *BOP1p:PtrBPL2* (Supplementary Table S2). Characteristic defects in *bop1 bop2* mutants include leafy petioles, loss of floral organ abscission, and flowers with a bract and extra petals on the abaxial side (Hepworth et al., 2005). Strong or medium complementation of the leaf phenotype was observed in 54% and 52% of *PtrBPL1* and *PtrBPL2* transformants, respectively (Figure 3; Supplementary Table S2). Floral patterning defects were significantly restored in 65% and 76% of *PtrBPL1* and *PtrBPL2* transformants scored, respectively (Supplementary Table S2). Floral organ abscission was significantly restored in 76% and 62% of *PtrBPL1* and *PtrBPL2* transformants scored, respectively (Figure 3; Supplementary Table S2). These data confirm that heterologous expression of *PtrBPL1* and *PtrBPL2* can complement *bop1 bop2* mutant phenotypes.

Overexpression of *PtrBPL1* and *PtrBPL2* alters secondary growth

Plants that overexpress *AtBOP1* or *AtBOP2* are short and bushy, with a wider pattern of secondary lignin deposition in stems (Khan et al., 2012b). Unlike trees, a continuous vascular cambium does not

10.3389/fpls.2023.1244583

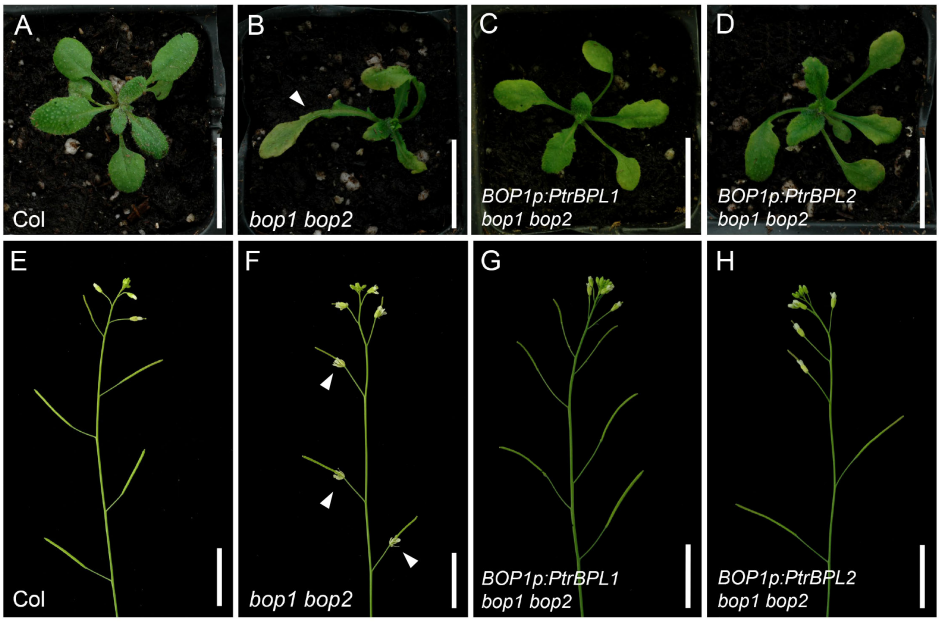

FIGURE 3
Complementation of Arabidopsis *bop1 bop2* leaf and flower defects with *PtrBPL1* and *PtrBPL2*. *PtrBPL1* and *PtrBPL2* coding regions were expressed under the control of the *AtBOP1* promoter in *bop1 bop2* plants. Representative plants are shown in the T2 generation. See Supplementary Table S2 for quantitative analysis of complementation for *bop1 bop2* defects in leaf morphology, floral patterning, and abscission. **(A, B)** Wild-type plant showing **(A)** smooth leaf petioles and **(B)** inflorescence with floral organ abscission. **(C, D)** A *bop1 bop2* mutant showing **(C)** leaves with a blade-on-petiole phenotype (arrow) and **(D)** inflorescence with asymmetric flowers and loss of floral organ abscission (arrows). **(E, F)** A *BOP1p:PtrBPL1 bop1 bop2* plant showing **(E)** smooth leaf petioles and **(F)** inflorescence with floral organ abscission restored. **(G, H)** A *BOP1p:PtrBPL2 bop1 bop2* plant showing **(G)** smooth leaf petioles and **(H)** inflorescence with floral organ abscission restored. Scale bars, 1.5 cm.

form except at the base of the stem. Instead, secondary growth is evident as the differentiation of abundant lignified interfascicular fibers (Ehlting et al., 2005).

To test the effect of *PtrBPL1* and *PtrBPL2* on stem development, Arabidopsis plants were transformed with a construct driving *PtrBPL1* and *PtrBPL2* expression from a strong, constitutive double cauliflower mosaic virus 35S promoter (D35S). Flowering *D35S:PtrBPL1* and *D35S:PtrBPL2* plants showed a loss of apical dominance and reduced stature in comparison to wild-type plants (Figure 4; Supplementary Table S3). The stems of 5-6 representative *D3SS : PtrBPL1* and *D35S:PtrBPL2* plants were hand-sectioned and stained with phloroglucinol to test for changes in lignin deposition. Several plants in this population showed an expanded pattern of lignin deposition in stems.

In the root-hypocotyl where a continuous vascular cambium forms, two phases of secondary growth take place (Chaffey et al., 2002; Nieminen et al., 2015). During the first phase, the xylem I is composed of lignified vessel cells in a matrix of non-lignified parenchyma. Flowering triggers the second phase, in which xylem II forms as a thick ring composed of lignified fibers interspersed with lignified vessels (Chaffey et al., 2002; Nieminen et al., 2015). Arabidopsis plants that overexpress *AtBOP1* and *AtBOP2* lack xylem II features in the upper part of the root (Woerlen et al., 2017) and hypocotyl (Liebsch et al., 2014).

Analysis of secondary growth in the hypocotyl of *D35S:PtrBPL1* and *D35S:PtrBPL2* lines showed at least one *D35S:PtrBPL1* line (n=3) missing xylem II fibers and vessels similar to *bop1-6D* and *35S:BOP2* control plants (Figure 4; Supplementary Figure S5). The xylem II ring in all *D35S:PtrBPL2* lines (n=3) was reduced in thickness compared to wild-type control plants. These data provide further evidence that *PtrBPL1* and *PtrBPL2* can functionally substitute in Arabidopsis plants.

PtrBPL1 and PtrBPL2 interact with TGA bZIP factors

BTB-ankyrin proteins perform a variety of function by utilizing TGA bZIP factors as interaction partners (Backer et al., 2019). For example, Arabidopsis BOP1 and BOP2 interact with clade I and clade III TGAs in yeast (Hepworth et al., 2005). Such complexes are implicated in the regulation of stem development and lignin deposition in plants (Wang et al., 2019; Zhang et al., 2019). Arabidopsis BOP1 and BOP2 also interact with PAN/TGA8 for patterning functions in the flower (Hepworth et al., 2005). A highly sensitive method for detecting protein-protein interactions, we used the yeast two-hybrid assay to assess PtrBPL interactions with AtTGA factors. PtrBPL1 and PtrBPL2 fused to the DNA-binding domain of the yeast transcription activator protein GAL4 were used as bait. AtTGA1, AtTGA4, AtTGA3, and AtTGA7 fused to the activation domain of GAL4 were used as prey. Figure 5 shows that PtrBPL1 and PtrBPL2 interact with AtTGA1, AtTGA4, AtTGA3, and AtTGA7 providing evidence of conserved functional partners in Arabidopsis and poplar.

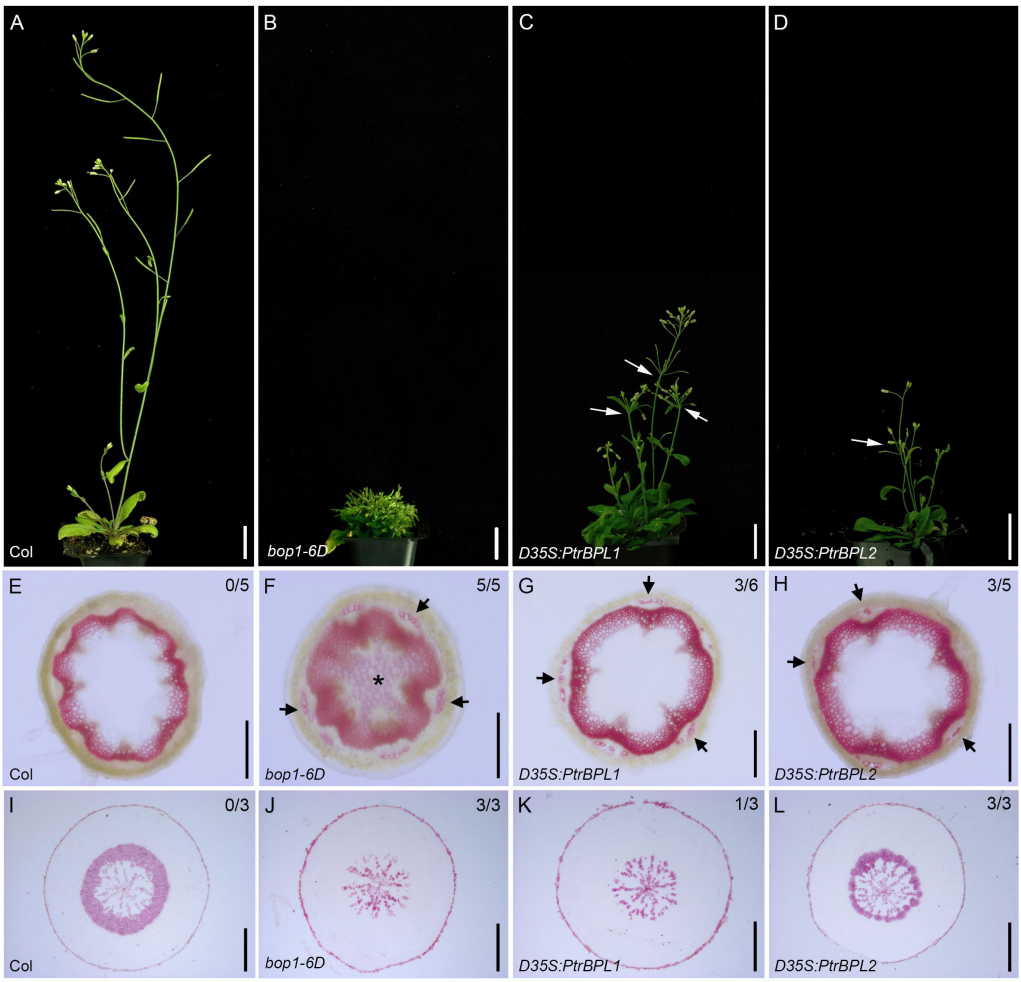

FIGURE 4
Overexpression of *PtrBPL1* and *PtrBPL2* in Arabidopsis plants. *PtrBPL1* and *PtrBPL2* coding regions were expressed under the control of a double 35S (*D35S*) cauliflower mosaic virus promoter in wild-type Arabidopsis plants. **(A-D)** Representative flowering plants are shown in the T1 generation. See Supplementary Table S3 for quantitative analysis. **(A)** Wild type plant, showing strong apical dominance and elongated internodes. **(B)** *bop1-6D* plant, showing a bushy, dwarf stature. **(C)** *D35S:PtrBPL1* plant, showing a bushy, semi-dwarf stature. Arrows, clustered flowers and siliques. **(D)** *D35S:PtrBPL2* plant, showing a bushy, semi-dwarf stature. Arrows, clustered flowers and siliques. **(E-H)** Transverse sections from the base of fully elongated stems were stained phloroglucinol-HCl to reveal lignin (pink). Top left, number of independent transgenic lines showing abnormal lignin deposition. Representative sections are shown for: **(E)** wild-type stem, showing a continuous vascular ring. **(F)** *bop1-6D* stem, showing a thicker vascular ring, lignified pith (asterisk) and lignified phloem fibers (arrows) **(G)** *D35S:PtrBPL1* stem, showing a thick vascular ring and lignified phloem fibers (arrows). **(H)** *D35S:PtrBPL2* stem, showing a thick vascular ring and lignified phloem fibers (arrows). **(I-L)** Transverse sections from the middle of the hypocotyl (1.5 mm below the rosette leaves) were stained phloroglucinol-HCl to reveal lignin (pink). Top left, number of independent transgenic lines showing abnormal lignin deposition. Representative sections are shown for: **(I)** Wild-type hypocotyl, showing a thick ring of xylem II. **(J)** *bop1-6D* hypocotyl, showing a lack of xylem II fibers and vessels. **(K)** *D35S:PtrBPL1* hypocotyl, showing a lack of xylem II fibers and vessels. **(L)** *D35S:PtrBPL2* hypocotyl, showing a xylem II ring of reduced thickness, compared to the wild type. Scale bars: **(A-D)** 1.5 cm; **(E-H)** 0.25 mm; **(I-L)** 0.5 mm.

Discussion

Trees display prominent radial growth in the stem in which secondary xylem and phloem tissues are produced by the vascular cambium. Current knowledge regarding the genetic regulation of cambium activity and secondary growth is still incomplete (Wang et al., 2021). Therefore, understanding gene families potentially involved in this process is desirable.

The BOP family of co-transcriptional regulators are conserved in dicots and monocots and contribute to numerous developmental processes. Studies in dicots such as tobacco (Wu et al., 2012), legumes (Frankowski et al., 2015; Couzigou et al., 2016; Magne et al., 2018), tomato (Xu et al., 2016; Izhaki et al., 2018) and monocots such as rice (Toriba et al., 2020), barley (Tavakol et al., 2015; Jost et al., 2016) and *Brachypodium* (Magne et al., 2020; Liu et al., 2022) reveal highly conserved functions, comparable to Arabidopsis, that influence organ patterning, inflorescence architecture, and abscission (Khan et al., 2014; Hepworth and Pautot, 2015). Taxon-specific roles in the maintenance of symbiotic nodule identity (Couzigou et al., 2012; Magne et al., 2018) and rhizome development (Toriba et al., 2020) have also been identified.

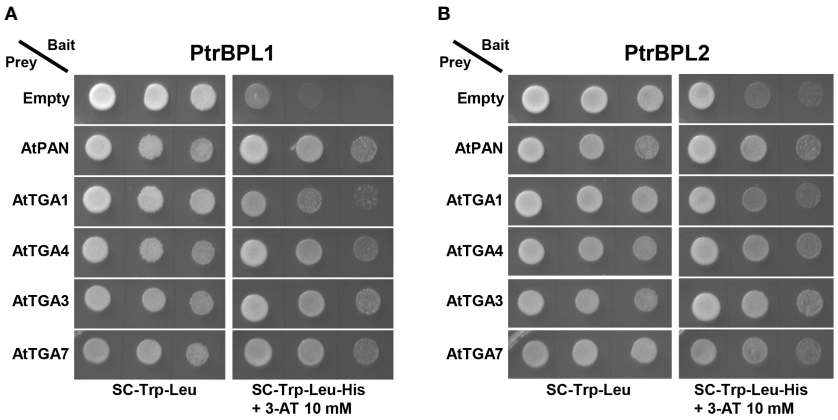

FIGURE 5
Pair-wise yeast two-hybrid assays showing **(A)** PtrBPL1 and **(B)** PtrBPL2 interaction with AtTGAs. PtrBPL1 and PtrBPL2 baits were fused to the DNA-binding domain of yeast GAL4. AtTGA1, AtTGA4, AtTGA3, and AtTGA7 preys were fused to the transcriptional activation domain of yeast GAL4. Plasmid constructs were co-transformed into yeast AH109 strain before serial dilutions (10^{-1}, 10^{-2}, 10^{-3}) were plated onto SC/-Trp/-Leu medium with or without histidine + 10 mM 3-AT. Growth on SC/-Trp/-Leu/-His/+3-AT above background confirms a protein-protein interaction. Dilutions were spotted in replicate onto SC/-Trp/-Leu/-His/+3-AT medium. Photos on SC/-Trp/-Leu were taken three days after plating. For all assays, interaction with AtPAN/TGA8 was used as a positive control and an empty prey vector was used as a negative control.

In flowering plants, BOPs are involved in boundary formation. These specific domains are important for the separation of meristematic regions from lateral organs (Aida and Tasaka, 2006; Žádníková and Simon, 2014). Compared to the shoot apical meristem, our knowledge of boundaries and their involvement in cambium meristems is limited. The conservation of BOPs across the plant kingdom (Khan et al., 2014) makes it plausible that orthologs in trees have roles in the vascular cambium and secondary growth.

The results shown here indicate that *PtrBPL1* and *PtrBPL2* play a role in secondary growth when overexpressed in Arabidopsis. *D35S:PtrBPL1* and *D35S:PtrBPL2* transgenic plants were characterized by dwarf stems with a thicker vascular ring and more developed phloem fibers whereas the increased activity of these genes in the hypocotyl interfered with xylem II production. Overexpression of either *PtrBPL1* or *PtrBPL2* resulted in phenotypes that were highly similar to those observed in Arabidopsis plants with overexpression of *AtBOP1* or *AtBOP2* (Khan et al., 2012b; Woerlen et al., 2017). Furthermore, the expression of *PtrBPL1* or *PtrBPL2* transgenes in a *bop1 bop2* mutant background was sufficient to rescue leaf and floral patterning defects. Abscission defects in the *bop1 bop2* mutant were also corrected. The *PtrBPL1p:GUS* and *PtrBPL2p:GUS* expression patterns in Arabidopsis plants were consistent with a role in boundary patterning and secondary growth. Finally, we identified a family of TGA bZIP factors in poplar with a clade structure similar that in Arabidopsis plants. Yeast two hybrid assays indicated that PtrBPL1 and PtrBPL2 can interact with AtTGAs known to mediate roles in plant development and lignin deposition. All of these results strongly suggest that BOP1/2-TGA modules characterized in Arabidopsis are conserved in *P. trichocarpa*. Therefore, it is feasible they contribute to stem development in trees.

In Arabidopsis plants, *BOP1* and *BOP2* genes are repressed by the class I KNOX homeodomain transcription factors SHOOT MERISTEMLESS (STM) and BREVIPEDICELLUS (BP) during meristem maintenance, stem development, and secondary xylem formation (Jun et al., 2010; Khan et al., 2012b; Liebsch et al., 2014; Khan et al., 2015; Woerlen et al., 2017). Consistent with these findings, *PtrBPL1* is significantly downregulated in the stem of hybrid poplar overexpressing the STM ortholog ARBORKNOX1 (ARK1) (Liu et al., 2015). Both ARK1 and ARK2 (ortholog of BP) are strongly expressed in the cambial zone (Groover et al., 2006; Du et al., 2009). In the ARK1 overexpressor, the boundary between the cambium and the secondary xylem was uneven and phloem fibers were reduced in number (Groover et al., 2006). In the ARK2 overexpressor, extra secondary phloem was produced at the expense of phloem fibers and secondary xylem leading to an overall decrease in the differentiation of lignified cell-types. Conversely, an *ark2* mutant generated by artificial miRNA silencing showed a premature differentiation of secondary xylem and phloem fibers, similar to the *bp* mutant in Arabidopsis (Du et al., 2009).

Studies in the tropical Cannabaceae tree *Parasponia andersonii* species complement these findings (Shen et al., 2021). CRISPR-Cas9 loss-of-function mutants in the *AtBOP1* ortholog *PanNODULE ROOT1 (PanNOOT1)* were altered in the development of xylem and phloem tissues without any obvious difference in cambium organization and size. Compared to the wild-type, the differentiation of secondary xylem and phloem was inhibited resulting in a reduced stem diameter. Transcriptomic data showed a reduction in the expression of lignin metabolism-related genes (Shen et al., 2021). In both Arabidopsis and cotton (*Gossypium hirsutum*) and the grass *Brachypodium distachyon* model, BOPs positively regulate the expression of lignin biosynthesis genes and lignin deposition in stems (Khan et al., 2012b; Zhang et al., 2019; Liu et al., 2022).

In Arabidopsis plants, BOP1 and BOP2 promote the expression of two homeobox genes to influence lignin deposition (Khan et al.,

2012a; Khan et al., 2012b; Woerlen et al., 2017). Poplar plants contain homeobox genes that are highly similar to *ARABIDOPSIS HOMEOBOX GENE 1* (*ATH1*) (Potri.018G054700/Potri.006G230700) and *KNOTTED-LIKE FROM ARABIDOPSIS THALIANA 6* (*KNAT6*) (Potri.010G043500/Potri.008G188700) suggesting that downstream pathway components are conserved. The homologous genes in *P. andersonii* were significantly downregulated in *Pannoot1* stems showing a similar regulation as in Arabidopsis plants (Shen et al., 2021). The *PagKNAT2/6b* gene from a hybrid poplar clone (*P. alb*a X *P. glandulosa*) is highly expressed in xylem and phloem. Compared to controls plants, transgenic poplar clones overexpressing *PagKNAT2/6b* showed a reduction in xylem formation by negatively regulating the expression of NAC domain transcription factor genes including *PagXYLEM NAC DOMAIN 1* as a direct target (Zhao et al., 2020).

Spatial and temporal differences between *PtrBPL1p:GUS* and *PtrBPL2p:GUS* expression were observed. In Arabidopsis plants, the *PtrBPL1* promoter was active in xylem I whereas *PtrBPL2* the promoter was active at the boundary of the cambial zone and secondary phloem (Figures 2A, B, D). By contrast, a *PanNOOT1p:GUS* reporter was expressed in all three tissues during secondary growth (Shen et al., 2021). A similar pattern to *PanNOOT1* was detected in aspen (*P. tremula*) and birch (*Betula pendula*) using high-spatial-resolution gene expression mapping (Sundell et al., 2017; Alonso-Serra et al., 2019; Shen et al., 2021). By contrast, *AtBOP1p:GUS* and *AtBOP2p:GUS* expression is normally repressed by BP in the cambial zone and secondary xylem of the root and hypocotyl (Liebsch et al., 2014; Khan et al., 2015; Woerlen et al., 2017). Thus, divergent transcriptional regulation may account for phenotypic differences in secondary growth between species. Compared to *AtBOP1* and *AtBOP2*, the *PtrBPL1* and *PtrBPL2* promoters had a higher number of predicted binding sites for MYB-related and NAC transcription factors, which as a group contribute strongly to secondary growth in plants (Nakano et al., 2015).

Considering all of the above, BOP-TGA modules characterized in Arabidopsis are likely conserved in poplar. Information gained from this study forms a basis for further exploration of networks that regulate cambium development and secondary growth in trees.

Data availability statement

The raw data supporting the conclusions of this article will be made available by the authors, without undue reservation.

Author contributions

SH and EL designed the research. SL, BD, GA, JM, and EL performed the research. AB carried out bioinformatics analysis. SL, JM, and SH wrote the article. All authors contributed to the article and approved the submitted version.

Funding

This work was supported by a Discovery Grant from the Natural Sciences and Engineering Research Council (NSERC) of Canada (RGPIN-2016-06193).

Acknowledgments

We thank Carl Douglas and Shawn Mansfield at the University of British Columbia for the gift of poplar cuttings, vectors, and poplar tissue cDNA. We thank Ying Wang and Kevin Xiong for help with cloning and Jenna O'Neill for images of GUS-stained seedlings.

Conflict of interest

The authors declare that the research was conducted in the absence of any commercial or financial relationships that could be construed as a potential conflict of interest.

Publisher's note

Supplementary material

The Supplementary Material for this article can be found online at: https://www.frontiersin.org/articles/10.3389/fpls.2023.1244583/full#supplementary-material

References

Aida, M., and Tasaka, M. (2006). Genetic control of shoot organ boundaries. *Curr. Opin. Plant Biol.* 9, 72–77. doi: 10.1016/j.pbi.2005.11.011

Alonso-Serra, J., Safronov, O., Lim, K. J., Fraser-Miller, S. J., Blokhina, O. B., Campilho, A., et al. (2019). Tissue-specific study across the stem reveals the chemistry and transcriptome dynamics of birch bark. *New Phytol.* 222, 1816–1831. doi: 10.1111/nph.15725

Backer, R., Naidoo, S., and van den Berg, N. (2019). The NONEXPRESSOR OF PATHOGENESIS-RELATED GENES 1 (NPR1) and related family: mechanistic insights in plant disease resistance. *Front. Plant Sci.* 10. doi: 10.3389/fpls.2019.00102

Bryant, N. D., Pu, Y., Tschaplinski, T. J., Tuskan, G. A., Muchero, W., Kalluri, U. C., et al. (2020). Transgenic poplar designed for biofuels. *Trends Plant Sci.* 25, 881–896. doi: 10.1016/j.tplants.2020.03.008

Chaffey, N., Cholewa, E., Regan, S., and Sundberg, B. (2002). Secondary xylem development in Arabidopsis: a model for wood formation. *Plant Physiol.* 114, 594–600. doi: 10.1034/j.1399-3054.2002.1140413.x

Chahtane, H., Zhang, B., Norberg, M., Lemasson, M., Thévenon, E., Bakó, L., et al. (2018). LEAFY activity is post-transcriptionally regulated by BLADE ON PETIOLE2 and CULLIN3 in Arabidopsis. *New Phytol.* 220, 579–592. doi: 10.1111/nph.15329

Chanoca, A., de Vries, L., and Boerjan, W. (2019). Lignin engineering in forest trees. *Front. Plant Sci.* 10. doi: 10.3389/fpls.2019.00912

Chen, C., Chen, H., Zhang, Y., Thomas, H. R., Frank, M. H., He, Y., et al. (2020). TBtools: an integrative toolkit developed for interactive analyses of big biological data. *Mol. Plant* 13, 1194–1202. doi: 10.1016/j.molp.2020.06.009

Clough, S. J., and Bent, A. F. (1998). Floral dip: a simplified method for *Agrobacterium*-mediated transformation of *Arabidopsis thaliana*. *Plant J.* 16, 735–743. doi: 10.1046/j.1365-313x.1998.00343.x

Cooke, J. E. K., and Rood, S. B. (2007). Trees of the people: the growing science of poplars in Canada and worldwide. *Can. J. Bot.* 85, 1103–1110. doi: 10.1139/b07-125

Couzigou, J. M., Magne, K., Mondy, S., Cosson, V., Clements, J., and Ratet, P. (2016). The legume *NOOT-BOP-COCH-LIKE* genes are conserved regulators of abscission, a major agronomical trait in cultivated crops. *New Phytol.* 209, 228–240. doi: 10.1111/nph.13634

Couzigou, J. M., Zhukov, V., Mondy, S., Heba, G. A., Cosson, V., Noel Ellis, T. N., et al. (2012). *NODULE ROOT* and *COCHLEATA* maintain nodule development and are legume orthologs of Arabidopsis *BLADE-ON-PETIOLE* genes. *Plant Cell* 24, 4498–4510. doi: 10.1105/ypc.112.103747

Du, J., Mansfield, S. D., and Groover, A. T. (2009). The *Populus* homeobox gene *ARBORKNOX2* regulates cell differentiation during secondary growth. *Plant J.* 60, 1000–1014. doi: 10.1111/j.1365-313x.2009.04017.x

Edgar, R. C. (2004). MUSCLE: multiple sequence alignment with high accuracy and high throughput. *Nucleic Acids Res.* 32, 1792–1797. doi: 10.1093/nar/gkh340

Ehlting, J., Mattheus, N., Aeschliman, D. S., Li, E., Hamberger, B., Cullis, I. F., et al. (2005). Global transcript profiling of primary stems from *Arabidopsis thaliana* identifies candidate genes for missing links in lignin biosynthesis and transcriptional regulators of fiber differentiation. *Plant J.* 42, 618–640. doi: 10.1111/j.1365-313x.2005.02403.x

Frankowski, K., Wilmowicz, E., Kućko, A., Zienkiewicz, A., Zienkiewicz, K., and Kopcewicz, J. (2015). Molecular cloning of the *BLADE-ON-PETIOLE* gene and expression analyses during nodule development in *Lupinus luteus*. *Plant Physiol.* 179, 35–39. doi: 10.1016/j.jplph.2015.01.019

Fu, Z. Q., Yan, S., Saleh, A., Wang, W., Ruble, J., Oka, N., et al. (2012). NPR3 and NPR4 are receptors for the immune signal salicylic acid in plants. *Nature* 486, 228–232. doi: 10.1038/nature11162

Gietz, R. D., and Schiestl, R. H. (2007). High-efficiency yeast transformation using the LiAc/SS carrier DNA/PEG method. *Nat. Protoc.* 2, 31–34. doi: 10.1038/nprot.2007.13

Goodstein, D. M., Shu, S., Howson, R., Neupane, R., Hayes, R. D., Fazo, J., et al. (2012). Phytozome: a comparative platform for green plant genomics. *Nucleic Acids Res.* 40, D1178–D1186. doi: 10.1093/nar/gkr944

Groover, A. T., Mansfield, S. D., DiFazio, S. P., Dupper, G., Fontana, J. R., Millar, R., et al. (2006). The *Populus* homeobox gene *ARBORKNOX1* reveals overlapping mechanisms regulating the shoot apical meristem and the vascular cambium. *Plant Mol. Biol.* 61, 917–932. doi: 10.1007/s11103-006-0059-y

Haughn, G. W., and Somerville, C. (1986). Sulfonylurea-resistant mutants of *Arabidopsis thaliana*. *Molec. Gen. Genet.* 204, 430–434. doi: 10.1007/bf00331020

He, L., Lei, Y., Li, X., Peng, Q., Liu, W., Jiao, K., et al. (2020). *Symmetric petals 1* encodes an ALOG domain protein that controls floral organ internal asymmetry in pea (*Pisum sativum L.*). *Int. J. Mol. Sci.* 21, 1–15. doi: 10.3390/ijms21114060

Hellens, R. P., Anne Edwards, E., Leyland, N. R., Bean, S., and Mullineaux, P. M. (2000). pGreen: a versatile and flexible binary Ti vector for *Agrobacterium*-mediated plant transformation. *Plant Mol. Biol.* 42, 819–832. doi: 10.1023/a:1006496308160

Hepworth, S. R., and Pautot, V. A. (2015). Beyond the divide: boundaries for patterning and stem cell regulation in plants. *Front. Plant Sci.* 6. doi: 10.3389/fpls.2015.01052

Hepworth, S. R., Zhang, Y., McKim, S., Li, X., and Haughn, G. W. (2005). BLADE-ON-PETIOLE-dependent signaling controls leaf and floral patterning in Arabidopsis. *Plant Cell* 17, 1434–1448. doi: 10.1105/tpc.104.030536

Izhaki, A., Alvarez, J. P., Cinnamon, Y., Genin, O., Liberman-Aloni, R., and Eyal, Y. (2018). The tomato *BLADE ON PETIOLE* and *TERMINATING FLOWER* regulate leaf axil patterning along the proximal-distal axes. *Front. Plant Sci.* 9. doi: 10.3389/fpls.2018.01126

Jansson, S., and Douglas, C. J. (2007). *Populus*: a model system for plant biology. *Annu. Rev. Plant Biol.* 58, 435–458. doi: 10.1146/annrrev.arplant58.032806.103956

Jost, M., Taketa, S., Mascher, M., Himmelbach, A., Yuo, T., Shahinnia, F., et al. (2016). A homolog of *BLADE-ON-PETIOLE 1* and *2* (*BOP1/2*) controls internode length and homeotic changes of the barley inflorescence. *Plant Physiol.* 171, 1113–1127. doi: 10.1104/pp.16.00124

Jun, J. H., Ha, C. M., and Fletcher, J. C. (2010). BLADE-ON-PETIOLE1 coordinates organ determinacy and axial polarity in Arabidopsis by directly activating *ASYMMETRIC LEAVES2*. *Plant Cell* 22, 62–76. doi: 10.1105/tpc.109.070763

Khan, M., Ragni, L., Tabb, P., Salasini, B. C., Chatfield, S., Datla, R., et al. (2015). Repression of lateral organ boundary genes by PENNYWISE and POUND-FOOLISH is essential for meristem maintenance and flowering in Arabidopsis. *Plant Physiol.* 169, 2166–2186. doi: 10.1104/pp.15.00915

Khan, M., Tabb, P., and Hepworth, S. R. (2012a). BLADE-ON-PETIOLE1 and 2 regulate Arabidopsis inflorescence architecture in conjunction with homeobox genes *KNAT6* and *ATH1*. *Plant Signal. Behav.* 7, 788–792. doi: 10.4161/psb.20599

Khan, M., Xu, H., and Hepworth, S. R. (2014). *BLADE-ON-PETIOLE* genes: setting boundaries in development and defense. *Plant Sci.* 215–216, 157–171. doi: 10.1016/j.plantsci.2013.10.019

Khan, M., Xu, M., Murmu, J., Tabb, P., Liu, Y., Storey, K., et al. (2012b). Antagonistic interaction of BLADE-ON-PETIOLE1 and 2 with BREVIPEDICELLUS and PENNYWISE regulates Arabidopsis inflorescence architecture. *Plant Physiol.* 158, 946–960. doi: 10.1104/pp.111.188573

Koncz, C., and Schell, J. (1986). The promoter of TL-DNA gene *5* controls the tissue-specific expression of chimaeric genes carried by a novel type of *Agrobacterium* binary vector. *Molec. Gen. Genet.* 204, 383–396. doi: 10.1007/bf00331014

Liebsch, D., Sunaryo, W., Holmlund, M., Norberg, M., Zhang, J., Hall, H. C., et al. (2014). Class I KNOX transcription factors promote differentiation of cambial derivatives into xylem fibers in the Arabidopsis hypocotyls. *Development* 141, 4311–4319. doi: 10.1242/dev.111369

Liu, L., Ramsay, T., Zinkgraf, M., Sundell, D., Street, N. R., Filkov, V., et al. (2015). A resource for characterizing genome-wide binding and putative target genes of transcription factors expressed during secondary growth and wood formation in *Populus*. *Plant J.* 82, 887–898. doi: 10.1111/tpj.12850

Liu, S., Magne, K., Daniel, S., Sibout, R., and Ratet, P. (2022). *Brachypodium distachyon* UNICULME4 and LAXATUM-A are redundantly required for development. *Plant Physiol.* 188, 363–381. doi: 10.1093/plphys/kiab456

Lu, Q., Tang, X., Tian, G., Wang, F., Liu, K., Nguyen, V., et al. (2009). Arabidopsis homolog of the yeast TREX-2 mRNA export complex: components and anchoring nucleoporin. *Plant J.* 61, 259–270. doi: 10.1111/j.1365-313X.2009.04048.x

Magne, K., Couzigou, J. M., Schiessl, K., Liu, S., George, J., Zhukov, V., et al. (2018). *MtNODULE ROOT1* and *MtNODULE ROOT2* are essential for indeterminate nodule identity. *Plant Physiol.* 178, 295–316. doi: 10.1104/pp.18.00610

Magne, K., Liu, S., Massot, S., Dalmais, M., Morin, H., Sibout, R., et al. (2020). Roles of *BdUNICULME4* and *BdLAXATUM-A* in the non-domesticated grass *Brachypodium distachyon*. *Plant J.* 103, 645–659. doi: 10.1111/tpj.14758

McKim, S. M., Stenvik, G. E., Butenko, M. A., Kristiansen, W., Cho, S. K., Hepworth, S. R., et al. (2008). The *BLADE-ON-PETIOLE* genes are essential for abscission zone formation in Arabidopsis. *Development* 135, 1537–1546. doi: 10.1242/dev.012807

Murmu, J., Bush, M. J., DeLong, C., Li, S., Xu, M., Khan, M., et al. (2010). Arabidopsis basic leucine-zipper transcription factors TGA9 and TGA10 interact with floral glutaredoxins ROXY1 and ROXY2 and are redundantly required for anther development. *Plant Physiol.* 154, 1492–1504. doi: 10.1104/pp.110.159111

Nakano, Y., Yamaguchi, M., Endo, H., Rejab, N. A., and Ohtani, M. (2015). NAC-MYB-based transcriptional regulation of secondary cell wall biosynthesis in land plants. *Front. Plant Sci.* 6, 288. doi: 10.3389/fpls.2015.00288

Nieminen, K., Blomster, T., Helariutta, Y., and Mähönen, A. P. (2015). Vascular cambium development. *Arabidopsis Book* 13, e0177. doi: 10.1199/tab.0177

Norberg, M., Holmlund, M., and Nilsson, O. (2005). The *BLADE ON PETIOLE* genes act redundantly to control the growth and development of lateral organs. *Development* 132, 2203–2213. doi: 10.1242/dev.01815

Pfaffl, M. W. (2001). A new mathematical model for relative quantification in real-time RT–PCR. *Nucleic Acids Res.* 29, e45–e45. doi: 10.1093/nar/29.9.e45

Rogers, L. A., and Campbell, M. M. (2004). The genetic control of lignin deposition during plant growth and development. *New Phytol.* 164, 17–30. doi: 10.1111/j.1469-8137.2004.01143.x

Sanchez, P., Nehlin, L., and Greb, T. (2012). From thin to thick: major transitions during stem development. *Trends Plant Sci.* 17, 113–121. doi: 10.1016/j.tplants.2011.11.004

Sannigrahi, P., Ragauskas, A. J., and Tuskan, G. A. (2010). Poplar as a feedstock for biofuels: A review of compositional characteristics. *Biofuel. Bioprod. Biorefin.* 4, 209–226. doi: 10.1002/bbb.206

Sehr, E. M., Agusti, J., Lehner, R., Farmer, E. E., Schwarz, M., and Greb, T. (2010). Analysis of secondary growth in the Arabidopsis shoot reveals a positive role of jasmonate signalling in cambium formation. *Plant J.* 63, 811–822. doi: 10.1111/j.1365-313x.2010.04283.x

Shen, D., Holmer, R., Kulikova, O., Mannapperuma, C., Street, N. R., Yan, Z., et al. (2021). The BOP-type co-transcriptional regulator NODULE ROOT1 promotes stem secondary growth of the tropical Cannabaceae tree *Parasponia andersonii*. *Plant J.* 106, 1366–1386. doi: 10.1111/tpj.15242

Song, J., Lu, S., Chen, Z. Z., Lourenco, R., and Chiang, V. L. (2006). Genetic transformation of *Populus trichocarpa* genotype Nisqually-1: a functional genomic tool for woody plants. *Plant Cell Physiol.* 47, 1582–1589. doi: 10.1093/pcp/pcl018

Sundell, D., Street, N. R., Kumar, M., Mellerowicz, E. J., Kucukoglu, M., Johnsson, C., et al. (2017). AspWood: High-spatial-resolution transcriptome profiles reveal uncharacterized modularity of wood formation in *Populus tremula*. *Plant Cell* 29, 1585–1604. doi: 10.1105/tpc.17.00153

Tavakol, E., Okagaki, R., Verderio, G., Vahid, S. J., Hussien, A., Bilgic, H., et al. (2015). The barley *Uniculme 4* gene encodes a BLADE-ON-PETIOLE-like protein that controls tillering and leaf patterning. *Plant Physiol.* 168, 164–174. doi: 10.1104/pp.114.252882

Taylor, G. (2002). *Populus*: Arabidopsis for forestry. Do we need a model tree? *Ann. Bot.* 90, 681–689. doi: 10.1093/aob/mcf255

Toriba, T., Tokunaga, H., Nagasawa, K., Nie, F., Yoshida, A., and Kyozuka, J. (2020). Suppression of leaf blade development by BLADE-ON-PETIOLE orthologs is a

common strategy for underground rhizome growth. *Curr. Biol.* 30, 509–516. doi: 10.1016/j.cub.2019.11.055

Toriba, T., Tokunaga, H., Shiga, T., Nie, F., Naramoto, S., Honda, E., et al. (2019). *BLADE-ON-PETIOLE* genes temporally and developmentally regulate the sheath to blade ratio of rice leaves. *Nat. Commun.* 10, 619. doi: 10.1038/s41467-019-08479-5

Unda, F., Kim, H., Hefer, C., Ralph, J., and Mansfield, S. D. (2017). Altering carbon allocation in hybrid poplar (*Populus alba* × *grandidentata*) impacts cell wall growth and development. *Plant Biotechnol. J.* 15, 865–878. doi: 10.1111/pbi.12682

Wang, D., Chen, Y., Li, W., Li, Q., Lu, M., Zhou, G., et al. (2021). Vascular cambium: the source of wood formation. *Front. Plant Sci.* 12. doi: 10.3389/fpls.2021.700928

Wang, S., Li, E., Porth, I., Chen, J. G., Mansfield, S. D., and Douglas, C. J. (2014). Regulation of secondary cell wall biosynthesis by poplar R2R3 MYB transcription factor PtrMYB152 in Arabidopsis. *Sci. Rep.* 4, 5054. doi: 10.1038/srep05054

Wang, Y., Salasini, B. C., Khan, M., Devi, B., Bush, M., Subramaniam, R., et al. (2019). Clade I TGACG-motif binding basic leucine zipper transcription factors mediate BLADE-ON-PETIOLE-dependent regulation of development. *Plant Physiol.* 180, 937–951. doi: 10.1104/pp.18.00805

Woerlen, N., Allam, G., Popescu, A., Corrigan, L., Pautot, V., and Hepworth, S. R. (2017). Repression of *BLADE-ON-PETIOLE* genes by KNOX homeodomain protein BREVIPEDICELLUS is essential for differentiation of secondary xylem in Arabidopsis root. *Planta* 245, 1079–1090. doi: 10.1007/s00425-017-2663-2

Wu, X. M., Yu, Y., Han, L. B., Li, C. L., Wang, H. Y., Zhong, N. Q., et al. (2012). The tobacco *BLADE-ON-PETIOLE2* gene mediates differentiation of the corolla abscission zone by controlling longitudinal cell expansion. *Plant Physiol.* 159, 835–850. doi: 10.1104/pp.112.193482

Xu, C., Park, S. J., Van Eck, J., and Lippman, Z. B. (2016). Control of inflorescence architecture in tomato by BTB/POZ transcriptional regulators. *Genes Dev.* 30, 2048–2061. doi: 10.1101/gad.288415.116

Žádníková, P., and Simon, R. (2014). How boundaries control plant development. *Curr. Opin. Plant Biol.* 17, 116–125. doi: 10.1016/j.pbi.2013.11.013

Zhang, B., Holmlund, M., Lorrain, S., Norberg, M., Bakó, L. S., Fankhauser, C., et al. (2017). BLADE-ON-PETIOLE proteins act in an E3 ubiquitin ligase complex to regulate PHYTOCHROME INTERACTING FACTOR 4 abundance. *elife* 6, e26759. doi: 10.7554/elife.26759

Zhang, Z., Wang, P., Luo, X., Yang, C., Tang, Y., Wang, Z., et al. (2019). Cotton plant defence against a fungal pathogen is enhanced by expanding BLADE-ON-PETIOLE1 expression beyond lateral-organ boundaries. *Commun. Biol.* 2, 238. doi: 10.1038/s42003-019-0468-5

Zhao, Y., Song, X., Zhou, H., Wei, K., Jiang, C., Wang, J., et al. (2020). *KNAT2/6b*, a class I KNOX gene, impedes xylem differentiation by regulating NAC domain transcription factors in poplar. *New Phytol.* 225, 1531–1544. doi: 10.1111/nph.16036

frontiers | Frontiers in Plant Science

TYPE Original Research
PUBLISHED 28 November 2023
DOI 10.3389/fpls.2023.1260596

OPEN ACCESS

EDITED BY
Verónica S. Di Stilio,
University of Washington, United States

REVIEWED BY
Eftychios Frangedakis,
University of Cambridge, United Kingdom
Shohei Yamaoka,
Kyoto University, Japan

*CORRESPONDENCE
John L. Bowman
john.bowman@monash.edu

RECEIVED 18 July 2023
ACCEPTED 08 September 2023
PUBLISHED 28 November 2023

CITATION
Singh S and Bowman JL (2023) The monoicous secondarily aquatic liverwort *Ricciocarpos natans* as a model within the radiation of derived Marchantiopsida. *Front. Plant Sci.* 14:1260596. doi: 10.3389/fpls.2023.1260596

The monoicous secondarily aquatic liverwort *Ricciocarpos natans* as a model within the radiation of derived Marchantiopsida

Shilpi Singh[1] and John L. Bowman[1,2]*

[1]School of Biological Sciences, Monash University, Melbourne, VIC, Australia, [2]Australian Research Council (ARC) Centre of Excellence for Plant Success in Nature and Agriculture, Monash University, Melbourne, VIC, Australia

Liverworts represent one of six embryophyte lineages that have a Devonian, or earlier, origin, and are, at present, represented by only *Marchantia polymorpha* as an established model. *Ricciocarpos natans* is a secondarily monoicous aquatic liverwort with a worldwide distribution, being found on all continents except Antarctica. *Ricciocarpos*, a monotypic genus, forms a sister relationship with *Riccia*, the largest genus of the Marchantiopsida (~250 species), diverging from their common ancestor in the mid-Cretaceous. *R. natans* is typically found on small stagnant ponds and billabongs (seasonal pools), where it assumes a typical 'aquatic' form with long scale keels for stabilization on the water surface. But, as water bodies dry, plants may become stranded and subsequently shift their development to assume a 'terrestrial' form with rhizoids anchoring the plants to the substrate. We developed *R. natans* as a model to address a specific biological question — what are the genomic consequences when monoicy evolves from ancestral dioicy where sex is chromosomally determined? However, *R. natans* possesses other attributes that makes it a model to investigate a variety of biological processes. For example, it provides a foundation to explore the evolution of sexual systems within *Riccia*, where it appears monoicy may have evolved many times independently. Furthermore, the worldwide distribution of *R. natans* postdates plate tectonic driven continent separation, and thus, provides an intriguing model for population genomics. Finally, the transition from an aquatic growth form to a terrestrial growth form is mediated by the phytohormone abscisic acid, and represents convergent evolution with a number of other aquatic embryophytes, a concept we explore further here.

KEYWORDS

Ricciocarpos natans, liverwort, aquatic macrophytes, abscisic acid, evo devo

Introduction

Why does one choose a particular species as a model system? For most of the 20th century plant biologists chose species based on attributes that facilitate experimental approaches to answer a specific biological question (Sussex, 1998). This approach led to a plethora of different species being investigated, each suited the questions being investigated. At one point, it became so parochial that each researcher worked on a different species, and as Ian Sussex once related, he was thinking about working on a particular species of plant, but was told by others that he should not, as that was professor X's species. Despite the parochialism, during that time a few species, namely maize, petunia and snapdragon, gained some traction as models, especially among geneticists (Stubbe, 1966; Rhoades, 1984; Coe, 2001; Schwarz-Sommer et al., 2003; Candela and Hake, 2008; Vandenbussche et al., 2016). It was not until the 1980's that the plant science community converged upon a dominant model system, *Arabidopsis thaliana* (Meyerowitz and Pruitt, 1985; Page and Grossniklaus, 2002; Somerville and Koornneef, 2002; Provart et al., 2015; Prunet and Meyerowitz, 2016). Subsequently, research with a small number of species amenable to genetic and molecular approaches facilitated rapid advances in our understanding of plant development, physiology, and even ecology. However, this canalization also led to other aspects of plant biology for which the model species were not appropriate, such as mycorrhizal fungal interactions and broader questions in evolution and ecology being neglected. With the advances of genomic sequencing and development of genome editing in the past decade, we are now in a position to return to the broader plant biology perspective of last century, where a wide spectrum of species could be developed as models given the specific biological question at hand. It is in this vein that we began research on the liverwort *Ricciocarpos natans*.

Materials and methods

Ricciocarpos culture

To determine optimal growth conditions in the laboratory (i.e. to mimic morphologies observed in nature), *Ricciocarpos* was growth in axenic aquatic culture, with liquid media containing various concentrations of Gamborg B-5 basal medium [PhytoTech Labs; www.phytotechlab.com; (Gamborg et al., 1968)], pH 6.0, with concentrations of 1x, 1/2, 1/4, 1/6, 1/8, 1/10, and 1/12 tested. Growth was under a 16-hour photoperiod at 20˚C. Light intensity was varied by growing plants at different distances from the light source. Conditions of 1/8 B-5 media and a light intensity of 80 μmol. $m^{-2}s^{-1}$ resulted a typical aquatic morphology with purple scale production. Addition of ABA at a concentration of 0.1μM to the above media successfully induced terrestrial characteristics of *Ricciocarpos* growing in liquid media; for the differential gene experiment, the addition of ABA was a single event at the initiation of the growth period.

Ricciocarpos accession relationships

The phylogenetic tree of *Ricciocarpos* was constructed using nucleotide sequences of 6 genes (nuclear: LOX1; chloroplast: *rbcL*, *rps4*, cpITS, *trn*L-F, 26S); while the Jerrybomberra Creek and Butner NC accessions were represented by most genes, the other accessions were represented by as few as one gene. Each sequence alignment was manually trimmed to exclude ambiguously aligned regions. The best substitution models for each of the six alignments obtained using the "optimize" function in raxmlGui2.0 (Edler et al., 2020). The six alignments were concatemerized producing a matrix consisting of 12,465 nucleotides representing 11 species/isolates. A maximum likelihood phylogeny was constructed, with nodal support calculated after 1000 replications, using raxmlGui2.0 (Edler et al., 2020).

Annotation of Ricciocarpos genome

Repeat Annotation: RepeatModeler (Smit and Hubley, 2008-2015) (version 1.0.8_RM4.0.7) was used for *de novo* repeat family identification. The output was used as a repeat library for RepeatMasker version 4.0.9 (Smit et al., 2013-2015).

RNA Extraction and Sequencing: RNA for sequencing was extracted from *R. natans* by submerging whole plants in liquid nitrogen and using a mortar and pestle to grind the tissue into a powder. For each line, 100mg of tissue was processed with the RNeasy mini kit (Qiagen), as per the manufacturer's instructions for purification of total RNA from plant tissues. The total RNA for each sample was quantified with the NanoDrop 2000 (Thermo Scientific). Library preparation used polyA mRNA selection and MGIEasy stranded mRNA chemistry. Sequencing used MGI Tech MGISEQ-2000RS hardware (400 million raw reads per lane, 100-pb paired-end reads).

Gene Prediction: A total of 106,736 transcript assemblies were made from ~57M pairs of paired-end Illumina RNA-seq reads with Trinity software-v2.12.0 described in Chapter 3. Ab-initio gene predictions were generated by AUGUSTUS-3.3.3 (Stanke et al., 2008). 37,626 transcript assemblies were constructed with RNA-seq-assisted prediction by PASA software (Haas et al., 2003) using RNA-seq transcript assemblies. Homology based gene prediction was done with EXONERATE alignments with the Marchantia v6.1 protein dataset to a repeat-soft-masked *Ricciocarpos* genome using RepeatMasker (Smit et al., 2013-2015). The Repeat library was generated using RepeatModeler (Smit and Hubley, 2008-2015).

The EVidenceModeler software, which combines ab-initio gene predictions, protein and transcript alignments into weighted consensus gene structures, was used to obtain consensus gene structures (Haas et al., 2008) in *R. natans*. Resultant gene structure annotations were updated by PASA. As *Marchantia* is used as model liverwort for comparison with *R. natans*, and is functionally well annotated, PASA-improved gene model proteins were subject to protein homology analysis to *Marchantia* to retrieve functional annotation of genes.

Differential gene expression analysis

RNA-seq filtered libraries, in triplicate, were used for each sample. Scaffold level assembly of *Ricciocarpos* (https://genomevolution.org/coge/; Genome id65508) was used as the reference for mapping filtered transcripts to *R. natans* genome assembly using samtools (Li and Durbin, 2009). Transcript abundance was estimated using HT-Seq count with -no strand specific parameter (-s = no) and other parameters were kept as default. Differential gene expression (DGE) analysis of ABA treated plants (terrestrial) in contrast to no ABA (aquatic) was performed with DESeq2 (Love et al., 2014).

Ricciocarpos natans, an aquatic monoicous liverwort

Liverworts are one of three bryophyte lineages (liverworts, mosses, hornworts) and comprise one of six land plant lineages that diverged from one another in the Devonian or earlier (Bowman, 2022). *Ricciocarpos natans*, hereafter *Ricciocarpos*, is a monoicous, largely aquatic, complex thalloid liverwort (Marchantiopsida) with a cosmopolitan distribution (Figures 1A–C). The genus is monotypic, being comprised of a single described species. Due to its resemblance to species of the genus *Riccia*, *Ricciocarpos* has traditionally been placed as one of the two genera of the Ricciaceae (Schuster, 1992), however, phylogenetic analyses using sequence data suggest it is more closely related to another genus, *Oxymitra*, and that they together are sister to *Riccia* [Figure 1A, (Villarreal et al., 2016)]. As liverworts were ancestrally dioicous and terrestrial, both monoicy and its aquatic habit are derived characters. However, development of *Ricciocarpos* as a model system could serve as a model for species in the genus *Riccia*, the largest genus by species number within the Marchantiopsida.

The morphology, anatomy and development of *Ricciocarpos* is similar to that of other complex thalloid liverworts. Growth occurs from a single apical cell in the shoot meristem, with the thallus undergoing periodic dichotomous branching [Figures 1D, E (Leitgeb, 1879; Garber, 1904)]. The dorsal surface is occupied by air chambers separated by unistratose (single cell layer) walls and forming an elaborate aerenchyma, with those at the dorsal surface having a complex air pore (Leitgeb, 1879; Kronestedt, 1981; Kronestedt, 1982a; Kronestedt, 1982b). The air chambers form schizogenously, i.e. *via* localized cell separation (Barnes and Land, 1907; Hirsh, 1910). The air in these chambers provides buoyancy such that the plants float on the water surface. As is typical of the Marchantiopsida, oil body cells are found as idioblasts (isolated cells differing from their neighbours) containing a single oil body (Kronestedt, 1983), and these likely function to deter herbivory as has been described for *Marchantia* (Kanazawa et al., 2020; Romani et al., 2020).

When *Ricciocarpos* is growing on an aquatic medium, ventral rhizoid production is suppressed, and large sword-like scales are produced that act as keels to stabilise the thallus on the water surface and prevent their overturning during windy periods [(Bischoff, 1835; Lindenberg, 1836; Kronestedt, 1981); e.g. Figure 2, Figures 3A, B]. The scales are unistratose, several cells wide (0.2-0.6 mm), and often with their length (10 mm) exceeding the width of the thallus (Kronestedt, 1981). The scales are often deeply pigmented, with a reddish-purple pigment that can almost appear black (Dillenius, 1741; Lindenberg, 1836; Schmidel, 1793). The pigment has been named riccionidin and its biosynthesis is related to that of the anthocyanin pathway (Kunz et al., 1994; Kunz and Becker, 1995; Albert et al., 2018; Kubo et al., 2018), and recent work on *Marchantia* has shown it to be an auronidin (Berland et al., 2019). This pigment appears to be polymerized in the cell wall, and thus provides both a possible sunscreen and also contributes mechanically to the stiffness of the scales (Kunz et al., 1994; Berland et al., 2019). Another attribute of the aquatic form is the periodic separation of thalli (Bischoff, 1835; Garber, 1904; Lewis, 1906; Pickett, 1925; Schmidel, 1793), *via* abscision and presumably involves programmed cell death (Figures 1D–F). Typical thalli have four shoot apices, and when each of these apices branch a short-lived thallus with eight shoot apices is formed that then undergoes abscission to produce two thalli with four apices once again [Figures 1D–F, (Ferreyra, 1990)]. This mode of vegetative reproduction allows for rapid proliferation of thalli on the water surface, with each 'individual' being able to float independently of the others. Consistent with its largely aquatic ecology, *Ricciocarpos* has lost the ability to form mycorrhizal fungal interactions (Stahl, 1949; Ligrone et al., 2007).

When *Ricciocarpos* is growing on a terrestrial medium, scale production is suppressed and instead unicellular thin-walled rhizoids as long as 15 mm are produced and these anchor the plant to the substrate (Kronestedt, 1981). In addition, the terrestrial form does not undergo fragmentation *via* abscission, but rather stay together forming a tight circular rosette, similar to many *Riccia* species (Bischoff, 1835; Garber, 1904; Lewis, 1906; Pickett, 1925).

Ricciocarpos is monoicous, producing first antheridia and then archegonia along the dorsal furrow [Figure 1F; (Garber, 1904)]. As the sex organs are produced in a temporally distinct manner, there is some scope for outcrossing. The heterochronic production of sex organs is likely what led to some early researchers to suggest dioicy (Campbell, 1895; Leitgeb, 1879). It is this derived feature, the evolution of monoicy from ancestral dioicy, without a major karyotype change [n = 9 (Siler, 1934), from the ancestral state of liverworts (Berrie, 1960)], that induced us to develop *Ricciocarpos* as a model to investigate the genomic consequences of a shift in sexual systems (Singh et al., 2023). The antheridia and archegonia are produced along the dorsal furrow in a single row (Leitgeb, 1879; Garber, 1904; Lewis, 1906; Rieth, 1959), and their development are typical of the Marchantiopsida (Leitgeb, 1879; Garber, 1904; Lewis, 1906). Following fertilization the sporophyte develops essentially embedded within the maternal thallus [Figure 1F; (Garber, 1904; Lewis, 1906; Rieth, 1959)]. The sporophytes consist of a capsule whose wall is unistratose, and largely lack both a foot and seta (Figure 1F). All spore mother cells under meiosis producing haploid spores [about 500 per sporangium; (Rieth, 1959)], with no evidence of elaters (Figure 1F). Following spore formation, the capsule wall breaks down releasing the spores into a cavity in maternal

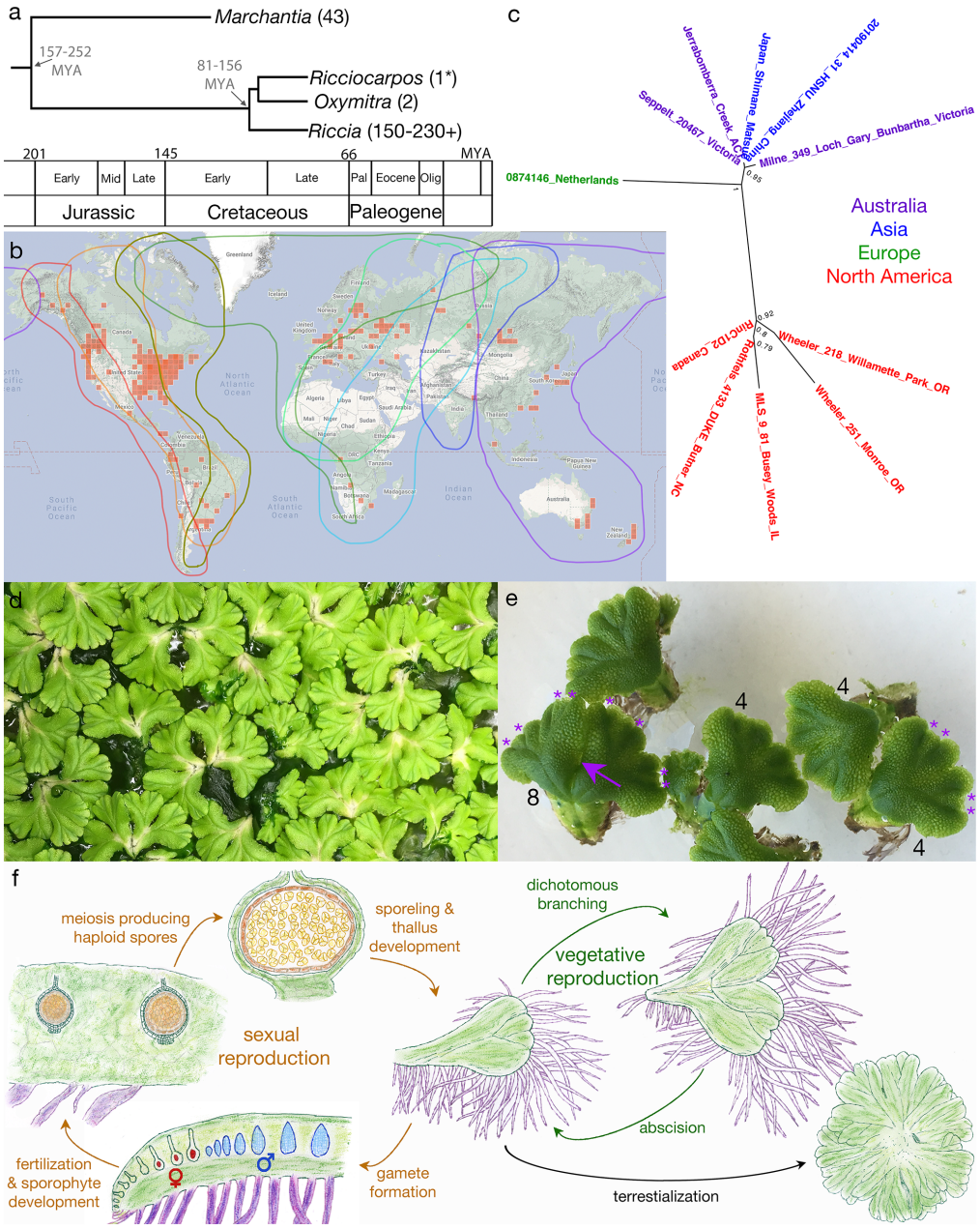

FIGURE 1
Overview of *Ricciocarpos*. **(A)** Phylogenetic relationship of *Ricciocarpos* to its closest extant relatives and to *Marchantia*, with approximate divergence times indicated (MYA, million years ago). Tree topology and estimated times are based on an analysis of 12 genes of mixed organellar and nuclear origin and calibrated with the known fossil record, with 95% posterior density intervals indicated [from (Villarreal et al., 2016)]. Numbers in parentheses indicate number of species in genera. **(B)** Present day distribution (red squares) of *Ricciocarpos* displayed at inaturalist.org (19 August 2022). The eight major flyways for migrating birds are outlined in different colours (Boere and Stroud, 2006). **(C)** Relationship between accessions of *R. natans*: the genome of the present paper is from Jerrabombera Creek, ACT (Australia), while the 1kp transcriptome (Wickett et al., 2014) was from plants isolated near Butner, NC (USA), and other accessions are from data in Genbank. Names are colour-coded based on geographical location. **(D)** Clonal population of *Ricciocarpos* growing in water amongst algae. **(E)** Dichotomous branching and separation of thallus fragments. The numbers indicate the number of apical meristems in the thalli, with the asterisks demarking them in two thalli. the arrow indicated where this thallus with eight apices will separate. **(F)** The life cycle of *Ricciocarpos*; sexual reproduction in brown and vegetative reproduction in green. Sporophyte tissues are shown in brown shades, whereas gametophyte tissues are green, except scales (purple), egg cells (red), antheridia (blue). Plants most often undergo vegetative reproduction *via* successive cycles of dichotomous branching and subsequent abscision of plants along the midline. If plants become stranded on a terrestrial substrate, production of long scales ceases and rhizoid are produced; in addition, abscision following branching no longer occurs, with plants forming a rosette. Growth in inductive conditions (aquatic growth and likely longer warmer days in spring) leads to production of first antheridia and then archegonia along the dorsal midline. Self- or cross-fertilization leads to production of sporophytes, again along the dorsal midline and essentially enclosed by the maternal gametophyte. As sporophytes lack both foot and seta, maternal nutrient contributions must be transferred *via* the calyptra. Following meiosis and release of spores from tetrads, the unistratose capsule wall (dark brown) breaks down, releasing the spores into a cavity in the maternal gametophyte to be dispersed as the gametophyte senesces. Adapted from (Bischoff, 1835; Garber, 1904).

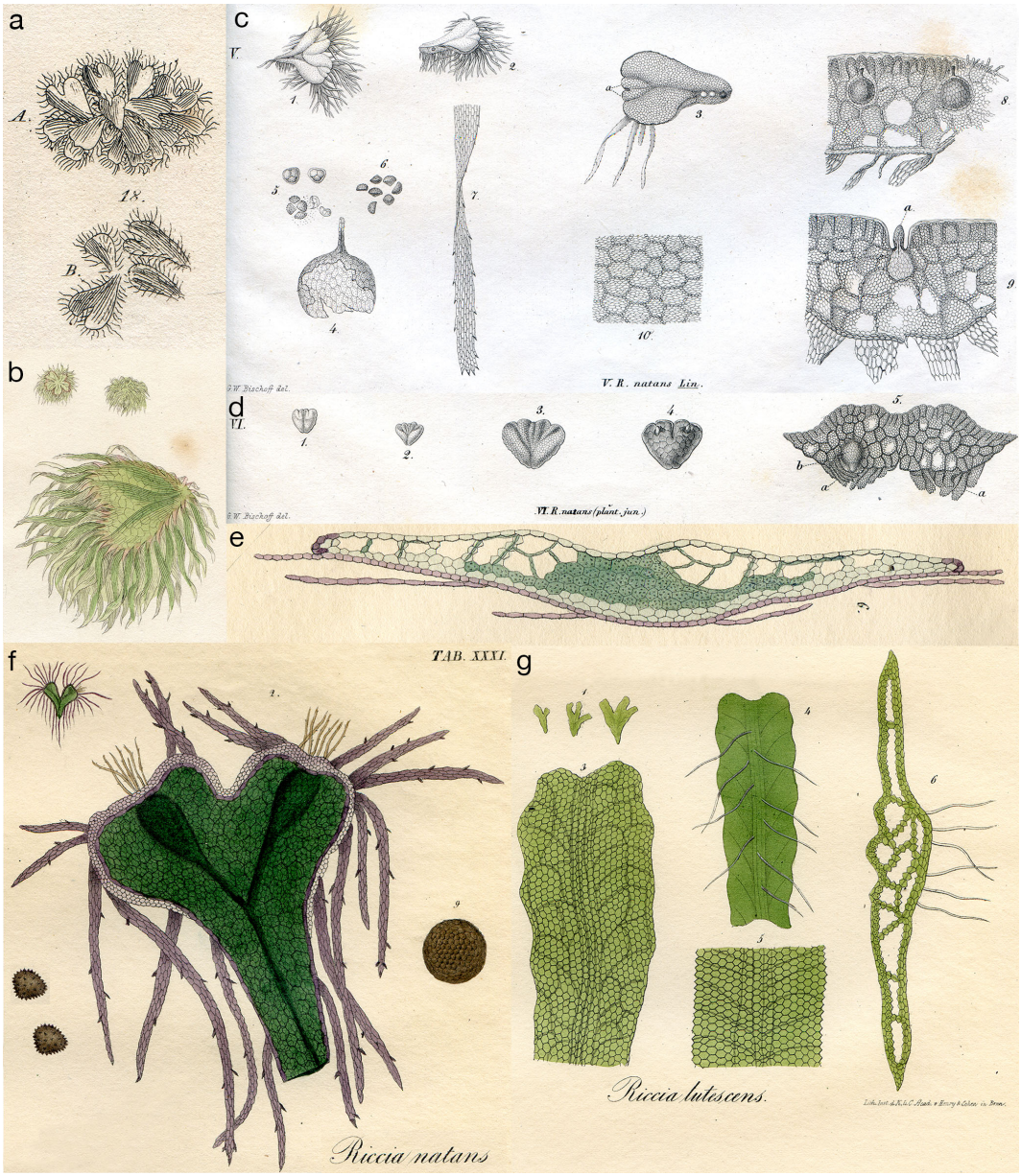

FIGURE 2
(A) A. dorsal surface; B. ventral surface; Plate 78, fig. 18 from Dillenius (Dillenius, 1741). **(B)** *Riccia natans* (Fringed *Riccia*), plate 77 in Smith's English Botany (Smith, 1804). **(C)** *Riccia natans*, Plate LXXI, fig. V of (Bischoff, 1835). (1) Mature frond; (2-3) fronds split into two halves along the intermediate groove, each half consisting of two unequal parts; (4) the sporangium; (5) developing spores; (6) mature spores; (7, 10) scale; (8) sporangium within thallus; (9) thallus cross section within antheridium **(A)**. **(D)** *Riccia natans* (plant juvenile), Plate LXX, fig. VI of (Bischoff, 1835). (1-3) Young fronds with quadricrenate apex, convex on both sides, attenuated on the outer edge, with an intermediate groove running out into two lateral grooves from the notches; (4) ventral side of 3; (5) frond cross section with young scales **(A)**. **(E, F)** *Riccia natans*, from Plate XXXI of (Lindenberg, 1836). **(E)** 6. cross section of mature frond. **(F)** 2. Mature frond; (9) sporangium; (left) mature spores. **(G)** *Riccia lutescens*, from Plate XXVI of (Lindenberg, 1836). (1, 3) Mature frond; (4) ventral view; (5) enlarged view of 4; (6) thallus cross section.

gametophyte, with dispersal either due to degeneration of the maternal gametophyte or *via* bird consumption (see below).

The discovery and early description of *Ricciocarpos*

The discovery and description of *Ricciocarpos* was given by Buddle in 1699 under the name '*Lichen parvus vernus cordiformis, ima parte fimbriatus, Lentis palustris modo aquae innatans*' in his *Hortus Siccus*, a herbarium that he assembled. A description was first published by Jacob Petiver (Petiver, 1695-1703), "*Lens palustris Roris Solis foliis cordatis*, observed by my Reverend friend Mr. Adam Buddle in some ponds about Henley in Suffolk", later corrected to 'Hadley' in Suffolk (Dillenius, 1741). It was later published under Buddle's original description in John Ray's *Synopsis methodica stirpium Britannicarum*, 3rd edition, and who noted that "It was suspected that it is being eaten by insects or

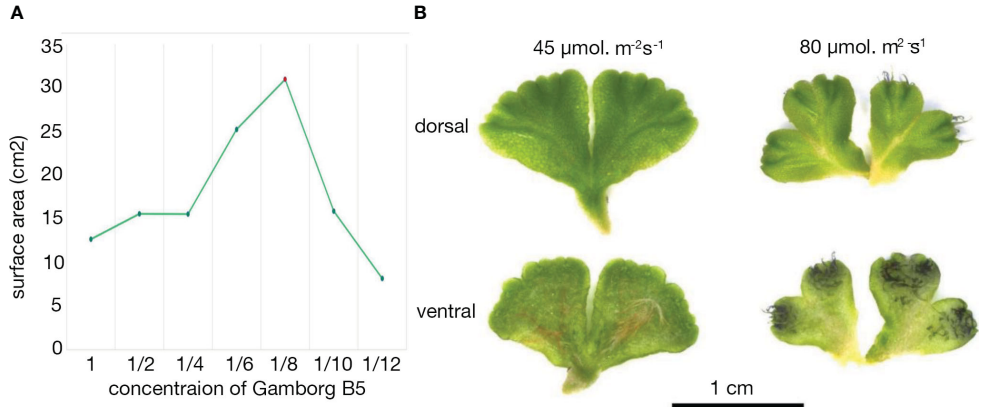

FIGURE 3
Growth of *Ricciocarpos* in culture. **(A)** Growth curve with varying Gamborg B-5 concentration. **(B)** Variation in induction of purple scales in *Ricciocarpos* with light intensity. The plate with ⅛ Gamborg B-5 media and higher light intensity produced growth with prominent purple scales compared to the plate with the same nutrient concentration and less intense light.

ducks" (Ray, 1724). The first published image (Figure 2A) was in Dillenius's *Historia Muscorum* (Dillenius, 1741). With respect to the cryptogams, Linneaus was a great lumper and placed *Ricciocarpos* with *Riccia* under the name *Riccia natans* (Linné, 1770); the species epithet 'natans' is derived from the Latin word for 'swimming'. As is often the case, Schmidel's description (of what he called *Riccia capillata*) added much detail, where he noted the dorsal air chambers and the serrated and coloured (black) nature of the ventral scales, and further suggested that it multiplied *via* dissociation along 'nerves' separating the lobes (Schmidel, 1793). A much less detailed drawing is presented in Smith's English Botany [Figure 2B; (Smith, 1804)]. Hooker was the first to describe the position of the sporophyte (Hooker, 1830), with Bischoff subsequently describing the structures of the sunken antheridia and sporophytes in some detail (Figure 2C), and also detailing the vegetative propagation *via* repeated division along the central channel of older plants into two plants (Bischoff, 1835). As with the case of many liverworts, new techniques for fixation and sectioning allowed Leitgeb to provide a detailed anatomical description of *Ricciocarpos*, with foci on development from the apical cell and the formation of air chambers (Leitgeb, 1879). Anatomical details of antheridia, archegonia and sporophyte development were clarified some years later (Garber, 1904; Lewis, 1906).

The genus name *Ricciocarpos* was coined by Corda (Corda, 1828) to separate *Ricciocarpos* from other *Riccia* species, but the first illustrations under the moniker *Ricciocarpos* are very poor [see Tab. 32. in (Sturm, 1832)]. Furthermore, Corda's distinguishing characters were shown not to be diagnostic (Bischoff, 1835), and thus it was subsequently often placed back into the genus *Riccia*. However, likely due to its similarity with other water plants and a lack of attention to detail, *Ricciocarpos* was described under other genera, e.g. *Salviniella* (*natans*) (Hübener, 1834). C. S. Rafinesque described *Ricciocarpos* growing on ponds on Long island, NY as *Lemna dimidiata*, perhaps ironically as he was didactic in correcting other botanist's nomenclature (Rafinesque, 1817). However, to his credit, Rafinesque also formulated a prescient early view of evolution: "*The truth is that Species and perhaps Genera also, are forming in organized beings by gradual deviations of shapes, forms and organs, taking place in the lapse of time. There is a tendency to deviations and mutations through plants and animals by gradual steps at remote irregular periods. This is a part of the great universal law of perpetual mutability in everything.*" (Rafinesque, 1833), which was later acknowledged by Darwin. Bischoff disparaged this proliferation of genus names, saying of some of his contemporaries, "*they could not resist the addiction to see their names behind a synonym, even if they were born as an invalid*", and in his description of *Ricciocarpos* he wished "*to protect us and our descendants from Babylonian confusion*" (Bischoff, 1835). Furthermore, "*In order to finally prevent such a polyonomatomania, which might threaten to infiltrate our Riccia even further*", Bischoff also drew "*attention to a plant which was discovered in February in the ditch of Lille near the Pont-de-France by Gay and (in the year 1834) to Prof. Al. Braun was notified*" (Figure 2D). Bischoff interpreted "*this plant, which at first glance could be taken to be a separate species, is in all probability only the Riccia natans in its youngest condition*" (Bischoff, 1835). Bischoff noted that while the dorsal surfaces were nearly identical, the ventral surfaces were different, which we now interpret to be due to the differences in the production of rhizoids rather than scales. The terrestrial form was actually described some years earlier as a distinct species, *Riccia lutescens*, that was "*found in abundance in an exsiccated swamp on the ground*" in western North Carolina (Schweinitz, 1821), consistent with the habitat of terrestrial *Ricciocarpos*. Bischoff's observations appear the first to equate the aquatic and terrestrial forms of *Ricciocarpos* to the same species. Lindenberg, who produced stunning drawings of *Ricciocarpos* (Figures 2E-G), also stated that when floating in the water large purple scales were produced, but "if the plant floats completely and consistently on the water, it is absolutely rootless, like *R. fluitans* in the same case; but as soon as it approaches the bank, or rests on the mud, it drives thin, delicate, rounded, hair-shaped, often articulated root fibers" [Figure 2E, (Lindenberg, 1836)]. Remarkably, despite these observations, Lindenberg also listed *R. lutescens* as a distinct species, with no cross reference to *Ricciocarpos* [Figure 2G,

(Lindenberg, 1836)]. While some equated the two forms as a single species (Lindberg, 1882), *R. lutescens* was often listed as a separate species in other publications into the mid-20th century, despite Lewis conclusively demonstrating that the terrestrial form could be converted into the aquatic form (Lewis, 1906). An additional distinct species name for the terrestrial form, *Riccia velutina*, was also proposed in the mid-19th century (Hooker, 1840). The original *R. lutescens* specimen of Schweinitz was typified as an isolectotype of *Ricciocarpos natans* (Stotler and Crandall-Stotler, 2017). A full account of the historical nomenclature of *Ricciocarpos*, including its orthographical variant (*Ricciocarpus natans*), has been previously described (Duthie and Garside, 1936; Perold, 1995).

Distribution and ecology of *Ricciocarpos*

Ricciocarpos has a nearly cosmopolitan distribution, being found throughout temperate habitats on six continents in both hemispheres, absent from extreme alpine habitats, the Arctic and Antarctica [Figure 1B; (Scott, 1985; Schuster, 1992)]. While not widely reported from the tropics, it can be found in both the neotropics of the Americas and tropics of the old world in Africa (Jones, 1957; Bischler-Causse et al., 2005). Notably, not long after *Ricciocarpos* was being described across western Europe, e.g. Germany (Schmidel, 1793) and in Provence and Montmorency in France (Candolle and Lamarck, 1805), it was also described in eastern North America (Muhlenberg, 1813), and noted by Robert Brown in Australia [(Brown and Bauer, 1814); Brown was botanist on the *Investigator* captained by Flinders and which circumnavigated Australia and he was the discoverer of both the nucleus and 'Brownian' motion], described by Joseph Dalton Hooker in the North Island of New Zealand (Hooker, 1855), collected as early as 1840 in Omgeni, Durban, South Africa (Drège, 1843) and as early as 1839 at Porto Alegre in southern Brazil (Montagne, 1839), and identified in Japan in the early 1850's (Perry et al., 1856). These early observations suggest its presence in these locales likely predated most human mediated dispersal. However, it was noted as early as the mid-19th century that *Ricciocarpos* was a suitable aquarium plant (Collier and Hooper, 1866) and this may have contributed to its dissemination in some local contexts. In regional floras, *Ricciocarpos* has been reported to be widely dispersed across the Americas, Eurasia, Africa, Australia and New Zealand [e.g. (Kashyap, 1929; Hassel de Menendez, 1962; Campbell, 1975; Scott, 1985; Piippo, 1990; Schuster, 1992; Fischer, 1995; Perold, 1995; Bischler-Causse et al., 2005; Frey et al., 2006; Lee and Gradstein, 2021; Acuña-Castillo et al., 2023)], with recent iNaturalist observations consistent with the published distribution (Figure 1B).

Ricciocarpos is thought to have diverged from its nearest extant relatives (the genera *Oxymitra* and *Riccia*) in the mid-Cretaceous (Villarreal et al., 2016), postdating the breakup of Pangea and indicating its present distribution has involved trans-oceanic dispersal. The evolution of both an aquatic lifestyle and monoicy likely evolved after the divergence of *Ricciocarpos* from *Oxymitra* and *Riccia*, and evolution of the two characters could be linked. The obvious vector for dispersal of aquatic plants over trans-oceanic distances, and shorter ones as well, is migratory waterbirds (Buch, 1954). For example, when *Ricciocarpos* was noted to be newly present at Lake Gjølsjø in eastern Norway, it was suspected that it was due to transport of plants from Swedish wetlands where *Ricciocarpos* is common, with the swan (*Cygnus olor*) the likely culprit (Skulberg, 1978). While it has not been demonstrated directly for *Ricciocarpos*, ectozoochory, including transequatorial dispersal of bryophyte diaspores in bird plumage has been documented (Lewis et al., 2014a). Endozoochory of moss spores or plant fragments *via* a number of bird species [e.g. upland goose (*Chloephaga picta*), white-bellied seedsnipe (*Attagis malouinus*), mallard (*Anas platyrhnchos*), skua (*Stercororius* sp.)] and even a flying fox (*Pteropus conspicillatus*), has been shown to be feasible (Parsons et al., 2007; Wilkinson et al., 2017; Lázaro et al., 2021; Maggio et al., 2022), and *Ricciocarpos* has been noted to be present in the faeces of mallards (Hartman, 1985). Thus, long distance dispersal *via* bird vectors (Viana et al., 2016) is a plausible mechanism to explain bryophyte species with disjunct, sometimes bipolar, geographic distributions (Schuster, 1983; Piñeiro et al., 2012; Lewis et al., 2014b). As *Ricciocarpos* is monoicous, only a single spore or thallus fragment is sufficient for dispersal to a new habitat, with evolution of monoicy an adaptation to its aquatic habit. Given the worldwide distribution of *Ricciocarpos* and its monoicous nature, it would be of interest to investigate the regional and global phylogenetic structure of the species and whether local adaptation can precede faster than dispersal.

In nature, the habitat of *Ricciocarpos* is limited to stagnant ponds and billabongs and their margins. Growth is most conspicuous during the summer months when plants may cover a significant fraction of the surface area. As temporary pools dry, the plants may become stranded on the margins, shifting to the terrestrial form with rhizoids anchoring the plants to the soil. If the waterholes refill while these stranded plants are still alive, pieces of plants originally stuck to the substrate will break free, possibly due to further growth being of the aquatic form, and the free thallus fragments can float to the pond surface once again. A similar scenario seems to occur in ponds that do not dry out, but freeze over. In this case plants growing in late autumn often sink to the bottom of the pond and over-winter there. With the coming of spring, as photosynthesis resumes, the plants then float back to the pond surface (Pickett, 1925). After some vegetative growth, first antheridia and then archegonia are produced in the late spring, with sporophytes maturing in the early summer (Garber, 1904; Pickett, 1925). If the population is undergoing the sexual life cycle, the spores can also act as over-wintering or desiccation tolerant propagules. Spores can apparently remain in the 'seed' bank for several years, with germination of *Ricciocarpos* observed following a ten year drought at Lake Ita, an ephemeral floodplain lake of the Lachlan River in the outback of southwestern New South Wales (Kelleway et al., 2021). Most reports suggest that *Ricciocarpos* primarily progresses through the sexual life cycle only in the aquatic form (Garber, 1904; Pickett, 1925; Maeda et al., 2016), but others have reported sexual reproduction in the terrestrial form (Lewis, 1906). One possible explanation is that sexual organs develop on the aquatic form, with sporophytes sometimes maturing after plants become stranded on the bank.

Ricciocarpos is often found in conjunction with a number of aquatic plants (often invasive weeds) including the angiosperms *Lemna*, *Wolffia*, *Spirodela* (i.e. the duckweeds), and *Utricularia* (the bladderworts), the fern *Azolla*, and in the northern hemisphere, another aquatic liverwort, *Riccia fluitans* (Scott, 1985; Schuster, 1992; Aoki et al., 2017). The specific community accompanying *Ricciocarpos* has been termed 'Ricciocarpetum natantis' (Scoppola et al., 1988), but to co-occurrence of different combination of free-floating, or pleustonic, plants appears to be random (Wolek, 1997; Wolek and Walanus, 2000). Competition among pleustonic plants is driven at least in part by nutrient supply (Peeters et al., 2016), with some evidence that increased eutrophication of Finnish lakes has facilitated the establishment and spread of *Ricciocarpos* where it had not been reported until after the 1930's (Toivonen, 1985).

A number of studies have registered the effects of water contaminants on *Ricciocarpos* growth. Pollution of waterways by factories producing the auxin analogues 2,4-D and dikamba led to the loss of severe reduction in local populations of both *Ricciocarpos* and *R. fluitans* in Lower Silesia, Poland (Kolon and Sarosiek, 1995). In transplantation experiments from fresh to water polluted with detergents or high nitrogen concentrations, *Ricciocarpos* was less tolerant than vascular aquatic plants and succumbed in the polluted water (Agami et al., 1976). However, that *Ricciocarpos* might tolerate moderate levels of certain water contaminants was suggested by its growth in a coal strip mine impoundment in Illinois (Chimney, 1984). Growth of *Ricciocarpos* in different concentrations of heavy metals (zinc, copper, lead, cobalt, chromium, nickel and vanadium) induced specific phenotypic responses suggesting the plant might be used as a bioindicator of chemical water pollution (Sarosiek et al., 1987a; Sarosiek et al., 1987b), as did subsequent experiments with cadmium (Oh and Koh, 2013). All these heavy metals, along with manganese and aluminium (Gimenes et al., 2020), affect growth when at higher concentrations. An open question is whether *Ricciocarpos* can accumulate any to provide a tool for phytoremediation. In a similar vein, experiments demonstrate that *Ricciocarpos* exhibits high ciprofloxacin (an antibiotic) tolerance, with a capacity for uptake and accumulation despite ciprofloxacin negatively affecting photosynthetic capacity (Gomes et al., 2018). *Ricciocarpos*, and aquatic plants in general, likely evolved mechanisms to cope with water contaminants, either internally, or alternatively involving active secretion of chemicals to modify their immediate environment, both chemically and altering the microbiome composition. *Ricciocarpos* may be a comparable model for such studies along with duckweeds (Fourounjian et al., 2020) and *Azolla* (Li et al., 2018).

Culture of Ricciocarpos

Ricciocarpos is amenable to growth in axenic culture under a variety of growth conditions (Woodfin, 1976; Lorenzen et al., 1981; Kunz and Becker, 1995). A culture of *Ricciocarpos natans* was obtained from Dr. Christine Cargill, curator of cryptogam collections at the Australian National Botanic Gardens in Canberra. This culture was originally isolated from Jerrabomberra Creek, near a bridge over the creek in Jerrabomberra Wetlands in the Australian Capital Territory (35° 18' S, 149° 9' E). We established axenic cultures with conditions adapted to our growth rooms. The aquatic form of *Ricciocarpos* grows on the surface of stagnant water bodies, such as ponds and billabongs, conditions which are not necessarily nutrient rich. Thus, *Ricciocarpos* was grown with varying concentrations of Gamborg B-5 media, pH 6.0, (Gamborg et al., 1968) to identify a 'wild-like' morphology of aquatic form of *Ricciocarpos*, based on previous descriptions of the species growing in nature. Plants were grown for 4 weeks and plant morphology, as well as the quantity of growth produced, with each varying nutrient concentration was compared. A peak of growth, measured by surface area, was observed when plants were grown in 1/8 B-5 media (Figure 3A). Increasing light intensity from 45 µmol. $m^{-2}s^{-1}$ to 80 µmol. $m^{-2}s^{-1}$ was sufficient to induce the production of pigmented scales on the ventral surface (Figure 3B); this range is similar to light intensities used in some previous *in vitro* culture conditions (Lorenzen et al., 1981; Kunz and Becker, 1995).

Genome

We recently reported an assembly of the *Ricciocarpos natans* genome based on approximately 200x coverage of Illumina sequencing followed by scaffold assembly using Hi-C [available at https://genomevolution.org/; (Singh et al., 2023)]. The current version (v1.0) consists of 38 large scaffolds covering 185.50 Mb genome assembly. Structural annotation of *Ricciocarpos* genome revealed 18,813 protein coding genes in *Ricciocarpos*, which is similar to gene number with the reference species *Marchantia polymorpha ruderalis*, hereafter *Marchantia*, with 19,473 genes (Bowman et al., 2017; Montgomery et al., 2020). *Marchantia* has 23,399 proteins and *Ricciocarpos* has 21,958 proteins suggesting that *Ricciocarpos* has 3,145 additional isomers. Blast searches to identify how many *Ricciocarpos* proteins have orthologs in *Marchantia* were performed using Blast-P with the *Ricciocarpos* protein set against the *Marchantia* protein set with filter parameters of percentage identity >30%, bitscore of >50 and e-value <=1e-05. This revealed that out of total number of 21,958 *Ricciocarpos* proteins orthologs were identified for 13,910 proteins

The accession from which the genome presented is derived was isolated from Jerrybomberra Creek, ACT, Australia, while the1kp transcriptome data was derived from mRNA isolated from a plant from near Butner, NC, USA. Their geographically distinct origins afforded the opportunity to examine sequence divergence between the two accessions. Surprisingly, it was noted that the two accessions differ on average by approximately 4% in the coding regions analysed, which is more than is typically observed for individual comparisons within eukaryotic species (<1%), and is closer to upper values of combined divergence for populations (Leffler et al., 2012) and to that (5%) observed for bacterial 'species' (Jain et al., 2018). The diversification of subspecies of the *Marchantia polymorpha* complex are thought to date to the late

Miocene, 5 Ma (highest posterior density 2-11 Ma) (Villarreal et al., 2016). The single nucleotide polymorphism frequency between *Marchantia polymorpha* subspecies is approximately 1.0-1.2% (Linde et al., 2020), while that between the Australian and North American *Ricciocarpos* isolates is approximately 4.1%. In the absence of fossil calibration, the nucleotide differences suggest divergence of the two *Ricciocarpos* populations perhaps in the early Miocene, 15-20 Ma.

We examined the phylogenetic relationships between *Ricciocarpos natans* accessions for which DNA sequence was available on Genbank, and found that sequences were distributed into at least two distinct clades (Figure 1C). One clade contained sequences from five accessions collected in Australia and Asia, including the Jerrybomberra Creek accession, while a second distinct clade was composed of sequences representing five accessions collected in North America. Ironically, a paucity of available DNA sequence from accessions collected in Europe, where *Ricciocarpos* was first described, prevented definitive placement of European accessions relative to the distinct two clades, with a single sequence with a long branch representing this continent. Given the sequence divergence between the Australasian and North American accessions, we suggest that these two clades might represent two distinct reproductively isolated *Ricciocarpos* populations and could be considered two separate species. Further work is required to ascertain whether there exist morphological or anatomical characters that define the two clades. Whether the European accessions might represent a third entity must await more sequence data from such accessions. Regardless of the phylogenetic position of the European accessions, it is of note that the divergence between the American and Australasian accessions could be related to distinct migratory bird flyways (Boere and Stroud, 2006). In this regard, it will be of interest whether genetic characterization of *Ricciocarpos* accessions from other geographic locations, such as South America, Africa, Central Asia and New Zealand also correlate with migratory patterns of birds.

The aquatic to terrestrial morphological transition in *Ricciocarpos*

Ricciocarpos is secondarily adapted to aquatic life and is found worldwide in stagnant water, e.g. ponds and billabongs. However, as water levels drop seasonally, *Ricciocarpos* plants may become stranded on the terrestrial margins. *Ricciocarpos* exhibits strong morphological differences based on the habitat in which it is growing, with a plant of the same genotype being able to transition from a free-floating aquatic form into a terrestrial form (Garber, 1904; Pickett, 1925). When growing in culture, the addition of abscisic acid (ABA) to the media of aquatically growing *Ricciocarpos* is sufficient to induce the transformation in growth habit from the aquatic to that of the terrestrial form (Hartung et al., 1994). This observation parallels similar experiments on another secondarily aquatic liverwort, *Riccia fluitans*, that usually grows submerged in water rather than floating on the surface. When *Riccia fluitans* is transferred from an aquatic medium to one exposed to the air, a transition from an aquatic growth form to a terrestrial form and during this transition process the concentration of ABA is increased 10-30 fold (Hellwege et al., 1992). Furthermore, treatment of *Riccia fluitans* with ABA can induce such characteristics even when the thallus is submerged in water (Hellwege et al., 1992), with concomitant changes in gene expression, including genes encoding Late Embryogenesis Abundant (LEA) proteins (Hellwege et al., 1996). The transition, which takes place over a couple weeks, includes changes to cell division patterns at the shoot apex such that the terrestrial form has larger air chambers and some air pores, in addition to the development of rhizoids (Althoff et al., 2022).

To further understand the aquatic to terrestrial transition in *Ricciocarpos*, we repeated earlier observations. In our growth conditions the morphological differences between aquatic and terrestrial forms of *Ricciocarpos* were successfully induced by addition of 0.1μM ABA (Figure 4A). The aquatic form is characterized by the development of long ventral scales that act as keels to keep the plants stable on the water surface (Figures 4B, C). The scales are usually heavily pigmented with riccionidin (Figure 4B), which is an auronidin localized to the cell wall and whose synthesis is biochemically related to that of anthocyanins that are common in other land plants (Kunz et al., 1994; Albert et al., 2018; Berland et al., 2019). In the aquatic form, the development of rhizoids is suppressed. Conversely, in the terrestrial form, the development of rhizoids is promoted, while that of scales is repressed. In addition, separation of the thallus *via* (presumably) programmed cell death, following dichotomous branching is a form of vegetative reproduction that allows dispersal of the plants across the water surface. Separation is suppressed in the terrestrial form such that plants form a rosette. When ABA is added to aquatically growing plants, a transition from production of scales to the production of rhizoids is observed and separation of thalli is suppressed (Figures 4A, C).

In the aquatic form, the scales that develop from the ventral epidermis are deeply pigmented with riccionidin at maturity. However, immature scales in which cell division is still occurring lack riccionidin pigmentation, but do contain conspicuous chloroplasts (Figure 5A). As scales differentiate, riccionidin accumulation first appears proximally and then gradually extends to the distal tip (Figure 5B). As scales mature riccionidin accumulation continues and chloroplasts are no longer conspicuous (Figures 5C-E). Pigmentation is particularly intense in the marginal cells with protuberances giving the scale a fringed appearance (Figures 5C-E). As the riccionidin accumulation occurs as a polymerized derivative embedded in the cell wall (Kunz et al., 1994; Berland et al., 2019), it may act to stiffen the scales to aid their function as keels. The production of the cell wall pigment may also preclude subsequence cell division (Albert et al., 2018). In the terrestrial form the scales remain small and are restricted to the region of the apical meristem (Kronestedt, 1982a). The rhizoids that develop in the terrestrial form following ABA treatment are smooth rhizoids (Figure 5F)

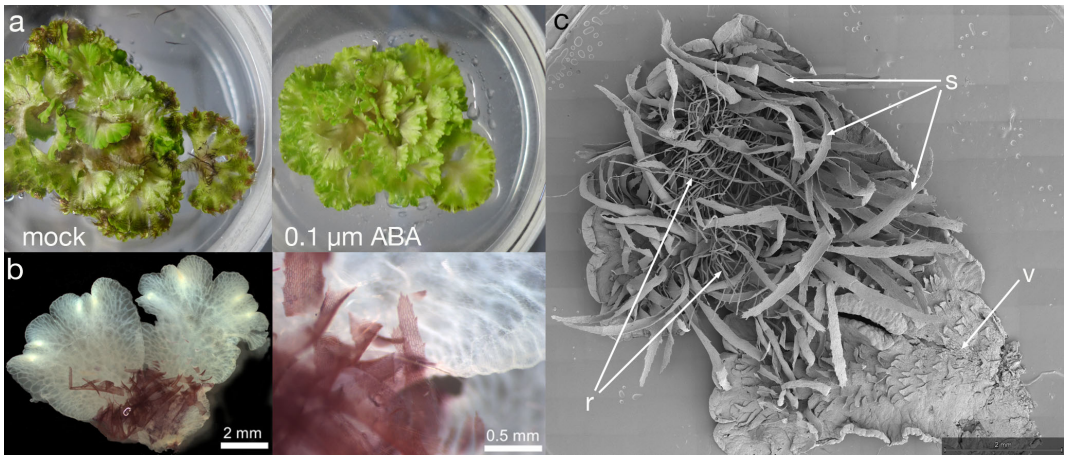

FIGURE 4
ABA induced formation of the terrestrial form. **(A)** When grown aquatically in ⅛ Gamborg B-5 media, plants produce copious ventral long scales, with their purple colour visible in the mocked plants (left); some of the thalli are flipped over to show the ventral scales. ABA treatment of leads to growth of the terrestrial form (right), lacking purple scales and. The diameter of petri plate is 9 cm. **(B)** The aquatic form of *Ricciocarpos* exhibits purple scales. The purple pigment of scales is cell wall bound, perhaps providing structural support. The image shows a thallus fixed in Formaldehyde Alcohol Acetic Acid - FAA and cleared in 100% Ethanol. **(C)** Both scales and rhizoids are observed in *Ricciocarpos* following a shift to ABA containing media. This plant was initially producing ventral scales, but began to produce rhizoids after ABA treatment; if treatment continues, eventually the scales will fall off and the plant will only have rhizoids; ventral thallus; s, scale; r, rhizoid.

To explore the role of ABA on gene expression in the *Ricciocarpos* thallus during the transition from an aquatic form to a terrestrial form, a differential expression analysis comparing plants growing aquatically to those grown for four weeks in the presence of ABA [0.1µM] was performed; given the time point the differentially expressed genes (DEG) will represent steady state levels following long-term ABA exposure. DEG were identified considering all data and observing the scaling at the gene level to identify differential expression (up or down). This analysis revealed that out of 15,440 genes with non-zero total read count with adjusted p-value < 0.05, a total of 2237 (15% of genes) are up-regulated (log2Foldchange > 0) and 2798 (18% of genes) are down-regulated (log2Foldchange < 0) (Figure 6A). A heatmap of the DEG facilitated hierarchical clustering to identify gene clusters displaying similar expression patterns amongst samples (Figure 6B). The heatmap was plotted with all significant genes with adjusted value < 0.05. The genes differentially expressed are grouped in 10 clusters.

Response of ABA related Genes: To determine changes in ABA-related genes, transcriptomes were analysed to identify expression of each known ortholog of *Marchantia* ABA biosynthesis and response genes (Bowman et al., 2017). DEG analysis of ABA-related genes revealed Rn_08915.1, an ortholog of *Marchantia* MpNCED (9-cis-epoxycarotenoid dioxygenase1; Mp2g07800) and of NCED1 (At3g63520) of Arabidopsis (Bowman et al., 2017), is up-regulated upon ABA treatment (Table 1). In contrast, the PYRABACTIN RESISTANCE1-like (PYR1-like) ABA receptor, an ortholog of MpPYL1 and the fourteen PYR-related genes of Arabidopsis (Bowman et al., 2017; Jahan et al., 2019) was not found to be differentially expressed when comparing aquatic and ABA treated samples.

ABA control expression of LEA-like genes: ABA reduces growth and enhances desiccation tolerance by increasing accumulation of intracellular sugars and various proteins such as those encoded by LEA-like genes (Akter et al., 2014; Hernández-Sánchez et al., 2022). Expression patterns of *Ricciocarpos* LEA genes are presented in Table 2. As expected, there is accumulation of several LEA genes upon ABA treatment, with Rn_05573.1 (LEA_1), Rn_18585.1 (LEA_1), and Rn_15939.1 (LEA_4) up-regulated in response to exogenous ABA application and Rn_16212.1 (LEA_2) and Rn_12186.1 (LEA_2) downregulated; LEA families as previously defined (Artur et al., 2018). In addition, several members of the NHL (*NDR1*, nonrace specific disease resistance 1; *HIN1*, hairpin-induced 1) gene family previously associated with disease resistance and ABA response (Bao et al., 2016) were differentially regulated, with Rn_11497.1, Rn_08770.1, and Rn_09383.1 downregulated in response to exogenous ABA.

Expression of the rhizoid gene, RSL1: The *Marchantia* gene Mp*RSL1* (Mp3g17930.1) is required for rhizoid initiation and is an ortholog of Arabidopsis *ROOT HAIR DEFECTIVE6* that acts in root hair development (Proust et al., 2016). The orthologous *Ricciocarpos* gene is Rn_00421, and consistent with the observed morphology of ABA treated *Ricciocarpos* plants, this gene is up-regulated upon ABA treatment. An analysis examining gene expression at shorter intervals during the aquatic to terrestrial transition should identify additional gene regulatory networks associated with the developmental changes.

Several limnetic or riparian plants exhibit phenotypic plasticity wherein morphology is dependent upon environmental conditions, e.g. whether growing submerged or floating on the water versus aerial growth or on a terrestrial substrate. In many cases the shift from an aquatic morphology to a terrestrial morphology is correlated or mediated with increased endogenous ABA levels. For example, in two liverworts that evolved a secondarily aquatic habit independently, *Riccia fluitans* and *Ricciocarpos natans*, the terrestrial form can be induced by ABA (Hellwege et al., 1992;

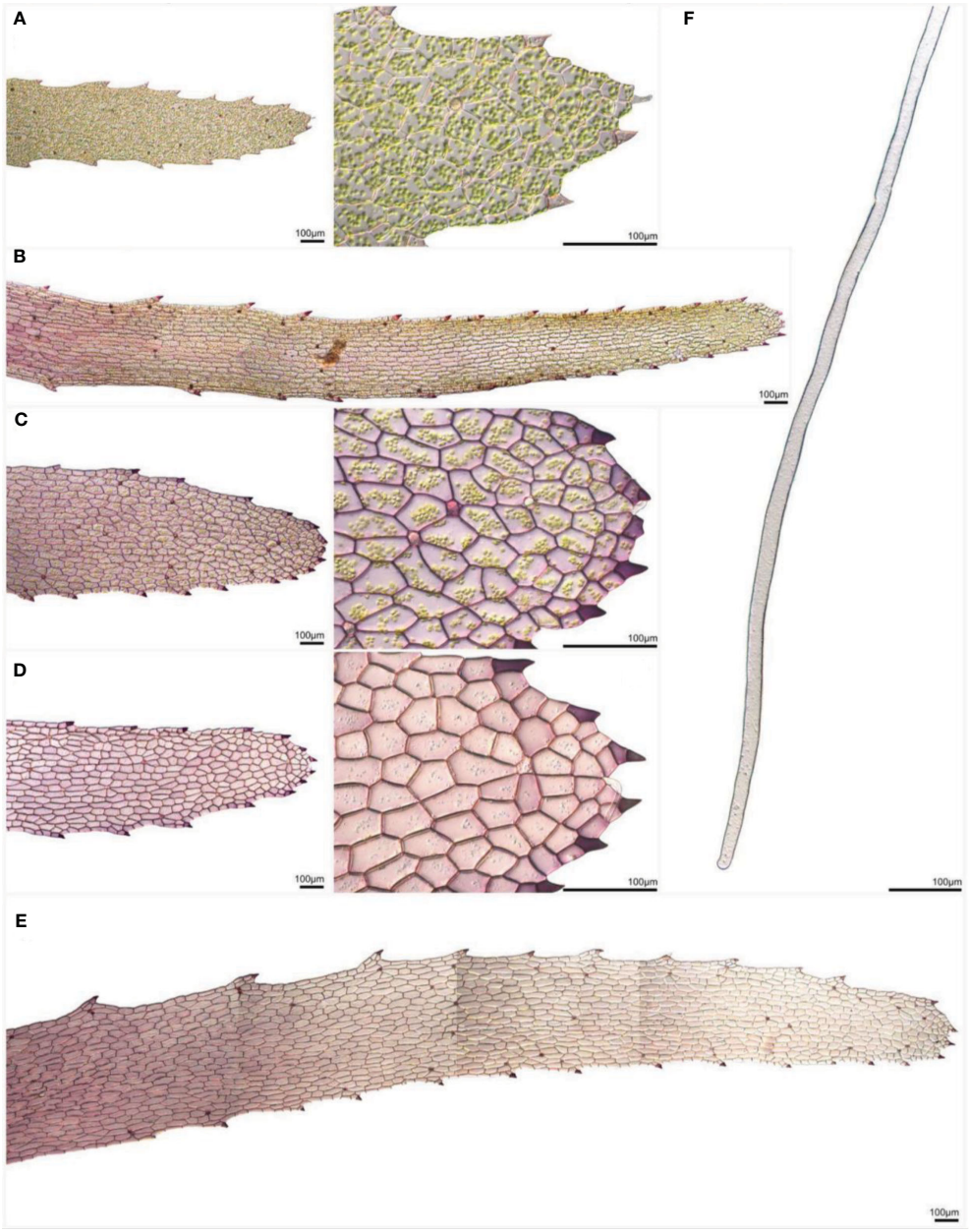

FIGURE 5
Scales and rhizoids of *Ricciocarpos*. **(A)** An immature scale in which little riccionidin is visible. (a') Magnification of **(A)** showing conspicuous chloroplasts. **(B)** In slightly older scales, the reddish-purple coloured riccionidin pigment initially appears at the proximal end of the scale and progresses towards the distal tip. **(C, D)** As scales differentiate, an increase in riccionidin pigmentation is distinctly visible. (c' and d') Magnifications of **(C, D)**, respectively, showing the loss of chloroplasts as scales mature. **(E)** Mature scales retain a gradient of pigmentation. **(F)** *Ricciocarpos* rhizoids are similar to the smooth rhizoids of *Marchantia* (Shimamura, 2016; Bowman et al., 2022).

Hartung et al., 1994; Hellwege et al., 1996; Althoff et al., 2022). In each of these species, the terrestrial form develops rhizoids, while the aquatic form does not, but other morphological changes appear to be species specific, such as the loss of scale production and loss of thallus separation appear to be specific to *Ricciocarpos*. Similar aquatic-terrestrial transitions are also observed in vascular plants in the form of heterophylly, wherein leaf morphology is polymorphic depending upon environmental conditions (Nakayama et al., 2017; Li et al., 2019). Such heterophylly has evolved multiple times independently within angiosperms, and while in many instances ABA in implicated, its involvement is not universal. For example, abscisic acid induces formation of floating leaves in the heterophyllous aquatic angiosperm *Potamogeton nodosus* (Anderson, 1978) and abscisic acid induces land form characteristics in the fern *Marsilea quadrifolia* (Liu, 1984). In contrast, aquatic-terrestrial heterophylly in *Rorippa aquatica* another phytohormone, gibberellic acid, regulates leaf morphology in conjunction with KNOX1 genes known to

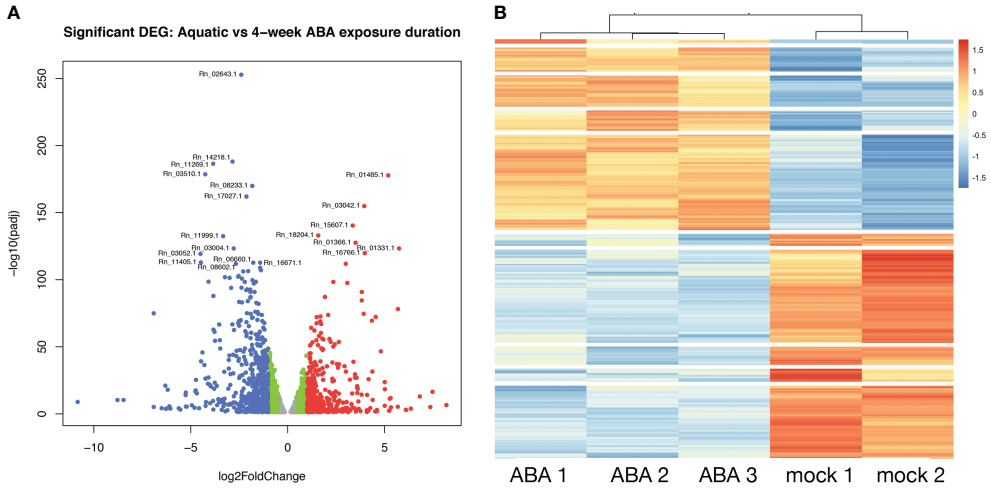

FIGURE 6
Differential gene expression between aquatic and terrestrial forms. **(A)** Differentially expressed genes in Aquatic vs 4-week ABA treated samples: adjusted p-values of <0.05 are plotted in the above graph with log2Foldchange between -0.5 to 0.5 represented in grey, genes with log2Foldchange in range -0.5 to -1 and 0.5 to 1 shown in green. The down-regulated and up-regulated genes with log2Foldchange greater than 1 or smaller than -1 are shown in red and blue color, respectively. **(B)** Heatmap showing differential gene expression in ABA treated *Ricciocarpos* in contrast to the control sample with no ABA treatment. Orange color signifies up regulated genes and blue color signifies down-regulated genes, scaled to normalized read counts.

influence leaf complexity (Nakayama et al., 2014) and in *Ranunculus trichophyllus* ABA works in conjunction with a third phytohormome, ethylene, to regulate heterophylly (Kim et al., 2018). Ethylene has also been implicated in heterophylly in other angiosperm species (Nakayama et al., 2017; Li et al., 2019). Both ethylene and ABA are implicated in adaptations to water stress, too much for the former and too little for the latter (Jackson, 2008; Sakata et al., 2013). Thus, these phytohormone signalling pathways are likely already active in the tissues that will develop heterophylly or other developmental modifications in aquatic plants, and can be integrated into gene regulatory networks controlling morphology as well as physiology.

Summary

While we developed *Ricciocarpos natans* as a 'model' system for examining genomic evolution during the transition for dioicy to monoicy (Singh et al., 2023), once some tools are developed for a species, other biological questions come calling. In today's age, only a

TABLE 1 ABA genes differentially expressed with ABA treated plants in comparison to aquatic *R. natans*.

Marchantia polymorpha Gene ID	Rn Gene ID	4 week	Gene Symbol	GO/PANTHER
Mp2g07800.1	Rn_08915.1	UP	Mp*NCED*: 9-cis-epoxycarotenoid dioxigenase	GO:0016702: oxidoreductase activity, acting on single donors with incorporation of molecular oxygen, incorporation of two atoms of oxygen
Mp1g24460.1	Rn_14445.1	X	Mp*SNRK2A*: SNF1-related protein kinase2	GO:0004672: protein kinase activity
Mp8g06370.1	Rn_10037.2	UP	Mp*AO*: abscisic aldehyde oxidase	GO:0016491: oxidoreductase activity
Mp2g25940.1	Rn_07898.1	DOWN	MpCYP707A: ABA 8'-hydroxylase	GO:0016705: oxidoreductase activity, acting on paired donors, with incorporation or reduction of molecular oxygen
Mp2g00670.1	Rn_08366.1	DOWN	MpABA1: zeaxanthin epoxidase	GO:0009688: abscisic acid biosynthetic process
Mp8g17460.1	Rn_17318.1	X	MpPYL1: PYR1-like abscisic acid receptor	PTHR31213:SF119 : ABSCISIC ACID RECEPTOR PYL4

X denotes not differentially expressed.

TABLE 2 LEA genes are differentially expressed with ABA treated plants in comparison to aquatic *R. natans*.

Marchantia polymorpha Gene ID	Rn Gene ID	4 week	Gene Symbol	LEA group	GO/PANTHER
Mp1g17670.1	Rn_16212.1	DOWN	No gene symbols are registered for this gene	LEA_2	PTHR31852:SF141:LATE EMBRYOGENESIS ABUNDANT PROTEIN, GROUP 2; PANTHER:PTHR31852:LATE EMBRYOGENESIS ABUNDANT (LEA) HYDROXYPROLINE-RICH GLYCOPROTEIN FAMILY
Mp3g04820.1	Rn_05573.1	UP	MpLEA-like12:Late-embryogenesis abundant protein	LEA_1	GO:0009793:embryo development ending in seed dormancy;
Mp7g19340.1	Rn_11497.1	DOWN	MpLEA-like58: Late-embryogenesis abundant protein	NHL	PANTHER:PTHR31234:LATE EMBRYOGENESIS ABUNDANT (LEA) HYDROXYPROLINE-RICH GLYCOPROTEIN FAMILY
Mp3g23740.1	Rn_18585.1	UP	MpLEA-like16:Late-embryogenesis abundant protein	LEA_4	GO:0009793:embryo development ending in seed dormancy
Mp1g01170.1	Rn_15939.1	UP	MpLEA-like2:Late-embryogenesis abundant protein	LEA_4	**PTHR47652:SF3**, LATE EMBRYOGENESIS ABUNDANT PROTEIN (LEA) FAMILY PROTEIN
Mp2g12370.1	Rn_08770.1	DOWN	MpLEA-like8:Late-embryogenesis abundant protein	NHL	PANTHER:PTHR31234:LATE EMBRYOGENESIS ABUNDANT (LEA) HYDROXYPROLINE-RICH GLYCOPROTEIN FAMILY
Mp8g07630.1	Rn_09383.1	DOWN	MpLEA-like59:Late-embryogenesis abundant protein	NHL	PANTHER:PTHR31234:LATE EMBRYOGENESIS ABUNDANT (LEA) HYDROXYPROLINE-RICH GLYCOPROTEIN FAMILY
Mp7g12850.1	Rn_12186.1	DOWN	MpLEA-like56:Late-embryogenesis abundant protein	LEA_2	PTHR31852:SF180:PROTEIN, PUTATIVE-RELATED

few prerequisites are required for establishing a model organism — e.g. ease of growth in culture, genomic resources, ability to introduce genome editing technologies. For *Ricciocarpos*, the former two have been established and it is likely that transformation using protocols for the related species, *Riccia fluitans* (Althoff and Zachgo, 2020), can be readily adapted to *Ricciocarpos*. Thus, *Ricciocarpos* is primed to be utilized to answer a spectrum of biological questions only limited by the imagination, and of course funding.

Data availability statement

The data presented in the study are deposited at https://genomevolution.org/coge/, accession code: 'Ricciocarpos'.

Author contributions

SS: Conceptualization, Formal Analysis, Investigation, Methodology, Writing – original draft. JB: Conceptualization, Formal Analysis, Funding acquisition, Supervision, Writing – original draft, Writing – review & editing.

Funding

The authors declare financial support was received for the research, authorship, and/or publication of this article. This work was supported by Monash University and funding from the Australian Research Council (CE200100015).

Acknowledgments

We thank Chris Cargill at the Australian National Botanic Gardens for the original *Ricciocarpos natans* isolate. We thank John Alvarez and Tom Fisher for helpful comments on the manuscript.

Conflict of interest

The authors declare that the research was conducted in the absence of any commercial or financial relationships that could be construed as a potential conflict of interest.

Publisher's note

References

Acuña-Castillo, R., Jiménez, J. E., Blanco Coto, M. A., and Bezerra Silva, L. E. (2023). Ricciocarpos natans (Marchantiophyta, Ricciaceae), new to Costa Rica, with A survey of its presence in Latin America. *Acta Botanica Mexicana* 130, E2177. doi: 10.21829/abm130.2023.2177

Agami, M., Litav, M., and Waisel, Y. (1976). The effects of various components of water pollution on the behavior of some aquatic macrophytes of the coastal rivers of Israel. *Aquat. Bot.* 2, 203–213. doi: 10.1016/0304-3770(76)90021-8

Akter, K., Kato, M., Sato, Y., Kaneko, Y., and Takezawa, D. (2014). Abscisic acid-induced rearrangement of intracellular structures associated with freezing and desiccation stress tolerance in the liverwort marchantia polymorpha. *J. Of Plant Physiol.* 171, 1334–1343. doi: 10.1016/j.jplph.2014.05.004

Albert, N. W., Thrimawithana, A. H., Mcghie, T. K., Clayton, W. A., Deroles, S. C., Schwinn, K. E., et al. (2018). Genetic analysis of the liverwort Marchantia polymorpha reveals that R2r3myb activation of flavonoid production in response to abiotic stress is an ancient character in land plants. *New Phytol.* 218, 554–566. doi: 10.1111/nph.15002

Althoff, F., Wegner, L., Ehlers, K., Buschmann, H., and Zachgo, S. (2022). Developmental plasticity of the amphibious liverwort Riccia fluitans. *Front. In Plant Sci.* 13, 909327. doi: 10.3389/fpls.2022.909327

Althoff, F., and Zachgo, S. (2020). Transformation of riccia fluitans, an amphibious liverwort dynamically responding to environmental changes. *Int. J. Of Mol. Biosci.* 21, 5410. doi: 10.3390/ijms21155410

Anderson, L. W. (1978). Abscisic acid induces formation of floating leaves in the heterophyllous aquatic angiosperm Potamogeton nodosus. *Science* 201, 1135–1138. doi: 10.1126/science.201.4361.1135

Aoki, C., Teixeira-Gamarra, M. C., Gamarra, R. M., Medeiros, S. C. H. D., Pott, V. J., Junior, G. A. D., et al. (2017). Abiotic factors drive the structure of aquatic plant assemblages in riverine habitats of the Brazilian "Pantanal". *Braz. J. Of Bot.* 40, 405–415. doi: 10.1007/s40415-016-0345-0

Artur, M. A. S., Zhao, T., Ligterink, W., Schranz, E., and Hilhorst, H. W. M. (2018). Dissecting thegenomicdiversificationof late embryogenesis abundant (Lea) protein gene families in plants. *Genome Biol. And Evol.* 11, 459–471. doi: 10.1093/gbe/evy248

Bao, Y., Song, W.-M., and Zhang, H.-X. (2016). Role of arabidopsis Nhl family in aba and stress response. *Plant Signaling Behav.* 11, E1180493. doi: 10.1080/15592324.2016.1180493

Barnes, C. R., and Land, W. J. G. (1907). Bryological papers I. The origin of air chambers - contributions from the hull botanical laboratory, 100. *Botanical Gazette* 44, 197–213. doi: 10.1086/329317

Berland, H., Albert, N. W., Stavland, A., Jordheim, M., Mcghie, T. K., Zhou, Y., et al. (2019). Auronidins are A previously unreported class of flavonoid pigments that challenges when anthocyanin biosynthesis evolved in plants. *Proc. Of Natl. Acad. Of Sci. U.S.A.* 116, 20232–20239. doi: 10.1073/pnas.1912741116

Berrie, G. K. (1960). The chromosome numbers of liverworts (Hepaticae and Anthocerotae). *Trans. Of Br. Bryological Soc.* 3, 688–705. doi: 10.1179/006813860804828963

Bischler-Causse, H., Gradstein, S. R., Jovet-Ast, S., Long, D. G., and Allen, N. S. (2005). Marchantiidae. *Flora Neotropica* 97, 1–262.

Bischoff, G. W. (1835). Bemerkungen über die lebermoose vozüglich aus den gruppen der marchantieen und riccieen. *Nova Acta Physico Med. A C L* 17 (2), 909–1088. Tafeln Lxvii-Lxxi.

Boere, G. C., and Stroud, D. A. (2006). "The flyway concept: what it is and what it isn't," in *Waterbirds Around The World*. Eds. G. C. Boere, C.A. Galbraith and D. A. Stroud (Edinburgh, Uk: The Stationery Office).

Bowman, J. L. (2022). The origin of A land flora. *Nat. Plants* 8, 1352–1369. doi: 10.1038/s41477-022-01283-y

Bowman, J. L., Arteaga-Vazquez, M., Berger, F., Briginshaw, L. N., Carella, P., Aguilar-Cruz, A., et al. (2022). The renaissance and enlightenment of marchantia as A model system. *Plant Cell* 34, 3512–3542. doi: 10.1093/plcell/koac219

Bowman, J. L., Kohchi, T., Yamato, K. T., Jenkins, J., Shu, S., Ishizaki, K., et al. (2017). Insights into land plant evolution garnered from the Marchantia polymorpha genome. *Cell* 171, 287–304. doi: 10.1016/j.cell.2017.09.030

Brown, R., and Bauer, F. (1814). *General Remarks, Geographical And Systematical, On The Botany Of Terra Australis* (W. Bulmer: London).

Buch, H. (1954). Om utbredning och spridningen av fissidens julianus, ricciocarpus natans och riccia fluitans I ostfennoskandia. *Memoranda Societatis Pro Fauna Et Flora Fennica* 29, 35–40.

Campbell, D. H. (1895). *The structure and development of mosses and ferns* (London: Macmillan And Co).

Campbell, E. O. (1975). Notes on the liverwort family ricciaceae in New Zealand. *Tuatara* 21, 121–129.

Candela, H., and Hake, S. (2008). The art and design of genetic screens: maize. *Nat. Rev. Genet.* 9, 192–203. doi: 10.1038/nrg2291

Candolle, A. P. D., and Lamarck, J.-B. P. A. (1805). *Flore Française, Paris, Chez H. Agasse, Rue Des Poitevins, N°. 6 (De L'imprimerie De Stoupe)*. Paris.

Chimney, M. J. (1984). First report of Ricciocarpus natans (L.) corda (Marchantiales-ricciaceae) from A strip mine impoundment. *Trans. Of Illinois Acad. Of Sci.* 77, 43–44.

Coe, E. H. J. (2001). The origins of maize genetics. *Nat. Rev. Genet.* 2, 898–905. doi: 10.1038/35098524

Collier, J. H., and Hooper, J. (1866). *The American Parlor Aquarium, Or, Fluvial Aqua Vivarium : Being A Familiar Treatise On The Fresh Water Aquarium; The Best Mode Of Construction And Arrangement; Including A Brief Sketch Of All The Fresh Water Fishes And Aquatic Plants Adapted To The Same, Found In The United States New York*. J. H Collier.

Corda, A. J. C. (1828). Genera hepaticarum. *Ph. M. Opiz Beiträgen Zur Naturgeschichte*, 12, 643–655.

Dillenius, J. J. (1741). *Historia Muscorum: A General History Of Land And Water, &C. Mosses And Corals, Containing All The Known Species* (London: J. Millan).

Drège, J. F. (1843). *Zwei Pflanzengeographische Documente, Stafleu & Cowan* (Taxonomic Literature). doi: 10.5962/bhl.title.87612

Duthie, A. V., and Garside, S. (1936). Studies in South African ricciaceae. *Trans. Of R. Soc. Of South Afr.* 2, 93–133. doi: 10.1080/00359193609520543

Edler, D., Klein, J., Antonelli, A., and Silverstro, D. (2020). Raxmlgui 2.0: A graphical interface and toolkit for phylogenetic analyses using Raxml. *Methods In Ecol. And Evol.* 12, 373–377. doi: 10.1111/2041-210X.13512

Ferreyra, A. N. (1990). Notas sobre la morfologia vegetativa Y la reproducción asexual en Ricciocarpus natans L. Corda marchantiales hepaticae. *Lilloa* 37, 51–54.

Fischer, E. (1995). The genera ricciocarpos and riccia (Hepaticae, Ricciaceae) in Rwanda. *Fragmenta Floristica Et Geobotanica* 40, 93–111.

Fourounjian, P., Fakhoorian, T., and Cao, X. H. (2020). "Importance of duckweeds in basic research and their industrial applications," in *The Duckweed Genomes*. Eds. X. H. Cao, P. Fourounjian and W. Wang (Springer Cham). doi: 10.1007/978-3-030-11045-1_1

Frey, W., Frahm, J.-P., Fischer, E., and Lobin, W. (2006). *The Liverworts, Mosses And Ferns Of Europe* Martins, Greathorkesley, Colchester, Essexc06 4ah (England: Harley Books, B.H. & A. Harley Ltd).

Gamborg, O. L., Miller, R. A., and Ojima, K. (1968). Nutrient requirements of suspension cultures of soybean root cells. *Exp. Cell Res.* 50, 151–158. doi: 10.1016/0014-4827(68)90403-5

Garber, J. F. (1904). The life history of Ricciocarpus natans. *Botanical Gazette* 37, 161–177. doi: 10.1086/328464

Gimenes, L. L. S., Freschi, G. P. G., Bianchini, I. J., and Cunha Santino, M. B. D. (2020). Growth of the aquatic macrophyte Ricciocarpos natans (L.) corda in different temperatures and in distinct concentrations of aluminum and manganese. *Aquat. Toxicol.* 224, 105484. doi: 10.1016/j.aquatox.2020.105484

Gomes, M. P., Brito, J. C. E. M. D., Bicalho, E. M., Silva, J. G., Gomides, M. D. F. A., Garcia, Q. S., et al. (2018). Ciprofloxacin vs. Temperature- antibiotic toxicity in the free-floating liverwort Ricciocarpus natans from A climate change perspective. *Chemosphere* 202, 410–419. doi: 10.1016/j.chemosphere.2018.03.048

Haas, B. J., Delcher, A. L., Mount, S. M., Wortman, J. R., Smith, R. K., Hannick, L. I., et al. (2003). Improving the arabidopsis genome annotation using maximal transcript alignment assemblies. *Nucleic Acids Res.* 31, 5654–5666. C.OMMAJ.R.X.X.X. doi: 10.1093/nar/gkg770

Haas, B. J., Salzberg, S. L., Zhu, W., Pertea, M., Allen, J. E., Orvis, J., et al. (2008). Automated eukaryotic gene structure annotation using evidencemodeler and the program to assemble spliced alignments. *Genome Biol.* 9, R7. doi: 10.1186/gb-2008-9-1-r7

Hartman, G. (1985). Foods of male mallard, before and during moult, as determined by faecal analysis. *Wildfowl J.* 36, 65–71.

Hartung, W., Hellwege, E. M., and Volk, O. H. (1994). The function of abscisic acid in bryophytes. *J. Of Hattori Botanical Lab.* 76, 59–65. 10.18968/jhbl.76.0_59

Hassel de Menendez, G. G. (1962). Estudio De Las Anthocerotales Y Marchantiales de la Argentina. *Opera Lilloana* 7, 1–97.

Hellwege, E. M., Dietz, K.-J., and Hartung, W. (1996). Abscisic acid causes changes in gene expression involved in the induction of the landform of the liverwort Riccia fluitans L. *Planta* 198, 423–432. doi: 10.1007/BF00620059

Hellwege, E. M., Volk, O. H., and Hartung, W. (1992). A physiological role of abscisic acid in the liverwort Riccia fluitans L. *J. Plant Physiol.* 140, 553–556. doi: 10.1016/S0176-1617(11)80788-1

Hernández-Sánchez, I. E., Maruri-López, I., Martinez-Martinez, C., Janis, B., Jiménez-Bremont, J. F., Covarrubias, A. A., et al. (2022). Leafing through literature: late embryogenesis abundant proteins coming of age—Achievements and perspectives. *J. Of Exp. Bot.* 73, 6525–6546. doi: 10.1093/jxb/erac293

Hirsh, P. E. (1910). The development of air chambers in the Ricciaceae. *Bull. Of Torrey Botanical Club* 37, 73–77. doi: 10.2307/2478961

Hooker, W. J. (1830). *Botanical Miscellany*. J. Murray: London.

Hooker, W. J. (1840). *Icones Plantarum Or Figures, With Brief Descriptive Characters And Remarks, Of New Or Rare Plants, Selected From The Author's Herbarium,* London: Longman, Rees, Orme, Brown, Green, & Longman.

Hooker, J. D. (1855). "The botany of the antarctic voyage of H. M. Discovery ships erebus and terror in the years 1839-1843 unde rthe command of captain sir james clark ross," in *Ii. Flora Novae-Zealandiae ii. Flowerless Plants* (London: Lovell Reeve).

Hübener, J.W., P. (1834). *Hepaticologia Germanica Oder Beschreibung Der Deutschen Lebermoose,* Mannheim: Schwan - Götz'sche Hofbuchlandlung.

Jackson, M. B. (2008). Ethylene-promoted elongation: an adaptation to submergence stress. *Ann. Of Bot.* 101, 229–248. doi: 10.1093/aob/mcm237

Jahan, A., Komatsu, K., Wakida-Sekiya, M., Hiraide, M., Tanaka, K., Ohtake, R., et al. (2019). Archetypal roles of an abscisic acid receptor in drought and sugar responses in liverworts. *Plant Physiol.* 179, 317–328. doi: 10.1104/pp.18.00761

Jain, C., Rodriguez-R, L. M., Phillippy, A. M., Konstantinidis, K. T., and Aluru, S. (2018). High throughput ani analysis of 90k prokaryotic genomes reveals clear species boundaries. *Nat. Commun.* 9, 5114. doi: 10.1038/s41467-018-07641-9

Jones, E. W. (1957). African hepatics: xiii. The ricciaceae in tropical Africa. *Trans. Of Br. Bryological Soc.* 3, 208–227. doi: 10.1179/006813857804829524

Kanazawa, T., Morinaka, H., Ebine, K., Shimada, T. L., Ishida, S., Minamino, N., et al. (2020). The liverwort oil body is formed by redirection of the secretory pathway. *Nat. Commun.* 11, 6152. doi: 10.1038/s41467-020-19978-1

Kashyap, S. R. (1929). *Liverworts of The Western Himalayas and the Panjab Plain. Part I* (Lahore: The University Of The Panjab).

Kelleway, J. J., Iles, J. A., Kobayashi, T., and Ling, J. E. (2021). Resilience Of A native soil seed bank in A floodplain lake subjected to cropping, grazing and extended drought. *Mar. And Freshw. Res.* 72, 787–799. doi: 10.1071/MF19386

Kim, J., Joo, Y., Kyung, J., Jeon, M., Park, J. Y., Lee, H. G., et al. (2018). A molecular basis behind heterophylly in an amphibious plant, Ranunculus trichophyllus. *PloS Genet.* 14, E1007208. doi: 10.1371/journal.pgen.1007208

Kolon, K., and Sarosiek, J. (1995). Das verschwinden der wasserlebermoose riccia fluitans und Ricciocarpos natans an irhen fundorten in niederschlesien und ihre empfindlichkeit gegeüber zwei herbiziden. *Cryptogamica Helv.* 18, 77–83.

Kronestedt, E. (1981). Anatomy of Ricciocarpus natans (L.) Corda, studied by scanning electron microscopy. *Ann. Of Bot.* 47, 817–827. doi: 10.1093/oxfordjournals.aob.a086081

Kronestedt, E. (1982a). Anatomy of Ricciocarpus natans, with emphasis on fine structure. *Nordic J. Of Bot.* 2, 353–367. doi: 10.1111/j.1756-1051.1982.tb01200.x

Kronestedt, E. (1982b). Structure and development of the air pores in Ricciocarpus natans. *Nordic J. Of Bot.* 2, 491–499. doi: 10.1111/j.1756-1051.1982.tb01214.x

Kronestedt, E. (1983). Cytology of oil–body cells in Ricciocarpus natans. *Nordic J. Of Bot.* 3, 547–558. doi: 10.1111/j.1756-1051.1983.tb01467.x

Kubo, H., Nozawa, S., Hiwatashi, T., Kondou, Y., Nakabayashi, R., Mori, T., et al. (2018). Biosynthesis of riccionidins and marchantins is regulated by R2r3- Myb transcription factors in marchantia polymorpha. *J. Of Plant Res.* 131, 849–864. doi: 10.1007/s10265-018-1044-7

Kunz, S., and Becker, H. (1995). Cell wall pigment formation of *in vitro* cultures of the liverwort Ricciocarpos natans. *Z. Naturforsch.* 50, 235–240. doi: 10.1515/znc-1995-3-412

Kunz, S., Burkhardt, G., and Becker, H. (1994). Riccionidins A and B, anthocyanidins from the cell walls of the liverwort Ricciocarpus natans. *Phytochemistry* 35, 233–235. doi: 10.1016/S0031-9422(00)90540-5

Lázaro, X. A., Mackenzie, R., and Jiménez, J. E. (2021). Evidence of endozoochory in upland geese chloephaga picta and white-bellied seedsnipes attagis malouinus in sub-antarctic Chile. *Ecol. And Evol.* 11, 9191–9197. doi: 10.1002/ece3.7725

Lee, G. E., and Gradstein, S. R. (2021). *Guide to the Genera of Liverworts and Hornworts Of Malaysia* (Tokyo, Japan: Hattori Botanical Laboratory).

Leffler, E. M., Bullaughey, K., Matute, D. R., Meyer, W. K., Ségurel, L., Venkat, A., et al. (2012). Revisiting an old riddle: what determines genetic diversity levels within species? *PloS Biol.* 10, E1001388. doi: 10.1371/journal.pbio.1001388

Leitgeb, H. (1879). *Untersuchungen über die lebermoose. Heft iv. Die riccieen* (Leuschner & Lubensky: Graz).

Lewis, C. E. (1906). The embryology and development of riccia lutescens and Riccia-crystallina. *Botanical Gazette* 41, 109–138. doi: 10.1086/328727

Lewis, L. R., Behling, E., Gousse, H., Qian, E., Elphick, C. S., Lamarre, J.-F., et al. (2014a). First evidence of bryophyte diaspores in the plumage of transequatorial migrant birds. *Peerj* 2, 424. doi: 10.7717/peerj.424

Lewis, L. R., Rozzi, R., and Goffinet, B. (2014b). Direct long-distance dispersal shapes A new world amphitropical disjunction in the dispersal-limited dung moss tetraplodon (Bryopsida: Splachnaceae). *J. Of Biogeography* 41, 2385–2395. doi: 10.1111/jbi.12385

Li, F.-W., Brouwer, P., Carretero-Paulet, L., Cheng, S., Vries, J. D., Delaux, P.-M., et al. (2018). Fern genomes elucidate land plant evolution and cyanobacterial symbioses. *Nat. Plants* 4, 460–472. doi: 10.1038/s41477-018-0188-8

Li, H., and Durbin, R. (2009). Fast and accurate short read alignment with burrows–wheeler transform. *Bioinformatics* 25, 1754–1760. doi: 10.1093/bioinformatics/btp324

Li, G., Hu, S., Hou, H., and Kimura, S. (2019). Heterophylly: phenotypic plasticity of leaf shape in aquatic and amphibious plants. *Plants* 8, 420. doi: 10.3390/plants8100420

Ligrone, R., Carafa, A., Lumini, E., Bianciotto, V., Bonfante, P., and Duckett, J. G. (2007). Glomeromycotean associations in liverworts- A molecular, cellular, and taxonomic analysis. *Am. Jounal Of Bot.* 94, 1756–1777. doi: 10.3732/ajb.94.11.1756

Lindberg, S. O. (1882). Bryological notes from the meetings of the society pro fauna et flora fennica. *Rev. Bryologique* 9, 81–85.

Linde, A.-M., Sawangproh, W., Cronberg, N., Szövényi, P., and Lagercrantz, U. (2020). Evolutionary history of the Marchantia polymorpha complex. *Front. In Plant Sci.* 11, 829. doi: 10.3389/fpls.2020.00829

Lindenberg, J. B. W. (1836). Monographie der riccieen. *Nova Acta Acad. Caes. Leopold.-Carol. Nat. Cur.* 18, 360–504. Tafeln Xix-Xxxvii.

Linné, C. V. (1770). *Systema Naturae Per Regna Tria Naturae, Secundum Classes, Ordines, Genera, Species, Cum Characteribus, Differentiis, Synonymis, Locis* Vindobonae: Typis Ioannis Thomae Von Trattner.

Liu, B.-L. L. (1984). Abscisic acid induces land form characteristics in Marsilea quadrifolia L. *Am. Jounal Of Bot.* 71, 638–644. doi: 10.1002/j.1537-2197.1984.tb14170.x

Lorenzen, H., Kaiser, U., and Foerster, M. (1981). Intensives wachstum von ricciocarpus natans (Lebermoos) in durchlüftungskultur. *Berichte Der Deutschen Botanischen Gesellschaft* 94, 719–725. doi: 10.1111/j.1438-8677.1981.tb03439.x

Love, M. I., Huber, W., and Anders, S. (2014). Moderated estimation of fold change and dispersion for RNA-seq data with DESeq2. *Genome biology* 15 (12), 1–21 doi: 10.1186/s13059-014-0550-8

Maeda, M., Akiyama, H., and Ashiya, M. (2016). Life history of Ricciocarpos natans L. 1. Development of sexual organs and sporophytes in rice field conditions. *Humans And Nat.* 27, 43–52. doi: 10.1590/0001-3765202220210436

Maggio, L. P., Schmitz, D., Putzke, J., Schaefer, C. E. G. R., and Pereira, A. B. (2022). Pellets of Stercorarius spp. (Skua) as plant dispersers in the Antarctic peninsula. *Anais Da Academia Bras. Cienc.* 94, E20210436.

Meyerowitz, E. M., and Pruitt, R. E. (1985). Arabidopsis thaliana and plant molecular genetics. *Science* 229, 1214–1218. doi: 10.1126/science.229.4719.1214

Montagne, C. (1839). Cryptogamae brasiliensis. *Annales Des. Sci. Naturelles Botanique Ser. 2 T.* 12, 42–55.

Montgomery, S. A., Tanizawa, Y., Galik, B., Wang, N., Ito, T., Mochizuki, T., et al. (2020). Chromatin organization in early land plants reveals an ancestral association between H3k27me3, transposons, and constitutive heterochromatin. *Curr. Biol.* 30, 573–588. doi: 10.1016/j.cub.2019.12.015

Muhlenberg, H. (1813). *Catalogus Plantarum Americae Septentrionalis* (Lancaster: William Hamilton).

Nakayama, H., Nakayama, N., Seiki, S., Kojima, M., Sakakibara, H., Sinha, N., et al. (2014). Regulation of the Knox-ga gene module induces heterophyllic alteration in North American lake cress. *Plant Cell* 26, 4733–4748. doi: 10.1105/tpc.114.130229

Nakayama, H., Sinha, N. R., and Kimura, S. (2017). How do plants and phytohormones accomplish heterophylly, leaf phenotypic plasticity, in response to environmental cues. *Front. In Plant Sci.* 8, 1717. doi: 10.3389/fpls.2017.01717

Oh, S., and Koh, S. C. (2013). Chl A fluorescence characterization and biomarker selection from Ricciocarpos natans under cadmium stress. *J. Of Environ. Sci. Int.* 22, 1403–1413. doi: 10.5322/JESI.2013.22.11.1403

Page, D. R., and Grossniklaus, U. (2002). The art and design of genetic screens: Arabidopsis thaliana. *Nat. Rev. Genet.* 3, 124–136. doi: 10.1038/nrg730

Parsons, J. G., Cairns, A., Johnson, C. N., Robson, S. K. A., Shilton, L. A., and Westcott, D. A. (2007). Bryophyte dispersal by flying foxes: A novel discovery. *Oecologia* 152, 112–114. doi: 10.1007/s00442-006-0639-1

Peeters, E. T. H. M., Neefjes, R. E. M., and Van Zuidam, B. G. (2016). Competition between free-floating plants is strongly driven by previously experienced phosphorus concentrations in thewater column. *PloS One* 11, E0162780. doi: 10.1371/journal.pone.0162780

Perold, S. M. (1995). The taxonomic history of the ricciaceae, (1937-1995) and A classification of sub-saharan ricciae. *Bothalia* 25, 211–231. doi: 10.4102/abc.v25i1.729

Perry, M. C., Lilly, L., and Jones, G. (1856). *Narrative of the expedition of an american squadron to the China seas and Japan : performed in the years 1852, 1853, and 1854, under the command of commodore M.C. Perry, United States navy, by order of the government of the United States* (Wahsington: Beverley Tucker).

Petiver, J. (1695-1703). *Musei petiveriani centuria prima-[Decima] rariora naturae; continens: viz. Animalia, fossilia, plantas, ex variis mundi plagis advecta, ordine digesta, et nominibus propriis signata,*. S. Smith and B. Walford.: Londini (London).

Pickett, F. L. (1925). The life history of Ricciocarpus Natans. *Bryologist* 28, 1–3. doi: 10.1639/0007-2745(1925)28[1:TLHORN]2.0.CO;2

Piippo, S. (1990). Annotated Catalogue of Chinese hepaticae and anthocerotae. *J. Of Hattori Botanical Lab.* 68, 1–192. doi: 10.18968/jhbl.68.0_1

Piñeiro, R., Popp, M., Hassel, K., Listl, D., Westergaard, K. B., Flatberg, K. I., et al. (2012). Circumarctic dispersal and long-distance colonization of South America: the moss genus cinclidium. *J. Of Biogeography* 39, 2041–2051. doi: 10.1111/j.1365-2699.2012.02765.x

Proust, H., Honkanen, S., Jones, V. A. S., Morieri, G., Prescott, H., Kelly, S., et al. (2016). Rsl class I genes controlled the development of epidermal structures in the common ancestor of land plants. *Curr. Biol.* 26, 93–99. doi: 10.1016/j.cub.2015.11.042

Provart, N. J., Alonso, J., Assmann, S. M., Bergmann, D., Brady, S. M., Brkljacic, J., et al. (2015). 50 years of Arabidopsis research: highlights and future directions. *New Phytol.* 209, 921–944. doi: 10.1111/nph.13687

Prunet, N., and Meyerowitz, E. M. (2016). Genetics and plant development. *Comptes Rendus Biologies* 339, 240–246. doi: 10.1016/j.crvi.2016.05.003

Rafinesque, C. S. (1817). First decade of undescribed American plants, or synopsis of new species, from the United States. *Am. Monthly Magazine And Crit. Rev.* 2, 43.

Rafinesque, C. S. (1833). Principles of the philosophy of New Genera and new species of plants and animals. *Atlantic J. And Friend Of Knowledge* 1, 163–164.

Ray, J. (1724). *Synopsis methodica stirpium britannicarum. 3rd ed* (Londini, Gulielmi & Joannis Innys).

Rhoades, M. M. (1984). The early years of maize genetics. *Annu. Rev. Of Genet.* 18, 1–29. doi: 10.1146/annurev.ge.18.120184.000245

Rieth, A. (1959). Bemerkungen über ricciocarpus natans (L.) corda. *Kulturpflanze* 7, 207–217. doi: 10.1007/BF02099389

Romani, F., Banic, E., Florent, S. N., Kanazawa, T., Goodger, J. Q. D., Mentink, R. A., et al. (2020). Oil body formation in marchantia polymorpha is controlled by Mpc1hdz and serves as A defense against arthropod herbivores. *Curr. Biol.* 30, 2815–2828. doi: 10.1016/j.cub.2020.05.081

Sakata, Y., Komatsu, K., and Takezawa, D. (2013). ABA as a universal plant hormone. *Prog. In Bot.* 75, 57–96. doi: 10.1007/978-3-642-38797-5_2

Sarosiek, J., Wazakowska Natkaniec, H., and Wiewiórka, Z. (1987a). The effect of heavy metals on the dynamics of A ricciocarpus natans (L.) corda population. *Symp. Biologica Hungaria* 35, 857–863.

Sarosiek, J., Wiewiórka, Z., and Mróz, L. (1987b). Bioindication of heavy metal toxicity of water by the liverwort Ricciocarpus natans (L.) corda. *Symp. Biologica Hungaria* 35, 827–833.

Schmidel, C. C. (1793). *Icones plantarvm et analyses partivm aeri incisae atqve vivis coloribvs insignatae* (Joannen Jocobum Palm: Erlangae).

Schuster, R. M. (1983). "Phytogeography of the bryophytes," in *New manual of bryology vol. 1*. Ed. R.M. Schuster (Hattori Botanical Laboratory: NiChinan, Miyazaki, Japan).

Schuster, R. M. (1992). *The hepaticae and anthocerotae of North America, vol. Vi* (Columbia University Press: New York).

Schwarz-Sommer, Z., Davies, B., and Hudson, A. (2003). An everlasting pioneer: the story of antirrhinum research. *Nat. Rev. Genet.* 4, 655–664. doi: 10.1038/nrg1127

Schweinitz, L. D. D. (1821). *Specimen florae americae septentrionalis cryptogamicae; sistens: muscos hepaticos huc usque'in am. Sept. Observatos* (Raleigh: J. Gales).

Scoppola, A., Spada, F., and Blasi, C. (1988). Framework for A chronological and coenological characterization of A Ricciocarpus natna (L.) corda stand in the subcoastal district in central Italy. *Documents Phytosociologiques* 11, 423–432.

Scott, G. A. M. (1985). *Southern Australian liverworts* (Australian Government Publishing Service: Canberra).

Shimamura, M. (2016). Marchantia polymorpha; taxonomy, phylogeny and morphology of A model plant. *Plant Cell Physiol.* 57, 230–256. doi: 10.1093/pcp/pcv192

Siler, M. B. (1934). Chromosome numbers in certain ricciaceae. *Proc. Of Natl. Acad. Of Sci. Of United States Of America* 20, 603–607. doi: 10.1073/pnas.20.12.603

Singh, S., Davies, K. M., Chagné, D., and Bowman, J. L. (2023). The fate of sex chromosomes during the evolution of monoicy from dioicy in liverworts. *Curr. Biol.* 33, 3597–3609. doi: 10.1016/J.Cub.2023.07.023

Skulberg, O. M. (1978). En ny lemnide I norsk flora - svanemat (Ricciocarpus natans) I gjølsjøen, halden'-vassdraget. *Blyttia* 36, 27–34.

Smit, A. F. A., and Hubley, R. (2008-2015). *Repeatmodeler open-1.0*.

Smit, A. F. A., Hubley, R., and Green, P. (2013-2015). *Repeatmasker open-4.0*.

Smith, J. E. (1804). *English botany or coloured figures of british plants vol. Xvii* (London: J. Taylor).

Somerville, C., and Koornneef, M. (2002). A fortunate choice: the history of arabidopsis as A model plant. *Nat. Rev. Genet.* 3, 883–889. doi: 10.1038/nrg927

Stahl, M. (1949). Die mycorrhiza der lebermoose mit besonderer beïcksichtigung der thallosen formen. *Planta* 37, 103–148. doi: 10.1007/BF01929705

Stanke, M., Diekhans, M., Baertsch, R., and Haussler, D. (2008). Using native and syntenically mapped cdna alignments to improve *de novo* gene finding. *Bioinformatics* 24, 637–644. doi: 10.1093/bioinformatics/btn013

Stotler, R. E., and Crandall-Stotler, B. (2017). A synopsis of the liverwort flora of North America North of Mexico. *Ann. Of Missouri Botanical Garden* 102, 574–709. doi: 10.3417/2016027

Stubbe, H. (1966). *Genetik und zytologie von antirrhinum L. Sect. Antirrhinum* (Jena: Gustav Fischer).

Sturm, J. (1832). *Deutschlands flora in abbildungen nach der natur* (Nürnberg: Gedruckt Auf Kosten Des Verfassers).

Sussex, I. (1998). Themes in plant development. *Annu. Rev. Plant Physiol. And Plant Mol. Biol.* 49, Xiii–Xxii. doi: 10.1146/annurev.arplant.49.1.0

Toivonen, H. (1985). Changes in the pleustic macrophyte flora of 54 small finnish lakes in 30 years. *Annales Botanici Fennici* 22, 37–44.

Vandenbussche, M., Chambrier, P., Bentoand, S. R., and Morel, P. (2016). Petunia, Your next supermodel? *Front. In Plant Sci.* 7, 72. doi: 10.3389/fpls.2016.00072

Viana, D. S., Santamaría, L., and Figuerola, J. (2016). Migratory birds as global dispersal vectors. *Trends In Ecol. Evol.* 31, 763–775. doi: 10.1016/j.tree.2016.07.005

Villarreal, A. J. C., Crandall-Stotler, B. J., Hart, M. L., Long, D. G., and Forrest, L. L. (2016). Divergence times and the evolution of morphological complexity in an early land plant lineage (Marchantiopsida) with A slow molecular rate. *New Phytol.* 209, 1734–1746. doi: 10.1111/nph.13716

Wickett, N. J., Mirarab, S., Nguyen, N., Warnow, T., Carpenter, E., Matasci, N., et al. (2014). Phylotranscriptomic analysis of the origin and early diversification of land plants. *Proc. Of Natl. Acad. Of Sci. Of United States Of America* 111, E4859–E4868. doi: 10.1073/pnas.1323926111

Wilkinson, D. M., Lovas-Kiss, A., Callaghan, D. A., and Green, A. J. (2017). Endozoochory of large bryophyte fragments by waterbirds. *Cryptogamie Bryologie* 38, 223–228. doi: 10.7872/cryb/v38.iss2.2017.223

Wolek, J. (1997). Species co-occurrence patterns in pleustonic plant communities (Class lemnetea): are there assembly rules governing pleustonic community assembly? *Fragmenta Floristica Et Geobotanica* 0, 3–100.

Wolek, J., and Walanus, A. (2000). Co-occurrence of lemnids in Argentina: A null model analysis. *Fragmenta Floristica Et Geobotanica* 45, 179–192.

Woodfin, C. M. (1976). Physiological studies on selected species of the liverwort family Ricciaceae. *J. Of Hattori Botanical Lab.* 41, 179–183.

frontiers | Frontiers in Plant Science

TYPE Original Research
PUBLISHED 18 December 2023
DOI 10.3389/fpls.2023.1288961

OPEN ACCESS

EDITED BY
Dianella G. Howarth,
St. John's University, United States

REVIEWED BY
Harold Suárez-Baron,
Pontificia Universidad Javeriana Cali, Colombia
Mariane S. Sousa-Baena,
Federal University of Rio Grande do Sul, Brazil

*CORRESPONDENCE
Verónica S. Di Stilio
distilio@uw.edu

RECEIVED 05 September 2023
ACCEPTED 27 November 2023
PUBLISHED 18 December 2023

CITATION
Zahid S, Schulfer AF and Di Stilio VS (2023) A eudicot *MIXTA* family ancestor likely functioned in both conical cells and trichomes.
Front. Plant Sci. 14:1288961.
doi: 10.3389/fpls.2023.1288961

A eudicot *MIXTA* family ancestor likely functioned in both conical cells and trichomes

Simra Zahid, Anjelique F. Schulfer and Verónica S. Di Stilio*

Department of Biology, University of Washington, Seattle, WA, United States

The *MIXTA* family of MYB transcription factors modulate the development of diverse epidermal features in land plants. This study investigates the evolutionary history and function of the *MIXTA* gene family in the early-diverging eudicot model lineage *Thalictrum* (Ranunculaceae), with R2R3 SBG9-A MYB transcription factors representative of the pre-core eudicot duplication and thus hereby referred to as "paleo*MIXTA*" (*PMX*). Cloning and phylogenetic analysis of *Thalictrum paleoMIXTA* (*ThPMX*) orthologs across 23 species reveal a genus-wide duplication coincident with a whole-genome duplication. Expression analysis by qPCR confirmed that the highest expression is found in carpels, while newly revealing high expression in leaves and nuanced differences between paralogs in representative polyploid species. The single-copy ortholog from the diploid species *T. thalictroides* (*TthPMX*, previously *TtMYBML2*), which has petaloid sepals with conical–papillate cells and trichomes on leaves, was functionally characterized by virus-induced gene silencing (VIGS), and its role in leaves was also assessed from heterologous overexpression in tobacco. Another ortholog from a species with conical–papillate cells on stamen filaments, *TclPMX*, was also targeted for silencing. Overexpression assays in tobacco provide further evidence that the *paleoMIXTA* lineage has the potential for leaf trichome function in a core eudicot. Transcriptome analysis by RNA-Seq on leaves of VIGS-treated plants suggests that *TthPMX* modulates leaf trichome development and morphogenesis through microtubule-associated mechanisms and that this may be a conserved pathway for eudicots. These experiments provide evidence for a combined role for *paleoMIXTA* orthologs in (leaf) trichomes and (floral) conical–papillate cells that, together with data from other systems, makes the functional reconstruction of a eudicot ancestor most likely as also having a combined function.

KEYWORDS

epidermis, MIXTA family, non-core eudicots, polyploidy, trichomes, conical cells, ranunculid, R2R3 MYB

Introduction

Plants have evolved diverse epidermal features to adapt to their environment (Javelle et al., 2011), and epidermal cell types are useful micromorphological markers of the different plant organs (Cavallini-Speisser et al., 2021). *MYB* genes are a prominent land plant gene family that encode transcription factors characterized by having one to four contiguous repeats, with most plants having two repeats, R2 and R3, that function in secondary metabolite production and cell identity (Stracke et al., 2001). The R2R3 MYB subgroup 9A *MIXTA/MIXTA-like* gene family has specialized roles in epidermal cells (Brockington et al., 2013), including the first characterized function in conical cells (Noda et al., 1994; Baumann et al., 2007; Di Stilio et al., 2009), trichomes (Jakoby et al., 2008; Yan et al., 2018; Qin et al., 2021), and ovule epidermal cells that make cotton fibers (MaChado et al., 2009). Certain *MIXTA-like* orthologs have evolved multiple functions in epidermal cell patterning, such as *Antirrhinum majus AmMYBML1* in regulating trichome branching and conical cells (Pérez-Rodríguez et al., 2005). In addition to the previously reviewed *MIXTA* family functions (Brockington et al., 2013), recent studies further support roles in glandular trichomes of mint (Qi et al., 2022) and *Nepetes* (Lamiaceae, Zhou et al., 2022) as well as in trichome patterning and morphogenesis in tomato leaves (Galdon-Armero et al., 2020). A novel function for *MIXTA* family orthologs in cuticle (Lashbrooke et al., 2015) is further supported in the early land plant model *Marchantia* (Xu et al., 2020) and in the orchid *Phalaenopsis* (a monocot, Lu et al., 2022). A *MIXTA* family ortholog from another orchid, *Dendrobium crumenatum*, is capable of rescuing the branched trichome phenotype of *Arabidopsis thaliana noeck* mutants, even though it does not produce trichomes in the orchid (Gilding and Marks, 2010). Since most of the functional information on *MIXTA* family genes comes from the core eudicots, additional functional studies of *MIXTA* family genes in early-diverging eudicots are warranted to inform the reconstruction of the ancestral gene function of this important transcription factor family in the eudicots, the most species-rich clade containing three quarters of all angiosperm species (Simpson, 2019).

Trichomes or epidermal hairs represent an emerging model for the study of single-cell differentiation that is structurally simple and easily accessible (Yang and Ye, 2013). Trichomes can be non-glandular or glandular (Feng et al., 2021): the former typically provides protection against UV-B radiation and dehydration, while the latter is a warehouse of defense metabolites against herbivores (Jaime et al., 2013; Yan et al., 2018; Chalvin et al., 2021). On the one hand, differentiation of unicellular trichomes is well understood in *A. thaliana*, where it is controlled by an activation–inhibition loop (Jakoby et al., 2008). Positive regulators GLABRA3 (GL3), GLABRA1 (GL1), and TRANSPARENT TESTA GLABRA1 (WD40) form a trimeric complex with basic helix–loop–helix proteins (bHLH) known as MYB-bHLH-WD40 that stimulates trichome differentiation in the epidermis (Pesch and Hülskamp, 2009). In the surrounding cells, transcription factors such as TRIPTYCHON (TRY) and TRICHOMELESS1,2 (TCL1 and TCL2) bind and inactivate the bHLH-WD40 complex, thereby suppressing trichome development (Gao et al., 2017). The regulatory network for multicellular trichomes, on the other hand, is less clear, with HD-ZIP IV transcription factors known to interact with *MIXTA* family orthologs during trichome development in maize, cucumber, and the asterid *Artemisia annua* (Vernoud et al., 2009; Wang et al., 2016; Yan et al., 2018), while a B-type cyclin plays this role in tomato (Gao et al., 2017). Hence, further investigation of trichome development and the underlying genetic regulators is warranted.

Thalictrum (meadow-rue) are herbaceous perennials in the family Ranunculaceae that lack petals and are pollinated by insects, the wind, or both, with associated floral morphotypes (Martínez-Gómez et al., 2023). *Thalictrum MIXTA* family orthologs are expressed in the epidermis of floral organs that contain conical–papillate cells (petaloid sepals or showy stamen filaments) that aid in attracting insect pollinators and were previously shown to affect conical–papillate cell elongation when overexpressed in tobacco (Di Stilio et al., 2009). However, the function of these non-core eudicot *MIXTA* orthologs remains untested in *Thalictrum*. As predicted then, this gene family represents a lineage that is sister to the core eudicot *MIXTA/MIXTA-like* duplication (Brockington et al., 2013). We will therefore hereby refer to "paleo*MIXTA*" (*PMX*) following the floral MADS box gene nomenclature (paleo*AP3*; Kramer et al., 1998) and *MX* shortcut for *MIXTA* (Brockington et al., 2013) and distinguish this gene lineage from the core eudicot *MIXTA/MIXTA-like*. Based on this new information, the published gene *TthMYBML2* (Di Stilio et al., 2009) is hereby renamed to *TthPMX*, and the others newly described here will follow this nomenclature scheme.

We chose to compare the gene functions in *T. thalictroides*, with conical–papillate cells in their petaloid sepals, and *T. clavatum*, with conical–papillate cells in their showy stamen filaments. The two species are closely related within clade I and represent the ancestral traits for the genus of diploid, hermaphrodite, and insect pollinated (Soza et al., 2012; Soza et al., 2013; Wang et al., 2019). Using virus-induced gene silencing (VIGS) as previously described (Di Stilio et al., 2010), we downregulated the paleo*MIXTA* ortholog in both species. We show evidence for a new role for this floral MYB transcription factor in leaf trichomes and further show that it is necessary for conical cell formation that contributes to petaloidy in sepals and stamens for these two species of *Thalictrum* with distinct floral morphologies.

This study aims broadly to provide functional information for members of the paleo*MIXTA* gene lineage via functional assays in flowers and leaves of early-diverging eudicots to ultimately contribute to an increased understanding of the functional evolution and molecular mechanisms of this important transcription factor family. To that end we (1) reconstruct the evolutionary history of *MIXTA* family orthologs from the genus *Thalictrum*, (2) investigate the function of two paleo*MIXTA* orthologs in the flowers and leaves of two distinct species, and (3) identify candidate genes underlying the *MIXTA* gene regulatory network (GRN) in leaves by RNA-Seq.

The evidence presented here from functional studies of *Thalictrum* paleo*MIXTA* representatives suggests that the

function of a putative pre-*MIXTA/MIXTA-like* core eudicot duplication ancestor likely consisted of a combined role in conical–papillate cells and trichomes. This multifunctional eudicot ancestral gene presumably could have parsed out its distinct roles among paralogs after the core eudicot *MIXTA/MIXTA-like* duplication as well as within taxa that underwent further lineage-specific duplications. Our finding of a duplication event within *Thalictrum* resulting in differential patterns of paralogous gene expression provides a potential basis for the evolution of increased epidermal trichomes found on the leaves and flowers of derived wind-pollinated polyploid taxa and thus represents an interesting avenue for future research.

Results

An early duplication in the *Thalictrum* paleo*MIXTA* lineage coincides with a genus-wide whole-genome duplication

A phylogenetic approach was used to investigate the evolutionary history of the *Thalictrum* (Ranunculaceae) MYB SBG9-A *MIXTA* gene family or paleo*MIXTA* (*PMX*, Figure 1A inset). To this end, a nucleotide alignment was constructed for 49 MYB SBG9-A *Thalictrum* sequences isolated from 23 species spanning the two main clades (Soza et al., 2012; Martínez-Gómez et al., 2023) and identified based on the conserved R2R3 and Subgroup 9-A domains (Supplementary Figure S1). The two SBG9-A outgroups chosen were columbine Aqcoe3G346800 (Ranunculaceae, *Aquilegia coerulea*) and California poppy EscalH2.4G309300 (Papaveraceae, *Eschscholzia californica* var. Aurantiaca Orange King Plant1.1 v1.1, DOE-JGI, http://phytozome.jgi.doe.gov/info/EcalifornicavarAurantiacaOrangeKingPlant1_1HAP2_v1_1).

A consensus phylogenetic tree was inferred using the Bayesian optimality criterion implemented in MrBayes (Figure 1A). *Thalictrum MIXTA* family sequences form two distinct clades with strong support, coincident with the two major clades previously described: clade I *Thalictrum* paleo*MIXTA* (*ThPMX*) containing only diploid species and clade II with subclades paleo*MIXTA1* (*ThPMX1*) and *ThPMX2* having both diploid and polyploid species. The gene tree suggests a gene duplication event at the base of the two subclades (Figure 1A, star), with paralogs from polyploid species distributed among the two resulting clades and instances of potential paralog loss (e.g., the 20-ploid *T. revolutum* has a gene copy in all clades except *ThPMX1a*). Each of these larger gene clades, in turn, underwent a subsequent duplication, designated as "a" and "b". Certain polyploid species, particularly those with high ploidy level, like *T. dasycarpum* (24x) and *T. revolutum* (20x), had additional species-level single-gene duplications that were consecutively numbered (e.g., *TpuPMX1b.1-TpuPMX1b.4*). Thus, *MIXTA* family orthologs only partially follow the species phylogeny, suggesting a reticulated evolutionary history for *Thalictrum* that could not be previously detected when using chloroplast loci and the transcribed spacers ITS and ETS (Soza et al., 2013; Martínez-Gómez et al., 2023).

Differential expression of *Thalictrum* paleo*MIXTA* paralogs in leaves and floral organs

To broadly investigate the spatial expression pattern of *Thalictrum paleoMIXTA*, we performed qPCR on leaves and dissected floral organs (sepals, stamens, and carpels) of recently open flowers, where expression is known to peak in other species (Pérez-Rodríguez et al., 2005; Lau et al., 2015; Lu et al., 2022). We chose diploid *T. thalictroides*, tetraploid *T. dioicum*, and high-level polyploid *T. dasycarpum* (24×) as representative species. *Thalictrum thalictroides* is in clade I and has the ancestral traits of insect pollination and hermaphrodite flowers, with petaloid sepals that contain conical cells. In contrast, *T. dioicum* and *T. dasycarpum* from clade II are wind-pollinated polyploids with small and inconspicuous unisexual flowers that contain long pendulous stamens or plumose stigmas on long styles (Soza et al., 2012; Martínez-Gómez et al., 2023).

There was a trend towards high *Thalictrum* paleo*MIXTA* expression for specific paralogs in the carpels of the three species in the leaves of *T. dioicum* carpellate (female) plants and in the sepals of carpellate *T. dasycarpum* flowers (Figure 1B). Stamens and sepals from staminate (male) flowers showed a lower combined relative expression across the three species. *T. thalictroides* had expression in all organs analyzed, likely from a combination of having conical–papillate cells in some organs and trichomes in others, with the highest expression in carpels, followed by sepals, leaves, and stamens. Similarly, both paralogs from *T. dioicum* showed a high carpel-specific expression, suggesting partial redundancy in function. In *T. dasycarpum*, the expression was low to undetectable in the leaves, and one paralog (*TdaPMX1b.2*) had a high expression in carpels while another (*TdaPMX1a*) had a higher expression in stamens. On closer inspection, the R2 and R3 MYB domains of the lowest-expressing copy (*TdaPMX1b.1*) had two single amino acid substitutions, K43N and S76N, in the R2 and R3 domain, respectively (Supplementary Figure S1). Single amino acid substitutions in the R2R3 domains can cause loss of promoter–site interactions in other MYB proteins, resulting in the downregulation of expression (Hichri et al., 2011; Dai et al., 2016). Taken together, specific paleo*MIXTA* paralogs showed a sex-dependent expression pattern in dioecious *Thalictrum*, with the lower-level polyploid *T. dioicum* showing an overlapping expression of paralogs and the higher level polyploid *T. dasycarpum* exhibiting more specialization of paralog expression patterns.

Targeted gene silencing reveals a leaf trichome morphogenesis role for paleoMIXTA

In order to investigate the gene function in a paleo*MIXTA* representative from an early-diverging eudicot, *Tth*paleo*MIXTA* (*TthPMX*) was targeted for downregulation by VIGS in *T. thalictroides*, on its own or together with *PHYTOENE DESATURASE* (*PDS*, as a "reporter" causing visible tissue photobleaching). The infection efficiency was 35%, with 15 out of 45 plants showing a range of photobleaching between 3 to 4 weeks

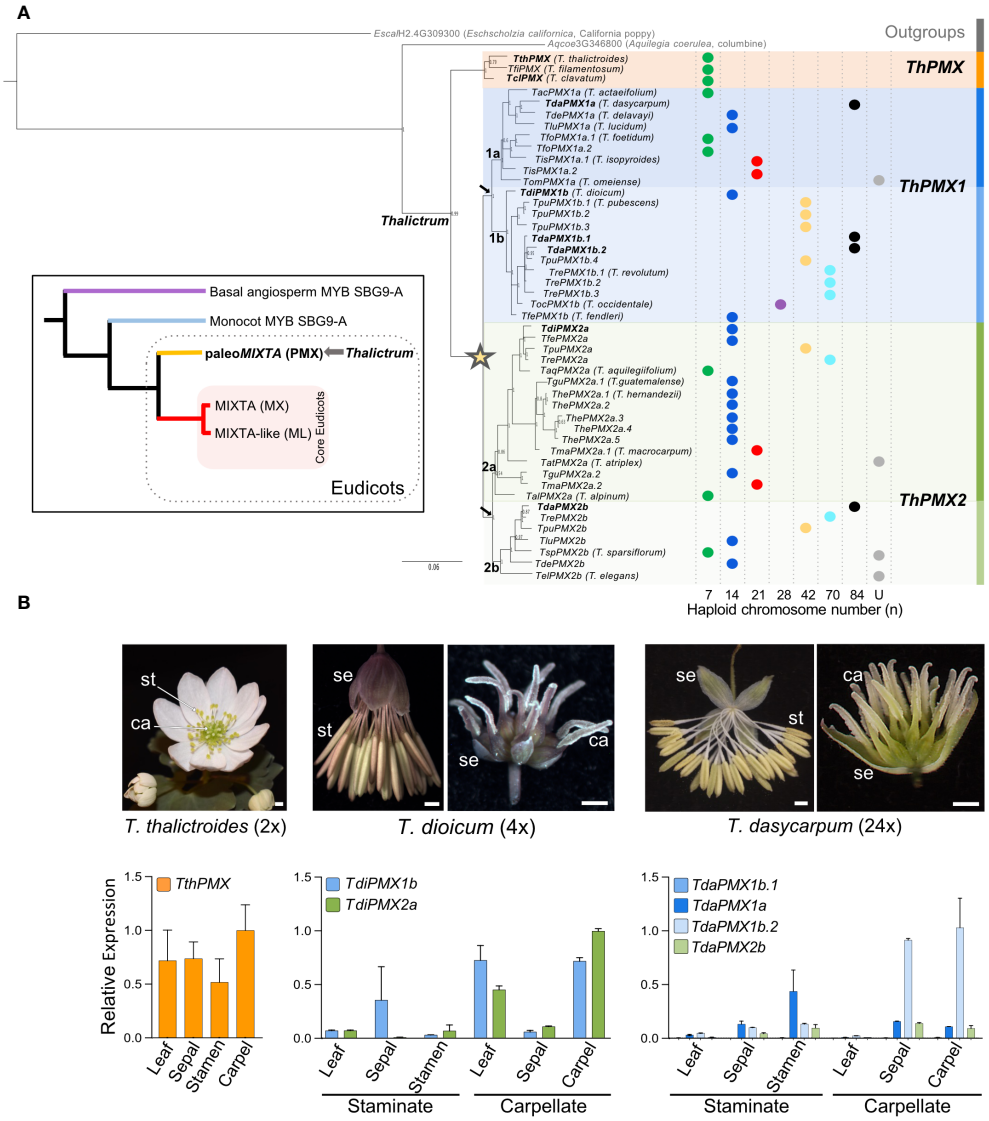

FIGURE 1
Gene phylogeny of the *Thalictrum MIXTA* family of MYB transcription factors (R2R3 Subgroup 9A). **(A)** Bayesian inference phylogeny with *Aquilegia coeruleae* (Ranunculaceae) and *Eschscholzia californica* as outgroups showing two major clades: clade I (orange) named *Thalictrum* paleo*MIXTA* (*ThPMX*) and clade II with an inferred gene duplication event (star) leading to subclades *ThPMX1* (blue) and *ThPMX2* (green). Another duplication in each clade (black arrows) leads to "a" and "b" subclades, and additional species-level duplications are designated with a period followed by a sequential number (e.g., *TdaPMX1b.1*–*TdaPMX1b.4*). Posterior probabilities are shown next to the nodes. Branch lengths indicate substitutions per site. Haploid (*n*) chromosome numbers are shown for each species as colored dots, from *n* = 7 (diploid) to *n* = 84 (24-ploid); U = unknown (data from Soza et al., 2013). Genes in bold are the subject of this study. Inset: Simplified tree of the *MIXTA* gene family in angiosperms [modified from Brockington et al. (2013)] highlighting the ranunculid *MIXTA* lineage (paleo*MIXTA*) that includes the *Thalictrum* orthologs. Organismal coding: purple = ANITA grade; blue = monocots; yellow = early-diverging eudicots; red = core eudicots. **(B)** Relative expression of *Thalictrum* paleo*MIXTA* in leaves and floral tissues of representative species from major clades. From left to right: Representative photos of hermaphrodite flowers of *T. thalictroides* (diploid) and staminate and carpellate flowers of dioecious *T. dioicum* (tetraploid) and *T. dasycarpum* (high-level polyploid). Quantitative RT-PCR showing the average expression level of *Thalictrum* paleo*MIXTA* orthologs relative to the average expression of two housekeeping genes *ThACTIN* and *ThEEF1-alpha*, normalized to the highest-expressing organ (carpel) and paralog. Color-coding matches the gene lineages shown in **(A)**. Error bars represent ± standard error of the mean. *N* = 4–7 flowers. Photo credits: Samantha Hartogs (*T. thalictroides* and *T. dasycarpum*); Kelsey Galimba (*T. dioicum*). se, sepals; st, stamens; ca, carpels.

after infiltration. Plants treated with the empty vector (EV = mock control) were indistinguishable from untreated wild-type plants, except for the previously described background effect of small necrotic lesions (Di Stilio et al., 2010) (Supplementary Figure S2). Viral transcripts (TRV1 and TRV2) were detected in treated plants and EV controls (Supplementary Figure S3A).

Targeted gene silencing was validated by qPCR, showing an approximately 11-fold decrease in the average expression of *TthPMX* in plants treated by VIGS compared to empty vector controls (Figure 2D). Fully photobleached and variegated (partially photobleached) leaves from plants treated with TRV2–*ThPDS*–*ThPMX* showed a correlated downregulation of both genes,

10.3389/fpls.2023.1288961

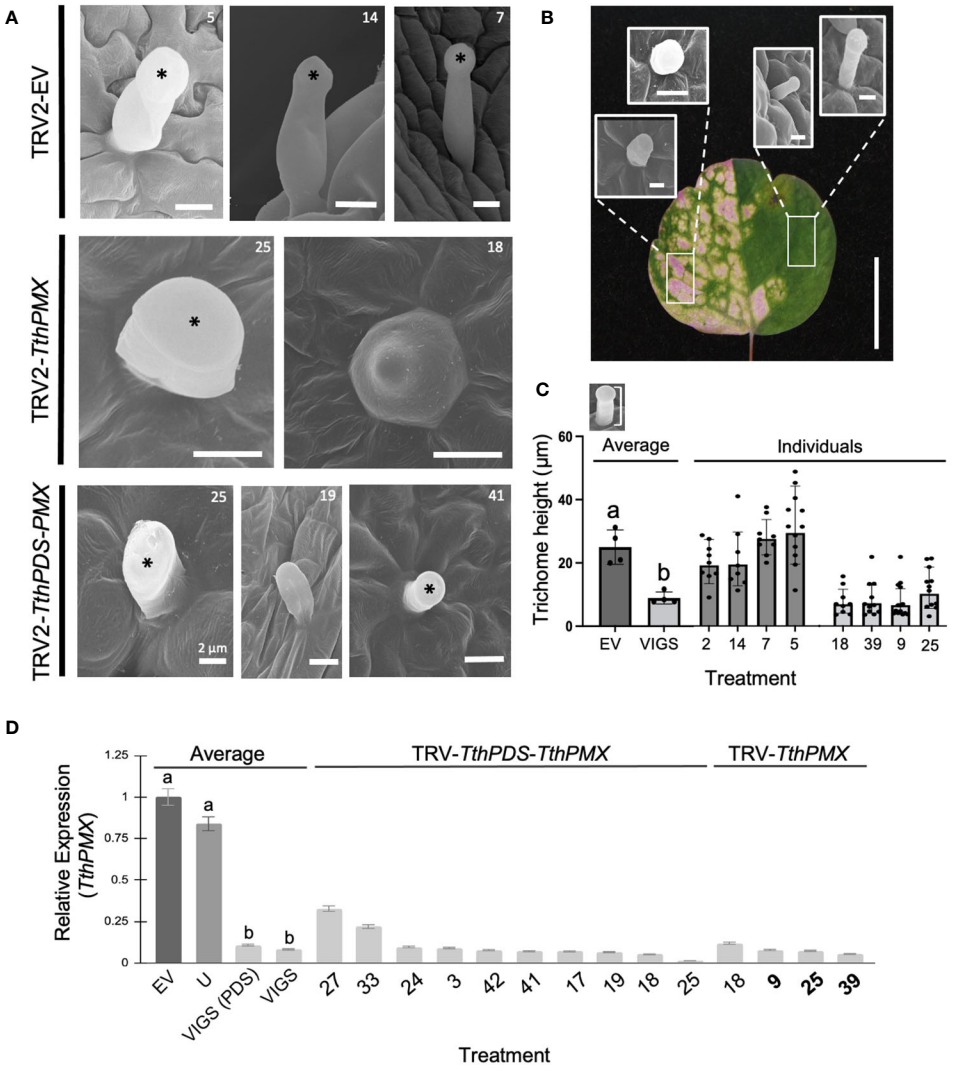

FIGURE 2
Targeted silencing of a *Thalictrum* paleo*MIXTA* ortholog affects leaf trichome morphogenesis. **(A)** Comparison of trichomes found on the abaxial epidermis of leaves of *Thalictrum thalictroides* in three representative empty vector control plants (TRV2-EV, top row) and four VIGS-treated plants with the construct TRV2-*Tth*paleo*MIXTA* (*TthPMX*). Asterisks indicate the position of the trichome head. Reduced "stubby" trichomes in plants undergoing targeted gene silencing for *TthPMX* represent three independent transgenic lines (middle and bottom row, transgenic line numbers shown for cross-reference). Scale bar = 10 µm, except as indicated. **(B)** Representative trichome phenotypes in green and photobleached sectors within a variegated leaf undergoing partial silencing of *TthPDS*. Rectangles show areas where the trichomes were sampled. Scale bar = 10 mm. **(C)** Quantitative difference in trichome cell height, measured as diagrammed in the top inset. Different letters indicate statistical significance between group means in one-way ANOVA with Tukey's HSD ($P \leq 0.0001$, $N = 4$ independent transgenic plants). **(D)** Molecular validation of VIGS experiments by qPCR for *TthPMX* as average expression level relative to *TthACTIN* and *TthEEF1* housekeeping genes, normalized against the empty vector controls. Error bars represent ± standard error of the mean. Different letters indicate statistically significant differences in one-way ANOVA with Tukey's comparison test ($P = 0.008$).

confirming the utility of *ThPDS* as a visual indicator of gene silencing (Supplementary Figure S3B).

To further establish the role of *T. thalictroides* paleo*MIXTA* in leaves, we quantified the epidermal features on their adaxial and abaxial epidermis from VIGS-treated plants, including the density and height of trichomes, the stomatal density, and the pavement cell shape. *T. thalictroides* has sparse trichomes on the abaxial leaf epidermis (Figures 2A, B). Under scanning electron microscopy (SEM), the trichomes appeared unicellular and capitate (enlarged toward the tip), which places them in the glandular category based on morphology (Simpson, 2019; Werker, 2000). The trichomes did not differ between the leaves of empty vector control and untreated plants (Figure 2A, top row). In contrast, the trichomes on the leaves of VIGS-treated plants showed either a "stubby", short-stalk phenotype (Figure 2A, middle and bottom rows) resembling a conical cell or one that appeared irregular in shape (Figures 2A, B; Supplementary Figure S4).

To further confirm that trichome developmental abnormalities resulted from the downregulation of the target gene, we compared sectors of photobleached and green tissues within variegated leaves (Figure 2B). Green leaf sectors had qualitatively taller trichomes than those found in photobleached sectors (Figure 2B;

Supplementary Figure S4). To further quantify this observation and to avoid the potential side effects of PDS downregulation, we measured the trichome height in single-construct VIGS (without *PDS*); the average trichome was 2.7-fold shorter in VIGS-treated leaves compared to the empty vector controls (Figure 3C, $p \leq 0.0001$, $N = 41$). Taken together, these results suggest that *T. thalictroides* paleo*MIXTA* plays a role in the elongation and morphogenesis of leaf trichomes.

We investigated additional epidermal features that have been reported to be influenced by other *MIXTA* family members, such as pavement cell morphology and stomatal density (Brockington et al., 2013). No significant qualitative differences were observed in the morphology of pavement cells between VIGS and control plants (Supplementary Figure S5A). Because stomatal density appeared to vary along the leaf, we sampled three regions on the abaxial side of transgenic plant leaves: top, middle, and base. In spite of some variations in stomatal density (visualized as a heat map, Supplementary Figure S5H), there was no statistically significant difference neither among leaf regions for a given treatment (Supplementary Figures S5I, J) nor between treatments when comparing averages (Supplementary Figure S5G, $N = 5$ independent transgenic plants per treatment).

Heterologous overexpression of *Thalictrum* paleo*MIXTA* induces ectopic and branched trichomes in tobacco leaves

Heterologous overexpression was previously pursued using an established bioassay in tobacco to observe changes in ovary wall cell morphology (Di Stilio et al., 2009), and fixed leaves from that experiment were used here for observations of their epidermal features under SEM. In the tobacco family Solanaceae, glandular, non-glandular, and defense trichomes are found (Bar and Shtein, 2019). Two types of non-glandular (types I and II), glandular (III and IV), and one type of defense trichome (type V) were identified on the upper and lower epidermis of wild-type tobacco leaves (Figures 3A–E).

Transgenic plants overexpressing *TthPMX* exhibited ectopic types II and IV branched trichomes (Figures 3F–H, arrows) and a higher density of type II trichomes adaxially and of types I, II, IV,

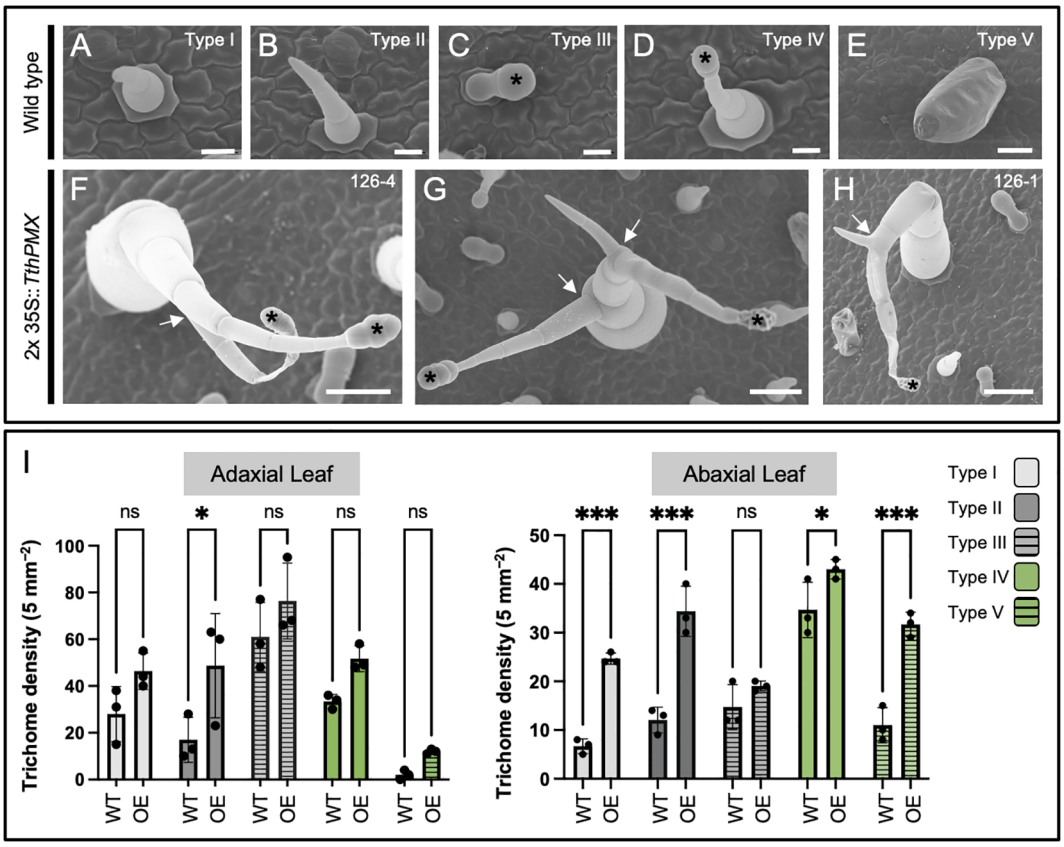

FIGURE 3
Overexpression of the *MIXTA* family ortholog *TthpaleoMIXTA* from *Thalictrum thalictroides* (Ranunculaceae) in tobacco leaves leads to ectopic and abnormal trichomes. **(A–E)** Trichome types I–V on the leaves of wild-type tobacco. Black asterisks indicate the position of the glandular head of capitate trichomes. **(F–H)** Ectopic branched trichomes on transgenic tobacco leaves; white arrows indicate abnormal branching. **(I)** Average trichome density ± SE by trichome type per 5 mm^2 on adaxial (left) and abaxial (right) leaf epidermis from three independent transgenic tobacco lines (2x35S::*TthPMX*) compared to wild type. Asterisks indicate statistically significant differences in trichome counts in a two-way ANOVA with Holm–Šídák's multiple comparisons. ns, not significant; *$P < 0.05$; ***$P < 0.001$. Scale bar = 50 µm.

and V abaxially (Figure 3I). Taken together, these findings suggest that *TthPMX* is a positive regulator of trichome development, capable of affecting their morphogenesis and patterning on the leaf epidermis of a core eudicot.

Identification of candidate genes in the leaf gene regulatory network of paleo*MIXTA*

To determine the molecular mechanisms underlying the role of paleo*MIXTA* in trichome development, we compared the transcriptomes of leaves from three mock-treated (empty vector) and three validated TRV2–*TthPMX* VIGS transgenic lines by RNA-Seq (Figure 4, transgenic line numbers in bold). There were 368,326,658 total reads, with a yield of 110,499 Mb and an average quality score of 35.84 (93.32% bases ≥3) (Supplementary Table S3). To independently validate the RNA-Seq results, we analyzed the expression counts for our target gene (*TthPMX*) and for genes known to have ubiquitous and stable expression (housekeeping genes). Leaves from VIGS-treated plants exhibited, on average, a fourfold decrease in *TthPMX* expression compared to controls, while the transcripts of the housekeeping genes *TthEEF1-alpha* and *TthACTIN* showed comparable expression levels in both treatments (Figure 4A).

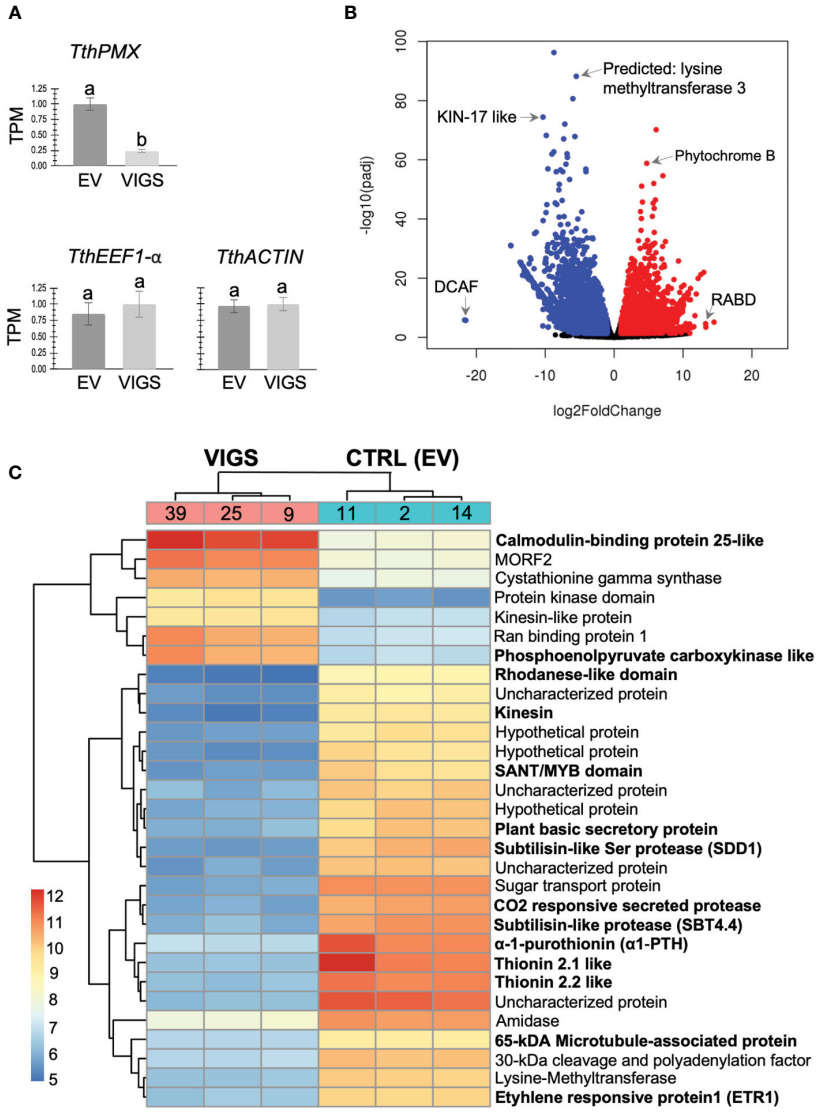

FIGURE 4
Identification of co-regulated candidate genes in the *Thalictrum* paleo*MIXTA* gene regulatory network. RNA-Seq analysis of differentially expressed genes (DEGs) in leaves from plants targeted for *TthPMX* downregulation (VIGS) vs. empty vector control (EV). **(A)** RNA-Seq validation with normalized count expression in transcripts per million of *Tth*paleo*MIXTA* and the housekeeping genes *TthEEF1-alpha* and *TthACTIN*. Means ± SE from three biological replicates; different letters indicate highly statistically significant difference ($p < 0.0001$) in one-way ANOVA followed by Tukey's multiple comparisons. **(B)** Volcano plot depicting log fold change in expression; red indicates upregulated differentially expressed genes (DEGs) and blue downregulated DEGs. Identified candidate genes amongst outliers are shown. **(C)** Hierarchical clustering and heat map of the top 30 DEGs with the highest or the lowest expression profiles. The color scale indicates the expression levels (log_2 fold change) relative to TRV2-EV controls. Genes identified via Diamond BLAST are listed; those of special interest are shown in bold and further discussed in the text.

The RNA-Seq analysis resulted in approximately equal numbers of significantly differentially expressed genes (DEGs) that were either upregulated (49%) or downregulated (50.3%) during the targeted silencing of *TthPMX*, using a cutoff $\log_2$ fold change of ±4, respectively. Differentially expressed genes were mapped onto a volcano plot, where the annotation of outliers identified a Ras-related protein (RABD) and phytochrome B that were significantly upregulated. Downregulated DEGs were identified as coding for DNA Damage Binding1, CULLIN4-associated factor homolog (DCAF), stress and UV damage response protein KIN-17-like, and lysine methyltransferase (Figure 4B). Annotation of the 30 highest- and lowest-expressing DEGs in the heat map uncovered a few more candidate genes upregulated in leaves undergoing VIGS of *ThPMX* (Figure 4C). These comprised orthologs of microtubule regulating *CALMODULIN-BINDING 25-LIKE* (*CaML-25*), kinesin-like protein (KLP), gluconeogenesis-associated phosphoenolpyruvate carboxy-kinase like (*PEPCK*), and multiple organellar RNA editing factor 2 (*MORF2*). The downregulated genes included those coding for motor proteins such as KINESIN and 65-kDa microtubule-associated protein (MAP65), defense peptides such as thionins (THI 2.1, THI 2.2, and α-1-purothionin), Rhodanese-like domain, epidermal specific subtilisin-like protease (SDD1; Von Groll et al., 2002), SANT/MYB domain proteins involved in chromatin remodeling, and ETHYLENE RESPONSIVE FACTOR 1 (ETF1) expressed highly in *Arabidopsis* mature trichomes (Jakoby et al., 2008). Taken together, the comparative transcriptomic analysis suggests that *TthpaleoMIXTA* influences trichome morphogenesis via the regulation of genes coding for candidate proteins involved in microtubule regulation, epidermal cell patterning, plant defense, and chromatin remodeling.

Thalictrum paleo*MIXTA* affects conical–papillate cell development in floral organs

VIGS leads to loss of conical–papillate cells on showy stamen filaments of *Thalictrum clavatum*

To further investigate the potential role of *ThPMX* in the epidermal features of flowers, we conducted functional studies by VIGS in two species of *Thalictrum* representing distinct flower morphologies, the "petaloid sepal" and "showy stamen" morphotypes (Martínez-Gómez et al., 2023). Untreated *T. clavatum* flowers are white to light pink and consist of a few small sepals and numerous stamens with showy or "petaloid" filaments (clavate, flattened, and wider at the top, and colored) as previously described (Di Stilio et al., 2010) (Figure 5A). Photobleaching of PDS is detectable in the floral center as a sign of effective gene silencing (Figure 5B). Conical–papillate cells are most prominent in the filaments of outer stamens (Figures 5C, D) and also present adaxially in sepals. In order to test the role of *TclPMX* in the conical–papillate cells of *T. clavatum* stamens, we used VIGS and observed the resulting floral cellular phenotypes under SEM. In wild-type plants, this gene is expressed at low levels in sepals and mostly in stamens and carpels, whereas *T. thalictroides* expresses relatively less in stamens (Figure 5N).

As in the leaf experiments, plants were visually assessed for photobleaching in leaves and flowers post-infiltration. *T. clavatum* began to show signs of photobleaching in leaves 13 days after infiltration, and the first buds opened 4 days later. The photobleached flowers tested positive for the TRV1 and TRV2 viruses as expected in all 10 plants that displayed the phenotype. The mock-treated plants displayed an identical TRV1 as well as a lower-molecular-weight TRV2 band, confirming the absence of insert (Supplementary Figure S6). The untreated plants did not show signs of TRV1 or TRV2 (Supplementary Figure S6A). Target gene silencing was validated by qPCR, showing a significant downregulation of approximately threefold in VIGS treatments compared to controls (P = 0.04). The SEM of stamens showed epidermal cells that looked flatter in VIGS treatments, either partially (Figure 5E) or fully along the filament (Figure 5F), and these observations were confirmed in the stamens of at least three independent transgenic plants.

VIGS leads to loss of conical–papillate cells on the petaloid sepals of *Thalictrum thalictroides*

Untreated *T. thalictroides* flowers have white petaloid sepals, stamens that are green to yellow, and carpels that are green toward the base (Figures 5G, I), therefore allowing for the detection of photobleaching in the flower center (Figure 5H). The conical–papillate cells are subtle in this species but can be observed adaxially at the base of the sepals under SEM (Figures 5J, K). Flowers showing signs of photobleaching similarly contained TRV virus (Supplementary Figure S6B), and the qPCR of dissected sepals showed a significant downregulation of *TthPMX* by approximately threefold (P = 0.02, N = 4 independent transgenic plants) (Figure 5O). Their sepal epidermis had flatter cells adaxially than the untreated controls (compare Figures 5J–M).

Thus, these results confirm a role for *TthPMX* in conical–papillate cells on the perianth in the non-core eudicot *Thalictrum*, previously suggested via heterologous expression in tobacco (Di Stilio et al., 2009). Taken together, the *T. clavatum* experiments suggest a more general function for *ThPMX* in epidermal protrusions beyond the perianth and into the reproductive organs.

Discussion

Evolutionary history of *Thalictrum MIXTA* family

Within the early-diverging eudicots, *Thalictrum* is in the order Ranunculales, sister to the rest of the eudicots. Since *MIXTA* and *MIXTA-like* are found exclusively within the core eudicots, we propose here that *Thalictrum* orthologs represent a "paleo" *MIXTA* lineage, analogous to how the *APETALA3* subfamily of floral MADS-box genes has a paleo*AP3* lineage in early-diverging eudicots sister to the euAP3/TM6 core eudicot gene duplication (Kramer et al., 1998). Therefore, *Thalictrum* paleo*MIXTA* is informative of the ancestral function of *MIXTA* family orthologs.

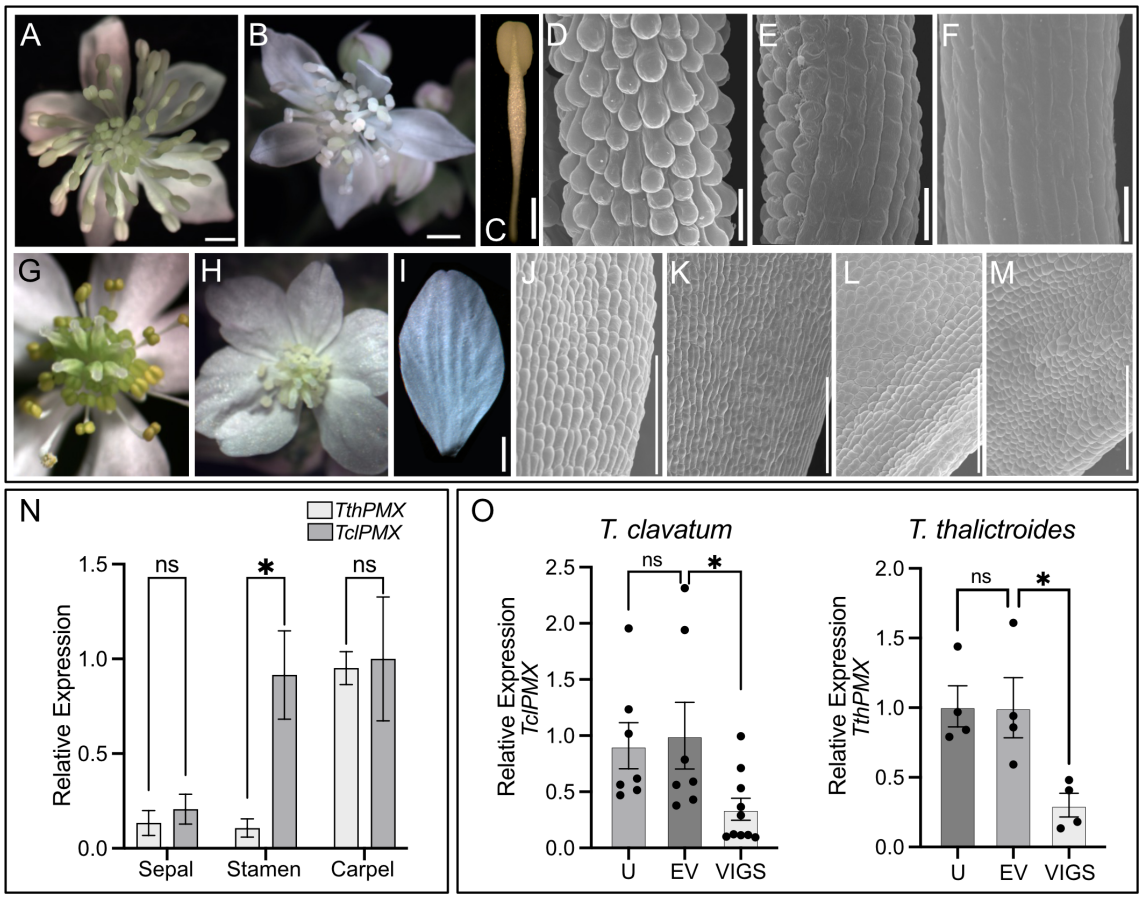

FIGURE 5
Thalictrum paleo*MIXTA* orthologs promote conical–papillate cells on the epidermis of flower organs. Virus-induced gene silencing (VIGS) of *ThPMX* in *Thalictrum clavatum* **(A–F)** and *T. thalictroides* **(G–M)**. **(A)** *T. clavatum* whole untreated flower. **(B)** VIGS-treated flower showing signs of photobleaching in the central region. **(C)** Control (untreated) outer stamen, whole view. **(D)** Detail of stamen filament in **(C)**, with protruding conical–papillate cells. **(E)** Stamen filament detail of flower treated with TRV2–PDS–*TclPMX*, showing signs of incomplete gene silencing; note the conical–papillate cells on the left half compared to the flatter cells on the right half. **(F)** Fully silenced stamen filament with flat epidermal cells. All filaments depicted are from fully mature outer stamens (before anther dehiscence). **(G)** *T. thalictroides* whole untreated flower. **(H)** VIGS-treated flower showing signs of photobleaching in the central region (immature stamens and carpels). **(I)** Control (untreated) outer sepal, whole view. **(J, K)** Detail of the adaxial epidermis of two untreated sepals with slightly protruding conical–papillate cells. **(L, M)** Detail of sepal adaxial epidermis undergoing VIGS in flowers from two independent plants treated with TRV2–*TthPDS*–*TthPMX*, with flatter epidermal cells. **(N)** Wild-type relative expression by qPCR of *TthPMX* and *TclPMX* in dissected floral organs of *T. thalictroides* and *T. clavatum*, respectively. **(O)** Molecular validation of VIGS experiments in *T. clavatum* and *T. thalictroides*. U, untreated; EV, empty vector control; VIGS, virus-induced gene silencing. The values shown in **(N, O)** are average expression levels relative to *TthACTIN* and *TthEEF1* housekeeping genes, normalized to the highest expressing organ in **(N)** (carpel) or to EV control in **(O)**. The asterisk denotes statistical significance at $P < 0.05$ by Dunnett's multiple-comparisons test, ns: not significant. The scale bar is 1 mm in **(A–C, G–I)** and 100 µm in **(D–F, J–M)**.

The phylogenetic inference of the *MIXTA-like* family in *Thalictrum* uncovered a lineage-specific duplication that coincides with a WGD event in the genus. This result suggests that, early in the history of the genus, the evolution of the *MIXTA-like* gene family was impacted by polyploidy, which is ubiquitous in *Thalictrum*.

T. thalictroides PMX is a positive regulator of leaf trichomes

The MYB family R2R3 SBG9-A gene *TthPMX* (previously *TthMYBML2*) from *T. thalictroides* had been shown to increase the height of ovary epidermal cells when overexpressed in tobacco (Di Stilio et al., 2009). This study provides evidence for the role of *TthPMX* in conical–papillate cells in the floral organs of *Thalictrum* while uncovering a novel function as a positive regulator of leaf trichome development. Most subgroup 9-A *MIXTA* family genes such as *Antirrhinum majus* (snapdragon) *AmMYBML1* (Pérez-Rodríguez et al., 2005) and *A. annua AaMIXTA1* (Shi et al., 2018) are positive regulators of trichome development. In tomato, the ectopic expression of *SlMIXTA* increases type I trichomes, whereas RNA silencing reduces them (Ewas et al., 2016; Schuurink and Tissier, 2020). However, certain *MIXTA-like* genes have developed inhibitory roles in trichome initiation, such as *Mimulus guttatus MgMYBML8* (Scoville et al., 2011) and

Arabidopsis MYB106 (Gilding and Marks, 2009). Hence, our finding that *Thalictrum* paleo*MIXTA* positively affects trichome development suggests that the negative role of MIXTA-like genes in trichome development could be a derived function in certain core eudicots.

Thalictrum paleo*MIXTA* modulates trichome morphogenesis via microtubule remodeling

Arabidopsis has become a model to study the morphogenesis and anisotropic development of epidermal cells (Yang et al., 2019). Microtubule binding proteins are important components of the plant cytoskeleton that have been implicated in the development of both conical cells and branched trichomes (Reddy et al., 2004). Previously, trichomes with short stalks were observed in *Arabidopsis* loss-of-function mutants for kinesin-like calmodulin-binding protein (KCBP) (Oppenheimer et al., 1997). However, the mechanisms of trichome morphogenesis in species outside of this derived model plant are poorly understood.

Our RNA-Seq data shows the downregulation of genes coding for the microtubule motor protein KINESIN, DCAF, KIN-17-like, and MAP65 and the upregulation of microtubule-regulating CaML-25 and KLP. In *Arabidopsis*, calmodulin-like proteins interact with kinesin microtubule motor proteins to regulate trichome morphogenesis (Oppenheimer et al., 1997; Reddy et al., 2004). In addition, there was downregulation of subtilisin-like proteases such as SDD1 that play a role in cell signaling and spacing of stomatal cells (Von Groll et al., 2002); however, their role in the spacing of other epidermal cells is unknown. While our qualitative SEM analysis of VIGS-treated plants did not uncover statistically significant differences in the morphology of pavement cells or the stomatal density, there was visible variability in stomatal densities among individual transgenic plants across the top, middle, and bottom leaf abaxial regions (Supplementary Figure S5H), thus warranting further investigation.

The top candidates included DEGS that are also highly expressed in mature *Arabidopsis* trichomes (top 5%), such as *PEPCK*, *ETF1*, *KINASE*, and *RABD*. These results together suggest that *MIXTA* family orthologs from phylogenetically distant plant species may have converged in regulating cell elongation in trichomes through similar microtubule-mediated mechanisms. Comparable genetic components point to the potential conservation of the genetic machinery for the development of epidermal extensions in eudicots.

A potential role for *Thalictrum* trichomes in plant defense

Thalictrum species are often cultivated for their wealth of biochemical compounds such as alkaloids, found in roots and leaves (Hao et al., 2021). It is currently unknown whether *Thalictrum* trichomes have the ability to synthesize or accumulate bio-compounds. Our study provides evidence that targeted silencing of *TthPMX* affects trichome morphology, and modulates genes related to plant stress and defense. Basic secretory protein (BSP), Rhodanese-like domain, multiple enzymes and genes encoding antimicrobial thionins were co-repressed in transgenic plants undergoing gene silencing. Glandular trichomes of *Artemisia annua* secrete Rhodanese-like domain protein for defense and detoxification (Wu et al., 2012), while leaf specific-thionins are small metabolites with roles in plant defense against pathogens and herbivores (Escudero-Martinez et al., 2017). Therefore, it appears likely that *Thalictrum* trichomes play a role in defense against herbivores. Moreover, the downregulation of secondary metabolites such as secretory proteins, sugar transport proteins and enzymes like methyltransferase, amidase, and protease in VIGS-treated plants supports a glandular role for *Thalictrum* trichomes that is consistent with their morphology (Figure 2).

A gene with many functions: *MIXTA family* genes regulate the development of multiple epidermal forms in different plant systems

It has been speculated that timing, developmental stage, or localization may determine the specialized cell forms that develop from the expression of *MIXTA-like* genes (Pérez-Rodríguez et al., 2005). Interestingly, our comparative transcriptomic approach revealed that *TthPMX* positively regulates a SANT/MYB domain-containing protein involved in local chromatin remodeling (Boyer et al., 2004), suggesting that paleo*MIXTA* genes could potentially reprogram epidermal cell fate via the regulation of chromatin remodeling complexes.

Functional studies of *MIXTA* family orthologs in the monocot and core eudicot clades suggest that they are sufficient to drive the development of multiple epidermal features. For instance, in the orchid *P. aphrodite*, both *PaMYB9A1/2* paralogs can drive the differentiation of conical cells and cuticle biosynthesis in petals (Lu et al., 2022). Similarly, snapdragon *AmMYBML1* can modulate the differentiation of trichomes in leaves and of conical cells in petals (Pérez-Rodríguez et al., 2005). In the liverwort *Marchantia polymorpha* (a bryophyte, or non-vascular plant), *MIXTA* family homologs play a role in cuticle in addition to papillate cells, representing a more ancestral function potentially common to all land plants (Xu et al., 2020).

Here, we show that *Thalictrum paleoMIXTA* from the early-diverging eudicots can modulate the development of leaf trichomes and floral conical–papillate cells. Hence, if the trichome and conical cell roles found here were extended to other early-diverging eudicots, it may be possible to reconstruct a combined function back to the last common ancestor of eudicots. In closing, our findings in *Thalictrum* join those in other plant systems to suggest a deeply conserved role for *MIXTA* family transcription factors in trichomes and conical–papillate, readily producing a diversity of epidermal features.

Methods

Plant materials

T. thalictroides bare root plants were purchased from Sundquist nursery (Poulsbo, WA) and mature *T. clavatum* plants from Gardens of the Blue Ridge Inc (Pineola, NC). Both sets of plants were vernalized at 4°C before infiltration. Voucher specimens are listed in Supplementary Table S1.

Phylogenetic analysis of *Thalictrum MIXTA* family genes

MIXTA family homologs were recovered from 23 species representative of all major clades in the *Thalictrum* phylogeny by PCR and cloning and/or direct sequencing (vouchers listed in Supplementary Table S1). Genomic DNA was extracted using the MP Bio101 FastDNA Kit, and complete or near-complete paleo*MIXTA* loci were amplified by PCR with locus-specific primers (Supplementary Table S2) and cloned with pCRII TOPO TA (Invitrogen, Carlsbad, CA, USA). Positive clones were purified using a 5 Prime FastPlasmid Miniprep kit and sequenced (Genewiz, South Plainfield, NJ, USA). At least eight colonies per diploid species or 15 colonies per polyploid species were sequenced to encompass all paralogs. The sequences were edited in Sequencher version 4.9 (Gene Codes Corporation, Ann Arbor, MI, USA) and aligned using MUSCLE (Edgar, 2004). INDELS were coded as gaps and missing data was coded as "?". The models of evolution for each data set were determined using jModelTest version 2.1 (Posada, 2008). The GTR+I+Γ model was selected based on the Akaike Information Criterion (Akaike, 1974). Bayesian inference analysis was conducted using MrBayes v.3.2 (Ronquist et al., 2012) with a parallel MCMC analysis of 50 million generations, sampling every 1,000 generations. Convergence was checked using the average standard deviation of split frequencies (<0.01) and the effective sample size (ESS) values (>200). The first 25% of trees were discarded as burn-in. The remaining trees were pooled to construct a 50% majority rule consensus tree and visualized using FigTree v1.4.4 (Rambaut et al., 2018).

Gene expression analysis

To determine paralog-specific expression, real-time quantitative PCR (qPCR) was carried out on a Bio-Rad CFX qPCR system, and the results were analyzed in BioRad CFX Manager3.0 software (Bio-Rad laboratories, Hercules, CA, USA). Locus-specific primers were designed in NCBI's Primer3 (Supplementary Table S2), and primer specificity was tested via melting curve analysis, resulting in a single peak per primer set. Quantification of expression for *TthPMX*, *TthPDS*, *TclPMX*, *TdiPM1b*, *TdiPMX2a*, *TdaPMX1a*, *TdaPMX1b.1*, *TdaPMX1b.2*, and *TdaPMX2b* was performed as previously described (Galimba et al., 2018). Briefly, each 10-µL reaction contained 5 µL of SYBR Green PCR Master Mix (Bio-Rad, Hercules, CA, USA), 0.5 µL (10 µM) of locus-specific primers, 1 µL of template cDNA, and 3 µL of water. The samples were amplified for 40 cycles in duplicate, including a no-template control. The reactions were normalized to the *Thalictrum* orthologs of two housekeeping genes, *ACTIN* and *EEF1* (*EUKARYOTIC ELONGATION FACTOR 1*), using the $2^{-\Delta\Delta CT}$ relative quantification method (Livak and Schmittgen, 2001). The standard deviation of Ct values of reference genes was calculated, and the average of three technical replicates was used to ensure minimal variation in gene expression. Average values and standard errors were graphed and compared statistically by single-factor ANOVA followed by Tukey's comparisons or Dunnett's multiple-comparisons test.

Construct preparation

T. clavatum and *T. thalictroides* share 99.8% nucleotide identity for PDS, allowing us to use the same PDS sequence across the two species. *TthPDS* had been previously cloned into TRV2 (Di Stilio et al., 2010) and was used here as a marker in a double construct with the target gene, also previously cloned (Di Stilio et al., 2009). Briefly, the TRV2–*TthPDS* construct was double-digested with XbaI and BamHI and then ligated to a *TclPMX* or *TthPMX* 400-bp fragment, half of which comprised the end of the C terminal and the other half the 3′UTR. The target sequences were obtained by PCR amplification from plasmid DNA containing the whole coding region of *TthPMX* (previously *TthMYBML2*, Di Stilio et al., 2009) using primers with added restriction sites (Supplementary Table S2).

Virus-induced gene silencing

The infiltration of *T. thalictroides* and *T. clavatum* was carried out as previously described (Di Stilio et al., 2010) with minor modifications. Briefly, TRV1, TRV2–*TthPMX/TclPMX*, and TRV2–*ThPDS–ThPMX* starter cultures were grown overnight with selective antibodies and subsequently used to inoculate 500-mL cultures. *Agrobacterium* was centrifuged at 4°C and 4,000*g* for 15 min before being resuspended in an infiltration medium (10 mM MES, 20 µM acetosyringone, and 10 mM MgCl2). Each culture was resuspended to a final OD600 of 2.0 and incubated for 3 h at room temperature. Islet L-77 (Lehle Seeds, Round Rock, TX, USA) was added at 100 uL/L as a surfactant.

Dormant tubers of both species that had been kept at 4°C for 3 weeks were removed from soil and rinsed, and a small razor blade incision was made away from the meristem before being submerged in an infiltration medium containing a 1:1 ratio of TRV1 and TRV2 cultures. *T. thalictroides* tubers were treated with a construct with the gene of interest alone or with both the target gene and the marker gene phytoene desaturase (*TthPDS*), whose downregulation induces photobleaching. *T. clavatum* tubers were treated with the double construct only. In total, 40 tubers were vacuum-infiltrated per species and then potted in 2.5″ Deepots™ (Stuewe & Sons, Tangent, OR, USA) using Sunshine Mix 4 soil (Sun Gro, Bellevue, WA, USA). The plants were kept in growth chambers under a 16-h

light–dark cycle at 22°C/18°C. An additional 15–20 plants per species were infiltrated with empty TRV2 (mock). This control was used to test for background viral effects. A total of 15 untreated plants were grown under the same conditions as an additional control.

Molecular validation of VIGS experiments

Fully expanded mature leaves and open flowers before anther dehiscence were collected from plants at 3 to 4 weeks post-infiltration, flash-frozen with liquid nitrogen, and stored at -80°C. Total RNA was extracted using the Spectrum Plant Total RNA Kit or Trizell reagent (Invitrogen, CA, USA) according to the manufacturer's protocol. The samples were treated with DNAase I (Thermo Scientific™, Waltham, MA, USA), and first-strand cDNA was synthesized using iScript cDNA synthesis kit (Sigma, Burlington, MA, USA). cDNA was synthesized using TRV1- and TRV2 -specific primers (for viral detection by RT-PCR) or the manufacturer's mix of random and polyT primers (for qPCR) and amplified using a 51 × 30 PCR cycle and locus-specific primers (Supplementary Table S2). The RT-PCR products were run on 1.2% agarose gel and photographed on GelDoc Image lab software package (Bio-Rad, Hercules, CA, USA).

To determine if target genes had been successfully downregulated, qPCR was conducted as explained above with *ThPDS*- and *ThPMX*-specific primers (Supplementary Table S2) on leaves or flowers (whole or dissected) at 4 to 10 samples each of untreated, mock (empty vector), and treatment. Average values and standard deviations for each biological replicate were graphed relative to the highest-expressing tissue.

Phenotypic analysis

Plants of both species were photographed using a Nikon D3400 hand-held camera and a dissecting microscope (Nikon SMZ800, Nikon Instruments Inc., Melville, NY, USA) equipped with a QImaging MicroPublisher 3.3 RTV digital camera (Surrey, BC, Canada).

Preparation of samples for scanning electron microscopy

Fully expanded mature leaves and open flowers were collected whole or dissected and fixed in 10% formaldehyde, 5% acetic acid, and 50% alcohol (FAA) for 1 h at RT and overnight at 4°C, dehydrated through an alcohol series, critical point-dried, mounted on stubs, and sputter-coated with gold. Observations were made on a JEOL NeoScope JCM-7000 (University of Washington Microscopy Facility). The leaves fixed in FAA from a previously published tobacco bioassay overexpressing *TthMYBML2* (here renamed to *TthPMX*) under a strong constitutive promoter (Di Stilio et al., 2009) were similarly prepared for SEM. The images were assembled in Affinity Publisher (Serif (Europe) Ltd) or Microsoft Powerpoint.

Quantification of epidermal features

T. thalictroides leaves and dissected floral organs were photographed under SEM. For leaf trichomes, a 1-mm^2 surface adjacent to the mid vein was sampled adaxially and abaxially in three regions: top, middle, and base. Trichomes were found only on the abaxial side and were measured from the base to the tip with Image J (Schneider et al., 2012) using either a straight or segmented line from four independent transgenic plants (at eight to 14 trichomes each).

Tobacco leaf trichomes were sampled in a 5-mm^2 area at the base adjacent to the mid vein both adaxially and abaxially. The trichome type was identified, and the number of trichomes found for each type (I–V) was averaged per treatment (three independent transgenic plant lines per treatment). Statistical significance was determined using a two-factor ANOVA followed by Holm–Šídák's test for multiple comparisons. Chimeric trichomes such as those with two or more types represented within one individual trichome were counted as a separate category and removed from the count data to avoid redundancy.

Comparative transcriptomic analysis

Four biological samples of *T. thalictroides* leaves were collected and validated from mock-treated and VIGS-treated lines (TRV2–*TthPMX*), and their total RNA was extracted for the RNA-Seq analysis. Sequencing was outsourced to Azenta-Genewiz (Burlington, MA, USA), where sample quality was evaluated in an Agilent 2100 Bioanalyzer (Agilent Technologies, Inc., CA, USA) before library preparation. mRNA sequencing was conducted using polyA selection on a HiSeq 4000, and the adapters were removed from the sequence reads with Trimmomatic v.0.36 (Bolger et al., 2014). The resulting reads were mapped to a *de novo Thalictrum thalictroides* transcriptome, assembled with Trinity v2.5 (Haas et al., 2013). Open reading frames were identified with EMBOSS GetOrf, and the transcriptome assembly was annotated using Diamond BLASTx.

Differential gene expression analysis (RNA-Seq)

To determine changes in transcript expression between controls and plants targeted for gene silencing, gene hit counts were used for downstream differential expression analysis (DEGs). Briefly, the standard bioinformatic analysis package (Azenta-Genewiz, South Plainfield, NJ, USA) consisted of DeSeq2 to generate normalized hit counts, Wald test to generate *p*-values for statistical significance (Wald, 1943) and $\log_2$ fold changes to quantify the expression change between groups. The Benjamini–Hochberg test (Benjamini and Hochberg, 1995) was used to generate adjusted *p*-values. Genes with adjusted *p*-values <0.05 and absolute $\log_2$ fold change >1 or ≤1 were regarded as differentially expressed. Significant DEGs were functionally annotated, and transcripts of interest, such as *TthPMX* and orthologs of the reference genes *EEF1-alpha* and *ACTIN*, were identified in the assemblies using BLAST. Transcript normalized counts (transcripts per million) were used to graph their relative expression as a validation

step. The average expression for three bio-replicates was normalized to mock-treated controls (empty vector, EV), and the statistical significance was calculated using single-factor ANOVA and Tukey's test for multiple comparison.

Data availability statement

The datasets presented in this study can be found in online repositories. The names of the repository/repositories and accession number(s) can be found below: SRA data: PRJNA1030785, NCBI SRA PRJNA1030785 and DRYAD dataset https://doi.org/10.5061/dryad.tdz08kq5k.

Author contributions

SZ: Writing – review & editing, Formal Analysis, Investigation, Visualization, Writing – original draft. AS: Investigation, Writing – review & editing. VD: Writing – review & editing, Conceptualization, Funding acquisition, Supervision.

Funding

The author(s) declare financial support was received for the research, authorship, and/or publication of this article. This work was funded by National Science Foundation (USA) Division of Environmental Biology (DEB), Evolutionary Processes, Mary Gates Research Scholarship and Frye-Hotson-Rigg award to AS, grant number 1911539 to VD; Hall International Fellowship and Lawrence Giles and Kruckeberg-Walker Awards to SZ (University of Washington, Department of Biology).

Acknowledgments

Cathie Martin (John Innes center, Norwich, UK) sent the transformed tobacco seeds. Kacie McCarty, Alessandra (Oddone) Sullivan, and Janet Solano ran the preliminary VIGS experiments. Jens Johnson and Valerie Soza contributed to an early version of the gene phylogeny. Patricia Salles and Christina Owen contributed to the cloning of *MIXTA* orthologs. Anthony García provided advice on RNA-seq analysis and assistance in locating the samples. We thank Wai Pang Chang (University of Washington microscopy facility) for help in the preparation and observation of SEM samples and the Student Technology Fee (STF) for funding the SEM. We thank Stephanie Ickert-Bond (U. of Alaska) for collecting *T. sparsiflorum* specimens and sharing seeds.

Conflict of interest

The authors declare that the research was conducted in the absence of any commercial or financial relationships that could be construed as a potential conflict of interest.

The author(s) declared that they were an editorial board member of Frontiers, at the time of submission. This had no impact on the peer review process and the final decision.

Publisher's note

Supplementary material

The Supplementary Material for this article can be found online at: https://www.frontiersin.org/articles/10.3389/fpls.2023.1288961/full#supplementary-material

References

Akaike, H. (1974). A new look at the statistical model identification. *IEEE Trans. Automat. Contr.* 19, 716–723. doi: 10.1109/TAC.1974.1100705

Bar, M., and Shtein, I. (2019). Plant trichomes and the biomechanics of defense in various systems, with Solanaceae as a model. *Botany* 97, 651–660. doi: 10.1139/cjb-2019-0144

Baumann, K., Perez-Rodriguez, M., Bradley, D., Venail, J., Bailey, P., Jin, H., et al. (2007). Control of cell and petal morphogenesis by R2R3 MYB transcription factors. *Development* 134, 1691–1701. doi: 10.1242/dev.02836

Benjamini, Y., and Hochberg, Y. (1995). Controlling the false discovery rate: A practical and powerful approach to multiple testing. *J. R. Stat. Soc.: Ser. B. (Methodological).* 57, 289–300. doi: 10.1111/j.2517-6161.1995.tb02031.x

Bolger, A. M., Lohse, M., and Usadel, B. (2014). Trimmomatic: a flexible trimmer for Illumina sequence data. *Bioinformatics* 30, 2114–2120. doi: 10.1093/bioinformatics/btu170

Boyer, L. A., Latek, R. R., and Peterson, C. L. (2004). The SANT domain: a unique histone-tail-binding module? *Nat. Rev. Mol. Cell Biol.* 5, 158–163. doi: 10.1038/nrm1314

Brockington, S. F., Alvarez-Fernandez, R., Landis, J. B., Alcorn, K., Walker, R. H., Thomas, M. M., et al. (2013). Evolutionary analysis of the MIXTA gene family highlights potential targets for the study of cellular differentiation. *Mol. Biol. Evol.* 30, 526–540. doi: 10.1093/molbev/mss260

Cavallini-Speisser, Q., Morel, P., and Monniaux, M. (2021). Petal cellular identities. *Front. Plant Sci.* 12. doi: 10.3389/fpls.2021.745507

Chalvin, C., Drevensek, S., Gilard, F., Mauve, C., Chollet, C., Morin, H., et al. (2021). Sclareol and linalyl acetate are produced by glandular trichomes through the MEP pathway. *Horticult. Res.* 8, 206. doi: 10.1038/s41438-021-00640-w

Dai, X., Zhou, L., Zhang, W., Cai, L., Guo, H., Tian, H., et al. (2016). A single amino acid substitution in the R3 domain of GLABRA1 leads to inhibition of trichome formation in Arabidopsis without affecting its interaction with GLABRA3: Ser92 in GL1 is critical for its function. *Plant. Cell Environ.* 39, 897–907. doi: 10.1111/pce.12695

Di Stilio, V. S., Kumar, R. A., Oddone, A. M., Tolkin, T. R., Salles, P., and McCarty, K. (2010). Virus-induced gene silencing as a tool for comparative functional studies in thalictrum. *PloS One* 5, e12064. doi: 10.1371/journal.pone.0012064

Di Stilio, V. S., Martin, C., Schulfer, A. F., and Connelly, C. F. (2009). An ortholog of MIXTA-like2 controls epidermal cell shape in flowers of Thalictrum. *New Phytol.* 183, 718–728. doi: 10.1111/j.1469-8137.2009.02945.x

Edgar, R. C. (2004). MUSCLE: multiple sequence alignment with high accuracy and high throughput. *Nucleic Acids Research* 32, 1792–1797. doi: 10.1093/nar/gkh340

Escudero-Martinez, C. M., Morris, J. A., Hedley, P. E., and Bos, J. I. B. (2017). Barley transcriptome analyses upon interaction with different aphid species identify thionins contributing to resistance: Barley transcriptional responses to aphids. *Plant. Cell Environ.* 40, 2628–2643. doi: 10.1111/pce.12979

Ewas, M., Gao, Y., Wang, S., Liu, X., Zhang, H., Nishawy, E. M. E., et al. (2016). Manipulation of SlMXl for enhanced carotenoids accumulation and drought resistance in tomato. *Sci. Bull.* 61, 1413–1418. doi: 10.1007/s11434-016-1108-9

Feng, Z., Bartholomew, E. S., Liu, Z., Cui, Y., Dong, Y., Li, S., et al. (2021). Glandular trichomes: new focus on horticultural crops. *Hortic. Res.* 8, 158. doi: 10.1038/s41438-021-00592-1

Galdon-Armero, J., Arce-Rodriguez, L., Downie, M., Li, J., and Martin, C. (2020). A scanning electron micrograph-based resource for identification of loci involved in epidermal development in tomato: elucidation of a new function for the mixta-like transcription factor in leaves[OPEN]. *Plant Cell* 32, 1414–1433. doi: 10.1105/tpc.20.00127

Galimba, K. D., Martínez-Gómez, J., Di Stilio, V. S., and S, V. (2018). Gene duplication and transference of function in the paleoAP3 lineage of floral organ identity genes. *Front. Plant Sci.* 9. doi: 10.3389/fpls.2018.00334

Gao, S., Gao, Y., Xiong, C., Yu, G., Chang, J., Yang, Q., et al. (2017). The tomato B-type cyclin gene, SlCycB2 , plays key roles in reproductive organ development, trichome initiation, terpenoids biosynthesis and Prodenia litura defense. *Plant Sci.* 262, 103–114. doi: 10.1016/j.plantsci.2017.05.006

Gilding, E. K., and Marks, M. D. (2009). NOECK, a gene related to MIXTA of snapdragon, controls cell size and shape in Arabidopsis trichomes in unexpected ways. *Plant Biol. (Rockville).* 2009, 181.

Gilding, E. K., and Marks, M. D. (2010). Analysis of purified glabra3-shapeshifter trichomes reveals a role for NOECK in regulating early trichome morphogenic events. *Plant J.* 64, 304–317. doi: 10.1111/j.1365-313X.2010.04329.x

Haas, B. J., Papanicolaou, A., Yassour, M., Grabherr, M., Blood, P. D., Bowden, J., et al. (2013). *De novo* transcript sequence reconstruction from RNA-seq using the Trinity platform for reference generation and analysis. *Nat. Protoc.* 8, 1494–1512. doi: 10.1038/nprot.2013.084

Hao, D.-C., Li, P., Xiao, P.-G., and He, C.-N. (2021). Dissection of full-length transcriptome and metabolome of Dichocarpum (Ranunculaceae): implications in evolution of specialized metabolism of Ranunculales medicinal plants. *PeerJ* 9, e12428. doi: 10.7717/peerj.12428

Hichri, I., Deluc, L., Barrieu, F., Bogs, J., Mahjoub, A., Regad, F., et al. (2011). A single amino acid change within the R2 domain of the VvMYB5b transcription factor modulates affinity for protein partners and target promoters selectivity. *BMC Plant Biol.* 11, 117. doi: 10.1186/1471-2229-11-117

Jaime, R., Rey, P. J., Alcántara, J. M., and Bastida, J. M. (2013). Glandular trichomes as an inflorescence defence mechanism against insect herbivores in Iberian columbines. *Oecologia* 172, 1051–1060. doi: 10.1007/s00442-012-2553-z

Jakoby, M. J., Falkenhan, D., Mader, M. T., Brininstool, G., Wischnitzki, E., Platz, N., et al. (2008). Transcriptional profiling of mature arabidopsis trichomes reveals that NOECK encodes the MIXTA-like transcriptional regulator MYB106. *Plant Physiol.* 148, 1583–1602. doi: 10.1104/pp.108.126979

Javelle, M., Vernoud, V., Rogowsky, P. M., and Ingram, G. C. (2011). Epidermis: the formation and functions of a fundamental plant tissue. *New Phytol.* 189, 17–39. doi: 10.1111/j.1469-8137.2010.03514.x

Kramer, E. M., Dorit, R. L., and Irish, V. F. (1998). Molecular evolution of genes controlling petal and stamen development: Duplication and divergence within the APETALA3 and PISTILLATA MADS-box gene lineages. *Genetics* 149, 765–783. doi: 10.1093/genetics/149.2.765

Lashbrooke, J., Adato, A., Lotan, O., Alkan, N., Tsimbalist, T., Rechav, K., et al. (2015). The tomato MIXTA-like transcription factor coordinates fruit epidermis conical cell development and cuticular lipid biosynthesis and assembly. *Plant Physiol.* 169, 2553–2571. doi: 10.1104/pp.15.01145

Lau, S.-E., Schwarzacher, T., Othman, R. Y., and Harikrishna, J. A. (2015). dsRNA silencing of an R2R3-MYB transcription factor affects flower cell shape in a Dendrobium hybrid. *BMC Plant Biol.* 15, 194. doi: 10.1186/s12870-015-0577-3

Livak, K. J., and Schmittgen, T. D. (2001). Analysis of relative gene expression data using real-time quantitative PCR and the $2^{-\Delta\Delta CT}$ method. *Methods* 25, 402–408. doi: 10.1006/meth.2001.1262

Lu, H.-C., Lam, S.-H., Zhang, D., Hsiao, Y.-Y., Li, B.-J., Niu, S.-C., et al. (2022). R2R3-MYB genes coordinate conical cell development and cuticular wax biosynthesis in Phalaenopsis aphrodite. *Plant Physiol.* 188, 318–331. doi: 10.1093/plphys/kiab422

MaChado, A., Wu, Y., Yang, Y., Llewellyn, D. J., and Dennis, E. S. (2009). The MYB transcription factor GhMYB25 regulates early fibre and trichome development. *Plant J.* 59, 52–62. doi: 10.1111/j.1365-313X.2009.03847.x

Martínez-Gómez, J., Park, S., Hartogs, S. R., Soza, V. L., Park, S., and Di Stilio, V. S. (2023). Flower morphology as a predictor of pollination mode in a biotic to abiotic pollination continuum. *Ann. Bot.* 132, 61–76. doi: 10.1093/aob/mcad069

Noda, K., Glover, B. J., Linstead, P., and Martin, C. (1994). Flower colour intensity depends on specialized cell shape controlled by a Myb-related transcription factor. *Nature* 369, 661–664. doi: 10.1038/369661a0

Oppenheimer, D. G., Pollock, M. A., Vacik, J., Szymanski, D. B., Ericson, B., Feldmann, K., et al. (1997). Essential role of a kinesin-like protein in Arabidopsis trichome morphogenesis. *Proc. Natl. Acad. Sci. U.S.A.* 94, 6261–6266. doi: 10.1073/pnas.94.12.6261

Pérez-Rodríguez, M., Jaffe, F. W., Butelli, E., Glover, B. J., and Martin, C. (2005). Development of three different cell types is associated with the activity of a specific MYB transcription factor in the ventral petal of *Antirrhinum majus* flowers. *Development* 132, 359–370. doi: 10.1242/dev.01584

Pesch, M., and Hülskamp, M. (2009). One, two, three…models for trichome patterning in Arabidopsis? *Curr. Opin. Plant Biol.* 12, 587–592. doi: 10.1016/j.pbi.2009.07.015

Posada, D. (2008). jModelTest: phylogenetic model averaging. *Mol. Biol. Evol.* 25, 1253–1256. doi: 10.1093/molbev/msn083

Qi, X., Chen, Z., Yu, X., Li, L., Bai, Y., Fang, H., et al. (2022). Characterisation of the Mentha canadensis R2R3-MYB transcription factor gene McMIXTA and its involvement in peltate glandular trichome development. *BMC Plant Biol.* 22, 1–11. doi: 10.1186/s12870-022-03614-9

Qin, W., Xie, L., Li, Y., Liu, H., Fu, X., Chen, T., et al. (2021). An R2R3-MYB transcription factor positively regulates the glandular secretory trichome initiation in artemisia annua L. *Front. Plant Sci.* 12. doi: 10.3389/fpls.2021.657156

Rambaut, A., Drummond, A. J., Xie, D., Baele, G., and Suchard, M. A. (2018). Posterior summarization in bayesian phylogenetics using tracer 1.7. *Syst. Biol.* 67, 901–904. doi: 10.1093/sysbio/syy032

Reddy, V. S., Day, I. S., Thomas, T., and Reddy, A. S. N. (2004). KIC, a novel calcium binding protein with one EF-hand motif, interacts with a microtubule motor protein and regulates trichome morphogenesis. *Plant Cell* 16, 185–200. doi: 10.1105/tpc.016600

Ronquist, F., Teslenko, M., van der Mark, P., Ayres, D. L., Darling, A., Höhna, S., et al. (2012). MrBayes 3.2: efficient bayesian phylogenetic inference and model choice across a large model space. *Syst. Biol.* 61, 539–542. doi: 10.1093/sysbio/sys029

Schneider, C. A., Rasband, W. S., and Eliceiri, K. W. (2012). NIH Image to ImageJ: 25 years of image analysis. *Nat. Methods* 9, 671–675. doi: 10.1038/nmeth.2089

Schuurink, R., and Tissier, A. (2020). Glandular trichomes: micro-organs with model status? *New Phytol.* 225, 2251–2266. doi: 10.1111/nph.16283

Scoville, A. G., Barnett, L. L., Bodbyl-Roels, S., Kelly, J. K., and Hileman, L. C. (2011). Differential regulation of a MYB transcription factor is correlated with transgenerational epigenetic inheritance of trichome density in *Mimulus guttatus*. *New Phytol.* 191, 251–263. doi: 10.1111/j.1469-8137.2011.03656.x

Shi, P., Fu, X., Shen, Q., Liu, M., Pan, Q., Tang, Y., et al. (2018). The roles of AaMIXTA1 in regulating the initiation of glandular trichomes and cuticle biosynthesis in Artemisia annua. *New Phytol.* Burlington, MA 217, 261–276. doi: 10.1111/nph.14789

Simpson, M. G. (2019). *Plant systematics* (Elsevier-Academic Press), 774. doi: 10.1016/B978-0-12-812628-8.50006-7

Soza, V. L., Brunet, J., Liston, A., Salles Smith, P., and Di Stilio, V. S. (2012). Phylogenetic insights into the correlates of dioecy in meadow-rues (Thalictrum, Ranunculaceae). *Mol. Phylogenet. Evol.* 63, 180–192. doi: 10.1016/j.ympev.2012.01.009

Soza, V. L., Haworth, K. L., and Stilio, V. S. D. (2013). Timing and consequences of recurrent polyploidy in meadow-rues (Thalictrum, ranunculaceae). *Mol. Biol. Evol.* 30, 1940–1954. doi: 10.1093/molbev/mst101

Stracke, R., Werber, M., and Weisshaar, B. (2001). The R2R3-MYB gene family in Arabidopsis thaliana. *Curr. Opin. Plant Biol.* 4, 447–456. doi: 10.1016/S1369-5266(00)00199-0

Vernoud, V., Laigle, G., Rozier, F., Meeley, R. B., Perez, P., and Rogowsky, P. M. (2009). The HD-ZIP IV transcription factor OCL4 is necessary for trichome patterning and anther development in maize. *Plant J.* 59, 883–894. doi: 10.1111/j.1365-313X.2009.03916.x

Von Groll, U., Berger, D., and Altmann, T. (2002). The subtilisin-like serine protease SDD1 mediates cell-to-cell signaling during arabidopsis stomatal development. *Plant Cell* 14, 1527–1539. doi: 10.1105/tpc.001016

Wald, A. (1943). Tests of statistical hypotheses concerning several parameters when the number of observations is large. *Trans. Am. Math. Soc.* 54, 426–482. doi: 10.1090/S0002-9947-1943-0012401-3

Wang, T. N., Clifford, M. R., Martínez-Gómez, J., Johnson, J. C., Riffell, J. A., and Di Stilio, V. S. (2019). Scent matters: differential contribution of scent to insect response in flowers with insect vs. wind pollination traits. *Ann. Bot.* 123, 289–301. doi: 10.1093/aob/mcy131

Wang, Y.-L., Nie, J., Chen, H.-M., Guo, C., Pan, J., He, H.-L., et al. (2016). Identification and mapping of Tril, a homeodomain-leucine zipper gene involved in multicellular trichome initiation in Cucumis sativus. *Theor. Appl. Genet.* 129, 305–316. doi: 10.1007/s00122-015-2628-4

Werker, E. (2000). "Trichome diversity and development," in *Advances in botanical research* (Academic Press), 1–35. doi: 10.1016/S0065-2296(00)31005-9

Wu, T., Wang, Y., and Guo, D. (2012). Investigation of glandular trichome proteins in artemisia annua L. Using comparative proteomics. *PloS One* 7, e41822. doi: 10.1371/journal.pone.0041822

Xu, B., Taylor, L., Pucker, B., Feng, T., Glover, B. J., and Brockington, S. F. (2020). The land plant-specific MIXTA-MYB lineage is implicated in the early evolution of the plant cuticle and the colonization of land. *New Phytol* 229, 2324–2338. doi: 10.1111/nph.16997

Yan, T., Li, L., Xie, L., Chen, M., Shen, Q., Pan, Q., et al. (2018). A novel HD-ZIP IV/MIXTA complex promotes glandular trichome initiation and cuticle development in Artemisia annua. *New Phytol.* 218, 567–578. doi: 10.1111/nph.15005

Yang, Y., Huang, W., Wu, E., Lin, C., Chen, B., and Lin, D. (2019). Cortical microtubule organization during petal morphogenesis in arabidopsis. *IJMS* 20, 4913. doi: 10.3390/ijms20194913

Yang, C., and Ye, Z. (2013). Trichomes as models for studying plant cell differentiation. *Cell. Mol. Life Sci.* 70, 1937–1948. doi: 10.1007/s00018-012-1147-6

Zhou, P., Dang, J., Shi, Z., Shao, Y., Sang, M., Dai, S., et al. (2022). Identification and characterization of a novel gene involved in glandular trichome development in Nepeta tenuifolia. *Front. Plant Sci.* 13. doi: 10.3389/fpls.2022.936244

frontiers | Frontiers in Plant Science

TYPE Original Research
PUBLISHED 15 February 2024
DOI 10.3389/fpls.2024.1336129

OPEN ACCESS

EDITED BY
Hirotomo Takatsuka,
Kanazawa University, Japan

REVIEWED BY
Yanping Jing,
Beijing Forestry University, China
Rui Malhó,
University of Lisbon, Portugal

*CORRESPONDENCE
Jian Chen
jianchen@ujs.edu.cn
Xiaojiang Zheng
xjzheng@nwu.edu.cn
Sheng Luan
sluan@berkeley.edu

RECEIVED 10 November 2023
ACCEPTED 02 February 2024
PUBLISHED 15 February 2024

CITATION
Jing Y, Zhao F, Lai K, Sun F, Sun C, Zou X, Xu M, Fu A, Sharifi R, Chen J, Zheng X and Luan S (2024) Plant elicitor Peptides regulate root hair development in *Arabidopsis*. *Front. Plant Sci.* 15:1336129. doi: 10.3389/fpls.2024.1336129

Plant elicitor Peptides regulate root hair development in *Arabidopsis*

Yanping Jing[1,2,3], Fugeng Zhao[4], Ke Lai[3], Fei Sun[3], Chenjie Sun[3], Xingyue Zou[3], Min Xu[3], Aigen Fu[3], Rouhallah Sharifi[5], Jian Chen[1,2*], Xiaojiang Zheng[3*] and Sheng Luan[6*]

[1]International Genome Center, Jiangsu University, Zhenjiang, China, [2]School of Life Sciences, Jiangsu University, Zhenjiang, China, [3]Chinese Education Ministry's Key Laboratory of Western Resources and Modern Biotechnology, Key Laboratory of Biotechnology Shaanxi Province, College of Life Sciences, Northwest University, Xi'an, Shaanxi, China, [4]College of Life Sciences, Nanjing University, Nanjing, Jiangsu, China, [5]Department of Plant Protection, College of Agriculture and Natural Resources, Razi University, Kermanshah, Iran, [6]Department of Plant and Microbial Biology, University of California, Berkeley, Berkeley, CA, United States

Plant Elicitor Peptides (Peps) induce plant immune responses and inhibit root growth through their receptors PEPR1 and PEPR2, two receptor-like kinases. In our study, we found a previously unknown function of Peps that enhance root hair growth in a PEPRs-independent manner. When we characterized the expression patterns of *PROPEP* genes, we found several gene promoters of *PROPEP* gene family were particularly active in root hairs. Furthermore, we observed that *PROPEP2* is vital for root hair development, as disruption of *PROPEP2* gene led to a significant reduction in root hair density and length. We also discovered that *PROPEP2* regulates root hair formation via the modulation of *CPC* and *GL2* expression, thereby influencing the cell-fate determination of root hairs. Additionally, calcium signaling appeared to be involved in PROPEP2/Pep2-induced root hair growth. These findings shed light on the function of Peps in root hair development.

KEYWORDS

PROPEP, root hair growth, Ca signaling, regulatory mechanism, plant elicitor peptide (Pep)

1 Introduction

Plants have developed highly conserved innate immune systems to protect themselves from external pathogens. These pathogens contain specific molecular patterns called PAMPs that are recognized by cell surface receptors in plants and result in PTI (pattern-triggered immunity) (Boller and Felix, 2009; Macho and Zipfel, 2014). Additionally, plants have the capability to release specific molecules termed damage- or danger-associated molecular patterns (DAMPs) in response to pathogen attacks or injuries, and these molecules also play a regulatory role in plant immunity (Endo et al., 2014; Macho and Zipfel, 2014).

InArabidopsis, a well-documented example of DAMPs is the family of plant elicitor peptides (Peps), which originate from the C-terminal regions of precursor proteins known as PROPEPs (Huffaker et al., 2006; Huffaker et al., 2013). Arabidopsis genome harbors eight *PROPEP*s, and they are responsible for generating eight small Pep peptides in response to pathogen invasion and physical injury (Huffaker et al., 2006; Bartels et al., 2013; Huffaker et al., 2013; Bartels and Boller, 2015; Klauser et al., 2015). Peps are recognized by a pair of closely related receptors, PEPR1 and PEPR2, which subsequently initiate downstream signaling events (Yamaguchi et al., 2006; Yamaguchi et al., 2010). These events include the elevation of cytosolic Ca^{2+} levels, the generation of reactive oxygen species, the expression of defense-related genes, the formation of calluses, lignin deposition, and inhibition of root growth (Millet et al., 2010; Bartels et al., 2013; Beck et al., 2014; Ma et al., 2014; Jing et al., 2019; Jing et al., 2020; Jing et al., 2023).

Root hairs are specialized tubular structures that develop from root epidermal cells. The dynamic adjustments in root hair growth, length, density, and morphology have a significant impact on the root's surface area that determines the efficiency of nutrient and water uptake by plants, interactions between plants and microorganisms, and the stability of plant anchorage (Grierson et al., 2014). In some plant species, such as rice, all epidermal cells can differentiate into root hairs in a random manner (Kim et al., 2006; Kim and Dolan, 2011; Tominaga-Wada et al., 2013). In other species, such as Arabidopsis, only specific short epidermal cells have the potential to become root hairs.

In the well-established model of root hair development in *Arabidopsis*, the fate of root hair cells is determined by the position of epidermal cells (Datta et al., 2011; Grierson et al., 2014). Epidermal cells located exclusively outside of two underlying cortical cells are designated to differentiate into root hairs. Conversely, those with only one underlying cortical cell become non-hair cells (Datta et al., 2011). This cell fate determination is regulated by multiple transcription factors (TFs). Notably, the *TRANSPARENT TESTA GLABRA* (*TTG*), *GLABRA3* (*GL3*), *ENHANCER OF GLABRA3* (*EGL3*), and *WEREWOLF* (*WER*) TFs are expressed in non-hair cells, forming the WER-GL3/EGL3-TTG complex (Galway et al., 1994; Di Cristina et al., 1996; Masucci et al., 1996; Bernhardt et al., 2003; Schiefelbein, 2003). This complex plays a positive role in regulating *GLABRA2* (*GL2*), a central TF responsible for inhibiting root hair formation in non-hair cells (Di Cristina et al., 1996; Masucci et al., 1996; Datta et al., 2011). In contrast, the *CAPRICE* (*CPC*) and *TRIPTYCHON* (*TRY*) TFs promote the formation of root hairs by suppressing *GL2* expression (Schiefelbein, 2003; Grierson et al., 2014).

In our endeavor to unravel the signaling pathway of Peps in plants, our previous work highlighted Pep1's role in stimulating root hair development when externally applied (Jing et al., 2019). In the present investigation, we provide evidence that both exogenous Peps and the overexpression of endogenous *PROPEP*s consistently promote the growth of root hairs. *PROPEP2* emerges as a critical regulator of root development, as the disruption of *PROPEP2* results in a significant reduction in both root hair density and length. Furthermore, we delve into the mechanism by which *PROPEP2* influences the determination of root hair cell fate through the modulation of CPC and GL2 expression. Simultaneously, PROPEP2 orchestrates calcium oscillations within root hair cells, directing the course of root hair development. These findings unveil a novel signaling pathway initiated by Pep/PROPEPs governing *Arabidopsis* root hair development.

2 Results

2.1 Regulation of root hair development by plant elicitor peptides

In previous investigations, we documented the immunomodulatory effects of Peps and their role in inhibiting root growth in *Arabidopsis* (Zheng et al., 2018; Jing et al., 2019; Shen et al., 2020). Additionally, seedlings treated with synthetic Pep1 or Pep2 caused intriguing root hair (RH)-related phenotypes. This led us to hypothesize that Peps might play a pivotal role in root hair development and growth. To scrutinize the impact of Peps on RH growth, we treated wild-type Col-0 (WT) seedlings with various synthetic Peps (Pep1-8) at 10 nM. Remarkably, all exogenous Peps significantly increased both the density and length of RH compared to controls (Figure 1). Notably, Pep1 and Pep2 nearly doubled both the number and length of RH (Figure 1). Furthermore, we engineered transgenic lines overexpressing each Pep precursor gene (*PROPEP*s) driven by the 35S promoter (Supplementary Figures 1–8). These overexpressed *PROPEP* lines exhibited higher RH density and longer RHs compared to the wild-type seedlings, mirroring the effects of exogenous Peps (Figure 2; Supplementary Figures 1–8). These results collectively suggested that both exogenous and endogenous Peps consistently promoted RH growth.

To elucidate the expression patterns of *PROPEP* genes to identify those naturally expressed in the RH, we generated transgenic lines with putative *PROPEP* promoters fused to a *β-glucuronidase* (GUS) gene reporter. GUS staining of these transgenic seedlings revealed extensive expression of all *PROPEP*s in both shoots and systems (Figure 3A). In root tissues, GUS activity in pro*PROPEP3/4/5/7/8:GUS* seedlings was primarily localized to vascular tissue, while the promoters of *PROPEP1/2/6* exhibited activity throughout the entire root (Figure 3B). Notably, the promoters of *PROPEP1/2/6* showed strong activity in root hair cells, implying their involvement in RH processes (Figure 3C). Additionally, we observed inducibility of *PROPEP* promoters by Peps, with GUS activity significantly enhanced in pro*PROPEP1/2/6:GUS* plants upon exposure to Peps (Supplementary Figure 9).

To determine the subcellular localization of each Pep, we fused *PROPEP*s with the *Green Fluorescent Protein* gene (*PROPEP-GFP*) and transiently expressed them in *Arabidopsis* protoplasts. Despite the expected cytosolic localization based on function and the absence of a signal peptide, we unexpectedly observed cytosol-localized GFP signals exclusively in cells expressing *PROPEP3-GFP* or *PROPEP5-GFP* (Figure 4A). In contrast, *PROPEP1*, *PROPEP2*, *PROPEP6*, *PROPEP7*, and *PROPEP8* were

10.3389/fpls.2024.1336129

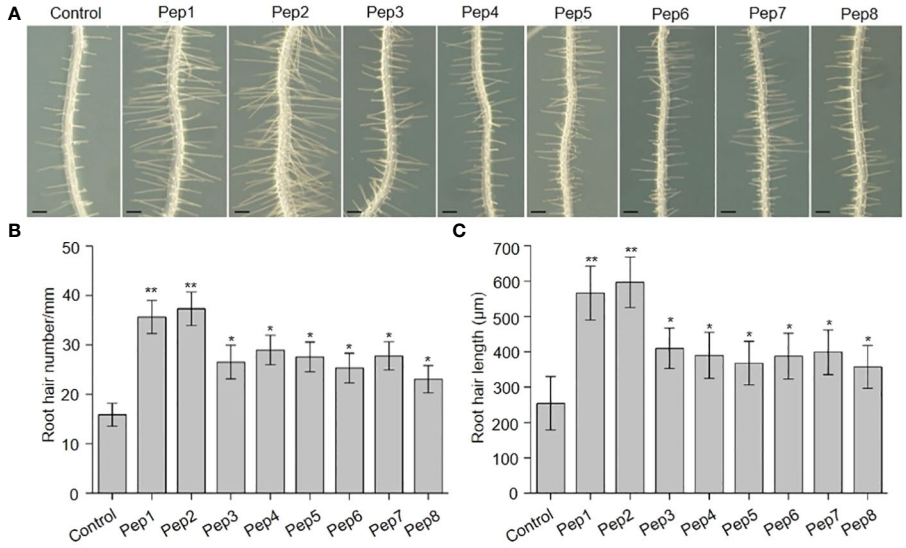

FIGURE 1
The effects of Peps on root hair development. **(A)** The growth phenotype of wild type root under Pep1-Pep8 treatment. Four-day-old WT plants were transplanted on half-strength Murashige and Skoog (MS) agar medium supplemented with or without 10 nM Pep1 to Pep8 for 48 h. Bars = 200 μm. **(B, C)** Statistics of the root hair number **(B)** and root hair length **(C)** as in **(A)**. Data are means ± SD (n = 15 roots per treatment). Asterisks in **(B, C)** indicate statistically significant differences compared with the untreated control. (Tukey's test; *p < 0.05, **p < 0.01).

found to target the tonoplast, while the GFP signal of *PROPEP4* overlapped with chloroplast fluorescence (Figure 4A). To validate the tonoplast localization of *PROPEP1* and *PROPEP2*, which have been extensively studied, we conducted lipophilic FM4-64 staining associated with plasma membrane. The GFP and FM4-64 fluorescence signals did not overlap (Figure 4B), confirming that GFP-PROPEP signals was not localized to the PM but the tonoplast.

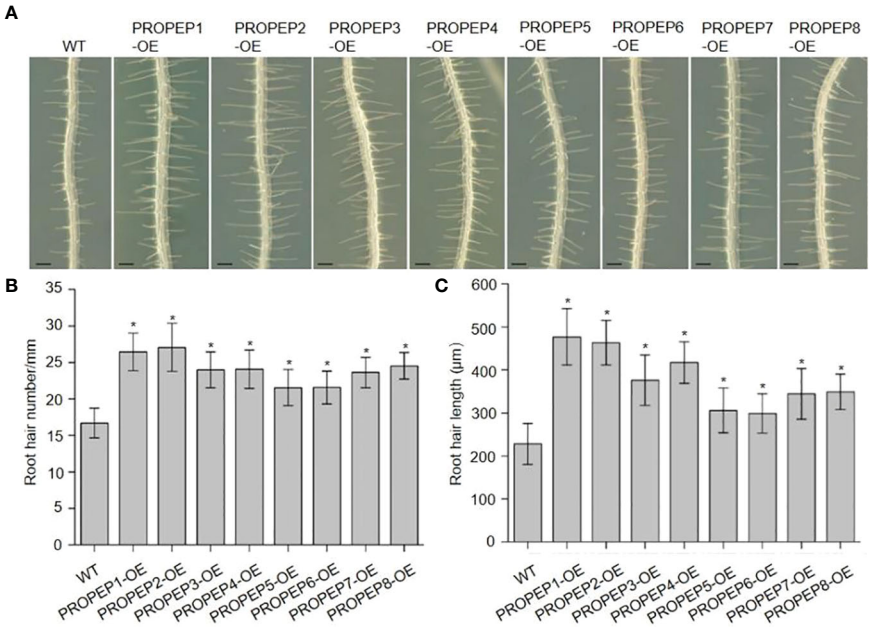

FIGURE 2
Over-expression of PROPEPs promote the root hair development. **(A)** The growth phenotype of root hair in wild type (WT)and wild type plants overexpressing *PROPEP*s (*PROPEP1-OE* to *PROPEP8-OE*). Four-day-old plants were transplanted on half-strength Murashige and Skoog (MS) agar medium for 48 h. Bars = 200 μm. **(B, C)** Statistics of the root hair number **(B)** and root hair length **(C)** as in **(A)**. Data are means ± SD (n = 15 roots per treatment). Asterisks in **(B, C)** indicate statistically significant differences compared with the WT plants. (Tukey's test; *p < 0.05).

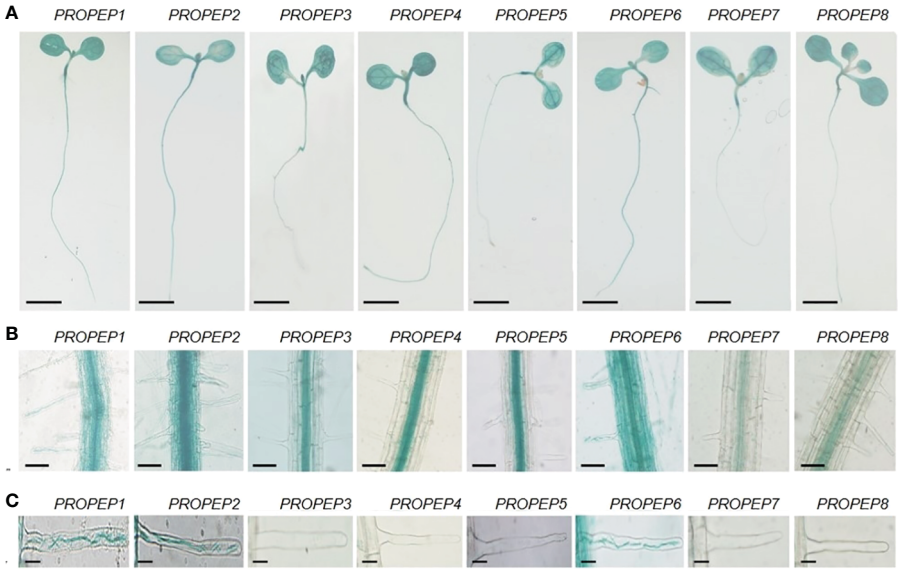

FIGURE 3
The tissue localization of PROPEPs. **(A)** Histochemical staining of GUS activity in 7-d-old transgenic plants harboring *proPROPEP1:GUS (PROPEP1)* to *proPROPEP8:GUS (PROPEP8)*. Bars =2 mm. **(B)** The GUS activity in roots of transgenic plants *PROPEP1* to *PROPEP8*. Bars =100 µm. **(C)** The GUS activity in root hairs of transgenic plants *PROPEP1* to *PROPEP8*. Bars =25 µm.

2.2 Disruption of *PROPEP2* suppresses root hair development

To further investigate the role of the PROPEP family in root hair growth, we isolated transfer DNA (T-DNA) insertional mutants for each gene, aiming to assess their RH phenotypes. Unexpectedly, all of mutants failed to yield detectable T-DNA insertions, except for *propep2*. Notably, *propep2* (SALK_206498) contained a T-DNA insertion within the intron of *PROPEP2*. RT-PCR analyses demonstrated the absence of a full-length *PROPEP2* transcript in *propep2* (Figures 5A, B), confirming its status as a knockout mutant. Consequently, the *propep2* mutant exhibited a significant reduction in both RH density and length compared to wild-type (WT) seedlings (Figures 5C–E).

To corroborate that the observed RH phenotype in the *propep2* mutant was indeed caused by the T-DNA insertion, we generated complementation lines by introducing a genomic fragment of *PROPEP2* into the mutant. Remarkably, transgenic expression of *PROPEP2* in the mutant led to the restoration of *PROPEP2* transcript levels to a comparable level as in WT plants in four independent *PROPEP2-COM* lines (Figure 5B), fully rescuing the RH defect (Figures 5C–E). The Pep2 peptide was released from its precursor protein PROPEP2, the disruption of PROPEP2 could not synthesis the Pep2 peptide anymore, we further used the exogenous Pep2 peptide to analyzed the root hair formation in *propep2* mutant. As shown in Figures 5F–H and Supplementary Figure 10, supplementing the *propep2* mutant with synthesized Pep2 also resulted in the recovery of RH growth (Figures 5F–H; Supplementary Figure 10). These findings provide compelling evidence that *PROPEP2* plays an indispensable role in RH growth in *Arabidopsis*. Moreover, other Peps, in addition to Pep2, also restored RH growth in the *propep2* mutant, suggesting that other PROPEPs (such as PROPEP1 and PROPEP6) with expression in RH may also regulate RH growth (Figures 5F–H).

2.3 *PROPEP2* relies on *CPC* and *GL2* in regulating root hair formation

As Peps affect both the density and length of root hairs, we aimed to investigate whether PROPEPs/Peps work together with other components known to have a role in determining RH cell fate. We focused on examining the expression patterns of *GL2* and *CPC* in relation to Pep2 treatment. The *GL2* gene encodes a homeodomain-leucine zipper protein primarily expressed in non-hair cells, suppressing hair cell differentiation (Di Cristina et al., 1996; Masucci et al., 1996). On the other hand, *CPC* encodes a small protein containing a MYB-like DNA-binding domain, lacking a transcription activation domain, and it acts as a negative transcription regulator of *GL2*, indirectly promoting hair cell differentiation (Wada et al., 1997, 2002; Schellmann et al., 2002; Kirik et al., 2004). Initially, we assessed whether Pep2 impacts the expression levels of *CPC* and *GL2* using real-time RT-PCR. Following Pep2 treatment, *CPC* transcripts increased significantly, while *GL2* expression sharply decreased (Figure 6A). We next examined whether the expression pattern of *CPC* and *GL2* was altered in the *propep2* mutant. Interestingly, *CPC* mRNA levels decreased, whereas *GL2* expression increased significantly, opposite to the data from Pep2 treated samples (Figures 6B, C), suggesting that *PROPEP2* modulates RH growth, at least in part, by regulating *CPC*

10.3389/fpls.2024.1336129

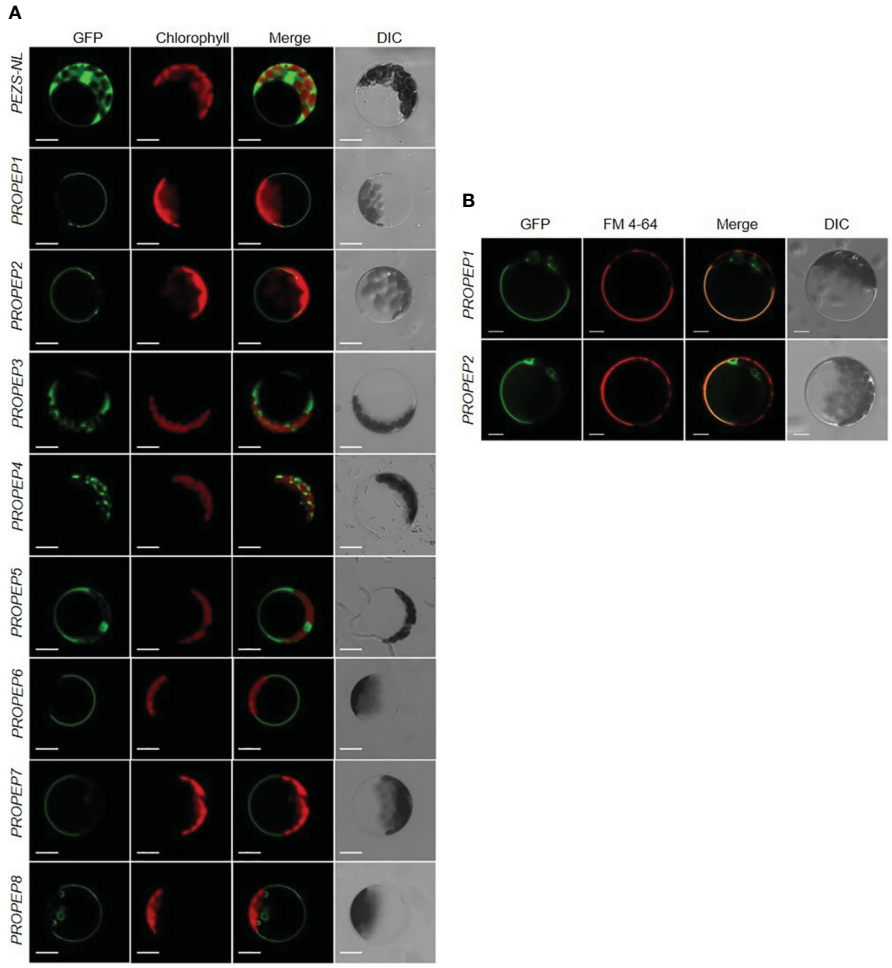

FIGURE 4
The subcellular localization assay of PROPEPs. **(A)** Arabidopsis mesophyll protoplasts were transiently transformed with a PEZS-NL vector expressed GFP signaling as the control. The coding sequence without the stop codon of *PROPEP1* to *PROPEP8* were cloned into pEZS-NL vector and transiently transformed into *Arabidopsis* mesophyll protoplasts. Columns from left to right show GFP signals (GFP), chlorophyll autofluorescence (Chlorophyll), merged images of GFP and chlorophyll (Merge), and bright-field differential interference contrast (DIC). Bars =5 μm. **(B)** FM 4-64 signaling was co-expressed with *PROPEP1-GFP* and PROPEP2-GFP in *Arabidopsis* protoplasts. The PROPEP1 and PROPEP2 fused GFP protein were transiently transformed into *Arabidopsis* mesophyll protoplasts and stained with 1 μM FM4-64 for 15 s before photographed. Columns from left to right show GFP signals (GFP), FM 4-64 fluorescence signals (FM 4-64), merged images of GFP and FM 4-64 (Merge), and bright-field differential interference contrast (DIC). Bars =5 μm.

and *GL2* expression levels. Furthermore, all *PROPEP*-overexpressing (OE) lines showed increased *CPC* expression and decreased *GL2* mRNA levels (Supplementary Figures 11A, B), further supporting the notion that *PROPEP*s regulate the *CPC* and *GL2* expression.

We also examined mutant plants for *cpc* and *gl2*. Consistent with previous research, *cpc* mutant seedlings had sparse root hairs, while *gl2* mutants had more root hairs than WT plants (Masucci et al., 1996; Wada et al., 2002). The expression of *PROPEP2* in *cpc* and *gl2* mutant did not show significant differences compared with this in WT root (Supplementary Figure 11C). After Pep2 treatment, the increase in root hair density induced by Pep2 was compromised in *cpc* mutants, although Pep2-triggered root hair elongation persisted (Figures 6D–F), suggesting that *CPC* acts downstream of Pep2 signal to regulates the root hair formation. However, the root hair density in *gl2* mutant was further increased after Pep2 treatment, which displays significant difference compared with this in WT root (Figures 6D–F).

2.4 Calcium signaling may be involved in *PROPEP2*-mediated root hair growth

Root hair growth is a finely tuned process in plants, regulated by a multitude of factors such as reactive oxygen species (ROS), cytoskeletal dynamics, and calcium signaling (Dunand et al., 2007; Pei et al., 2012; Zhang et al., 2016; Tan et al., 2019). Among these factors, the role of calcium, especially at the root hair tip, is critical for the elongation of these tubular cells (Takeda et al., 2008; Tan et al., 2019). To examine the link between Pep2 action and Ca signaling, we first observed that a reduction in calcium levels within the growth medium had an inhibitory effect on both the initiation and elongation of root hairs in wild-type (WT) seedlings (Figures 7A–C). Strikingly, the *propep2* mutant exhibited a complete absence of root hairs under conditions of reduced calcium availability (Figures 7A–C). Subsequently, we introduced the calcium-specific chelator EGTA into the growth medium. As

10.3389/fpls.2024.1336129

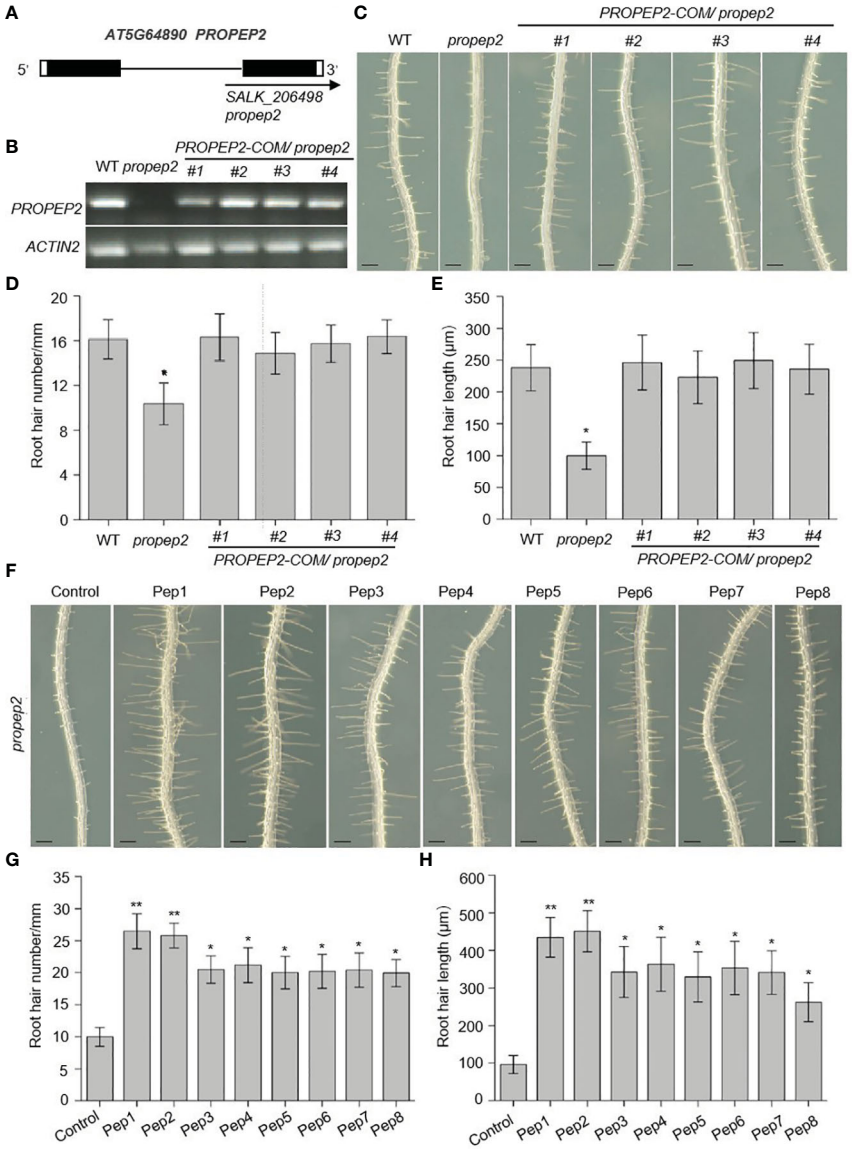

FIGURE 5
PROPEP2 regulates the root hair development. **(A)** Schematic map of T-DNA insertion location of *propep2* mutant. Black boxes, lines, and arrow represent exons, introns, and the position of the T-DNA insertion, respectively. The while boxes indicate the 5'or 3'UTRs. **(B)** RT-PCR analysis of the transcriptional level of *PROPEP2* in WT, *propep2* mutant and four independent complementation lines transformed with *PROPEP2* genomic DNA into *propep2* mutant (*PROPEP2-COM/propep2*). *Actin2* was used as internal standards. **(C)** The growth phenotype of root hairs in wild type (WT), *propep2* mutant and four *PROPEP2-COM/propep2* complementation lines. Four-day-old WT plants were transplanted on half-strength Murashige and Skoog (MS) agar medium for 48 h. Bars = 200 μm. **(D, E)** Statistics of the root hair number **(D)** and root hair length **(E)** as in **(C)**. Data are means ± SD (n = 15 roots per treatment). **(F)** The growth phenotype of root hairs in *propep2* mutant under Pep1-Pep8 treatment. Four-day-old plants were transplanted on half-strength Murashige and Skoog (MS) agar medium supplemented with or without 10 nM Pep1 to Pep8 for 48 h. Bars = 200 μm. **(G, H)** Statistics of the root hair number **(G)** and root hair length **(H)** as in **(F)**. Data are means ± SD (n = 15 roots per treatment). Asterisks in **(D, E, G, H)** indicate statistically significant differences compared with the control. (Tukey's test; *p < 0.05, **p < 0.01).

the EGTA concentration increased, both root hair density and length in WT roots progressively decreased, ultimately leading to a complete absence of root hairs when EGTA concentrations reached 500 mM (Supplementary Figure 12). Concurrently, the effectiveness of Pep2 in promoting root hair growth diminished with the introduction of EGTA. Similarly, the *propep2* mutant encountered significant challenges in root hair development when exposed to EGTA concentrations exceeding 50 mM. However, the supplementation of Pep2 partially reinstated root hair growth in the mutant, although to a lesser extent than observed in WT seedlings (Supplementary Figure 12). These findings implied the pivotal role of external calcium availability in facilitating Pep2-induced root hair growth.

To delve deeper into the calcium dynamics occurring within root hairs, we introduced a fluorescent protein-based $[Ca^{2+}]_{cytosol}$ sensor, GCaMP6 (Gao et al., 2023). The GCaMP6 was expressed in WT plant under the control of the *UBQ10* promoter (Gao et al., 2023). To generate *PROPEP2-OE*/GCaMP6 plants, we utilized the homozygous pUBQ10:GCaMP6/WT plant as the background and introduced the PROPEP2-OE construct. To generate pUBQ10:

10.3389/fpls.2024.1336129

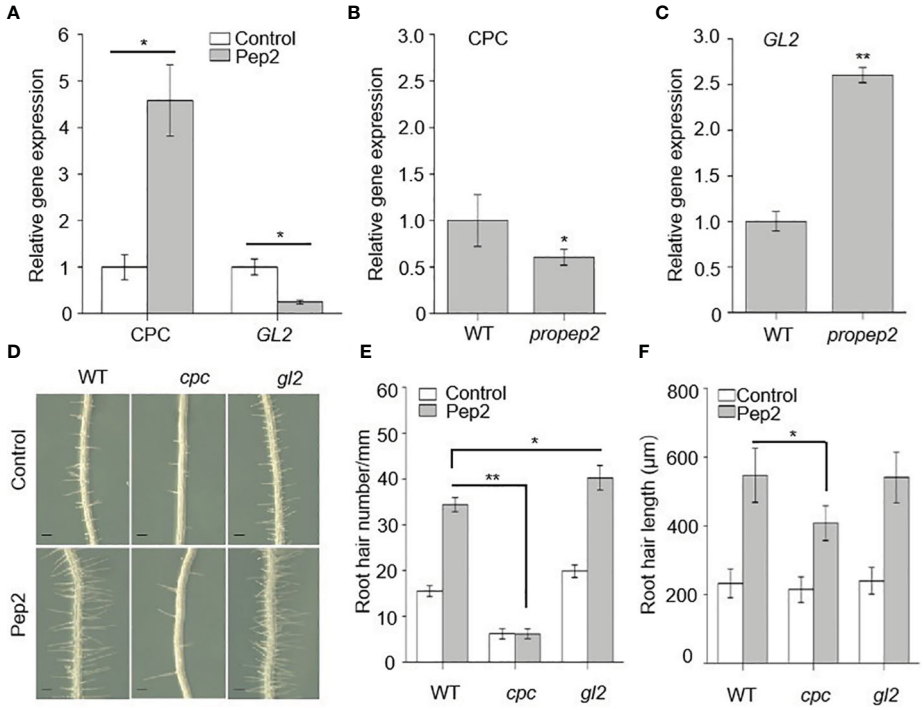

FIGURE 6
CPC and GL2 mediates the PROPEPs signals in root hair formation. **(A)** qRT-PCR analysis of *CPC* and *GL2* mRNA levels in wild type (WT) roots treated with 10 nM Pep2 for 24 h. The expression level of the untreated control (0 h) was set to 1.0, and Pep2 treatment levels were normalized to the control level. Data are means ± SD (n =3 individual reactions). **(B, C)** qRT-PCR analysis of *CPC* **(B)** and *GL2* **(C)** mRNA levels in 6-d-old WT and *propep2* roots. The expression level in WT root was set to 1.0. Data are means ± SD (n =3 individual reactions). **(D)** The growth phenotype of root hairs in wild type (WT), *cpc* and *gl2* mutant. Four-day-old plants were transplanted on half-strength Murashige and Skoog (MS) agar medium supplemented with or without 10 nm Pep2 for 48h. Bars = 200 μm. **(E, F)** Statistics of the root hair number **(E)** and root hair length **(F)** as in **(D)**. Data are means ± SD (n = 15 roots per treatment). Asterisks in **(A–C, E, F)** indicate statistically significant differences compared with the control. (Tukey's test; *p < 0.05, **p < 0.01).

GCaMP6/propep2 plants, we utilized the homozygous pUBQ10: GCaMP6/WT plant as the background and hybridized the pUBQ10:GCaMP6/WT with *propep2* mutant. As a result, the expression levels of GCaMP6 in various plant lines should be comparable. In *PROPEP2-OE* seedlings, the root hair tips exhibited significantly enhanced $[Ca^{2+}]_{cytosol}$ signals when compared to WT plants, both during the initiation and elongation stages of root hair growth (Figures 7D–F). Additionally, we generated *35S:PROPEP2-mRFP* transgenic plants, revealing extensive presence of PROPEP2 proteins in the root, including root hairs (Supplementary Figure 13). The $[Ca^{2+}]_{cytosol}$ signals in these plants were notably stronger than in WT, and these signals closely overlapped with PROPEP2-mRFP signals, emphasizing the correlation between *PROPEP2* expression and elevated $[Ca^{2+}]_{cytosol}$ levels (Supplementary Figure 13). Similarly, the application of Pep2 induced a substantial increase in $[Ca^{2+}]_{cytosol}$ levels, not only at the root hair tip but also throughout the entire root hair cell (Figure 7G; Supplementary Figure 14). These calcium dynamics were also observed with other Peps, mirroring the response to Pep2 (Supplementary Figure 14). In stark contrast, in the *propep2* mutant, there was an absence of discernible Ca^{2+} accumulation at the root hair tip (Figure 7G; Supplementary Figure 15). Moreover, the *PROPEP2* mutation resulted in a reduced response of Ca^{2+} elevation in root hairs to Pep2 compared to that in WT plants (Figure 7G; Supplementary Figure 15). We speculate that Pep2 intersects with Ca signaling to regulate root hair growth.

3 Discussion

Previous research has primarily focused on the immunomodulatory effects of Peps and their role in inhibiting overall root growth and have contributed significantly to our understanding of the functions of Peps in plant defense mechanisms. In this study, we demonstrate the multifaceted effects of Peps on root hair growth, unveil the expression patterns and subcellular localization of PROPEPs, and highlight the pivotal role of *PROPEP2* in this process. Additionally, we reveal the involvement of the CPC-GL2 module and calcium signature as downstream targets of PROPEPs/Peps in root hair differentiation, initiation, and elongation.

The development of plant root hairs is intricately regulated by a range of phytohormones, including auxins, ethylene, abscisic acid, and jasmonic acid. Phytohormones, notably auxins, primarily exert their influence on root hair development by promoting key processes such as root hair initiation, tip elongation, and the elongation of fully developed root hairs (Bruex et al., 2012; Lee

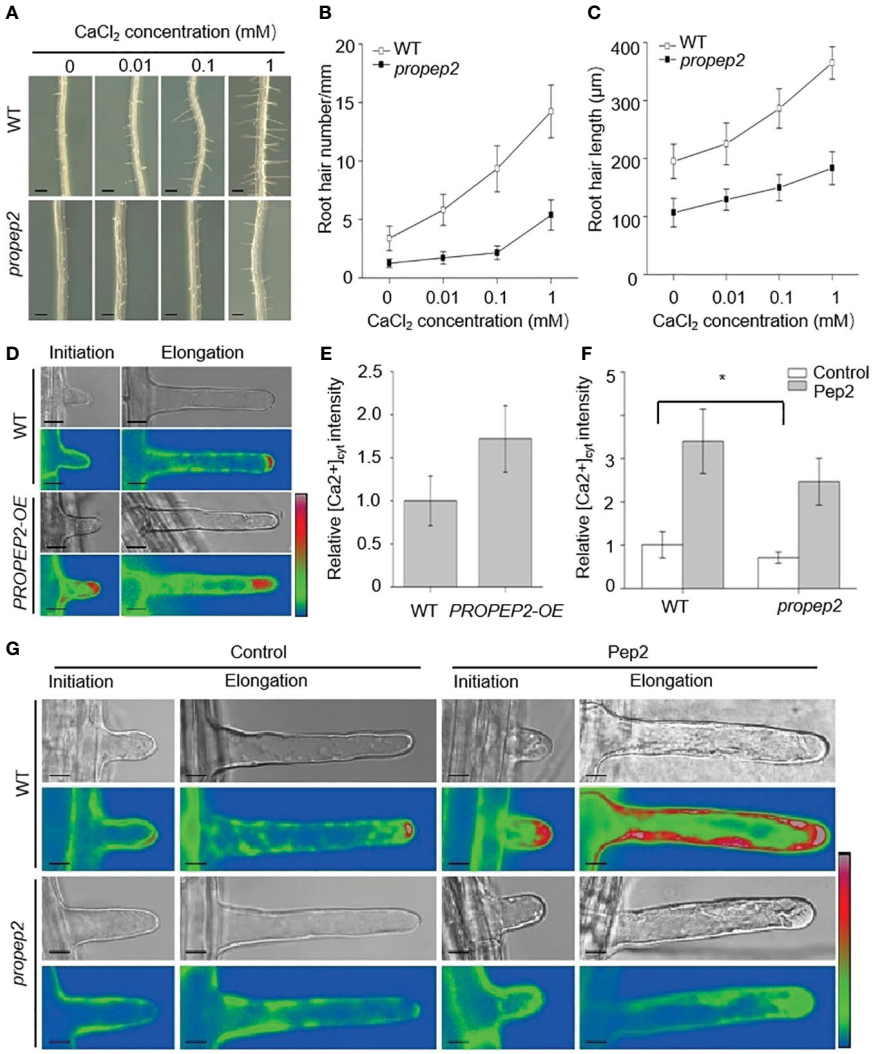

FIGURE 7
PROPEP2 mediates the root hair development dependent on Ca^{2+} concentrations changes. **(A)** The growth phenotype of root hairs in wild type (WT) and *propep2* mutant under $CaCl_2$ treatment. Four-day-old plants were transplanted on half-strength Murashige and Skoog (MS) agar medium supplemented with or without 0.01, 0.1 and 1mM CaCl2 for 48 h. Bars = 200 μm. **(B, C)** Statistics of the root hair number **(B)** and root hair length **(C)** as in **(A)**. Data are means ± SD (n = 15 roots per treatment). **(D)** Imaging of Ca^{2+} fluorescence signals in the initiation and elongation root hairs. The 6-day-old wild type (WT) and *PROPEP2*-overexpression line (*PROPEP2-OE*) expressing the genetically encoded intracellular Ca^{2+} indicator GCaMP6s were used. Bars = 10 μm. **(E)** Quantitative analysis of cytosolic Ca^{2+} signals in the elongation root hair as in **(D)**, Relative fluorescence was normalized against that in WT root hairs (1.0). Data are mean ± SD; (n = 35 root hairs of 10 roots per treatment). **(F)** Quantitative analysis of cytosolic Ca^{2+} signals in the elongation root hairs of WT and *propep2* plants, 6-day-old plants were transplanted on half-strength Murashige and Skoog (MS) agar medium supplemented with or without 10 nm Pep2 for 6 h. Relative fluorescence was normalized against that in WT root hairs without Pep2 treatment (1.0). Data are mean ± SD; (n = 35 root hairs of 10 roots per treatment). **(G)** Imaging of Ca^{2+} fluorescence signals in the initiation and elongation root hairs of WT and *propep2* plants. Six-day-old WT and *propep2* plants expressing GCaMP6s were transplanted on half-strength Murashige and Skoog (MS) agar medium supplemented with or without 10 nm Pep2 for 6 h. Bars = 10 μm. A pseudocolor scale bar for relative cytosolic Ca^{2+} level calibration in **(D, G)** is shown on the right. Asterisks in **(F)** indicate statistically significant differences compared with the untreated control. (Tukey's test; *p < 0.05).

and Cho, 2013; Zhang et al., 2016; Rymen et al., 2017). In addition to the pivotal role played by plant hormones in governing root hair development, recent scientific investigations have unveiled the significant involvement of hormone-like substances, specifically small peptides, in regulating various aspects of root hair development (Takahashi et al., 2019; Hsiao and Yamada, 2021). For instance, within plant cells, a class of small peptides known as Rapid Alkalinization Factors (RALFs) can be recognized by receptor-like kinases located in the plant cell membrane, such as FERONIA (FER) (Haruta et al., 2014). This recognition event triggers the formation of a protein complex involving FER and an intracellular receptor-like kinase called RIPK (Du et al., 2016). Together, they orchestrate the regulation of cytoplasmic alkalinization in root epidermal cells, consequently impacting the initiation of root hairs (Du et al., 2016). Another peptide, namely CLV3/ESR-related peptide 14 (CLE14), has been observed to enhance the expression of *CPC*, leading to the suppression of *GL2* transcription levels. This, in turn, promotes cell differentiation into hair cells, ultimately driving root hair development (Hayashi et al., 2018). In our study, we observed distinct tissue-specific expression

patterns of PROPEPs, and their proteins exhibited varying subcellular localization. Notably, the introduction of exogenous synthetic Peps (Pep1-8) or the utilization of transgenic PROPEPs-OE lines led to a significant enhancement in both root hair density and length in seedlings. These results imply that Pep/PROPEPs play a pivotal role throughout all stages of root hair development, and the subcellular localization of Pep may not be directly correlated with its function in regulating root hair growth. Notably, *propep2* mutant seedlings with impaired root hair growth displayed elevated *GL2* levels but reduced *CPC* expression compared to WT seedlings. In contrast, both the transgenic *PROPEP-OE* lines and seedlings treated with Pep2 exhibited higher *CPC* expression but lower *GL2* levels. These observations imply that, akin to CLE14 (Hayashi et al., 2018), Pep/PROPEPs promote the differentiation of root hair cells by modulating the CPC-GL2 regulatory module.

The polarization and growth of cells, such as pollen tubes and root hairs, have been demonstrated to coincide with highly organized and polarized cytoplasmic contents (Rosen et al., 1964; Emons, 1987). Calcium, among other factors, plays a crucial role in activating proteins and enzymes that contribute to the organization of cytoskeletal elements and membrane structures necessary for the development and maintenance of cell polarity (Bush, 1995). A localized gradient of cytoplasmic free Ca^{2+} toward the growing apex has been observed in growing root hairs and pollen tubes, and the intensity of this gradient correlates with the growth rate of these cells (Pierson et al., 1996; Felle and Hepler, 1997; Wymer et al., 1997). In line with this, the deprivation of calcium in the medium resulted in the inhibition of root hair growth in both *propep2* and WT plants. Conversely, either overexpression of *PROPEP2* or supplementation of Pep2 significantly enhanced the tip calcium gradient of root hairs (Figure 7). Exploring the calcium channels/transporters or calcium signature elements expressed in root hairs would be intriguing for further elucidating the crosstalk between calcium oscillation and Peps-triggered root hair growth.

Regarding the perception of Peps, it has been established that PEPR1 and PEPR2 serve as the principal receptors responsible for transmitting the Pep signal and triggering corresponding responses, albeit with varying affinities for different Peps. Notably, the mutation of PROPEP2 resulted in stunted root hair growth in plants. In contrast to the *propep2* mutant, neither *pepr1*, *pepr2*, nor the double mutant *pepr1 pepr2* displayed any discernible root hair deficit phenotype (Supplementary Figure 16). However, it is worth highlighting that exogenous application of Pep2 failed to stimulate root hair growth in *pepr1 pepr2*, underscoring the exclusive role of PEPR1/2 as the receptors for perceiving exogenous Peps (Supplementary Figure 16). Recent research introduced sucrose-induced receptor kinase 1 (SIRK1) as a novel receptor for Pep7, orchestrating sucrose-mediated water flux regulation and lateral root development (Wang et al., 2022). Consequently, we posit the existence of an unidentified perception system within the cell, which may facilitate the sensing of Peps and subsequently regulate root hair growth. In light of this, unraveling the signaling pathways downstream of Peps and PROPEPs becomes imperative for a holistic comprehension of root hair development. The identification of novel receptors and components participating in these pathways promises valuable insights into the mechanisms by which Peps govern root hair fate and growth.

4 Materials and methods

4.1 Plant materials and growth conditions

Arabidopsis (*Arabidopsis thaliana*) mutant lines *propep2* (SALK_206498), *cpc* (Wada et al., 2002), *gl2* (Wang et al., 2010) and transgenic line p*UBQ10:GCaMP6s* (Gao et al., 2023) were described previously. Homozygous mutant plants were identified by RT-PCR or DNA sequencing using primers described in Supplementary Table 1. The seedlings were grown on half-strength Murashige and Skoog (MS) medium, containing 1% sucrose and 0.8% phytogel (Sigma-Aldrich, St. Louis, MO, USA) in the growth chamber. The growth conditions had 90 μmol/m^2/s light intensity with a 16 h light/8 h dark photoperiod at 22°C.

4.2 Peptide synthesis

The peptides used in this study were synthesized by GL Biochem. The sequences (from the N terminus to the C terminus) were as follows:

Pep1, ATKVKAKQRGKEKVSSGRPGQHN;

Pep2, DNKAKSKKRDKEKPSSGRPGQTNSVPNAAIQVYKED;

Pep3, EIKARGKNKTKPTPSSGKGGKHN;

Pep4, GLPGKKNVLKKSRESSGKPGGTNKKPF;

Pep5, SLNVMRKGIRKQPVSSGKRGGVNDYDM;

Pep6, ITAVLRRRPRPPPYSSGRPGQNN;

Pep7, VSGNVAARKGKQQTSSGKGGGTN;

Pep8, GGVIVKSKKAARELPSSGKPGRRN;

4.3 Plasmid constructions and plant transformation

To produce transgenic *proPROPEP1:GUS* to *proPROPEP8:GUS* lines, the promoter regions upstream of the start codons of *PROPEP1* (1640-bp), *PROPEP2* (765-bp), *PROPEP3* (1437-bp), *PROPEP4* (1197-bp), *PROPEP5* (798-bp), *PROPEP6* (1707-bp), *PROPEP7* (1170-bp), *PROPEP8* (678-bp) were amplified and cloned into the *p*CAMBIA1300-GUS binary vector. For the transgenic PROPEP1 to PROPEP8 over-expression lines (termed as PROPEP1-OE to PROPEP8-OE), the coding sequence (CDS) without the stop codon of *PROPEP1* to *PROPEP8* were cloned into pEZS-NL to generate 35S-PROPEPs-GFP constructs and then cloned into the pART27 binary vector. The constructs were transformed into *Agrobacterium tumefaciens* strain GV3101 and further transformed into wild type plants using the floral-dip method (Clough and Bent, 1998). For construction of the genetic PROPEP2-OE harboring *GCaMP6s*, the CDS without the stop codon of *PROPEP2* was cloned into pEZS-NL to fuse with mRFP. The 35S-PROPEPs-mRFP construct was cloned into pART27

binary vector and then transformed into *pUBQ10:GCaMP6s* plants through GV3101 infection of floral-dip.

For construction of the genetic *PROPEP2* complementary lines (termed as *PROPEP2-COM*/*propep2*), the full-length genomic DNA of the PROPEP2 fragment (a 1557-bp fragment containing a 590-bp promoter and a 967-bp genomic region from translation initiation codon to 3' UTR domain) was amplified from the genomic DNA of wild-type seedlings and cloned into the binary vector pCAMBIA-1300. Then, the recombinant plasmid was transformed into the *Agrobacterium tumefaciens* strain GV3101 and further transformed into the propep2 mutant using the floral-dip method. The primers used to produce the constructs are listed in Supplementary Table 1.

4.4 Root hairs growth analyze

The root hairs growth was analyzed as previously described (Tan et al., 2019) with modifications. In brief, 4-day-old seedlings were transferred onto half-strength MS agar medium supplemented with different treatment conditions, and the plates were placed vertically in growth room for another 48h. The roots were covered by cover glass to push the angle of root hairs parallel to the surface of solid medium. Roots were photographed under an SZX16 microscope (Olympus). The 2 mm root hair distribution zone, which located 0.5 cm far away from the root tip was counted by using Image J software to analyze the root hairs length and root hair number. No less than 15 roots were analyzed for each treatment, three independent repetitions were performed.

4.5 RT-PCR and qRT-PCR analysis

Total RNA in roots were extracted using the TRIzol reagent (Invitrogen, Carlsbad, CA, USA), according to the manufacturer's protocol. Two μg RNA was used to synthesis the cDNA by using M-MLV Reverse Transcriptase (Promega, Madison, WI, USA). Real time qRT-PCR analysis was performed using the FastStart Universal SYBR Green mastermix (Roche Diagnostics, Hong Kong) on a CFX Connect Real Time System (Bio-Rad, Berkeley, CA, USA) using *Actin2* as internal standards. All individual reactions were performed in triplicate. The primers used are listed in Supplementary Table.

4.6 Histochemical GUS analysis

GUS activity was detected by histochemical staining of tissues as previously described (Liu et al., 2015). Briefly, T2 transgenic seedlings were incubated in GUS staining solution (2 mM 5-bromo-4-chloro-3-indolyl-b-D-glucuronide, 1 mM $K_3Fe(CN)_6$, 1 mM $K_4Fe(CN)_6{\cdot}3H_2O$, 10 mM Na_2EDTA, 0.1% Triton X-100, and 50 mM Na_3PO_4, pH 7.0) at 37°C for 6 h. After the tissue with 75% (vol/vol) ethanol was sufficiently decolorized to remove chlorophyll, individual representative plant tissues, the roots and root hairs were photographed under a microscope (Olympus, SZX16) equipped with a camera.

4.7 Subcellular localization assays in planta

Subcellular localization assays were performed as previously described (Mao et al., 2014) with slight modifications. Briefly, 4-week-old Arabidopsis rosette leaves were digested by Cellulase R-10 and Macerozyme R-10 (Yakult Pharmaceutical) to prepare the mesophyll protoplasts. The protoplasts were resuspended with suspension solution (154 mM NaCl, 125 mM $CaCl_2$, 5 mM KCl, 2 mM 4-Morpholineethanesulfonic acid (MES) adjusted to pH 5.7 with KOH) and further transfected with 20 μg recombinant plasmid DNA (PROPEP1 to PROPEP8-pEZS-NL-GFP) by using polyethylene glycol-mediated transformation protocol (Sheen, 2001). The transformed protoplasts were incubated in the dark at 23°C for 16 h before confocal imaging analysis. Imaging was performed on an LSM-710 argon/krypton laser scanning confocal microscope (Zeiss) with a 63 × objective. FM 4-64 excitation at 514 nm and emission at 600-700 nm. GFP signals were excited at 488 nm wavelength and collected emission between 495 and 550 nm. Z-stack images were collected with 1 μm steps and the scan speed was 8 s/scan.

4.8 Root hairs calcium imaging

For Peps-induced root hairs $[Ca^{2+}]_{cytosol}$ signals assays, the 6-day-old seedlings expressing GCaMP6s were supplemented with or without Peps for 6 h, the root hairs harboring GCaMP6s were monitored by a LSM-710 confocal microscope with a 20 × objective. The interval of data acquisition was 10 seconds, the Z-stack images were acquired from top to bottom of the cells with 1 μm steps and the scan speed was 6 s/scan. The excitation wavelengths for $[Ca^{2+}]_{cytosol}$ fluorescence signals was 488 nm. To quantitatively analyze fluorescence intensity, confocal images were captured under strictly identical acquisition parameters, which included laser power, photomultiplier settings, offset, zoom factor, and resolution, across all experimental root samples. The fluorescence intensity was analyzed by Image J software.

4.9 Statistical analysis

For all experiments, three independent repetitions were performed. One way ANOVA Tukey's test was used for statistical analysis. Asterisks in the figures denote significant differences as follows: *$P < 0.05$, **$P < 0.01$, and ***$P < 0.001$.

Data availability statement

The original contributions presented in the study are included in the article/Supplementary Material. Further inquiries can be directed to the corresponding authors.

Author contributions

YJ: Conceptualization, Data curation, Formal analysis, Funding acquisition, Investigation, Writing – original draft, Writing – review & editing. FZ: Data curation, Writing – original draft, Writing – review & editing. KL: Data curation, Writing – review & editing. FS: Data curation, Writing – review & editing. CS: Investigation, Writing – review & editing. XYZ: Investigation, Writing – review & editing. MX: Writing – original draft, Writing – review & editing. AF: Writing – original draft, Writing – review & editing. JC: Conceptualization, Formal analysis, Funding acquisition, Writing – original draft, Writing – review & editing. XJZ: Conceptualization, Data curation, Formal analysis, Funding acquisition, Writing – original draft, Writing – review & editing. SL: Conceptualization, Project administration, Resources, Supervision, Writing – original draft, Writing – review & editing. RS: Data curation, Writing – review & editing.

Funding

The author(s) declare financial support was received for the research, authorship, and/or publication of this article. This work was supported by Nation Nature Science Foundation of China (31900223 to XJZ, 32000201 to JC, and 32200258 to YJ), Basic Research Program of Shaanxi Province (22JHQ061 to XJZ), the Natural Science Foundation of Jiangsu Province (BK20211319 to JC), Qinchuangyuan Recruited High-level Innovation and Entrepreneurship Talents Project of Science and Technology Department of Shaanxi Province (QCYRCXM-2022-223 to XJZ), and the China Postdoctoral Science Foundation (2020M673626XB to YJ).

Conflict of interest

The authors declare that the research was conducted in the absence of any commercial or financial relationships that could be construed as a potential conflict of interest.

Publisher's note

Supplementary material

The Supplementary Material for this article can be found online at: https://www.frontiersin.org/articles/10.3389/fpls.2024.1336129/full#supplementary-material

References

Bartels, S., and Boller, T. (2015). Quo vadis, Pep? Plant elicitor peptides at the crossroads of immunity, stress, and development. *J. Exp. Bot.* 66, 5183–5193. doi: 10.1093/jxb/erv180

Bartels, S., Lori, M., Mbengue, M., van Verk, M., Klauser, D., Hander, T., et al. (2013). The family of Peps and their precursors in Arabidopsis: Differential expression and localization but similar induction of pattern-triggered immune responses. *J. Exp. Bot.* 64, 5309–5321. doi: 10.1093/jxb/ert330

Beck, M., Wyrsch, I., Strutt, J., Wimalasekera, R., Webb, A., Boller, T., et al. (2014). Expression patterns of flagellin sensing 2 map to bacterial entry sites in plant shoots and roots. *J. Exp. Bot.* 65, 6487–6498. doi: 10.1093/jxb/eru366

Bernhardt, C., Lee, M. M., Gonzalez, A., Zhang, F., Lloyd, A., and Schiefelbein, J. (2003). The bHLH genes GLABRA3 (GL3) and ENHANCER OF GLABRA3 (EGL3) specify epidermal cell fate in the Arabidopsis root. *Development* 130, 6431–6439. doi: 10.1242/dev.00880

Boller, T., and Felix, G. (2009). A renaissance of elicitors: Perception of microbe-associated molecular patterns and danger signals by pattern-recognition receptors. *Annu. Rev. Plant Biol.* 60, 379–406. doi: 10.1146/annurev.arplant.57.032905.105346

Bruex, A., Kainkaryam, R. M., Wieckowski, Y., Kang, Y. H., Bernhardt, C., Xia, Y., et al. (2012). A gene regulatory network for root epidermis cell differentiation in Arabidopsis. *PloS Genet.* 8, e1002446. doi: 10.1371/journal.pgen.1002446

Bush, D. (1995). Calcium regulation in plant cells and its role in signaling. *Annu. Rev. Plant Physiol. Plant Mol. Biol.* 46, 95–122. doi: 10.1146/annurev.pp.46.060195.000523

Clough, S., and Bent, A. (1998). Floral dip: A simplified method for Agrobacterium-mediated transformation of *Arabidopsis thaliana*. *Plant J.* 16, 735–743. doi: 10.1046/j.1365-313x.1998.00343.x

Datta, S., Kim, C., Pernas, M., Pires, N., Hélène, P., Tam, T., et al. (2011). Root hairs: development, growth and evolution at the plant-soil interface. *Plant Soil.* 346, 1–14. doi: 10.1007/s11104-011-0845-4

Di Cristina, M., Sessa, G., Dolan, L., Linstead, P., Baima, S., Ruberti, I., et al. (1996). The Arabidopsis Athb-10 (GLABRA2) is an HD-Zip protein required for regulation of root hair development. *Plant J.* 10, 393–402. doi: 10.1046/j.1365-313X.1996.10030393.x

Du, C., Li, X., Chen, J., Chen, W., Li, B., Li, C., et al. (2016). Receptor kinase complex transmits RALF peptide signal to inhibit root growth in Arabidopsis. *Proc. Natl. Acad. Sci. U.S.A.* 113 (51), 8326–8334.

Dunand, C., Crèvecoeur, M., and Penel, C. (2007). Distribution of superoxide and hydrogen peroxide in Arabidopsis root and their influence on root development: Possible interaction with peroxidases. *New Phytol.* 174, 332–341. doi: 10.1111/j.1469-8137.2007.01995.x

Emons, A. (1987). The cytoskeleton and secretory vesicles in root hairs of Equisetum and Limnobium and cytoplasmic streaming in root hairs of Equisetum. *Ann. Bot.* 60, 625–632. doi: 10.1093/oxfordjournals.aob.a087492

Endo, S., Betsuyaku, S., and Fukuda, H. (2014). Endogenous peptide ligand-receptor systems for diverse signaling networks in plants. *Curr. Opin. Plant Biol.* 21, 140–146. doi: 10.1016/j.pbi.2014.07.011

Felle, H., and Hepler, P. (1997). The cytosolic Ca^{2+}-concentration gradient of Sinapis alba root hairs as revealed by Ca^{2+}-selective microelectrode tests and fura-dextran ratio imaging. *Plant Physiol.* 114, 39–45. doi: 10.1104/pp.114.1.39

Galway, M., Masucci, J., Lloyd, A., Walbot, V., Davis, R., and Schiefelbein, J. (1994). The TTG gene is required to specify epidermal cell fate and cell patterning in the Arabidopsis root. *Dev. Biol.* 166, 740–754. doi: 10.1006/dbio.1994.1352

Gao, Q., Wang, C., Xi, Y., Shao, Q., Hou, C., Li, L., et al. (2023). RALF signaling pathway activates MLO calcium channels to maintain pollen tube integrity. *Cell Res.* 33, 71–79. doi: 10.1038/s41422-022-00754-3

Grierson, C., Nielsen, E., Ketelaarc, T., and Schiefelbein, J. (2014). Root hairs. *Arabidopsis Book*. doi: 10.1199/tab.0172

Haruta, M., Sabat, G., Stecker, K., Minkoff, B., and Sussman, M. (2014). A peptide hormone and its receptor protein kinase regulate plant cell expansion. *Science* 343, 408–411. doi: 10.1126/science.1244454

Hayashi, N., Tetsumura, T., Sawa, S., Wada, T., and Tominaga-Wada, R. (2018). CLE14 peptide signaling in *Arabidopsis* root hair cell fate determination. *Plant Biotechnol.* 35, 17–22. doi: 10.5511/plantbiotechnology.18.0122a

Hsiao, Y., and Yamada, M. (2021). The roles of peptide hormones and their receptors during plant root development. *Genes* 12, 22. doi: 10.3390/genes12010022

Huffaker, A., Pearce, G., and Ryan, C. (2006). An endogenous peptide signal in Arabidopsis activates components of the innate immune response. *Proc. Natl. Acad. Sci. U.S.A.* 103, 10098–10103. doi: 10.1073/pnas.0603727103

Huffaker, A., Pearce, G., Veyrat, N., Erb, M., Turlings, T., Sartor, R., et al. (2013). Plant elicitor peptides are conserved signals regulating direct and indirect antiherbivore defense. *Proc. Natl. Acad. Sci. U.S.A.* 110, 5707–5712. doi: 10.1073/pnas.1214668110

Jing, Y., Shen, N., Zheng, X., Fu, A., Zhao, F., Lan, W., et al. (2020). Danger-associated peptide regulates root immune responses and root growth by affecting ROS formation in Arabidopsis. *Int. J. Mol. Sci.* 21, 4590. doi: 10.3390/ijms21134590

Jing, Y., Zheng, X., Zhang, D., Shen, N., Wang, Y., Yang, L., et al. (2019). Danger-associated peptides interact with PIN-dependent local auxin distribution to inhibit root growth in Arabidopsis. *Plant Cell* 31, 1767–1787. doi: 10.1105/tpc.18.00757

Jing, Y., Zou, X., Sun, C., Qin, X., and Zheng, X. (2023). Danger-associate Peptide regulates root immunity in Arabidopsis. *Biochem. Biophys. Res. Commun.* 663, 163–170. doi: 10.1016/j.bbrc.2023.04.091

Kim, C., and Dolan, L. (2011). Root hair development involves asymmetric cell division in Brachypodium distachyon and symmetric division in Oryza sativa. *New Phytol.* 192 (3), 601–610.

Kim, D., Lee, S., Choi, S., Won, S., Heo, Y., Cho, M., et al. (2006). Functional conservation of a root hair cell-specific cis-element in angiosperms with different root hair distribution patterns. *Plant Cell.* 18, 2958–2970. doi: 10.1105/tpc.106.045229

Kirik, V., Simon, M., Huelskamp, M., and Schiefelbein, J. (2004). The ENHANCER OF TRY AND CPC1 gene acts redundantly with TRIPTYCHON and CAPRICE in trichome and root hair cell patterning in Arabidopsis. *Dev. Biol.* 268, 506–513. doi: 10.1016/j.ydbio.2003.12.037

Klauser, D., Desurmont, G., Glauser, G., Vallat, A., Flury, P., Boller, T., et al. (2015). The Arabidopsis Pep-PEPR system is induced by herbivore feeding and contributes to JA-mediated plant defence against herbivory. *J. Exp. Bot.* 66, 5327–5336. doi: 10.1093/jxb/erv250

Lee, R., and Cho, H. (2013). Auxin, the organizer of the hormonal/environmental signals for root hair growth. *Front. Plant Sci.* 4, 448. doi: 10.3389/fpls.2013.00448

Liu, J., Yang, L., Luan, M., Wang, Y., Zhang, C., Zhang, B., et al. (2015). A vacuolar phosphate transporter essential for phosphate homeostasis in Arabidopsis. *Proc. Natl. Acad. Sci. U.S.A.* 112, E6571–E6578. doi: 10.1073/pnas.1514598112

Ma, C., Guo, J., Kang, Y., Doman, K., Bryan, A. C., Tax, F., et al. (2014). AtPEPTIDE RECEPTOR2 mediates the AtPEPTIDE1-induced cytosolic Ca^{2+} rise, which is required for the suppression of glutamine dumper gene expression in Arabidopsis roots. *J. Integr. Plant Biol.* 56, 684–694. doi: 10.1111/jipb.12171

Macho, A., and Zipfel, C. (2014). Plant PRRs and the activation of innate immune signaling. *Mol. Cell.* 54, 263–272. doi: 10.1016/j.molcel.2014.03.028

Mao, D., Chen, J., Tian, L., Liu, Z., Yang, L., Tang, R., et al. (2014). Arabidopsis transporter MGT6 mediates magnesium uptake and is required for growth under magnesium limitation. *Plant Cell.* 26, 2234–2248. doi: 10.1105/tpc.114.124628

Masucci, J., Rerie, W., Foreman, D., Zhang, M., Galway, M., Marks, M., et al. (1996). The homeobox gene GLABRA2 is required for position-dependent cell differentiation in the root epidermis of Arabidopsis thaliana. *Development* 122, 1253–1260. doi: 10.1242/dev.122.4.1253

Millet, Y., Danna, C., Clay, N., Songnuan, W., Simon, M., Werck-Reichhart, D., et al. (2010). Innate immune responses activated in Arabidopsis roots by microbe-associated molecular patterns. *Plant Cell.* 22, 973–990. doi: 10.1105/tpc.109.069658

Pei, W., Du, F., Zhang, Y., He, T., and Ren, H. (2012). Control of the actin cytoskeleton in root hair development. *Plant Sci.* 187, 10–18. doi: 10.1016/j.plantsci.2012.01.008

Pierson, E., Miller, D., Callaham, D., van Aken, J., Hackett, G., and Hepler, P. (1996). Tip-localized calcium entry fluctuates during pollen tube growth. *Dev. Biol.* 174, 160–173. doi: 10.1006/dbio.1996.0060

Rosen, W., Gawlik, S., Dashek, W., and Siegesmund, K. (1964). Fine structure and cytochemistry of Lilium pollen tubes. *Am. J. Bot.* 51, 61–71. doi: 10.1002/j.1537-2197.1964.tb06601.x

Rymen, B., Kawamura, A., Sabine, S., Breuer, C., and Iwase, A. (2017). ABA suppresses root hair growth via the OBP4 transcriptional regulator. *Plant Physiol.* 173, 1750–1762. doi: 10.1104/pp.16.01945

Schellmann, S., Schnittger, A., Kirik, V., Wada, T., Okada, K., Beermann, A., et al. (2002). TRIPTYCHON and CAPRICE mediate lateral inhibition during trichome and root hair patterning in Arabidopsis. *EMBO J.* 21, 5036–5046. doi: 10.1093/emboj/cdf524

Schiefelbein, J. (2003). Cell-fate specification in the epidermis: a common patterning mechanism in the root and shoot. *Curr. Opin. Plant Biol.* 6, 74–78. doi: 10.1016/S136952660200002X

Sheen, J. (2001). Signal transduction in maize and Arabidopsis mesophyll protoplasts. *Plant Physiol.* 127, 1466–1475. doi: 10.1104/pp.010820

Shen, N., Jing, Y., Tu, G., Fu, A., and Lan, W. (2020). Danger-associated peptide regulates root growth by promoting protons extrusion in an AHA2-dependent manner in arabidopsis. *Int. J. Mol. Sci.* 21, 7963. doi: 10.3390/ijms21217963

Takahashi, F., Hanada, K., Kondo, T., and Shinozaki, K. (2019). Hormone-like peptides and small coding genes in plant stress signaling and development. *Curr. Opin. Plant Biol.* 51, 88–95. doi: 10.1016/j.pbi.2019.05.011

Takeda, S., Gapper, C., Kaya, H., Bell, E., Kuchitsu, K., and Dolan, L. (2008). Local positive feedback regulation determines cell shape in root hair cells. *Science* 319, 1241–1244. doi: 10.1126/science.1152505

Tan, Y., Yang, Y., Zhang, A., Fei, C., Gu, L., Sun, S., et al. (2019). Three CNGC family members, CNGC5, CNGC6, and CNGC9, are required for constitutive growth of arabidopsis root hairs as ca^{2+}-permeable channels. *Plant Commun.* 1, 100001. doi: 10.1016/j.xplc.2019.100001

Tominaga-Wada, R., Nukumizu, Y., Sato, S., and Wada, T. (2013). Control of plant trichome and root-hair development by a tomato (Solanum lycopersicum) R3 MYB transcription factor. *PloS One* 8, e54019. doi: 10.1371/journal.pone.0054019

Wada, T., Kurata, T., Tominaga, R., Koshino-Kimura, Y., Tachibana, T., Goto, K., et al. (2002). Role of a positive regulator of root hair development, CAPRICE, in Arabidopsis root epidermal cell differentiation. *Development* 129, 5409–5419. doi: 10.1242/dev.00111

Wada, T., Tachibana, T., Shimura, Y., and Okada, K. (1997). Epidermal cell differentiation in Arabidopsis determined by a Myb homolog, CPC. *Science* 277, 1113–1116. doi: 10.1126/science.277.5329.1113

Wang, J., Xi, L., Wu, X., Konig, S., Rohr, L., Neumann, T., et al. (2022). PEP7 acts as a peptide ligand for the receptor kinase SIRK1 to regulate aquaporin-mediated water influx and lateral root growth. *Mol. Plant* 15, 1615–1631. doi: 10.1016/j.molp.2022.09.016

Wang, S., Barron, C., Schiefelbein, J., and Chen, J. (2010). Distinct relationships between GLABRA2 and single-repeat R3 MYB transcription factors in the regulation of trichome and root hair patterning in Arabidopsis. *New Phytol.* 185, 387–400. doi: 10.1111/j.1469-8137.2009.03067.x

Wymer, C., Bibikova, T. N., and Gilroy, S. (1997). Cytoplasmic free calcium distribution during the development of root hairs of Arabidopsis thaliana. *Plant J.* 12, 427–439. doi: 10.1046/j.1365-313X.1997.12020427.x

Yamaguchi, Y., Huffaker, A., Bryan, A., Tax, F., and Ryan, C. (2010). PEPR2 is a second receptor for the Pep1 and Pep2 peptides and contributes to defense responses in Arabidopsis. *Plant Cell.* 22, 508–522. doi: 10.1105/tpc.109.068874

Yamaguchi, Y., Pearce, G., and Ryan, C. (2006). The cell surface leucine-rich repeat receptor for AtPep1, an endogenous peptide elicitor in Arabidopsis, is functional in transgenic tobacco cells. *Proc. Natl. Acad. Sci. U.S.A.* 10, 10104–10109. doi: 10.1073/pnas.0603729103

Zhang, S., Huang, L., Yan, A., Liu, Y., Liu, B., Yu, C., et al. (2016). Multiple phytohormones promote root hair elongation by regulating a similar set of genes in the root epidermis in Arabidopsis. *J. Exp. Bot.* 67, 6363–6372. doi: 10.1093/jxb/erw400

Zheng, X., Kang, S., Jing, Y., Ren, Z., Li, L., Zhou, J., et al. (2018). Danger-associated peptides close stomata by OST1-independent activation of anion channels in guard cells. *Plant Cell* 30, 1–18. doi: 10.1105/tpc.17.00701

frontiers | Frontiers in Plant Science

TYPE Original Research
PUBLISHED 05 July 2024
DOI 10.3389/fpls.2024.1397058

OPEN ACCESS

EDITED BY
Neelima Roy Sinha,
University of California, Davis, United States

REVIEWED BY
Tian Li,
Chinese Academy of Agricultural Sciences, China
Chuan Xia,
Chinese Academy of Agricultural Sciences (CAAS), China

*CORRESPONDENCE
Yan Zhang
zhangyanhfnu@gmail.com
Lingling Li
lingiae@163.com

RECEIVED 06 March 2024
ACCEPTED 03 June 2024
PUBLISHED 05 July 2024

CITATION
Wang H, Wei B, Qi L, Chen Y, Chen K, Liu D, Su X, Zhang Y and Li L (2024) Deciphering the maize gene ZmGF14–3: implications for plant height based on co-expression networks. *Front. Plant Sci.* 15:1397058. doi: 10.3389/fpls.2024.1397058

Deciphering the maize gene ZmGF14–3: implications for plant height based on co-expression networks

Hengsheng Wang[1,2,3], Bo Wei[4], Lulu Qi[1,2], Yansong Chen[1,2], Kelong Chen[3], Dong Liu[5], Xu Su[6], Yan Zhang[1,2]* and Lingling Li[1,2]*

[1]School of Biological and Food Engineering, Hefei Normal University, Hefei, Anhui, China, [2]Blueberry Engineering Technology Research Center of Anhui, Hefei Normal University, Hefei, Anhui, China, [3]College of Geographic Sciences, Qinghai Normal University, Xining, Qinhai, China, [4]School of Biology, Food and Environment, Hefei University, Hefei, Anhui, China, [5]Department of Horticulture and Landscape, Anqing Vocational and Technical College, Anqing, Anhui, China, [6]Key Laboratory of Biodiversity Formation Mechanism and Comprehensive Utilization of the Qinghai-Tibet Plateau in Qinghai Province, Qinghai Normal University, Xining, Qinhai, China

The evolutionary analysis showed that the GF14 family was conserved, however, there was limited evidence linking GF14s to plant height. In our investigations, we discovered a co-expression relationship between ZmGF14s and functionally characterized genes linked to plant height. In the co-expression network, we identified ZmGF14-3, a gene expression exhibiting a positive correlation with plant height in three maize varieties, we postulated that this gene could be intimately linked to plant height development. Subsequently, we cloned ZmGF14-3 from the maize B73 inbred line and overexpressed it in *Arabidopsis*, resulting in markedly dwarfed transgenic phenotypes. Measurements of endogenous phytohormones disclosed a significant reduction in concentrations of Gibberellic Acid 7 (GA_7) and Indole-3-Acetic Acid (IAA) in the overexpressed *Arabidopsis*, furthermore, qPCR results highlighted a pronounced decrease in the expression levels of plant height-related genes when compared to the wild type, therefore, it is plausible to posit that ZmGF14-3 plays a pivotal role in regulating the growth and development of maize through interactions with various phytohormone-related genes. Thus, delving into the potential interactions between ZmGF14-3 and these genes holds the promise of yielding valuable insights into the molecular mechanisms underpinning plant height development in maize.

KEYWORDS

plant height, ZmGF14-3, co-expression network, qRT-PCR, endogenous phytohormones

1 Introduction

In the past few decades, the increase in maize yield per unit area has primarily been attributed to higher planting density, rather than an enhancement in yield potential per plant (Sun et al., 2023). Maize have been adapted for high-density planting, however, high-density planting often makes plants susceptible to lodging, and reduce the yield. To counteract this issue, one cultivation strategy has been to adjust the plant height of maize within a suitable range, plant height is also an important grain yield-associated trait and a close correlation was confirmed between plant height and grain yield in maize (r^2 > 0.73) (Adel et al., 2016). Hence, plant height is an important trait for maize breeding.

There were two main biological factors that mainly influence height of maize plant, internode number and internode length, and expand in maize plant height are mainly attributable to increased internode elongation instead of enhance in internode number. Previous studies have established that the regulation of plant height is intricately governed by phytohormones and influenced by a multitude of associated Quantitative Trait Loci (QTLs). Currently, the molecular landscape of plant height in maize has been illuminated by the cloning and characterization of just over 60 genes associated with this trait. These genes span a spectrum of functions, encompassing signaling, transport, and phytohormone synthesis. Notable among them are genes such as *an1*, *br2*, *d1*, *d2*, *d3*, *d5*, *d8*, *d9*, *qPH3.1*, *DWF1*, and *DWF4*, each contributing to the complex regulatory network orchestrating maize plant height (Shang et al., 2020), Specifically, *Nana Plant 1* (*na1*) and *Nana Plant* 2 (*na2*) are distinctively marked by severe dwarfism, signifying their significant contributions to the brassinosteroid (BR) biosynthesis pathway. Their pivotal role in this pathway suggests a potential correlation with reductions in stem internode length (Zhao et al., 2022). *D3*, identified as a maize gene through transposon tagging, plays a crucial role in regulating gibberellin synthesis. The encoded protein exhibits activity at an early stage in the Gibberellin (GA) biosynthesis pathway (Winkler, 1995). *d8* and *d9* are key elements of the GA signal transduction channel that negatively regulate the GA response, which is involved in GA signal transduction pathways via DELLA proteins (Lawit et al., 2010). Genes involved in the expression of polar auxin transport, such as *ZmPIN1a* and *Brachytic2* (*br2*), are also regulated in the genetic control of plant height in maize (Pilu et al., 2007; Li et al., 2018). *ZmACS7* encodes ACC synthase 7 in the ethylene biosynthesis pathway of maize, resulting in dwarf phenotypes in the *zmacs7* mutant. The observed dwarfism emphasizes the pivotal role played by *ZmACS7* in plant growth, deepening our understanding of ethylene synthesis regulation and offering insights into the genetic factors that impact plant architecture (Li et al., 2020).

The GF14 (14–3-3) gene family is widely preserved in eukaryotes, spanning diverse organisms. GF14s proteins, crucial for cellular processes, have a unique structural composition with nine antiparallel α-helices. The persistent structural uniformity in GF14 proteins underscores their significance across various biological contexts. The widespread distribution and conservation of the GF14 genes family emphasize its foundational role in diverse eukaryotic organisms, making it intriguing for further exploration in understanding cellular processes and signaling pathways (Roy et al., 2023). GF14s frequently participate in the creation of heterodimers or homodimers, highlighting their dynamic inclination for molecular associations. Within these dimers, each GF14 protein exhibits an impressive proficiency to interact with distinct partners, unveiling the intricate versatility of GF14 proteins in coordinating diverse cellular interactions (Joshi et al., 2022). Hitherto, GF14–3s have been identified in plants such as rice, tobacco, *Brachypodium distachyon*, soybean, barley, cotton, *Arabidopsis* and maize, but only few have been phylogenetically and functionally characterized (Niti et al., 2017). In recent studies, the significance of GF14s has been increasingly emphasized, particularly in their involvement in carbon and nitrogen metabolism, as well as their crucial roles in responding to both biotic and abiotic stresses. These proteins serve as key regulatory factors within diverse stress signal transduction pathways, influencing the cellular responses to environmental challenges. Furthermore, GF14s play a pivotal role in the signal transduction processes associated with various phytohormones, including but not limited to GA, Brassinosterol (BR), Abscisic acid (ABA), and Ethylene (ET). This multifaceted involvement underscores the broad impact of GF14s in orchestrating intricate signaling networks critical for plant growth, development, and adaptation to changing environmental conditions (Qin et al., 2016). Despite limited evidence linking GF14s to plant height, ongoing investigations are progressively revealing the intricate roles these proteins play in regulating various aspects of plant morphology. This expanding body of research underscores the complexity of GF14 involvement in shaping the overall form and architecture of plants (Liu et al., 2016).

In this research, to further explore the relationship between ZmGF14s and plant height development, we employed weighted gene co-expression network analysis (WGCNA) on a previously published high-throughput RNA-seq dataset. The results showed that ZmGF14s exhibited a significant co-expression pattern with functionally characterized plant height-related genes in maize. Gene expression analysis suggested that only the expression value of ZmGF14–3 increased with the development of maize, indicating that ZmGF14–3 may play a crucial role in plant height regulation. Subsequently, we isolated ZmGF14–3 from the B73 maize inbred line and obtained *Arabidopsis* lines overexpressing ZmGF14–3 with a 35S promoter. Our results demonstrated that overexpression of ZmGF14–3 in *Arabidopsis* led to a reduction in plant height.

2 Materials and methods

2.1 Maize materials for co-expression network construction and high-throughput transcriptome sequencing data

In order to accurately and comprehensively depict the dynamic changes in gene expression during maize plant height development, in our previous research, three hybrids were chosen, which were defined as high (H, Dan 598×ES40), middle (M, Dan 598 × CML444) and low (L, Dan 598 × FAPW) group, and RNA

samples were collected at the jointing stage, big flare period and tasseling stage. Then, RNA-Seq was used to identify and characterize the expression of large quantities of genes, and develop a genome-wide co-expression network providing a gene expression overview for biological process analysis by combining algorithms (Wang et al., 2021). The RNA-seq datasets can available from Gene Expression Omnibus (GEO) in NCBI under accession number GSE115796.

2.2 Gene network construction

The weighted gene co-expression network analysis (WGCNA) R package (Version: 4.2.2) was used to construct a gene co-expression network. The expressed genes in the transcriptome data were cluster analyzed, and the soft threshold was calculated using the pick soft threshold function provided by WGCNA. To make the network show an approximate scale-free topology, a power of nine was chosen (model fitting index $R^2 = 0.8$). In order to ensure that the network was biologically relevant, the scale-free topology model and the mean connectivity of the network fit were estimated over a series of the soft threshold power β. All the coding sequences were hierarchical clustered by using topological overlap-based dissimilarity measure. Then, the resulting gene dendrogram was used for module detection based on the dynamic tree cut method (minModuleSize = 100 and mergeCutHeight = 0.25). If any two genes were connected in the weighted gene co-expression network, the topology overlap measure provided in WGCNA was used to determine edge weight. The weights ranged from 0 to 1, and reflected the strength of communication between the two genes. Only weights above 0.2 between any two genes were considered to stand for a strong co-expression relationship in our network. Finally, all expressed ZmGF14s and genes related to plant height were used as guide genes for the co-expression network construction, the Cytoscape_v 3.6.1 software was used to display the co-expression network (Hsieh et al., 2023).

2.3 RNA isolation and quantitative reverse transcription PCR

The primer Primier 5 software was used to design gene-specific qRT-PCR primers. A Spectrum™ Plant Total RNA Kit (SIGMA, Beijing, China) was used to extract total RNA from *Arabidopsis* stems, all RNA samples were treated with DNase to eliminate any potential trace contaminants of genomic DNA. A reverse transcription kit (Roche) was then used to synthesize first-strand cDNA (templates for qRT-PCR) using 1 mg of RNA, and the cDNA were transcripted by using PrimeScript™ RT Reagent Kit (Takara, Dalian, China). TransStart Top Green qPCR SuperMix kit (TANSGEN, Beijing China) were used for qRT-PCR, and performed in a CFX96 Real Time PCR Detection System (Bio-Rad). The thermal cycling conditions were as follows: an initial denaturation step of 5 min at 95°C, followed by 40 cycles of 10 s at 95°C for denaturation, 15 s at 60°C for annealing and 30 s at 72°C for extension (Wang et al., 2019). The primer pairs employed for qRT-PCR of cloned genes in this study are detailed in Supplementary Table S1, with the housekeeping gene ACTIN serving as a designated internal control, and formula $2^{-\Delta\Delta Ct}$ were used for calculating the expression level. The experiment was conducted in triplicate, a described method was used to calculate the relative expression level of the target gene.

2.4 Isolation of ZmGF14–3 cDNA

ZmGF14–3 was isolated from a cDNA library of B73 maize inbred line, and cloned into the 1301a vector, which contains the modified 35S promoter of *Escherichia coli* receptors. 5'-GGATCCATGGCTAAGTTTGTT-3' (Sense) and 5'-CCTAGG TACCGATTCAAACAA-3' (Antisense), containing the BamHI and PstI cloning sites, were used as primers to amplify ZmGF14–3 cDNA and subcloned in the corresponding sites of the 1301a vector. The 1301a-ZmGF14–3 construct was introduced into Agrobacterium tumefaciens C58C1 by heat shock. The floral-dip method were used in transforming Col-0 *Arabidopsis* plants, transgenic seedlings were selected on kanamycin medium (50 ug mL^{-1}). T2 plants that produced 100% kanamycin-resistant plants in the T3 generation were considered homozygous for the selection marker and arranged for further researches. Other experiments were performed using homozygous transgenic plants of T3 generation.

2.5 GA, ABA, and IAA quantification

Phytohormone were analyzed by using HPLC-MS/MS system (HPLC ExionLC™ AC; MS Sciex Triple Quadrupole 4500) (Liu et al., 2023). Prior to extraction, samples were fortified with deuterated standards for each compound. Following centrifugation and extraction, the pH of the supernatant was adjusted to 3.0 and partitioned twice with diethyl ether. The organic layers were then consolidated and evaporated using a centrifuge vacuum evaporator. The dry residue was thereafter resuspended in a water: methanol (9:1) solution, filtered, and injected in a HPLC system. The HPLC analytical conditions were as follows: column was HYPERSIL GOLD C18 column (3μm, 2.1mm*100 mm); solvent A was H_2O (0.1% FA); solvent B was MeOH; gradient program, 90% A from 0 to 0.2 min, 90% A at 3 min and kept to 8min, 10% A at 8.1 min and kept to 10 min; flow rate, 0.3 mL/min; temperature, 35°C; injection volume: 5μL. The mass spectrometer were adopted in negative ionization electrospray mode for different phytohormone measuring. Further method on the determination procedure are given by Jon et al (Jon et al., 2020). Accurate quantification of GA, ABA, and (Indole-3-Acetic Acid) IAA in *A. thaliana* stems was performed by Guocangjian Biotech (targetcrop.com) on UPLC-MS/MS platform.

2.6 Subcellular localization analysis

The ZmGF14–3 coding region, excluding the terminator, was cloned and subsequently fused with the subcellular localization

vector pCAMBIA1305, incorporating green fluorescent protein (GFP) tags (Abcam, ShangHai, China, ab275766) driven by the CaMV35S promoter. The ClonExpress MultiS One Step Cloning Kit (Vazyme, Najing, C113–01/02) were used to obtain the pCAMBIA1305-ZmGF14–3 vector through homologous recombination method, and the *N. benthamiana* epidermal cells were used as receptor cell for transforming recombinant plasmid pCAMBIA1305-ZmGF14–3 by *Agrobacterium tumefaciformis* infection. Then, the 13-day-old maize B73 etiolated seedlings were used as materials for preparing maize protoplasts. Additionally, the plasmid pCAMBIA1305 with 35S::ZmGF14–3-GFP fusion proteins was transformed to maize protoplasts using the PEG-mediated transformation method and the pCAMBIA1305 vector were also transformed as control, the DAPI (1 μg/mL) staining solution was used to nuclei stain. After incubation in darkness at 22°C for 16 h, the confocal laser scanning microscope (Zeiss LSM 800, Jena, Germany) were used for observing fluorescence signals. The confocal microscope were used to obtain microscopy images and analyzed by using the ZEN 3.1 software (https://www.zeiss.com.cn/microscopy/products/microscope-software/zen.html accessed on 18 September 2022). The DAPI and GFP were detected at excitation of 461 nm and 488 nm (Li et al., 2022).

2.7 Transformation of *Arabidopsis*

The coding sequence of ZmGF14–3 was cloned and inserted into the pMD18-T simple vector (TAKARA, Shanghai, China, Code No. 6011) for sequencing. The gene product was then placed under the control of the CAMV35S promoter and subcloned into the pCAMBIA1301a recombinant vector (Abcam, Shanghai, China, ab275753). The construct was introduced into *Agrobacterium tumefaciens* strain LBA4404 by the infection method and transformed into *Arabidopsis thaliana* (Lu et al., 2017).The seeds of transformed *Arabidopsis thaliana* were selected after being broadcast on MS culture plates with spectinomycin (2 mg/ml) and vernalization for 3 days. Resistant seedlings were planted in the soil, the specific primer PCR were used for identification of transformed plants. Their seeds were harvested separately. T3 homozygous seeds were identified by BASTA resistance and used for further experiments.

3 Results

3.1 Co–expression network of plant height–specific and ZmGF14s

Currently, a total of 28 ZmGF14s have been reported in maize (Wang et al., 2023). In our previous weighted gene co-expression network analyses (Wang et al., 2018), a total of 12 ZmGF14s were identified (Supplementary Table S2). We used these 12 ZmGF14s and all reported maize genes related to plant height as guide genes to construct a co-expression network. As a result, 10 ZmGF14s were identified in the new network, these genes are ZmGF14–1, ZmGF14–2, ZmGF14–3, ZmGF14–5, ZmGF14–6, ZmGF14–7, ZmGF14–8, ZmGF14–9, ZmGF14–10 and ZmGF14–11, and 30 functionally characterized plant height-related genes exhibited a co-expression relationship with these ZmGF14s (Figure 1; Supplementary Tables S3, S4). Among them some key hub ZmGF14s were identified, such as ZmGF14–7 (Co-expressed with

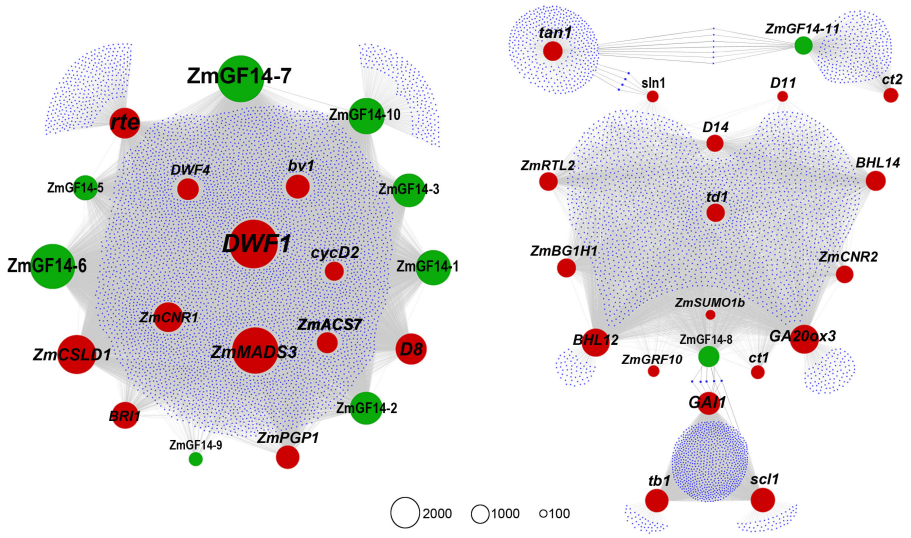

FIGURE 1
Weighted gene co-expression network of ZmGF14 genes and plant height related genes in maize. Black nodes represent reported plant height-related genes, grey nodes denote ZmGF14 genes, all other genes are depicted as small black nodes. Node size represents total connectivity. An edge indicates significant co-expression between two connected genes.

4080 genes), ZmGF14–6 (Co-expressed with 3066 genes), and ZmGF14–3 (Co-expressed with 2028 genes), showed co-expression with *DWF1*, *ZmGRF10*, *rte*, *ZmCNR01*, *D8*, and *bv1*. These results suggest that the 10 ZmGF14s may be potential candidates for regulating plant height.

3.2 Phylogenetic analysis of GF14s in different studied species and structural analyses of maize GF14 genes

For a deeper exploration into the evolutionary trajectory of ZmGF14s across maize and other species, we meticulously crafted a maximum likelihood tree encompassing all 155 GF14s identified from 12 meticulously surveyed species (Figure 2; Supplementary Table S5, Supplementary File S1). Based on the topology and bootstrap values of clade nodes, the tree can be categorized into four distinct clades, denoted as Clade I through IV. Within the four clades, 40, 19, 31 and 65 GF14s were clustered, respectively. Clade IV harbored the most GF14s members and Clade II the least, and Clade IV contained GF14s from 8 plant genomes, suggesting the evolutionary conservation and ancient origination of GF14s in these clades. Clade II exclusively comprised GF14s from animals and prokaryotes, suggesting a potentially unique evolutionary trajectory of GF14s across various clades.

We concentrated on GF14s within maize and additionally constructed a neighbor-joining (NJ) phylogenetic tree specifically comprising maize GF14s (Supplementary Figure S1). Our findings revealed that the topology of the neighbor-joining phylogenetic tree closely mirrored that of the maximum likelihood phylogenetic tree for GF14s, thereby underscoring the precision of phylogenetic reconstruction. Upon further analysis of maize GF14 gene structures, it was observed that only ZmGF14–5 lacked introns, while the others did not. Additionally, during the investigation of conserved motifs in GF14s, it was discovered that ZmGF14s with close phylogenetic relationships exhibited analogous motif

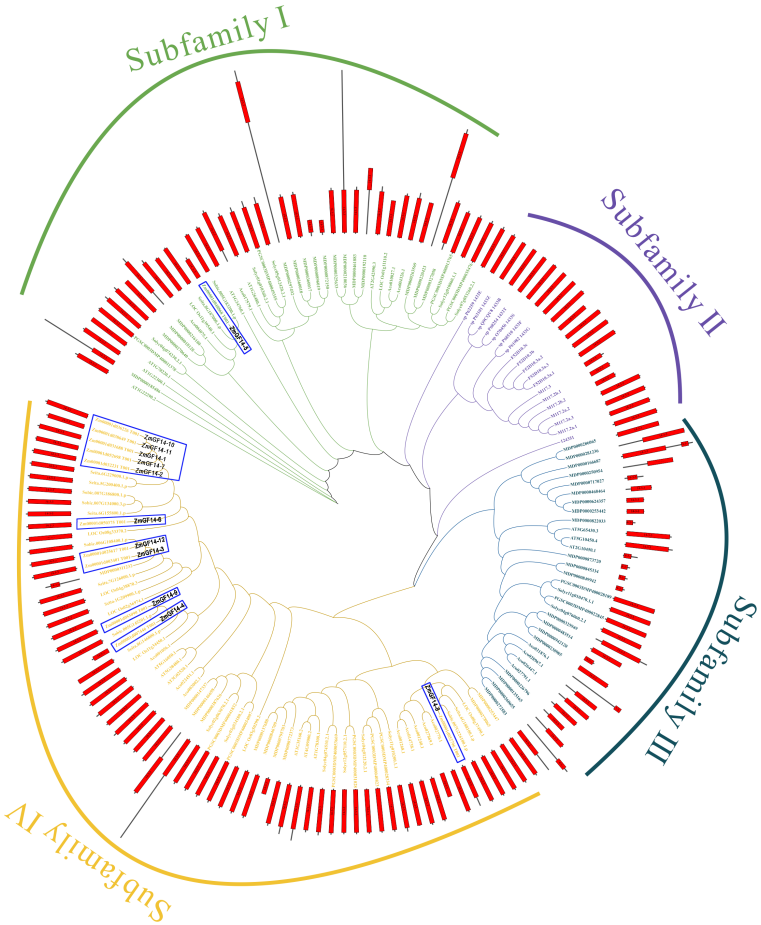

FIGURE 2
The maximum likelihood evolutionary tree was established for the selected GF14s, which contains 12 selected species and 4 outgroup species and their protein domains. Abbreviation of the species name can be found in Supplementary Table S5. The Figure can be divided into four clades, and different clades are shown in different colors. Green, purple, dark green, and orange represent clades I to V, respectively, while the topological structures on the domains are also marked, with red cuboids representing the GF14 (14–3-3) domain.

compositions, suggests that these genes may have similar biological functions.

3.3 Correlation analysis between ZmGF14s expression and genes associated with plant height

To delve deeper into the regulatory interplay between ZmGF14s and genes associated with plant height, we conducted an analysis to evaluate the correlation of gene expression levels across different developmental stages and maize varieties. This assessment was performed through the calculation of the Pearson correlation coefficient. All of the ZmGF14s genes, when compared with functionally characterized plant height-related genes, demonstrated varying degrees of significant correlation (Figure 3A; Supplementary Table S6). For example, the expression level of ZmGF14–1 exhibited a negative correlation with *GA20ox3* (r = -0.775, *p* -Value = 0.014) and a positive correlation with *DWF1* (r = 0.87, *p*-Value = 0.002). The expression levels of ZmGF14–3 showed positively correlated with *ZmMADS3*, *DWF1*, *D4* and *ZmCNR01* (*p-Value* < 0.05), and negatively correlated with *D11*, *D14*, *ct1* and *BHL14* (*p*-Value < 0.05). Prior investigations have revealed a heightened expression of ZmMADS3 in stem nodes. Ectopically expressing *ZmMADS3* led to reduced plant height, primarily attributed to a decrease in the number of nodes (Heuer et al., 2001). *ZmDWF1* is involved in BRs signal transduction, *zmdwf1* mutant exhibited severity dwarfed phenotype (Tao et al., 2004). *D11* is involved in GA biosynthesis, *d11* mutant exhibited severely developmental abnormalities and showed dwarfed phenotype (Wang et al., 2013). The obtained results posit that ZmGF14s may assume an indirect role within the regulatory framework governing the development of maize plant height. This can be attributed to their extensive involvement across a spectrum of phytohormone metabolic pathways, thereby exerting a discernible influence on the intricacies of plant height modulation.

3.4 Expression profiles of ZmGF14s across three developmental stages in three maize hybrids

To gain insights into the evolutionary relationships among maize GF14 proteins, we selectively chose ZmGF14s to construct a neighbor-joining (NJ) phylogenetic tree. The outcomes revealed a

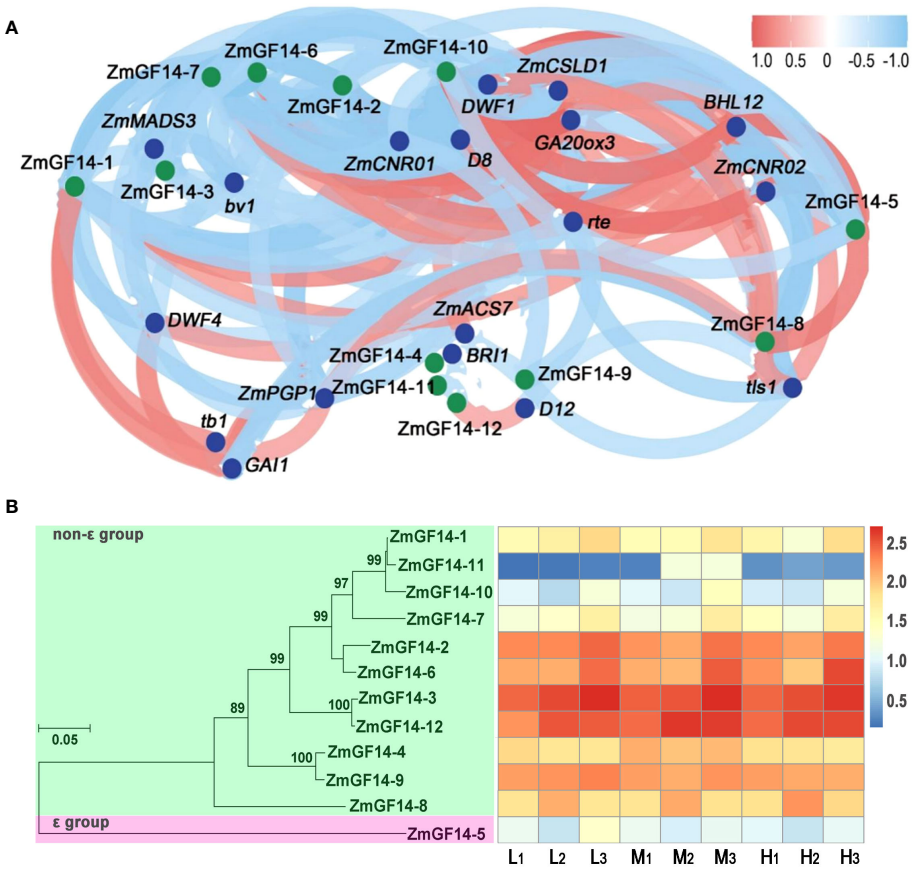

FIGURE 3
Correlation analysis of gene expression level between ZmGF14s and plant height-related genes and phylogenetic reconstruction. **(A)** Correlation analysis of gene expression level between ZmGF14s and plant height related genes; Blue dots in the figure represent reported height-related genes in maize, while green dots represent ZmGF14 family genes. **(B)** Phylogenetic reconstruction and expression profiles of ZmGFs genes in maize.

distinct classification of all ZmGF14s into two groups: the ϵ group and the non-ϵ group. Furthermore, we examined the relative expression levels of ZmGF14 genes in three maize hybrids (Low: L, Medium: M, High: H) across distinct developmental stages (1: joint stage, 2: trumpet stage, 3: tasseling stage). The analysis unveiled diverse expression patterns among the 12 ZmGF14 genes (Figure 3B; Supplementary Table S7). These variations in expression patterns imply that specific genes might play crucial roles in the developmental regulation of maize plant height across different growth stages. Notably, ZmGF14–2, 3, 6, and 12 exhibited relatively high expression levels across all hybrids and stages. Specifically, the expression of ZmGF14–3 consistently upregulated throughout the three developmental stages in all three hybrids, suggesting a gradual increase in ZmGF14–3 expression with maize growth and development.

3.5 Expression patterns and subcellular localization analysis of ZmGF14–3

Building upon the aforementioned findings, we observed that the ZmGF14–3 gene displayed a consistent upward trend in expression across three developmental stages within three maize hybrid lines, each distinguished by varying plant heights categorized as low (L), medium (M), and high (H). Consequently, we infer that ZmGF14–3 may play an important role in the plant height development. Based on these observations, ZmGF14–3 was selected as the focal point for further in-depth functional exploration. In general, gene expression profiles are indicative of their functions (Heyduk et al., 2022). To delve into the expression patterns of ZmGF14–3 throughout maize development, we gathered data on gene expression across nine distinct maize tissues using qRT-PCR. The results revealed that ZmGF14–3 displayed elevated expression levels in the stem (Figure 4A), aligning with the data obtained from our previously published transcriptome database.

To ascertain the subcellular localizations of ZmGF14–3, ZmGF14–3-GFP plasmids were introduced into maize protoplasts, with the empty protein (35S-GFP) GFP serving as the control group, diffusing uniformly throughout the cell. The findings revealed that ZmGF14–3 predominantly exhibited a punctate pattern of localization in protoplasts, primarily concentrating in the cytoplasm (Figure 4B).

3.6 Over-expression of ZmGF14–3 in *A. thaliana* and quantitation of GA, ABA, and IAA levels

To further explore the biological functions of ZmGF14–3, we heterologously expressed it in *Arabidopsis thaliana* for comprehensive functional research. This approach aims to elucidate the intricate roles and mechanisms associated with ZmGF14–3 in a different biological context, providing valuable

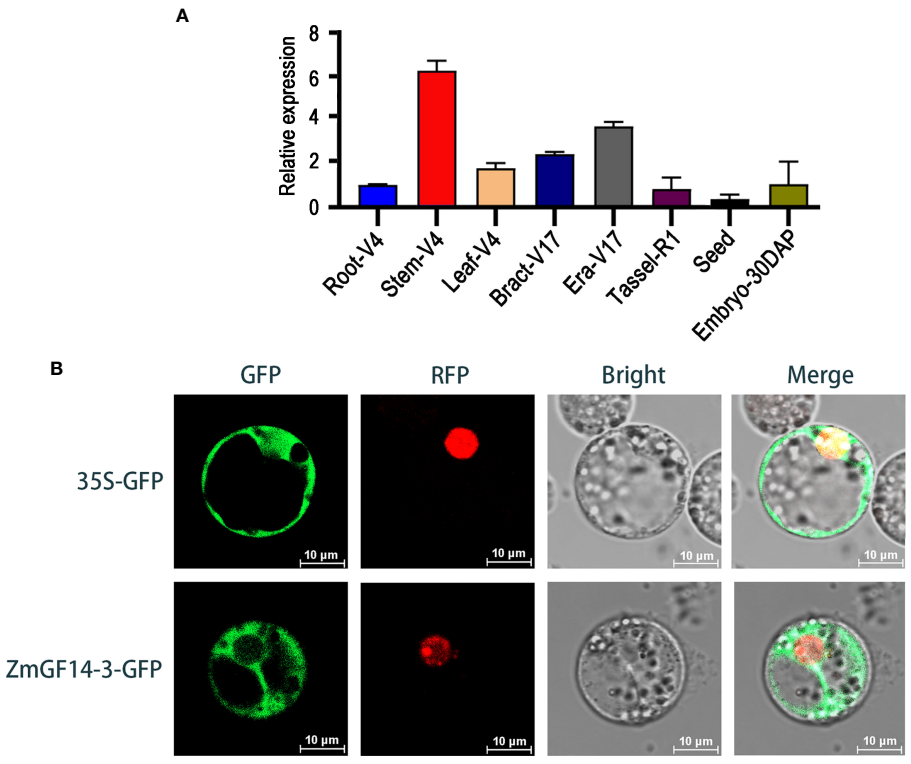

FIGURE 4
Expression patterns **(A)** and subcellular localization **(B)** analysis of ZmGF14–3.

10.3389/fpls.2024.1397058

insights into its potential functions. Each independent transgenic line underwent screening for hygromycin resistance. Subsequently, three distinct homozygous transgenic lines from the T3 generation (designated as OE#L1, OE#L2, and OE#L3), exhibiting the overexpression of ZmGF14–3, were meticulously chosen. At the flowering stage, we assessed the plant height of both the transgenic lines and the wild-type. Through rigorous statistical analysis, it became evident that transgenic plants manifested a considerably reduced height compared to their wild-type counterparts (p -Value < 0.05, as depicted in Figures 5A, B).

GF14s are essential genes that play a crucial role in regulating various aspects of plant growth and development, they are also involved in the metabolism of phytohormones, including GA, IAA and ABA, which are important for processes such as seed germination, root growth, and stress response (Qin et al., 2016). The phytohormone signaling pathway has undergone extensive

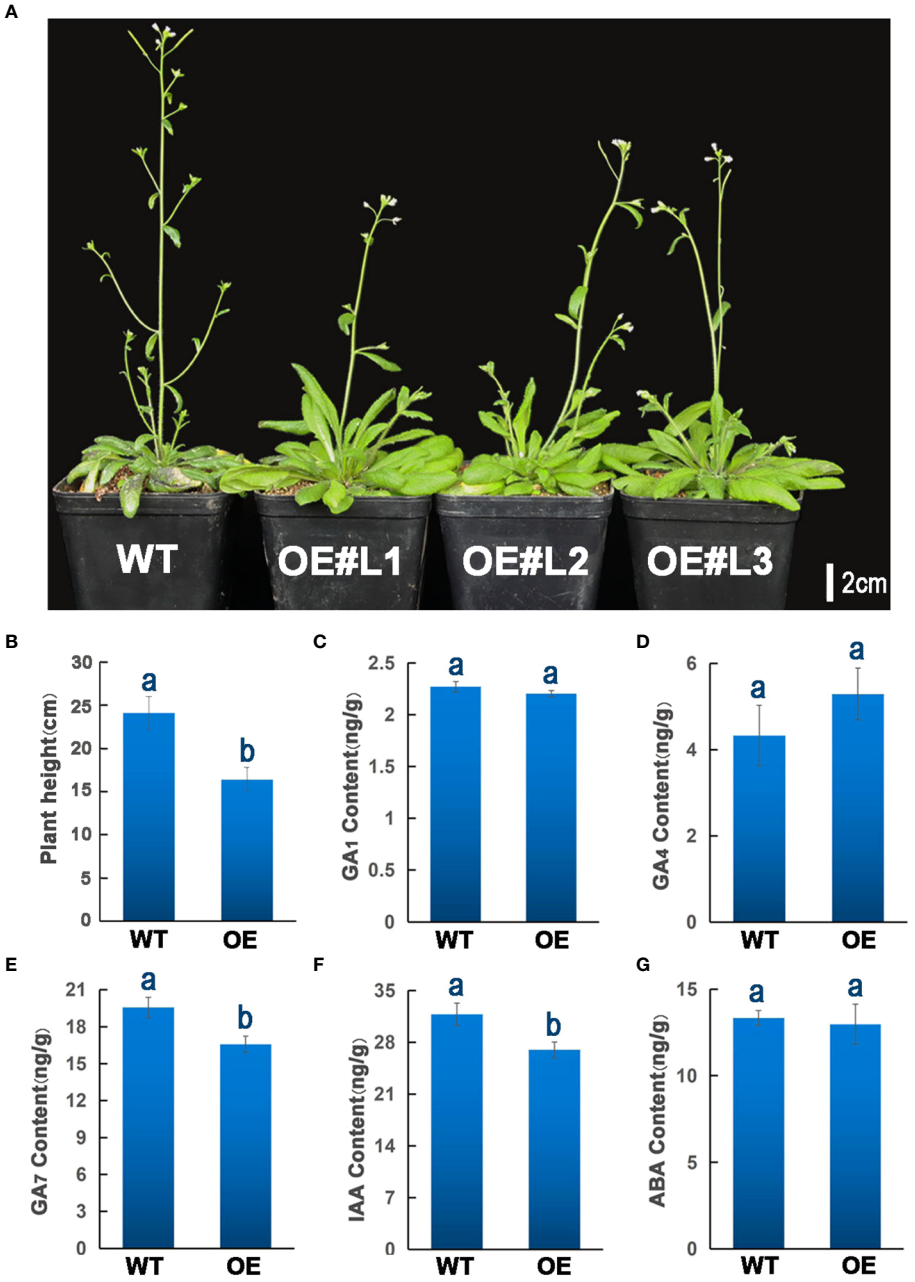

FIGURE 5
Over-expression of ZmGF14–3 in (A) *thaliana* and quantitation of GA, ABA, and IAA levels. **(A)** Over-Expression of ZmGF14–3 in (*A*) *thaliana*; **(B)** Statistical analysis of transgenic *Arabidopsis* and wild type plant height phenotypes; **(C–G)** Quantitation of GA_1, GA_4, GA_7, IAA and ABA levels in transgenic *Arabidopsis* and wild type plant. The data represent means ± SD from three biological samples. Different letters indicate a significant difference between WT plants and different transgenic lines by Student's t-test, * P < 0.05, the same letters indicate non-significant differences (P > 0.05).

10.3389/fpls.2024.1397058

exploration in *A. thaliana*, playing crucial roles in seed germination, stem elongation, flower transformation, and flowering. To investigate the impact of transgenic lines on phytohormone metabolism, we assessed the levels of GA, ABA, and IAA. The results unveil subtle distinctions in GA_1, GA_4, and ABA content between the overexpressing lines and the wild type (WT) (Figures 5C, D, G), while notably, a significant reduction in GA_7 and IAA levels is evident in the overexpressing lines compared to WT ($p < 0.05$) (Figures 5E, F). This marked decline hints at the potential involvement of ZmGF14–3 in the signaling pathways of GA_7 and IAA, thereby exerting a discernible influence on the developmental trajectory of plant height in the overexpressing *Arabidopsis*. These findings imply that ZmGF14–3 is putatively a key regulator in the phytohormone signaling pathway of *Arabidopsis*, thereby exerting an influence on the development of plant height.

3.7 The impact of ZmGF14–3 overexpression in *A. thaliana* on phytohormone responsE GENES

To further investigate the impact of ZmGF14–3 overexpression on various endogenous phytohormone-responsive genes in *Arabidopsis*, we assessed the expression levels of genes associated with different phytohormones (Figure 6). For instance, within the gibberellic acid (GA) biosynthetic pathway, GA20ox2 plays a crucial role in converting GA_{12} to GA_9, resulting in shortened

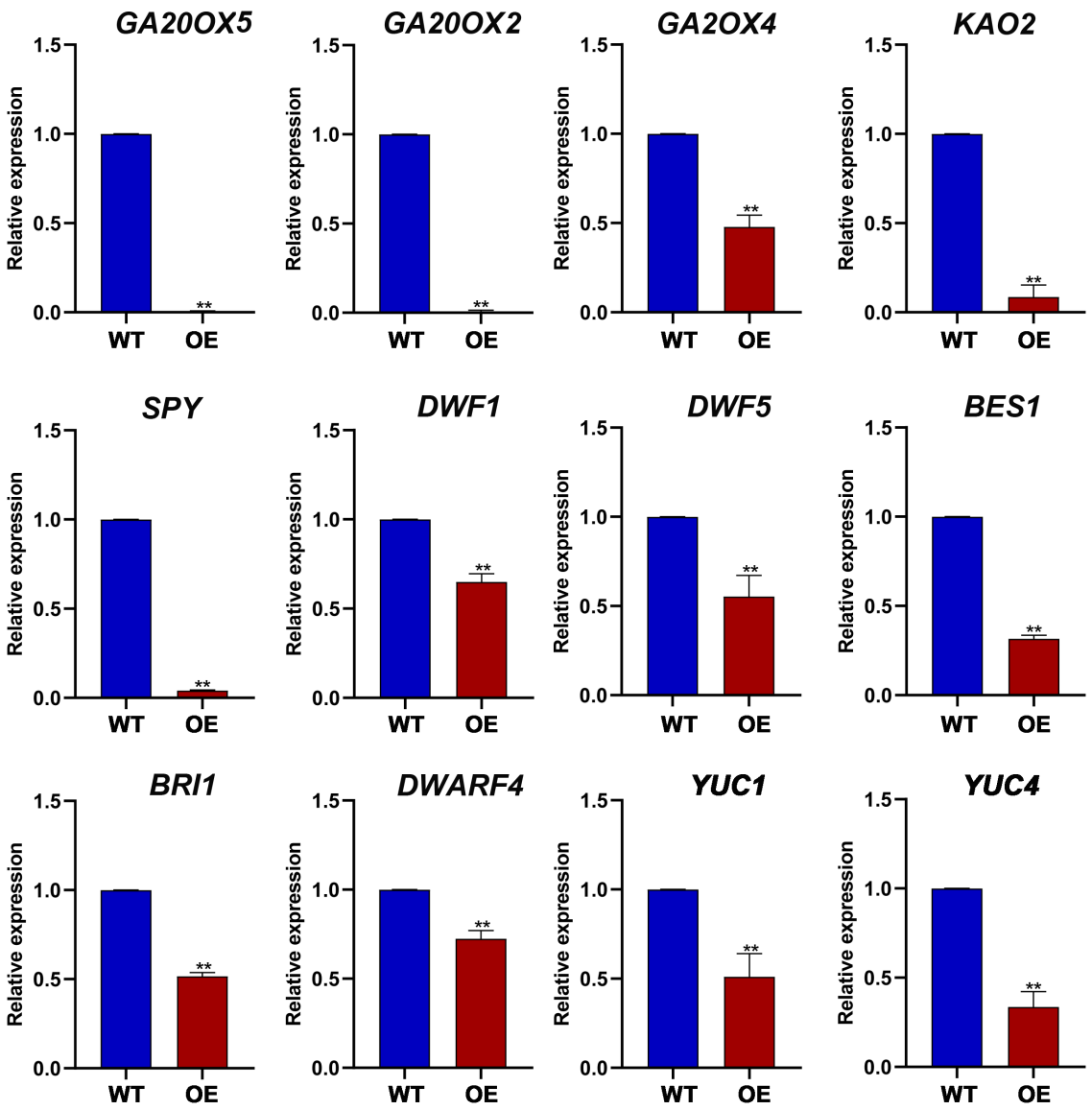

FIGURE 6
The expression levels of plant height related genes in transgenic *Arabidopsis* and wild type plants. ** indicates that the difference between OE and WT has reached a highly significant level (p-Value < 0.01).

internode length and pronounced dwarfism in the *ga20ox2* mutant of *Arabidopsis*. In *Arabidopsis* lines overexpressing ZmGF14–3, a notable decrease in the expression of GA20ox2 was observed, corresponding with the observed dwarf phenotype (Plackett et al., 2012). *DWF4* encodes a P450 protein responsible for catalyzing multiple 22a-hydroxylation reactions in the biosynthesis of BR. It serves as a key catalyst in a pivotal step that determines the overall flux in the biosynthetic pathway of BR, the *Arabidopsis dwf4* mutant exhibits a severely dwarfed phenotype accompanied by developmental abnormalities (Guo et al., 2010). In the biosynthetic pathway of plant growth phytohormones, the YUC gene family plays a pivotal role in regulating plant height and internode elongation. Research indicates that all YUC genes in *Arabidopsis* have overlapping functions, and the overexpression of each YUC gene results in excessive auxin production. Further studies demonstrate that the *Arabidopsis yuc1yuc4* double mutant exhibits pronounced dwarfing. In our investigation, the overexpression of ZmGF14–3 in *Arabidopsis* leads to a significant reduction in the expression levels of both *yuc1* and *yuc4* (Cheng et al., 2006). This result suggests that ZmGF14–3 may function as a key gene, capable of modulating the expression levels of associated genes within various phytohormones pathways, consequently impacting the developmental regulation of plant height.

4 Discussion

GF14s, serving as ubiquitous regulators, have been identified in a diverse array of plant species, including *Arabidopsis*, rice, wheat, soybean, cotton, rubber tree, alfalfa, and populus. This recognition began with the isolation of the first plant GF14 isoform from maize (Lu et al., 2022). The present study identified GF14s from 12 species, emphasizing the evolutionary patterns of ZmGF14s. Results found that in these GF14s, evolutionary pattern is conserved and could be identified in different surveyed eukaryotes, such as *mice*, *Micromonas pusilla*, and *Caenorhabditis elegans*, this suggests the ancient origin of GF14s. Generally speaking, conserved motifs and domains were generally regarded as important functional or regulatory elements (Zhu et al., 2022). In our results, 12 GF14s with similar conserved sequences were identified in a co-expression network associated with plant height in maize. Among them some key hub ZmGF14s exhibited co-expression with functionally validated genes associated with plant height, this results suggest that these genes may interact with plant height-related genes to regulate plant height development. Presently, GF14s exhibit interactions with a spectrum of genes related to energy metabolism, phytohormone signal transduction, redox homeostasis, stress response, and plant development. Recent studies have elucidated the additional involvement of GF14s and their binding proteins in the process of starch accumulation during cassava tuberization (Zhao et al., 2021). Currently, investigations into the GF14 gene family in plants are primarily focused on its pivotal role in regulating ion channels, hormone signaling pathways, and responses to diverse stresses, including but not limited to low temperature, salt, drought, osmotic stress, and mechanical stress (Gupta et al., 2023). While there is limited research on the regulation of plant height development by the GF14 gene family, sporadic literature reports suggest its potential key role in this aspect. Further investigations are warranted to deepen our understanding of the gene family's influence on plant height development. As an illustration, the dephosphorylation of the shade-induced transcription factor PIF7 plays a crucial role in light signal perception and stem elongation. Mutations in the phosphorylation-resistant sites of PIF7 enhance its interaction with GF14 proteins, thereby facilitating the elongation of the hypocotyl stem. This study unveils a novel mechanism wherein GF14s regulate stem elongation in shaded conditions by sequestering PIF7 in the cytoplasm (Xu et al., 2018). In another research, it was demonstrated that the expression of GF14s in rice significantly influences internode elongation. This is attributed to the role of GF14, which encodes a signaling protein capable of binding and inhibiting the function of the RSG (repression of shoot growth) protein. The RSG protein acts as a transcriptional repressor of the kaurene oxidase (KO) gene in the gibberellic acid (GA) biosynthetic pathway (Phanchaisri et al., 2012). Therefore, stem elongation is a crucial agronomic trait that significantly influences plant height. Moreover, the increase in maize plant height primarily results from enhanced internode elongation rather than an increase in the number of internodes (Gao et al., 2023). To research the possible functions of ZmGF14s in plant height development, the mRNA levels of all 12 ZmGF14s in stems were surveyed in three hybrids at three different developmental stages, all ZmGF14s exhibited different expression patterns, from the results of phylogenetic relationships and the expression pattern of the ZmGF14s, we speculated regarding the possible functions of certain genes in certain developmental processes. During maize development, out of these ZmGF14s, the expression level of the ZmGF14–3 may demonstrate an increasing trend. Furthermore, it has been observed that this gene is notably expressed at high levels in the stem, this compelling evidence strongly suggests that ZmGF14–3 plays a pivotal role in orchestrating the process of stem elongation, thereby exerting a profound influence on the overall development of plant height. Thus, research on the growth and development of plant height in maize should primarily concentrate on ZmGF14–3, a specific gene of ZmGF14s.

Moreover, additional studies indicate that GF14 gene family can indirectly influence plant height development by regulating phytohormone metabolic pagibberellinthways. GF14 genes are crucial regulatory factors involved in multiple stress signaling pathways, participating in the signal transduction pathways of various phytohormone such as s, brassinosteroids, ABA, and ET (Zhao et al., 2021). For instance, In the GA synthesis pathway, a class of RSG transcription factors can regulate the expression of genes involved in gibberellin biosynthesis. Previous studies have shown that using RSG as bait protein can screen for target proteins of GF14 and identified the interacting site RSGSer114. Additionally, GF14 protein can acts as a negative regulatory factor by binding to RSG through phosphorylation of Ser-114 in RSG. Exogenous application of gibberellin can phosphorylate RSG, altering its cellular localization and preventing it from entering the nucleus to regulate the expression

of target genes, thereby affecting gibberellin biosynthesis (Ito et al., 2014). *BZR1* and *BES1* play crucial roles as transcription factors in the brassinosteroid (BR) signaling pathway. When phosphorylated, BES1/BZR1 undergo structural changes that render them unstable and unable to bind to cis-elements, such as CPD, in downstream gene promoters. Instead, they are sequestered by GF14 proteins, leading to their degradation or retention in the cytoplasm (Nolan et al., 2017). GF14 proteins have the ability to recognize and interact with target proteins through specific amino acid sequences and phosphorylation forms. *OsBZR1*, *AtBZR1*, and *AtBES1* all possess a conserved GF14 binding domain. The study reveals that, via yeast two-hybrid experiments, five genes capable of interacting with *AtBZR1* were identified within the *Arabidopsis* GF14 family. In the case of rice, 8 GF14 proteins exhibiting interactions with OsBZR1 were screened. However, *BES1*/*BZR1* complexed with GF14 proteins are unable to translocate into the nucleus to regulate downstream gene expression, thereby hindering the transduction of BR signals and impacting plant height development (Lu et al., 2022). In *Arabidopsis*, some plant height-related genes involved in the GA pathway, such as *SPY*, *GA20ox4*, *KAO2*, *GA20ox2*, and *GA20ox5*, all exhibit significantly reduced expression levels in overexpression lines compared to the wild type (WT). After overexpression of ZmGF14–3 in *Arabidopsis*, genes involved in the Br metabolism pathway, such as *BES1*, *DWF5*, *DWF1*, *DWARF4*, and *BRI1*, as well as the IAA metabolism pathway gene *YUC1* and *YUC2*, all exhibited significantly reduced expression pattern. In summary, ZmGF14–3 may affect plant height development by regulating the expression levels of different phytohormone-related genes.

ZmGF14–3 demonstrated a co-expression relationship with pivotal genes associated with maize plant height, including *bv1*, *DWFI*, *ZmMADS3*, *BRI1*, *ZmCNR1*, *DWF4* and *ZmPGP1*. Among them, *bv1* plays a crucial role in auxin transport and exerts an influence on internode development. Maize mutants with *bv1* deficiencies exhibit a dwarf phenotype, underscoring the significance of *bv1* in the regulation of plant height (Avila et al., 2016). *DWF1* and *BRI1* play crucial roles in the signal transduction of brassinosteroids (BRs). The presence of mutations in *zmdwf1* and *bri1* genes resulted in a distinctive dwarfed phenotype. This highlights the significance of these genes in regulating plant growth and development through the BR signaling pathway (Jia et al., 2020). The *DWF4* gene encodes a C-22 hydroxylase, a pivotal enzyme in the brassinosteroid (BR) biosynthesis pathway. The overexpression of *ZmDWF4* in maize lines demonstrated a significant increase in BR levels, resulting in a remarkable enhancement in both grain yield and plant height (Liu et al., 2020). *ZmPGP1*, identified as an adenosine triphosphate (ATP) binding cassette (ABC) transporter, plays a pivotal role in facilitating polar auxin transport. Recent studies have compellingly demonstrated a significant correlation between the expression of *ZmPGP1* and the modulation of maize plant height, thereby emphasizing its key involvement in the intricate regulatory pathways governing plant growth (Li et al., 2019). As these genes have distinct functions in phytohormone metabolic pathways, it is plausible that ZmGF14–3 plays a crucial role in regulating the growth and development of maize by interacting with various phytohormone-related genes. Therefore, investigating the potential interactions between ZmGF14–3 and these genes could provide valuable insights into the molecular mechanisms underlying plant height development in maize. This exploration underscores the potential significance of GF14s in influencing pivotal factors for plant height, including cell elongation and internode development. Despite the current constraints in research, these insights lay the groundwork for delving into how GF14s contribute to overall plant growth, with a specific focus on height regulation. Subsequent inquiries in this domain hold the promise of revealing the nuanced roles of GF14s in shaping the architectural aspects of plants. This study is of great significance to the breeding of excellent maize varieties.

Data availability statement

The datasets presented in this study can be found in online repositories. The names of the repository/repositories and accession number(s) can be found in the article/Supplementary Material.

Author contributions

HW: Writing – original draft, Writing – review & editing, Funding acquisition. BW: Visualization, Writing – review & editing. LQ: Data curation, Writing – review & editing. YC: Formal analysis, Writing – review & editing. KC: Project administration, Writing – review & editing. DL: Software, Writing – review & editing. XS: Funding acquisition, Resources, Validation, Writing – review & editing. YZ: Data curation, Methodology, Writing – original draft. LL: Data curation, Funding acquisition, Project administration, Writing – review & editing.

Funding

The author(s) declare financial support was received for the research, authorship, and/or publication of this article. This research was supported by grants from the Natural Science Research Project of Colleges and Universities of Anhui Province (Grant No. KJ2021A0924 and 2022AH051780); The 2020 Provincial Quality Engineering Project of Higher Education (2020szsfkc0747); Talent Fund of Hefei University (Project No. 21–22RC32). Major Natural Science Research Project of Colleges and Universities of Anhui Province (Grant No.KJ2021ZD0113 and KJ2021ZD0164); Anqing Science and Technology Project (Grant No. 2022Z0003 and 2021Z0004). Natural Science Foundation of Anhui Province, China, grant number (NO. 2008085QC103), Hefei Normal University High-level Talents Research Start-up Fund, grant number (NO. 2020rcjj49 and 2020rcjj50). Anhui University Outstanding Top-of-the-line Talent Cultivation Project (grant No. gxbjZD2021073) and National Engineering Laboratory of Crop Stress Resistance Breeding (NELCOF20210104).

Conflict of interest

The authors declare that the research was conducted in the absence of any commercial or financial relationships that could be construed as a potential conflict of interest.

Publisher's note

All claims expressed in this article are solely those of the authors and do not necessarily represent those of their affiliated organizations, or those of the publisher, the editors and the reviewers. Any product that may be evaluated in this article, or claim that may be made by its manufacturer, is not guaranteed or endorsed by the publisher.

Supplementary material

The Supplementary Material for this article can be found online at: https://www.frontiersin.org/articles/10.3389/fpls.2024.1397058/full#supplementary-material

References

Adel, H. A. G., Hu, S., Chen, Y., Brenner, E. A., Kumar, B., Blanco, M., et al. (2016). Genetic architecture of plant height in maize phenotype-selected introgression families. *Plant Breed.* 135, 429–438. doi: 10.1111/pbr.12387

Avila, L. M., Cerrudo, D., Swanton, C., and Lukens, L. (2016). *Brevis plant1*, a putative inositol polyphosphate 5-phosphatase, is required for internode elongation in maize. *J. Exp. Bot.* 67, 1577–1588. doi: 10.1093/jxb/erv554

Cheng, Y. F., Dai, X. H., and Zhao, Y. D. (2006). Auxin biosynthesis by the yucca flavin monooxygenases controls the formation of floral organs and vascular tissues in *Arabidopsis*. *Gene. Dev.* 20, 1790–1799. doi: 10.1101/gad.1415106

Gao, J., Zhang, Y., Xu, C., Wang, X., Wang, P., and Huang, S. (2023). Abscisic acid collaborates with lignin and flavonoid to improve pre-silking drought tolerance by tuning stem elongation and ear development in maize (*Zea mays* L.). *Plant J.* 114, 437–454. doi: 10.1111/tpj.16147

Guo, Z., Fujioka, S., Blancaflor, E., Miao, S., Gou, X., and Li, J. (2010). TCP1 modulates brassinosteroid biosynthesis by regulating the expression of the key biosynthetic gene *DWARF4* in *Arabidopsis Thaliana*. *Plant Cell* 22, 1161–1173. doi: 10.1105/tpc.109.069203

Gupta, S., Misra, S., Kumar, M., Mishra, S. K., Tiwari, S., Narayan, S., et al. (2023). Enhancement of drought tolerance in transgenic *Arabidopsis thaliana* plants overexpressing chickpea Ca14–3-3 gene. *J. Plant Growth Regul.* 42, 1544–1557. doi: 10.1007/s00344–022-10639–9

Heuer, S., Hansen, S., Bantin, J., Brettschneider, R., Kranz, E., and Lorz, H. (2001). The maize mads box gene ZmMADS3 affects node number and spikelet development and is co-expressed with ZmMADS1 during flower development, in egg cells, and early embryogenesis. *Plant Physiol.* 127, 33–45. doi: 10.1104/pp.127.1.33

Heyduk, K., Mcassey, E. V., and Leebens-Mack, J. (2022). Differential timing of gene expression and recruitment in independent origins of CAM in the *Agavoideae* (*Asparagaceae*). *New Phytol.* 235, 2111–2126. doi: 10.1111/nph.18267

Hsieh, P., Lopes-Ramos, G. M., Zucknick, M., Sandve, G. K., and Kuijje, M. L. (2023). Adjustment of spurious correlations in co-expression measurements from RNA-sequencing data. *Bioinformatics* 39, 10. doi: 10.1093/bioinformatics/btad610

Ito, T., Nakata, M., Fukazawa, J., Ishida, S., and Takahashi, Y. (2014). Scaffold function of Ca^{2+}-dependent protein kinase: *NtCDPK1* transfers 14–3-3 to the substrate RSG after phosphorylation. *Plant Physiol.* 165, 1737–1750. doi: 10.1104/pp.114.236448

Jia, Z., Giehl, R. F. H., and Von Wiren, N. (2020). The root foraging response under low nitrogen depends on *DWARF1*-mediated brassinosteroid biosynthesis. *Plant Physiol.* 183, 998–1010. doi: 10.1104/pp.20.00440

Jon, C. S., Zou, Y. L., Zhao, J. H., Ri, H. C., Wang, L. Y., Kaw, H. Y., et al. (2020). Simultaneous determination of multiple phytohormones in tomato by ionic liquid-functionalized carbon fibers-based solid-phase microextraction coupled with liquid chromatography-mass spectrometry. *Anal. Chim. Acta* 1137, 143–155. doi: 10.1016/j.aca.2020.09.050

Joshi, R., Pohl, P., Strachotova, D., Herman, P., Obsil, T., and Obsilova, V. (2022). Nedd4–2 binding to 14–3-3 modulates the accessibility of its catalytic site and WW domains. *Biophys. J.* 7, 1299–1311. doi: 10.1016/j.bpj.2022.02.025

Lawit, S. J., Wych, H. M., Xu, D., Kundu, S., and Tomes, D. T. (2010). Maize DELLA proteins dwarf plant8 and dwarf plant9 as modulators of plant development. *Plant Cell Physiol.* 51, 1854–1868. doi: 10.1093/pcp/pcq153

Li, H., Guo, L., Yan, M., Hu, J., Lin, Q., Wang, P., et al. (2022). A rapid and efficient transient expression system for gene function and subcellular localization studies in the tea plant (*Camellia sinensis*) leaves. *Sci. Hortic-Amsterdam* 297, 110927. doi: 10.1016/j.scienta.2022.110927

Li, H., Wang, L., Liu, M., Dong, Z., Li, Q., Fei, S., et al. (2020). Maize plant architecture is regulated by the ethylene biosynthetic gene *ZmACS7 1*. *Plant Physiol.* 183, 1184–1199. doi: 10.1104/pp.19.01421

Li, P., Wei, J., Wang, H., Fang, Y., and Xu, C. (2019). Natural variation and domestication selection of *ZmPGP1* affects plant architecture and yield-related traits in maize. *Genes* 10, 9. doi: 10.3390/genes10090664

Li, Z., Zhang, X., Zhao, Y., Li, Y., Zhang, G., Peng, Z., et al. (2018). Enhancing auxin accumulation in maize root tips improves root growth and dwarfs plant height. *Plant Biotechnol. J.* 16, 86–99. doi: 10.1111/pbi.12751

Liu, N., Zhao, H., Hou, L., Zhang, C., Bo, W., Pang, X., et al. (2023). HPLC-MS/MS-based and transcriptome analysis reveal the effects of ABA and MeJA on jujube (*Ziziphus jujuba* Mill.) cracking. *Food Chem.* 421, 136155.1–136155.10. doi: 10.1016/j.foodchem.2023.136155

Liu, N., Zhao, Y. J., Wu, J. W., Wei, Y. M., and Zhao, X. Y. (2020). Overexpression of *ZmDWF4* improves major agronomic traits and enhances yield in maize. *Mol. Breed.* 40, 8. doi: 10.1007/s11032–020-01152–6

Liu, Q., Zhang, S. H., and Bin., L. (2016). 14–3-3 proteins: Macro-regulators with great potential for improving abiotic stress tolerance in plants. *Biochem. Bioph. Res. Co.* 477, 9–13. doi: 10.1016/j.bbrc.2016.05.120

Lu, L., Diao, Z., Yang, D., Wang, X., Zheng, X., Xiang, X., et al. (2022). The 14-3-3 protein GF14c positively regulates immunity by modulating the protein homoeostasis of the GRAS protein *OsSCL7* in rice. *Plant Cell Environ.* 4, 45. doi: 10.1111/pce.14278

Lu, X., Yang, L., Yu, M., Lai, J., Wang, C., Mcneil, D., et al. (2017). A novel Zea mays ssp. mexicana L. MYC-type ICE-like transcription factor gene *ZmmICE1*, enhances freezing tolerance in transgenic *Arabidopsis thaliana*. *Plant Physiol. Bioch.* 113, 78–88. doi: 10.1016/j.plaphy.2017.02.002

Niti, Y., Saurav, B., Shubho, C., and Dibyendu, N. S. (2017). Molecular characterization of the 14–3-3 gene family in rice and its expression studies under abiotic stress. *Planta* 247, 229–253. doi: 10.1007/s00425–017-2779–4

Nolan, T., Chen, J., and Yin, Y. (2017). Cross-talk of brassinosteroid signaling in controlling growth and stress responses. *Biochem. J.* 474, 2641–2661. doi: 10.1042/bcj20160633

Phanchaisri, B., Samsang, N., Yu, L. D., Singkarat, S., and Anuntalabhochai, S. (2012). Expression of *OsSPY* and 14–3-3 genes involved in plant height variations of ion-beam-induced KDML 105 rice mutants. *Mutat. Res-Fund. Mol. M.* 734, 56–61. doi: 10.1016/j.mrfmmm.2012.03.002

Pilu, R., Cassani, E., Villa, D., Curiale, S., Panzeri, D., Badone, F. C., et al. (2007). Isolation and characterization of a new mutant allele of brachytic 2 maize gene. *Mol. Breed.* 20, 83–91. doi: 10.1007/s11032–006-9073–7

Plackett, A. R. G., Powers, S. J., Fernandez-Garcia, N., Urbanova, T., Takebayashi, Y., Seo, M., et al. (2012). Analysis of the developmental roles of the *Arabidopsis* gibberellin 20-oxidases demonstrates that GA20ox1, -2, and -3 are the dominant paralogs. *Plant Cell* 24, 941–960. doi: 10.1105/tpc.111.095109

Qin, C., Cheng, L., Shen, J., Zhang, Y., and Shen, C. (2016). Genome-wide identification and expression analysis of the 14–3-3 family genes in medicago truncatula. *Front. Plant Sci.* 7. doi: 10.3389/fpls.2016.00320

Roy, M. J., Surudoi, M. G., Kropp, A., Hou, J., Dai, W., Hardy, J. M., et al. (2023). Structural mapping of PEAK pseudokinase interactions identifies 14–3-3 as a molecular switch for PEAK3 signaling. *Nat. Commun.* 14, 1. doi: 10.1038/s41467–023-38869–9

Shang, Q., Zhang, D., Li, R., Wang, K., and Shi, L. (2020). Mapping quantitative trait loci associated with stem-related traits in maize (*Zea mays* L). *Plant Mol. Biol.* 104, 583–595. doi: 10.1007/s11103–020-01062–3

Sun, X., Xiang, Y., Dou, N., Zhang, H., Pei, S., and Franco, A. V. (2023). The role of transposon inverted repeats in balancing drought tolerance and yield-related traits in maize. *Nat. Biotechnol.* 41, 120–127. doi: 10.1038/s41587–022-01470–4

Tao, Y., Zheng, J., Xu, Z., Zhang, X., Zhang, K., and Wang, G. (2004). Functional analysis of *ZmDWF1*, a maize homolog of the *Arabidopsis* brassinosteroids biosynthetic *DWF1*/*DIM* gene. *Plant Sci.* 167, 743–751. doi: 10.1016/j.plantsci.2004.05.012

Wang, H. S., Gu, L. J., Zhang, X. G., Liu, M. L., Jiang, H. Y., Cai, R. H., et al. (2018). Global transcriptome and weighted gene co-expression network analyses reveal hybrid-specific modules and candidate genes related to plant height development in maize. *Plant Mol. Biol.* 98, 187–203. doi: 10.1007/s11103–018-0763–4

Wang, H. S., Zhang, X. G., Hu, F. X., Liu, M. L., Zhao, Y., Wang, Y., et al. (2019). Systematic identification and characterization of candidate genes for the regulation of plant height in maize. *Euphytica* 215, 2. doi: 10.1007/s10681–019-2345–1

Wang, W., Tan, H., Sun, M., Han, Y., and Ni, T. (2021). Independent component analysis based gene co-expression network inference (ICAnet) to decipher functional modules for better single-cell clustering and batch integration. *Nucleic Acids Res.* 49, e54. doi: 10.1093/nar/gkab089

Wang, Y. J., Deng, D. X., Ding, H. D., Xu, X. M., Zhang, R., Wang, S. X., et al. (2013). Gibberellin biosynthetic deficiency is responsible for maize dominant *Dwarf11* (*d11*) mutant phenotype: physiological and transcriptomic evidence. *PloS One* 8, e66466. doi: 10.1371/journal.pone.0066466

Wang, Y. P., Xu, Q., Shan, H. C., Ni, Y., Xu, M. Y., Cheng, B. J., et al. (2023). Genome-wide analysis of *14–3-3* gene family in four gramineae and its response to mycorrhizal symbiosis in maize. *Front. Plant Sci.* 14. doi: 10.3389/fpls.2023.1117879

Winkler, R. G. (1995). The maize Dwarf3 gene encodes a cytochrome P450-mediated early step in Gibberellin biosynthesis. *Plant Cell 7* 8, 1307–1317. doi: 10.1105/tpc.7.8.1307

Xu, H., Qian, Z., Yupei, J., Chuanwei, Y., Qianyue, W., and Lin, L. (2018). Shade-induced nuclear localization of PIF7 is regulated by phosphorylation and 14–3-3 proteins in *Arabidopsis*. *Elife* 7, e31636. doi: 10.7554/eLife.31636

Zhao, X., Li, F., Li, K., and Wicke, S. (2021). The 14-3-3 proteins: regulators of plant metabolism and stress responses. *Plant Biol.* 23, 531–539. doi: 10.1111/plb.13268

Zhao, Y., Zhang, S., Lv, Y., Ning, F., Cao, Y., Liao, S., et al. (2022). Optimizing ear-plant height ratio to improve kernel number and lodging resistance in maize (*Zea mays* L.). *Field Crop Res.* 276, 108376–108388. doi: 10.1016/j.fcr.2021.108376

Zhu, J. W., He, X. H., Li, Y. Z., Zhang, Y. L., Yu, H. X., Xia, L. M., et al. (2022). Genome-wide analysis of the mango SPL family and overexpression of MiSPL13 confers early flowering and stress tolerance in transgenic *Arabidopsis*. *Sci. Horti-Amsterdam* 305, 1–15. doi: 10.1016/j.scienta.2022.111363

frontiers | Frontiers in Plant Science

TYPE Review
PUBLISHED 19 August 2024
DOI 10.3389/fpls.2024.1453951

OPEN ACCESS

EDITED BY
Verónica S. Di Stilio,
University of Washington, United States

REVIEWED BY
Florian Jabbour,
Muséum National d'Histoire Naturelle, France
Aniket Sengupta,
St. John's University, United States

*CORRESPONDENCE
Bharti Sharma
bsharma@cpp.edu

RECEIVED 24 June 2024
ACCEPTED 29 July 2024
PUBLISHED 19 August 2024

CITATION
Sharma B, Pandher MK, Alcaraz Echeveste AQ, Romo RK and Bravo M (2024) *Delphinium* as a model for development and evolution of complex zygomorphic flowers. *Front. Plant Sci.* 15:1453951. doi: 10.3389/fpls.2024.1453951

Delphinium as a model for development and evolution of complex zygomorphic flowers

Bharti Sharma*, Mankirat Kaur Pandher, Ana Quetzali Alcaraz Echeveste, Rene Kenny Romo and Marianellie Bravo

Department of Biological Sciences, California State Polytechnic University, Pomona, CA, United States

The complex zygomorphic flowers of the early-diverging eudicot *Delphinium* provide an opportunity to explore intriguing evolutionary, developmental, and genetic questions. The dorsal perianth organs, consisting of a spurred sepal and the nectar-bearing spurred petal(s) in *Delphinium*, contribute to the dorso-ventralization and zygomorphic flower morphology. The seamless integration of the two or three dorsal petaloid spurred organs is considered a synorganization, and the resulting organ complex is referred to as a hyperorgan. The hyperorgan shows variability within the tribe due to variation in the number, size, and shape of the spurs. Research in recent decades within this tribe has enhanced our understanding of morphological evolution of flowers. More recently, functional studies using the RNAi approach of Virus-Induced Gene Silencing (VIGS) have unraveled interesting results highlighting the role of gene duplication in the functional diversification of organ identity and symmetry genes. Research in this early-diverging eudicot genus bridges the gaps in understanding the morphological innovations that are mostly studied in model grass and core eudicot clades. This first comprehensive review synthesizes eco-evo-devo research on *Delphinium*, developing a holistic understanding of recent advancements and establishing the genus as an exceptional model for addressing fundamental questions in developmental genetics, particularly in the evolution of complex flowers. This progress highlights *Delphinium's* significant potential for future studies in this field.

KEYWORDS

***Delphinium*, zygomorphy, synorganization, model system, evo-devo, petaloid spurs**

1 Introduction

The flowering plants or angiosperms trace their evolutionary lineage back to around 140 million years ago (Mya) (Magallón et al., 2015; Sauquet et al., 2017, 2022). Considering the earth's evolutionary history, angiosperms have diverged dramatically in this brief period. As a result, the existing +350,000 angiosperms display a stunning array of floral

diversity (Endress, 2011; Christenhusz and Byng, 2016). This diversity provides an opportunity to understand complex evolutionary and genetic mechanisms that have sculpted novel and intriguing developmental innovations.

Nestled within this diversity is the early-diverging eudicot order Ranunculales, which includes the genus *Delphinium*, noted for its zygomorphic floral morphology. Floral symmetry is predominantly classified into two types: radial symmetry or actinomorphy with more than two planes of symmetry, and bilateral symmetry or zygomorphy with one plane of symmetry. The Delphinieae tribe, to which *Delphinium* belongs, is comprised of approximately 650–750 species, representing ~25% of the Ranunculaceae family (Figure 1, Jabbour and Renner, 2012b; Novikoff and Jabbour, 2014; Espinosa et al., 2017). Zygomorphy has evolved several times in angiosperms but only once in Ranunculaceae, in the ancestors of the tribe Delphinieae (Jabbour et al., 2009a; Citerne et al., 2010; Jabbour and Renner, 2012b; reviewed by Hileman, 2014a; Reyes et al., 2016). The arrangement of perianth organs in *Delphinium* zygomorphic flowers represents a fascinating example of morphological diversification this makes the genus popular for horticultural purposes (Figures 2A-C, Jabbour et al., 2009b). In *Delphinium*, the elaborate perianth is composed of two distinct whorls, each playing a crucial role in the flower's overall form and function. The two whorls of perianth organs in *Delphinium* are the sepals and petals, both are petaloid. Petaloidy is the term used to define organs attractive to pollinators, the display of petaloidy is not limited to perianth organs; showy bracts, leaves, and other organs can also be petaloid (Rasmussen et al., 2009; Sharma and Kramer, 2017).

The first whorl (W1) of perianth organs consists of four simple and flat petaloid sepals (Figure 2D, two lateral and two ventral) and one dorsal sepal that is spurred (Espinosa et al., 2021a). The asymmetrically elongated dorsal spurred sepal is particularly intriguing. It is noteworthy to mention that these spurs do not have nectaries. These spurs are petaloid, colored, and attractive (Figures 2C, E). Besides the aesthetic appeal of the flower, the petaloid sepals serve functional purposes in pollination and protecting reproductive organs (Macior, 1975). Spurs have independently evolved in Delphinieae relative to *Aquilegia*, which is also a member of the Ranunculaceae family (Delpeuch et al., 2022; Li et al., 2024a).

Within the second whorl (W2) are two lateral, showy petals that are trichome-rich in the center, often with a yellow spot and a pubescent texture (Figures 2B, F). These petals are not present in the genera *Aconitum* and *Gymnaconitum*, or in the subgenus *Consolida* of *Delphinium*. In addition to the showy petals are two (one in some species) dorsal, spurred petals (Figures 2G, H) that bear nectaries. These nectariferous petal(s) grow inside the hollow vicinity of the sepal spur whose three-dimensional morphology completely

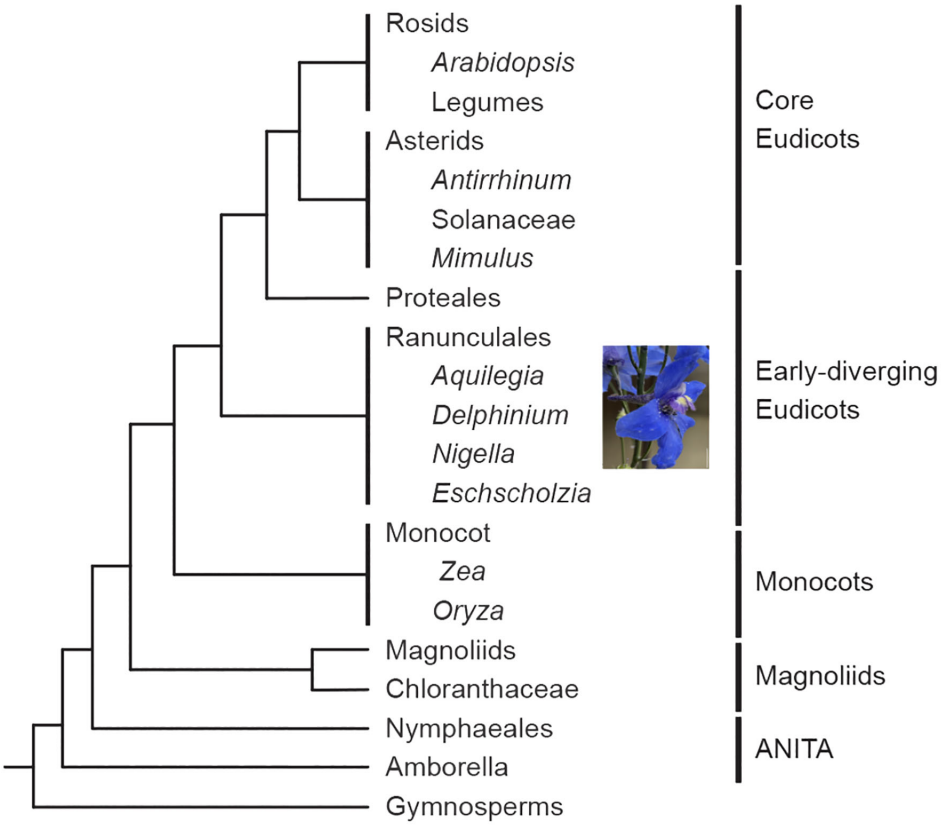

FIGURE 1
Simplified phylogeny of the angiosperms based on Moore et al. (2007) and Kramer and Hodges (2010) showing the position of *Delphinium* relative to other major model systems. Scale bar: 1 cm.

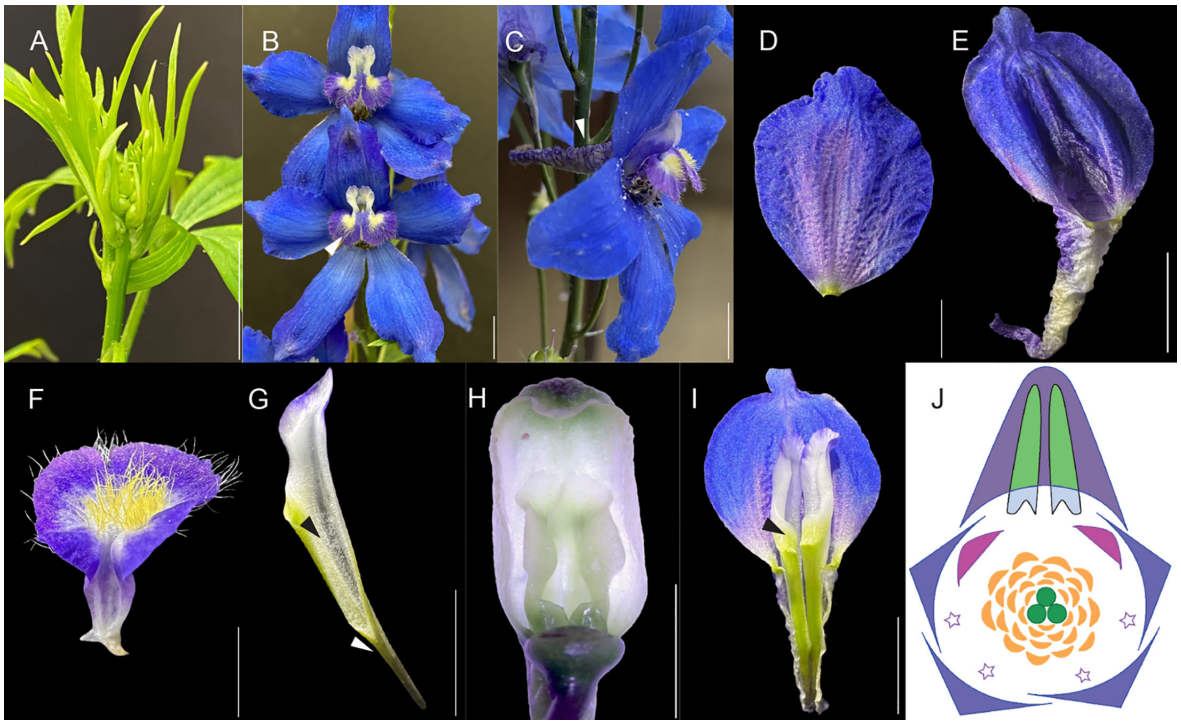

FIGURE 2
Photos of *Delphinium* x *belladonna "Bellamosum"* flower showing the arrangement of perianth organs, spur arrangement, and its floral organs appearance. **(A)** inflorescence, **(B)** front view with white arrow indicating trichome rich, non-spurred lateral petals, **(C)** side view with white arrow indicating sepal spur, **(D)** sepal, **(E)** spurred sepal, **(F)** non-spurred lateral petal, **(G)** spurred petal, black arrow pointing to the indented area, and white arrow pointing to three-dimensional cavity, **(H)** Spur-in-spur arrangement showing paired spurred petals residing within spurred sepal, **(I)** black arrow pointing to nectar-bearing spurred petal **(J)** floral diagram - in the dorsal region, there is a single-spurred sepal (purple), paired spurred petals (green spurs and light blue labium). Within the outer whorl, four sepals are present (blue-purple), and in the second whorl, reduced petals (stars), and two trichome-rich, non-spurred lateral petals (pink) are present. In the third whorl, stamens are present (yellow), and the fourth whorl contains carpels (green). Scale bars A-C, E, G, and I: 1 cm and D, F, and H: 0.5 cm.

envelops the tubular spurs of the petals while the labium of the dorsal petals remains open to pollinators. Under the labium, the spur is indented, the dorsal ends of each petal spur, below the indented portion, form a completely closed three-dimensional cavity (Jabbour et al., 2021, Figure 2G) The spurred petals function in attracting and guiding pollinators, ensuring effective pollination (Jabbour and Renner, 2012b). The close arrangement of these petals, growing snugly into the pocket of the spurred sepal, is a remarkable adaptation. This spur(s)-in-spur is considered a synorganization (Chen et al., 2018), and the resulting structure is referred to as a hyperorgan (Figures 2H, I, Jabbour et al., 2021). Besides being visually striking, it has been speculated that this spur (s)-in-spur configuration serves a protective function, shielding the delicate nectaries from environmental stressors and protecting the integrity of the nectar, preventing leakage and adulteration (Chen et al., 2018). Paired and nectariferous petal spurs are only observed in Delphinieae in the Ranunculaceae family (Jabbour and Renner, 2012b).

The micromorphological features of the dorsal sepal spur (W1) and petal spurs (W2) are quite distinct (Jabbour and Renner, 2012b; Zhao et al., 2023). This complex arrangement of perianth organs in *Delphinium* flowers reflects a sophisticated interplay between genetic predisposition and environmental adaptation, leading to the development of structures that optimize pollination efficiency and hence contribute to the fitness of this tribe (Jabbour et al., 2009b). The analysis of these features in studies detailed in this review provides invaluable insights into the broader patterns of floral evolution and diversification among angiosperms.

This is the first comprehensive review that compiles the insights derived from various morphological, developmental, and genetic studies that elucidate floral morphology and organ identity in *Delphinium*. Through a focused exploration of biogeography, morphology, and molecular studies on perianth organization and symmetry, we develop a primer on the overall progress made in unraveling the evolutionary strategies that shape the distinctive flowers in *Delphinium*. Moreover, this review endeavors to articulate future research directions, positioning *Delphinium* as a key model system for understanding the complexities of flower development and the evolutionary marvel of zygomorphic flowers in the vast and diverse world of angiosperms.

2 Biogeography and genetic diversity

The *Delphinium* subgenus, in addition to three genera, namely *Staphisagria*, *Aconitum*, and *Gymnaconitum* collectively form the Delphinieae tribe (Jabbour and Renner, 2012a; Zalko et al., 2021). *Staphisagria* was raised to the level genus after the resurrection of

the genus *Staphisagria* J. Hill (Jabbour and Renner, 2011b; Jabbour and Renner, 2012a). The evolutionary trajectory of this tribe is purported to have originated during the early Oligocene period, >32.3 million years ago (Jabbour and Renner, 2011a). The precise identification of their ancestral geographical region was rendered challenging by the unresolved status of their sister group of the tribe (Jabbour and Renner, 2012a). Recent studies suggest that the tribe Nigelleae is the sister group of Delphinieae (Lehtonen et al., 2016; Zhai et al., 2019).

The *Delphinium* genus is posited to have originated in East Asia during the late Oligocene around 24.27 Mya (Xiang et al., 2017). Subsequently, this genus underwent a notable evolutionary transition towards the perennial life cycle and a consequential expansion event in Asia during the late Miocene, approximately 9.7 Mya, facilitated by a phase of rapid diversification. Following this diversification across the Qinghai-Tibetan Plateau (QTP), *Delphinium* traversed into North America during the Pliocene, around 3 Mya, coinciding with the submergence of the Bering Strait (Brigham-Grette, 2001), and into East Africa (Figure 3, Jabbour and Renner, 2012a). Concomitantly, during this temporal epoch, *Delphinium* extended its geographical presence into the East African mountains, occurring between 0.7 and 4.4 Mya (Jabbour and Renner, 2012a; Chartier et al., 2016). This migration into East Africa was after the genus's diversification in the Irano-Turanian region, coupled with its expansion into the Balkans and Italy between 7-8 MYA (Figure 3, Xiang et al., 2017).

Within Delphinieae, variation in ploidy levels has been observed. The online Delphinieae Chromosome Database (DCDB) http://www.delphinieae.online has recently been updated and is now online. This database provides information on chromosome number, karyological data, and estimated ploidy levels of members of the Delphinieae tribe. The information is based on published resources that have been deemed accurate by the authors. The database contains information on 425 species of this tribe (Bosch et al., 2023). The diploid number of chromosomes in Delphinieae ranges from 2n=12 to 2n=64. The most frequently observed karyotype among Delphinieae species is 2n=16 and 2n=32 (Bosch et al., 2023 http://www.delphinieae.online). However, chromosome numbers ranging from 2n=14 to 52 are also present (Bosch et al., 2023). *Aconitum* has the most variation in chromosome numbers (Supplementary Table 1). The authors suggest that this information can be particularly useful for cytotaxonomical databases and for systematic and evolutionary research (Bosch et al., 2023). Besides this, a recent study by Luo et al. (2023) reported a comparative karyomorphological analysis and genome size of five taxa from *Delphinium* sub genus *Anthriscifolium*. The diploid genome size ranged from 3.02–3.92 pg, while for tetrapolid it ranged from 6.04–6.60 pg (Luo et al., 2023, Supplementary Table 2). Additionally, the genome of *S. picta* is being sequenced, and expression atlases are being produced (The RanOmics group et al., 2024).

Chloroplast (cp) genomes are valuable tools for studying evolutionary relationships and have been widely used in reconstructing phylogenetic relationships (Soltis and Soltis, 1998; Li et al., 2021, 2024). In Delphinieae, the cp genome has been sequenced for various species in recent years and is now being deployed to study phylogenetic and phylogeographic relationships within the genus (Duan et al., 2020; Li et al., 2020; Park et al., 2020; Song et al., 2024).

3 Pollinators and pollination

Pollinators play a pivotal role in the reproductive success of plants. The relationship of plants with their pollinators has been the central focus of evolutionary studies. Changes in plant-pollinator relationships are often due to changes in morphology, including but not limited to color, shape, novel organs, or changes in nectar

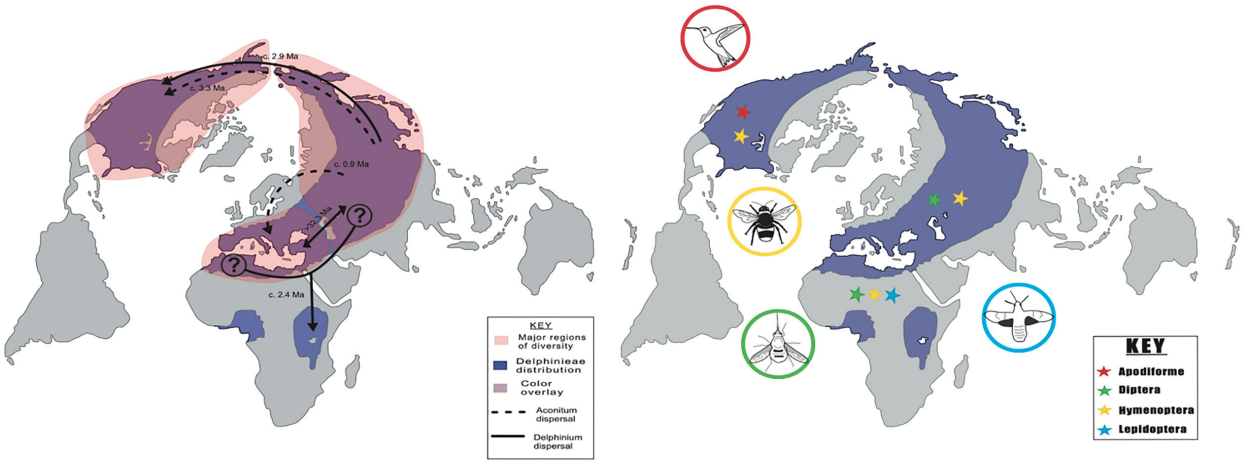

FIGURE 3
Regions of diversity, current day Delphinieae distribution and most common tribe pollinators. Adapted from Jabbour and Renner (2012a) (Left) Delphinieae's major regions of diversity, the Mediterranean region, Asia (Eurasia), and North America. The sampling data did not include species from West Africa, origin source and genetic divergence was not inferred. *Aconitum:* dashed line. *Delphinium:* solid line. (Right) Present day Delphinieae distribution area represented by purple shading. Four most frequented pollinator orders among the tribe and their general geographic distribution; Hymenoptera (yellow), Lepidoptera (blue), Diptera (green), and Apodiformes (red).

production or flowering time. Within the Delphinieae tribe, adaptation to insect pollination is observed. This might be an outcome of the floral morphology that features a floral parlor that not only attracts and guides the pollinators but also conceals the sugary nectar. Leppik (1964) defines parlor as a reception area for pollinators, in Delphinieae, the shared cavity in the hyperorgan is considered as a parlor. This unique morphology entices insects into repeatedly inserting and retracting their tongues or proboscises to access the nectar. These movements are implicated to maximize pollination and fit into the broader context of coevolutionary relationships that plants and pollinators share (Bosch et al., 1997). The existing studies have provided valuable insights into the interactions between the Delphinieae tribe and its pollinators. The observed pollinators within Delphinieae are bees (queen, bumblebees, and solitary in some cases), hummingbirds, hawkmoths, and the wind (Figure 3, Jabbour et al., 2009b; Jabbour and Renner, 2012b).

Amongst the insect pollinators, bee pollination is predominant, with more than 90% of Delphinieae species exhibiting this pollination mode. However, North American *Delphinium* species display variation. For instance, species such as *D. barbeyi, D. nuttallianum, D. tricorne*, in addition to bees rely on hummingbird-facilitated pollination (Jabbour and Renner, 2012b). In contrast, *D. cardinale*, and *D. nudicaule* rely exclusively on hummingbird-facilitated pollination. In East African species, *D. leroyi* hawkmoth pollination is observed (Johnson, 2008; Chartier et al., 2016). Bees and hawkmonth pollination have been observed in, *D. obcordatum* and *D. verdunense*, as well as in two species of *Staphisagria* subgenus (Supplementary Table 3, Jabbour and Renner, 2012a). In many Delphinieae species, effective pollinators are not specialized; however, bees pollinate the short-spurred species, the longest-spurred species are pollinated by hawkmoths, and medium-spurred varieties are pollinated by hummingbirds (Jabbour et al., 2009b). A similar pattern is also observed in *Aquilegia*, another genus within the Ranunculaceae that has evolved petal spurs independently (Hodges, 1997).

Within the *Staphisagria* species, the lowest activity of insects has been reported, which can be a result of imperfect herkogamy, leading to selfing (Bosch et al., 1997, 2001). The prevailing interferences suggest that Delphinieae has undergone very few pollinator switches (Jabbour and Renner, 2012b). The mean length of inner spurs ranges approximately from 4–30 mm in *Delphinium* and *Staphisagria* (Jabbour and Renner, 2012b). Bee-pollinated species in high-altitude southeast China, *D. tatsienense* and *D. oxycentrum*, and hawkmoth-pollinated species, *D. leroyi* in tropical Africa exhibit the longest spurs, 30, 34 and 37.5 mm respectively (Jabbour and Renner, 2012b). Bosch et al. report a clear correlation between altitudes and percentage of *Bombus* that visit the taxons growing in these altitudes (Bosch et al., 1997). Notably, no correlation between spur length and altitude was reported by Jabbour and Renner (2012b). It should be mentioned that Jabbour et al. (2021) suggest a re-assessment of relationship between the Delphinieae species and its pollinators. Such a re-assessment is necessary because traditionally outer spur lengths have been measured and reported in botanical and taxonomic treatments, although the nectar reward is provided by inner spurs (Jabbour and Renner, 2012b; Jabbour et al., 2021.

3.1 Nectaries and nectar secretion

A study by Antón and Kamińska (2015) analyzed the anatomy of floral spurs and the method of nectar exudation in four species of the Ranunculaceae family, including, *Aconitum lycoctonum* L., *Aquilegia vulgaris* L., *Consolida regalis* Gray, and *Delphinium elatum* L. These species share a general structural arrangement of nectaries, consisting of a single layer of internal epidermis, several layers of nectar-producing parenchyma cells, and underlying ground parenchyma. Despite this structural similarity, the method of nectar secretion varies among species. In *A. lycoctonum* and *A. vulgaris*, nectaries are located at the apices of the spurs, and nectar is produced through a holocrine method, where the epidermal cell wall erupts, resulting in nectar containing disrupted cell organelles such as mitochondria and nuclei. In contrast, in *D. elatum* and *C. regalis*, nectaries are located along the floor of the spur, with nectar exuding through microchannels into the cuticle; the secretory tissue is positioned along the ventral surface of the spur (Antoń and Kamińska, 2015).

Additionally, the study highlights the relationship between nectary spur length and pollinator type. The relatively long nectar spurs of the studied species are associated with long-tongued bumblebees, their primary pollinators (Jabbour and Renner, 2012b; Antón and Kamińska, 2015).

4 Diversity in floral organ morphology and synorganization in Delphinieae

Within the Delphinieae tribe, flowers exhibit remarkable morphological diversity, yet all share a common structural plan. As mentioned above, the calyx is petaloid and elaborate with a dorsal sepal sculpted into a pocket or hood (spur), varying in length and shape across the tribe (Chen et al., 2018). The dorsal enclosed spurred petal(s) comprise three components: a stalk, spur, and labium, with variations in number and their proportions across different Delphinieae clades (Jabbour and Renner, 2012b; Chen et al., 2018). Because of the variation in morphology (of both sepal and petal(s) spur) and in the number of petals, the overall three-dimensional structure of the hyperorgan itself shows variation, as explained with specific examples below (Figure 4). In many species of Delphinieae, ventral and lateral petals have been observed. Interestingly, the development of ventral petals (shown as stars in Figure 2J) is arrested at an early developmental stage. Their number varies from 4–8, and these petals have been referred to as reduced petals in the literature. There is one report that describes the stage at which the development is arrested and triangular reduced and aborted non-spurred petals are observed (Zalko et al., 2021). Besides, trichome-rich, showy, non-spurred lateral petals are observed in many species, including those in the genus

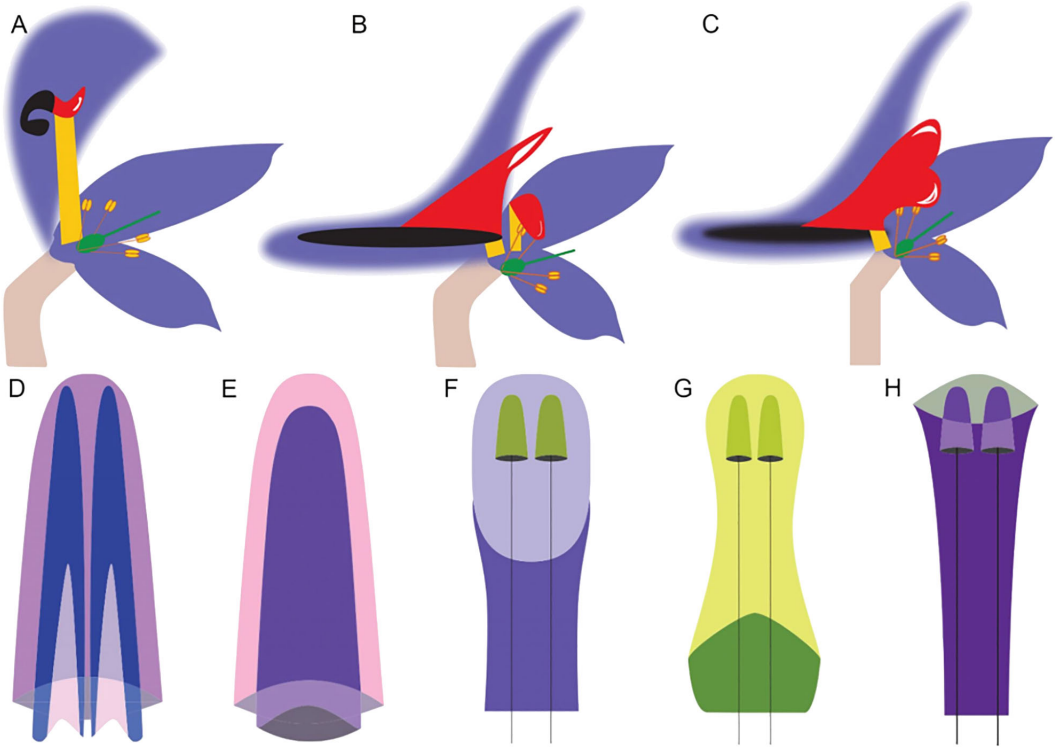

FIGURE 4
Differences in the morphology of the hyperorgan of the *Delphinieae* tribe. **(A-C)** (Adapted from Jabbour and Renner (2012b); Jabbour et al. (2021)), schematic longitudinal sections of perianth organization, Hooded type, Spurred type, and Spurred type with fused W2 organs, respectively. W1 organs are shown in purple, W2 organs stalk, labium, and spur are shown in yellow, red, and black, respectively. Half organs are drawn with faded lines. Gynoecium and androecium are represented by the green structure and protruding stamens. The number of carpels and stamens vary depending on the species. **(D)**, Spurred type hyperorgan with two spurs inside a third found in *Staphisagria*, *Delphinastrum*, *Oligophyllon*, *Anthriscifolium*, and *Delphinium*. **(E)**, Spurred-type with fused W2 organ with one spur inside a second found in *Consolida*. **(F, G)**, Hooded type hyperorgan with two short spurs on long pedicels enveloped by a helmet or cap shaped sepal found in *Aconitum*. **(H)** Hooded type hyperorgan with two short spurs on long pedicels covered by a portruding sepal found in *Gymnaconitum*..

Staphisagria and the subgenera *Delphinium*, *Anthriscifolium*, *Delphinastrum*, and *Oligophyllon* of the genus *Delphinium* (Zalko et al., 2021).

The morphological diversity of the hyperorgan of the tribe Delphinieae has been categorized into three types based on perianth organization: hooded-type, spurred-type, and spurred-type with fused W2 organs (Figures 4A-C, Jabbour and Renner, 2012b). Within the hooded-type perianths, further variations are noted, such as the dorsal sepal appearing as a helmet or as a cap, protruding and elaborating over the curved nectar-bearing petals (Figures 4D-H). Helmet, cap-type, protruding short spurs carried on a long pedicle with a stalk much longer than the labium can be found in the genus *Aconitum*. (Jabbour et al., 2021). The *Delphinium* subgenus and *Staphisagria* exhibit spurred-type hyperorgan morphology where the two most dorsal petals are spurred and encased within a dorsal spurred sepal. The spurred type with fused W2 organs is observed in *Consolida* which is a subgenus of *Delphinium* (DuPasquier et al., 2021; Espinosa et al., 2021b). Similarly to *Aconitum*, reduced primordia also evolved in subgenus *Consolida* alongside the fusion of the W2 dorsal primordia as well as the development of basal wings on the sides of the W2 adult organs (Jabbour and Renner, 2012b).

5 Petals and their molecular basis in *Delphinium* and standing questions on petaloidy of sepals

The evolution of petals stands as one of the major factors underlying the fitness and perhaps rapid radiation and diversification of angiosperms (Drea et al., 2007; Whittall and Hodges, 2007). Within the Ranunculaceae family, the morphological diversity in perianth organs is notable. The floral diversity is especially exemplified by nectaries and elaborate floral perianth organs. Most commonly, a bipartite perianth that is composed of sepals in the outer whorl and petals in the second whorl is observed in this family (Kosuge, 1994; Jensen and Kadereit, 1995). However, the family is also characterized by a perianth that includes elaborate spurs, asepalous and apetalous taxa, and organs with ambiguous identities that can represent either sepals or petals (Rasmussen et al., 2009). Such diversity is specifically noted in genera such as *Nigella* (forked petals with pseudonectaries), *Aquilegia* (nectar-bearing petal spurs, petaloid sepals), and in recent years more extensively discussed in *Delphinium*. Within the tribe Delphinieae, both whorls of perianth organs are petaloid,

and the complex perianth has spurred and non-spurred forms of sepals and petals. The hyperorgan makes the flowers elaborate. This kind of diversity between and within the whorls begs obvious explanation from a developmental genetics perspective. Simply, the obvious question that entreats exploration is - What genetic programs contribute to the establishment of distinct petaloid perianth organs in *Delphinium*? Do the nectar and non-nectar-bearing spurs share a common or distinct genetic organ identity program?

The genetic bases of floral organ identity establishment were put forth by the "ABC", "ABCE" and "Quartet" models (Bowman et al., 1991; Coen and Meyerowitz, 1991; Honma and Goto, 2001; Theissen and Saedler, 2001). As proposed by these models based on functional studies in core eudicots, the expression of A+E is required for sepal identity, A+B+E for the establishment of petal identity. Conservation of A function outside core eudicots is not observed (Litt, 2007).

Gene duplications within ABCE genes has resulted in multiple paralogs. In the Ranunculaceae family, two such duplication events have occurred (~70–120 Mya) within the B class *APETALA3* (*AP3*) gene lineage that have resulted in *AP3-1*, *AP3-2* and *AP3-3* lineages (Kramer et al., 2004; Rasmussen et al., 2009; Zhao et al., 2023). The homologs of these are retained in *Delphinium*, *DeajAP3-1*, *DeajAP3-2*, and *DeajAP3-3*. Similarly, in *Delphinium* the other B gene homolog, *PISTILLATA* (*PI*) has two copies *DeajPI1* and *Deaj PI2*. Three homologs of the E class gene, *SEPALLATA (SEP) Deaj Sep1*, *DeajSEP-2*, and *DeajSEP-3* have also been reported (Zhao et al., 2023).

A recent study by Zhao et al. (2023) reports the function of B-class genes based on the functional study conducted using VIGS. How the functional roles of these duplicate genes have evolved and how the resulting genetic networks have contributed to sculpting the complex zygomorphic flowers and the diversification of the tribe Delphinieae, is something that needs to be explored meticulously with functional genetics.

The expression of B genes in developing *Delphinium* flowers shows some conserved expression patterns but also highlights differentiated expression among paralogs (Supplementary Table 4). The expression patterns of D*eajAP3-1* and *DeajAP3-2* are broad, but both are strongly expressed in stamens. *DeajAP3-3* is highly expressed in the dorsal petal spurs. Both *PI* paralogs are differentially expressed. *DeajPI1* is highly expressed across all developmental stages and all floral organs except in developed carpels. *DeajPI2* expression is most prominent in stamens at later developmental stages but in early developmental stages across all organs, it shows a milder expression. The E class *SEP* paralogs also show differential expression, *DeajSEP3* gene is shown to be expressed across all organs and developmental stages, while the expression of *SEP1* and *2* homologs is broad and weak. *DeajSEP2* is not expressed in matured stage (S12) dorsal nectiferous petals and stamens (Zhao et al., 2023).

The availability of genetic resources, specifically a functional tool such as VIGS, as recently reported by Zhao et al., 2023, has made it possible to unravel the functional role of important genes that orchestrate the establishment of floral organ identity in *Delphinium ajacis* (*Deaj*). Functional knockdown of the *AP3-3* homolog in *Delphinium ajacis* (*DeajAP3-3*), a species that exhibits a fused single-spurred dorsal petal and lacks lateral non-spurred petals, results in the homeotic conversion of spurred nectary bearing petal into fused double spurred sepal. The knocking down of *DeajAP3-3* and *DeajAP3-1* together resulted in the reduced petals homeotically converted into sepals, exhibiting more than two outer whorls of sepals followed by the stamens and carpels. The dorsal petal homeotically transforms into a fused, double-spurred sepal. The phenotypes obtained by gene knockdown of all three homologs of *AP3-3* (TRV2-*DeajANS-DeajAP3-1*, and *DeajAP3-2, DeajAP-3*) are classic B knockout phenotypes, with outer whorls consisting of sepals and inner whorls comprising carpels. Also, the dorsal single-spurred petal homeotically transforms into a fused double-spurred sepal (Figure 5). Interestingly, the reduced petals are homeotically transformed into sepals. The exact phenotype is also obtained when both *PI* homologs (TRV2-*DeajANS-DeajPI1 and DeajPI1)* are knocked down together (Figure 5). These results highlight that AP3-3 and PI proteins are in an indispensable partnership and they function together as obligate heterodimers. *AP3-1* and *AP3-2* have a role in stamen identity whereas *AP3-3* and *AP3-1* together have functional overlap in regulating petal identity.

It is important to note that in B gene knockdowns, the dorsal petal spur's identity changes from fused single-spurred petals into fused double-spurred sepals through homeotic transformation. Although the spur identity changes, the 3D spur development and outgrowth still occur due to complete homeosis, however, it is interesting that the homeotic organ has two spurs with fused labium but unfused spur outgrowth (Figure 5). The dorsal spur outgrowth in *Delphinium* also contributes to zygomorphy, hence it can be implicated that the organ identity program of dorsal spurs is downstream of the zygomorphy program. In actinomorphic *Aquilegia*, spur outgrowth is lost with the downregulation of *AP3-3 or PI* homologs (Kramer et al., 2007; Sharma et al., 2011), however, this is complete homeosis as sepals are not spurred in *Aquilegia*. This further implies that the evolution of spur in dorsal petaloid organs in *Delphinium* might have caused the shift from actinomorphy to zygomorphy. As a future avenue, it will be interesting to explore how zygomorphy contributes to spur formation in both petaloid whorls.

As mentioned above, lateral petals are not present in *D. ajacis* but recent studies by Zhang et al. (2024a) have used *D. anthriscifolium*, which exhibits lateral petals, as a model system to provide new insights. In this species, the *DeanAP3-3* knockdown resulted in all petals, including dorsal spurred (2), lateral (2), and reduced petals (4), being homeotically transformed into flat non-spurred sepals. This result contrasts with the findings of Zhao et al. (2023), where the dorsal petal was homeotically transformed into fused double-spurred sepals, and the reduced petal identity remained unaffected. The discrepancy could be due to a stronger gene silencing effect in the Zhang et al. (2024a) study. Alternatively, as suggested by Zhang et al. (2024a), there may be interspecific differences in the regulatory mechanisms of the *AP3-3* homolog. In *D. ajacis*, the *AP3-3* homolog may specifically regulate dorsal petal identity, while in *D. anthriscifolium*, it may control the identity of dorsal, lateral, and reduced petals (Zhao et al., 2023; Zhang et al., 2024a). In another study by Zhang et al. (2024b), the role of the class I HD-Zip transcription factor *LATERAL MERISTEM IDENTITY I*

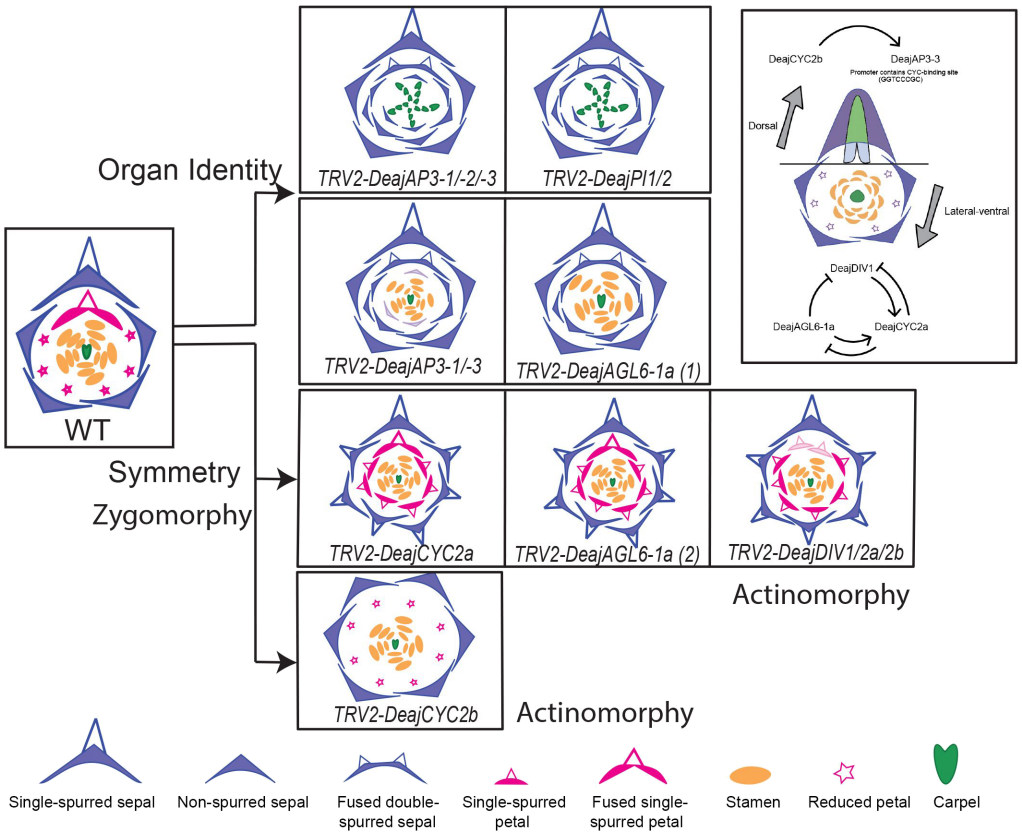

FIGURE 5
Relationship between floral organ identity and symmetry genes as observed in *D. ajacis*. Knockdown phenotypes of different floral organ identity and symmetry genes are compared to observe patterns. Gene knockdown that produces similar phenotype are placed in the same row. Through this comparison, floral organ identity genes and symmetry genes can be clearly separated, and interestingly, the role of *DeajAGL6-1a* in both organ identity and symmetry can be observed here. To the right, regulatory links between floral symmetry and organ identity genes are shown in the dorsal and lateral-ventral region. Arrows indicate positive regulation, while blunt arrows represent negative regulation; the dotted line separates dorsal and lateral-ventral regions. Floral organ diagrams adapted from Zhao et al., 2023.

(*DeanLMI1*) gene homolog in petal asymmetric development was demonstrated using VIGS.

6 Developmental and genetic bases of zygomorphy in Delphinieae and the crossroads where symmetry and *MADS-box* genes intersect

Zygomorphy is a derived state in angiosperms and is often associated with pollinator specialization (Ronse De Craene et al., 2003; Zhang et al., 2013). The ancestral state for Ranunculaceae flowers is spiral phyllotaxy and an open floral ground plan, typically associated with actinomorphy. The transition from the ancestral state of actinomorphy to the derived zygomorphy happened once in Ranunculaceae in the ancestor of the Delphinieae tribe that further diverged into *Staphisagria, Aconitum*, *Gymnaconitum*, and *Delphinium* (Zalko et al., 2021). Generally, zygomorphy is associated with whorled phyllotaxy, however, in Delphiniae the floral organs are arranged on an ontogenic spiral (Payer, 1857). In developmental studies conducted on *D. staphisagria* and *D. grandiflorum*, the zygomorphy is established in a later developmental stage that coincides with the dorsal sepals and petal spur development (Jabbour et al., 2009b). The organogenesis process is predominantly centripetal the sepals develop first followed by petals, stamens, and finally carpels (Schöffel, 1932).

Reported by Jabbour et al. (2009b), the majority of the development and organ identity establishment happens in *Delphinium* in the first quarter of development, the developmental scale in this study was based on the base width of the floral bud to an adult flower. However, it is important to note that after petal primordia initiation, petal development is delayed and reinitiated later; it is at this time when the dorsal petals acquire the three-dimensional spur shape. The hood/helmet/spur in sepals develops after the petal spur. The establishment of zygomorphy happens when the bud is 2mm (Kosuge and Tamura, 1988; Jabbour et al., 2009b) in *D. grandiflorum;* however, a delay is reported in *D. staphisagria*. These developmental studies implicate that zygomorphy establishment is correlated with the 3D growth of the spur(s) in petals and subsequently in sepals.

Gene duplication within organ identity and symmetry genes has facilitated novel functions of the duplicated homologs, driving diversification and evolutionary radiation (Kramer and Zimmer, 2006; Sharma et al., 2014). These phenomena contribute

significantly to the phenotypic complexity and adaptability. The *CYCLOIDEA* (*CYC*) and *DIVARICATA* (*DIV*) are integral to the regulation of floral symmetry and development in flowering plants. *CYC*, a TCP transcription factor, plays a critical role in establishing bilateral symmetry (zygomorphy) by regulating the development of dorsal petals (Zhang et al., 2010; Howarth et al., 2011; Zhang et al., 2013). *DIV*, another key player in floral symmetry, often works in conjunction with other genes to influence petal development and symmetry (Hileman, 2014b; Madrigal et al., 2019).

Within the Ranunculaceae family, there are two *CYC* clades, *RanaCyL1* and *RanaCyL2* (Jabbour et al., 2014). Delphinieae-specific duplication events have further resulted in two paralogs of each, *DelCYC1a*, *DelCYC1b*, *DelCYC2a*, and *DelCYC2b* (Zhao et al., 2023). In a recent study, Zhao et al. (2023) investigated the expression and function of homologs of *CYCLOIDEA, and DIVARICATA*. The *DeajCYC1a* homolog was expressed in ventral sepals only at stage 12 (Supplementary Table 4). This gene is more broadly expressed in *D. anthriscifolium* and *S. picta*, two other members of the Delphinieae tribe (Zhao et al., 2023). Notably, these species have lateral petals, that are absent in *D. ajacis*, and have only 4 reduced petals compared to six in *D. ajacis*. It is tempting to speculate the role of the *CYC1* homolog in regulating lateral petal development. No expression data on *DeajCYC1b* was reported in this study.

Furthermore, *DeajCYC2a* is not expressed in floral organs across any developmental stages (1, 2, 4, 9, 12, 16). *DeajCYC2b* was shown to be moderate to highly and broadly expressed in the dorsal regions of sepals and petals, particularly in stages 4 and 6 (highly), and in the spurred petals and sepals of stages 9, and 12 (moderately, Supplementary Table 4). *DeajDIV1* has broader expression patterns, with high expression in stages 9 and 12, especially in all petaloid organs (Zhao et al., 2023). *DeajDIV2a* also have a broader expression pattern, with high expression in stage 9 dorsal and ventral petals. *DeajDIV2b's* expression is low and is only noticed in floral organs of stages 9 and 12 (Supplementary Table 4, Zhao et al., 2023).

Functional analyses were conducted on all *CYC2* homologs and *DIV* homologs using VIGS (Figure 5, Zhao et al., 2023). A change in symmetry from zygomorphy towards actinomorphy is observed in all knockdowns, with *TRV2-DeajCYC2b* phenotypes exhibiting almost perfect actinomorphy. *DeajCYC2b* is specifically implicated in regulating dorsal spur development (Supplementary Table 4, Zhao et al., 2023). Silenced flowers exhibit six sepals and no spur growth is observed in dorsal sepals (Figure 5). The fused dorsal petals are transformed into a reduced petal and no spur formation is seen. This is different from B gene silencing where dorsal fused petals homeotically transform into fused double spurred sepals.

The silenced *DeajCYC2a* flowers contained mostly six sepals with spurs in the W1. The W2 petal phenotypes were also striking, with silenced flowers having seven spurred petals, including the dorsal fused petal with spur, and six other petals with spurs in place of reduced petals (Figure 5). The phenotype obtained suggests that *DeajCYC2a* may be expressed at a very low level, which was not detected in the expression studies. Alternatively, *DeajCYC2a* may have been transiently expressed during a specific developmental stage that was not captured in the expression data. The *DeajDIV1/2a/2b* knockdown phenotypes were quite similar to *DeajCYC2a*, with the difference that W2 dorsal petals are not fused in strongly silenced flowers. These phenotypes implicate a role of *DeajCYC2a* and *DeajDIV* homologs in the establishment of lateral and ventral identity of flowers by repressing the development of reduced petals and spurs in sepals (Supplementary Table 4, Zhao et al., 2023).

The *DeajCYC2* homologs underwent asymmetrical evolution, *DeajCYC2a* have experienced deletions and diverged markedly. Interestingly, in the expression studies presented by Zhao et al. (2023), *DeajCYC2a* is not expressed in floral organs of three different stages (9,12,16) in three *Delphinium* species (*D. ajacis*, *D. anthriscifolium* and *S. picta*, Zhao et al., 2023). However, its downregulation results in shifting the symmetry towards actinomorphy with all sepals that are spurred including extra spurred sepal(s), additionally all reduced petals homeotically transform into spurred petals (Figure 5). Based on functional data obtained from silencing *CYC2* homologs, this study inferred a plausible hypothesis that the ancestor of Delphinieae might have been actinomorphic with spurs in all petaloid organs, referred as all-spur-first hypothesis.

The expansive study by Zhao et al. (2023) also reported various regulatory pathways that link the interactions of floral organ identity and floral symmetry genes. One compelling piece of evidence was that the promotor region of *D. ajacis AP3-3* (*DeajAP3-3*) contains a CYC-binding site, GGTCCCGC, and the expression of *DeajCYC2b* precedes *DeajAP3-3* (Figure 5). This finding suggests *DeajCYC2b* can possibly act as a positive regulator for the *AP3-3* gene. Another intriguing finding of the study by Zhao et al. (2023) was the role of *AGL6* gene homologs in regulating spur development. *AGL6* are members of the type II MADS-box gene family (Dreni and Zhang, 2016). In *Delphinium* there are two *AGL6* homologs, *DeajAGL61a* and *DeajAGL61b*, both are broadly expressed across all floral organs (Supplementary Table 4). The resultant phenotype of downregulating *TRV2-DeajAGL61a* resembled that of *TRV2-DeajCYC2a* and to some extent of TRV2 *DeajDIV1/2a/2b* (Figure 5). As mentioned above, in the silenced flowers, the symmetry shifts towards actinomorphy, all sepals in W1 and petals in W2 were spurred, resulting in multiple spur-in-spur structures. Similar to *CYC2a* and *DIV* homologs, the reduced petals were homeotically transformed into spurred petals, the dorsal petal was fused and single-spurred. Analysis of the knockdown phenotypes of *AGL6* homolog implicated complex interactions between *AGL6*, *CYC*, and *DIV* homologs. Forming a feedback loop directly or indirectly the plausible hypothesis is, *AGL61a* and *DIV1* homologs promote the expression of *CYC2a* while *CYC2a* represses both. Additionally, *AGL6* represses *DIV1*. This study not only revealed the role of *AGL6* homolog in repressing spur formation but also in lateral and ventral petal development (Zhao et al., 2023). The exact functioning of how this feedback loop works needs further exploration.

7 Summary

Within angiosperms, the transitions from actinomorphy to zygomorphy have occurred several times independently. In the case of Delphinieae, this transition is also accompanied by the evolution of the spur(s)-in-spur synorganized hyperorgan. Variability in the size, number, and morphology of spurred organs contributes to the diversity in hyperorgan architecture observed across the tribe. As Delphinieae expanded geographically from East Asia to North America and Africa, their life cycles evolved from facultative annuals/biennials to perennials. Although bees are the primary pollinators across the tribe, some species are also pollinated by hawkmoths and hummingbirds.

Recent genetic and functional studies have revealed the co-option of *CYC*, and *DIV* homologs in regulating floral symmetry. Gene duplications in *CYC* genes, MADS-box organ identity, and *AGL6* genes have resulted in the evolution of complex morphology of *Delphinium* flowers. Particularly, the role of *DeajAGL61a* gene homologs in suppressing spur development and the possibility of its genetic interactions with *DeajCYC2a* in regulating floral symmetry have been intriguing findings.

Overall, this early-diverging eudicot genus provides a unique opportunity to understand the evolutionary and genetic mechanisms underlying zygomorphy and complex flower evolution. This review aims to comprehensively highlight the novelty and potential of *Delphinium* as a model system for evo-devo studies.

8 Future directions

Published work related to flower ecology and evo-devo in Delphinieae has set an excellent foundation for understanding the evolutionary and developmental processes underlying floral diversity. This work has underscored the opportunities for delving deeper into and using the morphological innovations in these complex flowers as the raw material to study the evolution of functional traits. Below, we highlight some key questions that can be addressed in future research.

- Resolving the Delphinieae species-level phylogeny to clarify the unresolved questions related to the origination of the tribe. How has the biogeographical expansion affected the morphology and the pollination syndrome in *Delphinium* begs more attention.
- A compelling question related to floral morphology is elucidating the genetic networks that control distinct petaloidy of spurred and non-spurred petals and sepals and understanding how zygomorphy regulates or modulates spur development in sepals and petals.
- Sequencing *Delphinium's* genome will facilitate comparative genomic and transcriptomic studies. Given the size of the genome, this is a major undertaking, so an alternative approach would be to sequence gene-rich regions.
- Exploration of the biophysical and cell division aspects that sculpt the spur(s)-in-spur three-dimensional growth of the dorsal hyperorgan will help understand the phenomenon underlying complex three-dimensional organ growth.
- An intriguing avenue for research lies in understanding the evolution and rewiring of genetic pathways that underpin annual, biennial, and perennial lifestyles in the tribe Delphinieae. Comparative -omics studies in extant species in each life cycle group can yield a wealth of knowledge that can inform targeted crop improvements, thereby advancing agricultural sustainability and productivity.

Author contributions

BS: Conceptualization, Formal analysis, Funding acquisition, Project administration, Resources, Supervision, Validation, Visualization, Writing – original draft, Writing – review & editing. MP: Funding acquisition, Investigation, Writing – original draft, Writing – review & editing. AA: Funding acquisition, Investigation, Writing – original draft, Writing – review & editing. RR: Formal Analysis, Funding acquisition, Writing – original draft, Writing – review & editing. MB: Funding acquisition, Writing – original draft, Writing – review & editing.

Funding

The author(s) declare financial support was received for the research, authorship, and/or publication of this article. BS is supported by the Provost Teacher-Scholar Award, Strategic Interdisciplinary Research Grant, and Agriculture Research Institute grant 20-04-122. This project was supported by an USDA NIFA Hispanic Serving Institution grant to the California State University Agricultural Research Institute, award number 2019-38422-30208 to MP and RR. MP and RR are also supported by the CPP STARS Program. AEQA- Is supported through Grant no- T32GM137812 through NIH, B2D program. MB is supported by McNair Scholars Program.

Acknowledgments

The authors would like to thank members of the Sharma lab, especially graduate student, Ms. Sarah Ramirez, and undergraduate student Christian Suarez and the reviewers for their comments on the manuscript. We would also like to thank Dr. Valerie Mellano for providing seeds for *Delphinium X belladonna "Bellamosum"*. The authors especially thank Dr. Elena M. Kramer for discussing and providing comments on this manuscript.

Conflict of interest

The authors declare that the research was conducted in the absence of any commercial or financial relationships that could be construed as a potential conflict of interest.

Publisher's note

All claims expressed in this article are solely those of the authors and do not necessarily represent those of their affiliated organizations, or those of the publisher, the editors and the reviewers. Any product that may be evaluated in this article, or claim that may be made by its manufacturer, is not guaranteed or endorsed by the publisher.

Supplementary material

The Supplementary Material for this article can be found online at: https://www.frontiersin.org/articles/10.3389/fpls.2024.1453951/full#supplementary-material

References

Antoń, S., and Kamińska, M. (2015). Comparative floral spur anatomy and nectar secretion in four representatives of Ranunculaceae. *Protoplasma* 252, 1587–1601. doi: 10.1007/s00709-015-0794-5

Bosch, M., López-Pujol, J., Blanché, C., and Simon, J. (2023). DCDB: chromosome database of tribe delphinieae (Ranunculaceae): structure, exploitation, and recent development. *Methods Mol. Biol.* 2703, 173–192. doi: 10.1007/978-1-0716-3389-2_13

Bosch, M., Simon, J., Blanché, C., and Molero, J. (1997). Pollination ecology in tribe Delphinieae (Ranunculaceae) in W Mediterranean area: floral visitors and pollinator behaviour. *Lagascalia* 19, 545–562.

Bosch, M., Simon, J., Molero, J., and Blanché, C. (2001). Breeding systems in tribe *Delphinieae* (Ranunculaceae) in the western Mediterranean area. *Flora* 196, 101–113. doi: 10.1016/S0367-2530(17)30025-7

Bowman, J. L., Smyth, D. R., and Meyerowitz, E. M. (1991). Genetic interactions among floral homeotic genes of *Arabidopsis*. *Development* 112, 1–20. doi: 10.1242/dev.112.1.1

Brigham-Grette, J. (2001). New perspectives on Beringian Quaternary paleogeography, stratigraphy, and glacial history. *Quaternary. Sci. Rev.* 20, 15–24. doi: 10.1016/S0277-3791(00)00134-7

Chartier, M., Dressler, S., Schönenberger, J., Mora, A. R., Sarthou, C., Wang, W., et al. (2016). The evolution of afro-montane Delphinium (Ranunculaceae): Morphospecies, phylogenetics and biogeography. *TAXON* 65, 1313–1327. doi: 10.12705/656.6

Chen, Y., Jabbour, F., Novikov, A., Wang, W., and Gerber, S. (2018). A study of floral shape variation in Delphinieae (Ranunculaceae) using geometric morphometrics on herbarium specimens. *Bot. Lett.* 165, 368–376. doi: 10.1080/23818107.2018.1427145

Christenhusz, M., and Byng, J. (2016). The number of known plant species in the world and its annual increase. *Phytotaxa* 261, 201–217. doi: 10.11646/phytotaxa.261.3.1

Citerne, H., Jabbour, F., Nadot, S., and Damerval, C. (2010). "The evolution of floral symmetry," in *Advances in botanical research*. Eds. J.-C. Kader and M. Delseny (United Kingdom: Elsevier Science & Technology), 85–137. doi: 10.1016/S0065-2296(10)54003-5

Coen, E. S., and Meyerowitz, E. M. (1991). The war of the whorls: genetic interactions controlling flower development. *Nature* 353, 31–37. doi: 10.1038/353031a0

Delpeuch, P., Jabbour, F., Damerval, C., Schönenberger, J., Pamperl, S., Rome, M., et al. (2022). A flat petal as ancestral state for Ranunculaceae. *Front. Plant Sci.* 13. doi: 10.3389/fpls.2022.961906

Drea, S., Hileman, L. C., De Martino, G., and Irish, V. F. (2007). Functional analyses of genetic pathways controlling petal specification in poppy. *Development* 134, 4157–4166. doi: 10.1242/dev.013136

Dreni, L., and Zhang, D. (2016). Flower development: the evolutionary history and functions of the AGL6 subfamily MADS-box genes. *J. Exp. Bot.* 67, 1625–1638. doi: 10.1093/jxb/erw046

Duan, H., Lu, Y., Duan, X., Zhou, X., Wang, C., Tian, F., et al. (2020). Characterization of the complete chloroplast genome of Delphinium grandiflorum L. *Mitochondrial. DNA Part B.* 5, 35–36. doi: 10.1080/23802359.2019.1692707

DuPasquier, P.-E., Andro-Durand, V., Batory, L., Wang, W., and Jabbour, F. (2021). Nomenclatural revision of delphiniumsubg.Consolida (DC.) huth (Ranunculaceae). *PhytoKeys* 180, 81–110. doi: 10.3897/phytokeys.180.67126

Endress, P. K. (2011). Angiosperm ovules: diversity, development, evolution. *Ann. Bot.* 107, 1465–1489. doi: 10.1093/aob/mcr120

Espinosa, F., Damerval, C., Le Guilloux, M., Deroin, T., Wang, W., Pinedo-Castro, M., et al. (2021a). Homeosis and delayed floral meristem termination could account for abnormal flowers in cultivars of Delphinium and Aquilegia (Ranunculaceae). *Bot. J. Linn. Soc.* 195, 485–500. doi: 10.1093/botlinnean/boaa063

Espinosa, F., Deroin, T., Malécot, V., Wang, W., Pinedo, M., Nadot, S., et al. (2021b). Historical note on the taxonomy of the genus Delphinium L. (Ranunculaceae) with an amended description of its floral morphology. *adan* 43, 9–18. doi: 10.5252/adansonia2021v43a

Espinosa, F., Deroin, T., Xiang, K.-L., Wang, W., Castro, M. P., Byng, J. W., et al. (2017). The turkish endemic pseudodelphinium turcicum (Ranunculaceae): an unusual population of delphinium with peloric flowers that has persisted in the wild for 20 years. *Int. J. Plant Sci.* 178, 546–555. doi: 10.1086/692764

Hileman, L. C. (2014a). Bilateral flower symmetry—how, when and why? *Curr. Opin. Plant Biol.* 17, 146–152. doi: 10.1016/j.pbi.2013.12.002

Hileman, L. C. (2014b). Trends in flower symmetry evolution revealed through phylogenetic and developmental genetic advances. *Philos. Trans. R. Soc. London. Ser. B. Biol. Sci.* 369, 20130348. doi: 10.1098/rstb.2013.0348

Hodges, S. A. (1997). Floral nectar spurs and diversification. *Int. J. Plant Sci.* 158, S81–S88. doi: 10.1086/297508

Honma, T., and Goto, K. (2001). Complexes of MADS-box proteins are sufficient to convert leaves into floral organs. *Nature* 409, 525–529. doi: 10.1038/35054083

Howarth, D. G., Martins, T., Chimney, E., and Donoghue, M. J. (2011). Diversification of CYCLOIDEA expression in the evolution of bilateral flower symmetry in Caprifoliaceae and Lonicera (Dipsacales). *Ann. Bot.* 107, 1521–1532. doi: 10.1093/aob/mcr049

Jabbour, F., Cossard, G., Le Guilloux, M., Sannier, J., Nadot, S., and Damerval, C. (2014). Specific duplication and dorsoventrally asymmetric expression patterns of cycloidea-like genes in zygomorphic species of ranunculaceae. *PloS One* 9, e95727. doi: 10.1371/journal.pone.0095727

Jabbour, F., Nadot, S., and Damerval, C. (2009a). Evolution of floral symmetry: a state of the art. *Comptes. Rendus. Biol.* 332, 219–231. doi: 10.1016/j.crvi.2008.07.011

Jabbour, F., and Renner, S. S. (2011a). *Consolida* and *Aconitella* are an annual clade of *Delphinium* (Ranunculaceae) that diversified in the Mediterranean basin and the Irano-Turanian region. *TAXON* 60, 1029–1040. doi: 10.1002/tax.604007

Jabbour, F., and Renner, S. S. (2011b). Resurrection of the genus Staphisagria J. Hill, sister to all the other Delphinieae (Ranunculaceae). *PhytoKeys*, 21–26. doi: 10.3897/phytokeys.7.2010

Jabbour, F., and Renner, S. S. (2012a). A phylogeny of Delphinieae (Ranunculaceae) shows that Aconitum is nested within Delphinium and that Late Miocene transitions to long life cycles in the Himalayas and Southwest China coincide with bursts in diversification. *Mol. Phylogenet. Evol.* 62, 928–942. doi: 10.1016/j.ympev.2011.12.005

Jabbour, F., and Renner, S. S. (2012b). Spurs in a spur: perianth evolution in the delphinieae (Ranunculaceae). *Int. J. Plant Sci.* 173, 1036–1054. doi: 10.1086/667613

Jabbour, F., Ronse De Craene, L. P., Nadot, S., and Damerval, C. (2009b). Establishment of zygomorphy on an ontogenic spiral and evolution of perianth in the tribe Delphinieae (Ranunculaceae). *Ann. Bot.* 104, 809–822. doi: 10.1093/aob/mcp162

Jabbour, F., Zalko, J., Morel, A., Frachon, S., and Bouchart-Dufay, I. (2021). "Ontogeny and evolution of the hyperorgan of delphinieae," in *Systematics and the Exploration of Life*. Eds. P. Grandcolas and M. Maurel (Wiley), 171–184. doi: 10.1002/9781119476870.ch9

Jensen, U., and Kadereit, J. W. (1995). *Systematics and Evolution of the Ranunculiflorae* (Vienna: Springer Vienna). doi: 10.1007/978-3-7091-6612-3_20

Johnson, S. (2008). Hawkmooth pollination and hybridization in Delphinium leroyi (Ranunculaceae) on the Nyika Plateau, Malawi. *Nordic. J. Bot.* 21, 599–605. doi: 10.1111/j.1756-1051.2001.tb00819.x

Kosuge, K. (1994). "Petal evolution in ranunculaceae," in *Early Evolution of Flowers*. Eds. P. K. Endress and E. M. Friis (Springer Vienna, Vienna), 185–191. doi: 10.1007/978-3-7091-6910-0_11

Kosuge, K., and Tamura, M. (1988). Morphology of the petal in aconitum. *Bot. Mag. Tokyo.* 101, 223–237. doi: 10.1007/BF02488601

Kramer, E. M., and Hodges, S. A. (2010). *Aquilegia* as a model system for the evolution and ecology of petals. *Phil. Trans. R. Soc B.* 365, 477–490. doi: 10.1098/rstb.2009.0230

Kramer, E. M., Holappa, L., Gould, B., Jaramillo, M. A., Setnikov, D., and Santiago, P. M. (2007). Elaboration of B gene function to include the identity of novel floral organs in the lower eudicot *aquilegia*. *Plant Cell* 19, 750–766. doi: 10.1105/tpc.107.050385

Kramer, E. M., Jaramillo, M. A., and Di Stilio, V. S. (2004). Patterns of gene duplication and functional evolution during the diversification of the *AGAMOUS* subfamily of MADS box genes in angiosperms. *Genetics* 166, 1011–1023. doi: 10.1534/genetics.166.2.1011

Kramer, E. M., and Zimmer, E. A. (2006). "Gene duplication and floral developmental genetics of basal eudicots," in *Advances in Botanical Research* (Elsevier), 353–384. doi: 10.1016/S0065-2296(06)44009-X

Lehtonen, S., Christenhusz, M. J. M., and Falck, D. (2016). Sensitive phylogenetics of Clematis and its position in Ranunculaceae. *Bot. J. Linn. Soc.* 182, 825–867. doi: 10.1111/boj.12477

Leppik, E. E. (1964). Floral evolution in the ranunculaceae. *Iowa. State. J. Sci.* 39, 1–101.

Li, S., Fan, J., Xue, C., Shan, H., and Kong, H. (2024a). Spur development and evolution: An update. *Curr. Opin. Plant Biol.* 81, 102573. doi: 10.1016/j.pbi.2024.102573

Li, Q., Guo, X., Yuan, F., Nima, C., Dongzhi, D., Duojie,, et al. (2020). Characterization of the complete chloroplast genome of the Musk Larkspur Delphinium brunonianum (Ranunculales: Ranunculaceae). *Mitochondrial. DNA Part B.* 5, 2394–2396. doi: 10.1080/23802359.2020.1775522

Li, D.-M., Li, J., Wang, D.-R., Xu, Y.-C., and Zhu, G.-F. (2021). Molecular evolution of chloroplast genomes in subfamily Zingiberoideae (Zingiberaceae). *BMC Plant Biol.* 21, 558. doi: 10.1186/s12870-021-03315-9

Li, D.-M., Pan, Y.-G., Wu, X.-Y., Zou, S.-P., Wang, L., and Zhu, G.-F. (2024b). Comparative chloroplast genomics, phylogenetic relationships and molecular markers development of Aglaonema commutatum and seven green cultivars of Aglaonema. *Sci. Rep.* 14, 11820. doi: 10.1038/s41598-024-62586-y

Litt, A. (2007). An evaluation of A-function: evidence from the *APETALA1* and *APETALA2* gene lineages. *Int. J. Plant Sci.* 168, 73–91. doi: 10.1086/509662

Luo, X.-Y., Nie, T.-J., Liu, H., Ding, X.-F., Huang, Y., Guo, C.-C., et al. (2023). Karyotype and genome size variation in Delphinium subg. Anthriscifolium (Ranunculaceae). *PhytoKeys* 234, 145–165. doi: 10.3897/phytokeys.234.108841

Macior, L. W. (1975). The pollination ecology of *delphinium tricorne* (RANUNCULACEAE). *Am. J. Bot.* 62, 1009–1016. doi: 10.1002/j.1537-2197.1975.tb11765.x

Madrigal, Y., Alzate, J. F., and González, F. (2019).). Evolution of RADIALIS and DIVARICATA gene lineages in flowering plants with an expanded sampling in non-core eudicots. *Am. J. Bot.* 106(3): 334–351. doi: 10.1002/ajb2.1243

Magallón, S., Gómez-Acevedo, S., Sánchez-Reyes, L. L., and Hernández-Hernández, T. (2015). A metacalibrated time-tree documents the early rise of flowering plant phylogenetic diversity. *New Phytol.* 207, 437–453. doi: 10.1111/nph.13264

Moore, M. J., Bell, C. D., Soltis, P. S., and Soltis, D. E. (2007). Using plastid genome-scale data to resolve enigmatic relationships among basal angiosperms. *Proc. Natl. Acad. Sci. U.S.A.* 104, 19363–19368. doi: 10.1073/pnas.0708072104

Novikoff, A., and Jabbour, F. (2014). Floral anatomy of delphinieae (Ranunculaceae): comparing flower organization and vascular patterns. 35–44. doi: 10.5281/ZENODO.161001

Park, S., An, B., and Park, S. (2020). Recurrent gene duplication in the angiosperm tribe Delphinieae (Ranunculaceae) inferred from intracellular gene transfer events and heteroplasmic mutations in the plastid matK gene. *Sci. Rep.* 10, 2720. doi: 10.1038/s41598-020-59547-6

Payer, J.-B. (1857). *Traite d'organogenie comparee de la fleur par J.-B. Payer: Texte* (Masson).

Rasmussen, D. A., Kramer, E. M., and Zimmer, E. A. (2009). One size fits all? Molecular evidence for a commonly inherited petal identity program in Ranunculales. *Am. J. Bot.* 96, 96–109. doi: 10.3732/ajb.0800038

Reyes, E., Sauquet, H., and Nadot, S. (2016). Perianth symmetry changed at least 199 times in angiosperm evolution. *TAXON* 65, 945–964. doi: 10.12705/655.1

Ronse De Craene, L. P., Soltis, P. S., and Soltis, D. E. (2003). Evolution of floral structures in basal angiosperms. *Int. J. Plant Sci.* 164, S329–S363. doi: 10.1086/377063

Sauquet, H., Ramírez-Barahona, S., and Magallón, S. (2022). What is the age of flowering plants? *J. Exp. Bot.* 73, 3840–3853. doi: 10.1093/jxb/erac130

Sauquet, H., Von Balthazar, M., Magallón, S., Doyle, J. A., Endress, P. K., Bailes, E. J., et al. (2017). The ancestral flower of angiosperms and its early diversification. *Nat. Commun.* 8, 16047. doi: 10.1038/ncomms16047

Schöffel, K. (1932). UNTERSUCHUNGEN ÜBER DEN BLÜTENBAU DER RANUNCULACEEN. *Z. Fu{{i}}ür. Wissenschaftliche. Biologie. Abteilung. E. Planta.* 17, 315–371.

Sharma, B., Guo, C., Kong, H., and Kramer, E. M. (2011). Petal-specific subfunctionalization of an *APETALA3* paralog in the Ranunculales and its implications for petal evolution. *New Phytol.* 191, 870–883. doi: 10.1111/j.1469-8137.2011.03744.x

Sharma, B., and Kramer, E. M. (2017). Aquilegia B gene homologs promote petaloidy of the sepals and maintenance of the C domain boundary. *EvoDevo* 8, 22. doi: 10.1186/s13227-017-0085-7

Sharma, B., Yant, L., Hodges, S. A., and Kramer, E. M. (2014). Understanding the development and evolution of novel floral form in Aquilegia. *Curr. Opin. Plant Biol.* 17, 22–27. doi: 10.1016/j.pbi.2013.10.006

Soltis, D. E., and Soltis, P. S. (1998). "Choosing an approach and an appropriate gene for phylogenetic analysis," in *Molecular Systematics of Plants II*. Eds. D. E. Soltis, P. S. Soltis and J. J. Doyle (Springer US, Boston, MA), 1–42. doi: 10.1007/978-1-4615-5419-6_1

Song, C., Zhu, J., and Li, H. (2024). Complete chloroplast genomes of eight Delphinium taxa (Ranunculaceae) endemic to Xinjiang, China: insights into genome structure, comparative analysis, and phylogenetic relationships. *BMC Plant Biol.* 24, 600. doi: 10.1186/s12870-024-05279-y

Theissen, G., and Saedler, H. (2001). Floral quartets. *Nature* 409, 469–471. doi: 10.1038/35054172

The RanOmics group, Becker, A., Bachelier, J. B., Carrive, L., Conde e Silva, N., Damerval, C., et al. (2024). A cornucopia of diversity—Ranunculales as a model lineage. *J. Exp. Bot.* 75, 1800–1822. doi: 10.1093/jxb/erad492

Whittall, J. B., and Hodges, S. A. (2007). Pollinator shifts drive increasingly long nectar spurs in columbine flowers. *Nature* 447, 706–709. doi: 10.1038/nature05857

Xiang, K.-L., Aytaç, Z., Liu, Y., Espinosa, F., Jabbour, F., Byng, J. W., et al. (2017). Recircumscription of *Delphinium* subg. *Delphinium* (Ranunculaceae) and implications for its biogeography. *TAXON* 66, 554–566. doi: 10.12705/663.3

Zalko, J., Frachon, S., Morel, A., Deroin, T. x. F., Xiang, K.-L., et al. (2021). Floral organogenesis and morphogenesis of *staphisagria* (Ranunculaceae): implications for the evolution of synorganized floral structures in delphinieae. *Int. J. Plant Sci.* 182, 59–70. doi: 10.1086/711471

Zhai, W., Duan, X., Zhang, R., Guo, C., Li, L., Xu, G., et al. (2019). Chloroplast genomic data provide new and robust insights into the phylogeny and evolution of the Ranunculaceae. *Mol. Phylogenet. Evol.* 135, 12–21. doi: 10.1016/j.ympev.2019.02.024

Zhang, W., Kramer, E. M., and Davis, C. C. (2010). Floral symmetry genes and the origin and maintenance of zygomorphy in a plant-pollinator mutualism. *Proc. Natl. Acad. Sci. U.S.A.* 107, 6388–6393. doi: 10.1073/pnas.0910155107

Zhang, W., Steinmann, V. W., Nikolov, L., Kramer, E. M., and Davis, C. C. (2013). Divergent genetic mechanisms underlie reversals to radial floral symmetry from diverse zygomorphic flowered ancestors. *Front. Plant Sci.* 4. doi: 10.3389/fpls.2013.00302

Zhang, P., Xie, Y., Xie, W., Li, L., Zhang, H., Duan, X., et al. (2024a). Roles of the APETALA3-3 ortholog in the petal identity specification and morphological differentiation in Delphinium anthriscifolium flowers. *Hortic. Res.* 11, uhae097. doi: 10.1093/hr/uhae097

Zhang, H., Xue, F., Guo, L., Cheng, J., Jabbour, F., DuPasquier, P.-E., et al. (2024b). The mechanism underlying asymmetric bending of lateral petals in *Delphinium* (Ranunculaceae). *Curr. Biol.* 34, 755–768.e4. doi: 10.1016/j.cub.2024.01.004

Zhao, H., Liao, H., Li, S., Zhang, R., Dai, J., Ma, P., et al. (2023). Delphinieae flowers originated from the rewiring of interactions between duplicated and diversified floral organ identity and symmetry genes. *Plant Cell* 35, 994–1012. doi: 10.1093/plcell/koac368

Frontiers in
Plant Science

Cultivates the science of plant biology and its applications

The most cited plant science journal, which advances our understanding of plant biology for sustainable food security, functional ecosystems and human health.

Discover the latest Research Topics

See more →

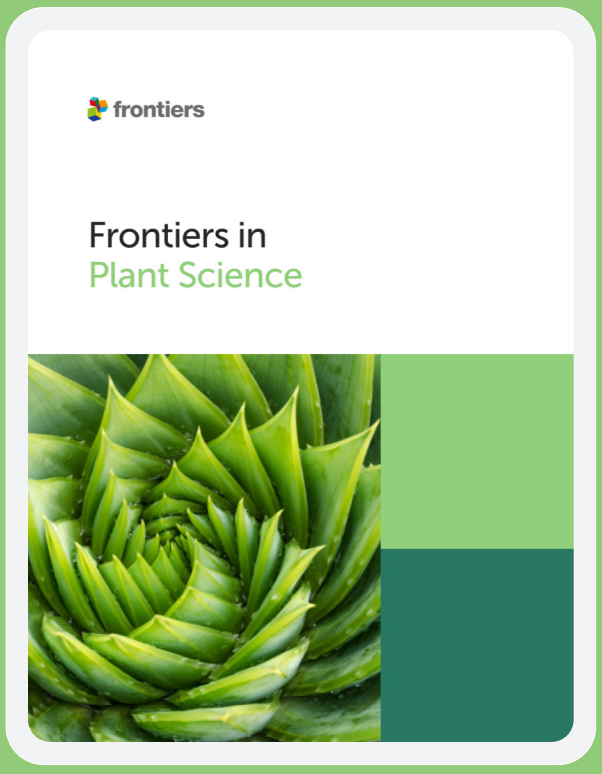

Frontiers

Avenue du Tribunal-Fédéral 34
1005 Lausanne, Switzerland
frontiersin.org

Contact us

+41 (0)21 510 17 00
frontiersin.org/about/contact